Computational Fluid and Solid Mechanics

Dominique Chapelle
Klaus-Jürgen Bathe

The Finite Element Analysis of Shells–Fundamentals

Second Edition

Springer

Computational Fluid and Solid Mechanics

Series Editor

K.J. Bathe
Massachusetts Institute of Technology, Cambridge, MA, USA

For other titles published in this series, go to
http://www.springer.com/series/4449

Dominique Chapelle · Klaus-Jürgen Bathe

The Finite Element Analysis of Shells – Fundamentals

Second Edition

Springer

Dominique Chapelle
INRIA Paris-Rocquencourt
France

Klaus-Jürgen Bathe
Massachusetts Institute of
Technology
USA

ISSN 1860-482X e-ISSN 1860-4838
ISBN 978-3-642-16407-1 e-ISBN 978-3-642-16408-8
DOI 10.1007/978-3-642-16408-8
Springer Heidelberg Dordrecht London New York

Library of Congress Control Number: 2010937756

Cover design: deblik, Berlin

Printed on acid-free paper

Springer is part of Springer Science+Business Media (www.springer.com)

To our fruitful collaboration and long-lasting friendship

Preface – Second Edition

Since our writing of the first edition of this book, some important advances in finite element methods for shell analyses have been achieved. In this new edition, we present some of these new developments. In addition, we have endeavored to strengthen the presentation throughout the text.

The major changes and additions in the book pertain to the section on the presentation of general variational formulations and finite element approximations, the new sections on 3D-shell models and finite element discretizations, on dynamic analyses, and on triangular elements. We also added more explanations in the text, and many new examples and figures in order to render the book more complete.

We endeavored to achieve more completeness also because the analysis of shells represents one of the most challenging fields in *all* of mechanics, and encompasses various fundamental and generally applicable components. Specifically, the material presented in this book regarding geometric descriptions, tensors and mixed variational formulations is fundamental and applicable also in other areas of mechanics.

However, in the writing of this second edition, we have not changed our basic objective, that is, in the book we continue to focus on the fundamentals of shell analysis and the synergy between the physical and mathematical understanding – as we have described in more detail in the Preface of the first edition.

Finally, in addition to the acknowledgments made in the first edition, Dominique Chapelle would like to warmly thank his colleague and friend Philippe Moireau for his feedback on this second edition, and Klaus-Jürgen Bathe would like to acknowledge his very valuable collaboration on advancing methods for shell analysis, reflected by references and results in this book, with his former student and now a Professor at KAIST, Phill-Seung Lee.

D. Chapelle and K.J. Bathe

Preface – First Edition

Since the first developments of finite element methods for the analysis of shells, about half a century ago, the possibilities to analyze shells in designs and to study, in general, the behavior of shell structures have vastly increased. However, at the same time as shell finite element procedures were rapidly introduced in many everyday practices of engineering analysis, also, a large research effort was directed towards increasing the capabilities of shell finite element methods, for linear and nonlinear analyses. This research effort is still ongoing because of the great challenges in shell structural analyses. These challenges are largely due to the diversity of shell structural behaviors and the difficulties to solve for such behaviors in a reliable and uniformly effective, ideally optimal, manner. The difficulties are apparent when considering complex shells of arbitrary curvatures, material conditions, boundary supports, loading, and in particular of small thickness. Furthermore, these challenges have grown during the last decades, and probably will continue to grow, because increasingly more daring – but also more beautiful – shell structures have been designed and analyzed than previously thought possible.

The earliest studies of shell structures using analytical methods were performed well over a century ago. At that time, and indeed until the development of the finite element method, researchers used all the available *physical and mathematical understanding* to formulate shell theories and solve shell problems. While the shell theories were quite general in nature, the actual solutions obtained to a shell problem were mostly very approximate, that is, when compared with the actual physical behavior of the shell considered.

With the development of the modern finite element method, the approach towards the practical solution of shell problems changed. Finite element procedures were largely developed based on physical understanding without the use of mathematical shell theories. Indeed, various shell finite element methods were proposed by simply superimposing plate bending and plane stress membrane behaviors. With this approach many shell structures were successfully analyzed, but of course only to a certain level of accuracy. In fact, the significant limitations of such element formulations became also apparent and, to some extent, recourse to the use of shell theories was sought to develop more powerful finite element methods.

The effective study of shell structures clearly requires a deep physical understanding of shell structural behaviors. The development of more powerful finite element methods requires in addition a strong knowledge of mathematical theories. Indeed, it is clearly the *synergy between physical and mathematical understanding* that will advance our knowledge of shell structural behaviors and the development of finite element methods. This, in fact, corresponds to the approach taken many years ago in the study of shell structures, but is now a path more difficult to follow. Namely, the mathematical theories now available are much more advanced and are still developing.

Our objective with this book is to provide a text in which the fundamentals of shell theories, mathematical analyses, and finite element methods are presented with a view towards the synergy mentioned above. Hence we endeavor to present and emphasize the physical concepts of shell analyses and their mathematical bases. With the text directed towards finite element solutions, we explore the complexity of the physical behaviors of shells in order to explain the difficulties to obtain uniformly optimal finite element procedures. While, of course, already quite effective finite element methods are available, our aim is, as well, to provide important fundamental considerations – including basic testing procedures – for the development of more powerful methods.

An important aspect of a shell finite element method is that it be reliable. We discuss this aspect in depth and direct our attention only towards the development of such finite element methods. Only finite element analysis procedures that are reliable and effective can be employed confidently and will be used for many years to come. With such shell analysis techniques, engineers can confidently replace some expensive laboratory testing and, using finite element analysis, experiment at much less expense with exciting new design concepts. In this way, the full benefits of computer-aided engineering are attained.

This text is not intended to be a survey of finite element methods for shell analyses. Indeed, it is a text in which we – to a large extent – only discuss our experiences with shell analysis methods with the focus on the endeavors mentioned above.

The writing of this book required a large effort and we would like to thank all those who have supported us, and made it possible for us, to complete this work.

Dominique Chapelle is grateful to his colleagues at INRIA-Rocquencourt – and in particular to his colleagues in the MACS project – for providing him with a very stimulating and pleasant environment. He would like to extend his special thanks to Marina Vidrascu for her precious help in obtaining some of the numerical results presented in the book.

Klaus-Jürgen Bathe is grateful to the Department of Mechanical Engineering, M.I.T., for the excellent environment made available for his teaching, research and scholarly writing, and to the many students who have con-

tributed in his research group. He would like to acknowledge as well that – to improve his teaching and research efforts – his involvement in ADINA R&D, Inc. has been very valuable.

We both would like to thank Michel Bernadou, Carlo Lovadina and Olivier Pironneau for their valuable comments regarding this book.

Finally, we would like to thank all our loved ones for their continuous support and understanding regarding our scientific endeavors.

D. Chapelle and K.J. Bathe

Contents

1. Introduction

In this chapter, we briefly discuss shell structures – noting also that, actually, the analysis of shell structures gave the impetus for the development of finite element procedures – and we summarize the general approach of analysis of a shell problem. We then give the objectives of this book; namely, to present fundamentals regarding physical considerations, mathematical models and modern finite element procedures for the analysis of shells.

1.1 Shells: from Nature to Engineering Designs

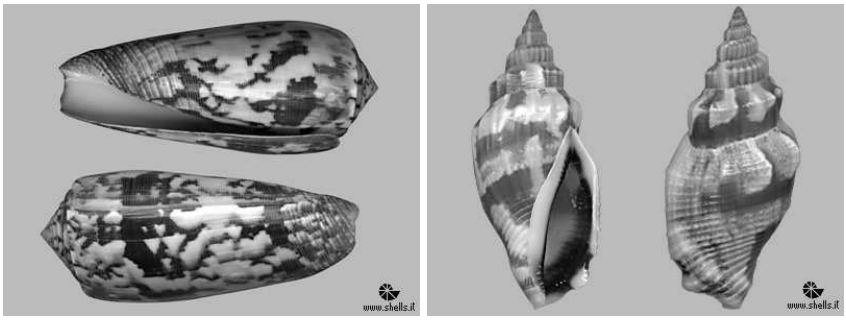

Fig. 1.1. Examples of sea-shells: Conus Striatus (left), Strombus Erythrinus Elegans (right) - Courtesy of A. Petronzi and C. Pirazzini (www.shells.it)

Simply said, a shell structure is a three-dimensional structure, thin in one direction and long in the other two directions. Such structures are abundantly found in nature, see e.g. Figure 1.1. Although thin and light, they span over relatively large areas, and hold applied loads in a very effective way. It seems that with shell structures, nature has maximized the ability to span over large areas with a minimum amount of material – the shell of an egg is an impressive example. Also, of course, shell structures in nature can be very beautiful and have indeed inspired many artists.

In engineering designs, shell structures are found abundantly and are employed in essence for the same reasons: they span over large areas, are light

D. Chapelle, K.-J. Bathe, *The Finite Element Analysis of Shells – Fundamentals*,
Computational Fluid and Solid Mechanics, 2nd ed., DOI 10.1007/978-3-642-16408-8_1,

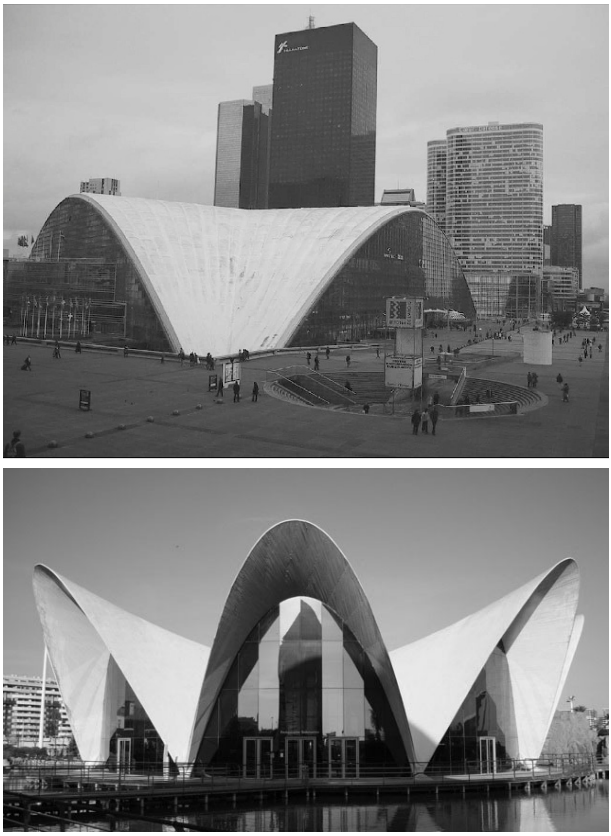

Fig. 1.2. Buildings made of shell structures: CNIT building in Paris-la-Défense (top, roof-span 220m), Valencia aquarium (bottom, courtesy B.H.V. Topping)

and hold applied loads very effectively. Frequently, they can also be built to be beautiful structures. In civil engineering, shell structures constitute large roofs or elegant bridges, see e.g. Figure 1.2; in the automobile industry, the bodies of cars are shells; in aeronautical engineering, the airplane bodies and rockets are shell structures; and in naval architecture, the ship hulls constitute shells. In each of these cases, a thin structure covers a wide area and holds large externally applied loads. Indeed, the objective in the design of such structures is to make the shell as thin as possible in order to make the structure light and use the minimum amount of material; yet have a safe, functional and – when applicable – beautiful structure.

The detailed analysis of a shell structure – as required to obtain an effective design – frequently presents a most difficult and challenging problem. The difficulty of analysis lies in that a shell resists the applied loads largely by its curvature; that is, given the same material and thickness, if the curva-

ture is changed, the shell can have a totally different load carrying capacity. Hence, the thickness, curvature and of course the boundary conditions of a shell structure play crucial roles in its behavior.

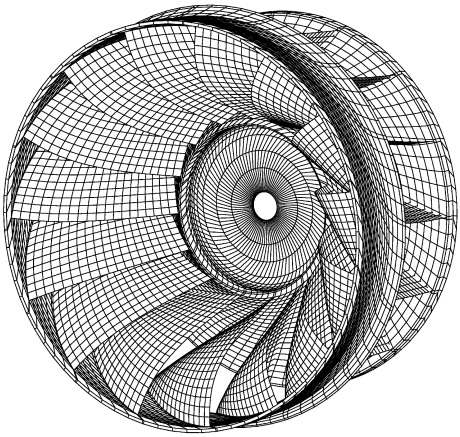

Fig. 1.3. Shell model of a turbine wheel

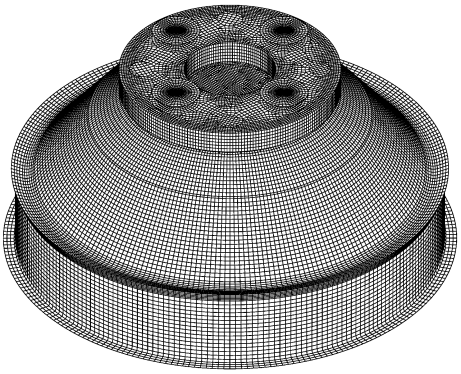

Fig. 1.4. Shell model of a pulley

The peculiarities of shell structural behavior, the difficulties of analysis, and the wide use of shell structures have instigated a large research effort in shell analysis. Various shell theories have been developed and approximate solution techniques have been proposed. However, the most significant advance in shell structural analysis has been made with the development of finite element methods (Bathe, 1996). While finite element procedures are now widely applied in many analysis areas, it is interesting to note that, indeed, it was the analysis of shell structures that gave the impetus for the development

of practical finite element methods (Argyris, 1954; Argyris & Kelsey, 1955; Turner et al., 1956). Since these first solutions, over five decades ago, significant research and development efforts in finite element methods for shells have been conducted and as a result quite effective, general and reliable solution techniques have become available. Figures 1.3 to 1.5 show some finite element models of shell structures as currently used in engineering practice. Although linear analyses of these structures *seem* to be obtained in engineering practice in almost a routine manner, there are many important aspects that need to be understood in order to perform an effective analysis. Of course, a general nonlinear analysis frequently represents a major solution effort and requires even more insight into the structural behavior and solution techniques used.

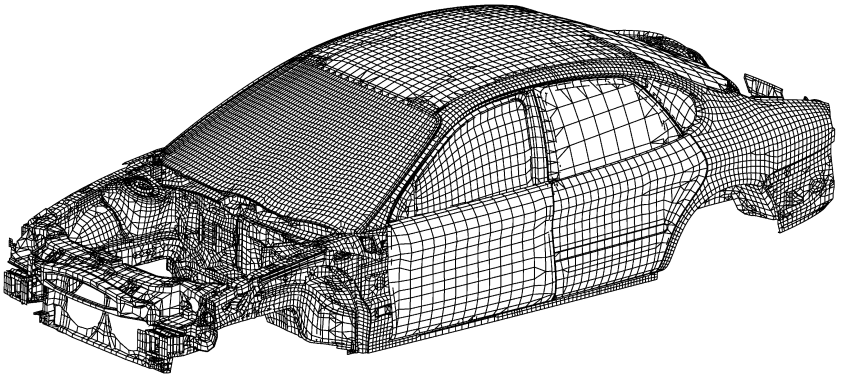

Fig. 1.5. Shell model of a motor car

The objective in this book is to present fundamental formulations, theories and results regarding modern finite element discretization procedures for shell structures. We naturally emphasize the shell analysis procedures that we have researched but aim to give a rather comprehensive discussion. The presentation focuses on the physical and mathematical aspects of general shell structural analyses.

1.2 The Finite Element Analysis of Shells as Approached in this Book

It is important to realize that *in any finite element analysis, the solution of the mathematical model of a physical structure (or more generally physical phenomenon) is numerically approximated using finite element procedures.* The fact that a mathematical model is solved allows the discussion of the behavior and convergence of the mathematical model as parameters thereof are changed. This fact moreover allows the analysis of convergence of the

finite element methods to the exact solution of the mathematical model, and as part thereof, the discussion of the effectiveness of the finite element methods used (Bathe, 1996).

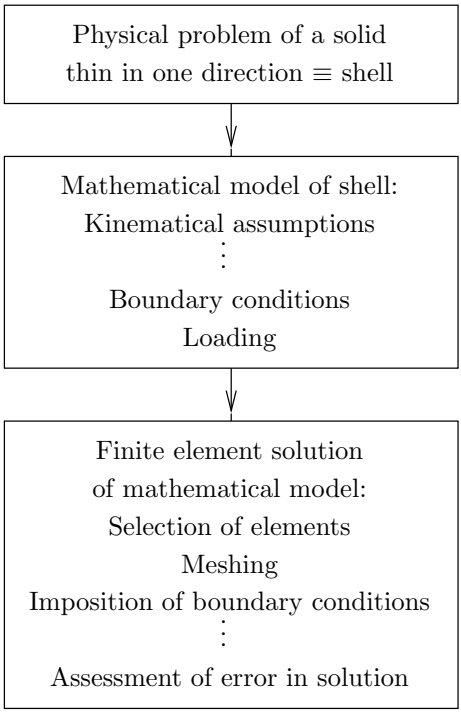

Fig. 1.6. Finite element analysis of a shell problem

Figure 1.6 summarizes the solution process of a shell analysis. We note that the mathematical model (the shell geometry, material data, loading, boundary conditions...) is selected to describe the physical structure and the solution of this mathematical model is approximated using the finite element method. Clearly, the mathematical model must be well-posed for any solution attempt to make sense. The finite element solution results must then be sufficiently close to the exact solution of the mathematical model, and here the concern of using reliable and efficient finite element methods enters. Of course, the finite element solution can only predict any response actually contained in the mathematical model. Hence, once a solution has been obtained, it may well be necessary to change the mathematical model in order to obtain more insight into the actual response of the physical shell structure, see (Bathe, 1996) and (Bucalem & Bathe, 201x)

In the early engineering applications of finite element methods, the mathematical model was frequently not thought of and questions of convergence

were investigated in a rather intuitive manner. This approach was taken because the mathematical tools were largely not yet developed, and even if already available, not known by the engineering researchers who developed finite element methods.

An important objective of this book is to introduce finite element methods for shells using a modern mathematical approach but without clouding the physical aspects.

The approach we therefore take is to present first the basic mathematical tools needed for the formulation of shell theories, and for the discussion of shell structural behaviors and finite element solutions. We then present general mathematical models of shell structures and an analysis of these models. We consider plate structures as special cases of the shell models.

The effective finite element solution of general shell structures requires the use of mixed finite element procedures. Such discretization schemes are much more difficult to formulate and analyze than the pure displacement-based techniques. We present some modern mixed finite element discretization procedures with important mathematical considerations regarding the techniques. Particular attention is given to the reliability of the finite element methods in shell solutions, which is a very important aspect for methods to be used in practice (Bathe, 2009).

The modeling of complex shell structures requires judgment on the use of the available discretization techniques, and we discuss and illustrate various aspects thereof.

The major part of the book focuses on the linear analysis of shell structures, for which we aim to give a thorough discussion of the mathematical models and discretization procedures. However, in the last chapter of the book, we also discuss briefly how the earlier presented considerations and methods are directly applicable in nonlinear analysis.

As we mentioned at the beginning of this chapter, shell structures are widely encountered in engineering practice. In addition to what we might call "true shells" (because the structures are curved), there are as well the special shell analysis cases of plates, folded plate structures and complex beam structures. These structural components are frequently also used as part of a complex shell, which might contain smooth curved surfaces strengthened by beams and plates. In addition, the shell might be constructed of composite materials, which further increases the analysis complexity. All these structures can be analyzed using general shell finite element procedures. Hence, when considering shell finite element analysis in a broad sense, the analysis area is very large and diverse, see for example (Zienkiewicz & Taylor, 1989/1991; Bernadou, 1996; Bathe, 2001a)

With the multitude of different shells encountered, and the peculiarities in their behaviors, it is difficult, but a great intellectual challenge, to develop finite element techniques effective for general shell analysis. This book

presents some of these efforts and, in many respects, provides a basis for further developments in this very challenging field.

2. Geometrical Preliminaries

The description of the geometry is essential for the definition of a shell structure. Our objective in this chapter is to survey the main geometrical concepts, to introduce the related notation and to recall some essential results that will be needed in this book.

2.1 Vectors and Tensors in Three-Dimensional Curvilinear Coordinates

In this section, we provide a brief review of tensor analysis and differential geometry. For more details on these concepts, the reader can refer to (Green & Zerna, 1968), see also (Bernadou, 1996; Ciarlet, 1998).

2.1.1 Vectors and tensors

In the following discussion, we distinguish between

- the three-dimensional (3D) *physical space* – also called the *Euclidean space* – that we denote by $\mathcal{E}$, in which we can define the geometry and the kinematics of all the mechanical objects that we want to consider (3D bodies, plates, shells...);
- the 3D *mathematical space*, denoted by $\mathbb{R}^3$, simply defined as the set of all triples of real numbers, i.e. quantities of the type (ξ^1, ξ^2, ξ^3) where ξ^1, ξ^2 and ξ^3 are reals[1].

We assume that an origin O is given in $\mathcal{E}$, so that we can identify points and vectors. Then, by choosing a basis in $\mathcal{E}$, i.e. three independent vectors $\vec{\imath}_1$, $\vec{\imath}_2$ and $\vec{\imath}_3$ that are attached to O, we obtain a natural (we can say "canonical") one-to-one mapping from $\mathbb{R}^3$ to $\mathcal{E}$ defined by

$$(\xi^1, \xi^2, \xi^3) \mapsto \xi^1 \vec{\imath}_1 + \xi^2 \vec{\imath}_2 + \xi^3 \vec{\imath}_3. \tag{2.1}$$

[1] The reason why we use superscripts in this notation will be explained in the sequel, see Remark 2.1.2.

D. Chapelle, K.-J. Bathe, *The Finite Element Analysis of Shells – Fundamentals*, Computational Fluid and Solid Mechanics, 2nd ed., DOI 10.1007/978-3-642-16408-8_2,

It is then said that ξ^1, ξ^2 and ξ^3 are the *components* of the vector "$\xi^1\vec{\imath}_1 + \xi^2\vec{\imath}_2 + \xi^3\vec{\imath}_3$" in the $(\vec{\imath}_1, \vec{\imath}_2, \vec{\imath}_3)$ basis. If we now consider the point identified with this vector, i.e. M such that

$$\vec{OM} = \xi^1\vec{\imath}_1 + \xi^2\vec{\imath}_2 + \xi^3\vec{\imath}_3, \tag{2.2}$$

then ξ^1, ξ^2 and ξ^3 are also called the *coordinates* of M in the *coordinate system* defined by O and $(\vec{\imath}_1, \vec{\imath}_2, \vec{\imath}_3)$.

A *tensor* is an object that generalizes vectors to a higher dimension. For example, we can consider the family of couples of base vectors, that we write

$$\vec{\imath}_m \otimes \vec{\imath}_n, \qquad m, n = 1, 2, 3, \tag{2.3}$$

calling the symbol $\otimes$ the *tensor product*[2], and we can use these couples as base vectors for a higher-order vector space that we call the space of second-order tensors, denoted by $\mathcal{E} \otimes \mathcal{E}$. Similarly, we can consider tensors of any order. In order to immediately identify the order of a given tensor, we place over the corresponding symbol a number of arrows equal to its order (or a parenthesized number as left superscript for orders higher than 2). For example, ${}^{(4)}S$ denotes a fourth-order tensor, and $\vec{\vec{T}}$ denotes a second-order tensor that decomposes on the basis given in (2.3) as follows

$$\vec{\vec{T}} = \sum_{m=1}^{3}\sum_{n=1}^{3} T^{mn}\vec{\imath}_m \otimes \vec{\imath}_n. \tag{2.4}$$

Note that, of course, a first-order tensor is a vector. By extension, we will say that a scalar is a zero-order tensor. Of course, a zero-order tensor has no components since it does not depend on any basis.

The main operations on tensors that we will consider are

- Tensor product: the tensor product of two tensors is the tensor with an order equal to the sum of the two orders, and components equal to the product of the components. For instance, for two second order tensors $\vec{\vec{U}}$ and $\vec{\vec{T}}$, we have

$$\vec{\vec{U}} \otimes \vec{\vec{T}} = \sum_{m=1}^{3}\sum_{n=1}^{3}\sum_{k=1}^{3}\sum_{l=1}^{3} U^{mn}T^{kl}\vec{\imath}_m \otimes \vec{\imath}_n \otimes \vec{\imath}_k \otimes \vec{\imath}_l. \tag{2.5}$$

- Dot product: the dot product on tensors generalizes the classical concept on vectors. It takes the last order of the first argument and the first order

[2] In some texts the tensor product symbol is not used and (2.3) is simply written as $\vec{\imath}_m\,\vec{\imath}_n$.

of the second argument and combines them using the vector dot product. For example, for two second-order tensors $\vec{\vec{U}}$ and $\vec{\vec{T}}$, we have

$$\vec{\vec{U}} \cdot \vec{\vec{T}} = \sum_{m=1}^{3} \sum_{n=1}^{3} \sum_{k=1}^{3} \sum_{l=1}^{3} U^{mn} T^{kl} (\vec{\imath}_n \cdot \vec{\imath}_k)\, \vec{\imath}_m \otimes \vec{\imath}_l. \tag{2.6}$$

Note that the result is a tensor of order $s-2$, where s is the sum of the two orders.

- Double-dot product: the double-dot product combines the last order of the first tensor with the first order of the second one like the dot product and, in addition, it also combines the last but one of the first tensor with the second of the second tensor. Namely, for two second-order tensors, we get

$$\vec{\vec{U}} : \vec{\vec{T}} = \sum_{m=1}^{3} \sum_{n=1}^{3} \sum_{k=1}^{3} \sum_{l=1}^{3} U^{mn} T^{kl} (\vec{\imath}_n \cdot \vec{\imath}_k)(\vec{\imath}_m \cdot \vec{\imath}_l) \tag{2.7}$$

This produces a tensor of order $s-4$, i.e. a scalar in (2.7).

- Transposition of second-order tensors: for a second-order tensor $\vec{\vec{T}}$, we define the *transposed* tensor $\vec{\vec{T}}^T$ by

$$\vec{\vec{T}}^T = \sum_{m=1}^{3} \sum_{n=1}^{3} T^{nm} \vec{\imath}_m \otimes \vec{\imath}_n. \tag{2.8}$$

2.1.2 Covariant and contravariant bases. Metric tensor

The *contravariant basis* $(\vec{\imath}^1, \vec{\imath}^2, \vec{\imath}^3)$ is inferred from the original (also called *covariant*) basis $(\vec{\imath}_1, \vec{\imath}_2, \vec{\imath}_3)$ by the relations

$$\boxed{\vec{\imath}_m \cdot \vec{\imath}^n = \delta_m^n, \qquad \forall m, n = 1, 2, 3,} \tag{2.9}$$

where δ denotes the Kronecker symbol[3]. Note that the relations (2.9) uniquely determine the contravariant base vectors. Then the components of any vector $\vec{u}$ in the covariant basis $(\vec{\imath}_1, \vec{\imath}_2, \vec{\imath}_3)$ will be called the *contravariant components*, denoted by (u^1, u^2, u^3), and these components can be easily calculated by the formula

$$\boxed{u^m = \vec{u} \cdot \vec{\imath}^m, \qquad m = 1, 2, 3,} \tag{2.10}$$

[3] $\delta_m^n = 1$ if $m = n$ and 0 otherwise.

i.e. by using the contravariant basis. Of course, similar expressions hold for higher-order tensors.

In addition, the contravariant basis can be used as an alternative to the covariant basis to express components of vectors and tensors. For example, the components of a vector $\vec{u}$ in the contravariant basis are called the *covariant components*. They are denoted by (u_1, u_2, u_3) and can be computed by

$$\boxed{u_m = \vec{u} \cdot \vec{\imath}_m, \qquad m = 1, 2, 3.} \tag{2.11}$$

For a higher-order tensor, mixed forms combining covariant and contravariant orders can be used. For example the expression

$$\vec{\vec{T}} = \sum_{m=1}^{3} \sum_{n=1}^{3} T^{m}_{\cdot n} \vec{\imath}_m \otimes \vec{\imath}^n \tag{2.12}$$

involves the contravariant-covariant components of the second-order tensor $\vec{\vec{T}}$. Note that the "$\cdot$" symbol in $T^{m}_{\cdot n}$ is used to identify the position of the contravariant and covariant vectors in the decomposition considered (in particular, in general $T^{m}_{\cdot n} \neq T_{n}^{\cdot m}$).

From now on, we will use the *Einstein summation convention*, i.e. we will not write summation signs for all indices that appear once as a subscript and once as a superscript in an expression. For example, instead of (2.12) we will simply write

$$\vec{\vec{T}} = T^{m}_{\cdot n} \vec{\imath}_m \otimes \vec{\imath}^n. \tag{2.13}$$

In this case, the indices m and n can be replaced by any other letters. For this reason, they are called dummy indices.

Combinations of covariant and contravariant indices can be very effectively used to compute the results of dot and double-dot products. For example, for two vectors $\vec{u}$ and $\vec{v}$ we have

$$\vec{u} \cdot \vec{v} = (u^m \vec{\imath}_m) \cdot (v_n \vec{\imath}^n) = u^m v_n (\vec{\imath}_m \cdot \vec{\imath}^n) = u^m v_n \delta^m_n = u^m v_m. \tag{2.14}$$

Similarly, for second-order tensors we obtain

$$\vec{\vec{U}} \cdot \vec{\vec{T}} = U^{mk} T_{kn} \, \vec{\imath}_m \otimes \vec{\imath}^n = U^{m}_{\cdot k} T^{k}_{\cdot n} \, \vec{\imath}_m \otimes \vec{\imath}^n = U_{m}^{\cdot k} T_{kn} \, \vec{\imath}^m \otimes \vec{\imath}^n = \dots \tag{2.15}$$

and

$$\vec{\vec{U}} \, : \, \vec{\vec{T}} = U^{mk} T_{km} = U^{m}_{\cdot k} T^{k}_{\cdot m} = U_{m}^{\cdot k} T_{k}^{\cdot m} = U_{mk} T^{km}. \tag{2.16}$$

Note how the Einstein convention makes all these expressions natural.

We now introduce the *metric tensor*, $\vec{\vec{g}}$, with covariant-covariant components defined by

$$\boxed{g_{mn} = \vec{\imath}_m \cdot \vec{\imath}_n, \qquad m, n = 1, 2, 3.} \tag{2.17}$$

For any two vectors $\vec{u}$ and $\vec{v}$,

$$\vec{u} \cdot \vec{\vec{g}} \cdot \vec{v} = u^m g_{mn} v^n = (u^m \vec{\imath}_m) \cdot (v^n \vec{\imath}_n) = \vec{u} \cdot \vec{v}. \tag{2.18}$$

This justifies the term "metric tensor", since the dot product allows to compute lengths of vectors, hence distances. The other components of the metric tensor are easily obtained. We have

$$\boxed{g^{mn} = \vec{\imath}^m \cdot \vec{\imath}^n,} \tag{2.19}$$

and

$$\boxed{g^m_{\cdot n} = g_n^{\cdot m} = \delta^m_n.} \tag{2.20}$$

The components of the metric tensor can be used to obtain contravariant components from covariant components and vice-versa. Indeed, for a vector $\vec{u}$,

$$\boxed{u^m = \vec{u} \cdot \vec{\imath}^m = (u_n \vec{\imath}^n) \cdot \vec{\imath}^m = g^{mn} u_n,} \tag{2.21}$$

and similarly

$$\boxed{u_m = g_{mn} u^n.} \tag{2.22}$$

For tensors, similar conversions can be performed by using appropriate components of the metric tensor as many times as necessary. For instance,

$$\boxed{T_{mn} = g_{mk} T^k_{\cdot n} = g_{nk} T_m^{\cdot k} = g_{mk} g_{nl} T^{kl}.} \tag{2.23}$$

Remark 2.1.1. In the special case where the (covariant) basis $(\vec{\imath}_1, \vec{\imath}_2, \vec{\imath}_3)$ is orthonormal, the contravariant basis is identical to the covariant one and the metric tensor satisfies the properties

$$g_{mn} = g^{mn} = \delta^n_m. \tag{2.24}$$

As a consequence, covariant and contravariant components of vectors and tensors are all equal in this case. ■

Example 2.1.1
Consider the three vectors $(\vec{\imath}_1, \vec{\imath}_2, \vec{\imath}_3)$ defined by their coordinates in some given orthonormal basis as follows

$$\vec{\imath}_1 = \begin{pmatrix} 2 \\ 0 \\ 0 \end{pmatrix}, \quad \vec{\imath}_2 = \begin{pmatrix} 1 \\ 1 \\ 0 \end{pmatrix}, \quad \vec{\imath}_3 = \begin{pmatrix} 1 \\ 2 \\ 3 \end{pmatrix}. \tag{2.25}$$

Clearly, these three vectors are linearly independent, hence they can be used as a covariant basis. With their components in the orthonormal basis we can directly compute the covariant-covariant components of the metric tensor (shown in matrix form)

$$(g_{mn}) = \begin{pmatrix} 4 & 2 & 2 \\ 2 & 2 & 3 \\ 2 & 3 & 14 \end{pmatrix}. \tag{2.26}$$

Then, noting that

$$g_{mn} g^{np} = g_m^{\cdot p} = \delta^p_m \tag{2.27}$$

implies that the matrices of coefficients (g_{mn}) and (g^{mn}) are the inverses of each other, we have

$$(g^{mn}) = \begin{pmatrix} \frac{19}{36} & -\frac{11}{18} & \frac{1}{18} \\ -\frac{11}{18} & \frac{13}{9} & -\frac{2}{9} \\ \frac{1}{18} & -\frac{2}{9} & \frac{1}{9} \end{pmatrix}. \tag{2.28}$$

In order to derive the contravariant base vectors, we note that (2.10) implies the identity

$$\vec{u} = (\vec{u} \cdot \vec{\imath}^{\,n})\vec{\imath}_n, \tag{2.29}$$

which, used with $\vec{u} = \vec{\imath}^{\,m}$, gives

$$\vec{\imath}^m = (\vec{\imath}^m \cdot \vec{\imath}^n)\vec{\imath}_n = g^{mn}\vec{\imath}_n. \tag{2.30}$$

Using this formula to compute the contravariant base vectors, we obtain

$$\vec{\imath}^1 = \begin{pmatrix} \frac{1}{2} \\ -\frac{1}{2} \\ \frac{1}{6} \end{pmatrix}, \quad \vec{\imath}^2 = \begin{pmatrix} 0 \\ 1 \\ -\frac{2}{3} \end{pmatrix}, \quad \vec{\imath}^3 = \begin{pmatrix} 0 \\ 0 \\ \frac{1}{3} \end{pmatrix}, \tag{2.31}$$

and we can easily check that the relations (2.9) are satisfied. ■

We denote the Euclidean norm of a vector $\vec{v}$ by $\|\vec{v}\|_{\mathcal{E}}$. According to the above discussion we have

$$\boxed{\|\vec{v}\|_{\mathcal{E}}^2 = \vec{v} \cdot \vec{v} = \vec{v} \cdot \vec{\vec{g}} \cdot \vec{v} = v_m g^{mn} v_n,} \tag{2.32}$$

among other possible expressions. We also have the corresponding inner-product

$$\boxed{\langle \vec{u}, \vec{v} \rangle_{\mathcal{E}} = \vec{u} \cdot \vec{v} = u_m g^{mn} v_n.} \tag{2.33}$$

We can extend these definitions to higher-order tensors. For example, for second-order tensors, we set

$$\|\vec{\vec{T}}\|_{\mathcal{E}}^2 = T_{mn} g^{mk} g^{nl} T_{kl}, \tag{2.34}$$

with the corresponding inner-product

$$\langle \vec{\vec{U}}, \vec{\vec{T}} \rangle_{\mathcal{E}} = U_{mn} g^{mk} g^{nl} T_{kl}. \tag{2.35}$$

Note that we use the same notation as for the norm and the inner-product of first-order tensors, since no confusion is possible. We can also easily see that

$$\langle \vec{\vec{U}}, \vec{\vec{T}} \rangle_{\mathcal{E}} = \vec{\vec{U}}^T : \vec{\vec{T}}. \tag{2.36}$$

However, this formula is restricted to second-order tensors, whereas (2.35) can be extended to any order.

We now define the *invariants* of a second-order tensor $\vec{\vec{T}}$. From the equation

$$\vec{\vec{T}} \cdot \vec{u} = T^{m}_{\cdot n} u^n \vec{\imath}_m, \tag{2.37}$$

we infer that the quantities $T^{m}_{\cdot n}$ are the coefficients of the matrix corresponding to the linear mapping

$$\vec{u} \mapsto \vec{\vec{T}} \cdot \vec{u} \tag{2.38}$$

in the covariant basis. We then call the trace and the determinant of this matrix the invariants of the tensor, because they do not depend on the particular covariant basis chosen. Namely we have

$$\boxed{\mathrm{tr}\vec{\vec{T}} = T^{m}_{\cdot m},} \tag{2.39}$$

$$\boxed{\det\vec{\vec{T}} = \begin{vmatrix} T^1_{\cdot 1} & T^1_{\cdot 2} & T^1_{\cdot 3} \\ T^2_{\cdot 1} & T^2_{\cdot 2} & T^2_{\cdot 3} \\ T^3_{\cdot 1} & T^3_{\cdot 2} & T^3_{\cdot 3} \end{vmatrix}.} \tag{2.40}$$

We will say that the second-order tensor $\vec{\vec{T}}$ is *symmetric* if it holds that $\vec{\vec{T}}^T = \vec{\vec{T}}$. Recalling (2.8), this means that

$$T^{mn} = T^{nm}, \qquad m, n = 1, 2, 3, \tag{2.41}$$

which is equivalent to

$$T_{mn} = T_{nm}, \qquad m, n = 1, 2, 3. \tag{2.42}$$

and also equivalent to

$$T^{m}_{\cdot n} = T_{n}^{\cdot m}, \qquad m, n = 1, 2, 3 \tag{2.43}$$

since $T^{m}_{\cdot n} = g^{mk} T_{kn}$ and $T_{n}^{\cdot m} = g^{mk} T_{nk}$, so that we can simply denote the mixed components by T^{m}_{n} [4]. Note that the metric tensor is obviously symmetric.

[4] Note that this does not imply that $T^{m}_{n} = T^{n}_{m}$, i.e. symmetry of the mixed components.

2.1.3 Curvilinear coordinate systems

It is sometimes useful, natural, or even necessary like in shell analysis, to express relevant quantities using a *curvilinear coordinate system*. Such a coordinate system is defined by the datum of

- a bounded open[5] subset of $\mathbb{R}^3$, denoted by Ω, that we call the *reference domain*;
- a smooth[6] injective[7] mapping $\vec{\Phi}$ from $\bar{\Omega}$, the closure[8] of Ω, into $\mathcal{E}$. We call this mapping the *chart*.

Any point M in $\vec{\Phi}(\bar{\Omega})$ is then uniquely defined by its coordinates in this curvilinear coordinate system, i.e. the three real numbers (ξ^1, ξ^2, ξ^3) such that

$$\vec{OM} = \vec{\Phi}(\xi^1, \xi^2, \xi^3). \tag{2.44}$$

A *coordinate curve* is defined by freezing any two of the coordinates and varying the third one. For example, the curve defined by

$$\xi^1 \mapsto \vec{\Phi}(\xi^1, \tilde{\xi}^2, \tilde{\xi}^3), \tag{2.45}$$

for a given choice of $(\tilde{\xi}^2, \tilde{\xi}^3)$, is a ξ^1-coordinate curve. Of course, in general, these coordinate curves are really curved. Particular examples of curvilinear coordinate systems are provided by spherical and cylindrical coordinates.

At any point M of coordinates (ξ^1, ξ^2, ξ^3) in $\vec{\Phi}(\Omega)$, we can consider the vectors $\vec{g}_m$, defined by

$$\boxed{\vec{g}_m = \frac{\partial \vec{\Phi}(\xi^1, \xi^2, \xi^3)}{\partial \xi^m}, \qquad m = 1, 2, 3.} \tag{2.46}$$

We henceforth assume that the vectors $(\vec{g}_1, \vec{g}_2, \vec{g}_3)$ are linearly independent at all points M in $\vec{\Phi}(\bar{\Omega})$. Then we call $(\vec{g}_1, \vec{g}_2, \vec{g}_3)$ the *covariant basis at M*. We emphasize that, unlike the global basis $(\vec{\imath}_1, \vec{\imath}_2, \vec{\imath}_3)$ considered in the previous sections, the basis $(\vec{g}_1, \vec{g}_2, \vec{g}_3)$ is a *local basis*; i.e., it varies with the point considered. This is an obvious consequence of the curvedness of the coordinate system since, by the definition (2.46), the vectors of the covariant basis at M are tangent to the three coordinate curves passing through M. Figure 2.1 shows an example of a curvilinear coordinate system.

[5] i.e. which does not contain its boundary
[6] i.e. which can be differentiated as many times as needed
[7] i.e. two different elements necessarily have different images through $\vec{\Phi}$
[8] i.e. Ω itself, together with its boundary $\partial\Omega$

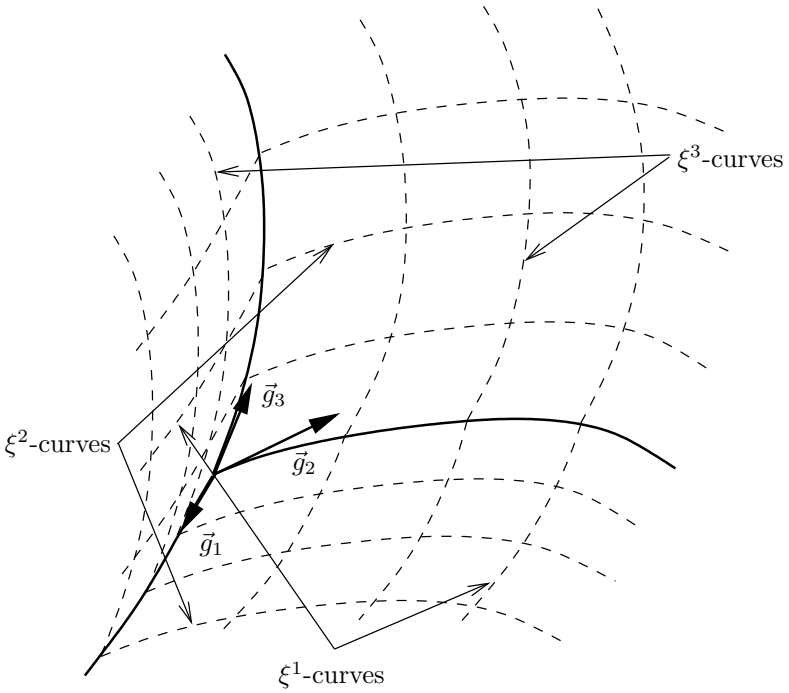

Fig. 2.1. Curvilinear coordinate system

Remark 2.1.2. Using superscripts in the notation of the coordinate symbols (ξ^1, ξ^2, ξ^3) is consistent with the definition of the covariant basis, since we can write

$$d\vec{\Phi} = \vec{g}_i \, d\xi^i, \tag{2.47}$$

where the symbol "d" denotes the differential. ■

Remark 2.1.3. Consider the particular chart given by

$$\vec{\Phi}(\xi^1, \xi^2, \xi^3) = \xi^1 \vec{\imath}_1 + \xi^2 \vec{\imath}_2 + \xi^3 \vec{\imath}_3. \tag{2.48}$$

Then the local covariant basis corresponds to $(\vec{\imath}_1, \vec{\imath}_2, \vec{\imath}_3)$ everywhere, and the coordinate system is in fact rectilinear in this case. ■

Using the local basis, we can define components of vectors and tensors as before, but these components are now defined locally. For instance, the twice-covariant components of the metric tensor are given by

$$\boxed{g_{mn} = \vec{g}_m \cdot \vec{g}_n, \qquad m, n = 1, 2, 3,} \tag{2.49}$$

and all other formulae from (2.19) to (2.23) still hold (by substituting $\vec{g}$ for $\vec{\imath}$ when needed) with, in particular, the contravariant basis $(\vec{g}^1, \vec{g}^2, \vec{g}^3)$ uniquely defined by

$$\boxed{\vec{g}_m \cdot \vec{g}^n = \delta_m^n, \qquad \forall m, n = 1, 2, 3.} \tag{2.50}$$

In order to perform integrations using a curvilinear coordinate system, we need to express the infinitesimal volume corresponding to the coordinate differentials $(d\xi^1, d\xi^2, d\xi^3)$. This infinitesimal volume, denoted by dV, is given by

$$dV = |[\vec{g}_1, \vec{g}_2, \vec{g}_3]|\, d\xi^1 d\xi^2 d\xi^3, \tag{2.51}$$

where $[\vec{g}_1, \vec{g}_2, \vec{g}_3]$ is the mixed product of the three vectors, namely

$$[\vec{g}_1, \vec{g}_2, \vec{g}_3] = \vec{g}_1 \cdot (\vec{g}_2 \wedge \vec{g}_3), \tag{2.52}$$

with the symbol "$\wedge$" denoting the vector cross product. We can show that

$$\boxed{|[\vec{g}_1, \vec{g}_2, \vec{g}_3]| = \sqrt{g},} \tag{2.53}$$

where g denotes the determinant of the matrix of coefficients $(g_{mn})_{m,n=1,2,3}$.

Proof of (2.53). Let Φ_m denote the components of $\vec{\Phi}$ in an orthonormal basis. Then we have

$$g_{mn} = \vec{g}_m \cdot \vec{g}_n = \frac{\partial \Phi_p}{\partial \xi^m} \frac{\partial \Phi_p}{\partial \xi^n}. \tag{2.54}$$

Hence

$$\det(g_{mn}) = \det(G^T G) = (\det G)^2, \tag{2.55}$$

where G denotes the (3×3) matrix of coefficients

$$G_{mn} = \frac{\partial \Phi_m}{\partial \xi^n}, \tag{2.56}$$

i.e. the matrix of the components of the covariant basis in the orthonormal system, and G^T denotes the transpose of G. Hence

$$\det G = [\vec{g}_1, \vec{g}_2, \vec{g}_3], \tag{2.57}$$

and (2.53) immediately follows. ∎

Therefore, the integral of a function f in curvilinear coordinates will take the form

$$\int_{\xi^1,\xi^2,\xi^3} f(\xi^1, \xi^2, \xi^3)\sqrt{g}\, d\xi^1 d\xi^2 d\xi^3. \tag{2.58}$$

2.1.4 Covariant differentiation

In our subsequent discussions, we will often be concerned with derivatives of *invariant quantities*. We call invariant a quantity that does not depend on a particular choice of coordinate system. For example, a scalar field defined in a region of the physical space (this field may represent a temperature, a pressure,...) is invariant. Likewise, a vector field (e.g. a velocity or displacement field) or, more generally speaking, a tensor field are invariant. Also, the invariants of a tensor are, of course, invariant. By contrast, the components of a tensor field (except for a zero-order tensor) depend on the specific coordinate system used and are hence obviously not invariant.

Clearly, the gradient of an invariant quantity must also be an invariant quantity, hence *the gradient of a tensor is also a tensor*. Note that in this statement we omitted the word "field" which will henceforth be implicit when considering derivatives (or gradients) of tensors. We now want to express the components (in a given basis) of the gradient of a tensor using the components of the tensor itself.

Let us start with a zero-order tensor (scalar field) T. By definition, the gradient of T is the first-order tensor, denoted by $\vec{\nabla}T$, such that, for any vector $\vec{u}$, the quantity $\vec{\nabla}T \cdot \vec{u}$ gives the "variation of T along $\vec{u}$". Namely

$$\vec{\nabla}T \cdot \vec{u} = \frac{d}{dx}[T(\xi^1(x), \xi^2(x), \xi^3(x))], \tag{2.59}$$

for any parametrization $x \mapsto (\xi^1(x), \xi^2(x), \xi^3(x))$ chosen so that $\vec{u}$ is the tangent vector of the curve given by $\vec{\Phi}(\xi^1(x), \xi^2(x), \xi^3(x))$. By the chain rule, we have

$$\frac{d}{dx}\vec{\Phi}(\xi^1(x), \xi^2(x), \xi^3(x)) = (\xi^1)'(x)\vec{g}_1 + (\xi^2)'(x)\vec{g}_2 + (\xi^3)'(x)\vec{g}_3 = \vec{u}. \tag{2.60}$$

Hence an appropriate parametrization must satisfy

$$(\xi^m)' = u^m, \qquad m = 1, 2, 3. \tag{2.61}$$

Using the chain rule in (2.59) we infer

$$\vec{\nabla} T \cdot \vec{u} = T_{,1} u^1 + T_{,2} u^2 + T_{,3} u^3, \tag{2.62}$$

where we adopt the classical notation

$$T_{,m} = \frac{\partial T}{\partial \xi^m}, \qquad m = 1, 2, 3. \tag{2.63}$$

Hence the covariant components of $\vec{\nabla} T$ are simply the ordinary derivatives of T along each coordinate curve, and of course

$$\vec{\nabla} T = T_{,m} \, \vec{g}^m. \tag{2.64}$$

For a first-order tensor (namely, a vector), the mathematics is slightly more complicated. For a vector $\vec{u}$, by definition, the gradient of $\vec{u}$ is a second-order tensor, denoted by $\vec{\vec{\nabla}} \vec{u}$, such that

$$\vec{\vec{\nabla}} \vec{u} \cdot \vec{v} = \frac{d}{dx} [\vec{u}(\xi^1(x), \xi^2(x), \xi^3(x))], \tag{2.65}$$

for a parametrization $x \mapsto (\xi^1(x), \xi^2(x), \xi^3(x))$ such that $(\xi^m)' = v^m$ $(m = 1, 2, 3)$ (i.e. the corresponding tangent vector is $\vec{v}$). By applying the chain rule, we obtain

$$\begin{aligned} \vec{\vec{\nabla}} \vec{u} \cdot \vec{v} &= (\vec{u}_{,m} v^m) \\ &= (u_{n,m} \vec{g}^n + u_n \vec{g}^n{}_{,m}) v^m \\ &= (u_{n,m} \vec{g}^n + u_k \vec{g}^k{}_{,m}) v^m \\ &= (u_{n,m} + u_k \vec{g}^k{}_{,m} \cdot \vec{g}_n) \vec{g}^n v^m, \end{aligned}$$

where we used the identity

$$\vec{w} = (\vec{w} \cdot \vec{g}_n) \, \vec{g}^n \tag{2.66}$$

with $\vec{w} = \vec{g}^k{}_{,m}$ in order to obtain the decomposition of this vector on the contravariant basis. Then, since $\vec{g}^k \cdot \vec{g}_n = \delta^k_n$ implies $\vec{g}^k{}_{,m} \cdot \vec{g}_n = -\vec{g}^k \cdot \vec{g}_{n,m}$, we obtain

$$\vec{\vec{\nabla}} \vec{u} \cdot \vec{v} = (u_{n,m} - u_k \vec{g}_{n,m} \cdot \vec{g}^k) \vec{g}^n v^m \tag{2.67}$$

We classically define the 3D *Christoffel symbols*

$$\boxed{\bar{\Gamma}^k_{nm} = \vec{g}_{n,m} \cdot \vec{g}^k.} \tag{2.68}$$

Hence, the (n, m) covariant-covariant component of $\vec{\vec{\nabla}}\vec{u}$, that we denote by $u_{n||m}$, is

$$\boxed{u_{n||m} = u_{n,m} - \bar{\Gamma}^k_{nm} u_k,} \tag{2.69}$$

and then, of course,

$$\vec{\vec{\nabla}}\vec{u} = u_{n||m}\, \vec{g}^n \otimes \vec{g}^m \tag{2.70}$$

We call $u_{n||m}$ the *covariant derivative* of u_n. If we want to use the contravariant components of $\vec{u}$, it can easily be checked that the (n, m) contravariant-covariant component of $\underline{\underline{\nabla}}\vec{u}$, denoted by $u^n_{\cdot||m}$ and called the covariant derivative of u^n, is given by

$$\boxed{u^n_{\cdot||m} = u^n{}_{,m} + \bar{\Gamma}^n_{mk} u^k,} \tag{2.71}$$

and therefore also

$$\vec{\vec{\nabla}}\vec{u} = u^n_{\cdot||m}\, \vec{g}_n \otimes \vec{g}^m. \tag{2.72}$$

There is no simple expression of the components of the gradient for which the second index is in contravariant position.

Remark 2.1.4. By definition, the derivative of a vector $\vec{u}$ along the m-th coordinate line satisfies

$$\vec{u}_{,m} = \vec{\vec{\nabla}}\vec{u} \cdot \vec{g}_m = u_{n||m}\vec{g}^n \tag{2.73}$$

hence the coefficients $(u_{n||m})_{n=1,2,3}$ (respectively $(u^n_{\cdot||m})_{n=1,2,3}$) are the covariant (respectively contravariant) components of the vector $\vec{u}_{,m}$. ■

For higher-order tensors, covariant differentiation formulae are more complex. We only give the expressions of covariant derivatives of second-order tensors.

$$T_{mn||p} = T_{mn,p} - \bar{\Gamma}^k_{mp} T_{kn} - \bar{\Gamma}^k_{np} T_{mk}, \tag{2.74}$$

$$T^m_{\cdot n||p} = T^m_{\cdot n,p} + \bar{\Gamma}^m_{kp} T^k_{\cdot n} - \bar{\Gamma}^k_{np} T^m_{\cdot k}, \tag{2.75}$$

$$T^{\cdot n}_{m\,\cdot||p} = T_m{}^{\cdot n}{}_{,p} - \bar{\Gamma}^k_{mp} T_k{}^{\cdot n} + \bar{\Gamma}^n_{kp} T_m{}^{\cdot k}, \tag{2.76}$$

$$T^{mn}_{\cdot\ \cdot||p} = T^{mn}{}_{,p} + \bar{\Gamma}^m_{kp} T^{kn} + \bar{\Gamma}^n_{kp} T^{mk}, \tag{2.77}$$

and we have

$${}^{(3)}\vec{\nabla}\vec{\vec{T}} = T_{mn||p}\, \vec{g}^m \otimes \vec{g}^n \otimes \vec{g}^p, \tag{2.78}$$

and similarly when using the other tensor representations.

Remark 2.1.5. The gradient of the metric tensor is zero. Indeed, in a global orthonormal coordinate system, the covariant and contravariant components of the metric tensor are the same, namely the components of the Kronecker symbol, and covariant differentiation is the same as usual differentiation. Hence, all the components of the gradient in this coordinate system are zero and, since the gradient is a tensor, it is the zero tensor. ■

Another important property of covariant derivatives is that they follow "usual rules" (i.e. the same as ordinary derivatives) for the differentiation of products. For example, for two vectors $\vec{u}$ and $\vec{v}$, recalling that covariant and ordinary differentiation are the same for a scalar, we have

$$(u_m v^m)_{,n} = (u_m v^m)_{||n} = u_{m||n} v^m + u_m v^m_{\cdot||n}. \tag{2.79}$$

Likewise, we have

$$(T^{mn} v_n)_{||p} = T^{mn}_{\cdot\ \cdot||p} v_n + T^{mn} v_{n||p}, \tag{2.80}$$

and all other covariant derivatives of products are similarly obtained in this natural fashion.

2.2 The Shell Geometry

The purpose of this section is to introduce the geometric concepts (notations, definitions and basic properties) needed in the analysis of mathematical shell models.

2.2.1 Geometric definition of a shell

We consider a shell to be a solid medium geometrically defined by a *mid-surface* immersed in the physical space $\mathcal{E}$, and a parameter representing the *thickness* of the medium around this surface. In general, the midsurface of a given shell is defined by a collection of *two-dimensional charts*, i.e. smooth injective mappings from domains of $I\!R^2$ (the reference domains associated with each chart) into $\mathcal{E}$. Note indeed that the mid-surface of a general shell

may consist of the collection of several smooth surfaces assembled along folds, and that even a smooth surface cannot always be defined by a single two-dimensional (2D) chart (e.g. a sphere). However, in complex configurations, the analysis will be decomposed according to each chart and each reference domain (by writing that the global energy is the sum of energies on all subparts). Therefore, without loss of generality, we now focus on shells defined using a single chart.

We thus consider a shell with a midsurface (denoted by $\mathcal{S}$) defined by a 2D chart $\vec{\phi}$ which is an injective mapping from the closure of a bounded open subset of $\mathbb{R}^2$, denoted by ω, into $\mathcal{E}$, hence $\mathcal{S} = \vec{\phi}(\bar{\omega})$. We assume that $\vec{\phi}$ is such that, at each point of the midsurface, the vectors

$$\boxed{\vec{a}_\alpha = \frac{\partial \vec{\phi}(\xi^1, \xi^2)}{\partial \xi^\alpha},} \tag{2.81}$$

are linearly independent, so that they form a basis of the plane tangent to the midsurface at this point. We define the unit normal vector

$$\boxed{\vec{a}_3 = \frac{\vec{a}_1 \wedge \vec{a}_2}{\|\vec{a}_1 \wedge \vec{a}_2\|}.} \tag{2.82}$$

The 3D medium corresponding to the shell is then defined by the 3D chart given by

$$\boxed{\vec{\Phi}(\xi^1, \xi^2, \xi^3) = \vec{\phi}(\xi^1, \xi^2) + \xi^3 \vec{a}_3(\xi^1, \xi^2),} \tag{2.83}$$

for (ξ^1, ξ^2, ξ^3), in Ω, where Ω is the 3D reference domain defined by

$$\Omega = \left\{ (\xi^1, \xi^2, \xi^3) \in \mathbb{R}^3 \mid (\xi^1, \xi^2) \in \omega,\ \xi^3 \in \left]-\frac{t(\xi^1, \xi^2)}{2}, +\frac{t(\xi^1, \xi^2)}{2}\right[\right\}. \tag{2.84}$$

In this definition, $t(\xi^1, \xi^2)$ represents the *thickness* of the shell at the point of coordinates (ξ^1, ξ^2). We denote by $\mathcal{B}$ the region of the Euclidean space occupied by the shell body, namely

$$\mathcal{B} = \vec{\Phi}(\bar{\Omega}). \tag{2.85}$$

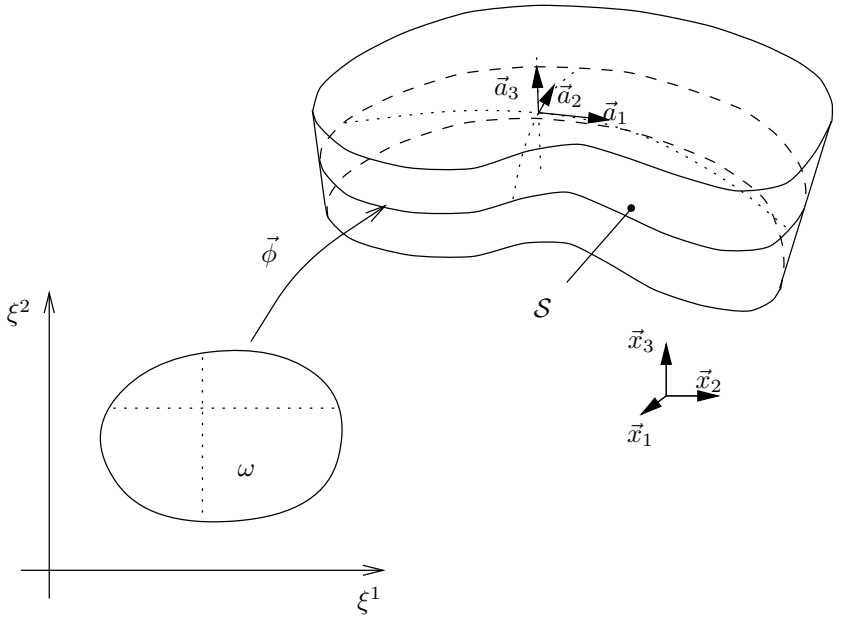

Fig. 2.2. Geometric description of a shell

Figure 2.2 shows an example of shell described by its midsurface and the thickness parameter. The notation $(\vec{x}_1, \vec{x}_2, \vec{x}_3)$ will be used in the sequel, like in this figure, to denote a reference orthonormal basis.

The 3D chart $\vec{\Phi}$ and the reference domain Ω provide a natural parametrization of the shell body, i.e. describe the shell with a natural (since it is based on the midsurface) curvilinear coordinate system. In order to be able to easily express and manipulate tensors in this specific coordinate system, we now introduce some basic concepts of surface differential geometry.

2.2.2 Differential geometry on the midsurface

We can introduce and use *surface tensors* on the midsurface of the shell in a manner very similar to what we did in three dimensions in Section 2.1. At each point, recalling that $(\vec{a}_1, \vec{a}_2)$ is a basis of the tangent plane, we call this basis the *covariant basis* and we define the *contravariant basis* of the tangent plane $(\vec{a}^1, \vec{a}^2)$ by

$$\boxed{\vec{a}_\alpha \cdot \vec{a}^{\,\beta} = \delta_\alpha^\beta, \qquad \alpha, \beta = 1, 2.} \tag{2.86}$$

First-order surface tensors are vectors of the tangent plane, hence they are uniquely determined by their components in either one of the above-defined

bases. To distinguish surface tensors from 3D tensors, we denote the former by symbols with a number of underbars corresponding to their order (or with a parenthesized number as left *subscript* for orders higher than 2). For example, a first-order surface tensor is denoted such as in "$\underline{v}$"; however, the notation of the bases $(\vec{a}_1, \vec{a}_2)$ and $(\vec{a}^1, \vec{a}^2)$ is an exception to this rule. Note that we use Greek indices for the components of surface tensors, in order to distinguish them from components of 3D tensors denoted with latin indices, hence Greek indices will henceforth implicitly vary in $\{1, 2\}$.

The restriction of the metric tensor to the tangent plane, also called the *first fundamental form* of the surface, is given by its components

$$\boxed{a_{\alpha\beta} = \vec{a}_\alpha \cdot \vec{a}_\beta,} \tag{2.87}$$

or alternatively in contravariant form by

$$\boxed{a^{\alpha\beta} = \vec{a}^\alpha \cdot \vec{a}^\beta.} \tag{2.88}$$

Of course, we also have

$$\boxed{a^\alpha_{\cdot\beta} = a^{\cdot\alpha}_\beta = \delta^\alpha_\beta.} \tag{2.89}$$

The first fundamental form can be used to convert covariant components into contravariant ones, such as in

$$v^\alpha = a^{\alpha\lambda} v_\lambda, \tag{2.90}$$

where we use the Einstein convention (with Greek indices varying from 1 to 2).

We denote the Euclidean norm of surface tensors by $\|\cdot\|_\mathcal{E}$, and the corresponding inner-product by $\langle\, \cdot, \cdot \,\rangle_\mathcal{E}$, like for 3D geometry. Of course, in order to evaluate these quantities we can use the first fundamental form. For example we have

$$\langle\, \underline{u}, \underline{v} \,\rangle_\mathcal{E} = u_\alpha a^{\alpha\beta} v_\beta, \tag{2.91}$$

$$\|\underline{v}\|^2_\mathcal{E} = v_\alpha a^{\alpha\beta} v_\beta, \tag{2.92}$$

$$\langle\, \underline{\underline{T}}, \underline{\underline{U}} \,\rangle_\mathcal{E} = T_{\alpha\beta} a^{\alpha\lambda} a^{\beta\mu} U_{\lambda\mu}, \tag{2.93}$$

$$\|\underline{\underline{T}}\|^2_\mathcal{E} = T_{\alpha\beta} a^{\alpha\lambda} a^{\beta\mu} T_{\lambda\mu}. \tag{2.94}$$

The first fundamental form is also useful to express surface integrals. Indeed, the infinitesimal area corresponding to the differentials $(d\xi^1, d\xi^2)$ of the coordinates can be expressed as

$$\boxed{dS = \sqrt{a}\, d\xi^1 d\xi^2,} \tag{2.95}$$

with

$$\boxed{a = a_{11}a_{22} - (a_{12})^2.} \tag{2.96}$$

Proof of (2.95). The infinitesimal surface area is given by

$$dS = \|\vec{a}_1 \wedge \vec{a}_2\|\, d\xi^1 d\xi^2. \tag{2.97}$$

and we show in Section 2.2.3 that

$$\|\vec{a}_1 \wedge \vec{a}_2\| = \sqrt{\det(a_{\alpha\beta})} = \sqrt{a}. \tag{2.98}$$

■

Note that second-order surface tensors also have invariants. Namely

$$\boxed{\mathrm{tr}\underline{\underline{T}} = T^{\alpha}_{\cdot\,\alpha},} \tag{2.99}$$

$$\boxed{\det\underline{\underline{T}} = \begin{vmatrix} T^1_{\cdot 1} & T^1_{\cdot 2} \\ T^2_{\cdot 1} & T^2_{\cdot 2} \end{vmatrix}.} \tag{2.100}$$

Another crucial second-order tensor is the *second fundamental form* of the surface, denoted by $\underline{\underline{b}}$. It is defined by

$$\boxed{b_{\alpha\beta} = \vec{a}_3 \cdot \vec{a}_{\alpha,\beta}.} \tag{2.101}$$

The second fundamental form is also called the *curvature tensor*, because it contains all the information on the curvature of the surface. Consider indeed $\underline{n}$, a unit vector in the tangent plane, and the curve obtained by intersecting

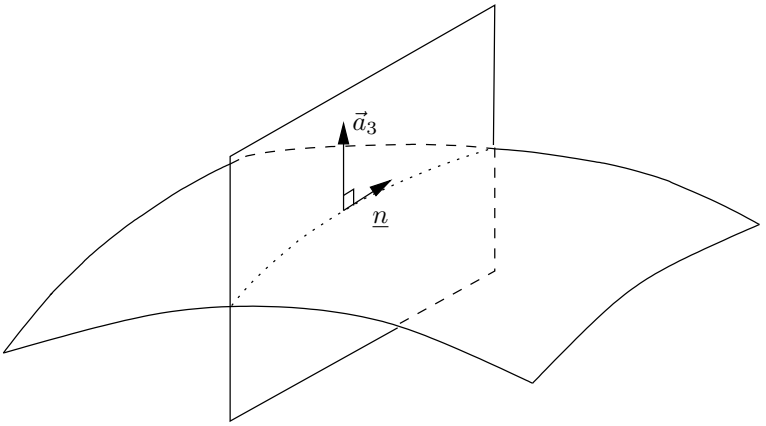

Fig. 2.3. Intersection of the surface with a plane containing $\vec{a}_3$

the midsurface with the plane defined by $\underline{n}$ (considered as a vector of $\mathcal{E}$) and $\vec{a}_3$, see Figure 2.3. A parametrization of this curve by its arc-length will be of the form

$$x \mapsto \vec{\phi}(\xi^1(x), \xi^2(x)), \tag{2.102}$$

with $(\xi^\alpha)'(x) = n^\alpha$ $(\alpha = 1, 2)$ at the point in consideration, as

$$\underline{n} = \frac{\partial \vec{\phi}}{\partial \xi^\alpha} \frac{d\xi^\alpha}{dx} = \frac{d\xi^\alpha}{dx} \vec{a}_\alpha, \tag{2.103}$$

recalling that x represents the arc-length. Then, noting that

$$b_{\alpha\beta} = -\vec{a}_{3,\beta} \cdot \vec{a}_\alpha, \tag{2.104}$$

(since $\vec{a}_3 \cdot \vec{a}_\alpha = 0$), we infer

$$\begin{aligned} \underline{n} \cdot \underline{\underline{b}} \cdot \underline{n} &= b_{\alpha\beta} n^\alpha n^\beta = b_{\alpha\beta} (\xi^\alpha)'(\xi^\beta)' = -(\xi^\beta)' \vec{a}_{3,\beta} \cdot (\xi^\alpha)' \vec{a}_\alpha \\ &= -\frac{d\vec{a}_3}{dx} \cdot \underline{n} = \vec{a}_3 \cdot \frac{d\underline{n}}{dx}, \end{aligned} \tag{2.105}$$

since $\vec{a}_3 \cdot \underline{n} = 0$ along the intersection curve. Hence, noting that $\vec{a}_3$ is the unit normal vector to this (planar) curve at the point of consideration, this implies that $\underline{n} \cdot \underline{\underline{b}} \cdot \underline{n}$ is the curvature of the curve, counted positively when $\vec{a}_3$ points towards the center of curvature (for example, it is negative in Fig. 2.3). Therefore, by considering the quantity

$$\frac{b_{\alpha\beta} v^\alpha v^\beta}{a_{\alpha\beta} v^\alpha v^\beta} \tag{2.106}$$

when $\underline{v}$ varies ($\underline{v}$ non-zero but not necessarily of unit length) we obtain all the curvatures of such curves passing through one specific point, since the denominator normalizes the numerator by the square of the norm of $\underline{v}$ and varying $\underline{v}$ in the tangent plane thus amounts to rotating the intersecting plane around $\vec{a}_3$ in Fig. 2.3. The tensors $\underline{\underline{a}}$ and $\underline{\underline{b}}$ are both symmetric (see Remark 2.2.1 below), hence the quantity (2.106) can be seen as a Rayleigh quotient. Therefore there exist two directions corresponding to its minimun and its maximum, and these directions are $\underline{\underline{a}}$-orthogonal, i.e. they are orthogonal in the usual sense since $\underline{\underline{a}}$ is the surface metric tensor. The values of the curvature along these directions are called the *principal curvatures*. The half-sum and the product of the principal curvatures are classically called the *mean* curvature and *Gaussian* curvature, respectively.

The mean and Gaussian curvatures of the surface can be respectively obtained by

$$\boxed{H = \frac{1}{2}(b_1^1 + b_2^2) = \frac{1}{2}\mathrm{tr}\underline{\underline{b}}} \tag{2.107}$$

and

$$\boxed{K = b_1^1 b_2^2 - b_2^1 b_1^2 = \det\underline{\underline{b}}.} \tag{2.108}$$

Here we have

$$b_\beta^\alpha = a^{\alpha\lambda} b_{\lambda\beta} = -a^{\alpha\lambda}\vec{a}_{3,\beta}\cdot\vec{a}_\lambda = -\vec{a}_{3,\beta}\cdot\vec{a}^\alpha = \vec{a}^\alpha{}_{,\beta}\cdot\vec{a}_3, \tag{2.109}$$

since $\vec{a}^\alpha \cdot \vec{a}_3 = 0$. Note that H and K are defined using invariants of the curvature tensor, hence they do not depend on the specific coordinate system considered.

Proof of (2.107) and (2.108). We can change the coordinate system so that, at the point in consideration, the covariant basis coincides with orthonormal vectors tangent to the directions of principal curvatures. In this new coordinate system (and at this specific point), covariant and contravariant components are the same[9] and the new coefficients of $\underline{\underline{b}}$, denoted by $\tilde{b}_{\alpha\beta}$ are such that $\tilde{b}_{11}$ and $\tilde{b}_{22}$ are the principal curvatures, and $\tilde{b}_{12} = \tilde{b}_{21} = 0$. Hence, (2.107) and (2.108) hold in this specific coordinate system and, since

[9] Note that covariant and contravariant components coincide in *any* orthonormal coordinate system, and this can be used to easily compute the mean and Gaussian curvatures with the above formulae.

these two expressions correspond to the two invariants of $\underline{\underline{b}}$, we infer that they must hold in any coordinate system. ■

We also define the *third fundamental form* by

$$\boxed{c_{\alpha\beta} = b^{\lambda}_{\alpha} b_{\lambda\beta}.} \tag{2.110}$$

Remark 2.2.1. The three fundamental forms are symmetric. This is obvious for $\underline{\underline{a}}$ (as it is for the metric tensor in 3D). For $\underline{\underline{b}}$, it is directly inferred from (2.101), noting that

$$\vec{a}_{\alpha,\beta} = \frac{\partial^2 \phi}{\partial \xi^{\alpha} \partial \xi^{\beta}} = \vec{a}_{\beta,\alpha}. \tag{2.111}$$

As for $\underline{\underline{c}}$, we have

$$c_{\alpha\beta} = b^{\lambda}_{\alpha} b_{\lambda\beta} = b_{\alpha\mu} a^{\mu\lambda} b_{\lambda\beta} = b_{\alpha\mu} b^{\mu}_{\beta} = c_{\beta\alpha}. \tag{2.112}$$

■

Remark 2.2.2. $\vec{a}_3 \cdot \vec{a}_3 = 1$ implies $\vec{a}_{3,\alpha} \cdot \vec{a}_3 = 0$, i.e. $\vec{a}_{3,\alpha}$ lies in the tangent plane. Hence we have

$$\vec{a}_{3,\alpha} = (\vec{a}_{3,\alpha} \cdot \vec{a}_{\lambda}) \vec{a}^{\lambda}, \tag{2.113}$$

and thus, recalling (2.104),

$$\vec{a}_{3,\alpha} = -b_{\alpha\lambda} \vec{a}^{\lambda} = -b^{\lambda}_{\alpha} \vec{a}_{\lambda}. \tag{2.114}$$

■

We now come to covariant differentiation of surface tensors. We start with a vector $\underline{u}$. In order to differentiate this vector, which, of course, can only be done along the surface (since the vector field is not defined outside the surface), we can see it as a vector of $\mathcal{E}$. We consider the quantity

$$\frac{d}{dx}[\underline{u}(\xi^1(x), \xi^2(x))] = (\xi^{\alpha})'(x) \frac{\partial \underline{u}}{\partial \xi^{\alpha}}, \tag{2.115}$$

i.e. the derivative of $\underline{u}$ along a curve lying on the surface and described by $(\xi^1(x), \xi^2(x))$. We have

$$\begin{aligned}\frac{\partial \underline{u}}{\partial \xi^\alpha} &= u_{\beta,\alpha}\vec{a}^\beta + u_\beta \vec{a}^\beta{}_{,\alpha} \\ &= u_{\beta,\alpha}\vec{a}^\beta + u_\lambda \vec{a}^\lambda{}_{,\alpha} \\ &= (u_{\beta,\alpha} + u_\lambda \vec{a}^\lambda{}_{,\alpha} \cdot \vec{a}_\beta)\,\vec{a}^\beta + (u_\lambda \vec{a}^\lambda{}_{,\alpha} \cdot \vec{a}_3)\,\vec{a}_3, \end{aligned} \tag{2.116}$$

where we used the identity

$$\vec{w} = (\vec{w} \cdot \vec{a}_\beta)\,\vec{a}^\beta + (\vec{w} \cdot \vec{a}_3)\,\vec{a}_3, \tag{2.117}$$

since $\vec{a}_3$ is a unit-vector normal to the tangent plane, and we applied this identity with $\vec{w} = \vec{a}^\lambda{}_{,\alpha}$. Hence, defining the *surface Christoffel symbols*

$$\boxed{\Gamma^\lambda_{\beta\alpha} = \vec{a}_{\beta,\alpha} \cdot \vec{a}^\lambda} \tag{2.118}$$

and noting that $\vec{a}_\beta \cdot \vec{a}^\lambda = \delta^\lambda_\beta$ implies

$$\Gamma^\lambda_{\beta\alpha} = -\vec{a}_\beta \cdot \vec{a}^\lambda{}_{,\alpha}, \tag{2.119}$$

we obtain from (2.116)

$$\frac{\partial \underline{u}}{\partial \xi^\alpha} = (u_{\beta,\alpha} - \Gamma^\lambda_{\beta\alpha} u_\lambda)\,\vec{a}^\beta + b^\lambda_\alpha u_\lambda \vec{a}_3. \tag{2.120}$$

Finally, calling $\underline{v}$ the tangent vector of the curve $(\xi^1(x), \xi^2(x))$, namely $v^\alpha = (\xi^\alpha)'$, we define the surface gradient of $\underline{u}$, denoted by $\underline{\underline{\nabla}}\,\underline{u}$, as the second-order surface tensor which, acting on $\underline{v}$ through the dot product, yields the tangential part of (2.115). Thus, denoting by $u_{\beta|\alpha}$ the covariant-covariant components of $\underline{\underline{\nabla}}\,\underline{u}$, we have

$$\boxed{u_{\beta|\alpha} = u_{\beta,\alpha} - \Gamma^\lambda_{\beta\alpha} u_\lambda,} \tag{2.121}$$

and $u_{\beta|\alpha}$ is called a *surface covariant derivative* of u_β. Note that the expressions of surface Christoffel symbols and of surface covariant derivatives are very similar to their 3D counterparts, with Greek indices instead of Latin indices. Likewise, we can obtain the formulae for contravariant components and for higher-order tensors by adapting the corresponding 3D expressions.

Since we are primarily concerned with shells (hence with surfaces), we will from now on omit the term "surface" when referring to quantities which pertain to surface differential geometry, and instead specify "3D" when referring to 3D differential geometry.

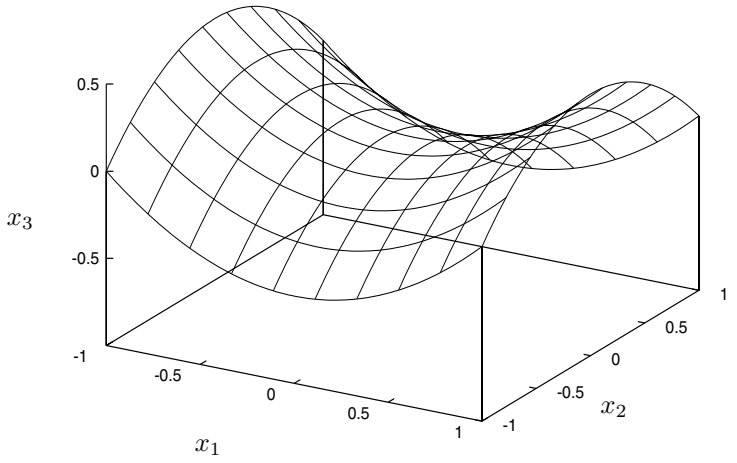

Fig. 2.4. Hyperbolic paraboloid

Example 2.2.1
Consider the surface described by the chart defined by its coordinates in the reference coordinate system as follows

$$\vec{\phi}(\xi^1,\xi^2) = \begin{pmatrix} \xi^1 \\ \xi^2 \\ \frac{(\xi^1)^2-(\xi^2)^2}{2} \end{pmatrix}, \qquad \omega =]-1,1[^2. \tag{2.122}$$

This surface, called a hyperbolic paraboloid, is shown in Figure 2.4. Note that – for dimensional (and physical) correctness – since a position vector has the dimension of a length we need to specify the unit in which (2.122) is to be understood. In other words, we can say that the chart is, in fact,

$$\vec{\phi} = \begin{pmatrix} L\xi^1 \\ L\xi^2 \\ L\frac{(\xi^1)^2-(\xi^2)^2}{2} \end{pmatrix}, \qquad \omega =]-1,1[^2, \tag{2.123}$$

where L is a reference length that is taken equal to one in the unit considered for this example. For further considerations on dimensions, see also Remark 4.1.3. We then have

$$\vec{a}_1 = \begin{pmatrix} 1 \\ 0 \\ \xi^1 \end{pmatrix}, \ \vec{a}_2 = \begin{pmatrix} 0 \\ 1 \\ -\xi^2, \end{pmatrix}, \tag{2.124}$$

$$(a_{\alpha\beta})_{\alpha,\beta=1,2} = \begin{pmatrix} 1+(\xi^1)^2 & -\xi^1\xi^2 \\ -\xi^1\xi^2 & 1+(\xi^2)^2 \end{pmatrix}, \tag{2.125}$$

$$a = \det(a_{\alpha\beta}) = 1 + (\xi^1)^2 + (\xi^2)^2, \tag{2.126}$$

$$\vec{a}_1 \wedge \vec{a}_2 = \begin{pmatrix} -\xi^1 \\ \xi^2 \\ 1 \end{pmatrix} \Rightarrow \ \vec{a}_3 = \frac{1}{\sqrt{a}} \begin{pmatrix} -\xi^1 \\ \xi^2 \\ 1 \end{pmatrix}. \tag{2.127}$$

Noting that

$$a_{\alpha\beta}a^{\beta\gamma} = \delta^\gamma_\alpha \tag{2.128}$$

implies that the matrices $(a_{\alpha\beta})$ and $(a^{\alpha\beta})$ are the inverses of each other, we infer

$$(a^{\alpha\beta})_{\alpha,\beta=1,2} = \frac{1}{a} \begin{pmatrix} 1+(\xi^2)^2 & \xi^1\xi^2 \\ \xi^1\xi^2 & 1+(\xi^1)^2 \end{pmatrix}. \tag{2.129}$$

We can now easily compute the contravariant base vectors

$$\vec{a}^1 = a^{11}\vec{a}_1 + a^{12}\vec{a}_2 = \frac{1}{a} \begin{pmatrix} 1+(\xi^2)^2 \\ \xi^1\xi^2 \\ \xi^1 \end{pmatrix}, \tag{2.130}$$

$$\vec{a}^2 = a^{21}\vec{a}_1 + a^{22}\vec{a}_2 = \frac{1}{a} \begin{pmatrix} \xi^1\xi^2 \\ 1+(\xi^1)^2 \\ -\xi^2 \end{pmatrix}. \tag{2.131}$$

Furthermore

$$\vec{a}_{1,1} = \begin{pmatrix} 0 \\ 0 \\ 1 \end{pmatrix}, \quad \vec{a}_{1,2} = \vec{a}_{2,1} = \vec{0}, \quad \vec{a}_{2,2} = \begin{pmatrix} 0 \\ 0 \\ -1 \end{pmatrix}, \tag{2.132}$$

hence

$$b_{11} = \frac{1}{\sqrt{a}}, \qquad b_{12} = b_{21} = 0, \qquad b_{22} = -\frac{1}{\sqrt{a}}, \tag{2.133}$$

$$\Gamma^1_{11} = -\Gamma^1_{22} = \frac{\xi^1}{a}, \qquad \Gamma^2_{11} = -\Gamma^2_{22} = -\frac{\xi^2}{a}, \tag{2.134}$$

and all the other Christoffel symbols are equal to zero. Next we can use again (2.129) to compute the mixed components of the curvature tensor. We obtain

$$b^1_1 = \frac{1+(\xi^2)^2}{a^{3/2}}, \qquad b^2_1 = -b^1_2 = \frac{\xi^1\xi^2}{a^{3/2}}, \qquad b^2_2 = -\frac{1+(\xi^1)^2}{a^{3/2}}, \tag{2.135}$$

Note that $b^1_2 \neq b^2_1$. The mean and Gaussian curvatures are

$$H = \frac{(\xi^2)^2 - (\xi^1)^2}{2a^{3/2}}, \qquad K = -\frac{1}{a^2}. \tag{2.136}$$

Finally, the components of the third fundamental form are

$$c_{11} = \frac{1+(\xi^2)^2}{a^2}, \qquad c_{12} = c_{21} = -\frac{\xi^1\xi^2}{a^2}, \qquad c_{22} = \frac{1+(\xi^1)^2}{a^2}. \tag{2.137}$$

■

The curvature tensor enjoys an additional symmetry property, which involves its covariant derivatives, namely

$$\boxed{b_{\alpha\beta|\lambda} = b_{\alpha\lambda|\beta}, \qquad \forall \alpha, \beta, \lambda = 1, 2.} \tag{2.138}$$

This is called the *Codazzi Equation*.

Proof of (2.138).

$$\frac{\partial \vec{a}_{\alpha,\beta}}{\partial \xi^\lambda} = \frac{\partial \vec{a}_{\alpha,\lambda}}{\partial \xi^\beta} \tag{2.139}$$

implies

$$\begin{aligned} 0 &= \left(\frac{\partial \vec{a}_{\alpha,\beta}}{\partial \xi^\lambda} - \frac{\partial \vec{a}_{\alpha,\lambda}}{\partial \xi^\beta}\right) \cdot \vec{a}_3 \\ &= \frac{\partial}{\partial \xi^\lambda}(\vec{a}_{\alpha,\beta} \cdot \vec{a}_3) - \vec{a}_{\alpha,\beta} \cdot \vec{a}_{3,\lambda} - \left[\frac{\partial}{\partial \xi^\beta}(\vec{a}_{\alpha,\lambda} \cdot \vec{a}_3) - \vec{a}_{\alpha,\lambda} \cdot \vec{a}_{3,\beta}\right] \\ &= b_{\alpha\beta,\lambda} + b_{\lambda\mu}\vec{a}^\mu \cdot \vec{a}_{\alpha,\beta} - b_{\alpha\lambda,\beta} - b_{\beta\mu}\vec{a}^\mu \cdot \vec{a}_{\alpha,\lambda} \end{aligned} \tag{2.140}$$

using (2.101) and (2.114). Next, recalling the expression of Christoffel symbols (2.118), we have

$$\begin{aligned} 0 &= b_{\alpha\beta,\lambda} + b_{\lambda\mu}\Gamma^{\mu}_{\alpha\beta} - b_{\alpha\lambda,\beta} - b_{\beta\mu}\Gamma^{\mu}_{\alpha\lambda} \\ &= b_{\alpha\beta,\lambda} - b_{\beta\mu}\Gamma^{\mu}_{\alpha\lambda} - b_{\alpha\mu}\Gamma^{\mu}_{\beta\lambda} - (b_{\alpha\lambda,\beta} - b_{\lambda\mu}\Gamma^{\mu}_{\alpha\beta} - b_{\alpha\mu}\Gamma^{\mu}_{\beta\lambda}) \\ &= b_{\alpha\beta|\lambda} - b_{\alpha\lambda|\beta}, \end{aligned} \tag{2.141}$$

from the covariant differentiation rule of second-order tensors (see (2.74)). ■

We recall that a surface is called *elliptic, parabolic* or *hyperbolic* according to whether its Gaussian curvature K is positive, zero, or negative, respectively. For example, an ellipsoid is an elliptic surface; a cylinder, a cone, and developable surfaces in general are all parabolic surfaces; a hyperbolic paraboloid (see Example 2.2.1) is a hyperbolic surface, as reflected in its name. Of course, general surfaces need not be of uniform nature in this respect, but this distinction can always be made pointwise.

For a parabolic or a hyperbolic surface, it is clear that the ratio (2.106) vanishes at least for one direction in the tangent plane. Of course, this occurs when

$$b_{\alpha\beta}v^{\alpha}v^{\beta} = 0, \tag{2.142}$$

for a vector $\underline{v}$ corresponding to the direction considered. We call these specific directions the *asymptotic directions* of the surface. If we perform a change of coordinates such that the first coordinate corresponds to an asymptotic direction at the point in consideration, which is always possible locally for a smooth chart, we obtain

$$b_{11} = 0 \tag{2.143}$$

in the new coordinate system. Recalling our discussion on the second fundamental form, we can interpret (2.143) and conclude that the curve obtained by intersecting the surface with the plane defined by the asymptotic direction and the vector normal to the surface has zero curvature at this point.

Furthermore, since the Gaussian curvature is the product of the two principal curvatures, i.e. the product of the minimum and maximum values of (2.106), we can be more specific about the number of asymptotic directions. For a hyperbolic surface, there are exactly two asymptotic directions, which lie in between the directions of principal curvatures. For a parabolic surface, there is either one single asymptotic direction which is also a direction of principal curvature if only one of the extreme values is zero, or all directions are asymptotic directions if the two principal curvatures are zero, namely if the second fundamental form is the zero tensor (e.g. for a plane).

For a hyperbolic surface, we can give an interesting characterization of the asymptotic directions as follows.

Proposition 2.2.1 *For a hyperbolic surface, the tangential plane intersects the surface along two directions which are the asymptotic directions.*

Proof. Consider a point, given by the curvilinear coordinates $(\bar{\xi}^1, \bar{\xi}^2)$, at which the surface is hyperbolic. Recalling the definition of the covariant basis (2.81), the second order Taylor expansion of the chart around this point gives

$$\begin{aligned}\vec{\phi}(\xi^1,\xi^2) &= \vec{\phi}(\bar{\xi}^1,\bar{\xi}^2)\\ &\quad +(\xi^\alpha-\bar{\xi}^\alpha)\vec{a}_\alpha(\bar{\xi}^1,\bar{\xi}^2)\\ &\quad +\frac{1}{2}(\xi^\alpha-\bar{\xi}^\alpha)(\xi^\beta-\bar{\xi}^\beta)\frac{\partial^2\vec{\phi}}{\partial\xi^\alpha\partial\xi^\beta}(\bar{\xi}^1,\bar{\xi}^2)\\ &\quad +O(\|\xi^1-\bar{\xi}^1,\xi^2-\bar{\xi}^2\|^3),\end{aligned} \tag{2.144}$$

with $\|\xi^1,\xi^2\| = \sqrt{(\xi^1)^2+(\xi^2)^2}$. We then have

$$\begin{aligned}\frac{\partial^2\vec{\phi}}{\partial\xi^\alpha\partial\xi^\beta} &= \vec{a}_{\alpha,\beta}\\ &= (\vec{a}_{\alpha,\beta}\cdot\vec{a}^\lambda)\,\vec{a}_\lambda+(\vec{a}_{\alpha,\beta}\cdot\vec{a}_3)\,\vec{a}_3\\ &= \Gamma^\lambda_{\alpha\beta}\vec{a}_\lambda+b_{\alpha\beta}\vec{a}_3\end{aligned} \tag{2.145}$$

recalling (2.101) and (2.118). Hence

$$\begin{aligned}\vec{\phi}(\xi^1,\xi^2) &= \vec{\phi}(\bar{\xi}^1,\bar{\xi}^2)+(\xi^\alpha-\bar{\xi}^\alpha)\vec{a}_\alpha\\ &\quad +\frac{1}{2}(\xi^\alpha-\bar{\xi}^\alpha)(\xi^\beta-\bar{\xi}^\beta)(\Gamma^\lambda_{\alpha\beta}\vec{a}_\lambda+b_{\alpha\beta}\vec{a}_3)\\ &\quad +O(\|\xi^1-\bar{\xi}^1,\xi^2-\bar{\xi}^2\|^3),\end{aligned} \tag{2.146}$$

where the covariant base vectors, Christoffel symbols and coefficients of the second fundamental form are all taken at the point of coordinates $(\bar{\xi}^1,\bar{\xi}^2)$.

The position of the surface with respect to the plane tangent to this surface at the point $(\bar{\xi}^1,\bar{\xi}^2)$ is then characterized by the quantity

$$\begin{aligned}[\vec{\phi}(\xi^1,\xi^2)-\vec{\phi}(\bar{\xi}^1,\bar{\xi}^2)]\cdot\vec{a}_3(\bar{\xi}^1,\bar{\xi}^2) &= \frac{1}{2}(\xi^\alpha-\bar{\xi}^\alpha)(\xi^\beta-\bar{\xi}^\beta)b_{\alpha\beta}(\bar{\xi}^1,\bar{\xi}^2)\\ &\quad +O(\|\xi^1-\bar{\xi}^1,\xi^2-\bar{\xi}^2\|^3),\end{aligned} \tag{2.147}$$

since $\vec{a}_3(\bar{\xi}^1,\bar{\xi}^2)$ is normal to the plane in consideration. Moreover, if we use a coordinate system aligned with the asymptotic directions at the point considered, we have $b_{11}=b_{22}=0$ (and $b_{12}\neq 0$), hence

$$[\vec{\phi}(\xi^1,\xi^2)-\vec{\phi}(\bar{\xi}^1,\bar{\xi}^2)]\cdot\vec{a}_3(\bar{\xi}^1,\bar{\xi}^2) = (\xi^1-\bar{\xi}^1)(\xi^2-\bar{\xi}^2)b_{12}(\bar{\xi}^1,\bar{\xi}^2) + O(\|\xi^1-\bar{\xi}^1,\xi^2-\bar{\xi}^2\|^3). \quad (2.148)$$

It is then clear that the surface locally "behaves like" $(\xi^1-\bar{\xi}^1)(\xi^2-\bar{\xi}^2)b_{12}(\bar{\xi}^1,\bar{\xi}^2)$, i.e. it intersects the tangential plane along two curves that are tangent to the coordinate curves, hence to the asymptotic directions. ■

Example 2.2.2

We consider again the surface used in Example 2.2.1, and we change the coordinate system by a rotation of angle $\pi/4$, namely we set

$$\begin{cases} y^1 = \frac{\sqrt{2}}{2}(\xi^1+\xi^2) \\ y^2 = \frac{\sqrt{2}}{2}(-\xi^1+\xi^2) \end{cases} \Leftrightarrow \begin{cases} \xi^1 = \frac{\sqrt{2}}{2}(y^1-y^2) \\ \xi^2 = \frac{\sqrt{2}}{2}(y^1+y^2) \end{cases} \quad (2.149)$$

In this new coordinate system, the chart becomes

$$\vec{\phi} = \begin{pmatrix} \frac{\sqrt{2}}{2}(y^1-y^2) \\ \frac{\sqrt{2}}{2}(y^1+y^2) \\ -y^1y^2 \end{pmatrix} \quad (2.150)$$

and we can see that all the coordinate curves (obtained by freezing either y^1 or y^2) are in fact straight lines. We infer that, considering a unit vector $\underline{n}$ directed along any coordinate curve, the intersection of the surface with the plane defined by $\underline{n}$ and $\vec{a}_3$ is a straight line, hence $b_{\alpha\beta}n^\alpha n^\beta = 0$ since we recall that this quantity gives the curvature of the intersection. Therefore the coordinate curves defined by (y^1,y^2) are directed along the asymptotic directions at all points of the surface. We show the hyperbolic paraboloid with the (y^1,y^2) coordinate curves in Figure 2.5. ■

Remark 2.2.3. Note that the argument used in Example 2.2.2 can easily be extended to more generally show that, when a straight line is contained in a surface, this line provides an asymptotic direction at all of its points. A line which is tangent to an asymptotic direction at all points is called an *asymptotic line*. ■

2.2.3 3D differential geometry for shells

We now focus on the natural 3D curvilinear coordinate system based on a parametrization of the midsurface of the shell. Using the definition of the 3D

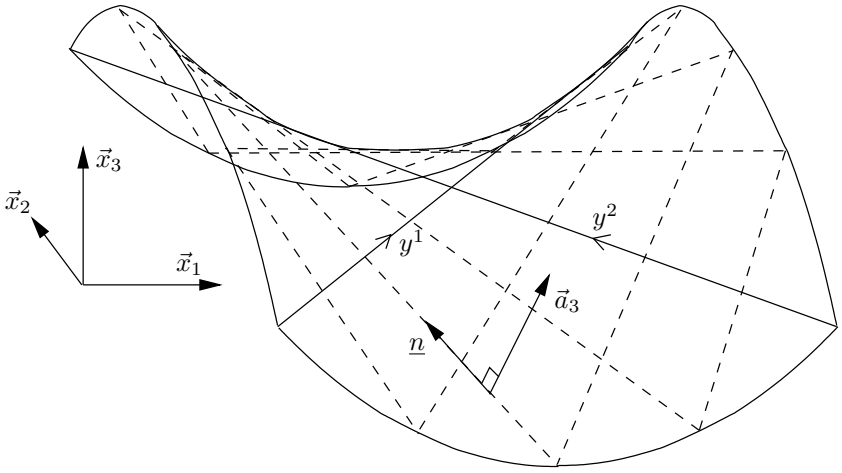

Fig. 2.5. Hyperbolic paraboloid with straight coordinate curves

chart given in (2.83), we can derive the 3D covariant base vectors. We have, recalling (2.114),

$$\vec{g}_\alpha = \frac{\partial \vec{\Phi}}{\partial \xi^\alpha} = \vec{a}_\alpha + \xi^3 \vec{a}_{3,\alpha} = \vec{a}_\alpha - \xi^3 b_\alpha^\lambda \vec{a}_\lambda, \tag{2.151}$$

hence

$$\boxed{\vec{g}_\alpha = (\delta_\alpha^\lambda - \xi^3 b_\alpha^\lambda)\vec{a}_\lambda.} \tag{2.152}$$

Moreover,

$$\boxed{\vec{g}_3 = \frac{\partial \vec{\Phi}}{\partial \xi^3} = \vec{a}_3.} \tag{2.153}$$

From (2.152) and (2.153) we can directly derive the components of the 3D metric tensor. We obtain

$$\boxed{\begin{cases} g_{\alpha\beta} = \vec{g}_\alpha \cdot \vec{g}_\beta = a_{\alpha\beta} - 2\xi^3 b_{\alpha\beta} + (\xi^3)^2 c_{\alpha\beta} \\ g_{\alpha 3} = \vec{g}_\alpha \cdot \vec{g}_3 = 0 \\ g_{33} = \vec{g}_3 \cdot \vec{g}_3 = 1 \end{cases}} \tag{2.154}$$

Note that the expression of $g_{\alpha\beta}$ suggests an interpretation of the "fundamental form" terminology, since the components of the three fundamental forms compose the coefficients of the polynomial expansion (along the transverse coordinate) of the tangential components of the 3D metric tensor.

Next, we can show that the g quantity appearing in volume measures is given by

$$\boxed{g = a\big(1 - 2H\xi^3 + K(\xi^3)^2\big)^2.} \tag{2.155}$$

Proof of (2.98) and (2.155). We have from (2.82)

$$\|\vec{a}_1 \wedge \vec{a}_2\| = (\vec{a}_1 \wedge \vec{a}_2) \cdot \vec{a}_3 = [\vec{a}_1, \vec{a}_2, \vec{a}_3], \tag{2.156}$$

which is thus a positive number. Therefore, we infer from (2.152) and(2.153) that

$$\|\vec{a}_1 \wedge \vec{a}_2\| = (|[\vec{g}_1, \vec{g}_2, \vec{g}_3]|)_{\xi^3=0}. \tag{2.157}$$

Using (2.53) and (2.154), we get

$$\|\vec{a}_1 \wedge \vec{a}_2\| = (\sqrt{\det(g_{mn})})_{\xi^3=0} = \sqrt{\det(a_{\alpha\beta})} \tag{2.158}$$

and (2.98) is proved. Then, from (2.53) and (2.52) we have

$$g = [\vec{g}_1 \cdot (\vec{g}_2 \wedge \vec{g}_3)]^2 = [\vec{g}_3 \cdot (\vec{g}_1 \wedge \vec{g}_2)]^2. \tag{2.159}$$

Substituting (2.152)-(2.153) into (2.159) and using

$$\vec{a}_1 \wedge \vec{a}_2 = \sqrt{a}\,\vec{a}_3, \tag{2.160}$$

(directly inferred from (2.82) and (2.98)), recalling (2.107) and (2.108) a direct calculation gives (2.155). ∎

We note from (2.155) that the mapping $\vec{\Phi}$ is well defined (hence so is the system of curvilinear coordinates) provided that the expression $1 - 2H\xi^3 + K(\xi^3)^2$ is always strictly positive. This is clearly equivalent to requiring that, $\forall(\xi^1, \xi^2) \in \bar{\omega}$,

$$\boxed{t(\xi^1, \xi^2) < 2|R_{\min}(\xi^1, \xi^2)|} \tag{2.161}$$

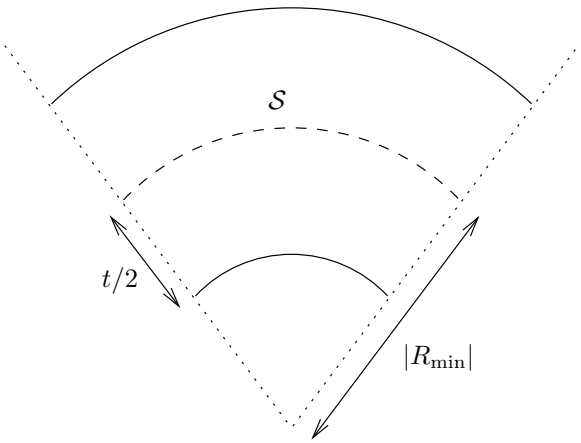

Fig. 2.6. Why "$t/2 < |R_{\min}|$" must hold

where $R_{\min}(\xi^1, \xi^2)$ is the radius of curvature of smallest modulus of the surface at point $\vec{\phi}(\xi^1, \xi^2)$. We therefore henceforth suppose that Condition (2.161) is satisfied everywhere. See Figure 2.6 for a geometric interpretation of this condition.

Remark 2.2.4. The quantities relative to surface differential geometry are in fact restrictions to ω (i.e. calculated for $\xi^3 = 0$) of 3D quantities. In particular, we have

$$a_{\alpha\beta} = (g_{\alpha\beta})_{\xi^3=0}, \tag{2.162}$$

$$a = (g)_{\xi^3=0}, \tag{2.163}$$

$$\Gamma^{\gamma}_{\alpha\beta} = (\bar{\Gamma}^{\gamma}_{\alpha\beta})_{\xi^3=0}, \tag{2.164}$$

$$b_{\alpha\beta} = (\bar{\Gamma}^{3}_{\alpha\beta})_{\xi^3=0}. \tag{2.165}$$

■

3. Elements of Functional and Numerical Analysis

A deeper understanding of finite element methods, and the development of improved finite element methods, can only be achieved with an appropriate mathematical and numerical assessment of the proposed techniques. The basis of such an assessment rests on identifying whether certain properties are satisfied by the finite element scheme and these properties depend on the framework within which the finite element method has been formulated.

In this chapter we first review fundamental concepts of functional analysis, and then present different basic frameworks of variational formulations and finite element discretizations that we will use in the later chapters for shell solutions. For completeness, we prove the stability and convergence properties of the abstract finite element discretizations for each of the frameworks of variational formulations considered. This chapter therefore provides the foundation used for the later assessment of the reliability and effectiveness of shell finite element schemes.

3.1 Sobolev Spaces and Associated Norms

In our forthcoming discussions, our approach will be that of numerical analysis, i.e. we will be concerned with the convergence of finite element solutions to the exact solution of mathematical models of shell structures. Such a study requires that

- we can identify some space in which the problem corresponding to the mathematical model is well-posed, and ideally can be shown to have a unique solution;
- a norm suitable for this space has been chosen to measure the error made in the approximate finite element solutions.

In this section, we recall some definitions and properties of spaces and norms which are crucial for the problems that we want to consider. For a more detailed presentation of these concepts, we refer to, e.g., (Adams, 1975).

D. Chapelle, K.-J. Bathe, *The Finite Element Analysis of Shells – Fundamentals*,
Computational Fluid and Solid Mechanics, 2nd ed., DOI 10.1007/978-3-642-16408-8_3,

3.1.1 General concepts in vector spaces

Let $\mathcal{V}$ be a general vector space. We recall that the essential property of a vector space is that any linear combination of elements of the space still belongs to the same space.

A *norm* on $\mathcal{V}$ is a function

$$v \in \mathcal{V} \mapsto \|v\| \in I\!R^+ \tag{3.1}$$

such that

$$\boxed{\|v\| = 0 \Rightarrow v = 0,} \tag{3.2}$$

$$\boxed{\|\lambda v\| = |\lambda| \|v\|, \quad \forall \lambda \in I\!R,} \tag{3.3}$$

$$\boxed{\|v + w\| \leq \|v\| + \|w\|, \quad \forall (v, w) \in \mathcal{V} \times \mathcal{V}.} \tag{3.4}$$

The property expressed in (3.4) is called the *triangle inequality* because of its direct interpretation in the Euclidean space, see Figure 3.1.

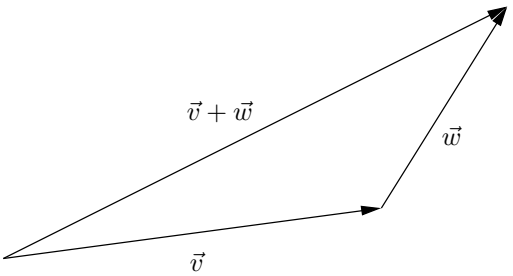

Fig. 3.1. Triangle inequality in $\mathcal{E}$: $\|\vec{v} + \vec{w}\|_{\mathcal{E}} \leq \|\vec{v}\|_{\mathcal{E}} + \|\vec{w}\|_{\mathcal{E}}$

Remark 3.1.1. For any $(v, w) \in \mathcal{V} \times \mathcal{V}$,

$$\big|\|v\| - \|w\|\big| = \max\big(\|v\| - \|w\|, \|w\| - \|v\|\big), \tag{3.5}$$

which we can bound using the triangle inequality, since

$$\|v\| - \|w\| = \|v - w + w\| - \|w\| \leq \|v - w\| + \|w\| - \|w\| = \|v - w\|, \tag{3.6}$$

and also, of course,

$$\|w\| - \|v\| \leq \|w - v\| = \|v - w\|. \tag{3.7}$$

Therefore,

$$\boxed{\big|\|v\| - \|w\|\big| \leq \|v - w\|,} \tag{3.8}$$

and this shows that the mapping given by the norm – as defined in (3.1) – is *continuous*. ■

A subset[1] $\mathcal{W}$ of $\mathcal{V}$ is said to be *closed* if any converging sequence of elements of $\mathcal{W}$ has its limit in $\mathcal{W}$.

A *linear form* is a continuous linear real-valued function defined on $\mathcal{V}$. We recall that a linear real-valued function F is continuous if and only if there exists a constant C such that

$$\boxed{|F(v)| \leq C\|v\|, \qquad \forall v \in \mathcal{V}.} \tag{3.9}$$

Continuity is a direct consequence of (3.9) since, due to the linearity, it obviously implies

$$|F(v) - F(w)| \leq C\|v - w\|, \qquad \forall (v, w) \in \mathcal{V} \times \mathcal{V}. \tag{3.10}$$

The space of all linear forms on $\mathcal{V}$ is a vector space, called the *dual space* of $\mathcal{V}$ and denoted by $\mathcal{V}'$. It can be equipped with the norm

$$\boxed{\|F\|_{\mathcal{V}'} = \sup_{v \in \mathcal{V},\, v \neq 0} \frac{F(v)}{\|v\|}.} \tag{3.11}$$

Note that this definition implies

$$|F(v)| \leq \|F\|_{\mathcal{V}'}\|v\|, \qquad \forall v \in \mathcal{V}, \tag{3.12}$$

and that $\|F\|_{\mathcal{V}'}$ is indeed the smallest constant C such that (3.9) holds. We will also use the so-called duality product notation defined by

$$\langle\, F, v \,\rangle_{\mathcal{V}' \times \mathcal{V}} = F(v). \tag{3.13}$$

A *bilinear form* is a real-valued function defined on $\mathcal{V} \times \mathcal{V}$ and both linear and continuous in each argument. This holds for A if and only if there exists a constant C such that

[1] Note that the space $\mathcal{V}$ itself can be considered as a subset.

$$\boxed{|A(v,w)| \leq C\|v\|\,\|w\|, \qquad \forall (v,w) \in \mathcal{V} \times \mathcal{V}.} \tag{3.14}$$

We sometimes also denote bilinear forms with semicolons, such as in $A(v;w)$. In particular, we always use the semicolon notation when the space $\mathcal{V}$ is a product space, such as in $A(v_1,v_2;w_1,w_2)$ when $\mathcal{V} = \mathcal{V}_1 \times \mathcal{V}_2$, in preference to the cumbersome notation $A((v_1,v_2),(w_1,w_2))$.

We say that a sequence $(v_n)_{n\geq 0}$ of $\mathcal{V}$ is *weakly converging* to $\tilde{v}$ (or that $\tilde{v}$ is the weak limit of (v_n)) if, for any F in $\mathcal{V}'$, $F(v_n)$ converges to $F(\tilde{v})$ in $\mathbb{R}$. Note that, if (v_n) converges in the usual sense to $\tilde{v}$ namely

$$\lim_{n\to\infty} \|v_n - \tilde{v}\| = 0, \tag{3.15}$$

then it converges weakly too since, for any linear form F, we have

$$|F(v_n) - F(\tilde{v})| \leq C\|v_n - \tilde{v}\| \tag{3.16}$$

by the linearity and continuity of F. In general, however, the converse property does not hold, i.e. weak convergence does not necessarily imply usual convergence, except in finite-dimensional spaces[2]. We will provide a counterexample in an infinite-dimensional space in Section 3.1.2 (Example 3.1.3). To further distinguish between the two notions, usual convergence is also sometimes called *strong convergence*.

Two norms $\|\cdot\|_1$ and $\|\cdot\|_2$ are said to be *equivalent norms* if there exist two strictly positive reals c and C such that, for all v in $\mathcal{V}$,

$$\boxed{c\|v\|_1 \leq \|v\|_2 \leq C\|v\|_1.} \tag{3.17}$$

It can be shown that, in a finite-dimensional space, all norms are equivalent. By contrast, in an infinite-dimensional space this is not true (see also Remark 3.1.4).

A *Cauchy sequence* of $\mathcal{V}$ is a sequence $(v_n)_{n\geq 0}$ of elements of $\mathcal{V}$ such that for any strictly positive real r, there exists an integer N_r such that, for all n and p larger than N_r,

$$\|v_n - v_p\| \leq r. \tag{3.18}$$

This property simply means that the elements of the sequence are restricted to an arbitrarily small region of the space, provided that we consider only elements of a sufficiently high rank.

[2] Indeed, in a finite-dimensional space equipped with a basis $(e_i)_{i=1}^N$, the function F_i that gives the i-th component of a vector in the basis is a linear form, hence weak convergence implies convergence of all components, and thus also convergence in the usual sense.

A *Banach space* is a normed vector space which is complete, i.e. in which all Cauchy sequences converge in the associated norm to an element of the space. Again, this is always true in a finite-dimensional space, but not otherwise (see also Remark 3.1.4). Note that any closed subspace of a Banach space also gives a Banach space (for the same norm).

A *Hilbert space* is a Banach space in which the norm is associated with an *inner product*. This means that there exists a bilinear form, denoted by $\langle \cdot, \cdot \rangle$ and called inner product, such that

$$\langle v, w \rangle = \langle w, v \rangle, \quad \forall (v, w) \in \mathcal{V} \times \mathcal{V}, \tag{3.19}$$

namely the bilinear form is *symmetric*, and

$$\langle v, v \rangle = \|v\|^2, \quad \forall v \in \mathcal{V}. \tag{3.20}$$

The Euclidean space $\mathcal{E}$, with the associated natural norm, is an example of a (finite-dimensional) Hilbert space.

A very important property of Hilbert spaces is the *Cauchy-Schwarz inequality*

$$\boxed{|\langle v, w \rangle| \leq \|v\| \, \|w\|, \quad \forall (v, w) \in \mathcal{V} \times \mathcal{V},} \tag{3.21}$$

which is readily established by noting that, for any λ,

$$\|\lambda v + w\|^2 = \langle v, v \rangle \lambda^2 + 2 \langle v, w \rangle \lambda + \langle w, w \rangle$$

is a positive quantity. Choosing $\lambda = -\langle v, w \rangle / \langle v, v \rangle$, we obtain (3.21). Note that this argument does not use the strict positivity of the norm, namely (3.2). Hence for any symmetric bilinear form A which is such that

$$A(v, v) \geq 0, \quad \forall v \in \mathcal{V}, \tag{3.22}$$

in which case we can say that A is "positive", we also have the following Cauchy-Schwarz inequality

$$\boxed{|A(v, w)| \leq A(v, v)^{\frac{1}{2}} \, A(w, w)^{\frac{1}{2}}, \quad \forall (v, w) \in \mathcal{V} \times \mathcal{V}.} \tag{3.23}$$

Hilbert spaces belong to a more general class of Banach spaces called *reflexive spaces* (see Adams, 1975). All these spaces enjoy the important property that, from any bounded sequence $(v_n)_{n \geq 0}$, one can extract a subsequence (i.e. a sequence of the form $(v_{n_p})_{p \geq 0}$ with $n_{p+1} > n_p$, $\forall p \geq 0$) that is weakly converging. This property – known as the Kakutani theorem – makes weak convergence particularly useful for our purposes. More specifically, we will often use the following result, inferred from this property.

Proposition 3.1.1 *Consider a bounded sequence $(v_n)_{n\geq 0}$ in a reflexive space. If all weakly-converging subsequences of (v_n) have the same limit, then the whole sequence (v_n) converges weakly to this limit.*

Proof. We thus consider a bounded sequence (v_n) for which all weakly-converging subsequences have the same limit l, and we proceed by contradiction. Suppose that (v_n) does not converge weakly to l. This means that there exists a linear form F such that $F(v_n)$ does not converge to $F(l)$. Namely, taking the negation of the convergence property, there exists a given strictly positive real number r such that, for any integer N, there exists another integer $n_N \geq N$ for which

$$|F(v_{n_N}) - F(l)| \geq r. \tag{3.24}$$

Obviously, we can then construct a subsequence of (v_n), denoted by (v_{n_p}) such that, for any p,

$$|F(v_{n_p}) - F(l)| \geq r. \tag{3.25}$$

The sequence (v_{n_p}) is bounded, hence we can extract a weakly-converging subsequence from it. Since this latter subsequence is also a subsequence of the original sequence (v_n) it must converge weakly to l, but this is in obvious contradiction with (3.25). ∎

We also record the *Riesz representation theorem* which shows that, if $\mathcal{V}$ is a Hilbert space, then for any linear form F there exists an element f of $\mathcal{V}$ such that

$$F(v) = \langle f, v \rangle, \qquad \forall v \in \mathcal{V}. \tag{3.26}$$

Note that we then have

$$\|F\|_{\mathcal{V}'} = \|f\|_{\mathcal{V}}, \tag{3.27}$$

Indeed,

$$\|F\|_{\mathcal{V}'} = \sup_{v\in\mathcal{V}} \frac{\langle f, v \rangle}{\|v\|_{\mathcal{V}}}, \tag{3.28}$$

and

$$\sup_{v\in\mathcal{V}} \frac{\langle f, v \rangle}{\|v\|_{\mathcal{V}}} \geq \frac{\langle f, f \rangle}{\|f\|_{\mathcal{V}}} = \|f\|_{\mathcal{V}}, \tag{3.29}$$

whereas, by the Cauchy-Schwarz inequality (3.21),

$$\sup_{v\in\mathcal{V}} \frac{\langle f, v\rangle}{\|v\|_{\mathcal{V}}} \leq \|f\|_{\mathcal{V}}. \tag{3.30}$$

Note that (3.26) and (3.27) also give

$$F(f) = \|f\|_{\mathcal{V}}^2 = \|F\|_{\mathcal{V}'}^2. \tag{3.31}$$

Furthermore, the fact that (3.27) holds means that (3.28) can be evaluated by finding $f \in \mathcal{V}$, and taking the usual norm of f.

Example 3.1.1
Consider the Euclidean space $\mathcal{E}$. A linear form F necessarily has the expression

$$F(\vec{v}) = av_1 + bv_2 + cv_3, \qquad \forall \vec{v} \in \mathcal{E}, \tag{3.32}$$

where (a, b, c) are real coefficients. Then, setting

$$\vec{f} = a\vec{g}_1 + b\vec{g}_2 + c\vec{g}_3, \tag{3.33}$$

(namely $f^1 = a$, $f^2 = b$ and $f^3 = c$), we have for any $\vec{v}$,

$$\begin{aligned} \vec{f}\cdot\vec{v} &= (a\vec{g}_1 + b\vec{g}_2 + c\vec{g}_3)\cdot(v_1\vec{g}^1 + v_2\vec{g}^2 + v_3\vec{g}^3) \\ &= av_1 + bv_2 + cv_3 \\ &= F(\vec{v}). \end{aligned} \tag{3.34}$$

Hence $\vec{f}$ is the vector that represents the linear form F according to the Riesz representation theorem. Note that the covariant/contravariant notation makes the association between vectors and linear forms straightforward as, with (3.33), (3.32) can be rewritten as

$$F(\vec{v}) = f^m v_m. \tag{3.35}$$

and we have, by (3.31),

$$\|F\|_{\mathcal{E}'}^2 = \|\vec{f}\|_{\mathcal{E}}^2 = (\vec{f})^2 = f^m f_m = F(\vec{f}). \tag{3.36}$$

■

Before closing this section, we record another very useful property. Considering two tensors ${}^{(m)}U$ and ${}^{(n)}T$ of arbitrary strictly positive orders m and n, we have

$$\|{}^{(m)}U \cdot {}^{(n)}T\|_{\mathcal{E}} \leq \|{}^{(m)}U\|_{\mathcal{E}}\, \|{}^{(n)}T\|_{\mathcal{E}}. \tag{3.37}$$

This is readily established by considering an orthonormal coordinate system and using the Cauchy-Schwarz inequality. Of course, similar equations hold for surface tensors.

3.1.2 L^2 and other Sobolev spaces

Let $\mathcal{O}$ be an open domain of $\mathbb{R}^n$ ($n \geq 1$). The fundamental Sobolev space denoted by $L^2(\mathcal{O})$ is the space of functions defined on $\mathcal{O}$ such that the square of the function is integrable on $\mathcal{O}$ in the generalized sense of Lebesgue's integration theory (see Adams, 1975). We define the associated norm and inner product

$$\|v\|_{L^2(\mathcal{O})} = \Big(\int_{\mathcal{O}} v^2 \, d\mathcal{O}\Big)^{1/2}, \tag{3.38}$$

$$\langle\, v, w \,\rangle_{L^2(\mathcal{O})} = \int_{\mathcal{O}} vw \, d\mathcal{O}, \tag{3.39}$$

and it can be shown that $L^2(\mathcal{O})$ is complete for this norm, hence it is a Hilbert space. The corresponding Cauchy-Schwarz inequality reads

$$\Big|\int_{\mathcal{O}} vw \, d\mathcal{O}\Big| \leq \Big(\int_{\mathcal{O}} v^2 \, d\mathcal{O}\Big)^{1/2} \Big(\int_{\mathcal{O}} w^2 \, d\mathcal{O}\Big)^{1/2}. \tag{3.40}$$

Note that $L^2(\mathcal{O})$ is, of course, an infinite-dimensional vector space. When there is no ambiguity on the domain considered, we will simply use the notation L^2 instead of $L^2(\mathcal{O})$.

Remark 3.1.2. Lebesgue's integration theory is essential to prove the completeness of L^2 because some elements of L^2 (which, for example, can be defined as limits of more regular functions such as finite element functions) cannot be integrated using standard Riemann integrals, or even improper integrals, see for example (Brenner & Scott, 1994). Therefore, when the only available information on a given function is that it belongs to L^2 – as may be the case with abstract solutions of various variational problems in mechanics – it is not guaranteed that the integral of the square of this function could be computed using standard or improper Riemann integrals, but it is still allowed to write this integral in the Lebesgue generalized sense. Moreover, such integrals enjoy, in particular, the usual properties of Hilbertian inner products (such as the Cauchy-Schwarz inequality, the triangle inequality...) which allow to manipulate these quantities (e.g. in order to bound them) without actually computing them. As a matter of fact, such formal manipulations are all that will be needed in the analysis of these abstract quantities, and the only direct integral computations that will have to be carried out for

practical purposes concern finite element functions (e.g. to compute stiffness matrices) and this only involves standard Riemann integrals. ■

Example 3.1.2
Consider $\mathcal{O} =]0,1[$ in $\mathbb{R}$. The function $x \mapsto |x - 1/2|^\alpha$ is in $L^2(\mathcal{O})$ if and only if $\alpha > -1/2$. Note that, when $-1/2 < \alpha < 0$, the function is not defined at 0, hence elements of $L^2(\mathcal{O})$ in general need not be continuous functions. Another example of non-continuous function in $L^2(]0,1[)$ is given in Figure 3.2. Note that the two functions depicted only differ by their values at $1/2$, hence they coincide in L^2 (since the L^2-norm of the difference is zero). These two examples show that we cannot define point values of L^2-functions. ■

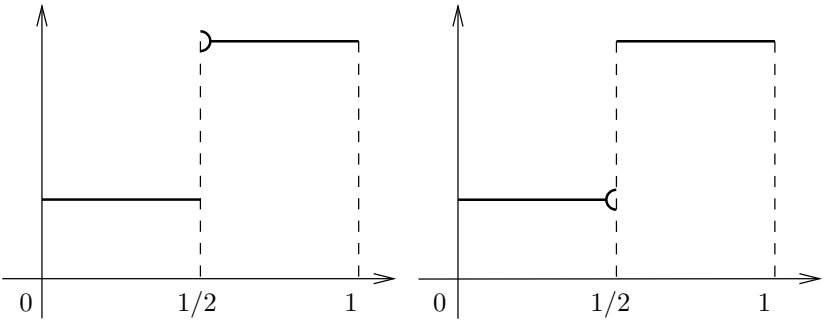

Fig. 3.2. Two alternate versions of a step function

Example 3.1.3
The sequence $(e_n)_{n\geq 1}$ defined by

$$e_n = \sqrt{2}\sin(n\pi x) \tag{3.41}$$

is obviously in $L^2(]0,1[)$, with

$$\|e_n\|_{L^2} = 1. \tag{3.42}$$

Let us prove that (e_n) is weakly converging to zero. Of course, because of (3.42), (e_n) cannot converge to zero in the usual sense, hence this will show that weak and strong convergence are not equivalent in Sobolev spaces. In fact, it can be shown that (e_n) is a Hilbert basis of $L^2(]0,1[)$, i.e. any element f of $L^2(]0,1[)$ can be decomposed into the series

$$f = \sum_{n=1}^{\infty} \langle f, e_n \rangle_{L^2} e_n, \tag{3.43}$$

which is converging in $L^2(]0,1[)$, and

$$\|f\|_{L^2}^2 = \sum_{n=1}^{\infty} (\langle f, e_n \rangle_{L^2})^2. \tag{3.44}$$

Note that this gives, indeed, the Fourier decomposition of f. From the Riesz representation theorem, any linear form F can be put in the form

$$F(v) = \langle f, v \rangle_{L^2} \tag{3.45}$$

where f is an element of $L^2(]0,1[)$. But

$$F(e_n) = \langle f, e_n \rangle_{L^2} \tag{3.46}$$

converges to zero since the series in (3.44) is converging. Therefore (e_n) converges weakly to zero. ■

We introduce a classical compact notation for partial derivatives in $\mathbb{R}^n$. Let $\mathbf{m} = (m_1, m_2, \ldots, m_n)$ be an n-tuple of integers and

$$|\mathbf{m}| = \sum_{i=1}^{n} m_i. \tag{3.47}$$

We define

$$\partial_{\mathbf{m}} f = \frac{\partial^{|\mathbf{m}|} f}{(\partial \xi^1)^{m_1} (\partial \xi^2)^{m_2} \ldots (\partial \xi^n)^{m_n}}. \tag{3.48}$$

Using this notation, we define the higher-order Sobolev spaces $H^p(\mathcal{O})$, for a non-zero integer p, as follows[3]

$$\boxed{H^p(\mathcal{O}) = \{v \in L^2(\mathcal{O}) \mid \partial_{\mathbf{m}} v \in L^2(\mathcal{O}),\ \forall \mathbf{m} \text{ s.t.} |\mathbf{m}| \leq p\},} \tag{3.49}$$

where the differentiation must be understood in the generalized distribution sense – which, of course, coincides with the usual differentiation when the function considered is differentiable with the usual rules – see Appendix C.

The norm and inner product associated with $H^p(\mathcal{O})$ are

$$\boxed{\|v\|_{H^p(\mathcal{O})} = \Big(\sum_{|\mathbf{m}| \leq p} \|\partial_{\mathbf{m}} v\|_{L^2(\mathcal{O})}^2 \Big)^{1/2},} \tag{3.50}$$

[3] By "s.t." we mean "such that" abbreviated.

$$\langle v, w \rangle_{H^p(\mathcal{O})} = \sum_{|\mathbf{m}| \leq p} \langle \partial_{\mathbf{m}} v, \partial_{\mathbf{m}} w \rangle_{L^2(\mathcal{O})}, \tag{3.51}$$

and it can be shown that they make $H^p(\mathcal{O})$ a Hilbert space.

Remark 3.1.3. The norm definition in (3.50) implicitly assumes that the coordinates considered correspond to dimensionless quantities. When this is not true (e.g., when the coordinates have the dimension of length) we – of course – need to multiply each derivative by an appropriate coefficient to make the expression consistent as regards dimension. ■

Remark 3.1.4. We have the following infinite chain of inclusions.

$$\ldots \subset H^2(\mathcal{O}) \subset H^1(\mathcal{O}) \subset L^2(\mathcal{O}). \tag{3.52}$$

We will use the notation $H^0(\mathcal{O}) = L^2(\mathcal{O})$ so that the definitions (3.49), (3.50) and (3.51) also hold for $p = 0$. Note that (3.52) implies that the H^p-norm ($p \geq 0$) is also a norm in H^q for $q > p$. However the two norms are, of course, not equivalent, and a sequence of H^q elements which is a Cauchy-sequence for the H^p-norm converges in general to an element of H^p, i.e. H^q is not complete for the H^p-norm. ■

In fact, the inclusions featured in (3.52) have the remarkable property that they are *compact inclusions*. This result is a consequence of the *Rellich-Kondrachov Theorem*, see e.g. (Adams, 1975), and means that a sequence that converges weakly in H^p ($p > 0$) converges strongly to the same limit in H^q for any $q < p$.

Example 3.1.4
In order for the function $x \mapsto x^\alpha$ to be in $H^1(]0,1[)$, we must first have $\alpha > -1/2$ ($x^\alpha \in L^2(\mathcal{O})$) and then, for $\alpha \neq 0$, $(x^\alpha)' = \alpha x^{\alpha-1} \in L^2(\mathcal{O})$ i.e. $\alpha > 1/2$. Of course, $x \mapsto 1$ is in $H^1(]0,1[)$ too, so that the condition is eventually $\alpha \in \{0\} \cup]1/2, +\infty[$. ■

In the Sobolev space $H^p(\mathcal{O})$, we also define a semi-norm, denoted by $|\cdot|_{H^p(\mathcal{O})}$, as follows

$$|v|_{H^p(\mathcal{O})} = \Big(\sum_{|\mathbf{m}|=p} \|\partial_{\mathbf{m}} v\|^2_{L^2(\mathcal{O})} \Big)^{1/2}. \tag{3.53}$$

We recall that a semi-norm is a positive-valued function that enjoys the same properties as a norm except for that expressed in (3.2), i.e. some non-zero

elements may have zero semi-norm. Here, in particular, for $p \geq 1$ all constant functions have zero semi-norm. Note that, for $p = 0$ (namely in $L^2(\mathcal{O})$), the definition of the semi-norm reduces to that of the norm. Moreover, for $p \geq 1$,

$$\boxed{\|v\|^2_{H^p(\mathcal{O})} = \sum_{k=0}^{p} |v|^2_{H^k(\mathcal{O})}.} \tag{3.54}$$

It is often important to know how a function of a specific Sobolev space behaves in a region of smaller dimension (i.e. at points in 1D, points and lines in 2D, and points, lines and surfaces in 3D), or if the function can be defined at all in such subregions. In particular, on the boundary of the domain, denoted by $\partial\mathcal{O}$, it is crucial to identify what type of *boundary condition* can be imposed on functions. For example, in 1D, we know (from Example 3.1.2) that the value of a function of $L^2(\mathcal{O})$ cannot be defined at a point, hence we cannot prescribe, as a boundary condition, the value of such a function at end-points. In fact, it can be shown that

- In 1D: functions of H^1 are continuous (note that this is consistent with Example 3.1.4);
- In 2D and 3D: only functions of H^2 (and higher orders) are continuous (i.e. have meaningful point values).

Important consequences of these statements are that when convergence is obtained in H^1, then in 1D also pointwise convergence is guaranteed, whereas in 2D and 3D H^2-convergence is needed to ensure pointwise convergence.

Example 3.1.5
Consider the domain given by the ball of radius 1/2 in $\mathbb{R}^2$, and the function f defined by $|\mathrm{Log}(r)|^\alpha$ for $0 < \alpha < 1/2$, where r denotes the distance to the origin. Then f is in $L^2(\mathcal{O})$, since

$$\int_{\mathcal{O}} f^2 \, d\mathcal{O} = 2\pi \int_0^{\frac{1}{2}} r|\mathrm{Log}(r)|^{2\alpha} \, dr, \tag{3.55}$$

which is bounded since the function under the second integral is continuous in zero. Moreover, f is in $H^1(\mathcal{O})$ since

$$\begin{aligned} |f|^2_{H^1(\mathcal{O})} &= 2\pi \int_0^{\frac{1}{2}} \Big(\frac{df}{dr}\Big)^2 r \, dr, \\ &= 2\pi\alpha^2 \int_0^{\frac{1}{2}} \frac{|\mathrm{Log}(r)|^{2\alpha-2}}{r} \, dr, \\ &= \frac{2\pi\alpha^2}{1-2\alpha} \big[|\mathrm{Log}(r)|^{2\alpha-1}\big]_0^{\frac{1}{2}}, \end{aligned} \tag{3.56}$$

which is also finite. However, of course f is not continuous at the origin. ■

In order to be able to effectively work with restrictions of functions to the boundary $\partial\mathcal{O}$, we need to prescribe some regularity requirements on this boundary. Throughout the book, we will assume that all the domains considered have a Lipschitz-continuous boundary, namely that the boundary can be parametrized by a finite number of Lipschitz-continuous functions (see e.g. (Ciarlet, 1978) for more details on this issue). We recall that a (scalar) function f is Lipschitz-continuous over a domain when there exists a constant C such that

$$|f(x_1) - f(x_2)| \leq C\|x_1 - x_2\|, \tag{3.57}$$

for any (x_1, x_2) in this domain. Figure 3.3 shows an example in which one domain has a Lipschitz-continuous boundary and the other does not because a cusp is present (the arrows represent tangent vectors on the boundary).

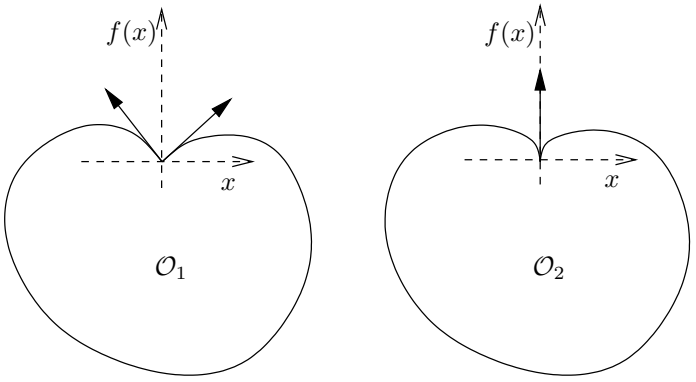

Fig. 3.3. Example: $\mathcal{O}_1$ has a Lipschitz-continuous boundary, $\mathcal{O}_2$ does not

Then, the restrictions of functions of H^1 to the boundary $\partial\mathcal{O}$ define functions of $L^2(\partial\mathcal{O})$, called the *traces* of the functions and denoted by "tr" (note that the context makes it easy to distinguish from the trace of a second-order tensor), and we have

$$\boxed{\|\mathrm{tr} f\|_{L^2(\partial\mathcal{O})} \leq C\|f\|_{H^1(\mathcal{O})},} \tag{3.58}$$

where C is a constant that depends only on $\mathcal{O}$. However, functions of $L^2(\partial\mathcal{O})$ are not always traces of functions of $H^1(\mathcal{O})$, therefore the question arises of how we can prescribe the value of an H^1-function on the boundary, e.g. in a boundary value problem. In fact, it can be shown that all functions of

$H^1(\partial\mathcal{O})$ are traces of $H^1(\mathcal{O})$ functions, hence boundary values that define a function in $H^1(\partial\mathcal{O})$ (e.g. piecewise-polynomial continuous functions on the boundary, such as with finite element shape functions) are admissible. We summarize this discussion by the following chain of inclusions (see e.g. Lions & Magenes, 1972)

$$\boxed{H^1(\partial\mathcal{O}) \subset \mathrm{tr}(H^1(\mathcal{O})) \subset L^2(\partial\mathcal{O}).} \tag{3.59}$$

We now recall an inequality which is crucial in boundary value problems set in Sobolev spaces. Suppose that $\mathcal{O}$ is a connected[4] bounded domain (with a Lipschitz-continuous boundary, as assumed above). Consider Γ_0, a part of this boundary of strictly positive measure[5], and the subspace $\mathcal{V}$ of $H^1(\mathcal{O})$ made of all functions v for which

$$\mathrm{tr}v|_{\Gamma_0} = 0, \tag{3.60}$$

where this equality should be understood as holding in $L^2(\Gamma_0)$. We can easily show that $\mathcal{V}$ – equipped with the norm of $H^1(\mathcal{O})$ – is a complete space, hence it is a Hilbert space. It can be interpreted as the subspace of functions of $H^1(\mathcal{O})$ subject to zero boundary condition on Γ_0. Then we have the inequality (see e.g. (Dautray & Lions, 1988–1993) for a proof)

$$\boxed{\|v\|_{L^2(\mathcal{O})} \leq C|v|_{H^1(\mathcal{O})}, \qquad \forall v \in \mathcal{V}.} \tag{3.61}$$

We will call this inequality the *Poincaré inequality*, although – strictly speaking – the Poincaré (or Poincaré-Friedrichs) inequality usually refers to the case when $\Gamma_0 = \partial\mathcal{O}$ in the literature. Note that the Poincaré inequality implies that the H^1-semi-norm is – in fact – a norm in $\mathcal{V}$, equivalent to the H^1-norm, as we have

$$\gamma\|v\|_{H^1(\mathcal{O})} \leq |v|_{H^1(\mathcal{O})} \leq C\|v\|_{H^1(\mathcal{O})}, \qquad \forall v \in \mathcal{V}, \tag{3.62}$$

since the right inequality holds by definition and the left inequality directly follows from (3.61).

For the space of H^1-functions subject to zero boundary condition on the whole boundary $\partial\mathcal{O}$ we have the classical notation $H_0^1(\mathcal{O})$, namely,

$$\boxed{H_0^1(\mathcal{O}) = \{v \in H^1(\mathcal{O}) \mid \mathrm{tr}v|_{\partial\mathcal{O}} = 0\}.} \tag{3.63}$$

[4] A connected domain is a domain which is "in one single piece".

[5] The measure corresponds to the length for a curve and the area for a surface

We also use the following classical notation for the dual space of $H_0^1(\mathcal{O})$,

$$\boxed{H^{-1}(\mathcal{O}) = H_0^1(\mathcal{O})'.} \tag{3.64}$$

Example 3.1.6
Let us consider $\mathcal{O} =]0, L[$ in $\mathbb{R}$ and the function $f(x) = \delta(x - L/2)$ where δ denotes the Dirac "delta function", see also Appendix C. Then f defines an element of $H^{-1}(\mathcal{O})$, since for any $v \in H_0^1(\mathcal{O})$ the quantity $f(v) = v(L/2)$ is well-defined by the trace theorem and we also have

$$|f(v)| \leq C\|v\|_{H^1(\mathcal{O})}.$$

Note that f can represent e.g. a concentrated force in a 1D bar model. We can then compute the Riesz representation of f in $H_0^1(\mathcal{O})$, denoted by v_f, which by some simple distribution calculations (or "integration by parts") we find to satisfy

$$-v_f'' + v_f = \delta(x - L/2).$$

We note that this equation governs the response of the 1D bar model, fixed at both ends, supported by uniformly-distributed springs and subjected to a point load of unit magnitude. The solution is

$$v_f(x) = -H(x - L/2)\sinh(x - L/2) + \frac{\sinh(-L/2)\sinh(x)}{\sinh(-L)},$$

where H denotes the Heaviside step function and sinh the hyperbolic sine function. We plot v_f in Figure 3.4. ■

In order to define Sobolev norms of vectors of $\mathbb{R}^n$, i.e. of n-tuples $\mathbf{v} = (v_i)_{i=1}^n$, we use the norms of the components of these quantities. Namely, we have

$$\|\mathbf{v}\|_{H^p(\mathcal{O})} = (\sum_{i=1}^{n} \|v_i\|_{H^p(\mathcal{O})}^2)^{1/2}. \tag{3.65}$$

We now extend the definitions of Sobolev spaces to the Euclidean space $\mathcal{E}$. Let Λ be a domain in $\mathcal{E}$, and let $(O, \vec{x}_1, \vec{x}_2, \vec{x}_3)$ be an orthonormal frame. We define $\mathcal{C}$ as the canonical one-to-one mapping from $\mathbb{R}^3$ to $\mathcal{E}$ associated with the coordinate system. Namely, for any (x_1, x_2, x_3) in $\mathbb{R}^3$, $\mathcal{C}(x_1, x_2, x_3)$ is the point M in $\mathcal{E}$ such that

$$\vec{OM} = x_1\vec{x}_1 + x_2\vec{x}_2 + x_3\vec{x}_3. \tag{3.66}$$

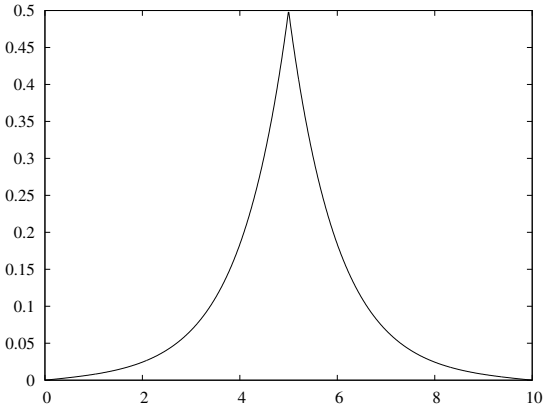

Fig. 3.4. Riesz representation of the Dirac "function" in $H_0^1(]0, L[)$ with $L = 10$

Using the domain $\mathcal{O}$ of $\mathbb{R}^3$ given by $\mathcal{O} = \mathcal{C}^{-1}(\Lambda)$, we define the Sobolev space $H^p(\Lambda)$ $(p \geq 0)$ as the space of functions f defined over Λ such that $f \circ \mathcal{C}$ is in $H^p(\mathcal{O})$ with the corresponding norm, i.e.

$$\|f\|_{H^p(\Lambda)} = \|f \circ \mathcal{C}\|_{H^p(\mathcal{O})}. \tag{3.67}$$

By this definition we have, for example,

$$\|f\|^2_{L^2(\Lambda)} = \int_{\mathcal{O}} [f \circ \mathcal{C}(x_1, x_2, x_3)]^2 \, dx_1 dx_2 dx_3. \tag{3.68}$$

In order to simplify the notation, we will omit the mapping $\mathcal{C}$ in such expressions – since the variables are clearly given by the infinitesimal volume – and henceforth write

$$\|f\|^2_{L^2(\Lambda)} = \int_{\mathcal{O}} f^2 dx_1 dx_2 dx_3. \tag{3.69}$$

Similarly, the H^1-semi-norm is defined by

$$|f|^2_{H^1(\Lambda)} = \int_{\mathcal{O}} [(\frac{\partial f}{\partial x_1})^2 + (\frac{\partial f}{\partial x_2})^2 + (\frac{\partial f}{\partial x_2})^2] \, dx_1 dx_2 dx_3, \tag{3.70}$$

and, of course, the H^1-norm is still given by

$$\|f\|^2_{H^1(\Lambda)} = \|f\|^2_{L^2(\Lambda)} + |f|^2_{H^1(\Lambda)}. \tag{3.71}$$

Note that these expressions are invariant by a change of *orthonormal* coordinate system. Similar expressions valid for any *general* curvilinear coordinate system are

$$\|f\|^2_{L^2(\Lambda)} = \int_{\mathcal{O}} f^2 \, dV \tag{3.72}$$

and

$$|f|^2_{H^1(\Lambda)} = \int_{\mathcal{O}} g^{mn} f_{,m} f_{,n} \, dV = \int_{\mathcal{O}} (\vec{\nabla} f)^2 \, dV, \tag{3.73}$$

where (recall (2.51) and (2.53))

$$dV = \sqrt{g} \, d\xi^1 d\xi^2 d\xi^3. \tag{3.74}$$

Indeed, Equations (3.69) and (3.72) (respectively (3.70) and (3.73)) give the same result in an orthonormal coordinate system, and the integrals in (3.72) and in (3.73) are clearly invariant quantities.

For vectors and tensors, the expressions of Sobolev norms are defined using similar rules. In particular, we have

$$\|\vec{v}\|^2_{L^2(\Lambda)} = \int_{\mathcal{O}} g^{mn} v_m v_n \, dV = \int_{\mathcal{O}} (\vec{v})^2 \, dV \tag{3.75}$$

and

$$\|\vec{\vec{T}}\|^2_{L^2(\Lambda)} = \int_{\mathcal{O}} g^{mk} g^{nl} T_{mn} T_{kl} \, dV. \tag{3.76}$$

Note that, in order to make the notation simpler, we denote Sobolev spaces by the same symbol for tensors of any order (e.g. $L^2(\Lambda)$). Of course, when derivatives are needed we use covariant differentiation to obtain invariant quantities. Hence, in particular,

$$\|\vec{v}\|^2_{H^1(\Lambda)} = \int_{\mathcal{O}} g^{mk} g^{nl} v_{m||n} v_{k||l} \, dV + \|\vec{v}\|^2_{L^2(\Lambda)} \tag{3.77}$$

and

$$\|\vec{\vec{T}}\|^2_{H^1(\Lambda)} = \int_{\mathcal{O}} g^{mk} g^{nl} g^{pq} T_{mn||p} T_{kl||q} \, dV + \|\vec{\vec{T}}\|^2_{L^2(\Lambda)}. \tag{3.78}$$

We can eventually extend the definition of Sobolev norms to surface-related quantities by substituting the surface metric tensor $\underline{\underline{a}}$ for the 3D metric tensor $\vec{\vec{g}}$, the surface covariant differentiation for the 3D covariant differentiation and the infinitesimal area dS for the infinitesimal volume dV (and of course by using the appropriate sets for all variables). For instance, for a first order tensor (namely, a vector in the tangential plane), we thus have

$$\|\underline{v}\|^2_{L^2(\mathcal{S})} = \int_\omega a^{\alpha\beta} v_\alpha v_\beta \, dS, \tag{3.79}$$

$$\|\underline{v}\|^2_{H^1(\mathcal{S})} = \int_\omega a^{\alpha\lambda} a^{\beta\mu} v_{\alpha|\beta} v_{\lambda|\mu} \, dS + \|\underline{v}\|^2_{L^2(\mathcal{S})}. \tag{3.80}$$

3.2 Variational Formulations and Finite Element Approximations

Having defined the functional spaces in which we will seek solutions and introduced the norms that we will use to measure the errors in finite element solutions, we now want to focus on the generic variational formulations used in the analysis of shell problems. In each case we show that the variational finite element problem is well-posed, and unique solutions are obtained.

We consider first the pure displacement formulation, for which the Lax-Milgram theorem and Céa's Lemma establish the uniqueness and optimality of the finite element solution (Propositions 3.2.1 and 3.2.2). However, as we will see in the next chapters, for a given mesh the error in the finite element solution can be – for various geometry and boundary conditions – highly dependent on the thickness of the shell.

To obtain much more accurate finite element solutions, in general, a mixed formulation need be used, in which the displacements and strains (or stresses) are interpolated. We thus consider a general mixed variational formulation. The continuous problem is well-posed provided the relevant 'continuous' ellipticity and inf-sup conditions (on the infinite-dimensional spaces) are satisfied (Proposition 3.2.3). The corresponding finite element problem is also well-posed with a unique solution that is optimal within the chosen finite element spaces, provided the corresponding 'discrete' ellipticity and inf-sup conditions are satisfied (Proposition 3.2.4). The important point is that this optimality of the finite element solution be independent of the geometry, boundary conditions and the thickness of the shell.

In practice, we usually have variational problems slightly different from those considered in Propositions 3.2.3 and 3.2.4, but the major results are applicable with some natural modifications (Propositions 3.2.5 to 3.2.11).

Finally, we briefly consider in this section interpolation and 'a priori' error estimates, and the effect of numerical integration in the finite element solutions.

3.2.1 Basic error estimates for displacement-based and mixed formulations

Most shell formulations that we consider in this book are linear *variational formulations*, i.e. they take the generic form
Find U in $\mathcal{V}$ such that

$$\boxed{A(U,V) = F(V), \quad \forall V \in \mathcal{V},} \tag{3.81}$$

where $\mathcal{V}$ is a Hilbert space (resulting of a combination of Sobolev spaces), A is a bilinear form, and F is a linear form. Typically, (3.81) expresses the *principle of virtual work*, U is the unknown displacement field, V a virtual displacement field, $A(U,V)$ represents the internal virtual work and $F(V)$ the external virtual work. In this section we give conditions that make this problem (and some variants of it) well-posed, and we recall some important properties of finite element approximations.

In the sequel we use the symbol C to denote a generic positive constant which thus takes different values at successive occurrences (including in the same equation). Likewise, γ denotes a generic *strictly positive* constant.

A fundamental result regarding (3.81) is provided by the *Lax-Milgram theorem* (the original reference is (Lax & Milgram, 1954), see also, e.g., (Dautray & Lions, 1988–1993)).

Proposition 3.2.1 *(Lax-Milgram Theorem). Assume that the bilinear form A is* elliptic*, i.e. that there exists a constant $\gamma > 0$ such that*

$$A(V,V) \geq \gamma \|V\|_{\mathcal{V}}^2, \quad \forall V \in \mathcal{V}. \tag{3.82}$$

Then Problem (3.81) has a unique solution U, and this solution is bounded from above and below by the data (i.e. the loading represented by F), namely

$$\boxed{\gamma \|F\|_{\mathcal{V}'} \leq \|U\|_{\mathcal{V}} \leq C \|F\|_{\mathcal{V}'}.} \tag{3.83}$$

Proof. For any $U \in \mathcal{V}$, the function

$$V \mapsto A(U, V),$$

is clearly a linear form, which we can represent by an element of $\mathcal{V}$ using the Riesz representation theorem. Denoting by AU this element we thus have

$$A(U, V) = \langle\, AU, V \,\rangle_{\mathcal{V}}, \quad \forall V \in \mathcal{V},$$

and A defines a linear application from $\mathcal{V}$ to $\mathcal{V}$. By a slight abuse of notation, we also denote by F the element of $\mathcal{V}$ which represents the linear form F, namely,

$$F(V) = \langle\, F, V \,\rangle_{\mathcal{V}}, \quad \forall V \in \mathcal{V}.$$

Then solving (3.81) is obviously equivalent to

$$AU = F,$$

and this will have a unique solution for any F – and with the bounds (3.83) – if and only if A is a homeomorphism (namely, a bijective linear function with a continuous inverse). The ellipticity property (3.82) gives

$$\|AV\|_{\mathcal{V}} \geq \gamma \|V\|_{\mathcal{V}}, \quad \forall V \in \mathcal{V}, \tag{3.84}$$

hence, A is injective (one-to-one) and the range of A, $\mathrm{Im}A$, is closed. This implies

$$\mathcal{V} = \mathrm{Im}A \oplus \mathrm{Im}A^{\perp}.$$

Let us consider an arbitrary $W \in \mathrm{Im}A^{\perp}$. By definition, we have

$$\langle\, AV, W \,\rangle_{\mathcal{V}} = A(V, W) = 0, \quad \forall V \in \mathcal{V},$$

and in particular $A(W, W) = 0$, which implies $W = 0$ by the ellipticity of A. Therefore, $\mathcal{V} = \mathrm{Im}A$, namely, A is surjective (onto), hence bijective, and the continuity of A^{-1} directly follows from (3.84), hence A is a homeomorphism and the proof is complete. ∎

Remark 3.2.1. Instead of "elliptic" and "ellipticity" we will also use the terms "coercive" and "coercivity". ∎

We now consider a finite element approximation of (3.81). We assume that we are given a *finite element space*, denoted by $\mathcal{V}_h$, which is a finite-dimensional subspace of $\mathcal{V}$. The symbol h represents the typical element size (or the maximum of all element sizes), and we should keep in mind that we

can reduce h (i.e. refine the mesh) in order to obtain a better approximation, which is why we have h as an index in the notation "$\mathcal{V}_h$". The classical finite element procedure amounts to solving:
Find U_h in $\mathcal{V}_h$ such that

$$\boxed{A(U_h, V) = F(V), \quad \forall V \in \mathcal{V}_h.} \tag{3.85}$$

Then we have the following result, sometimes called Céa's Lemma, see (Céa, 1964).

Proposition 3.2.2 *(Céa's Lemma). Assuming that the bilinear form A is elliptic, the finite element problem (3.85) has a unique solution, and this solution satisfies*

$$\boxed{\|U - U_h\|_{\mathcal{V}} \leq C \inf_{V \in \mathcal{V}_h} \|U - V\|_{\mathcal{V}},} \tag{3.86}$$

with C constant.

We emphasize that the constant C appearing in (3.86) does not depend on the mesh parameter h, i.e. on the particular mesh (and element sizes) considered. In fact, this will be true of all quantities called "constants" throughout the book, so we will not – in general – recall this independence in each specific case. Of course, the constant of (3.86) does depend on physical quantities related to the geometry or the material properties of the problem considered.

Remark 3.2.2. The property stated in Proposition 3.2.2 ensures that the finite element solution is *optimal* with respect to the approximation capabilities of the finite element space $\mathcal{V}_h$. ■

Proof of Proposition 3.2.2. That (3.85) has a unique solution follows from the Lax-Milgram theorem applied to $\mathcal{V}_h$ instead of $\mathcal{V}$. Then, from (3.81) and (3.85) we infer

$$A(U - U_h, V) = 0, \quad \forall V \in \mathcal{V}_h. \tag{3.87}$$

Hence, for any W in $\mathcal{V}_h$,

$$\begin{aligned} A(U - U_h, U - U_h) &= A(U - U_h, U - W) + A(U - U_h, W - U_h) \\ &= A(U - U_h, U - W), \end{aligned} \tag{3.88}$$

using (3.87) with $V = W - U_h$. Next we use the coercivity and the continuity of A and we thus obtain

$$\begin{aligned}\gamma\|U-U_h\|_{\mathcal{V}}^2 &\leq A(U-U_h,U-U_h)=A(U-U_h,U-W)\\ &\leq C\|U-U_h\|_{\mathcal{V}}\|U-W\|_{\mathcal{V}},\end{aligned} \tag{3.89}$$

hence

$$\|U-U_h\|_{\mathcal{V}}\leq C\|U-W\|_{\mathcal{V}}. \tag{3.90}$$

Since this holds for any W in $\mathcal{V}_h$, it implies (3.86). ■

Remark 3.2.3. In this book we will only consider *symmetric* bilinear forms in variational formulations such as (3.81). We recall that the bilinear form A is symmetric when

$$A(V,W)=A(W,V),\qquad \forall (V,W)\in\mathcal{V}\times\mathcal{V}. \tag{3.91}$$

However, this property is not needed to establish the Lax-Milgram Theorem and Céa's Lemma. ■

We will also consider variational formulations of a different type, namely, *Find* (U,Σ) *in* $\mathcal{V}\times\mathcal{T}$ *such that*

$$\boxed{\begin{cases} A(U,V)+B(V,\Sigma)=F(V), & \forall V\in\mathcal{V}\\ B(U,\Xi)=0, & \forall \Xi\in\mathcal{T}\end{cases}} \tag{3.92}$$

where $\mathcal{V}$ and $\mathcal{T}$ are both Hilbert spaces, A and B are bilinear forms, A is symmetric, and F is a linear form. This type of formulation, called a *mixed formulation* typically arises when some stresses (represented by Σ) are considered as independent unknowns in the mechanical problem.

Remark 3.2.4. Classical formulations of the type (3.81) are sometimes called *displacement-based formulations* in order to emphasize that, unlike mixed formulations, they only involve displacements as unknowns. ■

Remark 3.2.5. Defining the subspace

$$\boxed{\mathcal{V}_0=\{V\in\mathcal{V}\mid B(V,\Xi)=0,\qquad \forall\Xi\in\mathcal{T}\},} \tag{3.93}$$

we can see that the second equation in (3.92) expresses that the displacement solution U lies in $\mathcal{V}_0$. Hence, the mixed formulation considered in (3.92) cor-

responds to a *constrained problem* (see Chapter 7 for more details and examples). ■

The theory of general mixed formulations and their corresponding finite element approximations is vast and deep, refer in particular to (Brezzi & Fortin, 1991), and see also (Brezzi & Bathe, 1990; Roberts & Thomas, 1991). However, in shell analysis we encounter major difficulties related to the diversity and complexity of physical behaviors – not only to the mathematical aspects of mixed formulations. Hence, the field of shell analysis is most complex and mathematically quite encompassing, and indeed many of the fundamental results we will give are also directly applicable to somewhat less complex areas of analysis, like formulations for incompressible media and the analysis of plates.

For the mixed formulation (3.92) we have the following result.

Proposition 3.2.3 *Assume that*

- *A is coercive on $\mathcal{V}_0$, i.e. there exists $\gamma > 0$ such that*

$$\boxed{A(V,V) \geq \gamma \|V\|_{\mathcal{V}}^2, \quad \forall V \in \mathcal{V}_0,} \tag{3.94}$$

- *there exists $\delta > 0$ such that*

$$\boxed{\inf_{\Xi \in \mathcal{T},\, \Xi \neq 0} \sup_{V \in \mathcal{V},\, V \neq 0} \frac{B(V,\Xi)}{\|V\|_{\mathcal{V}} \|\Xi\|_{\mathcal{T}}} \geq \delta.} \tag{3.95}$$

Then (3.92) has a unique solution (U, Σ) and this solution satisfies

$$\boxed{\|U\|_{\mathcal{V}} + \|\Sigma\|_{\mathcal{T}} \leq C \|F\|_{\mathcal{V}'}} \tag{3.96}$$

for some constant C.

Proof. As already noted, if there exists a solution (U, Σ) to (3.92) then U necessarily is in $\mathcal{V}_0$. Also, taking test functions $V \in \mathcal{V}_0$ in the first equation of (3.92) we obtain

$$A(U,V) = F(V), \quad \forall V \in \mathcal{V}_0. \tag{3.97}$$

Since the subspace $\mathcal{V}_0$ is closed in $\mathcal{V}$, it is by itself a Hilbert space when equipped with the norm of $\mathcal{V}$. Hence, since A is assumed to be coercive on

$\mathcal{V}_0$ we can apply the Lax-Milgram theorem – namely, Proposition 3.2.1 – to infer that (3.97) has a unique solution and that this solution satisfies

$$\|U\|_{\mathcal{V}} \leq C\|F\|_{\mathcal{V}'}.$$

Then, using again the Riesz representation theorem, we denote by B^T the linear application from $\mathcal{T}$ to $\mathcal{V}$ such that

$$\langle\, B^T\Xi, V\,\rangle_{\mathcal{V}} = B(V,\Xi), \quad \forall V \in \mathcal{V},$$

and we can see that the first equation of (3.92) is equivalent to

$$B^T\Sigma = F - AU, \tag{3.98}$$

where F here denotes the element of $\mathcal{V}$ representing the linear form F by the Riez theorem, as in the proof of the Lax-Milgram theorem. Moreover the inf-sup condition (3.95) directly gives

$$\|B^T\Xi\|_{\mathcal{V}} \geq \delta\|\Xi\|_{\mathcal{T}}, \quad \forall \Xi \in \mathcal{T}, \tag{3.99}$$

hence, B^T is injective and has closed range, and we can write

$$\mathcal{V} = \mathrm{Im}B^T \oplus (\mathrm{Im}B^T)^{\perp}.$$

Let us consider an arbitrary element $W \in (\mathrm{Im}B^T)^{\perp}$. By definition,

$$\langle\, B^T\Xi, W\,\rangle_{\mathcal{V}} = B(W,\Xi) = 0, \quad \forall \Xi \in \mathcal{T},$$

hence $(\mathrm{Im}B^T)^{\perp} = \mathcal{V}_0$. On the other hand, (3.97) can be rewritten as

$$\langle\, F - AU, V\,\rangle_{\mathcal{V}} = 0, \quad \forall V \in \mathcal{V}_0,$$

which entails that $F - AU \in \mathcal{V}_0^{\perp} = \mathrm{Im}B^T$. Therefore, (3.98) has a unique solution Σ, for which (3.99) implies

$$\|\Sigma\|_{\mathcal{T}} \leq C\|F - AU\|_{\mathcal{V}} \leq C(\|F\|_{\mathcal{V}'} + \|U\|_{\mathcal{V}}) \leq C\|F\|_{\mathcal{V}'},$$

which concludes the proof. ∎

Remark 3.2.6. Condition (3.95) is known as the *continuous inf-sup condition*. This condition and the ellipticity condition (3.94) appear as *sufficient conditions* for the mixed formulation (3.92) to be well-posed, but by the

Banach theorem[6] it is straightforward to see that they are also *necessary conditions*. Namely, given some bilinear forms A and B with A symmetric positive, in order to have existence and uniqueness of a solution (U, Σ) *for any* choice of F in (3.92), we indeed *must* have the conditions (3.94) and (3.95) ensured. ■

Remark 3.2.7. When considering sums of norms involving quantities of different natures such as in (3.96), we should keep in mind that – for practical purposes (such as for assessing the accuracy of finite element approximations, see Chapter 8) – normalizing constants need be used for all terms in the sum to have the same dimension (or to be all dimensionless). ■

Remark 3.2.8. Defining the quantity

$$\|\Xi\|_{IS} = \sup_{V\in\mathcal{V},\, V\neq 0} \frac{B(V,\Xi)}{\|V\|_{\mathcal{V}}}, \tag{3.100}$$

we have, by (3.95),

$$\|\Xi\|_{IS} \geq \delta\|\Xi\|_{\mathcal{T}}, \qquad \forall \Xi \in \mathcal{T}, \tag{3.101}$$

and it can be easily seen that (3.100) defines a norm in $\mathcal{T}$. Furthermore, the boundedness of B implies

$$\|\Xi\|_{IS} \leq C\|\Xi\|_{\mathcal{T}}, \qquad \forall \Xi \in \mathcal{T}. \tag{3.102}$$

Hence, with (3.101) and (3.102) we have that the norm given by (3.100) is equivalent to the norm of $\mathcal{T}$. Therefore we can interpret the continuous inf-sup condition (3.95) as a condition that guarantees this equivalence of norms. ■

We will now establish another inf-sup condition result, which we will later use in some other mixed formulations.

Lemma 3.2.1. *Assuming* (3.95)*, we also have*

$$\boxed{\inf_{V\in\mathcal{V}_0^{\perp},\, V\neq 0} \sup_{\Xi\in\mathcal{T},\, \Xi\neq 0} \frac{B(V,\Xi)}{\|V\|_{\mathcal{V}}\|\Xi\|_{\mathcal{T}}} \geq \delta,} \tag{3.103}$$

with the same constant $\delta > 0$.

[6] This theorem states that any one-to-one continuous linear mapping from one Banach space into another has a continuous inverse, see (Banach, 1932).

Remark 3.2.9. We have "exchanged" the roles of the spaces in (3.103) compared to the original inf-sup condition (3.95) in which we are taking the supremum over the displacement space. ∎

Proof of Lemma 3.2.1. We again consider the mapping B^T defined in the proof of Proposition 3.2.3, where we have shown that B^T is a homeomorphism from $\mathcal{T}$ to $\mathcal{V}_0^\perp$. With this, we define the mapping $(B^T)'$ from $(\mathcal{V}_0^\perp)'$ to $\mathcal{T}'$ naturally associated with B^T, namely, characterized by

$$\langle\, (B^T)'\phi, \Xi \,\rangle_{\mathcal{T}'\times\mathcal{T}} = \langle\, \phi, B^T\Xi \,\rangle_{(\mathcal{V}_0^\perp)'\times\mathcal{V}_0^\perp}, \quad \forall (\phi,\Xi) \in (\mathcal{V}_0^\perp)'\times\mathcal{T}. \tag{3.104}$$

As a standard result from functional analysis (see e.g. (Adams, 1975)), we have that $(B^T)'$ is also a homeomorphism, and that the continuity constants for $(B^T)'$ and its inverse are the same as those of B^T and its inverse. In particular, we have

$$\|(B^T)'\phi\|_{\mathcal{T}'} \geq \delta\|\phi\|_{(\mathcal{V}_0^\perp)'}, \quad \forall \phi \in (\mathcal{V}_0^\perp)'.$$

Then, we can use the Riesz representation theorem in both spaces $(\mathcal{V}_0^\perp)'$ and $\mathcal{T}'$ to define the other closely-related mapping B from $\mathcal{V}_0^\perp$ to $\mathcal{T}$ such that, for any $V \in \mathcal{V}_0^\perp$, taking $\phi \in (\mathcal{V}_0^\perp)'$ associated with V,

$$BV = \Xi,$$

where $\Xi \in \mathcal{T}$ is associated with $(B^T)'\phi \in \mathcal{T}'$ through the Riesz representation theorem. Here again, we clearly have that B is a homeomorphism from $\mathcal{V}_0^\perp$ to $\mathcal{T}$, with the same continuity constants as B^T for the direct and inverse mappings, and in particular

$$\|BV\|_{\mathcal{T}} \geq \delta\|V\|_{\mathcal{V}}, \quad \forall V \in \mathcal{V}_0^\perp. \tag{3.105}$$

Let us now characterize B. For any $(V,\Gamma) \in \mathcal{V}_0^\perp \times \mathcal{B}$ we have

$$\langle\, BV, \Gamma \,\rangle_{\mathcal{T}} = \langle\, (B^T)'\phi, \Gamma \,\rangle_{\mathcal{T}'\times\mathcal{T}},$$

for $\phi \in (\mathcal{V}_0^\perp)'$ associated with V. Hence, using (3.104)

$$\langle\, BV, \Gamma \,\rangle_{\mathcal{T}} = \langle\, \phi, B^T\Xi \,\rangle_{(\mathcal{V}_0^\perp)'\times\mathcal{V}_0^\perp} = \langle\, V, B^T\Xi \,\rangle_{\mathcal{V}} = B(V,\Xi),$$

and we can see that (3.105) directly implies (3.103). ∎

A finite element procedure for the mixed formulation (3.92) is obtained by using the finite element subspaces $\mathcal{V}_h$ and $\mathcal{T}_h$ for $\mathcal{V}$ and $\mathcal{T}$, respectively,

and by considering the problem:
Find (U_h, Σ_h) *in* $\mathcal{V}_h \times \mathcal{T}_h$ *such that*

$$\boxed{\begin{cases} A(U_h, V) + B(V, \Sigma_h) = F(V), & \forall V \in \mathcal{V}_h \\ B(U_h, \Xi) = 0, & \forall \Xi \in \mathcal{T}_h \end{cases}} \tag{3.106}$$

Unlike for the displacement-based formulation (3.81), the mixed formulation requires additional conditions in order for finite element procedures to be well-posed and optimal. Let us define

$$\mathcal{V}_{h0} = \{V \in \mathcal{V}_h \mid B(V, \Xi) = 0, \quad \forall \Xi \in \mathcal{T}_h\}, \tag{3.107}$$

where in general we do not have $\mathcal{V}_{h0} \subset \mathcal{V}_0$. We then have the following fundamental result.

Proposition 3.2.4 *Under the assumptions of Proposition 3.2.3, if we further assume that*

- *A is coercive on* $\mathcal{V}_{h0}$*, i.e. there exists* $\gamma > 0$ *(independent of h) such that*

$$\boxed{A(V, V) \geq \gamma \|V\|_{\mathcal{V}}^2, \quad \forall V \in \mathcal{V}_{h0},} \tag{3.108}$$

- *there exists* $\delta > 0$ *(independent of h) such that*

$$\boxed{\inf_{\Xi \in \mathcal{T}_h,\, \Xi \neq 0} \sup_{V \in \mathcal{V}_h,\, V \neq 0} \frac{B(V, \Xi)}{\|V\|_{\mathcal{V}} \|\Xi\|_{\mathcal{T}}} \geq \delta.} \tag{3.109}$$

Then (3.106) has a unique solution (U_h, Σ_h) *and this solution satisfies*

$$\boxed{\begin{aligned} &\|U - U_h\|_{\mathcal{V}} + \|\Sigma - \Sigma_h\|_{\mathcal{T}} \\ &\qquad \leq C \inf_{V \in \mathcal{V}_h, \Xi \in \mathcal{T}_h} \{\|U - V\|_{\mathcal{V}} + \|\Sigma - \Xi\|_{\mathcal{T}}\} \end{aligned}} \tag{3.110}$$

for some constant C.

Remark 3.2.10. Note that, when considering the solution of (3.81) with the conditions (3.91) and (3.82) satisfied for the continuous problem, these

conditions are also automatically satisfied for the finite element problem in (3.85), i.e. they hold when substituting $\mathcal{V}_h$ for $\mathcal{V}$. However, considering the solution of (3.92) and assuming that (3.94) and (3.95) are satisfied, the "discrete versions" (3.108) and (3.109) are *not* automatically satisfied. Whether or not they are satisfied depends on the choice of the finite element spaces $\mathcal{V}_h$ and $\mathcal{T}_h$. Condition (3.109) is particularly difficult to enforce (see Chapters 7 to 9) and we call it the *discrete inf-sup condition* or simply *the inf-sup condition.* ■

In order to prove Proposition 3.2.4, we first need a result pertaining to the decomposition of the discrete displacement space into the direct sum

$$\mathcal{V}_h = \mathcal{V}_{h0} \oplus \mathcal{V}_{h1}, \tag{3.111}$$

where $\mathcal{V}_{h0}$ and $\mathcal{V}_{h1}$ are orthogonal subspaces, i.e. all elements of $\mathcal{V}_{h0}$ are orthogonal to all elements of $\mathcal{V}_{h1}$. Then, for any $V \in \mathcal{V}_h$ we have

$$V = \Pi_0 V + \Pi_1 V, \tag{3.112}$$

where Π_0 and Π_1 denote the orthogonal projections onto $\mathcal{V}_{h0}$ and $\mathcal{V}_{h1}$, respectively, and we also have

$$\|V\|_{\mathcal{V}}^2 = \|\Pi_0 V\|_{\mathcal{V}}^2 + \|\Pi_1 V\|_{\mathcal{V}}^2. \tag{3.113}$$

Lemma 3.2.2. *Under Assumption (3.109) (with $\delta > 0$), we have*

$$\boxed{\sup_{\Xi \in \mathcal{T}_h,\, \Xi \neq 0} \frac{B(V,\Xi)}{\|\Xi\|_{\mathcal{T}}} \geq \delta \|V\|_{\mathcal{V}}, \qquad \forall V \in \mathcal{V}_{h1}.} \tag{3.114}$$

Proof. Recalling that $\mathcal{V}_{h1} = \mathcal{V}_{h0}^{\perp}$, this condition is the discrete counterpart of (3.103), hence it can be proven exactly as in the proof of Lemma 3.2.1. ■

In order to establish the estimate (3.110), we will use a general strategy that consists in considering the mixed bilinear form defined by

$$\boxed{\begin{aligned} M(V,\Xi;W,\Gamma) &= A(V,W) + B(V,\Gamma) + B(W,\Xi), \\ &\forall (V,\Xi),(W,\Gamma) \in (\mathcal{V}_h \times \mathcal{T}_h)^2, \end{aligned}} \tag{3.115}$$

and in proving that this bilinear form provides *stability* on the finite element spaces using the natural norm of the product space $\mathcal{V} \times \mathcal{T}$, namely

$$\|V,\Xi\|_{\mathcal{V}\times\mathcal{T}} = \big(\|V\|_{\mathcal{V}}^2 + \|\Xi\|_{\mathcal{T}}^2\big)^{\frac{1}{2}}. \tag{3.116}$$

This stability result is stated in the following lemma.

Lemma 3.2.3. *Under the assumptions of Proposition 3.2.4, the bilinear form M is stable on $\mathcal{V}_h \times \mathcal{T}_h$. Namely, for all (V,Ξ) in $\mathcal{V}_h \times \mathcal{T}_h$ there exists (W,Γ) in $\mathcal{V}_h \times \mathcal{T}_h$ such that*

$$\|W,\Gamma\|_{\mathcal{V}\times\mathcal{T}} \le C\|V,\Xi\|_{\mathcal{V}\times\mathcal{T}}, \tag{3.117}$$

and

$$M(V,\Xi;W,\Gamma) \ge \gamma\|V,\Xi\|_{\mathcal{V}\times\mathcal{T}}^2. \tag{3.118}$$

Remark 3.2.11. The property defined (and established) in Lemma 3.2.3 is called *stability* because it guarantees that a small perturbation of the loading in the finite element problem induces a small perturbation in the solution. Namely, consider the problem of finding $(\delta U_h, \delta\Sigma_h)$ in $\mathcal{V}_h \times \mathcal{T}_h$ such that

$$\begin{cases} A(\delta U_h, V) + B(V,\delta\Sigma_h) = \delta F(V), \quad \forall V \in \mathcal{V}_h \\ B(\delta U_h,\Xi) = \delta H(\Xi), \quad \forall \Xi \in \mathcal{T}_h \end{cases} \tag{3.119}$$

or equivalently

$$M(\delta U_h,\delta\Sigma_h;V,\Xi) = \delta F(V) + \delta H(\Xi), \quad \forall (V,\Xi) \in \mathcal{V}_h \times \mathcal{T}_h. \tag{3.120}$$

Then the property of Lemma 3.2.3 implies that this problem has a unique solution (the corresponding matrix is invertible), and we have (W,Γ) in $\mathcal{V}_h \times \mathcal{T}_h$ such that

$$\|W,\Gamma\|_{\mathcal{V}\times\mathcal{T}} \le C\|\delta U_h,\delta\Sigma_h\|_{\mathcal{V}\times\mathcal{T}}, \tag{3.121}$$

and

$$M(\delta U_h,\delta\Sigma_h;W,\Gamma) \ge \gamma\|\delta U_h,\delta\Sigma_h\|_{\mathcal{V}\times\mathcal{T}}^2. \tag{3.122}$$

Hence

$$\begin{aligned} \|\delta U_h,\delta\Sigma_h\|_{\mathcal{V}\times\mathcal{T}}^2 &\le CM(\delta U_h,\delta\Sigma_h;W,\Gamma) = C\big(\delta F(W) + \delta H(\Gamma)\big) \\ &\le C\big(\|\delta F\|_{\mathcal{V}'} + \|\delta H\|_{\mathcal{T}'}\big)\|W,\Gamma\|_{\mathcal{V}\times\mathcal{T}} \\ &\le C\big(\|\delta F\|_{\mathcal{V}'} + \|\delta H\|_{\mathcal{T}'}\big)\|\delta U_h,\delta\Sigma_h\|_{\mathcal{V}\times\mathcal{T}}, \end{aligned} \tag{3.123}$$

and therefore

$$\|\delta U_h, \delta \Sigma_h\|_{\mathcal{V}\times\mathcal{T}} \leq C\big(\|\delta F\|_{\mathcal{V}'} + \|\delta H\|_{\mathcal{T}'}\big), \tag{3.124}$$

This shows that the perturbation in the solution is bounded by that of the data, which is the usual definition of stability. ■

Proof of Lemma 3.2.3. Consider an arbitrary (V, Ξ) in $\mathcal{V}_h \times \mathcal{T}_h$. We decompose the proof into 3 steps.

i) *Stability in* $\Pi_1 V$. Noting that (3.114) is equivalent to

$$\sup_{\Xi\in\mathcal{T}_h,\ \|\Xi\|_{\mathcal{T}}=\|\Pi_1 V\|_{\mathcal{V}}} B(V,\Xi) \geq \delta\|\Pi_1 V\|_{\mathcal{V}}^2, \qquad \forall V \in \mathcal{V}_h, \tag{3.125}$$

we infer that there exists Γ_1 in $\mathcal{T}_h$ such that

$$\|\Gamma_1\|_{\mathcal{T}} = \|\Pi_1 V\|_{\mathcal{V}}, \qquad B(V,\Gamma_1) \geq \frac{\delta}{2}\|\Pi_1 V\|_{\mathcal{V}}^2. \tag{3.126}$$

Setting $W_1 = 0$, we get

$$\|W_1, \Gamma_1\|_{\mathcal{V}\times\mathcal{T}} = \|\Pi_1 V\|_{\mathcal{V}} \leq \|V\|_{\mathcal{V}}, \tag{3.127}$$

and

$$M(V,\Xi;W_1,\Gamma_1) = B(V,\Gamma_1) \geq \frac{\delta}{2}\|\Pi_1 V\|_{\mathcal{V}}^2. \tag{3.128}$$

ii) *Stability in* $\Pi_0 V$. Taking $(W_2, \Gamma_2) = (V, -\Xi)$, we obtain

$$\|W_2, \Gamma_2\|_{\mathcal{V}\times\mathcal{T}} = \|V, \Xi\|_{\mathcal{V}\times\mathcal{T}}, \tag{3.129}$$

and

$$\begin{aligned} &M(V,\Xi;W_2,\Gamma_2) \\ &\qquad = A(V,V) = A(\Pi_0 V + \Pi_1 V, \Pi_0 V + \Pi_1 V) \\ &\qquad \geq A(\Pi_0 V, \Pi_0 V) - C\big(\|\Pi_1 V\|_{\mathcal{V}}^2 + \|\Pi_0 V\|_{\mathcal{V}}\|\Pi_1 V\|_{\mathcal{V}}\big), \end{aligned} \tag{3.130}$$

using the boundedness of A. Then, taking into account (3.108) and using the inequality (B.1) in Appendix B with

$$a = \|\Pi_0 V\|_{\mathcal{V}}, \qquad b = \|\Pi_1 V\|_{\mathcal{V}}, \tag{3.131}$$

and an appropriate value for η, we obtain

$$M(V,\Xi;W_2,\Gamma_2) \geq \gamma_2 \|\Pi_0 V\|_{\mathcal{V}}^2 - C_2 \|\Pi_1 V\|_{\mathcal{V}}^2, \tag{3.132}$$

where we now use (as an exception) indices with the constants γ and C because we will need to carefully combine several such constants in this proof.

iii) *Stability in Ξ and conclusion.* Using now the discrete inf-sup bound (3.109), there exists W_3 in $\mathcal{V}_h$ such that

$$\|W_3\|_{\mathcal{V}} = \|\Xi\|_{\mathcal{T}}, \qquad B(W_3,\Xi) \geq \frac{\delta}{2}\|\Xi\|_{\mathcal{T}}^2. \tag{3.133}$$

Taking $\Gamma_3 = 0$, we have

$$\|W_3,\Gamma_3\|_{\mathcal{V}\times\mathcal{T}} = \|\Xi\|_{\mathcal{T}}, \tag{3.134}$$

and

$$\begin{aligned} M(V,\Xi;W_3,\Gamma_3) &= A(V,W_3) + B(W_3,\Xi) \\ &\geq \frac{\delta}{2}\|\Xi\|_{\mathcal{T}}^2 - C\|V\|_{\mathcal{V}}\|\Xi\|_{\Gamma}, \end{aligned} \tag{3.135}$$

using the boundedness of A and (3.133). Applying again the inequality (B.1), we obtain

$$M(V,\Xi;W_3,\Gamma_3) \geq \gamma_3\|\Xi\|_{\mathcal{T}}^2 - C_3\|V\|_{\mathcal{V}}^2. \tag{3.136}$$

Finally, we consider the combination

$$(W,\Gamma) = \lambda_1(W_1,\Gamma_1) + \lambda_2(W_2,\Gamma_2) + \lambda_3(W_3,\Gamma_3), \tag{3.137}$$

where $(\lambda_1,\lambda_2,\lambda_3)$ are strictly positive coefficients to be chosen. Gathering the above results, we have

$$\|W,\Gamma\|_{\mathcal{V}\times\mathcal{T}} \leq C\|V,\Xi\|_{\mathcal{V}\times\mathcal{T}} \tag{3.138}$$

(where C depends on $(\lambda_1,\lambda_2,\lambda_3)$, of course) and, setting $\gamma_1 = \delta/2$,

$$\begin{aligned} M(V,\Xi;W,\Gamma) \geq\ & (\lambda_1\gamma_1 - \lambda_2 C_2 - \lambda_3 C_3)\,\|\Pi_1 V\|_{\mathcal{V}}^2 \\ & + (\lambda_2\gamma_2 - \lambda_3 C_3)\,\|\Pi_0 V\|_{\mathcal{V}}^2 + \lambda_3\gamma_3\|\Xi\|_{\mathcal{T}}^2. \end{aligned} \tag{3.139}$$

Setting then

$$\lambda_3 = \frac{\gamma_2}{2C_3}\lambda_2, \qquad \lambda_2 = \frac{\gamma_1}{2C_2+\gamma_2}\lambda_1, \tag{3.140}$$

we ensure that all the coefficients in the above lower bound are strictly positive, hence

$$M(V,\Xi;W,\Gamma) \geq \gamma\,(\|V\|_{\mathcal{V}}^2 + \|\Xi\|_{\mathcal{T}}^2). \tag{3.141}$$

■

Remark 3.2.12. If M were a coercive bilinear form, namely,

$$M(V,\Xi;V,\Xi) \geq \gamma\|V,\Xi\|_{\mathcal{V}\times\mathcal{T}}^2, \qquad \forall (V,\Xi) \in \mathcal{V}\times\mathcal{T}, \tag{3.142}$$

the stability conditions of Lemma 3.2.3 would be automatically satisfied (consider $(W,\Gamma) = (V,\Xi)$ in this case) for any choice of the finite element subspaces $\mathcal{V}_h$ and $\mathcal{T}_h$ and – in fact – we could then use Proposition 3.2.2 (Céa's Lemma) to directly obtain the error bound (3.110). Here, we do not have the coercivity property (note that, e.g., $M(0,\Xi;0,\Xi) = 0$ for any Ξ in $\mathcal{T}$), hence we have instead proven the more general stability condition of Lemma 3.2.3. ■

Remark 3.2.13. Note that – for example – if the matrix associated with the bilinear form M in the discrete space has an eigenvector (Φ_U, Φ_Σ) corresponding to a zero eigenvalue, then stability is obviously not satisfied since

$$M(\Phi_U,\Phi_\Sigma;V,\Xi) = 0, \qquad \forall (V,\Xi) \in \mathcal{V}\times\mathcal{T},$$

Of course, the main difficulties we will have to face will be more frequently related to "small" eigenvalues, which may tend to zero when the mesh is refined. ■

Now that we have established the stability result of Lemma 3.2.3, the proof of Proposition 3.2.4 is a simple extension of that of Céa's Lemma.

Proof of Proposition 3.2.4. The existence and uniqueness of (U_h,Σ_h) follows from Proposition 3.2.3 applied with the spaces $\mathcal{V}_h$ and $\mathcal{T}_h$ instead of the spaces $\mathcal{V}$ and $\mathcal{T}$.

Next, in order to establish (3.110), we use Lemma 3.2.3 with $(V,\Xi) = (U_h - \tilde{U}, \Sigma_h - \tilde{\Sigma})$, where $(\tilde{U},\tilde{\Sigma})$ is an arbitrary element of $\mathcal{V}_h \times \mathcal{T}_h$. Therefore there exists (W,Γ) in $\mathcal{V}_h \times \mathcal{T}_h$ such that

$$\|W,\Gamma\|_{\mathcal{V}\times\mathcal{T}} \leq C\|U_h - \tilde{U}, \Sigma_h - \tilde{\Sigma}\|_{\mathcal{V}\times\mathcal{T}}, \tag{3.143}$$

and

$$M(U_h - \tilde{U}, \Sigma_h - \tilde{\Sigma}; W,\Gamma) \geq \gamma\|U_h - \tilde{U}, \Sigma_h - \tilde{\Sigma}\|_{\mathcal{V}\times\mathcal{T}}^2. \tag{3.144}$$

Note that the system (3.92) can be rewritten as

$$M(U,\Sigma;V,\Xi) = F(V), \qquad \forall (V,\Xi) \in \mathcal{V}\times\mathcal{T}, \tag{3.145}$$

and that – similarly – the system (3.106) is equivalent to

$$M(U_h,\Sigma_h;V,\Xi) = F(V), \qquad \forall (V,\Xi) \in \mathcal{V}_h\times\mathcal{T}_h. \tag{3.146}$$

Therefore,

$$M(U-U_h,\Sigma-\Sigma_h;V,\Xi) = 0, \qquad \forall (V,\Xi) \in \mathcal{V}_h\times\mathcal{T}_h, \tag{3.147}$$

which can be used in (3.144) to obtain

$$\begin{aligned} &M(U_h-\tilde{U},\Sigma_h-\tilde{\Sigma};W,\Gamma) \\ &\quad = M(U-\tilde{U},\Sigma-\tilde{\Sigma};W,\Gamma) \geq \gamma \|U_h-\tilde{U},\Sigma_h-\tilde{\Sigma}\|^2_{\mathcal{V}\times\mathcal{T}}. \end{aligned} \tag{3.148}$$

Then, the boundedness of M gives

$$\begin{aligned} &M(U-\tilde{U},\Sigma-\tilde{\Sigma};W,\Gamma) \\ &\qquad \leq C\|U-\tilde{U},\Sigma-\tilde{\Sigma}\|_{\mathcal{V}\times\mathcal{T}}\|W,\Gamma\|_{\mathcal{V}\times\mathcal{T}} \\ &\qquad \leq C\|U-\tilde{U},\Sigma-\tilde{\Sigma}\|_{\mathcal{V}\times\mathcal{T}}\|U_h-\tilde{U},\Sigma_h-\tilde{\Sigma}\|_{\mathcal{V}\times\mathcal{T}}, \end{aligned} \tag{3.149}$$

where we have used (3.143). Combining this inequality with (3.148), we now obtain

$$\|U_h-\tilde{U},\Sigma_h-\tilde{\Sigma}\|_{\mathcal{V}\times\mathcal{T}} \leq C\|U-\tilde{U},\Sigma-\tilde{\Sigma}\|_{\mathcal{V}\times\mathcal{T}}. \tag{3.150}$$

It now remains to use the triangle inequality

$$\begin{aligned} \|U-U_h,\Sigma-\Sigma_h\|_{\mathcal{V}\times\mathcal{T}} \quad \leq \quad & \|U-\tilde{U},\Sigma-\tilde{\Sigma}\|_{\mathcal{V}\times\mathcal{T}} \\ & +\|U_h-\tilde{U},\Sigma_h-\tilde{\Sigma}\|_{\mathcal{V}\times\mathcal{T}} \end{aligned} \tag{3.151}$$

to infer

$$\|U-U_h,\Sigma-\Sigma_h\|_{\mathcal{V}\times\mathcal{T}} \leq C\|U-\tilde{U},\Sigma-\tilde{\Sigma}\|_{\mathcal{V}\times\mathcal{T}}, \tag{3.152}$$

and, since this is valid for $(\tilde{U},\tilde{\Sigma})$ arbitrary in $\mathcal{V}_h\times\mathcal{T}_h$, we have (3.110). ∎

Remark 3.2.14. Condition (3.109) is known as the *discrete inf-sup condition* (or simply "inf-sup condition"), and sometimes also referred to as the "Brezzi-Babuška condition" (Brezzi, 1974; Babuška, 1973). ∎

This type of convergence result is directly applicable to finite element discretizations of formulations in mechanics describing fully incompressible

media, e.g. the Stokes problem and incompressible elasticity. However, the problems of structural mechanics that we are concerned with – and in particular shell problems – do not provide mixed variational formulations which are exactly of the type given in (3.92). We instead need to consider mixed formulations of the slightly different type
Find $(U^\varepsilon, \Sigma^\varepsilon)$ *in* $\mathcal{V} \times \mathcal{T}^+$ *such that*

$$\boxed{\begin{cases} A(U^\varepsilon, V) + B(V, \Sigma^\varepsilon) = F(V), & \forall V \in \mathcal{V} \\ B(U^\varepsilon, \Xi) - \varepsilon^2 D(\Sigma^\varepsilon, \Xi) = 0, & \forall \Xi \in \mathcal{T}^+ \end{cases}} \tag{3.153}$$

where ε represents a small parameter – typically related to the thickness of the structure – the space $\mathcal{T}^+$ is a Sobolev space more regular than the above-defined $\mathcal{T}$ space, namely

$$\mathcal{T}^+ \subset \mathcal{T}, \qquad \|\cdot\|_{\mathcal{T}} \leq C \|\cdot\|_{\mathcal{T}^+}, \tag{3.154}$$

and D is a symmetric bilinear form bounded and coercive on $\mathcal{T}^+$. We will also assume that $\mathcal{T}^+$ is dense in $\mathcal{T}$, meaning that any element of $\mathcal{T}$ has elements of $\mathcal{T}^+$ arbitrarily close to it, namely,

$$\forall \Xi \in \mathcal{T},\ \forall \eta > 0,\ \exists \Xi^\eta \in \mathcal{T}^+ \text{ s.t. } \|\Xi - \Xi^\eta\|_{\mathcal{T}} \leq \eta.$$

Note that we use ε as a superscript in the unknowns of (3.153) to indicate that the solution now depends on the parameter ε. In our class of models $\mathcal{T}^+$ will be L^2, whereas the larger space $\mathcal{T}$ will be dependent on the specific type of formulation considered. In particular, for plate formulations the space $\mathcal{T}$ can be explicitly characterized – see Chapter 7, equations (7.79)–(7.81) – while for shell formulations in general only a definition based on the abstract norm $\|\cdot\|_{IS}$ given in Remark 3.2.8 is at hand. In some other cases such as beam formulations and nearly-incompressible elasticity, the space $\mathcal{T}$ is also (essentially) L^2. We will address this case separately below, since we can then obtain stronger results in the mathematical analysis.

For the category of problems formulated in (3.153), we can show the following result, obtained under slightly stronger assumptions – namely, the coercivity of A on the whole space $\mathcal{V}$ – than for Proposition 3.2.3.

Proposition 3.2.5 *Assuming that A is coercive on $\mathcal{V}$ and that* (3.95) *holds, recalling also that D is a symmetric bilinear form bounded and coercive on $\mathcal{T}^+$, the problem* (3.153) *has a unique solution $(U^\varepsilon, \Sigma^\varepsilon)$ in $\mathcal{V} \times \mathcal{T}^+$, and this solution satisfies*

$$\|U^\varepsilon\|_{\mathcal{V}} + \|\Sigma^\varepsilon\|_{\mathcal{T}} + \varepsilon \|\Sigma^\varepsilon\|_{\mathcal{T}^+} \leq C \|F\|_{\mathcal{V}'}, \tag{3.155}$$

for some constant C independent of ε. In addition, $(U^\varepsilon, \Sigma^\varepsilon)$ converges to the solution of (3.92)*, namely,*

$$\|U - U^\varepsilon\|_{\mathcal{V}} + \|\Sigma - \Sigma^\varepsilon\|_{\mathcal{T}} \overset{\varepsilon \to 0}{\longrightarrow} 0. \tag{3.156}$$

We postpone the proof until that of Proposition 3.2.7, which will be obtained under less restrictive coercivity assumptions, see Remark 3.2.15.

We proceed to extend our analysis of finite element discretizations of (3.92) to those of (3.153). Therefore, we consider the problem
Find $(U_h^\varepsilon, \Sigma_h^\varepsilon)$ in $\mathcal{V}_h \times \mathcal{T}_h$ such that

$$\boxed{\begin{cases} A(U_h^\varepsilon, V) + B(V, \Sigma_h^\varepsilon) = F(V), & \forall V \in \mathcal{V}_h \\ B(U_h^\varepsilon, \Xi) - \varepsilon^2 D(\Sigma_h^\varepsilon, \Xi) = 0, & \forall \Xi \in \mathcal{T}_h \end{cases}} \tag{3.157}$$

Here the second finite element space $\mathcal{T}_h$ should be a discretization space for $\mathcal{T}^+$, due to the presence of D in the formulation, and then $\mathcal{T}_h$ also gives an admissible discrete space for $\mathcal{T}$, since we have the dense inclusion $\mathcal{T}^+ \subset \mathcal{T}$ (namely, $\mathcal{T}^+$ is more regular). We then establish the following result.

Proposition 3.2.6 *Under the assumptions of Proposition 3.2.5 and supposing that* (3.109) *also holds, then (3.157) has a unique solution $(U_h^\varepsilon, \Sigma_h^\varepsilon)$ and this solution satisfies*

$$\boxed{\begin{aligned} &\|U^\varepsilon - U_h^\varepsilon\|_{\mathcal{V}} + \|\Sigma^\varepsilon - \Sigma_h^\varepsilon\|_{\mathcal{T}} + \varepsilon \|\Sigma^\varepsilon - \Sigma_h^\varepsilon\|_{\mathcal{T}^+} \\ &\quad \leq C \inf_{V \in \mathcal{V}_h, \Xi \in \mathcal{T}_h} \left\{ \|U^\varepsilon - V\|_{\mathcal{V}} + \|\Sigma^\varepsilon - \Xi\|_{\mathcal{T}} + \varepsilon \|\Sigma^\varepsilon - \Xi\|_{\mathcal{T}^+} \right\}, \end{aligned}} \tag{3.158}$$

for some constant C independent of ε.

As for Proposition 3.2.4 the proof of this proposition will essentially be based on the stability of a mixed bilinear form, defined here by

$$\boxed{\begin{aligned} M_\varepsilon(V, \Xi; W, \Gamma) = A(V, W) + B(V, \Gamma) + B(W, \Xi) \\ - \varepsilon^2 D(\Xi, \Gamma), \\ \forall (V, \Xi), (W, \Gamma) \in (\mathcal{V}_h \times \mathcal{T}_h)^2. \end{aligned}} \tag{3.159}$$

Proof of Proposition 3.2.6. We define the norm in which we will establish the stability of M_ε as

$$\|V, \Xi\|_\varepsilon = \left(\|V\|_{\mathcal{V}}^2 + \|\Xi\|_{\mathcal{T}}^2 + \varepsilon^2 \|\Xi\|_{\mathcal{T}^+}^2\right)^{\frac{1}{2}}. \tag{3.160}$$

Considering an arbitrary element of $\mathcal{V}_h \times \mathcal{T}_h$ (V, Ξ), we now decompose the proof into 2 steps.

i) *Stability in V and $\varepsilon\|\Xi\|_{\mathcal{T}^+}$.* Taking $(W_1, \Gamma_1) = (V, -\Xi)$, we have

$$\|W_1, \Gamma_1\|_\varepsilon = \|V, \Xi\|_\varepsilon, \tag{3.161}$$

and

$$M_\varepsilon(V, \Xi; W_1, \Gamma_1) = A(V, V) + \varepsilon^2 D(\Xi, \Xi) \geq \gamma_1(\|V\|_{\mathcal{V}}^2 + \varepsilon^2 \|\Xi\|_{\mathcal{T}^+}^2), \tag{3.162}$$

using the coercivity of A and D.

ii) *Stability in $\|\Xi\|_{\mathcal{T}}$.* Like in Step iii) of the proof of Lemma 3.2.3, we use the discrete inf-sup condition (3.109) to find W_2 in V_h such that

$$\|W_2\|_{\mathcal{V}} = \|\Xi\|_{\mathcal{T}}, \qquad B(W_2, \Xi) \geq \frac{\delta}{2} \|\Xi\|_{\mathcal{T}}^2. \tag{3.163}$$

Taking $\Gamma_2 = 0$, we then have

$$\|W_2, \Gamma_2\|_\varepsilon = \|\Xi\|_{\mathcal{T}} \leq \|V, \Xi\|_\varepsilon, \tag{3.164}$$

and (see proof of Lemma 3.2.3)

$$M_\varepsilon(V, \Xi; W_2, \Gamma_2) \geq \gamma_2 \|\Xi\|_{\mathcal{T}}^2 - C_2 \|V\|_{\mathcal{V}}^2. \tag{3.165}$$

We conclude the stability proof like for Lemma 3.2.3, then the existence and uniqueness of the solution of (3.157) with the best approximation result (3.158) are established like in the proof of Proposition 3.2.4. ∎

In practice, in structural mechanics formulations the coercivity assumption used in the Propositions 3.2.5 and 3.2.6 does not naturally hold. However, this assumption can be avoided by requiring another type of condition, as established in (Chapelle & Bathe, 2010). In order to present this alternative setting, we first define the mapping $\Sigma(\cdot)$ from $\mathcal{V}$ into $\mathcal{T}^+$ such that

$$D(\Sigma(V), \Xi) = B(V, \Xi), \quad \forall \Xi \in \mathcal{T}^+, \tag{3.166}$$

which is a well-defined continuous linear mapping since D is coercive on $\mathcal{T}^+$. We next define the new bilinear form

$$A_0(U,V) = B(U,\Sigma(V)), \tag{3.167}$$

which is symmetric since

$$\begin{aligned} A_0(V,U) &= B(V,\Sigma(U)) = D(\Sigma(V),\Sigma(U)) \\ &= D(\Sigma(U),\Sigma(V)) = B(U,\Sigma(V)) = A_0(U,V). \end{aligned}$$

It is also positive since

$$A_0(U,U) = D(\Sigma(U),\Sigma(U)).$$

Now, assuming that (3.153) has a solution, the second equation can be rewritten as

$$\Sigma^\varepsilon = \varepsilon^{-2}\Sigma(U^\varepsilon). \tag{3.168}$$

Hence, substituting in the first equation of (3.153) we obtain

$$A(U^\varepsilon,V) + \varepsilon^{-2}A_0(U^\varepsilon,V) = F(V), \quad \forall V \in \mathcal{V}, \tag{3.169}$$

namely, we have eliminated Σ^ε from the variational formulation using in essence "static condensation" – see e.g. (Bathe, 1996) – but here in the continuous problem. Therefore, the mixed formulation (3.153) is strictly equivalent to (3.169) together with the relation (3.168). Since (3.169) involves in solid mechanics only displacements (and in fluid mechanics only velocities), the formulation looks like the displacement formulation of solids (velocity formulation of fluids). Clearly, for this problem to be well-posed we need to require the coercivity of the bilinear form "$A + \varepsilon^{-2}A_0$", which holds for all values of $0 < \varepsilon \leq \varepsilon_{\max}$ if and only if it holds in particular for $\varepsilon = 1$. In general, this coercivity property is a very natural feature of the displacement-based formulation. We then have the following result.

Proposition 3.2.7 *Assuming that $A + A_0$ is coercive on $\mathcal{V}$ and that* (3.95) *holds, recalling also that D is a symmetric bilinear form bounded and coercive on $\mathcal{T}^+$, the problem* (3.153) *has a unique solution $(U^\varepsilon, \Sigma^\varepsilon)$ in $\mathcal{V} \times \mathcal{T}^+$, and this solution satisfies*

$$\|U^\varepsilon\|_{\mathcal{V}} + \|\Sigma^\varepsilon\|_{\mathcal{T}} + \varepsilon\|\Sigma^\varepsilon\|_{\mathcal{T}^+} \leq C\|F\|_{\mathcal{V}'}, \tag{3.170}$$

for some constant C independent of ε. In addition, $(U^\varepsilon, \Sigma^\varepsilon)$ converges to the solution of (3.92)*, namely,*

$$\|U - U^\varepsilon\|_{\mathcal{V}} + \|\Sigma - \Sigma^\varepsilon\|_{\mathcal{T}} \overset{\varepsilon\to 0}{\longrightarrow} 0, \tag{3.171}$$

and

$$\varepsilon\|\Sigma^\varepsilon\|_{\mathcal{T}^+} \overset{\varepsilon\to 0}{\longrightarrow} 0. \tag{3.172}$$

Proof. We will anticipate on the results of Chapter 5, since (3.169) is a so-called penalized formulation as analyzed in that chapter. In order to apply these results, let us first note that

$$\begin{aligned} A_0(V,V)=0 &\iff D(\Sigma(V),\Sigma(V))=0 \\ &\iff \Sigma(V)=0 \\ &\iff B(V,\Xi)=0,\ \forall \Xi\in\mathcal{T}^+ \\ &\iff B(V,\Xi)=0,\ \forall \Xi\in\mathcal{T} \\ &\iff V\in\mathcal{V}_0 \end{aligned}$$

where we have used the fact that $\mathcal{T}^+$ is dense in $\mathcal{T}$. Then, taking $V\in\mathcal{V}_0$ as a particular choice of test function in (3.92), we can see that U is the solution of

$$A(U,V)=F(V),\quad \forall V\in\mathcal{V}_0,$$

with U also in $\mathcal{V}_0$ as noted in Remark 3.2.5, hence this is the candidate limit problem for the penalized formulation. And since $A+A_0$ is coercive on $\mathcal{V}$, we can apply Proposition 5.1.2 and we infer that Problem (3.169) has a unique solution (for every value of ε), satisfying

$$\|U^\varepsilon\|_{\mathcal{V}}\le C\|F\|_{\mathcal{V}'},\quad \|U-U^\varepsilon\|_{\mathcal{V}}\overset{\varepsilon\to0}{\longrightarrow}0,\quad \varepsilon^{-2}A_0(U^\varepsilon,U^\varepsilon)\overset{\varepsilon\to0}{\longrightarrow}0. \tag{3.173}$$

Then, defining Σ^ε by (3.168), we have that $(U^\varepsilon,\Sigma^\varepsilon)$ satisfies (3.153), hence

$$B(V,\Sigma^\varepsilon)=F(V)-A(U^\varepsilon,V),\qquad \forall V\in\mathcal{V},$$

and with (3.95) we obtain

$$\|\Sigma^\varepsilon\|_{\mathcal{T}}\le C\|F\|_{\mathcal{V}'}.$$

In addition, taking $V=U^\varepsilon$ in (3.169) we obtain

$$\varepsilon^2 D(\Sigma^\varepsilon,\Sigma^\varepsilon)=\varepsilon^{-2}A_0(U^\varepsilon,U^\varepsilon)\le F(U^\varepsilon)\le C\|F\|^2_{\mathcal{V}'},$$

hence, by using the coercivity of D,

$$\varepsilon\|\Sigma^\varepsilon\|_{\mathcal{T}^+}\le C\|F\|_{\mathcal{V}'}.$$

To obtain the convergence of Σ^ε we subtract the first equation of (3.153) from the first equation of (3.92), which gives

$$B(V, \Sigma - \Sigma^\varepsilon) = A(U - U^\varepsilon, V), \quad \forall V \in \mathcal{V},$$

and we can again use the inf-sup condition (3.95) to obtain

$$\|\Sigma - \Sigma^\varepsilon\|_{\mathcal{T}} \leq C\|U - U^\varepsilon\|_{\mathcal{V}} \overset{\varepsilon\to 0}{\longrightarrow} 0.$$

Finally, (3.172) directly follows from $\varepsilon^2 D(\Sigma^\varepsilon, \Sigma^\varepsilon) = \varepsilon^{-2} A_0(U^\varepsilon, U^\varepsilon)$ and (3.173). ∎

Remark 3.2.15. Of course, when A is coercive on the whole space $\mathcal{V}$ then we automatically have the coercivity of $A + A_0$, since A_0 is a positive bilinear form. This shows that Proposition 3.2.5 is in fact a particular case of Proposition 3.2.7. ∎

Regarding the discrete formulation (3.157), since the stability proof for the bilinear form M_ε crucially relies on the coercivity of A on the whole space $\mathcal{V}$, we now introduce the augmented bilinear form

$$\tilde{M}_\varepsilon(V, \Xi; W, \Gamma) = M_\varepsilon(V, \Xi; W, \Gamma) + \alpha D\big(\Sigma(V) - \varepsilon^2 \Xi, \Sigma(W) - \varepsilon^2 \Gamma\big), \quad (3.174)$$

for some positive constant α. We first note that $(U^\varepsilon, \Sigma^\varepsilon)$ satisfies

$$\tilde{M}_\varepsilon(U^\varepsilon, \Sigma^\varepsilon; V, \Xi) = F(V), \quad \forall (V, \Xi) \in \mathcal{V} \times \mathcal{T}, \quad (3.175)$$

since the additional term in $\tilde{M}_\varepsilon(U^\varepsilon, \Sigma^\varepsilon; V, \Xi)$ vanishes due to $\Sigma(U^\varepsilon) = \varepsilon^2 \Sigma^\varepsilon$. We then consider the new discrete problem:
Find $(\tilde{U}_h^\varepsilon, \tilde{\Sigma}_h^\varepsilon)$ *in* $\mathcal{V}_h \times \mathcal{T}_h$ *such that*

$$\boxed{\tilde{M}_\varepsilon(\tilde{U}_h^\varepsilon, \tilde{\Sigma}_h^\varepsilon; V, \Xi) = F(V), \quad \forall (V, \Xi) \in \mathcal{V}_h \times \mathcal{T}_h.} \quad (3.176)$$

We will now establish the convergence of this discretization procedure.

Proposition 3.2.8 *Under the assumptions of Proposition 3.2.7 and supposing that* (3.109) *also holds, then for any given* $\alpha \in]0, 1/(\varepsilon_{max})^2[$ *used in the definition of* $\tilde{M}_\varepsilon$, *for* $0 < \varepsilon \leq \varepsilon_{max}$ *the problem* (3.176) *has a unique solution* $(\tilde{U}_h^\varepsilon, \tilde{\Sigma}_h^\varepsilon)$ *and this solution satisfies*

$$\boxed{\begin{aligned} &\|U^\varepsilon - \tilde{U}_h^\varepsilon\|_{\mathcal{V}} + \|\Sigma^\varepsilon - \tilde{\Sigma}_h^\varepsilon\|_{\mathcal{T}} + \varepsilon\|\Sigma^\varepsilon - \tilde{\Sigma}_h^\varepsilon\|_{\mathcal{T}^+} \\ &\leq C \inf_{V \in \mathcal{V}_h, \Xi \in \mathcal{T}_h} \big\{\|U^\varepsilon - V\|_{\mathcal{V}} + \|\Sigma^\varepsilon - \Xi\|_{\mathcal{T}} + \varepsilon\|\Sigma^\varepsilon - \Xi\|_{\mathcal{T}^+}\big\}, \end{aligned}} \quad (3.177)$$

for some constant C *independent of* ε.

Proof. Since consistency is ensured – recall (3.175) – we will focus on establishing the stability of $\tilde{M}_\varepsilon$ for the norm

$$\|V, \Xi\|_\varepsilon = \left(\|V\|_{\mathcal{V}}^2 + \|\Xi\|_{\mathcal{T}}^2 + \varepsilon^2 \|\Xi\|_{\mathcal{T}^+}^2\right)^{\frac{1}{2}}.$$

We decompose the proof into two steps.

i) *Stability in V and $\varepsilon\|\Xi\|_{\mathcal{T}^+}$.* Taking $(W_1, \Gamma_1) = (V, -\Xi)$, we have

$$\|W_1, \Gamma_1\|_\varepsilon = \|V, \Xi\|_\varepsilon, \tag{3.178}$$

and

$$\begin{aligned} \tilde{M}_\varepsilon(V, \Xi; W_1, \Gamma_1) &= A(V, V) + \alpha D(\Sigma(V), \Sigma(V)) + \varepsilon^2(1 - \alpha\varepsilon^2) D(\Xi, \Xi) \\ &= A(V, V) + \alpha A_0(V, V) + \varepsilon^2(1 - \alpha\varepsilon^2) D(\Xi, \Xi) \\ &\geq \gamma_1(\|V\|_{\mathcal{V}}^2 + \varepsilon^2 \|\Xi\|_{\mathcal{T}^+}^2), \end{aligned} \tag{3.179}$$

using the coercivities of $A + A_0$ and D, and the fact that

$$1 - \alpha\varepsilon^2 \geq 1 - \alpha(\varepsilon_{\max})^2 > 0.$$

ii) *Stability in $\|\Xi\|_{\mathcal{T}}$.* We again use the discrete inf-sup condition (3.109) to find W_2 in V_h such that

$$\|W_2\|_{\mathcal{V}} = \|\Xi\|_{\mathcal{T}}, \qquad B(W_2, \Xi) \geq \frac{\delta}{2} \|\Xi\|_{\mathcal{T}}^2,$$

and with $\Gamma_2 = 0$ we have

$$\|W_2, \Gamma_2\|_\varepsilon = \|\Xi\|_{\mathcal{T}} \leq \|V, \Xi\|_\varepsilon.$$

This choice gives

$$\tilde{M}_\varepsilon(V, \Xi; W_2, \Gamma_2) \geq \gamma_2 \|\Xi\|_{\mathcal{T}}^2 - C_2(\|V\|_{\mathcal{V}}^2 + \varepsilon^2 \|\Xi\|_{\mathcal{T}^+}^2), \tag{3.180}$$

and we conclude the proof like for Proposition 3.2.6. ∎

Remark 3.2.16. The above proof is formally similar to that of Proposition 3.2.6, although the discrete problem considered here does not – strictly speaking – enter in the framework of (3.157) due to the additional term introduced in $\tilde{M}_\varepsilon$. This shows that the additional term automatically provides the stability in $\mathcal{V}_h$ that was instead provided by the full coercivity of A in

Prop. 3.2.6. In this respect we can say that this additional term is a "stabilizing term". In fact, the modified formulation (3.176) is an "augmented Lagrangian" formulation as defined and discussed in (Glowinski & Le Tallec, 1989). ■

If we directly consider the discrete system (3.157), we can eliminate the unknown Σ_h^ε from the variational formulation – similarly to what we did in the continuous setting – by defining the mapping $\Sigma_h(\cdot)$ from $\mathcal{V}$ into $\mathcal{T}_h$ such that

$$D(\Sigma_h(V), \Xi) = B(V, \Xi), \quad \forall \Xi \in \mathcal{T}_h. \tag{3.181}$$

This clearly defines a continuous linear mapping, and in fact we have

$$\Sigma_h(V) = \Pi_D^h \Sigma(V), \tag{3.182}$$

where Π_D^h denotes the projection operator onto $\mathcal{T}_h$ for the scalar product associated with the bilinear form D. We can also define the bilinear form

$$A_0^h(U, V) = B(U, \Sigma_h(V)), \tag{3.183}$$

which is again symmetric and positive, and we infer that (3.157) is equivalent to

$$A(U_h^\varepsilon, V) + \varepsilon^{-2} A_0^h(U_h^\varepsilon, V) = F(V), \quad \forall V \in \mathcal{V}_h, \tag{3.184}$$

together with

$$\Sigma_h^\varepsilon = \varepsilon^{-2} \Sigma_h(U_h^\varepsilon). \tag{3.185}$$

Note that, if we instead eliminate $\tilde{\Sigma}_h^\varepsilon$ from the modified problem (3.176) we obtain

$$A(\tilde{U}_h^\varepsilon, V) + \alpha A_0(\tilde{U}_h^\varepsilon, V) + (\varepsilon^{-2} - \alpha) A_0^h(\tilde{U}_h^\varepsilon, V) = F(V), \quad \forall V \in \mathcal{V}_h, \tag{3.186}$$

with

$$\tilde{\Sigma}_h^\varepsilon = \varepsilon^{-2} \Sigma_h(\tilde{U}_h^\varepsilon). \tag{3.187}$$

Remark 3.2.17. With the formulation (3.186), it is quite straightforward to interpret why stability is more easily obtained in the augmented mixed formulation (3.176) than in the original mixed formulation associated with (3.184). Namely, in (3.186) we retain the coercivity contribution provided by the unperturbed form A_0 in the term $A + \alpha A_0$. This strategy is called

"partial selective reduced integration" in (Arnold & Brezzi, 1993, 1997b), see also Section 7.2.2 and (Bathe, 1996). However, this construction involves the rather arbitrary numerical factor α, and formulations not requiring this construction are clearly preferable in practice. ■

We will now be concerned with the convergence of the original discrete mixed problem (3.157) under the assumptions of Proposition 3.2.7, namely, assuming $A + A_0$ is coercive, in particular. Considering (3.184) involving only displacements, we clearly need to have $A + \varepsilon^{-2} A_0^h$ coercive on $\mathcal{V}_h$ for all admissible values of ε – which is equivalent to $A + A_0^h$ coercive. However, this coercivity property does not follow from the coercivity of $A + A_0$, as it depends on the specific choice of the discrete spaces $\mathcal{V}_h$ and $\mathcal{T}_h$, indeed. Hence, this is a condition that we need to require from the discrete spaces, namely,

$$A(V,V) + A_0^h(V,V) \geq \gamma \|V\|_{\mathcal{V}}^2, \quad \forall V \in \mathcal{V}_h, \tag{3.188}$$

for some $\gamma > 0$ *independent of* h. We then can show the following approximation result.

Proposition 3.2.9 *Under the assumptions of Proposition 3.2.7 and supposing that* (3.109) *and* (3.188) *also hold, then (3.157) has a unique solution* $(U_h^\varepsilon, \Sigma_h^\varepsilon)$ *and this solution satisfies*

$$\begin{aligned} &\|U^\varepsilon - U_h^\varepsilon\|_{\mathcal{V}} + \|\Sigma^\varepsilon - \Sigma_h^\varepsilon\|_{\mathcal{T}} + \varepsilon \|\Sigma^\varepsilon - \Sigma_h^\varepsilon\|_{\mathcal{T}^+} \\ &\quad \leq C \inf_{V \in \mathcal{V}_h, \Xi \in \mathcal{T}_h} \big\{ \|U^\varepsilon - V\|_{\mathcal{V}} + \|\Sigma^\varepsilon - \Xi\|_{\mathcal{T}} + \varepsilon \|\Sigma^\varepsilon - \Xi\|_{\mathcal{T}^+} \big\}, \end{aligned} \tag{3.189}$$

for some constant C *independent of* ε.

Proof. The existence and uniqueness directly follow from the equivalence of (3.157) with (3.184) and (3.185), and from the coercivity of $A + \varepsilon^{-2} A_0^h$ on $\mathcal{V}_h$. As regards convergence, we will take advantage of the convergence result established in Proposition 3.2.8 for the particular choice

$$\alpha = (2\varepsilon_{\max})^{-2}.$$

Then (3.177) holds, and using this auxiliary solution, we will establish the convergence in three steps.

i) *Convergence in* U_h^ε.
The discrete solution U_h^ε satisfies (3.184), while $\tilde{U}_h^\varepsilon$ instead satisfies

$$\big[A + \alpha A_0 + (\varepsilon^{-2} - \alpha)A_0^h\big](\tilde{U}_h^\varepsilon, V) = F(V), \quad \forall V \in \mathcal{V}_h.$$

Subtracting the two variational equations yields, for any $V \in \mathcal{V}_h$,

$$\begin{aligned}(A + \varepsilon^{-2}A_0^h)(U_h^\varepsilon - \tilde{U}_h^\varepsilon, V) &= \alpha(A_0 - A_0^h)(\tilde{U}_h^\varepsilon, V)\\ &= \alpha\big[(A_0 - A_0^h)(U^\varepsilon, V) + (A_0 - A_0^h)(\tilde{U}_h^\varepsilon - U^\varepsilon, V)\big].\end{aligned}$$

Choosing as a particular test function $V = U_h^\varepsilon - \tilde{U}_h^\varepsilon$ and using the coercivity (3.188) with the continuities of A_0 and A_0^h, we obtain

$$\|U_h^\varepsilon - \tilde{U}_h^\varepsilon\|_{\mathcal{V}} \le C\left[\|U^\varepsilon - \tilde{U}_h^\varepsilon\|_{\mathcal{V}} + \sup_{V\in\mathcal{V}_h} \frac{(A_0 - A_0^h)(U^\varepsilon, V)}{\|V\|_{\mathcal{V}}}\right].$$

Then, a simple triangle inequality gives

$$\|U^\varepsilon - U_h^\varepsilon\|_{\mathcal{V}} \le C\left[\|U^\varepsilon - \tilde{U}_h^\varepsilon\|_{\mathcal{V}} + \sup_{V\in\mathcal{V}_h} \frac{(A_0 - A_0^h)(U^\varepsilon, V)}{\|V\|_{\mathcal{V}}}\right]. \tag{3.190}$$

In order to bound the consistency error term in the right-hand side, we use (3.167) and (3.183), then (3.168) and (3.182) to write

$$(A_0 - A_0^h)(U^\varepsilon, V) = B(V, \Sigma(U^\varepsilon) - \Sigma_h(U^\varepsilon)) = \varepsilon^2 B(V, (I - \Pi_D^h)\Sigma^\varepsilon).$$

Therefore,

$$\frac{|(A_0 - A_0^h)(U^\varepsilon, V)|}{\|V\|_{\mathcal{V}}} \le C\varepsilon^2 \|(I - \Pi_D^h)\Sigma^\varepsilon\|_{\mathcal{T}^+} \le C\varepsilon^2 \inf_{\Xi\in\mathcal{T}_h} \|\Sigma^\varepsilon - \Xi\|_{\mathcal{T}^+},$$

since D provides a norm that is equivalent to $\|\cdot\|_{\mathcal{T}^+}$, and then (3.190) yields

$$\|U^\varepsilon - U_h^\varepsilon\|_{\mathcal{V}} \le C\big[\|U^\varepsilon - \tilde{U}_h^\varepsilon\|_{\mathcal{V}} + \varepsilon^2 \inf_{\Xi\in\mathcal{T}_h} \|\Sigma^\varepsilon - \Xi\|_{\mathcal{T}^+}\big]. \tag{3.191}$$

ii) *Convergence in* $\|\Sigma_h^\varepsilon\|_{\mathcal{T}}$.
Recalling that Σ^ε satisfies

$$A(U^\varepsilon, V) + B(V, \Sigma^\varepsilon) = F(V), \quad \forall V \in \mathcal{V},$$

we have, for any given $\Gamma \in \mathcal{T}_h$,

$$B(V, \Gamma) = F(V) - A(U^\varepsilon, V) + B(V, \Gamma - \Sigma^\varepsilon), \quad \forall V \in \mathcal{V},$$

while Σ_h^ε satisfies

$$B(V, \Sigma_h^\varepsilon) = F(V) - A(U_h^\varepsilon, V), \quad \forall V \in \mathcal{V}_h.$$

Subtracting the two equations, we obtain

$$B(V, \Sigma_h^\varepsilon - \Gamma) = A(U^\varepsilon - U_h^\varepsilon, V) + B(V, \Sigma^\varepsilon - \Gamma), \quad \forall V \in \mathcal{V}_h.$$

Using the discrete inf-sup condition (3.109) and the continuities of A and B, we infer

$$\|\Sigma_h^\varepsilon - \Gamma\|_{\mathcal{T}} \leq C\big(\|U^\varepsilon - U_h^\varepsilon\|_{\mathcal{V}} + \|\Sigma^\varepsilon - \Gamma\|_{\mathcal{T}}\big),$$

which yields, combined with a triangle inequality,

$$\|\Sigma^\varepsilon - \Sigma_h^\varepsilon\|_{\mathcal{T}} \leq C\big[\|U^\varepsilon - U_h^\varepsilon\|_{\mathcal{V}} + \inf_{\Xi \in \mathcal{T}_h} \|\Sigma^\varepsilon - \Xi\|_{\mathcal{T}}\big]. \tag{3.192}$$

iii) *Convergence in* $\varepsilon\|\Sigma_h^\varepsilon\|_{\mathcal{T}^+}$.
We have by construction

$$\varepsilon^2 D(\Sigma^\varepsilon, \Xi) = B(U^\varepsilon, \Xi), \quad \forall \Xi \in \mathcal{T}^+,$$

and

$$\varepsilon^2 D(\Sigma_h^\varepsilon, \Xi) = B(U_h^\varepsilon, \Xi), \quad \forall \Xi \in \mathcal{T}_h.$$

From this we infer, for any given $\Gamma \in \mathcal{T}_h$,

$$\varepsilon^2 D(\Sigma_h^\varepsilon - \Gamma, \Sigma_h^\varepsilon - \Gamma) = B(U_h^\varepsilon - U^\varepsilon, \Sigma_h^\varepsilon - \Gamma) + \varepsilon^2 D(\Sigma^\varepsilon - \Gamma, \Sigma_h^\varepsilon - \Gamma),$$

and – recalling the coercivity of D on $\mathcal{T}^+$ – standard manipulations then give

$$\varepsilon\|\Sigma_h^\varepsilon - \Gamma\|_{\mathcal{T}^+} \leq C\Big(\|U^\varepsilon - U_h^\varepsilon\|_{\mathcal{V}} + \|\Sigma_h^\varepsilon - \Gamma\|_{\mathcal{T}} + \varepsilon\|\Sigma^\varepsilon - \Gamma\|_{\mathcal{T}^+}\Big),$$

hence, with the help of triangle inequalities,

$$\begin{aligned}\varepsilon\|\Sigma^\varepsilon - \Sigma_h^\varepsilon\|_{\mathcal{T}^+} \leq C\Big(&\|U^\varepsilon - U_h^\varepsilon\|_{\mathcal{V}} + \|\Sigma^\varepsilon - \Sigma_h^\varepsilon\|_{\mathcal{T}} \\ &+ \inf_{\Xi \in \mathcal{T}_h} \big\{\|\Sigma^\varepsilon - \Xi\|_{\mathcal{T}} + \varepsilon\|\Sigma^\varepsilon - \Xi\|_{\mathcal{T}^+}\big\}\Big).\end{aligned} \tag{3.193}$$

In order to obtain the final error estimate (3.189), it now just remains to gather the intermediate bounds (3.177), (3.191), (3.192) and (3.193). ∎

Remark 3.2.18. Note that we have used the solution of the discrete stabilized formulation (3.176) only as an intermediary in the convergence proof,

and that no such stabilization is actually included in the mixed formulation (3.157). ■

Remark 3.2.19. Regarding the coercivity assumption (3.188), we note that

$$A_0^h(V,V) = D(\Sigma_h(V), \Sigma_h(V)) = D(\Pi_D^h \Sigma(V), \Pi_D^h \Sigma(V)),$$

while A_0, which provides the desired coercivity in $A + A_0$, satisfies instead

$$A_0(V,V) = D(\Sigma(V), \Sigma(V)).$$

Hence, in order for $A + A_0^h$ to remain coercive, we need to have $\mathcal{T}_h$ "sufficiently large" to avoid losing the coercivity in the projection Π_D^h. However, this may be difficult to accommodate with the inf-sup condition (3.109), which is more easily satisfied when $\mathcal{T}_h$ is "sufficiently small". Nevertheless, we point out that the coercivity assumption (3.188) can be numerically tested by computing the smallest eigenvalue in the eigenproblem

$$A(\Phi, V) + A_0^h(\Phi, V) = \lambda(\Phi, V)_{\mathcal{V}}, \quad \forall V \in \mathcal{V}_h,$$

for a series of increasingly refined meshes, in the spirit of the inf-sup test presented in (Chapelle & Bathe, 1993). ■

In some cases, we will have that $\mathcal{T}^+ = \mathcal{T}$. This holds, in particular, for nearly incompressible formulations where $\mathcal{T}$ and $\mathcal{T}^+$ correspond to L^2 (with the mean value of the function subtracted in the norm of $\mathcal{T}$ when considering homogeneous boundary conditions all over the boundary for the displacements, since the pressure is then defined up to a constant), see (Brezzi & Fortin, 1991). Another such example is the mixed formulation corresponding to the Timoshenko beam model, see Section 7.2.1. In such cases the partial coercivity (3.94) is sufficient – namely, the coercivity on the whole space $\mathcal{V}$ is not needed – in order to establish the following well-posedness and convergence result.

Proposition 3.2.10 *Consider the case when $\mathcal{T}^+ = \mathcal{T}$. Assume that* (3.94) *and* (3.95) *both hold, that the bilinear form A is positive, namely*

$$A(V,V) \geq 0, \quad \forall V \in \mathcal{V}, \tag{3.194}$$

and that D is a symmetric bilinear form coercive on $\mathcal{T}$. Then the problem (3.153) *has a unique solution and this solution satisfies*

$$\|U^\varepsilon\|_{\mathcal{V}} + \|\Sigma^\varepsilon\|_{\mathcal{T}} \leq C\|F\|_{\mathcal{V}'}, \tag{3.195}$$

for some constant C independent of ε. In addition, $(U^\varepsilon, \Sigma^\varepsilon)$ converges to the solution of (3.92)*, namely,*

$$\|U - U^\varepsilon\|_{\mathcal{V}} + \|\Sigma - \Sigma^\varepsilon\|_{\mathcal{T}} \overset{\varepsilon \to 0}{\longrightarrow} 0. \tag{3.196}$$

Remark 3.2.20. The condition that A be positive as defined in (3.194) is – of course – weaker than the condition that A be coercive on $\mathcal{V}$. Condition (3.194) is frequently satisfied in practice. ■

Proof of Proposition 3.2.10. It suffices to show that $A + A_0$ is coercive in this case, in order to apply Proposition 3.2.7. For any $V \in \mathcal{V}$ we have

$$A_0(V,V)^{\frac{1}{2}} = D(\Sigma(V), \Sigma(V))^{\frac{1}{2}} = \sup_{\Xi \in \mathcal{T}} \frac{D(\Sigma(V), \Xi)}{D(\Xi, \Xi)^{\frac{1}{2}}} = \sup_{\Xi \in \mathcal{T}} \frac{B(V, \Xi)}{D(\Xi, \Xi)^{\frac{1}{2}}},$$

by the definition of $\Sigma(V)$, recall (3.166). Of course, we have $D(\Xi, \Xi)^{\frac{1}{2}} \leq C\|\Xi\|_{\mathcal{T}^+}$, and we now use the fact that $\mathcal{T}^+ = \mathcal{T}$ to infer

$$A_0(V,V)^{\frac{1}{2}} \geq C \sup_{\Xi \in \mathcal{T}} \frac{B(V, \Xi)}{\|\Xi\|_{\mathcal{T}}}. \tag{3.197}$$

On the other hand, since (3.95) holds we have

$$\mathcal{V} = \mathcal{V}_0 \oplus \mathcal{V}_0^\perp,$$

with $\mathcal{V}_0^\perp = \mathrm{Im} B^T$, and for any $V \in \mathcal{V}$ we can write the decomposition

$$V = V_0 + V_1, \quad V_0 \in \mathcal{V}_0, \quad V_1 \in \mathcal{V}_0^\perp.$$

Then

$$(A + A_0)(V,V) = A(V_0, V_0) + A(V_1, V_1) + 2A(V_0, V_1) + A_0(V_1, V_1),$$

and we can combine (3.197) with (3.103) to obtain

$$A_0(V_1, V_1) \geq \gamma \|V_1\|_{\mathcal{V}}^2.$$

Furthermore, since A is positive we can apply the Cauchy-Schwarz inequality and infer

$$(A + A_0)(V,V) \geq (1 - \eta) A(V_0, V_0) + (1 - 1/\eta) A(V_1, V_1) + \gamma \|V_1\|_{\mathcal{V}}^2,$$

for any $0 < \eta < 1$. Then we can choose η so that

$$(1-1/\eta)A(V_1,V_1)+\gamma\|V_1\|^2 \geq \frac{\gamma}{2}\|V_1\|_{\mathcal{V}}^2,$$

and since A is coercive on $\mathcal{V}_0$ we obtain the desired coercivity of $A+A_0$. ■

Remark 3.2.21. The assumption $\mathcal{T}^+ = \mathcal{T}$ was crucially used in this proof to obtain (3.197). In the general case, we only have

$$\|\Xi\|_{\mathcal{T}} \leq C\|\Xi\|_{\mathcal{T}^+}, \quad \forall \Xi \in \mathcal{T},$$

and (3.197) cannot be inferred from the previous equation. ■

We can then show the following result for corresponding finite element discretizations.

Proposition 3.2.11 *Under the assumptions of Proposition 3.2.10 and supposing that* (3.108) *and* (3.109) *also hold, Problem (3.157) has a unique solution* $(U_h^\varepsilon, \Sigma_h^\varepsilon)$*. Moreover this solution satisfies, for* $0<\varepsilon\leq\varepsilon_{max}$*,*

$$\begin{aligned}\|U^\varepsilon - U_h^\varepsilon\|_{\mathcal{V}} + \|\Sigma^\varepsilon - \Sigma_h^\varepsilon\|_{\mathcal{T}} \\ \leq C \inf_{V\in\mathcal{V}_h,\Xi\in\mathcal{T}_h}\big\{\|U^\varepsilon - V\|_{\mathcal{V}} + \|\Sigma^\varepsilon - \Xi\|_{\mathcal{T}}\big\},\end{aligned} \tag{3.198}$$

for some constant C *independent of* ε*.*

Proof. Similarly to the proof of Proposition 3.2.10, we will simply show that $A+A_0^h$ is coercive on $\mathcal{V}_h$ in order to apply Proposition 3.2.9, and we just sketch this proof. We first directly obtain the discrete counterpart of (3.197), namely,

$$A_0^h(V,V)^{\frac{1}{2}} \geq C \sup_{\Xi\in\mathcal{T}_h}\frac{B(V,\Xi)}{\|\Xi\|_{\mathcal{T}}}, \quad \forall V\in\mathcal{V}_h, \tag{3.199}$$

using similar arguments. Then, the coercivity proof can be concluded by employing the decomposition

$$\mathcal{V}_h = \mathcal{V}_{h0}\oplus\mathcal{V}_{h0}^{\perp} = \mathcal{V}_{h0}\oplus\mathcal{V}_{h1},$$

and the alternate discrete inf-sup condition (3.114) combined with (3.199) to show that

$$A_0^h(V_1,V_1)\geq\gamma\|V_1\|_{\mathcal{V}}^2, \quad \forall V_1\in\mathcal{V}_{h1}.$$ ■

Remark 3.2.22. We note that – in Propositions 3.2.3 to 3.2.11 – there is a very strong similarity between the assumptions used for the continuous and discrete mixed formulations. An interpretation of this fact is that

- The continuous formulations *define* the functional setting in which the problems are well-posed. Namely, the spaces $\mathcal{V}$ and $\mathcal{T}$ (and $\mathcal{T}^+$ when appropriate) need be *identified* so that the *given* bilinear forms provide continuity and stability over these spaces. Hence, the assumptions used can be considered as – sufficient, and also necessary, see Remark 3.2.6 – conditions for ensuring well-posedness.
- Then, in order to also obtain well-posed problems with the corresponding discrete formulations we – of course – need to satisfy similar assumptions. In addition, the fact that continuity and stability properties hold over the *same functional spaces* as for the continuous formulations and with *constants independent of* h implies that optimal approximations are obtained. Moreover, when the problem is ε-dependent the error estimates derived are *independent of* ε (provided all constants are independent of ε as specified above, of course).

■

3.2.2 Interpolation and *a priori* error estimates

As already pointed out, the key point in the bounds given in Equations (3.86), (3.110) and (3.189) is that the error made in the finite element approximation is *of the same order* as for the best approximation of the exact solution in the finite element subspace. Hence, at this stage the problem of deriving an error bound for the finite element approximation "reduces to" a problem that falls into the domain of *approximation theory*. There is an abundant literature on this matter which – of course – goes much beyond the scope of this book. However, we now give a few selected results which show how the error analysis can be typically completed.

We concentrate on the case of *Lagrange-type isoparametric finite elements* which are most useful for practical purposes. Since the finite element fields are then defined by their values at the nodes, a "natural candidate" that can be used to obtain an upper bound of the best approximation error is the *interpolation* of the exact solution, namely the finite element field that has the same nodal values as the exact solution. Denoting the interpolation operator by $\mathcal{I}$, we indeed have

$$\boxed{\inf_{V \in \mathcal{V}_h} \|U - V\|_{\mathcal{V}} \leq \|U - \mathcal{I}(U)\|_{\mathcal{V}}.} \tag{3.200}$$

Of course, in this equation we implicitly assume that the exact solution U is sufficiently regular for this interpolation operation to be meaningful. Namely, U must be a continuous function, which holds when U is in H^2 in 2D or 3D, recall our discussion in Section 3.1.2. Note that this does not require that the whole of $\mathcal{V}$ be included in H^2 (which would be in contradiction with the Lagrange-type shape functions used), but only that the exact solution U itself be in this space.

Without loss of generality, we now restrict the analysis to cases when $\mathcal{V}$ is a space of scalar fields (i.e. with only one component). Further, we concentrate on standard Sobolev spaces for which the domain $\mathcal{O}$ in which the variational problem is posed is a domain of $\mathbb{R}^n$ with n equals 2 or 3. These results will be later extended to Sobolev spaces based on surfaces in Chapter 6. In the present framework, we also assume that the norm used in $\mathcal{V}$ is either the L^2 or the H^1 norm, which will be the case in most situations that we will encounter. Then we have

$$\|U - \mathcal{I}(U)\|_{\mathcal{V}}^2 = \|U - \mathcal{I}(U)\|_{H^q(\mathcal{O})}^2 = \sum_{K \in \mathcal{M}_h} \|U - \mathcal{I}(U)\|_{H^q(K)}^2, \qquad (3.201)$$

for $q = 0$ or $q = 1$, and where $\mathcal{M}_h$ represents the set of elements in the mesh considered. Note that the value of $\mathcal{I}(U)$ inside an element K is completely determined by the values of U at the nodes of the said element, hence the local interpolation estimate given by $\|U - \mathcal{I}(U)\|_{H^q(K)}$ can be analyzed at the element level. Clearly, what we are after is – for the arbitrary sequence of meshes considered – an estimate of the type

$$\boxed{\|U - \mathcal{I}(U)\|_{H^q(K)} \leq C(h_K)^{p+1-q},} \qquad (3.202)$$

where p represents the order of the shape functions used (e.g. $p = 2$ for quadratic shape functions, namely P_2 or Q_2), and h_K the diameter of element K. When (3.201) holds in all the elements, we infer using (3.201)

$$\|U - \mathcal{I}(U)\|_{\mathcal{V}} \leq Ch^{p+1-q}, \text{ for } h = \sup_{K \in \mathcal{M}_h} h_K. \qquad (3.203)$$

It can be shown that (3.202) indeed holds under certain conditions on the geometry of the elements/meshes and on the regularity of the solution U.

It is useful to consider examples of such conditions with the implied interpolation estimates, in order to provide guidelines for the construction of appropriate meshes, and also for the purpose of further mathematical analysis. We refer to (Ciarlet & Raviart, 1972) for the proofs of the results stated in the examples that now follow.

- For P_1 triangular (or tetrahedral) elements, denoting by ρ_K the diameter of the sphere inscribed in element K (see Figure 3.5), under the condition

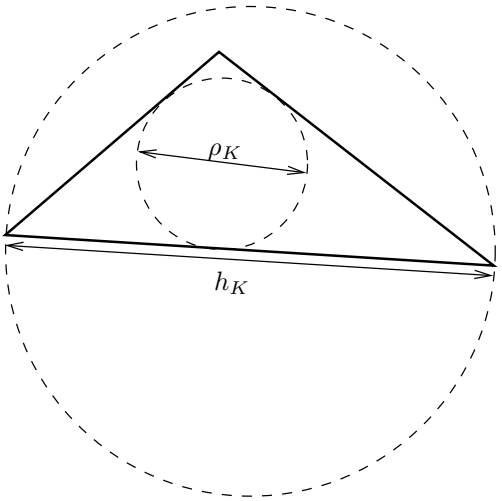

Fig. 3.5. Diameters in triangles

$$\boxed{0 < \gamma \leq \frac{\rho_K}{h_K}, \qquad \forall K \in \mathcal{M}_h,} \tag{3.204}$$

to be satisfied for all meshes $\mathcal{M}_h$ considered, we have

$$\|U - \mathcal{I}(U)\|_{H^q(K)} \leq C(h_K)^{2-q}\|U\|_{H^2(K)}. \tag{3.205}$$

- For Q_1 quadrilateral elements (in 2D), denoting by γ_K the supremum of the absolute values of cosines for the internal angles at the vertices of the element, we require that

$$\boxed{\gamma_K \leq C < 1, \qquad \forall K \in \mathcal{M}_h,} \tag{3.206}$$

in addition to Condition (3.204), in order to obtain the similar estimate

$$\|U - \mathcal{I}(U)\|_{H^q(K)} \leq C(h_K)^{2-q}\|U\|_{H^2(K)}. \tag{3.207}$$

- For P_2 triangular elements (in 2D), denoting by $\vec{x}_K^{(i)}$ (for $i = 1, 2, 3$) the position vectors corresponding to the vertices of an element and by $\vec{x}_K^{(ij)}$ $(i, j = 1, 2, 3)$ the position of the node located on the edge connecting the vertices i and j, we consider the straight triangle $\tilde{K}$ defined by the vertices, and the corresponding mid-edge nodes given by

$$\vec{x}_{\tilde{K}}^{(ij)} = \frac{1}{2}(\vec{x}_K^{(i)} + \vec{x}_K^{(j)}), \tag{3.208}$$

see Figure 3.6. Then, in addition to (3.204) we need to impose

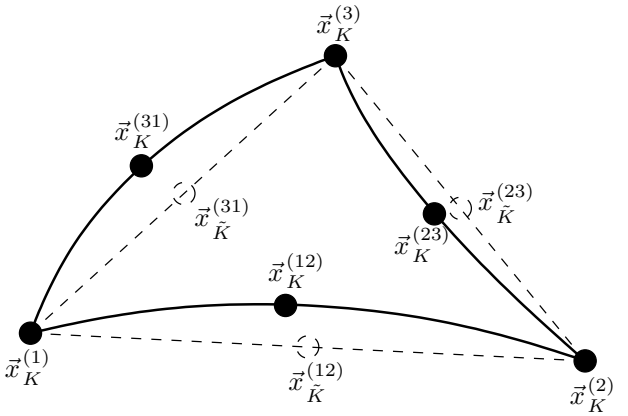

Fig. 3.6. P2-isoparametric triangle

$$\boxed{\|\vec{x}_{\tilde{K}}^{(ij)} - \vec{x}_K^{(ij)}\| \leq C(h_K)^2, \quad \forall (i,j),\ \forall K \in \mathcal{M}_h.} \tag{3.209}$$

in order to obtain

$$\|U - \mathcal{I}(U)\|_{H^q(K)} \leq C(h_K)^{3-q} \|U\|_{H^3(K)}. \tag{3.210}$$

Note that (3.209) is easily satisfied when, e.g., the distortion of a given edge is created by the fact that its three nodes are positioned on a smooth curved line (such as for the approximation of a curved boundary).

- For Q_2 quadrilateral elements (in 2D), we similarly define the position vectors of the vertices $\vec{x}_K^{(i)}$ (for $i = 1, \ldots, 4$), of the nodes on the edges $\vec{x}_K^{(ij)}$, and of the node inside the element $\vec{x}_K^{(9)}$. Likewise, we define the corresponding straight quadrilateral element $\tilde{K}$ with mid-edge nodes given by

$$\vec{x}_{\tilde{K}}^{(ij)} = \frac{1}{2}(\vec{x}_K^{(i)} + \vec{x}_K^{(j)}), \tag{3.211}$$

and with the center node

$$\vec{x}_{\tilde{K}}^{(9)} = \frac{1}{4}(\vec{x}_K^{(1)} + \vec{x}_K^{(2)} + \vec{x}_K^{(3)} + \vec{x}_K^{(4)}). \tag{3.212}$$

Then in addition to Conditions (3.204) and (3.206), we require that

$$\boxed{\begin{cases} \|\vec{x}_{\tilde{K}}^{(ij)} - \vec{x}_K^{(ij)}\| \leq C(h_K)^2 \\ \|\vec{x}_{\tilde{K}}^{(9)} - \vec{x}_K^{(9)}\| \leq C(h_K)^2 \end{cases}} \tag{3.213}$$

for all K in $\mathcal{M}_h$, in order to obtain

$$\|U - \mathcal{I}(U)\|_{H^q(K)} \leq C(h_K)^{3-q} \|U\|_{H^3(K)}. \tag{3.214}$$

Conditions to be imposed in various other types of finite element discretizations and the corresponding detailed analyses can be found in (Ciarlet & Raviart, 1972) and the references therein, see also the discussions in (Bathe, 1996) and (Lee & Bathe, 1993).

Using the local interpolation estimates (obtained under the above-mentioned conditions) together with (3.201), we infer global estimates of the type

$$\boxed{\|U - \mathcal{I}(U)\|_{H^q(\mathcal{O})} \leq Ch^{p+1-q} \|U\|_{H^{p+1}(\mathcal{O})},} \tag{3.215}$$

where the dependence of the estimate on the specific solution U considered is fully explicit in the right-hand side (namely, the bounding constant does not depend on U). We again note that some extra regularity (compared to that of the Sobolev space $\mathcal{V}$) is needed for the solution U in order to obtain the interpolation estimate.

Combining the interpolation estimate (3.215) with a best approximation estimate such as (3.86) we obtain

$$\boxed{\|U - U_h\|_{\mathcal{V}} \leq Ch^{p+1-q} \|U\|_{H^{p+1}(\mathcal{O})},} \tag{3.216}$$

which shows that the finite element procedure converges with an optimal order provided that the exact solution features the required regularity (in addition to all the other conditions used in the mathematical analysis leading to this estimate, including the conditions on the mesh geometry). Although this estimate is very valuable for the purpose of mathematical analysis, it cannot really be used in practice to quantitatively evaluate the error made in the finite element approximation because – notwithstanding the fact that it may be very difficult to obtain a sharp value of the bounding constant involved – it requires the knowledge of the exact solution. The numerical evaluation of the actual finite element error – which is crucial for mesh adaptation strategies, in particular – requires other approaches by which estimates that use only the discrete solution are constructed. These estimates are called *a posteriori* error estimates because they are computed once the finite element

analysis has been performed – and using only the finite element solution – as opposed to *a priori* error estimates as in (3.216). Since the *a posteriori* error estimates are used to assess the accuracy obtained in the finite element solution of a mathematical model, they are also an important ingredient of finite element analysis. However, we do not focus on this issue in this book and refer to (Verfürth, 1996; Bathe, 1996; Ainsworth & Oden, 2000; Babuška & Strouboulis, 2001; Grätsch & Bathe, 2005b,a) and the references therein.

Remark 3.2.23. In engineering practice, another norm called the L^∞-norm may be of interest for assessing solutions and errors. This norm is defined by

$$\|U\|_{L^\infty(\mathcal{O})} = \sup_{x\in\mathcal{O}} |U(x)|,$$

for all fields U so that this supremum exists. In particular, it may be valuable to bound pointwise values of solutions, e.g. to ensure that stresses do not exceed a given threshold in structural designs. When solution bounds are obtained in some Sobolev space $H^p(\mathcal{O})$ which is made of continuous functions – see the discussion in Section 3.1.2 – then L^∞ bounds follow, as in such cases

$$\|U\|_{L^\infty(\mathcal{O})} \leq C\|U\|_{H^p(\mathcal{O})}.$$

However, in most variational formulations that we will be concerned with, the natural Sobolev space associated with the formulation will be H^1, which is not made of continuous functions except in 1D. Nevertheless, in some such cases L^∞ error estimates can be obtained – albeit ensuring weaker convergence than in the natural norm, and only provided the solution enjoys some specific regularity properties – see e.g. (Ciarlet, 1978) and references therein. ■

3.2.3 Effect of numerical integration

It is also necessary to – at least briefly – address the issue of numerical integration. Indeed, we have so far assumed that exact values are used for the integrals involved in the expressions of the bilinear and linear forms applied on discrete (finite element) fields. This is in general not true in practice, as integrals cannot be exactly computed (except in very restrictive cases), hence must be substituted with approximate integration formulae. It is then very important to know which numerical integration rules should be used in order to retain optimal convergence properties for the finite element approximations.

We recall that the idea of the numerical integration of a function ϕ consists in using approximate formulae of the type

$$\int_K \phi\, dr ds \approx \sum_i \alpha_i \phi(r_i, s_i), \tag{3.217}$$

over each element K, where (r, s) denotes the local coordinates (hence we consider here the example of a 2D problem), (r_i, s_i) represents the coordinates of the "integration points", and the coefficients α_i are the corresponding "integration weights". For actual examples of numerical integration rules, see e.g. (Bathe, 1996).

In (Ciarlet, 1978) a second-order elliptic model problem (namely, a variational formulation containing derivatives of order one only) is analyzed in details as regards the influence of numerical integration when using P_2 isoparametric triangles for the finite element approximation. It is then shown that, under the same conditions that govern the optimality of interpolation estimates, namely (3.204) and (3.209), a numerical integration formula that exactly integrates polynomials of order two provides an approximation which converges in $O(h^2)$, namely with an optimal order (see (Ciarlet, 1978) for the more detailed conditions under which the result is obtained, in particular as regards the regularity of the data). However, there is no general theory that covers all types of finite element approximations and, in particular, results are quite scarce for quadrilateral isoparametric elements. Hence we must content ourselves with providing basic "rules of thumb" that are being used in practice. For second-order problems (such as for shell models based on the Reissner-Mindlin kinematical assumption, see Chapter 4), the usual recommendations are to use

1. For triangular (or tetrahedral) elements, an integration rule that exactly integrates polynomials of order $(2p-2)$ for P_p polynomial shape functions (as is mathematically substantiated in (Ciarlet, 1978) for $p = 1$ and 2);
2. For quadrilateral elements, the Gauss quadrature rule with $(p + 1)$ integration points in each direction for Q_p shape functions, see (Bathe, 1996).

Note that most finite element codes give the user a choice for the order of the integration rule, hence it is easy in practice – for a specific finite element analysis – to make sure that the error made with the numerical integration is not significant.

4. Shell Mathematical Models

In this chapter we describe and analyse the linear shell models that we consider in this book. We first describe the fundamental shell kinematics used. Then we discuss the "basic shell model" which is implicitly employed in general finite element solutions and from which other classical shell and plate models can be derived. We summarize the shell models that we call the "shear-membrane-bending model" and the "membrane-bending model", and introduce the proper mathematical framework in which they define well-posed problems. As special cases of these shell models we obtain well-known plate models.

4.1 Shell Kinematics

Most classical shell models are based on kinematical assumptions, which pertain to the admissible displacement profile through the shell thickness. The assumptions connect the displacements of points located on a material line that is orthogonal to the midsurface in the undeformed configuration. More specifically, it is usually assumed (and experimentally substantiated) that any such material line remains straight and unstretched during the deformations, which is expressed by the following equation

$$\boxed{\vec{U}(\xi^1,\xi^2,\xi^3) = \vec{u}(\xi^1,\xi^2) + \xi^3\theta_\lambda(\xi^1,\xi^2)\vec{a}^{\,\lambda}(\xi^1,\xi^2).} \tag{4.1}$$

In this equation we consider a material line in the direction of $\vec{a}_3$ at the coordinates (ξ_1,ξ_2). The displacement $\vec{u}(\xi_1,\xi_2)$ represents a global infinitesimal displacement of the line with all particles on the line displacing by the same amount. The displacement $\xi_3\theta_\lambda(\xi_1,\xi_2)\vec{a}^{\lambda}(\xi_1,\xi_2)$ is due to the rotation of the line measured by θ_1 and θ_2. Note that the rotation of an infinitely-thin straight material line is uniquely defined by a rotation vector normal to that line, hence without a component on $\vec{a}_3$ in our case, which is why we can represent this rotation vector by the surface tensor $\underline{\theta} = \theta_\lambda\vec{a}^{\lambda}$. We call this kinematical assumption the *Reissner-Mindlin kinematical assumption*, see in particular (Reissner, 1945; Mindlin, 1951), and also (Hencky, 1947).

D. Chapelle, K.-J. Bathe, *The Finite Element Analysis of Shells – Fundamentals*,
Computational Fluid and Solid Mechanics, 2nd ed., DOI 10.1007/978-3-642-16408-8_4,

Remark 4.1.1. The displacement $\xi^3\theta_1\vec{a}^1$ (respectively $\xi^3\theta_2\vec{a}^2$) corresponds to an infinitesimal rotation around an axis defined by the vector $\vec{a}_2$ (respectively $\vec{a}_1$) since $\vec{a}^\alpha \cdot \vec{a}_\beta = \delta^\alpha_\beta$, with an orientation of the rotation shown in Figure 4.1. Thus the θ_1-rotation gives a positive displacement in the direction of vector $\vec{a}^1$ for ξ^3 positive, and similarly for θ_2. ■

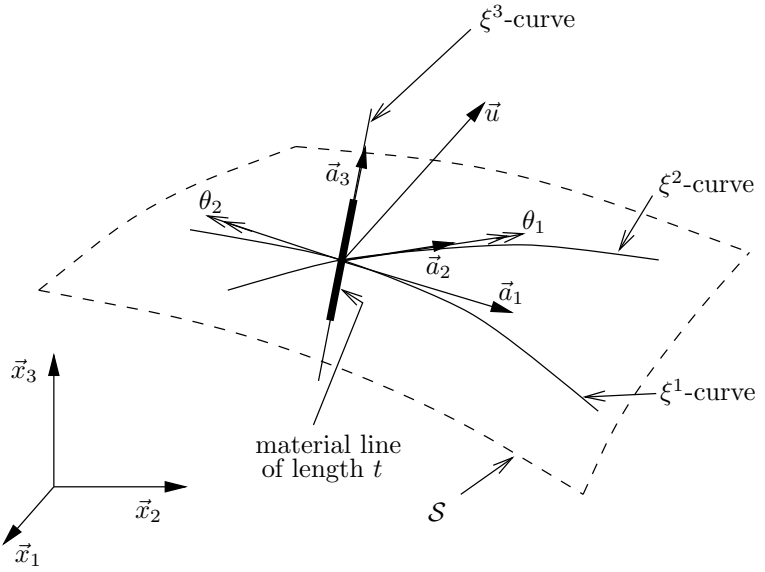

Fig. 4.1. Kinematic assumptions for the material line originally orthogonal to the midsurface $\mathcal{S}$ of the shell

The 3D Green-Lagrange strain tensor is given by half the increment in the 3D metric tensor (Bathe, 1996; Green & Zerna, 1968). For linear analysis, we use only the linear part of the Green-Lagrange strain tensor, for which the covariant components e_{ij} for a general displacement $\vec{U}(\xi^1, \xi^2, \xi^3)$ are

$$\boxed{e_{ij} = \frac{1}{2}(\vec{g}_i \cdot \vec{U}_{,j} + \vec{g}_j \cdot \vec{U}_{,i}), \qquad i, j = 1, 2, 3.} \tag{4.2}$$

For the specific displacement defined by (4.1), we can compute the covariant components of the linearized strain tensor as functions of $\vec{u}$ and $\underline{\theta}$. First we have

$$\frac{\partial \vec{u}}{\partial \xi^\alpha} = \frac{\partial}{\partial \xi^\alpha}(u_\lambda \vec{a}^\lambda + u_3 \vec{a}_3). \tag{4.3}$$

Using (2.120) and the definition of covariant differentiation (2.121) we obtain for the differentiation of $u_\lambda \vec{a}^\lambda$, which is a surface tensor,

$$\frac{\partial}{\partial \xi^\alpha}(u_\lambda \vec{a}^\lambda) = u_{\lambda|\alpha}\vec{a}^\lambda + b_\alpha^\lambda u_\lambda \vec{a}_3. \tag{4.4}$$

Hence

$$\begin{aligned} \frac{\partial \vec{u}}{\partial \xi^\alpha} &= u_{\lambda|\alpha}\vec{a}^\lambda + b_\alpha^\lambda u_\lambda \vec{a}_3 + u_{3,\alpha}\ \vec{a}_3 + u_3 \vec{a}_{3,\alpha} \\ &= (u_{\lambda|\alpha} - b_{\lambda\alpha}u_3)\,\vec{a}^\lambda + (u_{3,\alpha} + b_\alpha^\lambda u_\lambda)\,\vec{a}_3, \end{aligned} \tag{4.5}$$

recalling (2.114). Then, similarly to (4.4) we have

$$\frac{\partial}{\partial \xi^\alpha}(\theta_\lambda \vec{a}^\lambda) = \theta_{\lambda|\alpha}\vec{a}^\lambda + b_\alpha^\lambda \theta_\lambda \vec{a}_3. \tag{4.6}$$

Therefore

$$\frac{\partial \vec{U}}{\partial \xi^\alpha} = (u_{\lambda|\alpha} - b_{\lambda\alpha}u_3 + \xi^3\theta_{\lambda|\alpha})\,\vec{a}^\lambda + (u_{3,\alpha} + b_\alpha^\lambda u_\lambda + \xi^3 b_\alpha^\lambda \theta_\lambda)\,\vec{a}_3. \tag{4.7}$$

Moreover,

$$\frac{\partial \vec{U}}{\partial \xi^3} = \theta_\lambda \vec{a}^\lambda. \tag{4.8}$$

Substituting these expressions, (2.152) and (2.153) into (4.2), we obtain

$$\boxed{\begin{cases} e_{\alpha\beta} = \gamma_{\alpha\beta}(\vec{u}\,) + \xi^3 \chi_{\alpha\beta}(\vec{u}, \underline{\theta}) - (\xi^3)^2 \kappa_{\alpha\beta}(\underline{\theta}), \qquad \alpha, \beta = 1, 2 \\ e_{\alpha 3} = \zeta_\alpha(\vec{u}, \underline{\theta}), \qquad \alpha = 1, 2 \\ e_{33} = 0 \end{cases}} \tag{4.9}$$

where

$$\boxed{\begin{cases} \gamma_{\alpha\beta}(\vec{u}\,) = \frac{1}{2}(u_{\alpha|\beta} + u_{\beta|\alpha}) - b_{\alpha\beta}u_3 \\ \chi_{\alpha\beta}(\vec{u}, \underline{\theta}) = \frac{1}{2}(\theta_{\alpha|\beta} + \theta_{\beta|\alpha} - b_\beta^\lambda u_{\lambda|\alpha} - b_\alpha^\lambda u_{\lambda|\beta}) + c_{\alpha\beta}u_3 \\ \kappa_{\alpha\beta}(\underline{\theta}) = \frac{1}{2}(b_\beta^\lambda \theta_{\lambda|\alpha} + b_\alpha^\lambda \theta_{\lambda|\beta}) \\ \zeta_\alpha(\vec{u}, \underline{\theta}) = \frac{1}{2}(\theta_\alpha + u_{3,\alpha} + b_\alpha^\lambda u_\lambda) \end{cases}} \tag{4.10}$$

These tensors thus define the strain measures that correspond to the shell kinematics assumed in (4.1).

Remark 4.1.2. In the framework of the Reissner-Mindlin kinematical assumption, the tensors $\underline{\underline{\gamma}}$, $\underline{\underline{\chi}}$, and $\underline{\zeta}$ are called the membrane strain, bending strain, and shear strain tensors, respectively. The interpretation of this terminology follows from (4.9). ■

Remark 4.1.3. It is important to note that the use of tensorial components based on a chart requires some care in order to determine the dimension of a given quantity, namely which unit the quantity corresponds to. For example, a cylindrical shell structure of radius R, height L and thickness t, aligned along the $\vec{x}_3$ (Cartesian) base vector, can be described by the chart

$$\vec{\Phi}(\xi^1,\xi^2,\xi^3) = \begin{pmatrix} (R+\xi^3)\cos\frac{\xi^1}{R} \\ (R+\xi^3)\sin\frac{\xi^1}{R} \\ \xi^2 \end{pmatrix}, \tag{4.11}$$

$$\xi^1 \in [0, 2\pi R],\ \xi^2 \in [0, L],\ \xi^3 \in \big[-\frac{t}{2}, \frac{t}{2}\big],$$

which gives the following covariant base vectors

$$\vec{g}_1 = \begin{pmatrix} -\frac{R+\xi^3}{R}\sin\frac{\xi^1}{R} \\ \frac{R+\xi^3}{R}\cos\frac{\xi^1}{R} \\ 0 \end{pmatrix},\ \vec{g}_2 = \begin{pmatrix} 0 \\ 0 \\ 1 \end{pmatrix},\ \vec{g}_3 = \begin{pmatrix} \cos\frac{\xi^1}{R} \\ \sin\frac{\xi^1}{R} \\ 0 \end{pmatrix}. \tag{4.12}$$

We can see that the three covariant base vectors are dimensionless, hence the contravariant components of a given displacement vector $\vec{U}$ have the dimension of length, since

$$\vec{U} = U^i \vec{g}_i. \tag{4.13}$$

Similarly the contravariant base vectors are also dimensionless, since

$$\vec{g}^i \cdot \vec{g}_j = \delta^i_j, \qquad i,j = 1\ldots 3, \tag{4.14}$$

hence the covariant displacement components have the dimension of a length. In addition, the covariant components of the strain tensor are all dimensionless.

However, the same geometry can also be described by the alternative chart

$$\vec{\Phi}(\xi^1,\xi^2,\xi^3) = \begin{pmatrix} (R+\xi^3)\cos\xi^1 \\ (R+\xi^3)\sin\xi^1 \\ L\xi^2 \end{pmatrix}, \qquad \xi^1 \in [0,2\pi],\ \xi^2 \in [0,1],\ \xi^3 \in \big[-\frac{t}{2},\frac{t}{2}\big], \tag{4.15}$$

which gives

$$\vec{g}_1 = \begin{pmatrix} -(R+\xi^3)\sin\xi^1 \\ (R+\xi^3)\cos\xi^1 \\ 0 \end{pmatrix},\ \vec{g}_2 = \begin{pmatrix} 0 \\ 0 \\ L \end{pmatrix},\ \vec{g}_3 = \begin{pmatrix} \cos\xi^1 \\ \sin\xi^1 \\ 0 \end{pmatrix}. \tag{4.16}$$

The first two covariant base vectors now have the dimension of length, whereas $\vec{g}_3$ is still dimensionless. Hence, the contravariant components U^α of a displacement $\vec{U}$ are dimensionless, while U^3 has the dimension of a length. Further, the first two contravariant base vectors have the dimension of the inverse of a length, while $\vec{g}^3$ is still dimensionless. Therefore, the covariant components U_α have the dimension of a length squared (and U_3 still of a length). Likewise, it can be seen that the covariant components of the strains $e_{\alpha\beta}$ have the dimension of a length squared in this case.

Finally, as regards dimensions we should keep in mind that it is only when considering the components of quantities in a dimensionless basis (e.g. in a fixed orthonormal cartesian basis) that the dimensions (and therefore the units) are the usual ones. ■

We now proceed to introduce the shell models that we use in this book. We present these models within the framework of linearized elasticity and considering an isotropic material. Our approach can be easily extended to the case of a more general material having elastic symmetry with respect to surfaces $\xi^3 = \text{const.}$, see (Green & Zerna, 1968, Section 5.4).

As our focus in this book is on finite element methods rather than on mathematical modeling, we do not discuss the justification of shell models starting from 3D continuum mechanics. For a thorough presentation of existing mathematical justifications of shell models, we refer to (Ciarlet, 2000).

4.2 Derivation of Shell Models

Numerous shell models are encountered in the literature, see (Timoshenko & Woinowsky-Krieger, 1959; Naghdi, 1963; Flügge, 1973; Wunderlich, 1980; Calladine, 1983; Valid, 1995; Başar & Krätzig, 2000) and the references

therein. We henceforth focus on presenting the shell models that we believe are most useful for engineering practice, and we point out relationships between these shell models. These specific models also represent valuable prototypes for theoretical analysis purposes in that they feature generic ingredients that can be found in most other shell models.

4.2.1 The "basic shell model"

We start by introducing a mathematical shell model which is crucial for understanding the essential characteristics of most classical shell models, and also for analysing some widely used and efficient shell finite element methods (see in particular Section 6.3). Most classical shell models are based on the assumption that the state of the stresses in the shell corresponds to plane stress tangent to the midsurface of the shell, or at least approximately so. Of course, the combination of the plane stress assumption with the Reissner-Mindlin kinematical assumption, which itself implies $e_{33} = 0$, requires justification. A considerable amount of research has been devoted to these assumptions, see (Koiter, 1965; Novozhilov, 1970) and the references therein.

Let us then consider an isotropic linear elastic material. In a general curvilinear coordinate system, Hooke's law reads

$$\sigma^{ij} = H^{ijkl} e_{kl}, \tag{4.17}$$

with

$$H^{ijkl} = L_1\, g^{ij} g^{kl} + L_2 (g^{ik} g^{jl} + g^{il} g^{jk}), \tag{4.18}$$

where L_1 and L_2 are the Lamé constants, i.e.

$$L_1 = E \frac{\nu}{(1+\nu)(1-2\nu)}, \qquad L_2 = \frac{E}{2(1+\nu)} \tag{4.19}$$

if we classically denote Young's modulus by E and Poisson's ratio by ν. In the literature the Lamé constants L_1 and L_2 are usually denoted by λ and μ respectively, but we avoid this notation here since we already use λ and μ for indices of surface tensors.

We now specialize the constitutive equation to the curvilinear coordinate system attached to the midsurface (see Chapter 2). In this coordinate system, we have $\vec{g}_\alpha \cdot \vec{g}_3 = 0$ and $\|\vec{g}_3\| = 1$, see (2.154), hence

$$\vec{g}^3 = \vec{g}_3, \tag{4.20}$$

$$g^{33} = 1, \tag{4.21}$$

$$g^{\alpha 3} = \vec{g}^{\alpha} \cdot \vec{g}^{3} = 0. \tag{4.22}$$

This implies, in particular,

$$H^{\alpha\beta\gamma 3} (= H^{\alpha\beta 3\gamma} = H^{\gamma 3\alpha\beta} = H^{3\gamma\alpha\beta}) = 0, \qquad \forall \alpha, \beta, \gamma = 1, 2 \tag{4.23}$$

$$H^{\alpha 333} (= H^{3\alpha 33} = H^{33\alpha 3} = H^{333\alpha}) = 0, \qquad \forall \alpha = 1, 2. \tag{4.24}$$

Therefore

$$\begin{cases} \sigma^{\alpha\beta} = H^{\alpha\beta\lambda\mu} e_{\lambda\mu} + H^{\alpha\beta 33} e_{33} \\ \sigma^{\alpha 3} = 2H^{\alpha 3\lambda 3} e_{\lambda 3} \\ \sigma^{33} = H^{\lambda\mu 33} e_{\lambda\mu} + H^{3333} e_{33} \end{cases} \tag{4.25}$$

If we make use of the assumption that the normal stress σ^{33} is zero, we obtain the following modified constitutive equations

$$\boxed{\begin{cases} \sigma^{\alpha\beta} = C^{\alpha\beta\lambda\mu} e_{\lambda\mu} \\ \sigma^{\alpha 3} = \frac{1}{2} D^{\alpha\lambda} e_{\lambda 3} \end{cases}} \tag{4.26}$$

with

$$C^{\alpha\beta\lambda\mu} = H^{\alpha\beta\lambda\mu} - \frac{H^{\alpha\beta 33} H^{\lambda\mu 33}}{H^{3333}}, \tag{4.27}$$

hence

$$\boxed{C^{\alpha\beta\lambda\mu} = \frac{E}{2(1+\nu)} (g^{\alpha\lambda} g^{\beta\mu} + g^{\alpha\mu} g^{\beta\lambda} + \frac{2\nu}{1-\nu} g^{\alpha\beta} g^{\lambda\mu}),} \tag{4.28}$$

and

$$\boxed{D^{\alpha\lambda} = 4H^{\alpha 3\lambda 3} = \frac{2E}{1+\nu} g^{\alpha\lambda}.} \tag{4.29}$$

We finally define the *basic shell model* as the model represented by the following variational formulation

$$\int_\Omega [C^{\alpha\beta\lambda\mu} e_{\alpha\beta}(\vec{U}) e_{\lambda\mu}(\vec{V}) + D^{\alpha\lambda} e_{\alpha 3}(\vec{U}) e_{\lambda 3}(\vec{V})]\, dV = \int_\Omega \vec{F} \cdot \vec{V}\, dV, \tag{4.30}$$

where $\vec{U}$ is the unknown that satisfies the Reissner-Mindlin kinematical assumption and boundary conditions, and $\vec{V}$ denotes an arbitrary test function satisfying the same kinematical assumption, namely

$$\vec{V}(\xi^1, \xi^2, \xi^3) = \vec{v}(\xi^1, \xi^2) + \xi^3 \eta_\lambda(\xi^1, \xi^2) \vec{a}^{\,\lambda}(\xi^1, \xi^2), \tag{4.31}$$

and the appropriate boundary conditions (namely zero displacement wherever the displacement $\vec{U}$ is prescribed). The symbol $\vec{F}$ denotes the external 3D loading applied to the shell structure. Note that, regardless of the kinematical assumption, (4.30) corresponds to the 3D variational formulation of a linear elastic problem with $\sigma^{33} = 0$.

Remark 4.2.1. The variational problem (4.30) represents a mathematical shell model since the unknowns, as well as the test functions, are given by sets of tensors defined on the shell midsurface, namely $(\vec{u}, \underline{\theta})$ and $(\vec{v}, \underline{\eta})$, respectively. The values of the strains contained in the left-hand side can be computed directly from these tensors using the expressions (4.9) and (4.10) (and similar ones for $\vec{V}$). ■

Remark 4.2.2. In order to obtain the variational formulation (4.30) we eliminated the strain component e_{33} by using $\sigma^{33} = 0$ in the third equation of (4.25), which gives

$$e_{33} = -\frac{\nu}{1-\nu} g^{\alpha\beta} e_{\alpha\beta}. \tag{4.32}$$

This is in apparent contradiction to

$$e_{33} = 0, \tag{4.33}$$

which was obtained in (4.9) as a consequence of the Reissner-Mindlin kinematical assumption. However, we should note that (4.33) has no actual impact in the variational formulation considered – since e_{33} is not present in (4.30) – and in fact (4.32) (or analogous expressions when considering different material laws) can be used to recover the transverse strain once the in-plane strains are known, see Section 4.2.5. This is – indeed – similar to the approach followed in plane stress analysis, see e.g. (Bathe, 1996). Furthermore, that the above contradiction is only apparent can be fully substantiated mathematically by considering kinematical assumptions of a higher order in the thickness variable, see in particular Section 4.2.5 and (Chapelle et al., 2004a). ■

4.2.2 The "shear-membrane-bending model"

We refer in this book to a shear-membrane-bending model which we call abbreviated the "s-m-b model". Many researchers have contributed towards the development and study of this mathematical shell model and models close to it, see (Reissner, 1952; Naghdi, 1963) and the references therein.

The s-m-b model is directly and in a natural way obtained from the basic shell model discussed above by truncating the expressions to the lowest-order terms of their expansions with respect to the transverse coordinate ξ^3. Namely, we substitute

- $\gamma_{\alpha\beta} + \xi^3\chi_{\alpha\beta}$ for $e_{\alpha\beta}$ (see (4.9));
- $\sqrt{a}$ for $\sqrt{g}$ in the volume measure dV (recall (2.155));
- ${}^0C^{\alpha\beta\lambda\mu}$ and ${}^0D^{\alpha\lambda}$ for $C^{\alpha\beta\lambda\mu}$ and $D^{\alpha\lambda}$, with

$$\boxed{{}^0C^{\alpha\beta\lambda\mu} = \frac{E}{2(1+\nu)}(a^{\alpha\lambda}a^{\beta\mu} + a^{\alpha\mu}a^{\beta\lambda} + \frac{2\nu}{1-\nu}a^{\alpha\beta}a^{\lambda\mu}),} \tag{4.34}$$

$$\boxed{{}^0D^{\alpha\lambda} = \frac{2E}{1+\nu}a^{\alpha\lambda},} \tag{4.35}$$

to be compared with (4.28) and (4.29).

We further assume that the loading is constant through the thickness. Using these simplifications and performing the integration with respect to ξ^3 the following variational problem is obtained

$$\boxed{\begin{aligned}\int_\omega {}^0C^{\alpha\beta\lambda\mu}[t\gamma_{\alpha\beta}(\vec{u})\gamma_{\lambda\mu}(\vec{v}) + \frac{t^3}{12}\chi_{\alpha\beta}(\vec{u},\underline{\theta})\chi_{\lambda\mu}(\vec{v},\underline{\eta})]\,dS \\ + \int_\omega t\,{}^0D^{\alpha\lambda}\zeta_\alpha(\vec{u},\underline{\theta})\zeta_\lambda(\vec{v},\underline{\eta})\,dS = \int_\omega t\vec{F}\cdot\vec{v}\,dS,\end{aligned}} \tag{4.36}$$

for arbitrary test functions $(\vec{v},\underline{\eta})$.

In this expression the thickness t is, in general, a parameter that depends on (ξ_1,ξ_2). Hence, t remains in the expressions to be integrated.

We recall the expressions of the bending strain tensor $\underline{\underline{\chi}}$, the membrane strain tensor $\underline{\underline{\gamma}}$, and the shear strain tensor $\underline{\zeta}$ that are used in this formulation

$$\chi_{\alpha\beta}(\vec{u},\underline{\theta}) = \frac{1}{2}(\theta_{\alpha|\beta} + \theta_{\beta|\alpha} - b^\lambda_\beta u_{\lambda|\alpha} - b^\lambda_\alpha u_{\lambda|\beta}) + c_{\alpha\beta}u_3, \tag{4.37}$$

$$\gamma_{\alpha\beta}(\vec{u}\,) = \frac{1}{2}(u_{\alpha|\beta} + u_{\beta|\alpha}) - b_{\alpha\beta}u_3, \tag{4.38}$$

$$\zeta_\alpha(\vec{u}, \underline{\theta}) = \frac{1}{2}(\theta_\alpha + u_{3,\alpha} + b_\alpha^\lambda u_\lambda). \tag{4.39}$$

Remark 4.2.3. In applications of the s-m-b model, a slightly different formulation is frequently used, namely

$$\int_\omega {}^0C^{\alpha\beta\lambda\mu}[t\gamma_{\alpha\beta}(\vec{u}\,)\gamma_{\lambda\mu}(\vec{v}\,) + \frac{t^3}{12}\chi_{\alpha\beta}(\vec{u}, \underline{\theta})\chi_{\lambda\mu}(\vec{v}, \underline{\eta})]\, dS \tag{4.40}$$

$$+k\int_\omega t\, {}^0D^{\alpha\lambda}\zeta_\alpha(\vec{u}, \underline{\theta})\zeta_\lambda(\vec{v}, \underline{\eta})\, dS \quad = \quad \int_\omega t\vec{F}\cdot\vec{v}\, dS.$$

where a coefficient k is introduced in front of the shear term. This coefficient, smaller than one, is called the shear correction factor. The value of k accounts for the fact that the actual transverse shear strain is not constant through the thickness of the shell and must vanish on the outside surfaces. This is similar to the use of a shear correction factor in the Timoshenko beam theory, see e.g. (Bathe, 1996). ■

Remark 4.2.4. The introduction of the s-m-b model using the basic shell model as a starting point may seem somewhat arbitrary and we emphasize that this is by no means an attempt to justify the s-m-b model. However, this approach points out close connections between the models that we will use in the mathematical analysis of the models, including the asymptotic analysis of the models (making the thickness parameter tend to zero). ■

4.2.3 The "membrane-bending model"

We also introduce a membrane-bending model which we call abbreviated the "m-b model". For important contributions to the development of this model and similar ones, we refer in particular to (Kirchhoff, 1876; Love, 1927; Gol'denweizer, 1961; Koiter, 1965; Novozhilov, 1970), see also references therein.

In order to obtain the m-b model, a kinematical assumption stronger than the Reissner-Mindlin assumption, namely the *Kirchhoff-Love kinematical assumption*, must be made. This assumption states that the material line orthogonal to the midsurface in the undeformed configuration remains straight, unstretched, *and always orthogonal to the midsurface* during the deformations.

When considering a displacement of the type (4.1), the Kirchhoff-Love kinematical assumption clearly introduces a constraint between the translation and the rotation tensor. We identify this constraint in the following proposition.

Proposition 4.2.1 *A general displacement field* $\vec{U}(\xi^1, \xi^2, \xi^3)$ *satisfies the Kirchhoff-Love kinematical assumption if and only if the displacement field can be expressed in the form*

$$\vec{U}(\xi^1, \xi^2, \xi^3) = \vec{u}(\xi^1, \xi^2) + \xi^3 \theta_\lambda(\xi^1, \xi^2)\vec{a}^{\,\lambda}(\xi^1, \xi^2). \tag{4.41}$$

with

$$\theta_\lambda = -u_{3,\lambda} - b^\mu_\lambda u_\mu, \qquad \lambda = 1, 2, \tag{4.42}$$

i.e.

$$\underline{\zeta}(\vec{u}, \underline{\theta}) = 0. \tag{4.43}$$

Proof. As we mentioned to obtain (4.2), the linearized strain $e_{ij}(\vec{U})$ corresponds to half the (linearized) increment in the coefficient g_{ij} of the metric tensor when the body undergoes the displacement $\vec{U}$. Hence, a material line originally orthogonal to the midsurface, namely a ξ^3-curve, will remain orthogonal to the midsurface if and only if

$$e_{\lambda 3}(\vec{U})|_{\xi^3=0} = 0 \qquad \lambda = 1, 2. \tag{4.44}$$

Therefore, a displacement field satisfies the Kirchhoff-Love assumption if and only if

1. the field satisfies the Reissner-Mindlin assumption (i.e. it can be expressed as in (4.41));
2. we have (4.44), i.e. (4.43) (from (4.9)).

■

For a Kirchhoff-Love displacement, substituting the expression of the rotation $\underline{\theta}$ given by (4.42) into the bending strain tensor $\underline{\underline{\chi}}$ (see (4.37)) leads to

$$\chi_{\alpha\beta}(\vec{u}, \underline{\theta}) = -u_{3|\alpha\beta} - \frac{1}{2}(b^\mu_{\alpha|\beta} + b^\mu_{\beta|\alpha})u_\mu - b^\mu_\alpha u_{\mu|\beta} - b^\mu_\beta u_{\mu|\alpha} + c_{\alpha\beta}u_3. \tag{4.45}$$

Recalling the Codazzi Equation (2.138), we have

$$b^\mu_{\alpha|\beta} = b^\mu_{\beta|\alpha}, \tag{4.46}$$

and hence, for a Kirchhoff-Love displacement,

$$\chi_{\alpha\beta}(\vec{u},\underline{\theta}) = -\bar{\rho}_{\alpha\beta}(\vec{u}), \tag{4.47}$$

with

$$\boxed{\bar{\rho}_{\alpha\beta}(\vec{u}) = u_{3|\alpha\beta} + b^{\mu}_{\alpha|\beta}u_{\mu} + b^{\mu}_{\alpha}u_{\mu|\beta} + b^{\mu}_{\beta}u_{\mu|\alpha} - c_{\alpha\beta}u_3.} \tag{4.48}$$

We have the following important result, which provides an interpretation of the tensor $\underline{\underline{\bar{\rho}}}$.

Proposition 4.2.2 *For a smooth displacement field $\vec{u}$, the tensor $\underline{\underline{\bar{\rho}}}(\vec{u})$ is the tensor of linearized change of curvature of the midsurface.*

Proof. We consider *for the whole shell medium* the Kirchhoff-Love displacement field defined by (4.41) and (4.42). The Kirchhoff-Love kinematical assumption entails that the (ξ^1,ξ^2,ξ^3) parametrization of the shell remains of the type defined by Eqs. (2.81)–(2.84) *during the deformation process*. This implies that (2.154) also remains valid during the deformation, hence

$$\begin{cases} \delta g_{\alpha\beta} = \delta a_{\alpha\beta} - 2\xi^3\delta b_{\alpha\beta} + (\xi^3)^2\delta c_{\alpha\beta} \\ \delta g_{\alpha 3} = 0 \\ \delta g_{33} = 0 \end{cases} \tag{4.49}$$

where the δ symbol without indices denotes linearized increments of quantities. On the other hand, the linearized increment of the metric tensor is given by the linearized strain tensor multiplied by two. Considering (4.9), we note that the second and third equations of (4.49) are in agreement with $e_{\alpha 3} = \zeta_{\alpha}(\vec{u},\underline{\theta}) = 0$ and $e_{33} = 0$, and we infer by identifying the coefficients of the ξ^3-polynomial

$$\begin{cases} \delta a_{\alpha\beta} = 2\gamma_{\alpha\beta}(\vec{u}) \\ \delta b_{\alpha\beta} = -\chi_{\alpha\beta}(\vec{u},\underline{\theta}) = \bar{\rho}_{\alpha\beta}(\vec{u}) \\ \delta c_{\alpha\beta} = -2\kappa_{\alpha\beta}(\underline{\theta}) \end{cases} \tag{4.50}$$

where the second line provides the result needed. ∎

We now define the *m-b shell model* from the s-m-b model by taking in (4.36) both the unknown displacement and the test functions as displacements that satisfy the Kirchhoff-Love kinematical assumption. We thus obtain

$$\int_\omega {}^0C^{\alpha\beta\lambda\mu}[t\gamma_{\alpha\beta}(\vec{u})\gamma_{\lambda\mu}(\vec{v}) + \frac{t^3}{12}\bar{\rho}_{\alpha\beta}(\vec{u})\bar{\rho}_{\lambda\mu}(\vec{v})]\, dS = \int_\omega t\vec{F}\cdot\vec{v}\, dS, \tag{4.51}$$

for arbitrary test functions $\vec{v}$.

Remark 4.2.5. It is interesting to note that the two strain measures that appear in the m-b model correspond to the linear variations of the first two fundamental forms. ■

Remark 4.2.6. We should also note that the m-b shell model requires more regularity in the geometry than the s-m-b model – and also than the basic shell model – since derivatives of the curvature tensor are involved in the expression (4.48). This means that we need to differentiate the chart three times to calculate this expression (compared to only twice to compute the curvature components needed in the s-m-b and basic shell models), and that – in particular – discontinuities in the curvature are not allowed in this model. This restriction, however, can be relaxed by considering an alternative expression for the bending strains in this case, see (Blouza & Le Dret, 1999). ■

4.2.4 Plate models

Plate models can be inferred from shell models by considering the special case of planar midsurfaces. Then, of course, we have a constant normal vector $\vec{a}_3$ and the second and third fundamental forms are zero tensors, since there is no curvature. As a consequence we have, from (2.154),

$$g_{\alpha\beta} = a_{\alpha\beta} \tag{4.52}$$

and

$$g^{\alpha\beta} = a^{\alpha\beta}. \tag{4.53}$$

Also, we infer from (2.155)

$$g = a. \tag{4.54}$$

Considering the shell models, (4.53) implies

$${}^0C^{\alpha\beta\lambda\mu} = C^{\alpha\beta\lambda\mu}, \qquad {}^0D^{\alpha\beta} = D^{\alpha\beta}. \tag{4.55}$$

Moreover, the strain measures now take the simpler form

$$\begin{cases} \gamma_{\alpha\beta}(\vec{u}) = \frac{1}{2}(u_{\alpha|\beta} + u_{\beta|\alpha}) \\ \chi_{\alpha\beta}(\vec{u}, \underline{\theta}) = \frac{1}{2}(\theta_{\alpha|\beta} + \theta_{\beta|\alpha}) \\ \bar{\rho}_{\alpha\beta}(\vec{u}) = u_{3|\alpha\beta} \\ \kappa_{\alpha\beta}(\underline{\theta}) = 0 \\ \zeta_{\alpha}(\vec{u}, \underline{\theta}) = \frac{1}{2}(\theta_{\alpha} + u_{3,\alpha}) \end{cases} \tag{4.56}$$

This implies that the unknowns (u_1, u_2), which only appear – by themselves – in the membrane strains are completely decoupled from the other unknowns $(\underline{\theta}, u_3)$. From now on, we denote (u_1, u_2) by $\underline{u}$.

Remark 4.2.7. The truncations performed to obtain the s-m-b model from the basic shell model now correspond to exact equalities, hence the two models are identical. ■

As a result of the decoupling, the s-m-b model is now described by two variational problems. The first problem is

$$\boxed{\int_{\omega} t\, {}^0C^{\alpha\beta\lambda\mu} \gamma_{\alpha\beta}(\underline{u}) \gamma_{\lambda\mu}(\underline{v})\, dS = \int_{\omega} t \underline{F} \cdot \underline{v}\, dS,} \tag{4.57}$$

with

$$\underline{F} \cdot \underline{v} = F^1 v_1 + F^2 v_2, \tag{4.58}$$

for an arbitrary test function $\underline{v}$. We call (4.57) the *membrane problem*. The second problem is

$$\boxed{\begin{aligned} &\int_{\omega} \frac{t^3}{12} {}^0C^{\alpha\beta\lambda\mu} \chi_{\alpha\beta}(\underline{\theta}) \chi_{\lambda\mu}(\underline{\eta})\, dS \\ &\qquad + \int_{\omega} t\, {}^0D^{\alpha\lambda} \zeta_{\alpha}(u_3, \underline{\theta}) \zeta_{\lambda}(v_3, \underline{\eta})\, dS = \int_{\omega} t F_3 v_3\, dS, \end{aligned}} \tag{4.59}$$

for any test function $(v_3, \underline{\eta})$. We call this second problem the *Reissner-Mindlin plate model*.

Remark 4.2.8. Of course, a shear correction factor can also be used in the Reissner-Mindlin plate model, in which case it reads

$$\int_\omega \frac{t^3}{12} {}^0C^{\alpha\beta\lambda\mu}\chi_{\alpha\beta}(\underline{\theta})\chi_{\lambda\mu}(\underline{\eta})\, dS \tag{4.60}$$

$$+k\int_\omega t\, {}^0D^{\alpha\lambda}\zeta_\alpha(u_3,\underline{\theta})\zeta_\lambda(v_3,\underline{\eta})\, dS = \int_\omega tF_3v_3\, dS,$$

for any $(v_3, \underline{\eta})$. ■

For the m-b model, we also obtain two problems. The first of them is again the membrane problem given in (4.57). The second problem is described by

$$\boxed{\int_\omega \frac{t^3}{12} {}^0C^{\alpha\beta\lambda\mu}\bar{\rho}_{\alpha\beta}(u_3)\bar{\rho}_{\lambda\mu}(v_3)\, dS = \int_\omega tF_3v_3\, dS,} \tag{4.61}$$

for any test function v_3. We call this problem the *Kirchhoff-Love plate model*.

In practice, we usually choose an orthonormal coordinate system to describe the midsurface of the plate (which is always possible, unlike for a curved surface). The various quantities involved in the plate models are then easier to compute, as the Christoffel symbols vanish (hence the covariant derivatives are usual derivatives), $a^{\alpha\beta} = a_{\alpha\beta} = \delta^\beta_\alpha$, and $dS = d\xi^1 d\xi^2$. In this case, we can rewrite the plate models using column vectors that store the independent strain components. We thus define

$$\mathbf{g}(\underline{u}) = \begin{pmatrix} \gamma_{11}(\underline{u}) \\ \gamma_{22}(\underline{u}) \\ 2\gamma_{12}(\underline{u}) \end{pmatrix} = \begin{pmatrix} u_{1,1} \\ u_{2,2} \\ u_{1,2}+u_{2,1} \end{pmatrix}, \tag{4.62}$$

$$\mathbf{k}(\underline{\theta}) = \begin{pmatrix} \chi_{11}(\underline{\theta}) \\ \chi_{22}(\underline{\theta}) \\ 2\chi_{12}(\underline{\theta}) \end{pmatrix} = \begin{pmatrix} \theta_{1,1} \\ \theta_{2,2} \\ \theta_{1,2}+\theta_{2,1} \end{pmatrix}, \tag{4.63}$$

$$\mathbf{r}(u_3) = \begin{pmatrix} \bar{\rho}_{11}(u_3) \\ \bar{\rho}_{22}(u_3) \\ 2\bar{\rho}_{12}(u_3) \end{pmatrix} = \begin{pmatrix} u_{3,11} \\ u_{3,22} \\ 2u_{3,12} \end{pmatrix}, \tag{4.64}$$

and

$$\mathbf{z}(u_3,\underline{\theta}) = \begin{pmatrix} 2\zeta_1(u_3,\underline{\theta}) \\ 2\zeta_2(u_3,\underline{\theta}) \end{pmatrix} = \begin{pmatrix} \theta_1+u_{3,1} \\ \theta_2+u_{3,2} \end{pmatrix}. \tag{4.65}$$

In this notation, equivalent forms of the membrane problem (4.57), the Reissner-Mindlin model (4.60) and the Kirchhoff-Love model (4.61) are given by, respectively,

$$\boxed{\int_\omega \mathbf{g}(\underline{u})^T \mathbf{C}^{\mathrm{M}} \mathbf{g}(\underline{v})\; d\xi^1 d\xi^2 = \int_\omega t\underline{F}\cdot\underline{v}\; d\xi^1 d\xi^2,} \tag{4.66}$$

$$\boxed{\begin{aligned}\int_\omega \mathbf{k}(\underline{\theta})^T \mathbf{C}_{\mathrm{b}}^{\mathrm{RM}} \mathbf{k}(\underline{\eta})\; d\xi^1 d\xi^2 + \int_\omega \mathbf{z}(u_3,\underline{\theta})^T \mathbf{C}_{\mathrm{s}}^{\mathrm{RM}} \mathbf{z}(v_3,\underline{\eta})\; d\xi^1 d\xi^2 \\ = \int_\omega tF_3 v_3\; d\xi^1 d\xi^2,\end{aligned}} \tag{4.67}$$

$$\boxed{\int_\omega \mathbf{r}(u_3)^T \mathbf{C}^{\mathrm{KL}} \mathbf{r}(v_3)\; d\xi^1 d\xi^2 = \int_\omega tF_3 v_3\; d\xi^1 d\xi^2,} \tag{4.68}$$

where the T right-superscript denotes the usual transposition of matrices and vectors, and with

$$\mathbf{C}_{\mathrm{b}}^{\mathrm{RM}} = \frac{Et^3}{12(1-\nu^2)} \begin{pmatrix} 1 & \nu & 0 \\ \nu & 1 & 0 \\ 0 & 0 & \frac{1-\nu}{2} \end{pmatrix}, \tag{4.69}$$

$$\mathbf{C}_{\mathrm{s}}^{\mathrm{RM}} = \frac{Etk}{2(1+\nu)} \begin{pmatrix} 1 & 0 \\ 0 & 1 \end{pmatrix}, \tag{4.70}$$

$$\mathbf{C}^{\mathrm{M}} = \frac{12}{t^2}\mathbf{C}_{\mathrm{b}}^{\mathrm{RM}}, \tag{4.71}$$

$$\mathbf{C}^{\mathrm{KL}} = \mathbf{C}_{\mathrm{b}}^{\mathrm{RM}}. \tag{4.72}$$

4.2.5 Higher-order shell models, and the 3D-shell model

All the above-presented shell models are based on the Reissner-Mindlin kinematical assumption, which can be interpreted as a truncation of the expansion of displacements across the thickness of the structure. This truncated expansion contains terms up to degree one for the tangential displacements (recall that the terms of degree one correspond to rotations), and only of degree zero for the transverse displacements.

Although this fundamental modeling assumption leads to accurate predictions of shell behavior in a wide range of physical situations, we may – for

various specific reasons – consider models based on higher-order kinematical assumptions. Indeed, higher-order displacement assumptions to model shells (also coupled to 3D solids), albeit at a larger computational cost, have been used for a long time in practice, see e.g. (Bathe & Wilson, 1974). In these models, 3D higher-order isoparametric elements, like the Q2 element, with one element layer through the shell thickness are typically employed.

An obvious motivation for using a higher-order kinematical assumption is given when large through-the-thickness deformations are to be very accurately represented in the model, as e.g. it might be the case in metal forming applications. Note that the low degree of the expansion of the transverse displacement in Reissner-Mindlin kinematics implies zero transverse strains, recall (4.9). In some problem solutions it is most effective to simply recover the transverse strains once the in-plane strains are known, see Section 9.4.2 for an example. But in other problems we need to dispense with the plane stress assumption ("$\sigma^{33} = 0$") that – in fact – is required together with the Reissner-Mindlin kinematical assumption in order to obtain a satisfactory shell model, namely in particular for the shell model to be asymptotically consistent with full 3D continuum mechanics, see Chapter 5. Clearly, setting the through-the-thickness stress to be zero is restrictive in some problem solutions. For example, in a metal forming process, a sheet might be held on its top and botton surfaces which can lead to significant non-zero transverse stress and strain that are fully coupled to the other stress components.

Note that by dispensing with the plane stress assumption we are able to directly use an arbitrary 3D material law in a 3D formulation of mechanics. Hence, we will not use any modification of the 3D model or any specific procedure to enforce the plane stress assumption.

In order to obtain a shell model asymptotically consistent with 3D solid mechanics without resorting to any independent assumption on the stresses and with expansions of identical degrees on all the components of the displacement (which can be important for practical purposes, see below), it can be shown that at least all terms up to degree two are required, namely,

$$\vec{U}(\xi^1, \xi^2, \xi^3) = \vec{u}(\xi^1, \xi^2) + \xi^3 \vec{\theta}(\xi^1, \xi^2) + (\xi^3)^2 \vec{\varrho}(\xi^1, \xi^2), \tag{4.73}$$

need be considered instead of (4.1), see Chapter 5 and also (Delfour, 1999). We emphasize that the vector $\vec{\theta}$ is considered here as arbitrary in the Euclidean space, and not constrained to lie in the tangential plane as before. This leads to the following modified expressions of the strain components

$$\begin{cases} e_{\alpha\beta}(\vec{U}) = \gamma_{\alpha\beta}(\vec{u}) + \xi^3\, \hat{\chi}_{\alpha\beta}(\vec{u}, \vec{\theta}) + (\xi^3)^2\, k_{\alpha\beta}(\vec{\theta}, \vec{\varrho}) + (\xi^3)^3 l_{\alpha\beta}(\vec{\varrho}) \\ e_{\alpha 3}(\vec{U}) = \zeta_\alpha(\vec{u}, \vec{\theta}) + \xi^3\, m_\alpha(\vec{\theta}, \vec{\varrho}) + (\xi^3)^2\, n_\alpha(\vec{\varrho}) \\ e_{33}(\vec{U}) = \delta(\vec{\theta}) + \xi^3\, p(\vec{\varrho}) \end{cases}$$

(4.74)

where

$$\begin{cases} \gamma_{\alpha\beta}(\vec{u}) = \frac{1}{2}(u_{\alpha|\beta} + u_{\beta|\alpha}) - b_{\alpha\beta}u_3 \\ \hat{\chi}_{\alpha\beta}(\vec{u},\vec{\theta}) = \frac{1}{2}(\theta_{\alpha|\beta} + \theta_{\beta|\alpha} - b^\lambda_\alpha u_{\lambda|\beta} - b^\lambda_\beta u_{\lambda|\alpha}) - b_{\alpha\beta}\theta_3 + c_{\alpha\beta}u_3 \\ k_{\alpha\beta}(\vec{\theta},\vec{\varrho}) = \frac{1}{2}(\varrho_{\alpha|\beta} + \varrho_{\beta|\alpha} - b^\lambda_\alpha \theta_{\lambda|\beta} - b^\lambda_\beta \theta_{\lambda|\alpha}) - b_{\alpha\beta}\varrho_3 + c_{\alpha\beta}\theta_3 \\ l_{\alpha\beta}(\vec{\varrho}) = -\frac{1}{2}(b^\lambda_\alpha \varrho_{\lambda|\beta} + b^\lambda_\beta \varrho_{\lambda|\alpha}) + c_{\alpha\beta}\varrho_3 \\ \zeta_\alpha(\vec{u},\vec{\theta}) = \frac{1}{2}(\theta_\alpha + b^\lambda_\alpha u_\lambda + u_{3,\alpha}) \\ m_\alpha(\vec{\theta},\vec{\varrho}) = \frac{1}{2}(2\varrho_\alpha + \theta_{3,\alpha}) \\ n_\alpha(\vec{\varrho}) = \frac{1}{2}(-b^\lambda_\alpha \varrho_\lambda + \varrho_{3,\alpha}) \\ \delta(\vec{\theta}) = \theta_3 \\ p(\vec{\varrho}) = 2\varrho_3 \end{cases} \tag{4.75}$$

We point out that the tensors $\underline{\underline{\gamma}}$ and $\underline{\zeta}$ respectively correspond to the membrane and shear strain tensors previously defined in (4.10). The tensor $\underline{\underline{\hat{\chi}}}$ is a generalization of the bending strain tensor $\underline{\underline{\chi}}$, since θ_3 now appears in the expression. Likewise, the tensor $\underline{\underline{k}}$ is a generalization of the previously introduced tensor $-\underline{\underline{\kappa}}$. Note also that, despite similar expressions for $\underline{\underline{\hat{\chi}}}$ and $\underline{\underline{k}}$, we use a different notation to distinguish the two tensors and avoid confusion in their physical interpretations since they appear in expressions for strains with different orders in ξ^3. In addition, we emphasize that – unlike with classical shell models – we have the non-zero transverse strain e_{33}. The first term in the expression of these strains (δ) plays a distinctive role in the formulation – as will become clear in the forthcoming discussion. We call this quantity the "pinching strain".

We might mention that displacement assumptions different and of smaller degree may be used when simultaneously considering independent polynomial assumptions on the stresses, as has been proposed for plate models in (Alessandrini et al., 1999).

In our discussions of higher-order shell models, we will focus on the model obtained by using the kinematical assumption (4.73) directly in the 3D elastic energy, namely, in a variational form

$$\boxed{\int_\Omega H^{ijkl} e_{ij}(\vec{U}) e_{kl}(\vec{V})\, dV = \int_\Omega \vec{F}\cdot\vec{V}\, dV,} \tag{4.76}$$

with $\vec{V}$ satisfying the same kinematical assumption, viz.

$$\vec{V}(\xi^1,\xi^2,\xi^3) = \vec{v}(\xi^1,\xi^2) + \xi^3\vec{\eta}(\xi^1,\xi^2) + (\xi^3)^2\vec{\varsigma}(\xi^1,\xi^2). \tag{4.77}$$

We will call this shell mathematical model the *3D-shell model*, in particular due to the fact that the 3D variational formulation is used without any modification in the constitutive law. We will see that this terminology is also particularly adequate from a finite element perspective, see Chapter 6.

Before going into details, we already note that taking an expansion of identical degree for all displacement components at the shell section has important practical consequences since we can simply use the Cartesian coordinates of all nodal unknowns (without any specific treatment such as for rotation-induced displacements with the Reissner-Mindlin kinematical assumption). This equivalently implies that we can use nodes located across the shell section (instead of only on the midsurface) with standard displacement degrees of freedom. In particular, the kinematical assumption (4.73) used in the 3D-shell model is equivalent to, setting $\xi = 2\xi^3/t$,

$$\vec{U} = \frac{\xi(\xi-1)}{2}\vec{u}^{\,\mathrm{bot}} + \big(1-(\xi)^2\big)\vec{u}^{\,\mathrm{mid}} + \frac{\xi(1+\xi)}{2}\vec{u}^{\,\mathrm{top}}, \tag{4.78}$$

where $\vec{u}^{\,\mathrm{bot}}$, $\vec{u}^{\,\mathrm{mid}}$ and $\vec{u}^{\,\mathrm{top}}$ denote the displacements at the bottom, middle and top surfaces, respectively, with obvious transformation formulae between these quantities and $(\vec{u},\vec{\theta},\vec{\varrho})$. This formulation with top and bottom nodes can be convenient when the shell structure is to be coupled with other physical formulations through its outer surfaces, such as for modeling sandwich structures, piezoelectric patches, fluid-structure interaction, and so on, see (Chapelle & Ferent, 2003). However, when using (4.78) for thin shells care must be taken regarding the ill-conditioning that is introduced, and then the use of equivalent degrees-of-freedom at mid-surface nodes is more effective, see (Kim & Bathe, 2008) and (Bathe et al., 201x).

Of course, the use of such an element is then (per element) in computational cost about equivalent to using a usual isoparametric 3D element. To reduce the solution cost, shell mathematical models of essentially similar characteristics have been proposed using a quadratic expansion of the transverse displacements only (with linear tangential displacements). These models are often referred to as "seven-parameter models" as they involve seven degrees of freedom in one given shell section (compared to nine degrees of freedom for the kinematical assumption in (4.73)), see (Bischoff & Ramm, 2000; Sansour, 1995) and references therein. However, the simplicity gained by considering full Cartesian vectors in the 3D-shell model – instead of individual transverse components in seven-parameter models – is of considerable advantage, and even more so when large displacements and rotations are considered. Nevertheless, the essential fundamental features of these shell models are similar, and this also justifies that we henceforth restrict our discussions to the 3D-shell model of (4.76).

4.3 Mathematical Analysis of the Shell Models

We start by showing that the s-m-b shell model, as represented by the variational formulation (4.36), defines a well-posed mathematical problem. We then use this result to establish similar properties for the m-b model, the basic shell model and the 3D-shell model.

We recall that – throughout this book – the symbol C denotes a generic positive constant which may take different values at successive occurrences, while γ similarly denotes a generic *strictly positive* constant.

4.3.1 Analysis of the s-m-b shell model

Recalling Section 3.2, our objective here is to show that Problem (4.36) can be written in the form

$$A^N(\vec{u},\underline{\theta};\vec{v},\underline{\eta}) = F^N(\vec{v},\underline{\eta}), \tag{4.79}$$

for arbitrary test functions in some solution space $\mathcal{V}^N$, A^N being a symmetric and coercive bilinear form over $\mathcal{V}^N$, and F^N being a linear form over $\mathcal{V}^N$. Proceeding by inspection, we set

$$\begin{aligned} A^N(\vec{u},\underline{\theta};\vec{v},\underline{\eta}) = & \int_\omega {}^0C^{\alpha\beta\lambda\mu}[t\gamma_{\alpha\beta}(\vec{u})\gamma_{\lambda\mu}(\vec{v}) + \frac{t^3}{12}\chi_{\alpha\beta}(\vec{u},\underline{\theta})\chi_{\lambda\mu}(\vec{v},\underline{\eta})]\, dS \\ & + \int_\omega t\, {}^0D^{\alpha\lambda}\zeta_\alpha(\vec{u},\underline{\theta})\zeta_\lambda(\vec{v},\underline{\eta})\, dS, \end{aligned} \tag{4.80}$$

$$F^N(\vec{v},\underline{\eta}) = \int_\omega t\vec{F}\cdot\vec{v}\, dS, \tag{4.81}$$

where the symmetry of A^N is obvious. Furthermore, noting that all first-order derivatives of the arguments are used in the expression of A^N, we define

$$\boxed{\mathcal{V}^N = \big\{(\vec{v},\underline{\eta}) \in H^1(\mathcal{S})\times H^1(\mathcal{S})\big\} \cap \mathcal{BC},} \tag{4.82}$$

where $\mathcal{BC}$ symbolically denotes the essential boundary conditions imposed on the structure. We henceforth assume that these boundary conditions are homogeneous, so that $\mathcal{V}^N$ is a vector space. For example, if the shell structure is fully clamped we impose $(\vec{v},\underline{\eta}) = (\vec{0},\underline{0})$ over the whole boundary $\partial\mathcal{S}$ of the midsurface. Note that there is a slight abuse of notation in (4.82) since $\vec{v}$ is not directly a surface tensor, so that $\vec{v} \in H^1(\mathcal{S})$ should really be understood as $(\underline{v}, v_3) \in H^1(\mathcal{S}) \times H^1(\mathcal{S})$ with

$$\|\vec{v}\|^2_{H^1(\mathcal{S})} = \|\underline{v}\|^2_{H^1(\mathcal{S})} + \|v_3\|^2_{H^1(\mathcal{S})}. \tag{4.83}$$

The norm that we then consider in $\mathcal{V}^N$ is that obtained by the natural combination of H^1-norms, namely it is given by

$$\|\vec{v}, \underline{\eta}\|^2_{\mathcal{V}^N} = \|\vec{v}\|^2_{H^1(\mathcal{S})} + \|\underline{\eta}\|^2_{H^1(\mathcal{S})}, \tag{4.84}$$

and we point out that the considerations raised in Remark 3.2.7 hold here as well.

In this framework, we have the following result.

Proposition 4.3.1 *A^N is continuous, hence it is a bilinear form, i.e.*

$$|A^N(\vec{u}, \underline{\theta}; \vec{v}, \underline{\eta})| \leq C\|\vec{u}, \underline{\theta}\|_{\mathcal{V}^N}\|\vec{v}, \underline{\eta}\|_{\mathcal{V}^N}, \quad \forall (\vec{u}, \underline{\theta}), (\vec{v}, \underline{\eta}) \in \mathcal{V}^N \times \mathcal{V}^N. \tag{4.85}$$

Furthermore, assuming $\vec{F} \in L^2(\mathcal{S})$, F^N is also continuous, hence it is a linear form, i.e.

$$|F^N(\vec{v}, \underline{\eta})| \leq C\|\vec{v}, \underline{\eta}\|_{\mathcal{V}^N}, \qquad \forall (\vec{v}, \underline{\eta}) \in \mathcal{V}^N. \tag{4.86}$$

Proof. We have

$$\begin{aligned} |A^N(\vec{u}, \underline{\theta}; \vec{v}, \underline{\eta})| \quad \leq \quad & t_{\max} \int_\omega |{}^0C^{\alpha\beta\lambda\mu}\gamma_{\alpha\beta}(\vec{u})\gamma_{\lambda\mu}(\vec{v})| \, dS \\ & + \frac{(t_{\max})^3}{12} \int_\omega |{}^0C^{\alpha\beta\lambda\mu}\chi_{\alpha\beta}(\vec{u}, \underline{\theta})\chi_{\lambda\mu}(\vec{v}, \underline{\eta})| \, dS \\ & + t_{\max} \int_\omega |{}^0D^{\alpha\lambda}\zeta_\alpha(\vec{u}, \underline{\theta})\zeta_\lambda(\vec{v}, \underline{\eta})| \, dS, \end{aligned} \tag{4.87}$$

where $t_{\max}$ is the maximum thickness over the whole surface. We start by bounding the first term of this right-hand side, using the expression of ${}^0C^{\alpha\beta\lambda\mu}$ (4.34) and the symmetry of the membrane strain tensor. We get

$$\begin{aligned} & |{}^0C^{\alpha\beta\lambda\mu}\gamma_{\alpha\beta}(\vec{u})\gamma_{\lambda\mu}(\vec{v})| \\ & \quad = \quad \frac{E}{2(1+\nu)} \, |\langle \underline{\underline{\gamma}}(\vec{u}), \underline{\underline{\gamma}}(\vec{v}) \rangle_{\mathcal{E}} + \langle \underline{\underline{\gamma}}(\vec{u}), \underline{\underline{\gamma}}(\vec{v})^T \rangle_{\mathcal{E}} \\ & \qquad\qquad + \frac{2\nu}{1-\nu} \mathrm{tr}\underline{\underline{\gamma}}(\vec{u}) \, \mathrm{tr}\underline{\underline{\gamma}}(\vec{v}) \, | \\ & \quad = \quad \frac{E}{1+\nu} \, |\langle \underline{\underline{\gamma}}(\vec{u}), \underline{\underline{\gamma}}(\vec{v}) \rangle_{\mathcal{E}} + \frac{\nu}{1-\nu} \mathrm{tr}\underline{\underline{\gamma}}(\vec{u}) \, \mathrm{tr}\underline{\underline{\gamma}}(\vec{v}) \, | \\ & \quad \leq \quad \frac{E}{1+\nu} \, (\, |\langle \underline{\underline{\gamma}}(\vec{u}), \underline{\underline{\gamma}}(\vec{v}) \rangle_{\mathcal{E}}| + \frac{\nu}{1-\nu} \, | \, \mathrm{tr}\underline{\underline{\gamma}}(\vec{u}) \, \mathrm{tr}\underline{\underline{\gamma}}(\vec{v}) \, | \,), \end{aligned} \tag{4.88}$$

using the triangle inequality. Then we have the estimate

$$|\mathrm{tr}\underline{\underline{T}}|^2 \leq 2\|\underline{\underline{T}}\|_{\mathcal{E}}^2, \tag{4.89}$$

for any second-order surface tensor $\underline{\underline{T}}$, which can easily be established using an orthonormal coordinate system (locally) and applying a Cauchy-Schwarz inequality. Combining this and a Cauchy-Schwarz inequality on the first term of (4.88), we get

$$|{}^0C^{\alpha\beta\lambda\mu}\gamma_{\alpha\beta}(\vec{u})\gamma_{\lambda\mu}(\vec{v})| \leq \frac{E}{1-\nu}\|\underline{\underline{\gamma}}(\vec{u})\|_{\mathcal{E}}\|\underline{\underline{\gamma}}(\vec{v})\|_{\mathcal{E}}. \tag{4.90}$$

Using then the expression of the membrane strain tensor (4.38), we obtain

$$\begin{aligned}\|\underline{\underline{\gamma}}(\vec{u})\|_{\mathcal{E}} &= \|\frac{1}{2}\underline{\underline{\nabla}}\,\underline{u} + \frac{1}{2}(\underline{\underline{\nabla}}\,\underline{u})^T - \underline{\underline{b}}u_3\|_{\mathcal{E}} \\ &\leq \|\underline{\underline{\nabla}}\,\underline{u}\|_{\mathcal{E}} + \|\underline{\underline{b}}\|_{\mathcal{E}}\,|u_3|,\end{aligned} \tag{4.91}$$

since $\|\underline{\underline{\nabla}}\,\underline{u}\|_{\mathcal{E}} = \|(\underline{\underline{\nabla}}\,\underline{u})^T\|_{\mathcal{E}}$ and, of course, we have a similar expression for $\underline{\underline{\gamma}}(\vec{v})$. Defining $b_{\max}$ as the maximum of $\|\underline{\underline{b}}\|_{\mathcal{E}}$ over the surface, we get, by combining (4.90) and (4.91) and by using a Cauchy-Schwarz inequality,

$$\begin{aligned}&\int_\omega |{}^0C^{\alpha\beta\lambda\mu}\gamma_{\alpha\beta}(\vec{u})\gamma_{\lambda\mu}(\vec{v})|\,dS \\ &\quad\leq \frac{E}{1-\nu}\int_\omega (\|\underline{\underline{\nabla}}\,\underline{u}\|_{\mathcal{E}} + \|\underline{\underline{b}}\|_{\mathcal{E}}\,|u_3|)\,(\|\underline{\underline{\nabla}}\,\underline{v}\|_{\mathcal{E}} + \|\underline{\underline{b}}\|_{\mathcal{E}}\,|v_3|)\,dS \\ &\quad\leq \frac{E}{1-\nu}\left[\int_\omega (\|\underline{\underline{\nabla}}\,\underline{u}\|_{\mathcal{E}} + \|\underline{\underline{b}}\|_{\mathcal{E}}\,|u_3|)^2\,dS\right]^{\frac{1}{2}} \\ &\qquad\qquad \times\left[\int_\omega (\|\underline{\underline{\nabla}}\,\underline{v}\|_{\mathcal{E}} + \|\underline{\underline{b}}\|_{\mathcal{E}}\,|v_3|)^2\,dS\right]^{\frac{1}{2}} \\ &\quad\leq \frac{E}{1-\nu}\,(|\underline{u}|_{H^1(\mathcal{S})} + b_{\max}\|u_3\|_{L^2(\mathcal{S})}) \\ &\qquad\qquad \times(|\underline{v}|_{H^1(\mathcal{S})} + b_{\max}\|v_3\|_{L^2(\mathcal{S})}),\end{aligned} \tag{4.92}$$

using also triangle inequalities in the last step.

The two other terms in the right-hand side of (4.87) can be bounded by similar arguments (using also (3.37)). More specifically, we obtain

$$\int_\omega |{}^0C^{\alpha\beta\lambda\mu}\chi_{\alpha\beta}(\vec{u},\underline{\theta})\chi_{\lambda\mu}(\vec{v},\underline{\eta})|\,dS$$

$$\leq \frac{E}{1-\nu}\,(|\underline{\theta}|_{H^1(\mathcal{S})} + b_{\max}|\underline{u}|_{H^1(\mathcal{S})} + (b_{\max})^2\|u_3\|_{L^2(\mathcal{S})}) \tag{4.93}$$

$$\times(|\underline{\eta}|_{H^1(\mathcal{S})} + b_{\max}|\underline{v}|_{H^1(\mathcal{S})} + (b_{\max})^2\|v_3\|_{L^2(\mathcal{S})}),$$

$$\int_\omega |{}^0D^{\alpha\lambda}\zeta_\alpha(\vec{u},\underline{\theta})\zeta_\lambda(\vec{v},\underline{\eta})|\,dS$$

$$\leq \frac{E}{2(1+\nu)}\,(\|\underline{\theta}\|_{L^2(\mathcal{S})} + |u_3|_{H^1(\mathcal{S})} + b_{\max}\|\underline{u}\|_{L^2(\mathcal{S})}) \tag{4.94}$$

$$\times(\|\underline{\eta}\|_{L^2(\mathcal{S})} + |v_3|_{H^1(\mathcal{S})} + b_{\max}\|\underline{v}\|_{L^2(\mathcal{S})})$$

Combining the bounds (4.92)–(4.94) with (4.87), we finally obtain (4.85), with a constant C which depends on E, ν, $t_{\max}$ and $b_{\max}$. Equation (4.86) is obtained by similar (although much simpler) arguments. ■

In order to prove the coercivity of A^N, we need some preliminary results, the first of which being a Korn inequality for first-order surface tensors.

Lemma 4.3.1. *There exists a strictly positive constant α_K such that, for any first-order surface tensor $\underline{v}$ in $H^1(\mathcal{S})$,*

$$|\underline{v}|_{H^1(\mathcal{S})} \leq \alpha_K(\|\underline{\underline{\epsilon}}(\underline{v})\|_{L^2(\mathcal{S})} + \|\underline{v}\|_{L^2(\mathcal{S})}), \tag{4.95}$$

for

$$\underline{\underline{\epsilon}}(\underline{v}) = \frac{1}{2}[\underline{\underline{\nabla}}\,\underline{v} + (\underline{\underline{\nabla}}\,\underline{v})^T]. \tag{4.96}$$

Although this property is, in essence, inherited from similar 3D Korn inequalities, the detailed proof is complex and technical so that we do not provide it here, and instead refer to (Delfour, 2000) (see also (Ciarlet, 2000) for a similar inequality, albeit using components in a given curvilinear coordinate system). We now state and prove a second preliminary result.

Lemma 4.3.2. *Consider $\vec{v} \in H^1(\mathcal{S})$ and $\underline{\eta} \in H^1(\mathcal{S})$. Assume that*

$$(\underline{\underline{\gamma}}(\vec{v}), \underline{\underline{\chi}}(\vec{v},\underline{\eta}), \underline{\zeta}(\vec{v},\underline{\eta})) = (\underline{\underline{0}}, \underline{0}, \underline{0}) \tag{4.97}$$

all over $\mathcal{S}$. Then the displacements defined by (4.31) in $\mathcal{B}$ correspond to an infinitesimal rigid body motion, i.e. there exists a global translation vector $\vec{T}$ and an infinitesimal rotation vector $\vec{R}$ such that

$$\boxed{\vec{v}(\xi^1,\xi^2)=\vec{T}+\vec{R}\wedge\vec{\phi}(\xi^1,\xi^2),} \tag{4.98}$$

$$\boxed{\underline{\eta}(\xi^1,\xi^2)=\vec{R}\wedge\vec{a}_3(\xi^1,\xi^2).} \tag{4.99}$$

Remark 4.3.1. Note that (4.99) is admissible although $\underline{\eta}$ is a first-order surface tensor (namely, a vector of the tangential plane), since $\vec{R}\wedge\vec{a}_3$ is also a vector of the tangential plane. ■

Remark 4.3.2. Equations (4.98) and (4.99) define a rigid body motion in $\mathcal{B}$ since they imply by (4.31)

$$\vec{V}=\vec{T}+\vec{R}\wedge(\vec{\phi}+\xi^3\vec{a}_3), \tag{4.100}$$

i.e. the displacement $\vec{V}$ of any point M in $\mathcal{B}$ is given by

$$\vec{V}=\vec{T}+\vec{R}\wedge O\vec{M}. \tag{4.101}$$

■

Proof of Lemma 4.3.2. Assume that (4.97) holds and consider the 3D displacement field $\vec{V}$ defined in $\mathcal{B}$ by (4.31). This displacement field clearly is in $H^1(\mathcal{B})$. The 3D linearized Green-Lagrange strain tensor is given by, according to (4.9) and using (4.97),

$$\begin{cases} e_{\alpha\beta}=-(\xi^3)^2\kappa_{\alpha\beta}(\underline{\eta}), \quad \alpha,\beta=1,2 \\ e_{\alpha 3}=0, \quad \alpha=1,2 \\ e_{33}=0 \end{cases} \tag{4.102}$$

We then focus on

$$\kappa_{\alpha\beta}(\underline{\eta})=\frac{1}{2}(b^\lambda_\beta\eta_{\lambda|\alpha}+b^\lambda_\alpha\eta_{\lambda|\beta}). \tag{4.103}$$

Using $\underline{\zeta}(\vec{v},\underline{\eta})=\underline{0}$ we have

$$\begin{aligned} \eta_{\lambda|\alpha} &= -(v_{3|\lambda\alpha}+b^\mu_{\lambda|\alpha}v_\mu+b^\mu_\lambda v_{\mu|\alpha}) \\ &= -(\bar{\rho}_{\lambda\alpha}(\vec{v})-b^\mu_\alpha v_{\mu|\lambda}+c_{\lambda\alpha}v_3) \end{aligned} \tag{4.104}$$

Since $\underline{\zeta}(\vec{v},\underline{\eta})=\underline{0}$, we can easily check that (4.47) still holds in $L^2(\mathcal{S})$, hence

$$\eta_{\lambda|\alpha}=b_\alpha^\mu v_{\mu|\lambda}-c_{\lambda\alpha}v_3 \tag{4.105}$$

and recalling the definition of the third fundamental form (2.110) we infer

$$\kappa_{\alpha\beta}(\underline{\eta})=b_\alpha^\lambda b_\beta^\mu\gamma_{\lambda\mu}(\vec{v})=0. \tag{4.106}$$

Therefore, from (4.102) all 3D strains are identically zero throughout $\mathcal{B}$. This implies by classical results from 3D continuum mechanics (see e.g. Ciarlet, 1988) that the displacement field $\vec{V}$ corresponds to an infinitesimal rigid body motion. Hence there exist two vectors $\vec{T}$ and $\vec{R}$ such that (4.101) holds. Substituting then

$$\vec{OM}=\vec{\Phi}=\vec{\phi}+\xi^3\vec{a}_3 \tag{4.107}$$

and using the definition of $\vec{V}$ in (4.31), we finally obtain (4.98) and (4.99). ■

Remark 4.3.3. Note that the property established in Lemma 4.3.2 is very important from a physical and practical point of view, since it ensures that only genuine rigid body modes render the shell strains identically zero and result into zero deformation energy. This property will be satisfied by all the shell models discussed in this book, and also by the finite element procedures proposed for these models. ■

We are now in a position to prove the coercivity result.

Proposition 4.3.2 *Suppose that the essential boundary conditions enforced in $\mathcal{V}^N$ are such that no rigid body motion is possible, i.e. the only element $(\vec{v},\underline{\eta})$ in $\mathcal{V}^N$ satisfying (4.98) and (4.99) for some $(\vec{T},\vec{R})$ is $(\vec{0},\underline{0})$. Then the bilinear form A^N is coercive over $\mathcal{V}^N$.*

Proof. We consider an arbitrary $(\vec{v},\underline{\eta})\in\mathcal{V}^N$. Throughout this proof, it is implicitly assumed that all the deformation strain tensors used (namely $\underline{\underline{\gamma}}$, $\underline{\underline{\chi}}$ and $\underline{\zeta}$) apply to this same element considered, so we write these strain tensors without arguments. We decompose the proof into three steps.

i) Using Lemma 4.3.1, we get

$$\begin{aligned}|\underline{v}|^2_{H^1(\mathcal{S})} &\le C(\|\underline{\underline{\epsilon}}(\underline{v})\|^2_{L^2(\mathcal{S})}+\|\underline{v}\|^2_{L^2(\mathcal{S})})\\ &= C(\|\underline{\underline{\gamma}}+\underline{\underline{b}}v_3\|^2_{L^2(\mathcal{S})}+\|\underline{v}\|^2_{L^2(\mathcal{S})})\\ &\le C(\|\underline{\underline{\gamma}}\|^2_{L^2(\mathcal{S})}+\|\underline{v}\|^2_{L^2(\mathcal{S})}+\|v_3\|^2_{L^2(\mathcal{S})}),\end{aligned} \tag{4.108}$$

since $\|\underline{\underline{b}} v_3\|_{L^2(\mathcal{S})} \leq b_{\max}\|v_3\|_{L^2(\mathcal{S})}$. Then, we apply again Lemma 4.3.1, with $\underline{\eta}$ instead of $\underline{v}$, and we obtain

$$\begin{aligned}
|\underline{\eta}|^2_{H^1(\mathcal{S})} &\leq C(\|\underline{\underline{\epsilon}}(\underline{\eta})\|^2_{L^2(\mathcal{S})} + \|\underline{\eta}\|^2_{L^2(\mathcal{S})}) \\
&= C(\|\underline{\underline{\chi}} + \frac{1}{2}[\underline{\underline{b}} \cdot \underline{\underline{\nabla}}\, \underline{v} + (\underline{\underline{b}} \cdot \underline{\underline{\nabla}}\, \underline{v})^T] - \underline{\underline{c}} v_3\|^2_{L^2(\mathcal{S})} + \|\underline{\eta}\|^2_{L^2(\mathcal{S})}) \\
&\leq C(\|\underline{\underline{\chi}}\|^2_{L^2(\mathcal{S})} + |\underline{v}|^2_{H^1(\mathcal{S})} + \|v_3\|^2_{L^2(\mathcal{S})} + \|\underline{\eta}\|^2_{L^2(\mathcal{S})}), \\
&\leq C(\|\underline{\underline{\chi}}\|^2_{L^2(\mathcal{S})} + \|\underline{\underline{\gamma}}\|^2_{L^2(\mathcal{S})} + \|\underline{v}\|^2_{L^2(\mathcal{S})} + \|\underline{\eta}\|^2_{L^2(\mathcal{S})} \\
&\qquad + \|v_3\|^2_{L^2(\mathcal{S})}), \qquad (4.109)
\end{aligned}$$

using (4.108) to bound $|\underline{v}|^2_{H^1(\mathcal{S})}$. Next, we have

$$\begin{aligned}
|v_3|^2_{H^1(\mathcal{S})} &= \|2\underline{\zeta} - \underline{\eta} - \underline{\underline{b}} \cdot \underline{v}\|^2_{L^2(\mathcal{S})} \\
&\leq C(\|\underline{\zeta}\|^2_{L^2(\mathcal{S})} + \|\underline{\eta}\|^2_{L^2(\mathcal{S})} + \|\underline{v}\|^2_{L^2(\mathcal{S})}). \qquad (4.110)
\end{aligned}$$

Gathering (4.108)–(4.110), we thus obtain

$$\begin{aligned}
\|\vec{v}, \underline{\eta}\|^2_{\mathcal{V}^N} &\leq C(\|\underline{\underline{\chi}}\|^2_{L^2(\mathcal{S})} + \|\underline{\underline{\gamma}}\|^2_{L^2(\mathcal{S})} + \|\underline{\zeta}\|^2_{L^2(\mathcal{S})} \\
&\qquad + \|\underline{v}\|^2_{L^2(\mathcal{S})} + \|v_3\|^2_{L^2(\mathcal{S})} + \|\underline{\eta}\|^2_{L^2(\mathcal{S})}). \qquad (4.111)
\end{aligned}$$

ii) Consider the quantity

$$N(\vec{v}, \underline{\eta}) = (\|\underline{\underline{\chi}}\|^2_{L^2(\mathcal{S})} + \|\underline{\underline{\gamma}}\|^2_{L^2(\mathcal{S})} + \|\underline{\zeta}\|^2_{L^2(\mathcal{S})})^{\frac{1}{2}}. \qquad (4.112)$$

It clearly defines a norm in $\mathcal{V}^N$ by Lemma 4.3.2, since we assumed that the only rigid body motion allowed in $\mathcal{V}^N$ is the zero displacement. We now proceed to show that this norm is equivalent to the norm chosen for $\mathcal{V}^N$ (namely, the H^1-norm). By arguments similar to those used in the proof of Proposition 4.3.1, we already have

$$N(\vec{v}, \underline{\eta}) \leq C\|\vec{v}, \underline{\eta}\|_{\mathcal{V}^N}. \qquad (4.113)$$

We need to show that we also have

$$\|\vec{v}, \underline{\eta}\|_{\mathcal{V}^N} \leq CN(\vec{v}, \underline{\eta}). \qquad (4.114)$$

We proceed by contradiction. Suppose that (4.114) does not hold. Then there exists a sequence $(\vec{v}_n, \underline{\eta}_n)$ in $\mathcal{V}^N$ such that

$$\|\vec{v}_n, \underline{\eta}_n\|_{\mathcal{V}^N} = 1, \quad \forall n, \tag{4.115}$$

and $N(\vec{v}_n, \underline{\eta}_n)$ tends to zero when n tends to infinity. Since the sequence is uniformly bounded in the H^1-norm, there exists a subsequence that converges weakly (for this same norm) to some limit $(\vec{v}_\infty, \underline{\eta}_\infty)$. For simplicity we also denote this subsequence by $(\vec{v}_n, \underline{\eta}_n)$. Recalling that the weak convergence in H^1 implies strong convergence in L^2 (to the same limit), we infer that the subsequence $(\vec{v}_n, \underline{\eta}_n)$ is a Cauchy sequence for the L^2-norm. Since $N(\vec{v}_n, \underline{\eta}_n)$ tends to zero, $(\vec{v}_n, \underline{\eta}_n)$ is a Cauchy sequence for the norm given by N too, hence it is a Cauchy sequence for the norm that corresponds to the right-hand side of (4.111), hence it is a Cauchy sequence for the H^1-norm on the left-hand side. Therefore, the subsequence converges strongly to $(\vec{v}_\infty, \underline{\eta}_\infty)$ in the H^1-norm. Then, by (4.113), it converges strongly for the N-norm to the same limit, but since $N(\vec{v}_n, \underline{\eta}_n)$ tends to zero we have that

$$N(\vec{v}_\infty, \underline{\eta}_\infty) = 0, \tag{4.116}$$

hence $(\vec{v}_\infty, \underline{\eta}_\infty) = (\vec{0}, \underline{0})$ because N is a norm in $\mathcal{V}^N$, which is in contradiction with (4.115). Therefore (4.114) holds, and hence we now have a stronger result than (4.111), namely,

$$\|\vec{v}, \underline{\eta}\|^2_{\mathcal{V}^N} \leq C(\|\underline{\underline{\chi}}\|^2_{L^2(\mathcal{S})} + \|\underline{\underline{\gamma}}\|^2_{L^2(\mathcal{S})} + \|\underline{\zeta}\|^2_{L^2(\mathcal{S})}). \tag{4.117}$$

iii) We finally show that

$$\|\underline{\underline{\chi}}\|^2_{L^2(\mathcal{S})} + \|\underline{\underline{\gamma}}\|^2_{L^2(\mathcal{S})} + \|\underline{\zeta}\|^2_{L^2(\mathcal{S})} \leq C A^N(\vec{v}, \underline{\eta}; \vec{v}, \underline{\eta}), \tag{4.118}$$

which, with (4.117), will conclude the proof. Considering first the membrane term in the expression of $A^N(\vec{v}, \underline{\eta}; \vec{v}, \underline{\eta})$, we have

$$\begin{aligned} {}^0C^{\alpha\beta\lambda\mu}\gamma_{\alpha\beta}\gamma_{\lambda\mu} &= \frac{E}{2(1+\nu)}[\langle \underline{\underline{\gamma}}, \underline{\underline{\gamma}} \rangle_{\mathcal{E}} + \langle \underline{\underline{\gamma}}, \underline{\underline{\gamma}}^T \rangle_{\mathcal{E}} \\ &\qquad + \frac{2\nu}{1-\nu}(\mathrm{tr}\underline{\underline{\gamma}})^2] \\ &\geq \frac{E}{1+\nu} \|\underline{\underline{\gamma}}\|^2_{\mathcal{E}}, \end{aligned} \tag{4.119}$$

hence

$$\int_\omega t\, {}^0C^{\alpha\beta\lambda\mu}\gamma_{\alpha\beta}\gamma_{\lambda\mu}\, dS \geq \frac{E t_{\min}}{1+\nu} \|\underline{\underline{\gamma}}\|^2_{L^2(\mathcal{S})}, \tag{4.120}$$

where $t_{\min}$ denotes the minimum of the thickness parameter over the whole surface. Similarly

$$\int_\omega \frac{t^3}{12} {}^0C^{\alpha\beta\lambda\mu}\chi_{\alpha\beta}\chi_{\lambda\mu}\, dS \geq \frac{E(t_{\min})^3}{12(1+\nu)}\, \|\underline{\underline{\chi}}\|^2_{L^2(\mathcal{S})}, \tag{4.121}$$

and

$$\int_\omega t\, {}^0D^{\alpha\lambda}\zeta_\alpha\zeta_\lambda\, dS \geq \frac{2Et_{\min}}{1+\nu}\, \|\underline{\zeta}\|^2_{L^2(\mathcal{S})}. \tag{4.122}$$

Combining eventually (4.120)–(4.122), we get (4.118). ∎

Remark 4.3.4. The above proof of the coercivity of the bilinear form in the s-m-b model, with the two Lemmas 4.3.1 and 4.3.2, follows the same main lines as the original proof of the coercivity for the m-b shell model in (Bernadou & Ciarlet, 1975), on which the first proof for the s-m-b model was itself based (Coutris, 1978), see also (Bernadou et al., 1994a). Compared to that original proof, however, the one provided here is considerably simplified due to the use of the Korn inequality (4.95) written directly with surface tensors, and also to a much simpler proof of Lemma 4.3.2 (due to considering the complete shell body $\mathcal{B}$ instead of only the surface $\mathcal{S}$). ∎

We can now state the final result of this section.

Proposition 4.3.3 *Under the assumptions that*

- $\vec{F} \in L^2(\mathcal{S})$;
- *the essential boundary conditions enforced in* $\mathcal{V}^N$ *are such that no rigid body motion is possible, i.e. the only element* $(\vec{v}, \underline{\eta})$ *in* $\mathcal{V}^N$ *satisfying (4.98) and (4.99) for some* $(\vec{T}, \vec{R})$ *is* $(\vec{0}, \underline{0})$;

the s-m-b shell model gives a well-posed mathematical problem, i.e. there is a unique $(\vec{u}, \underline{\theta}) \in \mathcal{V}^N$ *such that*

$$A^N(\vec{u}, \underline{\theta}; \vec{v}, \underline{\eta}) = F^N(\vec{v}, \underline{\eta}) \tag{4.123}$$

holds for any $(\vec{v}, \underline{\eta}) \in \mathcal{V}^N$, *and we have*

$$\|\vec{u}, \underline{\theta}\|_{\mathcal{V}^N} \leq C\|\vec{F}\|_{L^2(\mathcal{S})}. \tag{4.124}$$

Proof. Immediate from Propositions 4.3.1 and 4.3.2, by using the Lax-Milgram Theorem (Prop. 3.2.1). ∎

4.3.2 Analysis of the m-b shell model

Following the procedure used for the analysis of the s-m-b model, we define, from the expression of the m-b model featured in (4.51),

$$A^K(\vec{u};\vec{v}) = \int_\omega {}^0C^{\alpha\beta\lambda\mu}[t\gamma_{\alpha\beta}(\vec{u})\gamma_{\lambda\mu}(\vec{v}) + \frac{t^3}{12}\bar{\rho}_{\alpha\beta}(\vec{u})\bar{\rho}_{\lambda\mu}(\vec{v})]\, dS \tag{4.125}$$

$$F^K(\vec{v}) = \int_\omega t\vec{F}\cdot\vec{v}\, dS. \tag{4.126}$$

Since second-order derivatives of the transverse displacements (along $\vec{a}_3$) are used in the expression of the tensor $\underline{\underline{\bar{\rho}}}$, we define the displacement space as

$$\boxed{\mathcal{V}^K = \left\{\vec{v} = (\underline{v}, v_3) \in H^1(\mathcal{S}) \times H^2(\mathcal{S})\right\} \cap \mathcal{BC},} \tag{4.127}$$

where, again, $\mathcal{BC}$ denotes homogeneous boundary conditions. Note that, in this space, clamped boundary conditions are imposed by setting $\underline{v} = \underline{0}$ and $\underline{\nabla} v_3 \cdot \underline{n} = 0$, where $\underline{n}$ denotes a vector of the tangential plane normal to the boundary. The norm that we use for $\mathcal{V}^K$ is given by

$$\|\vec{v}\|^2_{\mathcal{V}^K} = \|\underline{v}\|^2_{H^1(\mathcal{S})} + \|v_3\|^2_{H^2(\mathcal{S})}. \tag{4.128}$$

We now directly state and prove the well-posedness of the mathematical problem given by the m-b shell model.

Proposition 4.3.4 *Assume that:*

- $\vec{F} \in L^2(\mathcal{S})$*;*
- *the essential boundary conditions enforced in* $\mathcal{V}^K$ *are such that no rigid body motion is possible, i.e. the only element* $\vec{v}$ *in* $\mathcal{V}^K$ *satisfying (4.98) for some* $(\vec{T}, \vec{R})$ *is* $\vec{0}$*.*

Then, A^K *is a coercive bilinear form over the space* $\mathcal{V}^K$*, and* F^K *is a linear form over* $\mathcal{V}^K$*. Therefore there is a unique* $\vec{u} \in \mathcal{V}^K$ *that satisfies*

$$A^K(\vec{u},\vec{v}) = F^K(\vec{v}) \tag{4.129}$$

for any $\vec{v} \in \mathcal{V}^K$*, and we have*

$$\|\vec{v}\|_{\mathcal{V}^K} \leq C\|\vec{F}\|_{L^2(\mathcal{S})}. \tag{4.130}$$

Proof. We will use the continuity and coercivity of the bilinear form of the s-m-b model to prove similar properties for the m-b model. Consider any $\vec{v} \in \mathcal{V}^K$ and set

$$\underline{\eta} = -\underline{\nabla} v_3 - \underline{\underline{b}} \cdot \underline{v}, \tag{4.131}$$

hence $\underline{\eta}$ is the rotation tensor given by the Kirchhoff-Love kinematical assumption (see Equation (4.42)). Then, clearly $\underline{\eta} \in H^1(\mathcal{S})$. Define now the s-m-b displacement space $\mathcal{V}^N$ such that the essential boundary conditions on the rotations are obtained from the essential boundary conditions that prevail in $\mathcal{V}^K$ by (4.131). Then, $(\vec{v}, \underline{\eta}) \in \mathcal{V}^N$ and

$$\|\vec{v}, \underline{\eta}\|_{\mathcal{V}^N} \leq C \|\vec{v}\|_{\mathcal{V}^K}. \tag{4.132}$$

For any $\vec{u} \in \mathcal{V}^K$, we similarly define

$$\underline{\theta} = -\underline{\nabla} u_3 - \underline{\underline{b}} \cdot \underline{u}, \tag{4.133}$$

and we have $(\vec{u}, \underline{\theta}) \in \mathcal{V}^N$ with

$$\|\vec{u}, \underline{\theta}\|_{\mathcal{V}^N} \leq C \|\vec{u}\|_{\mathcal{V}^K}. \tag{4.134}$$

Note that, with (4.131) (resp. (4.133)), the shear strain tensor $\underline{\zeta}$ vanishes for $(\vec{v}, \underline{\eta})$ (resp. for $(\vec{u}, \underline{\theta})$). Hence

$$A^K(\vec{u}; \vec{v}) = A^N(\vec{u}, \underline{\theta}; \vec{v}, \underline{\eta}), \tag{4.135}$$

recalling (4.47). This implies, by (4.85),

$$|A^K(\vec{u}; \vec{v})| \leq C \|\vec{u}, \underline{\theta}\|_{\mathcal{V}^N} \|\vec{v}, \underline{\eta}\|_{\mathcal{V}^N} \leq C \|\vec{u}\|_{\mathcal{V}^K} \|\vec{v}\|_{\mathcal{V}^K}, \tag{4.136}$$

which shows that A^K is continuous.

Consider now a rigid-body motion in $\mathcal{V}^N$, i.e. an element $(\vec{v}, \underline{\eta})$ given by (4.98) and (4.99) for some vectors $(\vec{T}, \vec{R})$. Then, recalling Remark 4.3.2, $(\vec{v}, \underline{\eta})$ defines a rigid body motion in $\mathcal{B}$ through the Reissner-Mindlin kinematical assumption. Of course, the Green-Lagrange linearized strain tensor of this 3D displacement field is identically zero, hence, from (4.9), $\underline{\zeta}(\vec{v}, \underline{\eta})$ vanishes. Therefore, $(\vec{v}, \underline{\eta})$ satisfies the Kirchhoff-Love kinematical assumption and, since the tensors given by (4.98) and (4.99) are smooth, $\vec{v}$ is also in $\mathcal{V}^K$ (note that the boundary conditions are consistently enforced). Since the only rigid-body motion contained in $\mathcal{V}^K$ is the zero displacement, we infer that $\vec{T} = \vec{R} = 0$, hence $(\vec{v}, \underline{\eta})$ is identically zero. This implies that $\mathcal{V}^N$ satisfies the assumptions of Proposition 4.3.2 and thus

$$A^K(\vec{v};\vec{v}) = A^N(\vec{v},\underline{\eta};\vec{v},\underline{\eta}) \geq c\|\vec{v},\underline{\eta}\|^2_{\mathcal{V}^N}. \tag{4.137}$$

We complete the coercivity proof by noting that, using (4.131), we have

$$\begin{aligned}\|\vec{v}\|^2_{\mathcal{V}^K} &= \|v_3\|^2_{L^2(\mathcal{S})} + \|\underline{\nabla} v_3\|^2_{H^1(\mathcal{S})} + \|\underline{v}\|^2_{H^1(\mathcal{S})} \\ &= \|v_3\|^2_{L^2(\mathcal{S})} + \|\underline{\eta} + \underline{b}\cdot\underline{v}\|^2_{H^1(\mathcal{S})} + \|\underline{v}\|^2_{H^1(\mathcal{S})} \\ &\leq C\|\vec{v},\underline{\eta}\|^2_{\mathcal{V}^N}. \end{aligned} \tag{4.138}$$

Next, the continuity of F^K is immediate and, finally, the existence and uniqueness of a solution to the m-b model directly follows from the Lax-Milgram Theorem (Prop. 3.2.1), and so does the estimate (4.130). ∎

4.3.3 Analysis of the basic shell model

For the basic shell model, we define the following bilinear function, based on (4.30),

$$\begin{aligned} A^B(\vec{u},\underline{\theta};\vec{v},\underline{\eta}) = & \\ & \int_\Omega C^{\alpha\beta\lambda\mu}[\gamma_{\alpha\beta}(\vec{u}) + \xi^3\chi_{\alpha\beta}(\vec{u},\underline{\theta}) - (\xi^3)^2\kappa_{\alpha\beta}(\underline{\theta})] \\ & \qquad \times[\gamma_{\lambda\mu}(\vec{v}) + \xi^3\chi_{\lambda\mu}(\vec{v},\underline{\eta}) - (\xi^3)^2\kappa_{\lambda\mu}(\underline{\eta})]\, dV \\ & + \int_\Omega D^{\alpha\lambda}\zeta_\alpha(\vec{u},\underline{\theta})\,\zeta_\lambda(\vec{v},\underline{\eta})\, dV, \end{aligned} \tag{4.139}$$

and the linear function

$$F^B(\vec{v},\underline{\eta}) = \int_\Omega \vec{F}\cdot(\vec{v} + \xi^3\eta_\lambda\vec{a}^\lambda)\, dV. \tag{4.140}$$

By inspection, the natural displacement space for the basic shell model is the same as for the s-m-b model, namely

$$\boxed{\mathcal{V}^B = \big\{(\vec{v},\underline{\eta}) \in H^1(\mathcal{S}) \times H^1(\mathcal{S})\big\} \cap \mathcal{BC},} \tag{4.141}$$

and we also use the same norm, viz.

$$\|\vec{v},\underline{\eta}\|^2_{\mathcal{V}^B} = \|\vec{v}\|^2_{H^1(\mathcal{S})} + \|\underline{\eta}\|^2_{H^1(\mathcal{S})}. \tag{4.142}$$

In order to establish the well-posedness of the basic shell model, we need a number of preliminary results that relate 3D quantities to surface quantities.

Lemma 4.3.3. *There exist two strictly positive constants c and C such that, for any $(\xi^1, \xi^2, \xi^3) \in \Omega$,*

$$c\sqrt{a}(\xi^1, \xi^2) \leq \sqrt{g}(\xi^1, \xi^2, \xi^3) \leq C\sqrt{a}(\xi^1, \xi^2). \tag{4.143}$$

Proof. Directly inferred from (2.155) and (2.161). ∎

Lemma 4.3.4. *There exist two strictly positive constants c and C such that, for any $(\xi^1, \xi^2, \xi^3) \in \Omega$,*

$$\begin{aligned} c\, a^{\alpha\beta}(\xi^1, \xi^2)\, X_\alpha X_\beta \leq g^{\alpha\beta}(\xi^1, \xi^2, \xi^3)\, X_\alpha X_\beta \\ \leq C\, a^{\alpha\beta}(\xi^1, \xi^2)\, X_\alpha X_\beta,\ \forall (X_1, X_2) \in I\!R^2. \end{aligned} \tag{4.144}$$

Proof. Consider the function

$$(X_1, X_2; \xi^1, \xi^2, \xi^3) \in \mathcal{U}_2 \times \bar{\Omega} \mapsto \frac{g^{\alpha\beta}(\xi^1, \xi^2, \xi^3)\, X_\alpha X_\beta}{a^{\alpha\beta}(\xi^1, \xi^2)\, X_\alpha X_\beta}, \tag{4.145}$$

where $\mathcal{U}_2$ is the unit circle of $I\!R^2$. This function is well-defined (since the first fundamental form is positive definite over $\bar{\omega}$) and clearly continuous. Therefore, since it is defined over a compact set, it admits a minimum and a maximum value that we denote by c and C, respectively. The minimum value (in particular) is reached, hence it is strictly positive because $\underline{\underline{g}}$ is positive definite over $\bar{\Omega}$. Equation (4.144) follows with the same two constants c and C. ∎

Lemma 4.3.5. *There exist two strictly positive constants c and C such that, for any $(\xi^1, \xi^2, \xi^3) \in \Omega$,*

$$\begin{aligned} c\, a^{\alpha\lambda}(\xi^1, \xi^2) a^{\beta\mu}(\xi^1, \xi^2)\, Y_{\alpha\beta} Y_{\lambda\mu} \\ \leq g^{\alpha\lambda}(\xi^1, \xi^2, \xi^3) g^{\beta\mu}(\xi^1, \xi^2, \xi^3)\, Y_{\alpha\beta} Y_{\lambda\mu} \\ \leq C\, a^{\alpha\lambda}(\xi^1, \xi^2) a^{\beta\mu}(\xi^1, \xi^2)\, Y_{\alpha\beta} Y_{\lambda\mu}, \\ \forall (Y_{11}, Y_{12}, Y_{21}, Y_{22}) \in I\!R^4. \end{aligned} \tag{4.146}$$

Proof. Similar to that of Lemma 4.3.4. ∎

Proposition 4.3.5 *A^B is continuous, hence it is a bilinear form over the space $\mathcal{V}^B$. Moreover, assuming that the essential boundary conditions enforced in $\mathcal{V}^B$ are such that no rigid body motion is possible, i.e. the only element $(\vec{v}, \underline{\eta})$ in $\mathcal{V}^B$ satisfying (4.98) and (4.99) for some $(\vec{T}, \vec{R})$ is $(\vec{0}, \underline{0})$, then A^B is coercive over $\mathcal{V}^B$.*

Proof. We start by proving the coercivity of A^B. Consider any $(\vec{v}, \underline{\eta}) \in \mathcal{V}^B$. To make the equations more compact we write $\gamma_{\alpha\beta}$, $\chi_{\alpha\beta}$, $\kappa_{\alpha\beta}$ and ζ_α instead of $\gamma_{\alpha\beta}(\vec{v})$, $\chi_{\alpha\beta}(\vec{v}, \underline{\eta})$, $\kappa_{\alpha\beta}(\underline{\eta})$ and $\zeta_\alpha(\vec{v}, \underline{\eta})$, respectively. Recalling (4.28) and (4.29) and noting that, for any second order tensor $\underline{\underline{Y}}$, $g^{\alpha\beta} g^{\lambda\mu} Y_{\alpha\beta} Y_{\lambda\mu} = (g^{\alpha\beta} Y_{\alpha\beta})^2 \geq 0$, we have

$$\begin{aligned} A^B(\vec{v}, \underline{\eta}; \vec{v}, \underline{\eta}) \;\geq\; & \gamma \int_\Omega g^{\alpha\lambda} g^{\beta\mu} [\gamma_{\alpha\beta} + \xi^3 \chi_{\alpha\beta} - (\xi^3)^2 \kappa_{\alpha\beta}] \\ & \times [\gamma_{\lambda\mu} + \xi^3 \chi_{\lambda\mu} - (\xi^3)^2 \kappa_{\lambda\mu}] \, dV \\ & + \gamma \int_\Omega g^{\alpha\lambda} \zeta_\alpha \zeta_\lambda \, dV. \end{aligned} \tag{4.147}$$

Then, applying Lemmas 4.3.3, 4.3.4 and 4.3.5, we obtain

$$\begin{aligned} A^B(\vec{v}, \underline{\eta}; \vec{v}, \underline{\eta}) \;\geq\; & \gamma \int_\Omega a^{\alpha\lambda} a^{\beta\mu} [\gamma_{\alpha\beta} + \xi^3 \chi_{\alpha\beta} - (\xi^3)^2 \kappa_{\alpha\beta}] \\ & \times [\gamma_{\lambda\mu} + \xi^3 \chi_{\lambda\mu} - (\xi^3)^2 \kappa_{\lambda\mu}] \sqrt{a} \, d\xi^1 d\xi^2 d\xi^3 \\ & + \gamma \int_\Omega a^{\alpha\lambda} \zeta_\alpha \zeta_\lambda \sqrt{a} \, d\xi^1 d\xi^2 d\xi^3. \end{aligned} \tag{4.148}$$

Since the dependance on ξ^3 is explicit in the right-hand side of this inequality, we can perform a partial integration with respect to this variable across the thickness. We get

$$\begin{aligned} & A^B(\vec{v}, \underline{\eta}; \vec{v}, \underline{\eta}) \;\geq \\ & \gamma \int_\omega t \Big[a^{\alpha\lambda} a^{\beta\mu} \Big(\gamma_{\alpha\beta} \gamma_{\lambda\mu} + \frac{t^2}{12} \chi_{\alpha\beta} \chi_{\lambda\mu} - \frac{t^2}{6} \gamma_{\alpha\beta} \kappa_{\lambda\mu} + \frac{t^4}{80} \kappa_{\alpha\beta} \kappa_{\lambda\mu} \Big) \\ & \qquad + a^{\alpha\beta} \zeta_\alpha \zeta_\beta \Big] \, dS. \end{aligned} \tag{4.149}$$

For any strictly positive real r we have, using the Cauchy-Schwarz inequality,

$$
\begin{aligned}
|t^2 a^{\alpha\lambda} a^{\beta\mu} \gamma_{\alpha\beta} \kappa_{\lambda\mu}| &= |\langle \underline{\underline{\gamma}}, t^2 \underline{\underline{\kappa}} \rangle_{\mathcal{E}}| = |\langle \sqrt{r}\, \underline{\underline{\gamma}}, \frac{t^2}{\sqrt{r}} \underline{\underline{\kappa}} \rangle_{\mathcal{E}}| \\
&\leq \|\sqrt{r}\, \underline{\underline{\gamma}}\|_{\mathcal{E}} \| \frac{t^2}{\sqrt{r}} \underline{\underline{\kappa}} \|_{\mathcal{E}} \\
&\leq \frac{1}{2} (\|\sqrt{r}\, \underline{\underline{\gamma}}\|_{\mathcal{E}}^2 + \| \frac{t^2}{\sqrt{r}} \underline{\underline{\kappa}} \|_{\mathcal{E}}^2) \\
&\leq \frac{1}{2} (r \|\underline{\underline{\gamma}}\|_{\mathcal{E}}^2 + \frac{t^4}{r} \|\underline{\underline{\kappa}}\|_{\mathcal{E}}^2) \\
&\leq \frac{1}{2} a^{\alpha\lambda} a^{\beta\mu} (r \gamma_{\alpha\beta} \gamma_{\lambda\mu} + \frac{t^4}{r} \kappa_{\alpha\beta} \kappa_{\lambda\mu}) \qquad (4.150)
\end{aligned}
$$

Choosing $r = 10$, we obtain from (4.149)

$$
\begin{aligned}
& A^B(\vec{v}, \underline{\eta}; \vec{v}, \underline{\eta}) \\
&\geq \gamma \int_\omega t \big[a^{\alpha\lambda} a^{\beta\mu} (\frac{1}{6} \gamma_{\alpha\beta} \gamma_{\lambda\mu} + \frac{t^2}{12} \chi_{\alpha\beta} \chi_{\lambda\mu} + \frac{t^4}{240} \kappa_{\alpha\beta} \kappa_{\lambda\mu}) \\
&\qquad\qquad + a^{\alpha\beta} \zeta_\alpha \zeta_\beta \big]\, dS \\
&\geq \gamma \int_\omega t \big[a^{\alpha\lambda} a^{\beta\mu} (\frac{1}{6} \gamma_{\alpha\beta} \gamma_{\lambda\mu} + \frac{t^2}{12} \chi_{\alpha\beta} \chi_{\lambda\mu}) + a^{\alpha\beta} \zeta_\alpha \zeta_\beta \big]\, dS \\
&\geq \gamma\, (\|\underline{\underline{\gamma}}\|_{L^2(\mathcal{S})}^2 + \|\underline{\underline{\chi}}\|_{L^2(\mathcal{S})}^2 + \|\underline{\zeta}\|_{L^2(\mathcal{S})}^2), \qquad (4.151)
\end{aligned}
$$

since we have $t \geq t_{\min} > 0$ over the whole domain. The coercivity now directly follows from that of the s-m-b model, namely we can use step **ii)** of the proof of Proposition 4.3.2 (and more specifically Equation (4.114)) to complete the argument, since the spaces $\mathcal{V}^N$ and $\mathcal{V}^B$ (and their associated norms) are identical.

The continuity of A^B is established by similar (although simpler) arguments. ∎

Proposition 4.3.6 *Assuming $\vec{F} \in L^2(\mathcal{B})$, F^B is continuous, hence it is a linear form over $\mathcal{V}^B$.*

Proof. Using the Cauchy-Schwarz inequality and the triangle inequality in $L^2(\mathcal{B})$, we have, $\forall (\vec{v}, \underline{\eta}) \in \mathcal{V}^B$,

$$
\begin{aligned}
|F^B(\vec{v}, \underline{\eta})| &\leq \|\vec{F}\|_{L^2(\mathcal{B})} \|\vec{v} + \xi^3 \eta_\lambda \vec{a}^\lambda\|_{L^2(\mathcal{B})} \\
&\leq \|\vec{F}\|_{L^2(\mathcal{B})} (\|\vec{v}\|_{L^2(\mathcal{B})} + \|\xi^3 \eta_\lambda \vec{a}^\lambda\|_{L^2(\mathcal{B})}. \qquad (4.152)
\end{aligned}
$$

Note that $\vec{v}$ and $\xi^3\eta_\lambda\vec{a}^\lambda$ are in $L^2(\mathcal{B})$ since, with (4.143),

$$\int_\Omega \vec{v}^{\,2}\, dV \leq Ct_{\max}\int_\omega \vec{v}^{\,2}\, dS \tag{4.153}$$

and

$$\begin{aligned}\int_\Omega (\xi^3\eta_\lambda\vec{a}^\lambda)^2\, dV &= \int_\Omega (\xi^3)^2 a^{\lambda\mu}\eta_\lambda\eta_\mu\, dV \\ &\leq C(t_{\max})^3\int_\omega a^{\lambda\mu}\eta_\lambda\eta_\mu\, dS. \end{aligned}\tag{4.154}$$

Hence

$$\begin{aligned}|F^B(\vec{v},\underline{\eta})| &\leq C\|\vec{F}\|_{L^2(\mathcal{B})}(\|\vec{v}\|_{L^2(\mathcal{S})} + \|\underline{\eta}\|_{L^2(\mathcal{S})}) \\ &\leq C\|\vec{F}\|_{L^2(\mathcal{B})}\|\vec{v},\underline{\eta}\|_{\mathcal{V}^B}. \end{aligned}\tag{4.155}$$

■

We now can prove the well-posedness of the basic shell model.

Proposition 4.3.7 *Assume that:*

- $\vec{F} \in L^2(\mathcal{B})$*;*
- *the essential boundary conditions enforced in* $\mathcal{V}^B$ *are such that no rigid body motion is possible, i.e. the only element* $(\vec{v},\underline{\eta})$ *in* $\mathcal{V}^B$ *satisfying (4.98) and (4.99) for some* $(\vec{T},\vec{R})$ *is* $(\vec{0},\underline{0})$*.*

Then there is a unique $(\vec{u},\underline{\theta})$ *in* $\mathcal{V}^B$ *that satisfies*

$$A^B(\vec{u},\underline{\theta};\vec{v},\underline{\eta}) = F^B(\vec{v},\underline{\eta}), \tag{4.156}$$

for any $(\vec{v},\underline{\eta})$ *in* $\mathcal{V}^B$*, and we have*

$$\|\vec{u},\underline{\theta}\|_{\mathcal{V}^B} \leq C\|\vec{F}\|_{L^2(\mathcal{B})}. \tag{4.157}$$

Proof. Immediate from Propositions 4.3.5 and 4.3.6, using the Lax-Milgram Theorem (Prop. 3.2.1). ■

4.3.4 Analysis of the 3D-shell model

In order to analyze the 3D-shell model and in view of (4.76), we introduce the following bilinear function

$$A^{3Ds}(\vec{u},\vec{\theta},\vec{\varrho};\vec{v},\vec{\eta},\vec{\varsigma}) = \int_\Omega H^{ijkl} e_{ij}\big(\vec{u}+\xi^3\vec{\theta}+(\xi^3)^2\vec{\varrho}\big) e_{kl}\big(\vec{v}+\xi^3\vec{\eta}+(\xi^3)^2\vec{\varsigma}\big)\, dV, \tag{4.158}$$

and the linear function

$$F^{3Ds}(\vec{v},\vec{\eta},\vec{\varsigma}) = \int_\Omega \vec{F}\cdot\big(\vec{v}+\xi^3\vec{\eta}+(\xi^3)^2\vec{\varsigma}\big)\, dV. \tag{4.159}$$

Specifying the displacement space

$$\boxed{\mathcal{V}^{3Ds} = \big\{(\vec{v},\vec{\eta},\vec{\varsigma}) \in H^1(\mathcal{S})\times H^1(\mathcal{S})\times H^1(\mathcal{S})\big\} \cap \mathcal{BC},} \tag{4.160}$$

with the natural associated $H^1(\mathcal{S})$-norm, the variational problem (4.76) is clearly well-posed since it corresponds to a restriction of the variational space used in the original 3D problem – well-posed in H^1, see e.g. (Ciarlet, 1988). More specifically here, we can prove the following result.

Proposition 4.3.8 *Assume that:*

- $\vec{F} \in L^2(\mathcal{B})$*;*
- *the essential boundary conditions enforced in* $\mathcal{V}^{3Ds}$ *are such that no rigid body motion is possible, i.e. the only element* $(\vec{v},\vec{\eta},\vec{\varsigma})$ *in* $\mathcal{V}^{3Ds}$ *satisfying (4.98) and (4.99) for some* $(\vec{T},\vec{R})$ *is* $(\vec{0},\vec{0},\vec{0}\,)$*.*

Then there is a unique $(\vec{u},\vec{\theta},\vec{\varrho}\,)$ *in* $\mathcal{V}^{3Ds}$ *that satisfies*

$$A^{3Ds}(\vec{u},\vec{\theta},\vec{\varrho};\vec{v},\vec{\eta},\vec{\varsigma}) = F^{3Ds}(\vec{v},\vec{\eta},\vec{\varsigma}), \tag{4.161}$$

for any $(\vec{v},\vec{\eta},\vec{\varsigma})$ *in* $\mathcal{V}^{3Ds}$*, and we have*

$$\|\vec{u},\vec{\theta},\vec{\varrho}\,\|_1 \le C\|\vec{F}\|_{L^2(\mathcal{B})}. \tag{4.162}$$

Proof. The proof again relies on the continuities of A^{3Ds} and F^{3Ds}, and on the coercivity of A^{3Ds}. We start with establishing the latter, and to make the equations more compact we will write e_{ij} instead of $e_{ij}(\vec{v}+\xi^3\vec{\eta}+(\xi^3)^2\vec{\varsigma})$, and $\gamma_{\alpha\beta}$, $\hat{\chi}_{\alpha\beta}$, $k_{\alpha\beta}$, $l_{\alpha\beta}$, ζ_α, m_α, n_α, δ, p instead of $\gamma_{\alpha\beta}(\vec{v})$, $\hat{\chi}_{\alpha\beta}(\vec{v},\vec{\eta}\,)$, $k_{\alpha\beta}(\vec{\eta},\vec{\varsigma}\,)$,

$l_{\alpha\beta}(\vec{\varsigma})$, $\zeta_\alpha(\vec{v},\vec{\eta})$, $m_\alpha(\vec{\eta},\vec{\varsigma})$, $n_\alpha(\vec{\varsigma})$, $\delta(\vec{\eta})$ and $p(\vec{\varsigma})$, respectively. We decompose the coercivity argument into three steps.

i) We first show that

$$A^{3Ds}(\vec{v},\vec{\eta},\vec{\varsigma};\vec{v},\vec{\eta},\vec{\varsigma}) \geq \gamma\big(\|\underline{\underline{\gamma}}\|_0^2 + \|\underline{\underline{\hat{\chi}}}\|_0^2 + \|\underline{\underline{k}}\|_0^2 + \|\underline{\underline{l}}\|_0^2 + \|\underline{\varsigma}\|_0^2 + \|\underline{m}\|_0^2 + \|\underline{n}\|_0^2 + \|\delta\|_0^2 + \|p\|_0^2\big). \quad (4.163)$$

From (4.144) and (4.146), using $g^{ij}g^{kl}e_{ij}e_{kl} = (g^{ij}e_{ij})^2 \geq 0$, we have

$$\begin{aligned} A^{3Ds}(\vec{v},\vec{\eta},\vec{\varsigma};\vec{v},\vec{\eta},\vec{\varsigma}) &\geq \gamma\int_\Omega g^{ik}g^{jl}e_{ij}e_{kl}\,dV \\ &\geq \gamma\int_\Omega \big[g^{\alpha\lambda}g^{\beta\mu}e_{\alpha\beta}e_{\lambda\mu} + g^{\alpha\beta}e_{\alpha 3}e_{\beta 3} + (e_{33})^2\big]\,dV \\ &\geq \gamma\int_\Omega \big[a^{\alpha\lambda}a^{\beta\mu}e_{\alpha\beta}e_{\lambda\mu} + a^{\alpha\beta}e_{\alpha 3}e_{\beta 3} + (e_{33})^2\big]\,dV. \end{aligned} \quad (4.164)$$

Using now (4.143), then (4.74), and integrating through the thickness, we obtain

$$\begin{aligned} A^{3Ds}(\vec{v},\vec{\eta},\vec{\varsigma};\vec{v},\vec{\eta},\vec{\varsigma}) \geq \gamma\int_\omega t\Big\{ & a^{\alpha\lambda}a^{\beta\mu}[\gamma_{\alpha\beta}\gamma_{\lambda\mu} + \frac{t^2}{12}\hat{\chi}_{\alpha\beta}\hat{\chi}_{\lambda\mu} + \frac{t^2}{6}\gamma_{\alpha\beta}k_{\lambda\mu} \\ & + \frac{t^4}{80}k_{\alpha\beta}k_{\lambda\mu} + \frac{t^4}{40}l_{\alpha\beta}\hat{\chi}_{\lambda\mu} + \frac{t^6}{448}l_{\alpha\beta}l_{\lambda\mu}] \\ & + a^{\alpha\beta}[\zeta_\alpha\zeta_\beta + \frac{t^2}{12}m_\alpha m_\beta + \frac{t^2}{6}\zeta_\alpha n_\beta + \frac{t^4}{80}n_\alpha n_\beta] \\ & + [\delta^2 + \frac{t^2}{12}p^2]\Big\}\,dS. \end{aligned} \quad (4.165)$$

By the inequality (B.1), we then have

$$\begin{aligned} |\frac{t^2}{6}a^{\alpha\lambda}a^{\beta\mu}\gamma_{\alpha\beta}k_{\lambda\mu}| &= \frac{1}{6}|\langle\underline{\underline{\gamma}}, t^2\underline{\underline{k}}\rangle_{\mathcal{E}}| \\ &\leq \frac{1}{12}\big(r_1\|\underline{\underline{\gamma}}\|_{\mathcal{E}}^2 + \frac{t^4}{r_1}\|\underline{\underline{k}}\|_{\mathcal{E}}^2\big) \\ &\leq \frac{1}{12}a^{\alpha\lambda}a^{\beta\mu}(r_1\gamma_{\alpha\beta}\gamma_{\lambda\mu} + \frac{t^4}{r_1}k_{\alpha\beta}k_{\lambda\mu}), \end{aligned} \quad (4.166)$$

and similarly

$$|\frac{t^4}{40}a^{\alpha\lambda}a^{\beta\mu}l_{\alpha\beta}\hat{\chi}_{\lambda\mu}| \leq \frac{1}{80}a^{\alpha\lambda}a^{\beta\mu}(r_2t^6l_{\alpha\beta}l_{\lambda\mu} + \frac{t^2}{r_2}\hat{\chi}_{\alpha\beta}\hat{\chi}_{\lambda\mu}), \quad (4.167)$$

$$|\frac{t^2}{6}a^{\alpha\beta}\zeta_\alpha n_\beta| \leq \frac{1}{12}a^{\alpha\beta}(r_3\zeta_\alpha\zeta_\beta + \frac{t^4}{r_3}n_\alpha n_\beta), \tag{4.168}$$

with r_1, r_2, r_3 arbitrary strictly positive constants. With an appropriate choice for these constants – for example $r_1 = 10$, $r_2 = \frac{6}{35}$, $r_3 = 10$ – and recalling that $t \geq t_{\min} > 0$, Equation (4.165) gives

$$A^{3Ds}(\vec{v},\vec{\eta},\vec{\varsigma};\vec{v},\vec{\eta},\vec{\varsigma}) \geq \gamma \int_\omega \{a^{\alpha\lambda}a^{\beta\mu}[\gamma_{\alpha\beta}\gamma_{\lambda\mu} + \hat{\chi}_{\alpha\beta}\hat{\chi}_{\lambda\mu} + k_{\alpha\beta}k_{\lambda\mu} + l_{\alpha\beta}l_{\lambda\mu}]$$
$$+a^{\alpha\beta}[\zeta_\alpha\zeta_\beta + m_\alpha m_\beta + n_\alpha n_\beta] + [\delta^2 + p^2]\}\, dS, \tag{4.169}$$

namely, we have (4.163).
ii) Denoting

$$\|\eta_3,\vec{\varsigma}\|_\# = \Big(\|\underline{m}(\vec{\eta},\vec{\varsigma})\|_0^2 + \|\underline{n}(\vec{\varsigma})\|_0^2 + \|\underline{\underline{k}}\big((\underline{0},\eta_3),\vec{\varsigma}\big)\|_0^2 + \|\delta(\vec{\eta})\|_0^2 + \|p(\vec{\varsigma})\|_0^2\Big)^{1/2},$$

we now show that $\|\cdot\|_\#$ provides a norm equivalent to the H^1-norm (i.e. the norm prevailing in $\mathcal{V}^{3Ds}$) over the subspace of $\mathcal{V}^{3Ds}$ of displacements of the type $(\vec{0},\underline{0},\eta_3,\vec{\varsigma})$. First, in order to see that $\|\cdot\|_\#$ gives a norm, we observe that from $\delta(\vec{\eta}) = 0$ and $p(\vec{\varsigma}) = 0$ we obtain $\eta_3 = 0$ and $\varsigma_3 = 0$, respectively. Then, from $\underline{m}(\vec{\eta},\vec{\varsigma}) = 0$ and $\eta_3 = 0$ we have $\underline{\varsigma} = \underline{0}$. Bounding this norm as in

$$\|\eta_3,\vec{\varsigma}\|_\# \leq C\|\eta_3,\vec{\varsigma}\|_1 \tag{4.170}$$

is straightforward, hence to prove the equivalence it remains to show that we have the other inequality

$$\|\eta_3,\vec{\varsigma}\|_\# \geq \gamma\|\eta_3,\vec{\varsigma}\|_1. \tag{4.171}$$

To that purpose, we use the Korn inequality (4.95). We then have, from (4.75),

$$\begin{aligned}
|\underline{\varsigma}|_1^2 &\leq C(\|\underline{\underline{\epsilon}}(\underline{\varsigma})\|_0^2 + \|\underline{\varsigma}\|_0^2)\\
&\leq C(\|\underline{\underline{k}}\big((\underline{0},\eta_3),\vec{\varsigma}\big)\|_0^2 + \|\underline{b}\varsigma_3\|_0^2 + \|\underline{c}\eta_3\|_0^2 + \|\underline{\varsigma}\|_0^2)\\
&\leq C(\|\underline{\underline{k}}\big((\underline{0},\eta_3),\vec{\varsigma}\big)\|_0^2 + \|\varsigma_3\|_0^2 + \|\eta_3\|_0^2 + \|\underline{\varsigma}\|_0^2).
\end{aligned} \tag{4.172}$$

In addition, from the definitions of $\underline{n}$ and $\underline{m}$ in (4.75) we have

$$|\varsigma_3|_1^2 \leq C(\|\underline{n}(\vec{\varsigma})\|_0^2 + \|\underline{\varsigma}\|_0^3), \tag{4.173}$$

$$|\eta_3|_1^2 \leq C(\|\underline{m}(\vec{\eta},\vec{\varsigma})\|_0^2 + \|\underline{\varsigma}\|_0^2). \tag{4.174}$$

Gathering Eqs. (4.172)–(4.174), we obtain

$$\begin{aligned}\|\eta_3,\vec{\varsigma}\|_1^2 &\leq C(\|\underline{m}(\vec{\eta},\vec{\varsigma})\|_0^2+\|\underline{\underline{k}}\big((\underline{0},\eta_3),\vec{\varsigma}\big)\|_0^2\\ &\qquad +\|\underline{n}(\vec{\varsigma})\|_0^2+\|\varsigma_3\|_0^2+\|\eta_3\|_0^2+\|\underline{\varsigma}\|_0^2)\\ &\leq C(\|\eta_3,\vec{\varsigma}\|_{\#}^2+\|\eta_3,\vec{\varsigma}\|_0^2). \end{aligned}\tag{4.175}$$

Finally, in order to show that we can dispense with the L^2-norm term in the right-hand side of this inequality, we invoke the standard contradiction argument already used in the proof of Proposition 4.3.2.

iii) Coercivity bound.

We will repeatedly use the following basic inequality, directly inferred from (B.1) and valid for any norm and any (fixed) real number α,

$$\|\vec{v}_1+\alpha\vec{v}_2\|^2+\|\vec{v}_2\|^2\geq\gamma(\|\vec{v}_1\|^2+\|\vec{v}_2\|^2).\tag{4.176}$$

Using this inequality we obtain

$$\begin{aligned}\|\underline{\underline{\hat{\chi}}}(\vec{v},\vec{\eta})\|_0^2+\|\delta(\vec{\eta})\|_0^2 &= \|\underline{\underline{\hat{\chi}}}\big(\vec{v},(\underline{\eta},0)\big)-\underline{\underline{b}}\eta_3\|_0^2+\|\eta_3\|_0^2\\ &\geq \gamma(\|\underline{\underline{\hat{\chi}}}\big(\vec{v},(\underline{\eta},0)\big)\|_0^2+\|\eta_3\|_0^2),\end{aligned}\tag{4.177}$$

hence,

$$\begin{aligned}&\|\underline{\underline{\gamma}}(\vec{v})\|_0^2+\|\underline{\underline{\hat{\chi}}}(\vec{v},\vec{\eta})\|_0^2+\|\underline{\varsigma}(\vec{v},\vec{\eta})\|_0^2+\|\delta(\vec{\eta})\|_0^2\\ &\qquad\geq\gamma\Big(\|\underline{\underline{\gamma}}(\vec{v})\|_0^2+\|\underline{\varsigma}(\vec{v},\vec{\eta})\|_0^2+\|\underline{\underline{\hat{\chi}}}\big(\vec{v},(\underline{\eta},0)\big)\|_0^2+\|\eta_3\|_0^2\Big)\\ &\qquad\geq\gamma\Big(\|\vec{v},\underline{\eta}\|_1^2+\|\eta_3\|_0^2\Big),\end{aligned}\tag{4.178}$$

where the last inequality directly follows from the coercivity of the bilinear form A^N in the s-m-b model, recall Proposition 4.3.2. Furthermore,

$$\|\underline{\underline{k}}(\vec{\eta},\vec{\varsigma})\|_0^2+|\underline{\eta}|_1^2\geq\gamma\Big(\|\underline{\underline{k}}\big((\underline{0},\eta_3),\vec{\varsigma}\big)\|_0^2+|\underline{\eta}|_1^2\Big),\tag{4.179}$$

hence,

$$\begin{aligned}&\|\underline{\underline{k}}(\vec{\eta},\vec{\varsigma})\|_0^2+|\underline{\eta}|_1^2+\|\underline{m}(\vec{\eta},\vec{\varsigma})\|_0^2+\|\underline{n}(\vec{\varsigma})\|_0^2+\|\delta(\vec{\eta})\|_0^2+\|p(\vec{\varsigma})\|_0^2\\ &\geq\ \gamma\Big(\|\underline{\underline{k}}\big((\underline{0},\eta_3),\vec{\varsigma}\big)\|_0^2+\|\underline{m}(\vec{\eta},\vec{\varsigma})\|_0^2+\|\underline{n}(\vec{\varsigma})\|_0^2+\|\delta(\vec{\eta})\|_0^2+\|p(\vec{\varsigma})\|_0^2+|\underline{\eta}|_1^2\Big)\\ &=\ \gamma\Big(\|\eta_3,\vec{\varsigma}\|_{\#}^2+|\underline{\eta}|_1^2\Big)\\ &\geq\ \gamma\big(\|\eta_3,\vec{\varsigma}\|_1^2+|\underline{\eta}|_1^2\Big).\end{aligned}\tag{4.180}$$

Therefore, from (4.163), (4.178) and (4.180), we have

$$\begin{aligned} A^{3Ds}(\vec{v},\vec{\eta},\vec{\varsigma};\vec{v},\vec{\eta},\vec{\varsigma}) &\geq \gamma\big(\|\underline{\underline{\gamma}}\|_0^2 + \|\underline{\underline{\hat{\chi}}}\|_0^2 + \|\underline{\varsigma}\|_0^2 + \|\delta\|_0^2 \\ &\qquad + \|\underline{\underline{k}}\|_0^2 + \|\underline{m}\|_0^2 + \|\underline{n}\|_0^2 + \|p\|_0^2\big) \\ &\geq \gamma(\|\vec{v},\underline{\eta}\|_1^2 + \|\eta_3\|_0^2 + \|\underline{\underline{k}}\|_0^2 + \|\underline{m}\|_0^2 + \|\underline{n}\|_0^2 + \|p\|_0^2) \\ &\geq \gamma(\|\vec{v},\underline{\eta}\|_1^2 + \|\eta_3,\vec{\varsigma}\|_1^2) = \gamma\|\vec{v},\vec{\eta},\vec{\varsigma}\|_1^2. \end{aligned} \tag{4.181}$$

iv) Completion of the proof.
The continuity of the bilinear form is obtained by similar – although much more straightforward arguments. To obtain the *a priori* estimate (4.162) we use the continuity of F^{3Ds}, which gives for any $(\vec{v},\vec{\eta},\vec{\varsigma}) \in \mathcal{V}$

$$\begin{aligned} \Big|\int_\Omega \vec{F}\cdot(\vec{v}+\xi^3\vec{\eta}+(\xi^3)^2\vec{\varsigma})dV\Big| &\leq \|\vec{F}\|_{L^2(\mathcal{B})}\|\vec{v}+\xi^3\vec{\eta}+(\xi^3)^2\vec{\varsigma}\|_{L^2(\mathcal{B})} \\ &\leq C\|\vec{F}\|_{L^2(\mathcal{B})}\|\vec{v},\vec{\eta},\vec{\varsigma}\|_0. \end{aligned} \tag{4.182}$$

Then, from the H^1-coercivity of A^{3Ds} we infer

$$\begin{aligned} \gamma\|\vec{u},\vec{\theta},\vec{\varrho}\|_1^2 &\leq A^{3Ds}(\vec{u},\vec{\theta},\vec{\varrho};\vec{u},\vec{\theta},\vec{\varrho}) \\ &= F^{3Ds}(\vec{u},\vec{\theta},\vec{\varrho}) \leq C\|\vec{F}\|_{L^2(\mathcal{B})}\|\vec{u},\vec{\theta},\vec{\varrho}\|_0, \end{aligned} \tag{4.183}$$

and the *a priori* estimate directly follows. ∎

Remark 4.3.5. The assumptions on the loading used in the main results of this section (Prop. 4.3.3, 4.3.4, 4.3.7 and 4.3.8) are *sufficient* conditions for the corresponding variational formulations to be well-posed. More generally it is clear that any loading that provides a linear form over the functional space considered in each case also gives a well-posed problem. For example a transverse point-load is admissible for the m-b model since transverse displacements are then in H^2 for which pointwise values are meaningful, see Section 3.1.2. For the s-m-b model, however, point-loads are not admissible (since the displacement space is only H^1), namely, they do not give rise to solutions with finite energies. ∎

5. Asymptotic Behaviors of Shell Models

Implicit in the concept of a "shell" is the idea that the thickness is "small" compared to the other two dimensions. In practice, it is not unusual to deal with structures for which the thickness is smaller by several orders of magnitude, in which case the shell is said to be "thin" (consider, for example, the shell body of a motor car). Considering the role of the thickness parameter t in the shell models that we presented in the previous chapter (see for example Eqs. (4.36) and (4.51)), with different powers of t in the bilinear terms on the left-hand side, it is essential to determine how the mathematical properties and physical behaviors of the models are affected when this parameter becomes small. In particular, it is important to know whether the model converges, in some sense to be specified, towards a limit model when the thickness t "tends to zero", i.e. we need to study the *asymptotic behavior* of the shell models. When such convergence occurs, a possibly simpler limit model can sometimes be used instead of the original one when t is sufficiently small, but more generally, the issues discussed below are important.

The asymptotic behaviors of shell models display succinctly the shell structural behavior when the thickness becomes small – or in practice actually is small – and can dramatically differ depending on various factors, and in particular on the shell shape and boundary conditions. The impact of boundary conditions is exemplified in the static deformation cases shown in Figure 5.1, between which only the location of the boundary conditions is changed. One should note the dramatic difference in the orders of magnitude of the resulting displacements – the plotting amplification factor being given in each case in the figure. In order to understand such complex and important phenomena, asymptotic behaviors must be discussed.

Moreover, our goal is to investigate the influence of the thickness on the convergence of finite element methods, as we want to be able to identify numerical procedures for which there is no deterioration of convergence when the thickness becomes small. To that purpose, the analysis of the asymptotic behaviors of mathematical shell models clearly also represents a crucial prerequisite on which we concentrate in this chapter, whereas the issues arising in the finite element solutions themselves are addressed in the next chapters.

D. Chapelle, K.-J. Bathe, *The Finite Element Analysis of Shells – Fundamentals*,
Computational Fluid and Solid Mechanics, 2nd ed., DOI 10.1007/978-3-642-16408-8_5,

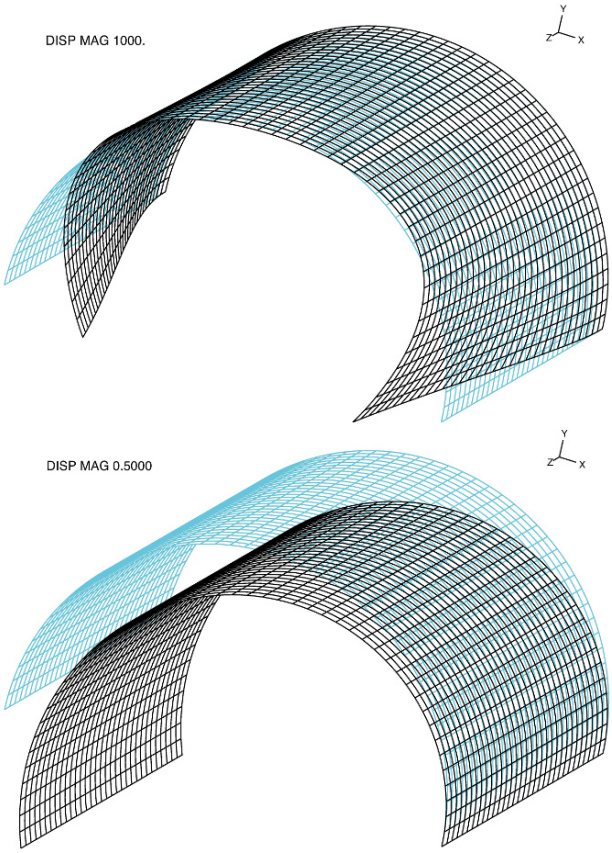

Fig. 5.1. Cylindrical structures loaded by self-weight – Steel material constants – Thickness/length ratio $2.5\,10^{-3}$ (dark grid represents deformed configuration). Top structure fixed on circular boundary – Bottom structure fixed on straight lateral boundary

5.1 General Asymptotic Analysis

We call L an overall characteristic dimension of the shell structure. We now define

$$\boxed{\varepsilon = \frac{t_{\min}}{L},} \tag{5.1}$$

where we recall that $t_{\min}$ denotes the minimum thickness over the whole surface. We then define

$$l = \frac{t}{\varepsilon}\ (= \frac{t}{t_{\min}} L). \tag{5.2}$$

Note that l varies over the surface when the thickness is not constant, and that

$$\min_{(\xi^1,\xi^2)\in\bar{\omega}} l(\xi^1,\xi^2) = L. \tag{5.3}$$

Namely, the quantity l is a scaled representation of the thickness defined so that its minimum is exactly equal to a given value L. Of course, when the thickness is constant l is also constant and of value L. We call l the *thickness profile*. If we now vary ε while keeping l fixed, we can define a family of shell structures that share the same midsurface and the same thickness profile (i.e. the ratio of thicknesses at two given points is the same), but for which the thickness is scaled by a global value corresponding to ε. These definitions thus allow us, in particular, to consider sequences of problems for which the overall thickness becomes smaller and smaller while the thickness profile is kept constant (as well as the midsurface), simply by making ε tend to zero.

Considering the s-m-b model (4.36) and the m-b model (4.51), we observe that these models can both be described by the following general variational formulation:
Find $U^\varepsilon \in \mathcal{V}$ *such that*

$$\boxed{\varepsilon^3 A_{\rm b}(U^\varepsilon, V) + \varepsilon A_{\rm m}(U^\varepsilon, V) = F^\varepsilon(V), \qquad \forall V \in \mathcal{V}.} \tag{5.4}$$

The meaning of the symbols appearing in this formulation is:

- U^ε: the unknown solution, namely the displacement of the midsurface for the m-b model, or this displacement *and* the rotation of the normal fiber for the s-m-b model;
- $\mathcal{V}$: the Sobolev space in which we seek the solution (we recall that the definition of this space takes into account the essential boundary conditions);
- V: a test function;
- $A_{\rm b}$: a scaled representation of the bending energy;
- $A_{\rm m}$: a scaled representation of the membrane energy for the m-b model, or of the membrane energy *and* of the shear energy for the s-m-b model;
- $F^\varepsilon(V)$: the external virtual work associated with V.

Namely, for the s-m-b model, we have

$$A^N(\vec{u},\underline{\theta};\vec{v},\underline{\eta}) = \varepsilon^3 A^N_{\rm b}(\vec{u},\underline{\theta};\vec{v},\underline{\eta}) + \varepsilon A^N_{\rm m}(\vec{u},\underline{\theta};\vec{v},\underline{\eta}), \tag{5.5}$$

with

$$A^N_{\rm b}(\vec{u},\underline{\theta};\vec{v},\underline{\eta}) = \int_\omega \frac{l^3}{12}\, {}^0C^{\alpha\beta\lambda\mu}\chi_{\alpha\beta}(\vec{u},\underline{\theta})\chi_{\lambda\mu}(\vec{v},\underline{\eta})\, dS, \tag{5.6}$$

$$A_{\rm m}^N(\vec{u},\underline{\theta};\vec{v},\underline{\eta}) =$$

$$\int_\omega l\,[{}^0C^{\alpha\beta\lambda\mu}\gamma_{\alpha\beta}(\vec{u})\gamma_{\lambda\mu}(\vec{v}) + {}^0D^{\alpha\lambda}\zeta_\alpha(\vec{u},\underline{\theta})\zeta_\lambda(\vec{v},\underline{\eta})]\,dS, \tag{5.7}$$

and for the m-b model

$$A^K(\vec{u};\vec{v}) = \varepsilon^3 A_{\rm b}^K(\vec{u};\vec{v}) + \varepsilon A_{\rm m}^N(\vec{u};\vec{v}), \tag{5.8}$$

with

$$A_{\rm b}^K(\vec{u};\vec{v}) = \int_\omega \frac{l^3}{12}\,{}^0C^{\alpha\beta\lambda\mu}\bar{\rho}_{\alpha\beta}(\vec{u})\bar{\rho}_{\lambda\mu}(\vec{v})\,dS, \tag{5.9}$$

$$A_{\rm m}^K(\vec{u};\vec{v}) = \int_\omega l\,{}^0C^{\alpha\beta\lambda\mu}\gamma_{\alpha\beta}(\vec{u})\gamma_{\lambda\mu}(\vec{v})\,dS. \tag{5.10}$$

Note that – in (5.4) – we indexed the unknown solution with ε, meaning that we consider the sequence of problems obtained when ε varies, which is the basis of the asymptotic analysis that we want to perform. We further emphasize that *the bilinear forms $A_{\rm b}$ and $A_{\rm m}$ depend only on the thickness profile l and not on the overall thickness parameter ε*. In addition, we also introduced ε as a superscript in the right-hand side of the formulation because it is likely to be impossible to obtain a well-posed asymptotic behavior while keeping the loading constant over the whole sequence of problems. More specifically, what we will be looking for in the asymptotic analysis is a scaling of the right-hand side in the form

$$\boxed{F^\varepsilon(V) = \varepsilon^\rho G(V),} \tag{5.11}$$

where G is an element of $\mathcal{V}'$ *independent of* ε and ρ is a real number, for which the scaled external work $G(U^\varepsilon)$ converges to a *finite and non-zero* limit when ε tends to zero. In this case, we will say that the given scaling provides an *admissible asymptotic behavior*. Of course, this is equivalent to requiring that the scaled internal work $\varepsilon^{3-\rho}A_{\rm b}(U^\varepsilon,U^\varepsilon) + \varepsilon^{1-\rho}A_{\rm m}(U^\varepsilon,U^\varepsilon)$ have a finite non-zero limit, since

$$\varepsilon^{3-\rho}A_{\rm b}(U^\varepsilon,U^\varepsilon) + \varepsilon^{1-\rho}A_{\rm m}(U^\varepsilon,U^\varepsilon) = G(U^\varepsilon). \tag{5.12}$$

Remark 5.1.1. In some cases the convergence may be such that U^ε tends to some limit in $\mathcal{V}$, but we want to allow for more general situations in which a weaker convergence property may hold energy-wise. ■

Remark 5.1.2. The search for a scaling of the loading that provides a definite (scaled) energy limit for the sequence of problems is very relevant for practical

purposes, as it gives most valuable information on the order of magnitude of loads that a thin shell structure may sustain (while of course remaining in the linear regime). ■

Of course, since our objective is to precisely identify the influence of ε on the solutions, all the constants (in particular those denoted by the symbols C and γ) that we use in this chapter must be understood as *constants independent of* ε. Also, we assume that the essential boundary conditions are prescribed in such a way that no rigid body motion is allowed, hence the shell model gives a well-posed problem for any value of ε (see Chapter 4).

The following result shows that the above-proposed objective of finding a given asymptotic scaling is meaningful (see also Blouza et al., 1999; Baiocchi & Lovadina, 2002).

Proposition 5.1.1 *For a given G in $\mathcal{V}'$, there is at most one real exponent ρ for which the corresponding scaling provides an admissible asymptotic behavior. In addition, if such a number exists we have*

$$\boxed{1 \leq \rho \leq 3.} \tag{5.13}$$

Before proving this proposition we establish the following two lemmas.

Lemma 5.1.1. *For the bilinear forms that correspond to the s-m-b and m-b models, there exist strictly positive constants c and C such that*

$$c\|V\|_{\mathcal{V}}^2 \leq A_{\mathrm{b}}(V,V) + A_{\mathrm{m}}(V,V) \leq C\|V\|_{\mathcal{V}}^2 \qquad \forall V \in \mathcal{V}. \tag{5.14}$$

Proof of Lemma 5.1.1. When we proved the boundedness and the coercivity of the bilinear forms corresponding to the s-m-b model (see Prop. 4.3.1 and Prop. 4.3.2) and to the m-b model (see Prop. 4.3.4), the thickness appeared as a distributed parameter for which the final result depended only on the condition

$$t_{\min} > 0. \tag{5.15}$$

Hence, we can apply these arguments for $\varepsilon = 1$, namely for $t = l$ (although this does not correspond to a physically acceptable value of the thickness, of course). We thus obtain the inequalities (5.14) and, since $\|V\|_{\mathcal{V}}$ and $A_{\mathrm{b}}(V,V) + A_{\mathrm{m}}(V,V)$ are thickness-independent quantities, we infer that c and C are thickness-independent too. ■

Proof of Proposition 5.1.1. Consider first two real numbers ρ_1 and ρ_2 – corresponding to the two sequences (U_1^ε) and (U_2^ε), respectively – such that

both $G(U_1^\varepsilon)$ and $G(U_2^\varepsilon)$ have finite non-zero limits. Due to the linearity of Problem (5.4), we have

$$\varepsilon^3 A_{\rm b}(\frac{U_1^\varepsilon}{\varepsilon^{\rho_1}}, V) + \varepsilon A_{\rm m}(\frac{U_1^\varepsilon}{\varepsilon^{\rho_1}}, V) = G(V), \qquad \forall V \in \mathcal{V}, \tag{5.16}$$

and also

$$\varepsilon^3 A_{\rm b}(\frac{U_2^\varepsilon}{\varepsilon^{\rho_2}}, V) + \varepsilon A_{\rm m}(\frac{U_2^\varepsilon}{\varepsilon^{\rho_2}}, V) = G(V), \qquad \forall V \in \mathcal{V}. \tag{5.17}$$

Hence, due to the existence and uniqueness of the shell model solutions,

$$\frac{U_1^\varepsilon}{\varepsilon^{\rho_1}} = \frac{U_2^\varepsilon}{\varepsilon^{\rho_2}}. \tag{5.18}$$

Therefore

$$\frac{G(U_1^\varepsilon)}{\varepsilon^{\rho_1}} = \frac{G(U_2^\varepsilon)}{\varepsilon^{\rho_2}}, \tag{5.19}$$

and the existence of non-zero finite limits for *both* $G(U_1^\varepsilon)$ and $G(U_2^\varepsilon)$ implies $\rho_1 = \rho_2$ (consider for example $G(U_1^\varepsilon) = \varepsilon^{\rho_1 - \rho_2} G(U_2^\varepsilon)$).

Then, consider the sequence (U^ε) corresponding to some $\rho > 3$. As soon as $\varepsilon \leq 1$, using (5.14) we obtain

$$\begin{aligned} \varepsilon^3 \|U^\varepsilon\|_{\mathcal{V}}^2 &\leq C\varepsilon^3 [A_{\rm b}(U^\varepsilon, U^\varepsilon) + A_{\rm m}(U^\varepsilon, U^\varepsilon)] \\ &\leq C[\varepsilon^3 A_{\rm b}(U^\varepsilon, U^\varepsilon) + \varepsilon A_{\rm m}(U^\varepsilon, U^\varepsilon)] = C\varepsilon^\rho G(U^\varepsilon) \\ &\leq C\varepsilon^\rho \|U^\varepsilon\|_{\mathcal{V}}. \end{aligned} \tag{5.20}$$

Dividing both sides by $\varepsilon^3 \|U^\varepsilon\|_{\mathcal{V}}$, we obtain

$$\|U^\varepsilon\|_{\mathcal{V}} \leq C\varepsilon^{\rho-3}, \tag{5.21}$$

which implies that U^ε converges strongly to 0 in $\mathcal{V}$, hence $G(U^\varepsilon)$ tends to zero and therefore the chosen scaling does not provide an admissible asymptotic behavior.

Consider finally the sequence (U^ε) corresponding to some $\rho < 1$. We take an element $\tilde{V} \in \mathcal{V}$ such that $G(\tilde{V}) \neq 0$ (such an element exists since G is not the zero linear form). Then, taking $\tilde{V}$ as the test function in (5.4) and using triangle and Cauchy-Schwarz inequalities, we obtain

$$\begin{aligned} &\varepsilon^\rho |G(\tilde{V})| \\ &\quad \leq \varepsilon \big[\varepsilon^2 |A_{\rm b}(U^\varepsilon, \tilde{V})| + |A_{\rm m}(U^\varepsilon, \tilde{V})|\big] \\ &\quad \leq \varepsilon \sqrt{\varepsilon^2 A_{\rm b}(U^\varepsilon, U^\varepsilon) + A_{\rm m}(U^\varepsilon, U^\varepsilon)} \sqrt{\varepsilon^2 A_{\rm b}(\tilde{V}, \tilde{V}) + A_{\rm m}(\tilde{V}, \tilde{V})} \end{aligned} \tag{5.22}$$

Therefore, recalling (5.12), we have

$$G(U^\varepsilon) \geq \varepsilon^{\rho-1} \frac{[G(\tilde{V})]^2}{\varepsilon^2 A_{\rm b}(\tilde{V},\tilde{V}) + A_{\rm m}(\tilde{V},\tilde{V})}, \tag{5.23}$$

When ε tends to zero, the denominator of the expression in the right-hand side tends to $A_{\rm m}(\tilde{V},\tilde{V}) \geq 0$. Therefore, since $\rho < 1$ the whole expression tends to infinity when ε tends to zero, hence so does $G(U^\varepsilon)$. This shows that such a scaling cannot provide an admissible asymptotic behavior. ■

Of course, due to the symmetry of the bilinear forms in consideration, the solution of the variational problem (5.4) is also the solution of the minimization problem

$$\mathcal{E}^\varepsilon(U^\varepsilon) = \min_{V\in\mathcal{V}} \mathcal{E}^\varepsilon(V), \tag{5.24}$$

with

$$\mathcal{E}^\varepsilon(V) = \frac{\varepsilon^3}{2} A_{\rm b}(V,V) + \frac{\varepsilon}{2} A_{\rm m}(V,V) - F^\varepsilon(V). \tag{5.25}$$

Clearly, for a scaling of the loading – corresponding to a given power ρ – such that $G(U^\varepsilon)$ has a finite non-zero limit, we will have

$$\mathcal{E}^\varepsilon(U^\varepsilon) = O(\varepsilon^\rho), \tag{5.26}$$

and, as a result of Proposition 5.1.1, we know that ρ must lie between 1 and 3. In order to determine which specific scaling may work, it will be important to consider a specific subspace characterized in the following Lemma.

Lemma 5.1.2. *The set defined by*

$$\boxed{\mathcal{V}_0 = \{V \in \mathcal{V} \mid A_{\rm m}(V,V) = 0\},} \tag{5.27}$$

is a closed subspace of $\mathcal{V}$. Also, $\mathcal{V}_0$ is a proper subspace, namely

$$\mathcal{V}_0 \neq \mathcal{V}. \tag{5.28}$$

Proof. If V is in $\mathcal{V}_0$, then for any real λ

$$A_{\rm m}(\lambda V, \lambda V) = \lambda^2 A_{\rm m}(V,V) = 0, \tag{5.29}$$

hence λV is in $\mathcal{V}_0$ too. Then, if V_1 and V_2 are in $\mathcal{V}_0$,

$$A_{\rm m}(V_1+V_2,V_1+V_2)=A_{\rm m}(V_1,V_1)+2A_{\rm m}(V_1,V_2)+A_{\rm m}(V_2,V_2)=0, \quad (5.30)$$

since by the Cauchy-Schwarz inequality

$$|A_{\rm m}(V_1,V_2)|\le\sqrt{A_{\rm m}(V_1,V_1)}\sqrt{A_{\rm m}(V_2,V_2)}. \quad (5.31)$$

Therefore $\mathcal{V}_0$ is a subspace of $\mathcal{V}$. In order to show that it is closed, we consider a sequence (V_n) of elements of $\mathcal{V}_0$ that converges to some limit $\bar{V}$ in $\mathcal{V}$. A bilinear form is continuous as a function of two variables, hence $A_{\rm m}(V_n,V_n)$ (which equals zero for any n) converges to $A_{\rm m}(\bar{V},\bar{V})$. Therefore $A_{\rm m}(\bar{V},\bar{V})=0$, i.e. $\bar{V}\in\mathcal{V}_0$, and since this holds for *any* converging sequence closedness follows. Finally, of course for the shell models considered we do not have $A_{\rm m}(V,V)=0$ for all $V\in\mathcal{V}$, hence $\mathcal{V}_0$ is a proper subspace. ∎

The displacement fields that belong to the subspace $\mathcal{V}_0$ have zero membrane energy, and also zero shear energy in the case of the s-m-b model. Therefore, they only give rise to bending energy, and for this reason $\mathcal{V}_0$ is called the *subspace of pure-bending displacements*. We can now use this subspace to infer from (5.24)-(5.25)

$$\mathcal{E}^\varepsilon(U^\varepsilon)\le\min_{V\in\mathcal{V}_0}\mathcal{E}^\varepsilon(V)=\min_{V\in\mathcal{V}_0}\{\frac{\varepsilon^3}{2}A_{\rm b}(V,V)-\varepsilon^\rho G(V)\}=-\frac{\varepsilon^\rho}{2}G(\tilde{U}), \quad (5.32)$$

where $\tilde{U}$ is the element of $\mathcal{V}_0$ that satisfies

$$\varepsilon^3A_{\rm b}(\tilde{U},V)=\varepsilon^\rho G(V),\qquad\forall V\in\mathcal{V}_0. \quad (5.33)$$

Hence we have $\tilde{U}=\varepsilon^{\rho-3}U^0$, where U^0 is the solution of the variational problem:
Find $U^0\in\mathcal{V}_0$ *such that*

$$\boxed{A_{\rm b}(U^0,V)=G(V),\qquad\forall V\in\mathcal{V}_0.} \quad (5.34)$$

Note that this problem is well-posed since, by (5.14), $A_{\rm b}$ is coercive and continuous on $\mathcal{V}_0$. We then infer from (5.32) that

$$\mathcal{E}^\varepsilon(U^\varepsilon)\le-\frac{\varepsilon^{2\rho-3}}{2}G(U^0). \quad (5.35)$$

Of course, in Equation (5.35) we have

$$G(U^0)=A_{\rm b}(U^0,U^0)\ge\gamma\|U^0\|_{\mathcal{V}}\ge0, \quad (5.36)$$

and $G(U^0)$ cannot be zero unless $U^0 = 0$ which, from the Lax-Milgram theorem (Prop. 3.2.1), is equivalent to the condition

$$G(V) = 0, \qquad \forall V \in \mathcal{V}_0. \tag{5.37}$$

This happens in particular when $\mathcal{V}_0$ only contains the zero element, a situation that we will refer to as *inhibited pure bending*, as opposed to *non-inhibited pure bending* when $\mathcal{V}_0$ does contain some non-zero elements. We now specialize our analysis for each of these types of situations.

5.1.1 Non-inhibited pure bending

We assume that pure bending is not inhibited – namely, that $\mathcal{V}_0$ contain some non-zero elements – and we also assume that (5.37) does not hold (see Remark 5.1.3 below). Then $G(U^0) > 0$ and, in order to have both (5.35) and (5.26) (with $\mathcal{E}^\varepsilon(U^\varepsilon) < 0$), it necessarily holds that $2\rho - 3 \geq \rho$, i.e. $\rho \geq 3$, which, combined with (5.13), implies that $\rho = 3$. In the next proposition, we show that $\rho = 3$ indeed provides an admissible asymptotic behavior in this case (see (Sanchez-Palencia, 1989a; Pitkäranta, 1992; Chenais & Paumier, 1994) for other proofs or elements thereof), namely that the relevant sequence of problems to be considered is
Find U^ε in V such that

$$\boxed{A_{\rm b}(U^\varepsilon, V) + \frac{1}{\varepsilon^2} A_{\rm m}(U^\varepsilon, V) = G(V), \qquad \forall V \in \mathcal{V}.} \tag{5.38}$$

Proposition 5.1.2 *Assume that*

$$\mathcal{V}_0 \neq \{0\}. \tag{5.39}$$

Then, setting $\rho = 3$, U^ε converges strongly in $\mathcal{V}$ to U^0, the solution of (5.34). Moreover, we have

$$\boxed{\lim_{\varepsilon \to 0} \frac{1}{\varepsilon^2} A_{\rm m}(U^\varepsilon, U^\varepsilon) = 0.} \tag{5.40}$$

Proof. We thus consider (5.38). Using (5.14) we have, as soon as $\varepsilon \leq 1$,

$$\begin{aligned} \|U^\varepsilon\|_{\mathcal{V}}^2 &\leq C[A_{\rm b}(U^\varepsilon, U^\varepsilon) + A_{\rm m}(U^\varepsilon, U^\varepsilon)] \\ &\leq C[A_{\rm b}(U^\varepsilon, U^\varepsilon) + \frac{1}{\varepsilon^2} A_{\rm m}(U^\varepsilon, U^\varepsilon)] = CG(U^\varepsilon) \\ &\leq C\|U^\varepsilon\|_{\mathcal{V}}. \end{aligned} \tag{5.41}$$

Hence, dividing both sides by $\|U^\varepsilon\|_{\mathcal{V}}$ we infer that the whole sequence (U^ε) is bounded. Therefore, we can extract a subsequence, that we also denote by (U^ε) for convenience, which converges weakly in $\mathcal{V}$ to some limit $\tilde{U}$. We now consider elements of this subsequence, for which we write (5.38), multiplying both sides by ε^2. We obtain

$$A_{\rm m}(U^\varepsilon, V) = \varepsilon^2[G(V) - A_{\rm b}(U^\varepsilon, V)], \quad \forall V \in \mathcal{V}. \tag{5.42}$$

Keeping V fixed, we now make ε go to zero in this equation. Weak convergence implies that $A_{\rm m}(U^\varepsilon, V)$ tends to $A_{\rm m}(\tilde{U}, V)$ and that $G(V) - A_{\rm b}(U^\varepsilon, V)$ tends to $G(V) - A_{\rm b}(\tilde{U}, V)$. Therefore, $A_{\rm m}(\tilde{U}, V) = 0$, and since this holds for any $V \in \mathcal{V}$ we have in particular $A_{\rm m}(\tilde{U}, \tilde{U}) = 0$, hence $\tilde{U} \in \mathcal{V}_0$. Then using test functions of $\mathcal{V}_0$ in (5.38), we obtain

$$A_{\rm b}(U^\varepsilon, V) = G(V), \quad \forall V \in \mathcal{V}_0, \tag{5.43}$$

since $|A_{\rm m}(U^\varepsilon, V)| \leq A_{\rm m}(U^\varepsilon, U^\varepsilon)^{1/2} A_{\rm m}(V, V)^{1/2} = 0$ by a Cauchy-Schwarz inequality. Making again ε go to 0 in this equation (for any given $V \in \mathcal{V}_0$), and using the properties of weak limits, we have

$$A_{\rm b}(\tilde{U}, V) = G(V), \quad \forall V \in \mathcal{V}_0. \tag{5.44}$$

Hence $\tilde{U}$ (which is in $\mathcal{V}_0$) solves the same problem as U^0, and therefore $\tilde{U} = U^0$ and we infer that the *whole sequence* (U^ε) converges weakly to U^0, recall Prop. 3.1.1.

To further show that convergence is – in fact – strong, we again use (5.14), with $V = U^\varepsilon - U^0$, and we obtain for $\varepsilon \leq 1$

$$\begin{aligned}
&\|U^\varepsilon - U^0\|_{\mathcal{V}}^2 \\
&\quad \leq \; C[A_{\rm b}(U^\varepsilon - U^0, U^\varepsilon - U^0) + A_{\rm m}(U^\varepsilon - U^0, U^\varepsilon - U^0)] \\
&\quad \leq \; C[A_{\rm b}(U^\varepsilon - U^0, U^\varepsilon - U^0) + \frac{1}{\varepsilon^2} A_{\rm m}(U^\varepsilon - U^0, U^\varepsilon - U^0)] \\
&\quad = \; C[A_{\rm b}(U^\varepsilon, U^\varepsilon) + \frac{1}{\varepsilon^2} A_{\rm m}(U^\varepsilon, U^\varepsilon) \\
&\qquad\qquad + A_{\rm b}(U^0, U^0) - 2A_{\rm b}(U^0, U^\varepsilon)].
\end{aligned} \tag{5.45}$$

Then, using (5.38), we have

$$A_{\rm b}(U^\varepsilon, U^\varepsilon) + \frac{1}{\varepsilon^2} A_{\rm m}(U^\varepsilon, U^\varepsilon) = G(U^\varepsilon) \tag{5.46}$$

and

$$A_{\rm b}(U^\varepsilon, U^0) = G(U^0), \tag{5.47}$$

while we obtain, by using (5.34),

$$A_{\rm b}(U^0, U^0) = G(U^0). \tag{5.48}$$

Hence, from (5.45) we infer

$$\|U^\varepsilon - U^0\|^2_{\mathcal{V}} \leq CG(U^\varepsilon - U^0), \tag{5.49}$$

and, since weak convergence implies that $G(U^\varepsilon - U^0)$ tends to zero, we also have strong convergence.

Finally, using (5.46), we have

$$\frac{1}{\varepsilon^2} A_{\rm m}(U^\varepsilon, U^\varepsilon) = G(U^\varepsilon) - A_{\rm b}(U^\varepsilon, U^\varepsilon), \tag{5.50}$$

and, due to the strong convergence, $A_{\rm b}(U^\varepsilon, U^\varepsilon)$ tends to $A_{\rm b}(U_0, U_0)$, hence to $G(U_0)$ by (5.48). Since $G(U^\varepsilon)$ tends to $G(U_0)$ too, the convergence property (5.40) follows. ∎

Remark 5.1.3. If $U^0 = 0$, which is – as earlier explained – equivalent to

$$G(V) = 0, \qquad \forall V \in \mathcal{V}_0, \tag{5.51}$$

then the sequence obtained with the scaling $\rho = 3$ is such that $G(U^\varepsilon)$ tends to $G(U^0) = 0$, therefore it does not provide an admissible asymptotic behavior. Equation (5.51) means that the specific loading applied does not activate the pure bending displacements. Although this is possible in theory, it is clearly not very likely to occur in practice, unless of course the loading is specifically chosen in order to satisfy this condition. We will investigate this issue further in Section 5.3.1. By contrast, when $U^0 \neq 0$ Proposition 5.1.2 shows that the scaling $\rho = 3$ provides an admissible asymptotic behavior when (5.39) holds. In fact, we obtained a much stronger result, as the sequence of solution was shown to converge strongly to a given limit solution in $\mathcal{V}$ (that we were able to characterize). Since we have a finite asymptotic solution provided that the loading is scaled in the form

$$F^\varepsilon(V) = \varepsilon^3 G(V), \tag{5.52}$$

we can say that "the stiffness of the shell structure is of the order of ε^3". ∎

Remark 5.1.4. From Eq.(5.38), we see that U^ε is the solution of the minimization problem

$$\min_{V\in\mathcal{V}}\Big\{\frac{1}{2}A_{\rm b}(V,V)+\frac{1}{2\varepsilon^2}A_{\rm m}(V,V)-G(V)\Big\}, \tag{5.53}$$

while, from Eq.(5.34), U^0 is the solution of the other minimization problem

$$\min_{V\in\mathcal{V}_0}\Big\{\frac{1}{2}A_{\rm b}(V,V)-G(V)\Big\}. \tag{5.54}$$

We can thus interpret the minimization problem (5.53) as a *penalized* form of the constrained minimization problem (5.54), i.e. the constraint $A_{\rm m}(V,V)=0$ – which is exactly satisfied in (5.54) – is only approximately enforced in (5.53) by the use of a large coefficient in front of the term $A_{\rm m}(V,V)$. ■

We further point out that, for the scaling of the energy that is relevant in this asymptotic behavior, namely

$$A_{\rm b}(U^\varepsilon,U^\varepsilon)+\frac{1}{\varepsilon^2}A_{\rm m}(U^\varepsilon,U^\varepsilon)=G(U^\varepsilon), \tag{5.55}$$

the additional convergence property (5.40) shows that the membrane part vanishes when ε tends to zero (as well as the shear part when appropriate). By contrast, the bending part $A_{\rm b}(U^\varepsilon,U^\varepsilon)$ tends to $A_{\rm b}(U^0,U^0)$ which is strictly positive, unless $U^0=0$ which is not the case in general (see Remark 5.1.3 above). In reference to this asymptotic distribution of the energy, we say that the asymptotic behavior of the shell is *bending-dominated* in this case.

Remark 5.1.5. The property (5.40) also directly implies that the membrane strains (and shear strains, when applicable) tend to zero in the L^2-norm faster than in $O(\varepsilon)$. Hence, these strains rapidly become "small" whereas the various parts in their detailed expressions remain finite. This indeed represents a key difficulty in designing effective shell finite element formulations as illustrated in (Lee & Bathe, 2005), see also (Kim & Bathe, 2008) for a related discussion. ■

5.1.2 Inhibited pure bending

We now consider the case of inhibited pure bending, namely when

$$\mathcal{V}_0=\{0\}. \tag{5.56}$$

Then we can define an inner product – and the corresponding norm – using the bilinear form $A_{\rm m}$. Indeed, by (5.56)

$$\|V\|_{\rm m}=\sqrt{A_{\rm m}(V,V)} \tag{5.57}$$

provides a well-defined norm on $\mathcal{V}$, that we call the *membrane energy norm*. A natural idea is then to study the problem

$$A_{\mathrm{m}}(U^{\mathrm{m}}, V) = G(V), \qquad \forall V \in \mathcal{V}, \tag{5.58}$$

as a candidate limit problem for the sequence of shell problems obtained with the scaling $\rho = 1$, namely

$$\boxed{A_{\mathrm{m}}(U^{\varepsilon}, V) + \varepsilon^2 A_{\mathrm{b}}(U^{\varepsilon}, V) = G(V), \qquad \forall V \in \mathcal{V}.} \tag{5.59}$$

In the framework of this conjecture, the term $\varepsilon^2 A_{\mathrm{b}}(U^{\varepsilon}, V)$ appearing in (5.59) can be interpreted as a perturbation term introduced into (5.58), the influence of which being made smaller and smaller as ε tends to zero.

Clearly, Problem (5.58) is not well-posed for U^{m} in $\mathcal{V}$, as A_{m} is not coercive for the norm in $\mathcal{V}$. In other words, the membrane norm is not equivalent to the original norm of $\mathcal{V}$. This implies that $\mathcal{V}$ is not complete for the membrane norm, i.e. that some sequences of $\mathcal{V}$ that are Cauchy sequences for the membrane norm do not converge to an element of $\mathcal{V}$. However, we can consider $\mathcal{V}_{\mathrm{m}}$, the space obtained from $\mathcal{V}$ by *completion* with respect to the membrane norm, i.e. the space containing $\mathcal{V}$ and all the limits of Cauchy sequences – for the membrane norm – of elements of $\mathcal{V}$. The space $\mathcal{V}_{\mathrm{m}}$ is then the set of all functions that have bounded membrane energy. By construction, $\mathcal{V}_{\mathrm{m}}$ is a complete space for the membrane norm, hence a Hilbert space in which we can apply the Lax-Milgram theorem. Therefore the problem:
Find $U^{\mathrm{m}} \in \mathcal{V}_{\mathrm{m}}$ *such that*

$$\boxed{A_{\mathrm{m}}(U^{\mathrm{m}}, V) = G(V), \qquad \forall V \in \mathcal{V}_{\mathrm{m}},} \tag{5.60}$$

has a unique solution *provided that* $G \in \mathcal{V}_{\mathrm{m}}'$. This, however, imposes a restriction on the loading, since it requires the corresponding external work be bounded *for any virtual displacement in* $\mathcal{V}_{\mathrm{m}}$, and not only in $\mathcal{V}$.

Note that – by construction – $\mathcal{V}_{\mathrm{m}}$ is a larger space than the original displacement space $\mathcal{V}$, as the A_{m}-norm provides less control on the displacements than the norm of $\mathcal{V}$ associated with the complete energy. Namely, the bending strains are not included in the A_{m}-norm, which implies in particular that the transverse displacements are controlled at best in L^2, since no derivatives of these displacement components are present in the membrane strains, see Section 5.2.1 for a further discussion in the case of elliptic surfaces. A consequence is that oscillations in transverse displacements may occur, for example near boundaries, see Remark 5.1.9.

Remark 5.1.6. Equation (5.60) is in fact equivalent to (5.58), because – by construction – the space $\mathcal{V}$ is dense in $\mathcal{V}_{\mathrm{m}}$, namely all elements of $\mathcal{V}_{\mathrm{m}}$

can be obtained as limits of sequences of elements of $\mathcal{V}$ (that converge for the membrane energy norm, of course). Hence we can obtain (5.60) by using these sequences as test functions in (5.58) and by passing to the limit. Likewise, the condition $G \in \mathcal{V}'_{\rm m}$, which is directly equivalent to

$$|G(V)| \leq C\|V\|_{\rm m} = C\sqrt{A_{\rm m}(V,V)}, \qquad \forall V \in \mathcal{V}_{\rm m}, \tag{5.61}$$

is also equivalent to

$$\boxed{|G(V)| \leq C\sqrt{A_{\rm m}(V,V)}, \qquad \forall V \in \mathcal{V},} \tag{5.62}$$

which will prove very convenient to work with in practice when we are not able to make the space $\mathcal{V}_{\rm m}$ fully explicit. ■

We now show that, provided that the loading satisfies the above-mentioned condition, the conjecture that we made regarding the asymptotic behavior is confirmed, see also (Sanchez-Palencia, 1989b; Piila & Pitkäranta, 1993a).

Proposition 5.1.3 *Assume that pure bending is inhibited – namely that (5.56) holds – and also that $G \in \mathcal{V}'_{\rm m}$. Then, setting $\rho = 1$, U^ε converges strongly in $\mathcal{V}_{\rm m}$ to $U^{\rm m}$, the solution of (5.60). Moreover, we have*

$$\boxed{\lim_{\varepsilon\to 0} \varepsilon^2 A_{\rm b}(U^\varepsilon, U^\varepsilon) = 0.} \tag{5.63}$$

Proof. Under the assumptions stated in this proposition, the asymptotic problem (5.59) is a classical singular perturbation problem such as described and analyzed in (Lions, 1973). However, we provide the full proof for completeness.

Using U^ε as a test function in (5.59), we obtain

$$\|U^\varepsilon\|^2_{\rm m} \leq A_{\rm m}(U^\varepsilon, U^\varepsilon) + \varepsilon^2 A_{\rm b}(U^\varepsilon, U^\varepsilon) = G(U^\varepsilon) \leq C\|U^\varepsilon\|_{\rm m}, \tag{5.64}$$

hence the sequence (U^ε) is bounded in $\mathcal{V}_{\rm m}$. In addition, if we combine (5.59) with (5.14) we have, for $\varepsilon \leq 1$,

$$\begin{aligned} \varepsilon^2\|U^\varepsilon\|^2_{\mathcal{V}} &\leq C\varepsilon^2[A_{\rm m}(U^\varepsilon, U^\varepsilon) + A_{\rm b}(U^\varepsilon, U^\varepsilon)] \\ &\leq C[A_{\rm m}(U^\varepsilon, U^\varepsilon) + \varepsilon^2 A_{\rm b}(U^\varepsilon, U^\varepsilon)] = CG(U^\varepsilon) \\ &\leq C, \end{aligned} \tag{5.65}$$

because $\|U^\varepsilon\|_{\mathrm{m}}$ is bounded. Since $\mathcal{V}_{\mathrm{m}}$ is a Hilbert space, out of the bounded sequence (U^ε) we can extract a subsequence – that we denote by (U^ε) also – which converges weakly (in $\mathcal{V}_{\mathrm{m}}$) to some limit $\tilde{U}$. Considering Eq. (5.59) for elements of this subsequence and keeping V fixed in $\mathcal{V}$, we now make ε go to zero. The term $A_{\mathrm{m}}(U^\varepsilon, V)$ converges to $A_{\mathrm{m}}(\tilde{U}, V)$. Furthermore, by the Cauchy-Schwarz inequality and (5.65),

$$\varepsilon^2 |A_{\mathrm{b}}(U^\varepsilon, V)| \leq C\varepsilon^2 \|U^\varepsilon\|_{\mathcal{V}} \|V\|_{\mathcal{V}} \leq C\varepsilon \|V\|_{\mathcal{V}}, \tag{5.66}$$

hence this term tends to zero. Therefore, we obtain in the limit

$$A_{\mathrm{m}}(\tilde{U}, V) = G(V), \qquad \forall V \in \mathcal{V}, \tag{5.67}$$

which, taking into account Remark 5.1.6, shows that $\tilde{U} = U^{\mathrm{m}}$. As a consequence, the whole original sequence (U^ε) is seen to converge weakly to U^{m} in $\mathcal{V}_{\mathrm{m}}$ (recall Prop. 3.1.1).

We now show that the convergence is – in fact – strong. We indeed have

$$\begin{aligned} \|U^\varepsilon - U^{\mathrm{m}}\|_{\mathrm{m}}^2 &= A_{\mathrm{m}}(U^\varepsilon - U^{\mathrm{m}}, U^\varepsilon - U^{\mathrm{m}}) \\ &= A_{\mathrm{m}}(U^\varepsilon, U^\varepsilon) + A_{\mathrm{m}}(U^{\mathrm{m}}, U^{\mathrm{m}}) \\ &\qquad -2A_{\mathrm{m}}(U^{\mathrm{m}}, U^\varepsilon). \end{aligned} \tag{5.68}$$

Using (5.60), we obtain $A_{\mathrm{m}}(U^{\mathrm{m}}, U^{\mathrm{m}}) = G(U^{\mathrm{m}})$ and $A_{\mathrm{m}}(U^{\mathrm{m}}, U^\varepsilon) = G(U^\varepsilon)$, and (5.59) gives $A_{\mathrm{m}}(U^\varepsilon, U^\varepsilon) = G(U^\varepsilon) - \varepsilon^2 A_{\mathrm{b}}(U^\varepsilon, U^\varepsilon)$. Hence, from (5.68), we infer

$$\begin{aligned} \|U^\varepsilon - U^{\mathrm{m}}\|_{\mathrm{m}}^2 &= G(U^{\mathrm{m}}) - G(U^\varepsilon) - \varepsilon^2 A_{\mathrm{b}}(U^\varepsilon, U^\varepsilon) \\ &\leq G(U^{\mathrm{m}}) - G(U^\varepsilon), \end{aligned} \tag{5.69}$$

since $\varepsilon^2 A_{\mathrm{b}}(U^\varepsilon, U^\varepsilon) \geq 0$. Weak convergence implies that $G(U^{\mathrm{m}}) - G(U^\varepsilon)$ tends to zero, therefore we also have strong convergence.

Finally, we rewrite the first line of (5.69) as

$$\varepsilon^2 A_{\mathrm{b}}(U^\varepsilon, U^\varepsilon) = G(U^{\mathrm{m}}) - G(U^\varepsilon) - \|U^\varepsilon - U^{\mathrm{m}}\|_{\mathrm{m}}^2, \tag{5.70}$$

hence the convergence property (5.63) directly follows from the strong convergence of U^ε towards U^{m}. ∎

Remark 5.1.7. The scaling $\rho = 1$ gives an admissible asymptotic behavior, and also stronger properties, since U^ε itself converges to a strong limit, albeit in a larger space (hence in a weaker norm) than in $\mathcal{V}$. Due to this convergence

result, we can say that "the stiffness of the shell structure is of the order of ε". ■

Remark 5.1.8. Considering the asymptotic distribution of the energy such as in $A_{\rm m}(U^\varepsilon, U^\varepsilon) + \varepsilon^2 A_{\rm b}(U^\varepsilon, U^\varepsilon)$, (5.63) shows that the second term tends to zero, whereas strong convergence implies that $A_{\rm m}(U^\varepsilon, U^\varepsilon)$ tends to $A_{\rm m}(U^{\rm m}, U^{\rm m}) = G(U^{\rm m})$ which cannot be zero except if the solution of the variational problem (5.60) is zero, namely if G itself is zero, which is a case that we do not consider. As a consequence, we will say that the asymptotic behavior is *membrane-dominated* in this case. ■

5.1.3 Summary of asymptotic behaviors

As a result of Propositions 5.1.2 and 5.1.3, we can see that a scaling of the loading corresponding to ρ other than 1 or 3, namely

$$1 < \rho < 3, \tag{5.71}$$

can possibly give rise to an admissible asymptotic behavior *only when*[1] pure bending is inhibited *and* the loading is such that $G \notin \mathcal{V}'_{\rm m}$. We will further analyze such behaviors and give some examples in Section 5.3.2.

We summarize the results obtained in the above asymptotic analysis with the diagram given in Figure 5.2. The question "$1 < \rho < 3$?" in the box corresponding to an ill-posed membrane problem means that if there exists a scaling that gives an admissible asymptotic behavior in this case it is necessarily such that $1 < \rho < 3$, but we do not know whether such a scaling always exists. Moreover, for an explanation and an example of the behavior referred to as "unstable membrane-dominated", see Section 5.3.1.

Note that, now that we have discussed the diversity of asymptotic behaviors which can be encountered with shell structures, we are in a position to understand the motivation examples given in the introduction to this chapter, recall Figure 5.1. Namely – as will be fully substantiated in Section 5.2 – the cylindrical structure with the boundary conditions along the straight boundary is not pure-bending inhibited, hence it is bending-dominated, whereas the boundary conditions applied along the circular boundary inhibit pure bending, and in this case the asymptotic behavior is mixed like for the Scordelis-Lo roof, see Section 5.3.2.

Remark 5.1.9. Another important phenomenon associated with asymptotic behaviors is the presence of *boundary layers*, due to incompatibilities between

[1] Disregarding cases with non-inhibited pure bending and $U^0 = 0$, see Remark 5.1.3.

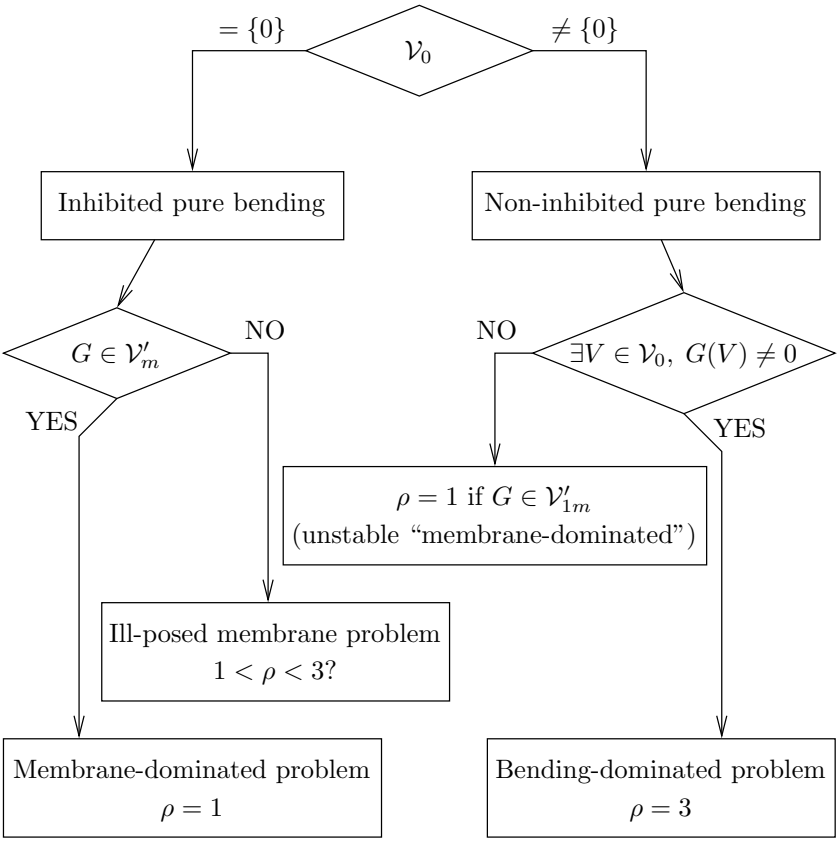

Fig. 5.2. Summary of asymptotic behaviors

the boundary conditions prescribed – essential or natural – and the displacement and stress state that can be supported by the shell, succinctly identified by the analysis of the limit problems. In particular, in membrane-dominated problems since transverse displacements are controlled at best in L^2 in the limit membrane problem, essential boundary conditions prescribed on transverse displacements do not hold in the limit, which gives rise to strong boundary layer effects. More generally, boundary layers have dimensions – in width and in amplitude – which vary with the thickness parameters, in ways which depend on the type of asymptotic behavior, the geometry (both of the mid-surface and of the boundary), and the specific boundary conditions enforced. For more detailed descriptions we refer in particular to (Häggblad & Bathe, 1990; Arnold & Falk, 1996; Dauge & Yosibash, 2000; Karamian et al., 2000; Pitkäranta et al., 2001) and references therein. As discussed in this literature, we also point out that similar phenomena called *internal layers* may

arise due to the propagation of singularities along the asymptotic lines of the midsurface. ■

5.1.4 Comparison of asymptotic behaviors for specific shell models

We emphasize that, in the above general asymptotic analysis, we did not distinguish between the s-m-b model and the m-b model. This suggests that these two models have very similar asymptotic behaviors. In order to compare these asymptotic behaviors in more detail, we consider the solutions of the two models for the *same loading*, namely the sequence of solutions $(\vec{u}_N^{\varepsilon}, \underline{\theta}_N^{\varepsilon}) \in \mathcal{V}^N$ that satisfies

$$A^N(\vec{u}_N^{\varepsilon}, \underline{\theta}_N^{\varepsilon}; \vec{v}, \underline{\eta}) = \varepsilon^{\rho} \int_{\omega} \vec{G} \cdot \vec{v}\, dS, \qquad \forall (\vec{v}, \underline{\eta}) \in \mathcal{V}^N, \tag{5.72}$$

for the s-m-b model, and the sequence of solutions $(\vec{u}_K^{\varepsilon}) \in \mathcal{V}^K$ that satisfies

$$A^K(\vec{u}_K^{\varepsilon}; \vec{v}) = \varepsilon^{\rho} \int_{\omega} \vec{G} \cdot \vec{v}\, dS, \qquad \forall \vec{v} \in \mathcal{V}^K, \tag{5.73}$$

for the m-b model. Note that we consider the same scaling ρ and the same surface loading $\vec{G}$ in the two models. In order for this loading to be admissible for both models, we take $\vec{G} \in L^2(\mathcal{S})$. Of course, we also need to assume that the essential boundary conditions are the same in the two models, and that these boundary conditions do not allow non-zero rigid body motions.

Denoting by $\mathcal{V}_0^N$ and $\mathcal{V}_0^K$ the subspaces of pure bending displacements for these two models (respectively), we can show that these two subspaces are very closely related, as expressed in the following proposition.

Proposition 5.1.4 *The subspaces $\mathcal{V}_0^N$ and $\mathcal{V}_0^K$ satisfy the following relation:*

$$\mathcal{V}_0^N = \{(\vec{v}, -\underline{\nabla} v_3 - \underline{\underline{b}} \cdot \underline{v}) \mid \vec{v} \in \mathcal{V}_0^K\}. \tag{5.74}$$

Proof. Taking any element $\vec{v}$ in $\mathcal{V}_0^K$, it is obvious that $(\vec{v}, -\underline{\nabla} v_3 - \underline{\underline{b}} \cdot \underline{v})$ gives an element of $\mathcal{V}_0^N$. Conversely, taking an arbitrary $(\vec{v}, \underline{\eta})$ in $\mathcal{V}_0^N$, $\underline{\zeta}(\vec{v}, \underline{\eta}) = \underline{0}$ implies

$$\underline{\eta} = -\underline{\nabla} v_3 - \underline{\underline{b}} \cdot \underline{v}, \tag{5.75}$$

hence $\underline{\nabla} v_3 \in H^1(\mathcal{S})$, and since $v_3 \in H^1(\mathcal{S})$ we infer that $v_3 \in H^2(\mathcal{S})$. Therefore $\vec{v} \in \mathcal{V}_0^K$. ■

According to Proposition 5.1.4, the elements (namely the displacement-rotation couples) of the s-m-b pure bending subspace consist of the displacements of the m-b pure bending subspace associated with the rotations directly

derived from these by using the Kirchhoff-Love assumption. Hence, we can say that these two subspaces are essentially the same. In addition, it follows that the conditions that govern whether or not pure bending is inhibited are identical for the two models (see also Section 5.2). This is a crucial prerequisite in the comparison between the asymptotic behaviors of the two models, since we know that – for a given model – this behavior is dramatically different according to whether or not pure bending is inhibited. We can thus start by considering the case of non-inhibited pure bending, as a situation that occurs concurrently for the two models.

Proposition 5.1.5 *Assume that pure bending is not inhibited. Then, for the scaling $\rho = 3$, denoting by $(\vec{u}_N^0, \underline{\theta}_N^0)$ the limit solution for the s-m-b model and by $\vec{u}_K^0$ the limit solution for the m-b problem, we have*

$$\vec{u}_N^0 = \vec{u}_K^0, \tag{5.76}$$

$$\underline{\theta}_N^0 = -\underline{\nabla} u_{K3}^0 - \underline{\underline{b}} \cdot \underline{u}_K^0. \tag{5.77}$$

Proof. The limit solution $(\vec{u}_N^0, \underline{\theta}_N^0)$ for the s-m-b model is in $\mathcal{V}_0^N$ and satisfies

$$A_{\rm b}^N(\vec{u}_N^0, \underline{\theta}_N^0; \vec{v}, \underline{\eta}) = \int_\omega \vec{G} \cdot \vec{v}\, dS, \qquad \forall (\vec{v}, \underline{\eta}) \in \mathcal{V}_0^N. \tag{5.78}$$

For any $(\vec{v}, \underline{\eta}) \in \mathcal{V}_0^N$, we have $\underline{\zeta}(\vec{v}, \underline{\eta}) = \underline{0}$, hence, by Proposition 4.2.1, it corresponds to a Kirchhoff-Love displacement and therefore we have (recall Eq.(4.47))

$$\underline{\underline{\chi}}(\vec{v}, \underline{\eta}) = -\underline{\bar{\rho}}(\vec{v}). \tag{5.79}$$

Note that this holds for $(\vec{u}_N^0, \underline{\theta}_N^0)$ also and that, by Prop. 5.1.4, $\vec{u}_N^0$ and $\vec{v}$ are in $\mathcal{V}_0^K$. Hence (5.78) implies

$$A_{\rm b}^K(\vec{u}_N^0; \vec{v}) = \int_\omega \vec{G} \cdot \vec{v}\, dS, \qquad \forall (\vec{v}, \underline{\eta}) \in \mathcal{V}_0^N. \tag{5.80}$$

Since – by Prop. 5.1.4 – *any* displacement $\vec{v}$ in $\mathcal{V}_0^K$ can be obtained by taking the first part of a couple $(\vec{v}, \underline{\eta})$ in $\mathcal{V}_0^N$, it follows that

$$A_{\rm b}^K(\vec{u}_N^0; \vec{v}) = \int_\omega \vec{G} \cdot \vec{v}\, dS, \qquad \forall \vec{v} \in \mathcal{V}_0^K, \tag{5.81}$$

which shows that we have (5.76). Finally, the relation (5.77) directly follows from $\underline{\zeta}(\vec{u}_N^0, \underline{\theta}_N^0) = 0$. ∎

We then consider the case of inhibited pure bending. In this case, we know from our previous discussions that the condition "$G \in \mathcal{V}_{\rm m}'$" is crucial in order

to obtain a well-defined membrane-dominated asymptotic behavior. In this respect also, it is straightforward to see that the two conditions corresponding to the s-m-b and m-b models are equivalent, and that they – indeed – are both equivalent to (see Remark 5.1.6)

$$|\int_\omega \vec{G}\cdot\vec{v}\,dS| \le C\left\{\int_\omega l^0 C^{\alpha\beta\lambda\mu}\gamma_{\alpha\beta}(\vec{v})\gamma_{\lambda\mu}(\vec{v})\,dS\right\}^{\frac{1}{2}}, \quad \forall \vec{v}\in\mathcal{V}^K. \tag{5.82}$$

Note that we can substitute "$\forall(\vec{v},\underline{\eta})\in\mathcal{V}^N$" for "$\forall\vec{v}\in\mathcal{V}^K$" in this equation and still have an equivalent condition using density considerations (i.e. the fact that every element in $\mathcal{V}^K$ can be reached by elements in $\mathcal{V}^N$). Since the membrane-dominated behaviors of the s-m-b and m-b models are well-posed under the same condition, it is meaningful to compare the asymptotic solutions.

Proposition 5.1.6 *Assume that (5.82) holds. Then, for the scaling $\rho = 1$, denoting by $(\vec{u}_N^{\,\mathrm{m}},\underline{\theta}_N^{\mathrm{m}})$ the limit solution for the s-m-b model and by $\vec{u}_K^{\,\mathrm{m}}$ the limit solution for the m-b model, we have*

$$\vec{u}_N^{\,\mathrm{m}} = \vec{u}_K^{\,\mathrm{m}}, \tag{5.83}$$

$$\underline{\theta}_N^{\mathrm{m}} = -\underline{\nabla} u_{K3}^{\mathrm{m}} - \underline{\underline{b}}\cdot\underline{u}_K^{\mathrm{m}}. \tag{5.84}$$

Proof. The limit solution $(\vec{u}_N^{\,\mathrm{m}},\underline{\theta}_N^{\mathrm{m}})$ for the s-m-b model is in $\mathcal{V}_{\mathrm{m}}^N$ and satisfies

$$A_{\mathrm{m}}^N(\vec{u}_N^{\,\mathrm{m}},\underline{\theta}_N^{\mathrm{m}};\vec{v},\underline{\eta}) = \int_\omega \vec{G}\cdot\vec{v}\,dS, \qquad \forall(\vec{v},\underline{\eta})\in\mathcal{V}_{\mathrm{m}}^N. \tag{5.85}$$

Clearly, considering the expression of A_{m}^N as the sum of a membrane term and of a shear term (see Eq.(5.7)), since the rotation does not produce any external work we must have

$$\underline{\zeta}(\vec{u}_N^{\,\mathrm{m}},\underline{\theta}_N^{\mathrm{m}}) = \underline{0}. \tag{5.86}$$

Therefore, (5.85) implies

$$A_{\mathrm{m}}^K(\vec{u}_K^{\,\mathrm{m}};\vec{v}) = \int_\omega \vec{G}\cdot\vec{v}\,dS, \qquad \forall(\vec{v},\underline{\eta})\in\mathcal{V}_{\mathrm{m}}^N. \tag{5.87}$$

Note that $\vec{u}_N^{\,\mathrm{m}}$ is in $\mathcal{V}_{\mathrm{m}}^K$, since $(\vec{u}_N^{\,\mathrm{m}},\underline{\theta}_N^{\mathrm{m}})\in\mathcal{V}_{\mathrm{m}}^N$ implies that $\underline{\underline{\gamma}}(\vec{u}_N^{\,\mathrm{m}})$ is in $L^2(\mathcal{S})$. Likewise, for any $(\vec{v},\underline{\eta})$ in $\mathcal{V}_{\mathrm{m}}^N$ $\vec{v}$ is in $\mathcal{V}_{\mathrm{m}}^K$, hence $A_{\mathrm{m}}^K(\vec{u}_K^{\,\mathrm{m}};\vec{v})$ is well-defined. Finally, considering any $\vec{v}$ in $\mathcal{V}_{\mathrm{m}}^K$, define $\underline{\eta}$ as

$$\underline{\eta} = -\underline{\nabla} v_3 - \underline{\underline{b}}\cdot\underline{v}. \tag{5.88}$$

Then $(\vec{v}, \underline{\eta}) \in \mathcal{V}_{\mathrm{m}}^N$ since $\underline{\underline{\gamma}}(\vec{v}) \in L^2(\mathcal{S})$ and $\underline{\zeta}(\vec{v}, \underline{\eta}) = \underline{0} \in L^2(\mathcal{S})$, hence it also holds that

$$A_{\mathrm{m}}^K(\vec{u}_K^{\mathrm{m}}; \vec{v}) = \int_\omega \vec{G} \cdot \vec{v}\, dS, \qquad \forall \vec{v} \in \mathcal{V}_{\mathrm{m}}^K, \tag{5.89}$$

which shows that we have (5.83), and (5.84) directly follows from (5.86). ■

Finally, in our discussion on the compared asymptotic behaviors of the s-m-b and m-b models, we have shown that the conditions that determine the category of asymptotic behavior (namely membrane-dominated or bending-dominated) and the well-posedness of the membrane-dominated behavior (when appropriate) are the same, and that the limit solutions are the same (considering only the displacement part in the s-m-b model). To summarize these properties, we can say that the s-m-b and m-b models are "asymptotically equivalent".

Remark 5.1.10. In (Ciarlet, 2000), an asymptotic analysis is performed on the 3D linear elastic problem corresponding to the same geometry that we consider here (namely the domain Ω, with varying ε, albeit with a constant thickness profile). It is then shown that convergence properties hold for the 3D solution towards the same limit solutions and under the same assumptions as for a given m-b problem. More specifically, these convergence properties hold for $\vec{u}_{3D}^{\,\varepsilon}$, the mean value of the 3D solution over the thickness. When pure bending is non-inhibited for the m-b problem, $\vec{u}_{3D}^{\,\varepsilon}$ converges to the pure bending limit solution, in the norm of $\mathcal{V}^K$, for the scaling of the loading that corresponds to $\rho = 3$ in our analysis. By contrast, when pure bending is inhibited, $\vec{u}_{3D}^{\,\varepsilon}$ converges in the membrane energy norm – for the scaling $\rho = 1$ – to the limit membrane solution, provided that the load given on the m-b problem satisfies the admissibility condition "$G \in \mathcal{V}_{\mathrm{m}}'$". Therefore, the 3D model and the m-b model (hence also the s-m-b model) can be said to be "asymptotically equivalent" as well. We also refer to (Piila & Pitkäranta, 1993b, 1995) for an alternative asymptotic analysis of the 3D formulation using the energy norm, albeit restricted to cylindrical geometries. ■

Before closing this section, we recall that the general asymptotic analysis performed here is not directly applicable to the basic shell model and 3D-shell model introduced in Section 4.2.1 and 4.2.5, since these mathematical models cannot be written in the generic form (5.4), hence we will specifically analyze the asymptotic behaviors of these models in Section 5.4.

5.2 Analysis of the Subspace of Pure Bending Displacements

In the previous section, in the light of our general analysis it clearly appeared that the specific contents of the subspace of pure bending displacements are crucial in order to determine the asymptotic behavior that a shell structure may undergo. In particular the existence of non-zero elements in this subspace governs – to a large extent – the category of asymptotic behavior obtained. Therefore, in this section we proceed to analyze in more detail the subspace of pure bending displacements.

In the case of the m-b model, the subspace of pure bending displacements (denoted by $\mathcal{V}_0^K$) is characterized by zero membrane energy. Note that this is equivalent to

$$\mathcal{V}_0^K = \{\vec{v} = (\underline{v}, v_3) \in \mathcal{V}^K \mid \underline{\underline{\gamma}}(\vec{v}) \equiv \underline{\underline{0}}\}, \tag{5.90}$$

and thus $\mathcal{V}_0^K$ is the subspace of displacements with vanishing membrane strains.

For the s-m-b model, the subspace of pure bending displacements (denoted by $\mathcal{V}_0^N$) is given by zero membrane *and* shear energy, namely by vanishing membrane and shear strains, i.e.,

$$\mathcal{V}_0^N = \{(\vec{v}, \underline{\eta}) \in \mathcal{V}^N \mid \underline{\underline{\gamma}}(\vec{v}) \equiv \underline{\underline{0}},\ \underline{\zeta}(\vec{v}, \underline{\eta}) \equiv \underline{0}\}. \tag{5.91}$$

We have shown in the previous section (Proposition 5.1.4) that the subspaces $\mathcal{V}_0^K$ and $\mathcal{V}_0^N$ are very closely related, in particular since the condition of zero shear strains can be written in the form

$$\boxed{\underline{\eta} = -(\underline{\nabla} v_3 + \underline{\underline{b}} \cdot \underline{v}),} \tag{5.92}$$

i.e. in the form of an explicit expression of $\underline{\eta}$ as a function of $\vec{v}$. Hence, the conditions of zero membrane strains are the crucial conditions for $\mathcal{V}_0^N$ also. For this reason, elements of the subspace of pure bending displacements are also called, in general, *inextensional displacements*. Also, we can therefore focus on the condition of zero membrane strains in the sequel.

Considering the system of partial differential equations given by

$$\boxed{\underline{\underline{\gamma}}(\vec{v}) \equiv \underline{\underline{0}},} \tag{5.93}$$

we then infer that the conditions which characterize the subspace of inextensional displacements make up an exactly determined set of equations, i.e. with

as many unknowns as equations if we write them component-wise (recall that $\underline{\underline{\gamma}}$ is a symmetric tensor). This highlights an essential feature of shells, which is that a situation of inhibited pure bending (i.e. one in which only the zero displacement satisfies the exactly determined set of homogeneous equations) is possible.

Furthermore, a remarkable property of the system of differential equations (5.93) is given in the following proposition (Sanchez-Hubert & Sanchez-Palencia, 1997).

Proposition 5.2.1 *The differential nature (elliptic, parabolic or hyperbolic) of System (5.93) is the same as the geometric nature of the midsurface at the point in consideration. In addition, when such a concept is relevant (namely in the hyperbolic and – by extension – parabolic case) the characteristics of the system are also the asymptotic lines of the surface.*

This fundamental result allows us to review several instances for which it is possible to tell whether or not pure bending is inhibited. Obviously this question also depends on the boundary conditions which we therefore need to take into consideration. We now examine shells for which the mid-surface is of uniform nature (everywhere elliptic, or parabolic, or hyperbolic). These should not be thought of as restrictive cases but – on the contrary – as essential ingredients that determine the behavior of more general structures obtained by assembling surfaces of various types. We also recall that we discussed the geometrical nature of surfaces and asymptotic lines in Section 2.2.2.

5.2.1 Elliptic surfaces

For a sufficiently smooth uniformly elliptic surface, for instance part of an ellipsoid, it can be shown that imposing zero displacements on a part of the boundary of non-zero measure is sufficient to inhibit pure bending displacements (Lods & Mardaré, 1998). Moreover, if this part extends to the whole boundary, then the membrane norm $\|\cdot\|_{\mathrm{m}}$ provides control on the H^1-norm of the tangential displacement $\underline{v}$ and on the L^2-norm of the transverse displacement v_3, namely we have (see (Sanchez-Hubert & Sanchez-Palencia, 1997; Ciarlet, 2000) and references therein)

$$c(\|\underline{v}\|^2_{H^1(\mathcal{S})} + \|v_3\|^2_{L^2(\mathcal{S})}) \leq \|\underline{\underline{\gamma}}(\vec{v})\|^2_{L^2(\mathcal{S})} \leq C(\|\underline{v}\|^2_{H^1(\mathcal{S})} + \|v_3\|^2_{L^2(\mathcal{S})}), \quad (5.94)$$

for strictly positive constants c and C. Note that this holds for both the s-m-b and m-b models, of course. Therefore the limit membrane problem – set in $\mathcal{V}_{\mathrm{m}}$ – retains a certain degree of regularity in this case.

By contrast, if the displacements are fixed on a limited part of the boundary only, it can be shown that $\mathcal{V}_{\mathrm{m}}$ is not a distribution space (Lions & Sanchez-Palencia, 1996), see Appendix C for fundamentals of distributions. This implies that there exist some indefinitely differentiable functions that do not

belong to the dual of $\mathcal{V}_{\rm m}$, and hence lead to ill-posed membrane problems when used as loadings. As a matter of fact, it is well known in engineering practice that any reasonable loading applied on such a structure gives a "physically unstable" membrane problem.

These results also imply that, in order to obtain non-inhibited pure bending in a uniformly-elliptic shell, the only boundary conditions that we can prescribe are those required to prevent rigid body motions, and it can be shown that non-trivial pure bending displacements then do indeed exist (see e.g. (Kirmse, 1993) in the case of a hemisphere).

5.2.2 Hyperbolic surfaces

For a hyperbolic surface (see for instance the hyperbolic paraboloid in Figure 2.5 with the lattice of straight asymptotic lines), we infer from Proposition 5.2.1 that the system (5.93) is of hyperbolic nature, and that its characteristics are the asymptotic lines of the surface. Therefore, the subspace of pure bending displacements is highly dependent on the boundary conditions which – together with (5.93) – define a Cauchy problem that – in general – is well-posed.

In order to make the analysis of the problem simpler, it is valuable to use the coordinate system defined by the asymptotic lines of the surface. This is always possible when the surface is sufficiently smooth. System (5.93) then becomes:

$$\begin{cases} v_{1|1} = 0 \\ v_{2|2} = 0 \\ \frac{1}{2}(v_{1|2} + v_{2|1}) = b_{12} v_3 \end{cases} \tag{5.95}$$

with $b_{12} \neq 0$, and therefore the third equation gives v_3 explicitly in terms of v_1 and v_2.

As an example, we display in Figure 5.3 the reference domain of a hyperbolic surface in this particular coordinate system. Suppose that v_1 and v_2 are fixed on the part (AB) of the boundary. Then the Cauchy problem is well-posed in the triangle (ABC) where therefore all displacements are zero. However, outside of this region there exist non-zero displacements which satisfy (5.95). For instance, we can arbitrarily set v_1 on the line (CE) and v_2 on the line (CD), and this determines the value of the fields over the whole domain.

Thus, unlike with elliptic surfaces, hyperbolic surfaces appear to easily lead to non-inhibited situations, provided that boundary conditions are imposed on a sufficiently restricted part of the boundary.

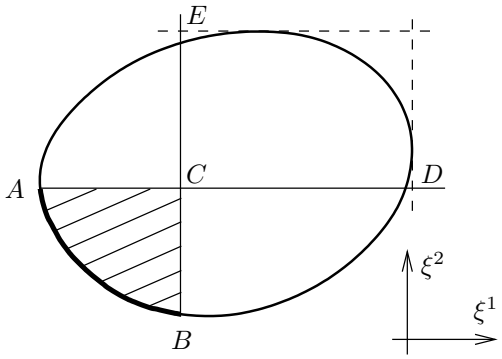

Fig. 5.3. Hyperbolic surface in the asymptotic coordinates

5.2.3 Parabolic surfaces

Parabolic surfaces, i.e. surfaces of zero Gaussian curvature (cylinders, cones, etc.), can be thought of as a "narrow category" between the two above-mentioned major types. In practical designs, however, these geometric shapes are – by far – the most employed. Therefore the analysis of their mechanical behavior is of particular importance.

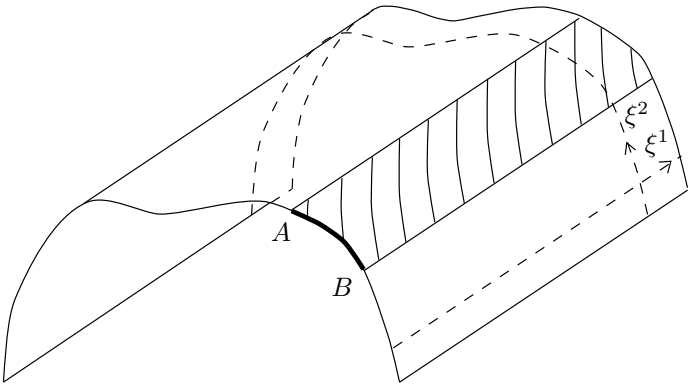

Fig. 5.4. Natural coordinates and inhibited region for a cylinder

For the sake of simplicity, we focus on the cylindrical case (the analysis for a cone would be similar). Note that, for example, a plane is a specific type of cylinder (with a straight line as a cross-section). We use the natural coordinate system (defined by the rulings and the cross-sections, see Figure 5.4) in which all Christoffel symbols are zero and the covariant basis is orthonormal. System (5.93) then reads

$$\begin{cases} v_{1,1} = 0 \\ v_{2,2} = b_{22} v_3 \\ v_{1,2} + v_{2,1} = 0 \end{cases} \tag{5.96}$$

As is easily seen, if we prescribe the displacements on some part of a cross-section, the entire corresponding band gets inhibited (see Figure 5.4 where the section is fixed on part (AB)), *except if the surface is a plane* in which case b_{22}=0 and *pure bending is never inhibited* since any non-zero transverse displacement satisfies the conditions. For general cylinders, if boundary conditions are only imposed along rulings (i.e. straight lines parallel to the axis of the cylinder), pure bending displacements also remain possible: v_1 and v_2 can in fact be set arbitrarily along any cross-section (subject to satisfying the end boundary conditions) and a complete field of pure bending displacements is thus fully determined.

Example 5.2.1
Assume that boundary conditions are only prescribed along rulings and that the radius of curvature is everywhere finite ($1/R = b_{22} \neq 0$). Then we can easily identify the plane-strain displacements (i.e. displacements that do not depend on the variable ξ^1, and for which $v_1 = 0$) that give inextensional displacements. Indeed, the inextensional system then reduces to

$$v_3 = R \frac{dv_2}{d\xi^2}. \tag{5.97}$$

The inextensional displacements of this type are then obtained by choosing any v_2 (function of ξ^2) that satisfies the appropriate boundary conditions and for which

$$\frac{dv_2}{d\xi^2} = 0 \tag{5.98}$$

wherever the boundary conditions require that $v_3 = 0$. The transverse displacement v_3 can then be derived from (5.97). In fact, as can be expected (5.97) is also the governing condition for inextensional displacements in a curved plane beam (namely an arch), see (Kikuchi, 1982). ■

Remark 5.2.1. For hyperbolic and parabolic surfaces with inhibited pure bending, the membrane energy space $\mathcal{V}_{\mathrm{m}}$ is more complicated than for a fully clamped elliptic surface (for which the tangential part of the displacement is in H^1 and the transverse part in L^2 as discussed in Section 5.2.1 above). Nevertheless, it is still a distribution space as shown in (Mardaré, 1998) where a detailed characterization of these spaces is also provided. ■

5.3 Influence of the Loading

In our above general asymptotic analysis of shell models, we identified the contents of the subspace of pure bending displacements as the key to the asymptotic behavior of a given shell structure. Recalling that this subspace only depends on the geometry of the midsurface and on the boundary conditions (see Section 5.2), it may be surprising that the loading does not appear to have a major influence on the shell behavior. Clearly, if a particular effect of the loading exists, it must be "concealed" in the assumptions made on this loading in our analysis. Two such assumptions have been used:

1. When pure bending is not inhibited, we used the assumption that Condition (5.51) does not hold, namely that the loading does activate pure bending displacements;
2. When pure bending is inhibited, we used the assumption "$G \in \mathcal{V}'_{\rm m}$", equivalent to Condition (5.62).

We therefore proceed to analyze these assumptions and – in particular – the consequences produced when they do not hold.

5.3.1 Effect of the loadings that do not activate the pure bending displacements

As noted in Remark 5.1.3, there may be situations in which pure bending is not inhibited and yet U^0 – the solution of (5.34) – is zero due to

$$G(V) = 0, \qquad \forall V \in \mathcal{V}_0. \tag{5.99}$$

We now investigate this specific issue further. More specifically, we will look for a scaling corresponding to $\rho < 3$ that provides an admissible asymptotic behavior (since $\rho = 3$ gives a zero limit). To that purpose, we will use a preliminary result stated in the following lemma.

Lemma 5.3.1. *$\mathcal{V}$ can be decomposed into the direct sum*

$$\mathcal{V} = \mathcal{V}_0 \oplus \mathcal{V}_1, \tag{5.100}$$

where $\mathcal{V}_1$ is the subspace of $\mathcal{V}$ uniquely determined by

$$A_{\rm b}(V_0, V_1) = 0, \qquad \forall (V_0, V_1) \in \mathcal{V}_0 \times \mathcal{V}_1. \tag{5.101}$$

Proof. Lemma 5.1.1 implies that $A_{\rm b} + A_{\rm m}$ defines an inner product of associated norm equivalent to the norm of $\mathcal{V}$. We call $\mathcal{V}_1$ the subspace of $\mathcal{V}$ orthogonal to $\mathcal{V}_0$ for this new inner product. The subspace $\mathcal{V}_1$ is well-defined, and uniquely determined by the orthogonality property

$$A_{\rm b}(V_0,V_1)+A_{\rm m}(V_0,V_1)=A_{\rm b}(V_0,V_1)=0,\ \forall (V_0,V_1)\in \mathcal{V}_0\times\mathcal{V}_1. \quad (5.102)$$

■

Using the decomposition provided by Lemma 5.3.1, we can write in a unique manner

$$U^\varepsilon = U_0^\varepsilon + U_1^\varepsilon, \quad (5.103)$$

with $(U_0^\varepsilon, U_1^\varepsilon)\in \mathcal{V}_0\times\mathcal{V}_1$. We now characterize U_0^ε and U_1^ε by using test functions taken from $\mathcal{V}_0$ and $\mathcal{V}_1$ in (5.4). With $V_0\in\mathcal{V}_0$, using (5.101) and (5.99) we obtain

$$\varepsilon^3 A_{\rm b}(U_0^\varepsilon,V_0)=\varepsilon^\rho G(V_0)=0, \quad (5.104)$$

and since this holds for any $V_0\in\mathcal{V}_0$, we infer that

$$U_0^\varepsilon = 0, \quad (5.105)$$

hence

$$U^\varepsilon = U_1^\varepsilon \in \mathcal{V}_1. \quad (5.106)$$

Using then $V_1\in\mathcal{V}_1$ in (5.4), we further obtain

$$\varepsilon^3 A_{\rm b}(U^\varepsilon,V_1)+\varepsilon A_{\rm m}(U^\varepsilon,V_1)=\varepsilon^\rho G(V_1),\qquad \forall V_1\in\mathcal{V}_1, \quad (5.107)$$

Note that, by definition

$$\mathcal{V}_1\cap\mathcal{V}_0=\{0\}, \quad (5.108)$$

i.e. the only pure bending displacement in $\mathcal{V}_1$ is the zero displacement. Therefore, we now have in $\mathcal{V}_1$ a situation identical to the inhibited pure bending situation in $\mathcal{V}$. We can thus define $\mathcal{V}_{1\rm m}$ as the completion of $\mathcal{V}_1$ for the norm $\|\cdot\|_{\rm m}$ associated with $A_{\rm m}$ (note that it is a norm in $\mathcal{V}_1$, although not in $\mathcal{V}$), and the limit problem:
Find $U_1^{\rm m}\in\mathcal{V}_{1\rm m}$ *such that*

$$A_{\rm m}(U_1^{\rm m},V_1)=G(V_1),\qquad \forall V_1\in\mathcal{V}_{1\rm m}. \quad (5.109)$$

We then state the following convergence result, which can be proved exactly like Proposition 5.1.3.

Proposition 5.3.1 *Assume that* $G\in\mathcal{V}'_{1\rm m}$. *Then, setting* $\rho=1$, U^ε *converges strongly in* $\mathcal{V}_{1\rm m}$ *to* $U_1^{\rm m}$, *the solution of (5.109). Moreover, we have*

$$\lim_{\varepsilon\to 0}\varepsilon^2 A_{\rm b}(U^\varepsilon,U^\varepsilon)=0. \quad (5.110)$$

Remark 5.3.1. The condition $G \in \mathcal{V}'_{1\mathrm{m}}$ is equivalent to (see Remark 5.1.6)

$$|G(V_1)| \leq C\sqrt{A_{\mathrm{m}}(V_1, V_1)}, \qquad \forall V_1 \in \mathcal{V}_1, \tag{5.111}$$

which is also equivalent to

$$|G(V)| \leq C\sqrt{A_{\mathrm{m}}(V, V)}, \qquad \forall V \in \mathcal{V} \tag{5.112}$$

since we can decompose any $V \in \mathcal{V}$ into $V_0 + V_1$ with $(V_0, V_1) \in \mathcal{V}_0 \times \mathcal{V}_1$, and drop all the terms containing V_0, recalling (5.99) and $A_{\mathrm{m}}(V_0, V_0) = 0$. ■

Therefore, for particular loadings that satisfy (5.99), it appears that the asymptotic behavior obtained is similar to the case of inhibited pure bending, i.e. it is membrane-dominated and the stiffness of the structure varies like ε. However, to understand the *general* behavior of a shell structure we – of course – need to consider various loading distributions, and in particular also the effect of perturbations on the loading used above. Such perturbed loading can be represented by substituting $G + \bar{G}$ for G in (5.4), assuming that G satisfies (5.99) but not $\bar{G}$, and that the amplitude of $\bar{G}$ is "small" compared to that of G. Note that $\bar{G}$, although activating the pure bending deformations, is assumed to correspond to the same asymptotic scaling as G – namely $\rho = 1$ – i.e. we use $F^\varepsilon = \varepsilon(G + \bar{G})$ in the right-hand side of (5.4). Then, due to the linearity of the problem, the new solution is $U^\varepsilon + \bar{U}^\varepsilon/\varepsilon^2$, where U^ε is the element of $\mathcal{V}_1$ that satisfies

$$A_{\mathrm{m}}(U^\varepsilon, V_1) + \varepsilon^2 A_{\mathrm{b}}(U^\varepsilon, V_1) = G(V_1), \qquad \forall V_1 \in \mathcal{V}_1, \tag{5.113}$$

and $\bar{U}^\varepsilon$ is the solution of

$$A_{\mathrm{b}}(\bar{U}^\varepsilon, V) + \frac{1}{\varepsilon^2} A_{\mathrm{m}}(\bar{U}^\varepsilon, V) = \bar{G}(V), \qquad \forall V \in \mathcal{V}. \tag{5.114}$$

This bending-dominated problem is well-posed and has a finite non-zero limit solution in $\mathcal{V}_0$ when ε tends to zero, since $\bar{G}$ was assumed to activate the pure-bending displacements. However, this convergence behavior holds for the norm of $\mathcal{V}$, whereas the convergence of U^ε takes place in the membrane norm, therefore we cannot directly compare the terms U^ε and $\bar{U}^\varepsilon/\varepsilon^2$. Nevertheless, we can compare the asymptotic orders of their respective deformation energies, i.e.

$$\mathcal{D}(V) = \varepsilon A_{\mathrm{m}}(V, V) + \varepsilon^3 A_{\mathrm{b}}(V, V) \tag{5.115}$$

for $V = U^\varepsilon$ and for $V = \bar{U}^\varepsilon/\varepsilon^2$. For U^ε, according to Prop. 5.3.1, the dominant part of the energy is $\varepsilon A_{\mathrm{m}}(U^\varepsilon, U^\varepsilon)$, and $A_{\mathrm{m}}(U^\varepsilon, U^\varepsilon)$ converges to a finite value. By contrast, for $\bar{U}^\varepsilon/\varepsilon^2$, Prop. 5.1.2 implies that the dominant

term is $\varepsilon^{-1}A_{\rm b}(\bar{U}^\varepsilon, \bar{U}^\varepsilon)$, where $A_{\rm b}(\bar{U}^\varepsilon, \bar{U}^\varepsilon)$ converges to a finite value. Thus, even though the amplitude of the perturbation is small, the effect of this perturbation becomes dominant when ε is sufficiently small, with a relative amplification factor proportional to $1/\varepsilon^2$ in the deformation energy.

Example 5.3.1
We consider an infinitely long circular cylinder of radius R and of constant thickness t, with the natural coordinate system introduced in Section 5.2.3. We use the s-m-b shell formulation (4.36). The cylinder is loaded by a (non-constant) internal pressure independent of the ξ^1 coordinate. Therefore the solution is independent of ξ^1 and, for symmetry reasons,

$$u_1 = \theta_1 = 0. \tag{5.116}$$

For certain choices of the pressure distribution, we can derive closed-form solutions of the problem by solving simple systems of linear equations. This will allow us to illustrate our above discussions. We use $L = R$ to define ε, namely

$$\varepsilon = \frac{t}{R}, \tag{5.117}$$

and we introduce the following three constants:

$$\beta_1 = \frac{1}{12(1-\nu^2)}, \qquad \beta_2 = \frac{1}{1-\nu^2}, \qquad \beta_3 = \frac{1}{2(1+\nu)}. \tag{5.118}$$

If a constant pressure is applied on the cylinder, pure bending displacements are clearly not activated. We therefore consider the following right-hand side:

$$F^\varepsilon(V) = \varepsilon \int_\omega p v_3 \, dS, \tag{5.119}$$

where p is a constant. Note that this is consistent with the membrane-type scaling. We obtain the following values for the displacements:

$$u_2 = \theta_2 = 0, \tag{5.120}$$

$$u_3 = \frac{pR}{E} \frac{1}{\beta_2 + \beta_1 \varepsilon^2}. \tag{5.121}$$

For a slice of unit length, the energy values corresponding to the bending and membrane parts are, respectively,

$$\mathcal{D}_b = \pi \beta_1 \frac{p^2 R^2}{E} \frac{\varepsilon^3}{(\beta_2 + \beta_1 \varepsilon^2)^2}, \tag{5.122}$$

$$\mathcal{D}_m = \pi\beta_2 \frac{p^2R^2}{E} \frac{\varepsilon}{(\beta_2 + \beta_1\varepsilon^2)^2}, \tag{5.123}$$

and the shear energy is zero.

Suppose now that the constant pressure above is perturbed by the term

$$\bar{F}^\varepsilon(V) = \varepsilon \int_\omega \bar{p}\cos(2\xi_2/R) v_3 \, dS, \tag{5.124}$$

where $\bar{p}$ is a constant much smaller than p. We can also compute analytically the solution corresponding to this perturbation. We obtain, for the displacements,

$$\bar{u}_2 = -\frac{\bar{p}R}{E}\left(\frac{1}{18\beta_1}\varepsilon^{-2} + \frac{5}{9\beta_2} + \frac{2}{9\beta_3}\right)\sin(2\xi_2/R), \tag{5.125}$$

$$\bar{u}_3 = \frac{\bar{p}R}{E}\left(\frac{1}{9\beta_1}\varepsilon^{-2} + \frac{4}{9\beta_2} + \frac{4}{9\beta_3}\right)\cos(2\xi_2/R), \tag{5.126}$$

$$\bar{\theta}_2 = \frac{\bar{p}}{E}\left(\frac{1}{6\beta_1}\varepsilon^{-2} + \frac{1}{3\beta_2}\right)\sin(2\xi_2/R), \tag{5.127}$$

and for the bending, membrane and shear energies, respectively,

$$\mathcal{D}_b = \frac{\pi}{18\beta_1}\frac{\bar{p}^2R^2}{E}\varepsilon^{-1}, \tag{5.128}$$

$$\mathcal{D}_m = \frac{2\pi}{9\beta_2}\frac{\bar{p}^2R^2}{E}\varepsilon, \tag{5.129}$$

$$\mathcal{D}_s = \frac{2\pi}{9\beta_3}\frac{\bar{p}^2R^2}{E}\varepsilon. \tag{5.130}$$

Of course, these results are fully consistent with the earlier given theoretical discussions. Here, even though $\bar{p}$ is much smaller than p, the effect of the perturbation is dominant in the displacements themselves when t is smaller than $R\sqrt{\bar{p}/p}$, and in the energy also when t is smaller than $R\bar{p}/p$. ■

Remark 5.3.2. In our above discussions, we have considered the effect of a perturbation in a loading that originally satisfies (5.99). We could alternatively consider the effect of a perturbation of the geometry (for example small geometrical flaws with respect to a specific design) for a fixed loading. Indeed, the property expressed by (5.99) pertains to a given loading applied on a given structure, as $\mathcal{V}_0$ is defined on the basis of a given geometry. For example, constant pressure does – in general – activate pure bending displacements when the surface considered is not a circular cylinder. The effect

of such a perturbation would thus be amplified by the change of asymptotic behavior, from a membrane-dominated to a bending-dominated behavior. ■

From our discussions, it follows that the membrane-type asymptotic behavior obtained when the loading satisfies (5.99) – and for which the stiffness of the structure varies like ε – is misleading because this behavior is "unstable". Namely, a small perturbation in the loading (or in the geometry of the structure) will – in general – produce large effects corresponding to a bending-dominated behavior (for which the stiffness of the structure varies like ε^3). Therefore, since – as previously mentioned – a situation where (5.99) holds is very likely to occur only as the result of a deliberate design, we in fact showed that such a design should be avoided (unless, of course, this "unstable" effect is specifically sought).

5.3.2 Effect of non-admissible membrane loadings

When pure bending is inhibited, we say that we have a non-admissible membrane loading if the condition "$G \in \mathcal{V}'_{\rm m}$" or – equivalently – if Condition (5.62) does not hold. We proceed to consider and discuss two examples in which this situation prevails. We also refer to (Pitkäranta et al., 1995) for another thoroughly analyzed example.

The "Scordelis-Lo Roof". This test-problem is widely used for the evaluation of shell finite element procedures. The geometry of the midsurface and the boundary conditions are described in Figure 5.5. The loading is a constant distributed vertical force. The thickness is taken as constant over the whole structure but – unlike in the original test problem – we allow it to vary in order to investigate the asymptotic behavior. Note that – due to symmetry – the computational domain can be taken as one fourth of the whole structure, see Fig. 5.5.

Clearly, in this case pure bending is inhibited (see Section 5.2.3). We then show that we have

$$G \notin \mathcal{V}'_{\rm m}, \tag{5.131}$$

namely we have a non-admissible membrane loading.

Proof of Eq.(5.131). We will construct a sequence of displacements (V_e) with clamped boundary conditions such that $A_{\rm m}(V_e; V_e)$ remains bounded, while $G(V_e)$ tends to infinity when e tends to zero, which will show that Condition (5.62) is violated.

We have

$$G(V) = \int_\omega \vec{g} \cdot \vec{v}\, dS, \tag{5.132}$$

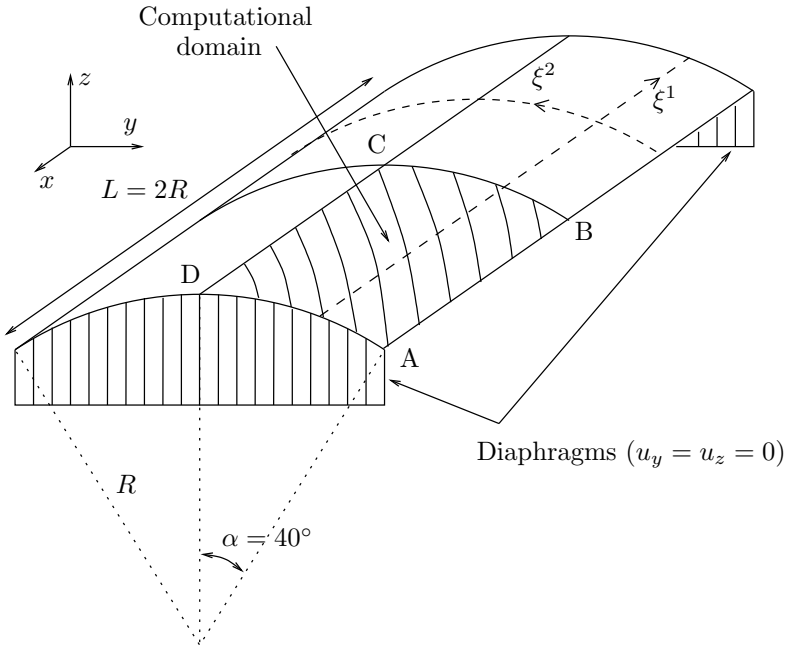

Fig. 5.5. Scordelis-Lo roof

where $\vec{v}$ represents the displacement vector that corresponds to V, and $\vec{g}$ is a constant force vector directed along the z-axis. We use the natural coordinate system of the cylinder such as displayed in Figs. 5.4 and 5.5. We observe that, for an arbitrary smooth function $\psi(\xi^2)$, the displacement field $\vec{v}(\psi)$ defined in covariant components by

$$\begin{cases} v_1(\psi) = 0 \\ v_2(\psi) = \psi(\xi^2) \\ v_3(\psi) = -R\psi'(\xi^2) \end{cases} \tag{5.133}$$

gives zero membrane strains according to System (5.96). Of course, except if ψ is identically zero, this displacement field does not satisfy the clamped boundary conditions (we recall that $\mathcal{V}_0 = \{0\}$). We then define

$$\vec{w}(\psi) = \tau(\xi^1)\vec{v}(\psi), \tag{5.134}$$

where τ is a smooth function of the type described in Figure 5.6. This new displacement field satisfies the prescribed boundary conditions, and gives the following membrane strains

$$\begin{cases} \gamma_{11}(\vec{w}(\psi)) = 0 \\ \gamma_{22}(\vec{w}(\psi)) = 0 \\ \gamma_{12}(\vec{w}(\psi)) = \frac{1}{2}\tau'(\xi^1)\psi(\xi^2) \end{cases} \tag{5.135}$$

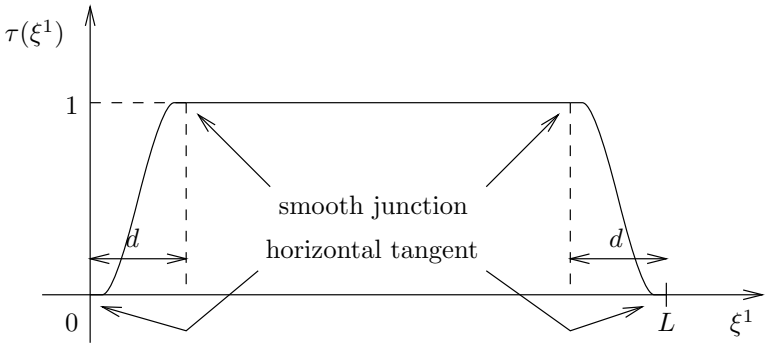

Fig. 5.6. Specifications of τ

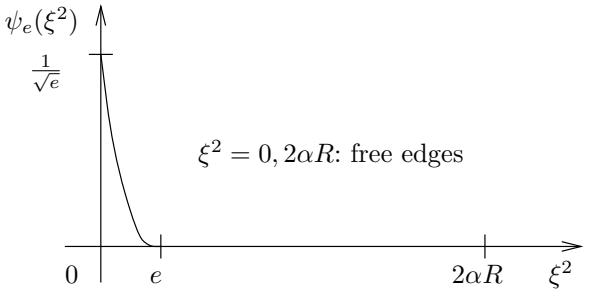

Fig. 5.7. Plot of ψ_e

We now consider a sequence of functions (ψ_e) defined as follows (see also Figure 5.7)

$$\begin{aligned} \psi_e(\xi^2) &= \tfrac{1}{\sqrt{e}}(1 - \tfrac{\xi^2}{e})^3 \quad \text{for } 0 \le \xi^2 \le e \\ &= 0 \qquad\qquad\qquad\quad \text{for } e \le \xi^2 \end{aligned} \tag{5.136}$$

and we construct the displacement sequence (V_e) associated with $(\vec{w}(\psi_e))$. If the model considered is the s-m-b model, we choose the rotation so that the shear strains are zero, namely

$$\underline{\eta} = -\underline{\nabla} v_3 - \underline{\underline{b}} \cdot \underline{v} \tag{5.137}$$

(see Eq. (4.42)). This is allowed since $\vec{w}(\psi_e)$ is sufficiently smooth (in particular, ψ_e is twice continuously differentiable in $\xi^2 = e$). Then we have

$$\begin{aligned} A_{\mathrm{m}}(V_e; V_e) &\propto \int_\omega [\gamma_{12}(\vec{w}(\psi_e))]^2 \, dS \\ &\propto \int_\omega [\psi_e(\xi^2)]^2 \, dS \\ &\propto \left(\frac{1}{\sqrt{e}}\right)^2 \times e = 1 \end{aligned}$$

whereas, since when e is small $w_2(\psi_e) = \tau(\xi^1)\psi_e(\xi^2)$ is much smaller than $w_3(\psi_e) = -R\tau(\xi^1)\psi_e'(\xi^2)$, we have from (5.132)

$$\begin{aligned} G(V_e) &= \int_\omega \vec{g} \cdot \vec{w}(\psi_e) \, dS \\ &\propto \int_\omega g_3 w_3(\psi_e) \, dS \\ &\propto |\psi_e'(\xi^2 = 0)| \times e \\ &\propto \frac{1}{\sqrt{e}}. \end{aligned}$$

Therefore, (5.62) is violated, which shows the result. ∎

Remark 5.3.3. In the literature, this test problem is analyzed with various types of boundary conditions enforced along the curved boundaries, namely some degrees of freedom may or may not be fixed. Note that the above argument is applicable to all such cases, because the sequence of displacement fields constructed here with clamped boundary conditions does also – of course – satisfy any of these other (homogeneous) boundary conditions, and thus is also a sequence for all such cases to show that (5.62) is violated. ∎

The violation of Condition (5.62) can be interpreted by saying that the membrane deformation energy by itself is unable to appropriately control some specific displacement fields that are excited by the loading, such as the sequence of displacements that we constructed in the above proof. This suggests that strong singularities will appear near the free boundaries in the shell structure when the thickness becomes small.

In fact, defining here ε as t/R it can be shown that a boundary layer of width proportional to $\varepsilon^{1/4}$ develops along the free edges, see (Sanchez-Hubert & Sanchez-Palencia, 2001), and also (Karamian et al., 2000; Pitkäranta et al., 2001; Briassoulis, 2002a). Denoting by ${}^1\vec{u}^\varepsilon$ the displacement solution corresponding to a uniform vertical distributed surface force $\vec{f}$ scaled by ε (e.g., representing the weight), we consider the scaled displacement components

$$\begin{cases} \tilde{u}_1^\varepsilon = \varepsilon^{\frac{1}{2}}\, {}^1u_1^\varepsilon \\ \tilde{u}_2^\varepsilon = \varepsilon^{\frac{3}{4}}\, {}^1u_2^\varepsilon \\ \tilde{u}_3^\varepsilon = \varepsilon\, {}^1u_3^\varepsilon \end{cases} \tag{5.138}$$

and the scaled circumferential coordinate

$$\tilde{\xi}^2 = \varepsilon^{-\frac{1}{4}}\, \xi^2, \tag{5.139}$$

designed to "zoom into" the boundary layer in the vicinity of the free edge ($\tilde{\xi}^2 = \xi^2 = 0$). Then the scaled displacement components $(\tilde{u}_1^\varepsilon, \tilde{u}_2^\varepsilon, \tilde{u}_3^\varepsilon)$ satisfy a sequence of variational problems (parametrized by ε) in the domains $[0, L] \times [0, l\,\varepsilon^{-1/4}]$, where l denotes the circumferential length of the computational domain, and these problems can be shown to have a well-defined (non-zero) limit solution when ε tends to zero (Sanchez-Hubert & Sanchez-Palencia, 2001). Moreover, the scaled energy

$$\varepsilon^{\frac{3}{4}} \int_{\mathcal{S}} \vec{f} \cdot {}^1\vec{u}^\varepsilon \, dS \tag{5.140}$$

converges to a finite (non-zero) value. From this, it immediately follows that the scaling corresponding to

$$\boxed{\rho = \frac{7}{4}} \tag{5.141}$$

provides an admissible asymptotic behavior. Note that, however, this scaling does not correspond to a (direct) convergence of the displacements, since the convergence can only be obtained by scaling the displacements and the circumferential coordinate as explained above. Denoting by $\vec{u}^\varepsilon$ the displacement sequence produced by the scaling (5.141) we have – of course – $\vec{u}^\varepsilon = \varepsilon^{3/4}\, {}^1\vec{u}^\varepsilon$, hence the converging quantities are given by

$$\begin{cases} \tilde{u}_1^\varepsilon = \varepsilon^{-\frac{1}{4}}\, u_1^\varepsilon \\ \tilde{u}_2^\varepsilon = u_2^\varepsilon \\ \tilde{u}_3^\varepsilon = \varepsilon^{\frac{1}{4}}\, u_3^\varepsilon \end{cases} \tag{5.142}$$

Numerical experiments provide a very valuable illustration of this theoretical discussion, see (Lee & Bathe, 2002). All the numerical results presented below have been obtained using a uniform mesh of 72×72 MITC4 elements – see Chapter 8 where these elements are discussed – in the computational domain (see Figure 5.5), for various values of the thickness ratio (unlike in the original benchmark proposed by Scordelis and Lo where only $\varepsilon = 10^{-2}$ was considered). The specific numerical values used are $R = 300$, $E = 3.\,10^6$, $\nu = 0$ and a vertical distributed surface force of 0.625 (with all values expressed in consistent units, namely inches and pounds in the original test problem). The given value of the force is only used for $\varepsilon = 10^{-2}$, as we consider scalings for other situations, see below.

The computed distributions of membrane and bending energies – scaled by the total strain energy for each value of ε – are shown in Figures 5.8 and 5.9[2] (note that they are represented over the computational domain ABCD, recall Figure 5.5). As expected, the strain energy increasingly concentrates in the boundary layer as the thickness decreases. In addition, we can check that the membrane and bending energies remain of the same order of magnitude. This is in accordance with the identity proven in (Baiocchi & Lovadina, 2002), that expresses the asymptotic proportion of bending energy (with respect to total strain energy) as

$$\boxed{R_b = \frac{\rho - 1}{2},} \tag{5.143}$$

namely, $R_b = 3/8$ here.

Further, we can represent the scaled vertical displacement

$$\tilde{u}_z^\varepsilon = \varepsilon^{\frac{1}{4}}\, u_z^\varepsilon \tag{5.144}$$

in the cross-section BC and against the scaled circumferential coordinate defined above. Note that – e.g. at point B – the quantity $\tilde{u}_z^\varepsilon$ can be expressed as

$$\tilde{u}_z^\varepsilon = \varepsilon^{\frac{1}{4}} (\cos\alpha\, u_3^\varepsilon + \sin\alpha\, u_1^\varepsilon) = \cos\alpha\, \tilde{u}_3^\varepsilon + \varepsilon^{\frac{1}{2}}\, \sin\alpha\, \tilde{u}_1^\varepsilon, \tag{5.145}$$

hence $\tilde{u}_z^\varepsilon$ features a well-defined limit behavior governed by that of $\tilde{u}_3^\varepsilon$. We show the numerical results in Figure 5.10, with the scaled coordinate defined as $5.35\,\tilde{\xi}^2$ so that it is 0 on the free boundary and approximately 1 at the location of the first peak of the solution, see (Lee & Bathe, 2002). We can thus check that a converging behavior appears to be obtained.

[2] We include here results of $\varepsilon = 10^{-5}$ and 10^{-6} merely in order to clearly identify the asymptotic behavior.

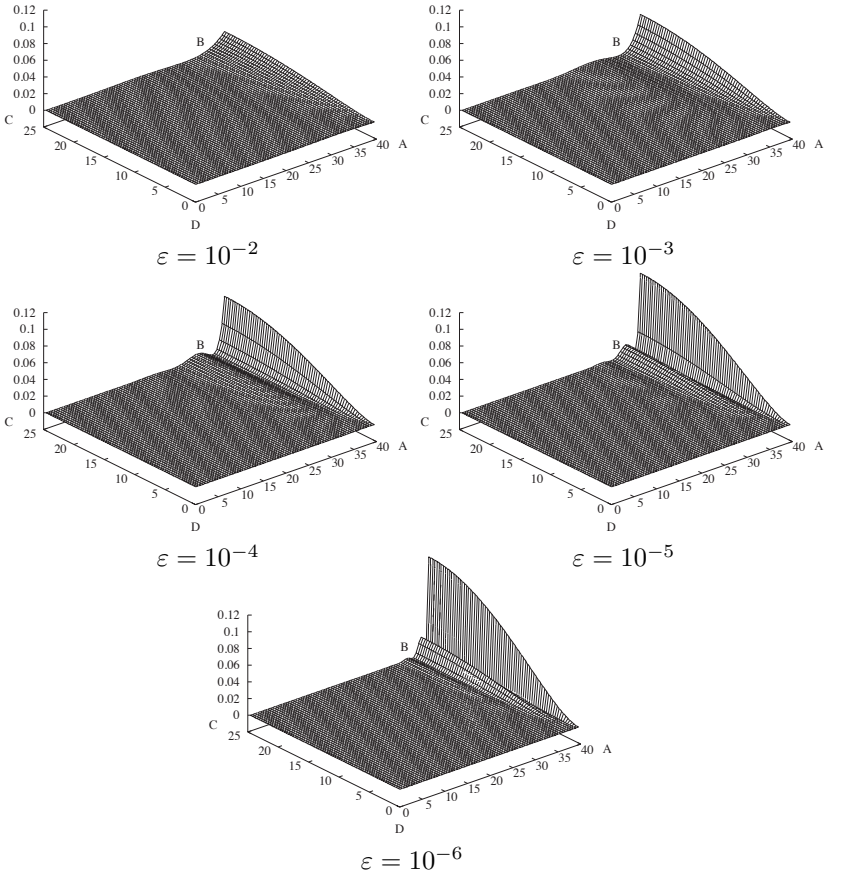

$\varepsilon = 10^{-2}$ $\varepsilon = 10^{-3}$

$\varepsilon = 10^{-4}$ $\varepsilon = 10^{-5}$

$\varepsilon = 10^{-6}$

Fig. 5.8. Distribution of membrane energy

Finally, in Table 5.1, we give the computed strain energy scaled by a proper factor as provided by the theoretical analysis, namely, we consider here the energy obtained for the loading proportional to ε (self-weight) and we multiply this energy by the factor

$$\left(\frac{\varepsilon}{0.01}\right)^{\rho-1} = \left(\frac{\varepsilon}{0.01}\right)^{\frac{3}{4}}. \tag{5.146}$$

We observe that a stable value is obtained for the scaled energy as the thickness decreases. The convergence behavior, however, is not definitely demonstrated in the numerical values (especially for the smallest value of the thickness). This is probably due to the relative coarsening of the mesh inside the

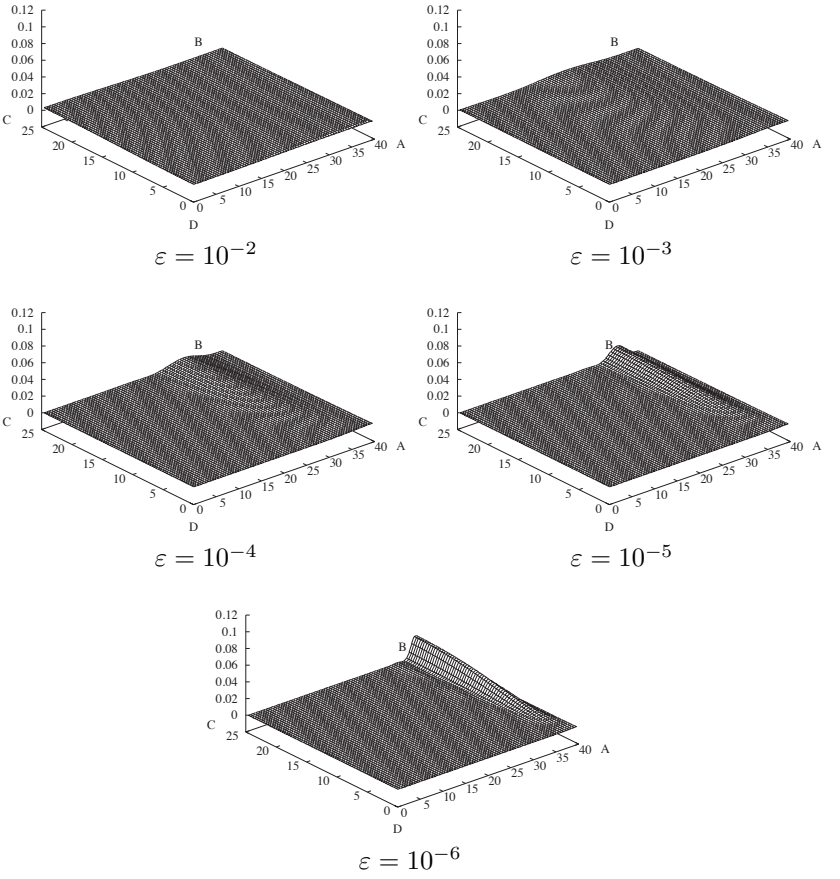

$\varepsilon = 10^{-2}$ $\varepsilon = 10^{-3}$

$\varepsilon = 10^{-4}$ $\varepsilon = 10^{-5}$

$\varepsilon = 10^{-6}$

Fig. 5.9. Distribution of bending energy

Table 5.1. Strain energy (W) scaled for $\rho = 1.75$

ε	10^{-2}	10^{-3}	10^{-4}	10^{-5}
W	1.451 10^4	1.493 10^4	1.479 10^4	1.428 10^4

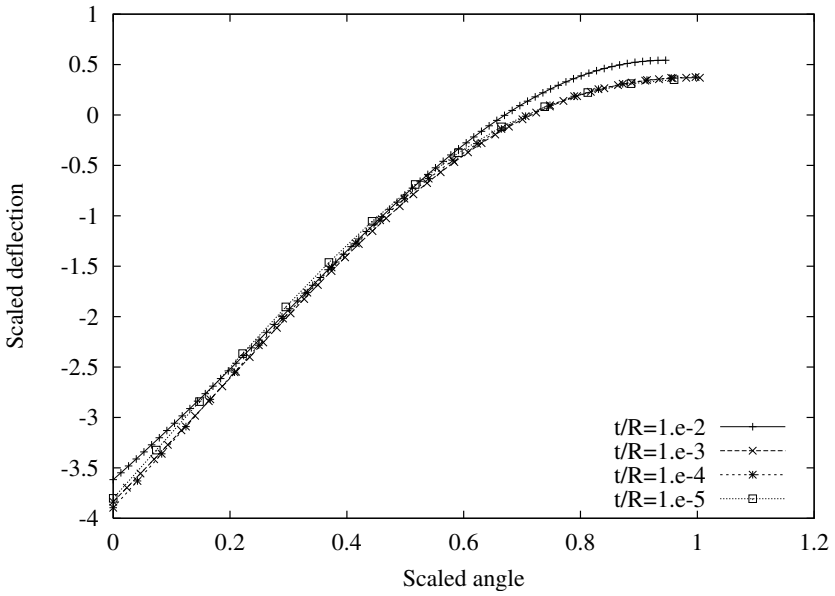

Fig. 5.10. Scaled deflection $\tilde{u}_z^\varepsilon$ inside the boundary layer

boundary layer in which the dominant displacements and energies concentrate (see in particular Figure 5.10 where the scaled mesh size appears to be about five times as large for $\varepsilon = 10^{-5}$ as for $\varepsilon = 10^{-2}$), which is – of course – detrimental to the accuracy of the solution.

Remark 5.3.4. In (Sanchez-Hubert & Sanchez-Palencia, 2001), it is also shown that the scaled problem satisfied by $(\tilde{u}_1^\varepsilon, \tilde{u}_2^\varepsilon, \tilde{u}_3^\varepsilon)$ is a penalized problem for which the penalized constraints are a subset of the inextensional constraints. Hence, locking is to be expected with displacement-based finite elements, see Chapter 7. However, the "locking factor" arising in this scaled penalized problem (namely, the penalization coefficient) is proportional to ε^{-1} only – compared to ε^{-2} for a bending-dominated problem – hence locking should be "softer" in this case. Nevertheless, in order to obtain an optimally accurate finite element solution it is necessary to use a locking-free finite element procedure. ■

Example of a "highly-sensitive shell". Following (Bathe et al., 2003a), see also (Lions & Sanchez-Palencia, 1994; Pitkäranta & Sanchez-Palencia, 1997), we say that we have a "highly-sensitive shell" when the space $\mathcal{V}_{\rm m}$ is not even a distribution space. In such cases – by definition – there exist infinitely smooth internal loadings that do not belong to the dual space $\mathcal{V}'_{\rm m}$. An example of a sensitive shell is depicted in Figure 5.11. We can investigate

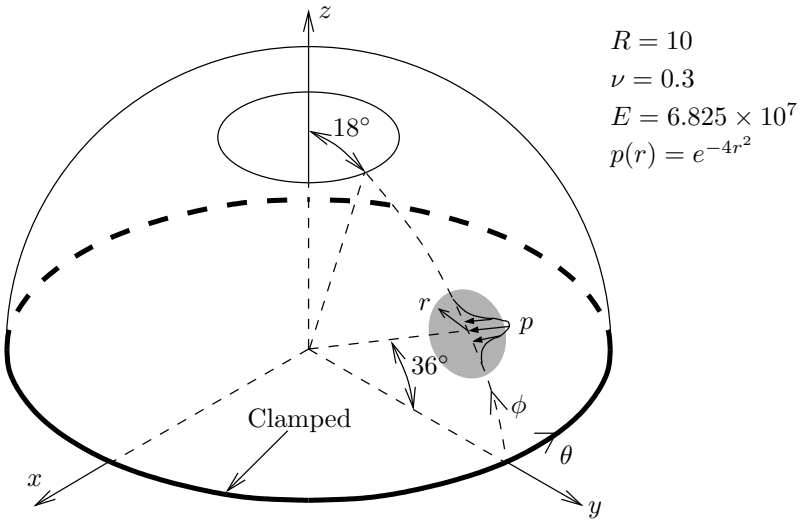

Fig. 5.11. A "highly-sensitive" shell: problem definition

this case by performing numerical experiments (Bathe et al., 2003a). The deformed shapes obtained using MITC4 elements (128 by 32 elements) are shown in Figure 5.12 for various values of the thickness parameter $\varepsilon = t/R$. In this figure, we denote by $\delta_{\max}$ the maximum value of the outward normal displacement and a scaling is applied so that the corresponding plotted maximum value is constant. The behavior observed is in accordance with the theoretical predictions of (Pitkäranta & Sanchez-Palencia, 1997) based on a simplified analysis. In particular, we observe that when the thickness is small the displacements are dominant in the immediate vicinity of the boundary, namely within a boundary layer. This boundary layer has a width of the order of $R/\log(1/\varepsilon)$, and the displacements therein oscillate in the circumferential direction with an angular wavelength inversely proportional to $\log(1/\varepsilon)$.

Further, in Figure 5.13 we show the computed ratio of bending to total strain energies R_b as a function of

$$\alpha = \log\Big(\frac{1}{\varepsilon}\Big). \tag{5.147}$$

We can see that – unlike in the previous example – this ratio does not appear to converge when the thickness decreases. This is also in agreement with the analysis of (Pitkäranta & Sanchez-Palencia, 1997) which predicts that each Fourier component of the loading of the form $\vec{F}_k \cos(k\theta)$ produces a strain energy proportional to

$$W_k = (F_k)^2 \frac{e^{2\mu k}}{c_0 + c_1 k^4 \varepsilon^2 e^{2\mu k}} = (F_k)^2 \frac{e^{2\mu k}}{c_0 + c_1 k^4 e^{2(\mu k - \alpha)}}, \tag{5.148}$$

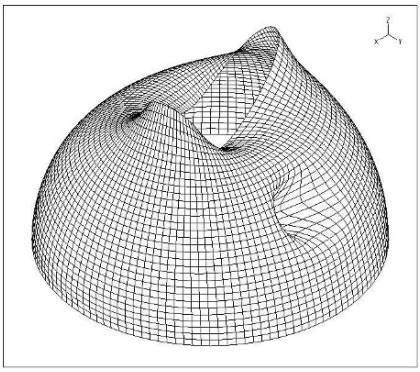

$\varepsilon = 10^{-2},\ \delta_{\max} = 1.66 \times 10^{-6}$

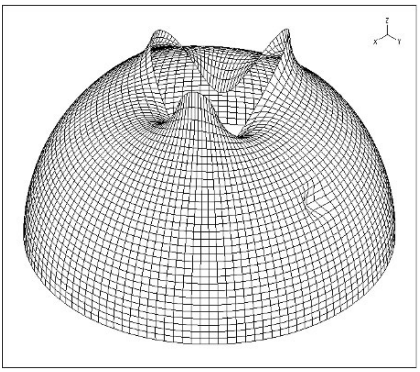

$\varepsilon = 10^{-3},\ \delta_{\max} = 2.53 \times 10^{-4}$

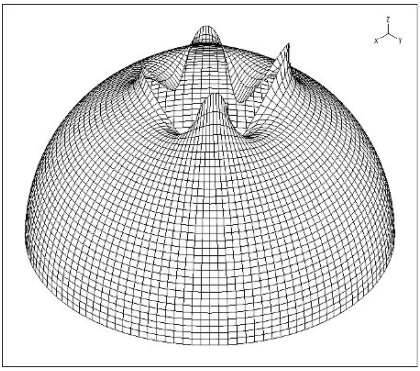

$\varepsilon = 10^{-4},\ \delta_{\max} = 4.03 \times 10^{-2}$

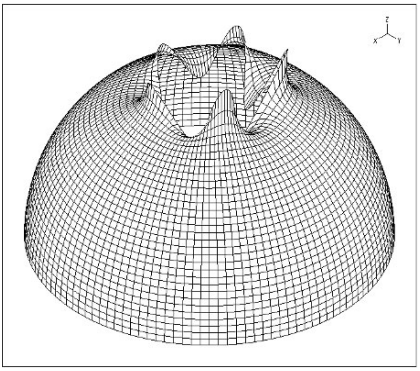

$\varepsilon = 10^{-5},\ \delta_{\max} = 7.19 \times 10^{0}$

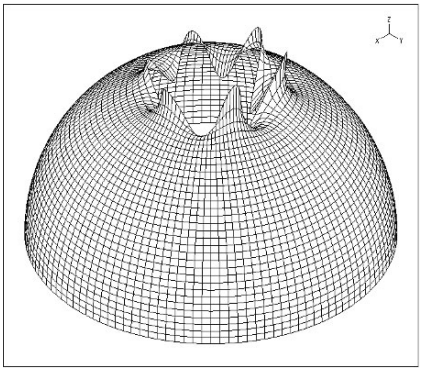

$\varepsilon = 10^{-6},\ \delta_{\max} = 1.35 \times 10^{3}$

Fig. 5.12. Deformed shapes for decreasing values of the thickness

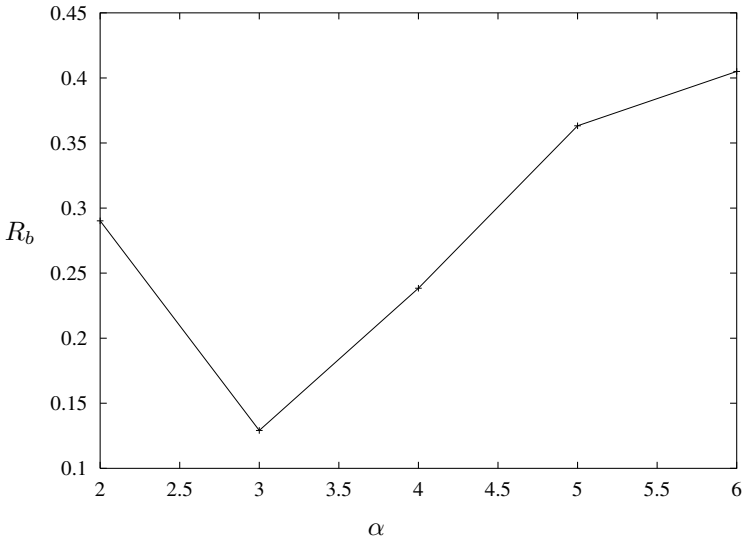

Fig. 5.13. Computed ratio of bending energy

where μ, c_0 and c_1 represent constants independent of k and ε, and F_k denotes a scalar quantity derived from $\vec{F}_k$. In addition, the ratio of bending energy to membrane energy in W_k can be seen to be proportional to the factor

$$k^4 e^{2(\mu k - \alpha)}.$$

This implies that, when α grows (i.e. when ε decreases) we have two distinct stages:

- When α is significantly smaller than μk the energy is bending-dominated and behaves like

$$W_k \approx \frac{(F_k)^2}{c_1 k^4} e^{2\alpha}. \tag{5.149}$$

- When α is significantly larger than μk the energy is membrane-dominated and behaves like

$$W_k \approx \frac{(F_k)^2}{c_0} e^{2\mu k}, \tag{5.150}$$

  hence it does not depend on α.

This behavior is represented in Figure 5.14 (where constants c_0, c_1 and μ are set to one, $F_k = 1$ and $k = 2$). Note that – in actual cases – the asymptotic value of the energy for the kth mode is given by (5.150).

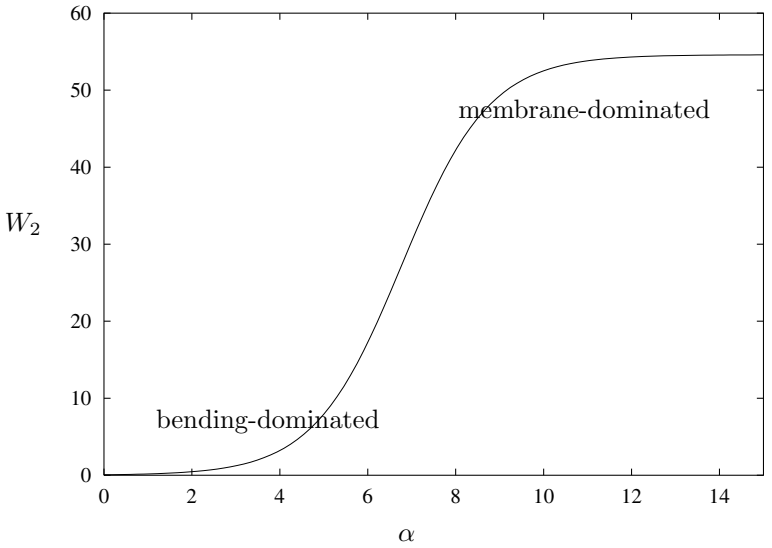

Fig. 5.14. Behavior of the energy for one mode

Then, since the problem is linear and the successive Fourier modes do not interact through the energy, the total energy is simply given by the sum of the energies of all components, and so are the fractions of the energy corresponding to bending and membrane. Therefore, we can see that the ratio R_b is likely to oscillate as α grows and reaches the threshholds corresponding to the successive values of μk. This is – of course – better seen when these values are well separated, so we show in Figure 5.15 the behavior obtained when a symmetric loading is also applied on the opposite side of the spherical cap, which cancels the Fourier modes corresponding to odd values of k. The predicted oscillations are then very clearly observed. In addition, we show in Figures 5.16 and 5.17 the computed distributions of membrane and bending energies scaled by the total strain energy (note that only half of the spherical cap is represented, since the problem is symmetric).

Remark 5.3.5. In (Pitkäranta & Sanchez-Palencia, 1997) the loading applied is a boundary traction, which is why the above coefficients F_k do not depend on ϕ. In our numerical experiments we used a different loading, but we conjecture that a similar simplified theoretical analysis would be applicable. ■

The above discussion and numerical results show that this example gives rise to complex (mixed) states of stresses and strains when the thickness is small. In particular, membrane and bending energies are always present in significant amounts, although it does not appear that we have a limit value

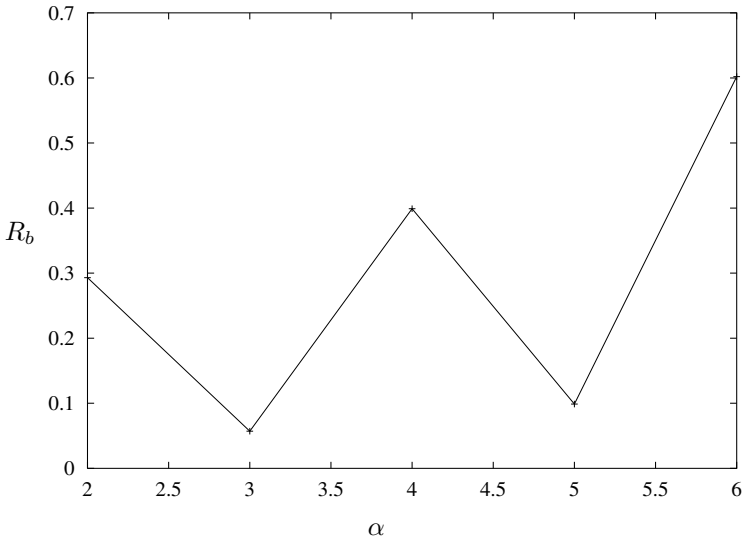

Fig. 5.15. Computed ratio of bending energy for two load application

for the ratios of energies when the thickness tends to zero. Hence it is very likely that we do not have an admissible scaling in this case, see (Baiocchi & Lovadina, 2002; Bathe et al., 2003a). We conclude that – in this case also – it is very important to employ finite element procedures that behave well for both membrane-dominated and bending-dominated behaviors. In particular, we can see from Figures 5.16 and 5.17 that the dominant displacements that arise in the vicinity of the free boundary (corresponding to $\phi = 72°$) are bending-dominated, hence the ability of finite elements to resist locking is of key importance in this problem also.

5.4 Asymptotic Analysis of the 3D-Based Shell Models

By "3D-based shell model" we here mean to refer to mathematical shell models presented earlier based on 3D variational formulations, namely,

- the basic shell model presented in Section 4.2.1 and analyzed (as regards well-posedness) in Section 4.3.3;
- the 3D-shell model presented in Section 4.2.5 and analyzed in Section 4.3.4.

Since these 3D-based shell models cannot be directly written in the generic form (5.4) for which we performed a general asymptotic analysis in Section 5.1, a specific analysis is required, which is the objective of this section. We start with the basic shell model.

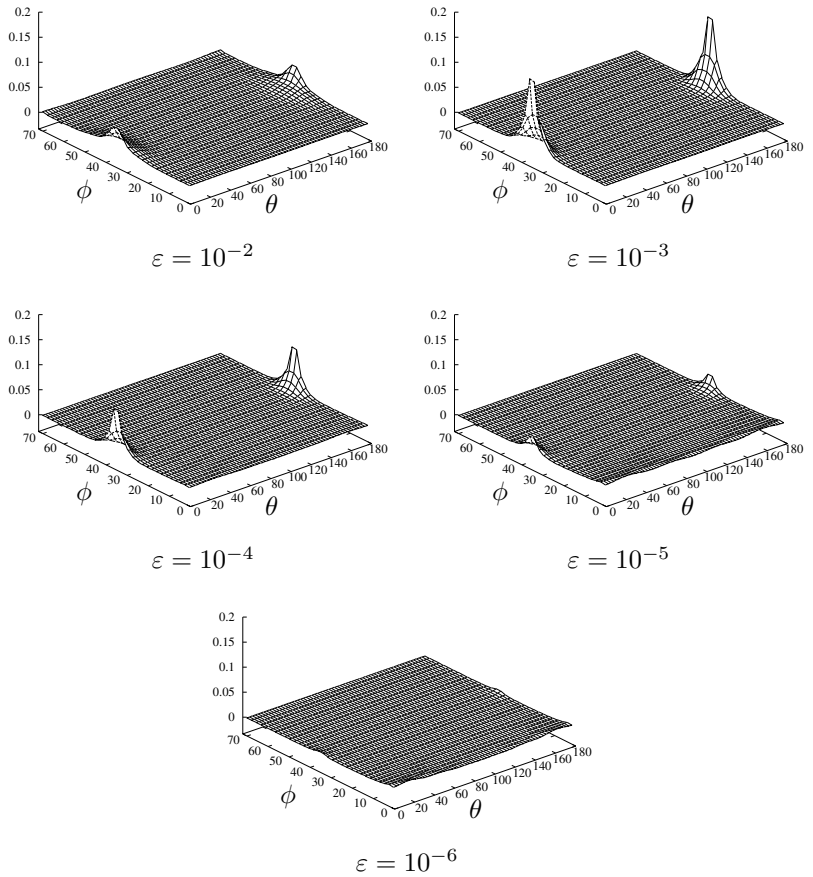

Fig. 5.16. Distribution of membrane energy

5.4.1 Asymptotic analysis of the basic shell model

In particular, a significant difference between the basic shell model and the above-analyzed models is that the loading that is acting on the basic shell model is three-dimensional. We define the 3D body-force as

$$\boxed{\vec{F}^{\varepsilon} = \varepsilon^{\rho-1}\vec{G},} \tag{5.151}$$

where we use the exponent $\rho - 1$ in order to be consistent with the above general asymptotic analysis, since the external work involves an integration

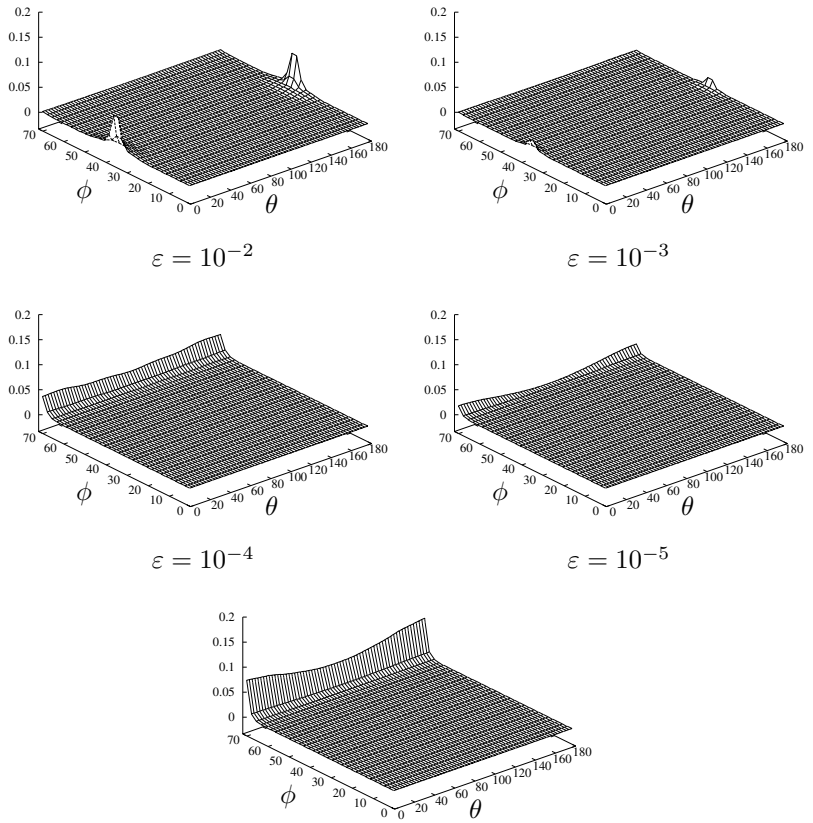

Fig. 5.17. Distribution of bending energy

over the thickness. The vector $\vec{G}$ represents a "force field" *independent of* ε. Furthermore, we assume that $\vec{G}$ is smooth enough to provide

$$\vec{G}(\xi^1, \xi^2, \xi^3) = \vec{G}_0(\xi^1, \xi^2) + \xi^3 \vec{G}_1(\xi^1, \xi^2) + (\xi^3)^2 \vec{B}(\xi^1, \xi^2, \xi^3), \tag{5.152}$$

where $\vec{G}_0$ and $\vec{G}_1$ are in $L^2(\mathcal{S})$, while $\vec{B}$ is a bounded function.

Like for the s-m-b model, we will use the subspace of pure bending displacements:

$$\mathcal{V}_0^B = \mathcal{V}_0^N = \left\{ (\vec{v}, \underline{\eta}) \in \mathcal{V}^N \mid \underline{\underline{\gamma}}(\vec{v}) \equiv \underline{0},\ \underline{\zeta}(\vec{v}, \underline{\eta}) \equiv \underline{0} \right\}. \tag{5.153}$$

We also introduce the bilinear forms that correspond – in the s-m-b model – to the abstract bilinear forms A_{b} and A_{m}, namely

$$A_{\rm b}^N(\vec{u},\underline{\theta};\vec{v},\underline{\eta}) = \int_\omega \frac{l^3}{12}\, {}^0C^{\alpha\beta\lambda\mu}\chi_{\alpha\beta}(\vec{u},\underline{\theta})\chi_{\lambda\mu}(\vec{v},\underline{\eta})\, dS, \tag{5.154}$$

$$A_{\rm m}^N(\vec{u},\underline{\theta};\vec{v},\underline{\eta}) = \int_\omega l\,[{}^0C^{\alpha\beta\lambda\mu}\gamma_{\alpha\beta}(\vec{u}\,)\gamma_{\lambda\mu}(\vec{v}\,) + {}^0D^{\alpha\lambda}\zeta_\alpha(\vec{u},\underline{\theta})\zeta_\lambda(\vec{v},\underline{\eta})]\, dS, \tag{5.155}$$

respectively.

In this section we again assume that essential boundary conditions are prescribed in such a way that no rigid body motion is allowed, hence the shell model gives a well-posed problem for any value of ε, as proven in Section 4.3.3.

We now successively analyze the asymptotic behaviors in the cases of non-inhibited and inhibited pure bending, denoting by $(\vec{u}^\varepsilon,\underline{\theta}^\varepsilon)$ the sequence of solutions obtained for the basic shell model (and for a given scaling to be specified). We refer to (Chapelle & Bathe, 2000) for a similar earlier analysis.

The case of non-inhibited pure bending. We suppose that $\mathcal{V}_0^B$ contains some non-zero elements. Like in the general asymptotic analysis, we will investigate the existence of an admissible asymptotic behavior for the scaling $\rho = 3$. To that purpose, we define the following (tentative) limit problem:
Find $(\vec{u}^0,\underline{\theta}^0) \in \mathcal{V}_0^B$ *such that*

$$\boxed{A_{\rm b}^N(\vec{u}^0,\underline{\theta}^0;\vec{v},\underline{\eta}) = \int_\omega l\,\vec{G}_0\cdot\vec{v}\, dS, \qquad \forall(\vec{v},\underline{\eta}) \in \mathcal{V}_0^B.} \tag{5.156}$$

We can then show the corresponding convergence result.

Proposition 5.4.1 *For the scaling* $\rho = 3$*, the sequence of solutions* $(\vec{u}^\varepsilon,\underline{\theta}^\varepsilon)$ *converges strongly in* $\mathcal{V}^B$ *to* $(\vec{u}^0,\underline{\theta}^0)$*, the solution of (5.156).*

Proof. We need to adapt the strategy used in the general analysis (Prop. 5.1.2). We divide the proof into 4 steps.

i) *Uniform bound on the solution.* We start by noting that, in the proof of the coercivity of the bilinear form which appears in the basic shell model (Chapter 4, Prop. 4.3.5), the constants obtained in the inequalities do not depend on the thickness parameter until the very last step of Eq.(4.151). Hence we have

$$A^B(\vec{v},\underline{\eta};\vec{v},\underline{\eta}) \geq \gamma\int_\omega t\,[a^{\alpha\lambda}a^{\beta\mu}(\frac{1}{6}\gamma_{\alpha\beta}\gamma_{\lambda\mu} + \frac{t^2}{12}\chi_{\alpha\beta}\chi_{\lambda\mu}) + a^{\alpha\beta}\zeta_\alpha\zeta_\beta]\, dS \tag{5.157}$$

where γ does not depend on t. Therefore, recalling that $l \geq L$, we also have

$$\begin{aligned} & A^B(\vec{v}, \underline{\eta}; \vec{v}, \underline{\eta}) \\ & \geq \gamma\, \varepsilon^3 \int_\omega l\, [a^{\alpha\lambda} a^{\beta\mu} (\frac{l^2}{12} \chi_{\alpha\beta} \chi_{\lambda\mu} + \frac{1}{6\varepsilon^2} \gamma_{\alpha\beta} \gamma_{\lambda\mu}) + \frac{1}{\varepsilon^2} a^{\alpha\beta} \zeta_\alpha \zeta_\beta]\, dS \\ & \geq \gamma\, \varepsilon^3 \int_\omega L\, [a^{\alpha\lambda} a^{\beta\mu} (\frac{L^2}{12} \chi_{\alpha\beta} \chi_{\lambda\mu} + \frac{1}{6} \gamma_{\alpha\beta} \gamma_{\lambda\mu}) + a^{\alpha\beta} \zeta_\alpha \zeta_\beta]\, dS, \quad (5.158) \end{aligned}$$

provided that $\varepsilon \leq 1$. Since $L \neq 0$ we infer

$$\begin{aligned} & A^B(\vec{v}, \underline{\eta}; \vec{v}, \underline{\eta}) \\ & \geq \gamma\, \varepsilon^3\, (\|\underline{\underline{\chi}}\|^2_{L^2(\mathcal{S})} + \|\underline{\underline{\gamma}}\|^2_{L^2(\mathcal{S})} + \|\underline{\zeta}\|^2_{L^2(\mathcal{S})}) \\ & \geq \gamma\, \varepsilon^3\, \|\vec{v}, \underline{\eta}\|^2_{\mathcal{V}^B}, \quad (5.159) \end{aligned}$$

using Eq.(4.117) and the assumption that prevents the existence of non-zero rigid body motions. Next, combining Eqs.(2.155) and (5.152) to expand the external virtual work in powers of ε and integrating over the thickness, we obtain

$$\int_\Omega \vec{G} \cdot (\vec{v} + \xi^3 \eta_\lambda \vec{a}^\lambda)\, dV = \int_\omega t\, \vec{G}_0 \cdot \vec{v}\, dS + R, \quad (5.160)$$

where – since all first-order terms in ξ^3 vanish due to the integration through the thickness – the remainder R is bounded as (recall $t \leq C\varepsilon$)

$$|R| \leq C\varepsilon^3 (\|\vec{v}\|_{L^2(\mathcal{S})} + \|\underline{\eta}\|_{L^2(\mathcal{S})}). \quad (5.161)$$

Therefore

$$\begin{aligned} |\varepsilon^2 \int_\Omega \vec{G} \cdot (\vec{v} + \xi^3 \eta_\lambda \vec{a}^\lambda)\, dV| & \leq C\varepsilon^3\, (\|\vec{v}\|_{L^2(\mathcal{S})} + \|\underline{\eta}\|_{L^2(\mathcal{S})}) \\ & \leq C\varepsilon^3\, \|\vec{v}, \underline{\eta}\|_{\mathcal{V}^B}. \quad (5.162) \end{aligned}$$

Hence, setting $(\vec{v}, \underline{\eta}) = (\vec{u}^\varepsilon, \underline{\theta}^\varepsilon)$ in the variational equation

$$A^B(\vec{u}^\varepsilon, \underline{\theta}^\varepsilon; \vec{v}, \underline{\eta}) = \varepsilon^2 \int_\Omega \vec{G} \cdot (\vec{v} + \xi^3 \eta_\lambda \vec{a}^\lambda)\, dV, \quad (5.163)$$

as well as in Eqs.(5.159) and (5.162), we obtain

$$\|\vec{u}^\varepsilon, \underline{\theta}^\varepsilon\|_{\mathcal{V}^B} \leq C. \quad (5.164)$$

ii) *Weak convergence.* Since the sequence $(\vec{u}^\varepsilon, \underline{\theta}^\varepsilon)$ is uniformly bounded, we can extract a subsequence (also denoted by $(\vec{u}^\varepsilon, \underline{\theta}^\varepsilon)$) that converges weakly in $\mathcal{V}^B$ to some limit $(\vec{u}^w, \underline{\theta}^w)$. Using the change of variables $\xi^3 = \varepsilon\xi$, the expression of A^B (4.139) gives

$$
\begin{aligned}
A^B(\vec{u}^\varepsilon, \underline{\theta}^\varepsilon; \vec{v}, \underline{\eta}) = \\
&\varepsilon \int_\omega \int_{\xi=-\frac{l}{2}}^{\frac{l}{2}} C^{\alpha\beta\lambda\mu}[\gamma_{\alpha\beta}(\vec{u}^\varepsilon) + \varepsilon\xi\, \chi_{\alpha\beta}(\vec{u}^\varepsilon, \underline{\theta}^\varepsilon) - \varepsilon^2(\xi)^2\kappa_{\alpha\beta}(\underline{\theta}^\varepsilon)] \\
&\qquad \times[\gamma_{\lambda\mu}(\vec{v}) + \varepsilon\xi\, \chi_{\lambda\mu}(\vec{v}, \underline{\eta}) - \varepsilon^2(\xi)^2\kappa_{\lambda\mu}(\underline{\eta})]\sqrt{g}\, d\xi^1 d\xi^2 d\xi \\
&+ \varepsilon \int_\omega \int_{\xi=-\frac{l}{2}}^{\frac{l}{2}} D^{\alpha\lambda}\zeta_\alpha(\vec{u}^\varepsilon, \underline{\theta}^\varepsilon)\, \zeta_\lambda(\vec{v}, \underline{\eta})\sqrt{g}\, d\xi^1 d\xi^2 d\xi. \qquad (5.165)
\end{aligned}
$$

Assuming sufficient regularity of the midsurface, we can write Taylor expansions of all geometrical quantities. In particular, in addition to Eq.(2.155) we have (recall Eqs.(4.28)–(4.29) compared to (4.34)–(4.35))

$$
C^{\alpha\beta\lambda\mu}(\xi^1, \xi^2, \xi^3) = {}^0C^{\alpha\beta\lambda\mu}(\xi^1, \xi^2) + \xi^3 \bar{C}^{\alpha\beta\lambda\mu}(\xi^1, \xi^2, \xi^3), \qquad (5.166)
$$

$$
D^{\alpha\beta}(\xi^1, \xi^2, \xi^3) = {}^0D^{\alpha\beta}(\xi^1, \xi^2) + \xi^3 \bar{D}^{\alpha\beta}(\xi^1, \xi^2, \xi^3), \qquad (5.167)
$$

where $\bar{C}^{\alpha\beta\lambda\mu}$ and $\bar{D}^{\alpha\beta}$ are bounded over Ω uniformly in ε. Therefore, using the weak convergence of $(\vec{u}^\varepsilon, \underline{\theta}^\varepsilon)$) and the bound (5.164) we obtain

$$
\begin{aligned}
&\lim_{\varepsilon\to 0} \varepsilon^{-1} A^B(\vec{u}^\varepsilon, \underline{\theta}^\varepsilon; \vec{v}, \underline{\eta}) \\
&= \int_\omega l\, [{}^0C^{\alpha\beta\lambda\mu}\gamma_{\alpha\beta}(\vec{u}^w)\gamma_{\lambda\mu}(\vec{v}) + {}^0D^{\alpha\lambda}\zeta_\alpha(\vec{u}^w, \underline{\theta}^w)\zeta_\lambda(\vec{v}, \underline{\eta})]\, dS, \\
&= A^N_{\mathrm{m}}(\vec{u}^w, \underline{\theta}^w; \vec{v}, \underline{\eta}). \qquad (5.168)
\end{aligned}
$$

On the other hand, using (5.163) and (5.162) we have

$$
\begin{aligned}
|\varepsilon^{-1} A^B(\vec{u}^\varepsilon, \underline{\theta}^\varepsilon; \vec{v}, \underline{\eta})| &= |\varepsilon \int_\Omega \vec{G} \cdot (\vec{v} + \xi^3\eta_\lambda \vec{a}^\lambda)\, dV| \\
&\leq \varepsilon^2 \|\vec{v}, \underline{\eta}\|_{\mathcal{V}^B}, \qquad (5.169)
\end{aligned}
$$

hence

$$
\lim_{\varepsilon\to 0} \varepsilon^{-1} A^B(\vec{u}^\varepsilon, \underline{\theta}^\varepsilon; \vec{v}, \underline{\eta}) = 0, \qquad (5.170)
$$

and therefore

$$A_{\rm m}^N(\vec{u}^w,\underline{\theta}^w;\vec{v},\underline{\eta})=0. \tag{5.171}$$

Since this holds for *any* $(\vec{v},\underline{\eta})\in\mathcal{V}^B$, we can choose in particular $(\vec{v},\underline{\eta})=(\vec{u}^w,\underline{\theta}^w)$, which implies that $(\vec{u}^w,\underline{\theta}^w)$ is in the subspace of pure bending displacements $\mathcal{V}_0^B$.

iii) *Characterization of* $(\vec{u}^w,\underline{\theta}^w)$. We now take $(\vec{v},\underline{\eta})$ in $\mathcal{V}_0^B$. According to Eq.(5.165) we have

$$\begin{aligned}\varepsilon^{-3}A^B(\vec{u}^\varepsilon,\underline{\theta}^\varepsilon;\vec{v},\underline{\eta})=&\\ \varepsilon^{-1}\int_\omega\int_{\xi=-\frac{l}{2}}^{\frac{l}{2}}&C^{\alpha\beta\lambda\mu}[\gamma_{\alpha\beta}(\vec{u}^\varepsilon)+\varepsilon\xi\,\chi_{\alpha\beta}(\vec{u}^\varepsilon,\underline{\theta}^\varepsilon)-\varepsilon^2(\xi)^2\kappa_{\alpha\beta}(\underline{\theta}^\varepsilon)]\\ &\times[\xi\,\chi_{\lambda\mu}(\vec{v},\underline{\eta})-\varepsilon(\xi)^2\kappa_{\lambda\mu}(\underline{\eta})]\sqrt{g}\,d\xi^1d\xi^2d\xi.\end{aligned} \tag{5.172}$$

We use Eqs.(2.155) and (5.166) to develop this expression in powers of ε. The term of order ε^{-1}, which is

$$\varepsilon^{-1}\int_\omega\int_{\xi=-\frac{l}{2}}^{\frac{l}{2}}\xi\,{}^0C^{\alpha\beta\lambda\mu}\gamma_{\alpha\beta}(\vec{u}^\varepsilon)\chi_{\lambda\mu}(\vec{v},\underline{\eta})\sqrt{a}\,d\xi^1d\xi^2d\xi, \tag{5.173}$$

vanishes because of the integration on ξ. Next, all the zero-order terms that contain $\gamma_{\alpha\beta}(\vec{u}^\varepsilon)$ tend to zero with ε because $\vec{u}^\varepsilon$ converges weakly to $\vec{u}^w$ which is an inextensional displacement. The only zero-order term without $\gamma_{\alpha\beta}(\vec{u}^\varepsilon)$ is

$$\begin{aligned}\int_\omega\int_{\xi=-\frac{l}{2}}^{\frac{l}{2}}(\xi)^2\,{}^0C^{\alpha\beta\lambda\mu}\chi_{\alpha\beta}(\vec{u}^\varepsilon,\underline{\theta}^\varepsilon)\chi_{\lambda\mu}(\vec{v},\underline{\eta})\sqrt{a}\,d\xi^1d\xi^2d\xi&\\ =\int_\omega\frac{l^3}{12}\,{}^0C^{\alpha\beta\lambda\mu}\chi_{\alpha\beta}(\vec{u}^\varepsilon,\underline{\theta}^\varepsilon)\chi_{\lambda\mu}(\vec{v},\underline{\eta})\,dS&\\ =A_{\rm b}^N(\vec{u}^\varepsilon,\underline{\theta}^\varepsilon;\vec{v},\underline{\eta}),&\end{aligned} \tag{5.174}$$

and – of course – all higher-order terms tend to zero with ε. Therefore,

$$\lim_{\varepsilon\to0}\varepsilon^{-3}A^B(\vec{u}^\varepsilon,\underline{\theta}^\varepsilon;\vec{v},\underline{\eta})=A_{\rm b}^N(\vec{u}^w,\underline{\theta}^w;\vec{v},\underline{\eta}). \tag{5.175}$$

Furthermore, using Eqs.(5.163) and (5.160) we have

$$\begin{aligned}\varepsilon^{-3}A^B(\vec{u}^\varepsilon,\underline{\theta}^\varepsilon;\vec{v},\underline{\eta})&=\varepsilon^{-1}\int_\Omega\vec{G}\cdot(\vec{v}+\xi^3\eta_\lambda\vec{a}^\lambda)\,dV\\ &=\int_\omega l\,\vec{G}_0\cdot\vec{v}\,dS+\varepsilon^{-1}R\end{aligned} \tag{5.176}$$

and, taking the limits of both sides, we obtain with (5.161)

$$A_{\rm b}^N(\vec{u}^w,\underline{\theta}^w;\vec{v},\underline{\eta}) = \int_\omega l\,\vec{G}_0\cdot\vec{v}\,dS. \tag{5.177}$$

Since this holds for *any* $(\vec{v},\underline{\eta})$ in $\mathcal{V}_0^B$ and since $(\vec{u}^w,\underline{\theta}^w)\in\mathcal{V}_0^B$, this implies that $(\vec{u}^w,\underline{\theta}^w)$ is the unique solution of the limit pure bending problem for the s-m-b shell model as represented by Eq.(5.156), namely

$$(\vec{u}^w,\underline{\theta}^w) = (\vec{u}^0,\underline{\theta}^0). \tag{5.178}$$

In addition, the whole original sequence $(\vec{u}^\varepsilon,\underline{\theta}^\varepsilon)$ therefore converges weakly to $(\vec{u}^0,\underline{\theta}^0)$.

iv) *Strong convergence.* Using Eq.(5.159) we have

$$\begin{aligned}\|\vec{u}^\varepsilon-\vec{u}^0,\underline{\theta}^\varepsilon-\underline{\theta}^0\|_{\mathcal{V}^B}^2 &\le C\varepsilon^{-3}A^B(\vec{u}^\varepsilon-\vec{u}^0,\underline{\theta}^\varepsilon-\underline{\theta}^0;\vec{u}^\varepsilon-\vec{u}^0,\underline{\theta}^\varepsilon-\underline{\theta}^0)\\ &= C\varepsilon^{-3}\,[A^B(\vec{u}^\varepsilon,\underline{\theta}^\varepsilon;\vec{u}^\varepsilon-\vec{u}^0,\underline{\theta}^\varepsilon-\underline{\theta}^0)\\ &\qquad -A^B(\vec{u}^0,\underline{\theta}^0;\vec{u}^\varepsilon-\vec{u}^0,\underline{\theta}^\varepsilon-\underline{\theta}^0)].\end{aligned} \tag{5.179}$$

We first consider the second term on the right-hand side of this equation, namely

$$II = \varepsilon^{-3}A^B(\vec{u}^0,\underline{\theta}^0;\vec{u}^\varepsilon-\vec{u}^0,\underline{\theta}^\varepsilon-\underline{\theta}^0), \tag{5.180}$$

and we expand it in powers of ε, using again Eqs.(2.155) and (5.166). Since $(\vec{u}^0,\underline{\theta}^0)$ is in $\mathcal{V}_0^B$, this is similar to the expansion performed in Step iii). The only term in ε^{-1} gives zero. Here, all the zero-order terms tend to zero because $(\vec{u}^\varepsilon-\vec{u}^0,\underline{\theta}^\varepsilon-\underline{\theta}^0)$ converges weakly to zero. Of course, all higher-order terms tend to zero also. Hence, II tends to zero.

We then treat the first term using Eqs.(5.163) and (5.160) with $(\vec{v},\underline{\eta}) = (\vec{u}^\varepsilon-\vec{u}^0,\underline{\theta}^\varepsilon-\underline{\theta}^0)$. We obtain

$$I = \varepsilon^{-3}A^B(\vec{u}^\varepsilon,\underline{\theta}^\varepsilon;\vec{u}^\varepsilon-\vec{u}^0,\underline{\theta}^\varepsilon-\underline{\theta}^0) = \int_\omega l\,\vec{G}_0\cdot(\vec{u}^\varepsilon-\vec{u}^0)\,dS+\varepsilon^{-1}R, \tag{5.181}$$

with, by (5.161),

$$|\varepsilon^{-1}R| \le C\varepsilon^2\|\vec{u}^\varepsilon-\vec{u}^0,\underline{\theta}^\varepsilon-\underline{\theta}^0\|_{\mathcal{V}^B} \tag{5.182}$$

which tends to zero since $\|\vec{u}^\varepsilon-\vec{u}^0,\underline{\theta}^\varepsilon-\underline{\theta}^0\|_{\mathcal{V}^B}$ is bounded. Hence I tends to zero also, due to the weak convergence of $\vec{u}^\varepsilon$ to $\vec{u}^0$. Therefore, we infer from (5.179) that $\|\vec{u}^\varepsilon-\vec{u}^0,\underline{\theta}^\varepsilon-\underline{\theta}^0\|_{\mathcal{V}^B}$ tends to zero, i.e. $(\vec{u}^\varepsilon,\underline{\theta}^\varepsilon)$ converges strongly to $(\vec{u}^0,\underline{\theta}^0)$ in $\mathcal{V}^B$. ∎

The case of inhibited pure bending. We now suppose that pure bending is inhibited, namely that the only element of $\mathcal{V}_0^B$ is the zero element. Following the approach previously used in the general analysis, we define the membrane energy norm by

$$\|\vec{v},\underline{\eta}\|_{\rm m} = \sqrt{A_{\rm m}^N(\vec{v},\underline{\eta};\vec{v},\underline{\eta})}, \tag{5.183}$$

the space $\mathcal{V}_{\rm m}^B$ obtained by completion of $\mathcal{V}^B$ for this norm, and the following tentative limit problem:
Find $(\vec{u}^{\rm m},\underline{\theta}^{\rm m}) \in \mathcal{V}_{\rm m}^B$ *such that*

$$\boxed{A_{\rm m}^N(\vec{u}^{\rm m},\underline{\theta}^{\rm m};\vec{v},\underline{\eta}) = \int_\omega l\,\vec{G}_0\cdot\vec{v}\,dS, \qquad \forall(\vec{v},\underline{\eta})\in\mathcal{V}_{\rm m}^B.} \tag{5.184}$$

Note that, since the continuity and coercivity properties of $A_{\rm m}^N$ with respect to the membrane energy norm are directly obtained by construction, the necessary and sufficient condition for this problem to be well-posed (i.e. to satisfy the assumptions of the Lax-Milgram theorem) is that the right-hand side be a linear form in $\mathcal{V}_{\rm m}^B$, namely that (see Remark 5.1.6)

$$|\int_\omega l\,\vec{G}_0\cdot\vec{v}\,dS| \le C\sqrt{A_{\rm m}^N(\vec{v},\underline{\eta};\vec{v},\underline{\eta})}, \qquad \forall(\vec{v},\underline{\eta})\in\mathcal{V}^B. \tag{5.185}$$

We then have the following convergence result.

Proposition 5.4.2 *Assume that Condition (5.185) holds. Then, for the scaling* $\rho = 1$*, the sequence of solutions* $(\vec{u}^\varepsilon,\underline{\theta}^\varepsilon)$ *converges strongly in* $\mathcal{V}_{\rm m}^B$ *to* $(\vec{u}^{\rm m},\underline{\theta}^{\rm m})$*, the solution of (5.184).*

Proof. We follow and adapt the strategy used in the general asymptotic analysis above (Prop. 5.1.3). We divide this proof into 3 parts.

i) *Uniform bound on the solution.* We start like in the proof of Prop. 5.4.1 and we infer from (5.157)

$$\begin{aligned} A^B(\vec{v},\underline{\eta};\vec{v},\underline{\eta}) &\ge \gamma\,\varepsilon\int_\omega l\,[\frac{1}{6}a^{\alpha\lambda}a^{\beta\mu}\gamma_{\alpha\beta}\gamma_{\lambda\mu} + a^{\alpha\beta}\zeta_\alpha\zeta_\beta]\,dS \\ &\ge \gamma\,\varepsilon\,A_{\rm m}^N(\vec{v},\underline{\eta};\vec{v},\underline{\eta}). \end{aligned} \tag{5.186}$$

Combining this bound with (5.159) we obtain

$$A^B(\vec{v},\underline{\eta};\vec{v},\underline{\eta}) \ge \gamma\,\varepsilon\,(\|\vec{v},\underline{\eta}\|_{\rm m}^2 + \varepsilon^2\|\vec{v},\underline{\eta}\|_{\mathcal{V}^B}^2). \tag{5.187}$$

Also, combining (5.160) and (5.161) with (5.185) gives

$$|\int_\Omega \vec{G}\cdot(\vec{v}+\xi^3\eta_\lambda\vec{a}^\lambda)\,dV| \le C\varepsilon\,(\|\vec{v},\underline{\eta}\|_{\rm m}+\varepsilon^2\|\vec{v},\underline{\eta}\|_{\mathcal{V}^B}). \tag{5.188}$$

Then, setting $(\vec{v},\underline{\eta})=(\vec{u}^\varepsilon,\underline{\theta}^\varepsilon)$ in the variational equation

$$A^B(\vec{u}^\varepsilon,\underline{\theta}^\varepsilon;\vec{v},\underline{\eta})=\int_\Omega \vec{G}\cdot(\vec{v}+\xi^3\eta_\lambda\vec{a}^\lambda)\,dV, \tag{5.189}$$

and in the previous two inequalities, we obtain the uniform bound

$$\|\vec{u}^\varepsilon,\underline{\theta}^\varepsilon\|_{\rm m}+\varepsilon\|\vec{u}^\varepsilon,\underline{\theta}^\varepsilon\|_{\mathcal{V}^B}\le C. \tag{5.190}$$

ii) *Weak convergence.* Since the subsequence $(\vec{u}^\varepsilon,\underline{\theta}^\varepsilon)$ is uniformly bounded in the two norms $\|\cdot\|_{\rm m}$ and $\varepsilon\|\cdot\|_{\mathcal{V}^B}$, we can extract a subsequence (also denoted by $(\vec{u}^\varepsilon,\underline{\theta}^\varepsilon)$) that converges weakly in $\mathcal{V}^B_{\rm m}$ to some weak limit $(\vec{u}^w,\underline{\theta}^w)$ and – of course – this subsequence remains bounded in the norm $\varepsilon\|\cdot\|_{\mathcal{V}^B}$.

We now suppose that the geometry is sufficiently regular to allow a second-order Taylor expansion of the coefficients $C^{\alpha\beta\lambda\mu}$ and $D^{\alpha\beta}$ in the form

$$\begin{aligned}&C^{\alpha\beta\lambda\mu}(\xi^1,\xi^2,\xi^3)\\&\quad={}^0C^{\alpha\beta\lambda\mu}(\xi^1,\xi^2)+\xi^3\bar{C}^{\alpha\beta\lambda\mu}(\xi^1,\xi^2)+(\xi^3)^2\hat{C}^{\alpha\beta\lambda\mu}(\xi^1,\xi^2,\xi^3),\end{aligned} \tag{5.191}$$

$$\begin{aligned}&D^{\alpha\beta}(\xi^1,\xi^2,\xi^3)\\&\quad={}^0D^{\alpha\beta}(\xi^1,\xi^2)+\xi^3\bar{D}^{\alpha\beta}(\xi^1,\xi^2)+(\xi^3)^2\hat{D}^{\alpha\beta}(\xi^1,\xi^2,\xi^3),\end{aligned} \tag{5.192}$$

where $\bar{C}^{\alpha\beta\lambda\mu}$ and $\bar{D}^{\alpha\beta}$ are bounded over ω, while $\hat{C}^{\alpha\beta\lambda\mu}$ and $\hat{D}^{\alpha\beta}$ are bounded over Ω (uniformly in ε).

Considering again Eq.(5.165) and using Eqs.(2.155), (5.191) and (5.192) to perform a Taylor expansion, we obtain

$$\varepsilon^{-1}A^B(\vec{u}^\varepsilon,\underline{\theta}^\varepsilon;\vec{v},\underline{\eta})=A^N_{\rm m}(\vec{u}^\varepsilon,\underline{\theta}^\varepsilon;\vec{v},\underline{\eta})+R', \tag{5.193}$$

with

$$|R'|\le C\,\varepsilon^2\,\|\vec{u}^\varepsilon,\underline{\theta}^\varepsilon\|_{\mathcal{V}^B}\|\vec{v},\underline{\eta}\|_{\mathcal{V}^B} \tag{5.194}$$

because all the first-order terms of the expansion vanish due to the integration over the thickness. Making ε tend to zero in (5.193) and keeping $(\vec{v},\underline{\eta})$ fixed, we have

$$\lim_{\varepsilon\to 0}\varepsilon^{-1}A^B(\vec{u}^\varepsilon,\underline{\theta}^\varepsilon;\vec{v},\underline{\eta})=A^N_{\rm m}(\vec{u}^{\,w},\underline{\theta}^w;\vec{v},\underline{\eta}),\tag{5.195}$$

due to the weak convergence of $(\vec{u}^\varepsilon,\underline{\theta}^\varepsilon)$ and to the boundedness of $\varepsilon\|\vec{u}^\varepsilon,\underline{\theta}^\varepsilon\|_{\mathcal{V}^B}$ in the remainder R'. On the other hand, using (5.160) and (5.161) we obtain

$$\lim_{\varepsilon\to 0}\varepsilon^{-1}\int_\Omega \vec{G}\cdot(\vec{v}+\xi^3\eta_\lambda\vec{a}^\lambda)\,dV=\int_\omega l\,\vec{G}_0\cdot\vec{v}\,dS.\tag{5.196}$$

Therefore, since – when multiplying Eq.(5.189) by ε^{-1} – the limits of both sides of the equality obtained must be equal, we infer that $(\vec{u}^{\,w},\underline{\theta}^w)$ is an element of $\mathcal{V}^B_{\rm m}$ that satisfies

$$A^N_{\rm m}(\vec{u}^{\,w},\underline{\theta}^w;\vec{v},\underline{\eta})=\int_\omega l\,\vec{G}_0\cdot\vec{v}\,dS,\tag{5.197}$$

for any $(\vec{v},\underline{\eta})$ in $\mathcal{V}^B$, hence also (by density) for any $(\vec{v},\underline{\eta})$ in $\mathcal{V}^B_{\rm m}$. We can then conclude that $(\vec{u}^{\,w},\underline{\theta}^w)=(\vec{u}^{\,\rm m},\underline{\theta}^{\rm m})$ and that the whole original sequence converges to $(\vec{u}^{\,\rm m},\underline{\theta}^{\rm m})$.

iii) *Strong convergence.* Define

$$\begin{aligned}&A^B_{\rm m}(\vec{u},\underline{\theta};\vec{v},\underline{\eta})\\&\quad=\varepsilon^{-1}\int_\Omega[C^{\alpha\beta\lambda\mu}\gamma_{\alpha\beta}(\vec{u}\,)\gamma_{\lambda\mu}(\vec{v}\,)+D^{\alpha\beta}\zeta(\vec{u},\underline{\theta})\zeta(\vec{v},\underline{\eta})]\,dV.\end{aligned}\tag{5.198}$$

The limit solution $(\vec{u}^{\,\rm m},\underline{\theta}^{\rm m})$ is in $\mathcal{V}^B_{\rm m}$, hence the limit membrane and shear deformation tensors $\underline{\underline{\gamma}}(\vec{u}^{\,\rm m})$ and $\underline{\zeta}(\vec{u}^{\,\rm m},\underline{\theta}^{\rm m})$ are in $L^2(\mathcal{S})$. Therefore, we can consider the quantity

$$I'=A^B_{\rm m}(\vec{u}^{\,\varepsilon}-\vec{u}^{\,\rm m},\underline{\theta}^\varepsilon-\underline{\theta}^{\rm m};\vec{u}^{\,\varepsilon}-\vec{u}^{\,\rm m},\underline{\theta}^\varepsilon-\underline{\theta}^{\rm m}),\tag{5.199}$$

and we have

$$I'=A^N_{\rm m}(\vec{u}^{\,\varepsilon}-\vec{u}^{\,\rm m},\underline{\theta}^\varepsilon-\underline{\theta}^{\rm m};\vec{u}^{\,\varepsilon}-\vec{u}^{\,\rm m},\underline{\theta}^\varepsilon-\underline{\theta}^{\rm m})+R'',\tag{5.200}$$

where R'' is the remainder of the Taylor expansion obtained by using Eqs.(2.155), (5.191) and (5.192). We thus have

$$\begin{aligned}|R''|&\le C\varepsilon^2\,(\|\underline{\underline{\gamma}}(\vec{u}^{\,\varepsilon}-\vec{u}^{\,\rm m})\|^2_{L^2(\mathcal{S})}+\|\underline{\zeta}(\vec{u}^{\,\varepsilon}-\vec{u}^{\,\rm m},\underline{\theta}^\varepsilon-\underline{\theta}^{\rm m})\|^2_{L^2(\mathcal{S})})\\&\le C\varepsilon^2\,\|\vec{u}^{\,\varepsilon}-\vec{u}^{\,\rm m},\underline{\theta}^\varepsilon-\underline{\theta}^{\rm m}\|^2_{\rm m},\end{aligned}\tag{5.201}$$

hence R'' tends to zero with ε. As a consequence, a necessary and sufficient condition for $(\vec{u}^{\,\rm m},\underline{\theta}^{\rm m})$ to converge strongly to $(\vec{u}^{\,\varepsilon},\underline{\theta}^\varepsilon)$ in $\mathcal{V}^B_{\rm m}$ is that I' tend to zero, which we proceed to show.

We develop I' into

$$\begin{aligned} I' &= A_{\rm m}^B(\vec{u}^\varepsilon, \underline{\theta}^\varepsilon; \vec{u}^\varepsilon, \underline{\theta}^\varepsilon) + A_{\rm m}^B(\vec{u}^{\rm m}, \underline{\theta}^{\rm m}; \vec{u}^{\rm m}, \underline{\theta}^{\rm m}) \\ &\quad -2A_{\rm m}^B(\vec{u}^\varepsilon, \underline{\theta}^\varepsilon; \vec{u}^{\rm m}, \underline{\theta}^{\rm m}). \end{aligned} \tag{5.202}$$

Using Taylor expansions, we clearly have

$$\begin{aligned} \lim_{\varepsilon\to 0} A_{\rm m}^B(\vec{u}^{\rm m}, \underline{\theta}^{\rm m}; \vec{u}^{\rm m}, \underline{\theta}^{\rm m}) &= A_{\rm m}^N(\vec{u}^{\rm m}, \underline{\theta}^{\rm m}; \vec{u}^{\rm m}, \underline{\theta}^{\rm m}) \\ &= \int_\omega l\,\vec{G}_0 \cdot \vec{v}\, dS, \end{aligned} \tag{5.203}$$

and – because of the weak convergence of $(\vec{u}^\varepsilon, \underline{\theta}^\varepsilon)$ – we also have

$$\begin{aligned} \lim_{\varepsilon\to 0} A_{\rm m}^B(\vec{u}^\varepsilon, \underline{\theta}^\varepsilon; \vec{u}^{\rm m}, \underline{\theta}^{\rm m}) &= A_{\rm m}^N(\vec{u}^{\rm m}, \underline{\theta}^{\rm m}; \vec{u}^{\rm m}, \underline{\theta}^{\rm m}) \\ &= \int_\omega l\,\vec{G}_0 \cdot \vec{v}\, dS. \end{aligned} \tag{5.204}$$

We then focus on the remaining term $A_{\rm m}^B(\vec{u}^\varepsilon, \underline{\theta}^\varepsilon; \vec{u}^\varepsilon, \underline{\theta}^\varepsilon)$. Since it only concerns $(\vec{u}^\varepsilon, \underline{\theta}^\varepsilon)$, we omit repeating these symbols in the expressions of the strains in the following derivation. We have

$$\begin{aligned} & A_{\rm m}^B(\vec{u}^\varepsilon, \underline{\theta}^\varepsilon; \vec{u}^\varepsilon, \underline{\theta}^\varepsilon) \\ &= \varepsilon^{-1} A^B(\vec{u}^\varepsilon, \underline{\theta}^\varepsilon; \vec{u}^\varepsilon, \underline{\theta}^\varepsilon) + \varepsilon^{-1} \int_\Omega C^{\alpha\beta\lambda\mu}\gamma_{\alpha\beta}\gamma_{\lambda\mu}\, dV \\ &\quad -\varepsilon^{-1} \int_\Omega C^{\alpha\beta\lambda\mu}[\gamma_{\alpha\beta} + \xi^3\chi_{\alpha\beta} - (\xi^3)^2\kappa_{\alpha\beta}] \\ &\qquad\qquad \times[\gamma_{\lambda\mu} + \xi^3\chi_{\lambda\mu} - (\xi^3)^2\kappa_{\lambda\mu}]\, dV \\ &= \varepsilon^{-1} \int_\Omega \vec{G} \cdot (\vec{u}^\varepsilon + \xi^3\theta_\lambda^\varepsilon \vec{a}^\lambda)\, dV \\ &\quad -2\,\varepsilon^{-1} \int_\Omega C^{\alpha\beta\lambda\mu}\gamma_{\alpha\beta}\,[\xi^3\chi_{\lambda\mu} - (\xi^3)^2\kappa_{\lambda\mu}]\, dV \\ &\quad -\varepsilon^{-1} \int_\Omega C^{\alpha\beta\lambda\mu}[\xi^3\chi_{\alpha\beta} - (\xi^3)^2\kappa_{\alpha\beta}][\xi^3\chi_{\lambda\mu} - (\xi^3)^2\kappa_{\lambda\mu}]\, dV. \end{aligned} \tag{5.205}$$

From Eqs.(5.160) and (5.161), using the weak convergence of $(\vec{u}^\varepsilon, \underline{\theta}^\varepsilon)$ in $\mathcal{V}_{\rm m}^B$, the boundedness of $\varepsilon\|\vec{u}^\varepsilon, \underline{\theta}^\varepsilon\|_{\mathcal{V}^B}$ and Condition (5.185), we infer

$$\lim_{\varepsilon\to 0} \varepsilon^{-1} \int_\Omega \vec{G} \cdot (\vec{u}^\varepsilon + \xi^3\theta_\lambda^\varepsilon \vec{a}^\lambda)\, dV = \int_\omega l\,\vec{G}_0 \cdot \vec{u}^{\rm m}\, dS. \tag{5.206}$$

For the second term in the right-hand side of (5.205), we perform a Taylor expansion using (2.155) and (5.191). The first-order terms vanish and we obtain, by the Cauchy-Schwarz inequality,

$$2\,\varepsilon^{-1}\int_{\Omega} C^{\alpha\beta\lambda\mu}\gamma_{\alpha\beta}\,[\xi^3\chi_{\lambda\mu}-(\xi^3)^2\kappa_{\lambda\mu}]\,dV \\ \leq\ C\varepsilon^2\|\underline{\underline{\gamma}}\|_{L^2(\mathcal{S})}\|\vec{u}^{\,\varepsilon},\underline{\theta}^{\varepsilon}\|_{\mathcal{V}^B}, \tag{5.207}$$

hence this term tends to zero with ε, since the membrane strain tensor is bounded in $L^2(\mathcal{S})$ and $\varepsilon\|\vec{u}^{\,\varepsilon},\underline{\theta}^{\varepsilon}\|_{\mathcal{V}^B}$ is bounded.

Furthermore, we have

$$\varepsilon^{-1}\int_{\Omega} C^{\alpha\beta\lambda\mu}[\xi^3\chi_{\alpha\beta}-(\xi^3)^2\kappa_{\alpha\beta}][\xi^3\chi_{\lambda\mu}-(\xi^3)^2\kappa_{\lambda\mu}]\,dV\geq 0, \tag{5.208}$$

since $C^{\alpha\beta\lambda\mu}$ defines a positive-definite bilinear form on second-order tensors. Finally, combining the above results, we see that I' is the sum of

1. a group of terms with definite limits when ε tends to zero, the combination of which yields zero;
2. a negative term.

Since I' must be positive due to the positive-definite characters of $C^{\alpha\beta\lambda\mu}$ and $D^{\alpha\beta}$, it follows that I' tends to zero, which completes the proof. ■

Conclusions on the asymptotic analysis of the basic shell model. From our previous discussions, we can conclude that the basic shell model displays the same asymptotic behaviors as the following s-m-b shell problem: *Find* $(\vec{u}^{\,\varepsilon},\underline{\theta}^{\varepsilon})\in\mathcal{V}^N$ *such that*

$$\boxed{\begin{aligned}&\varepsilon^3 A_{\rm b}^N(\vec{u}^{\,\varepsilon},\underline{\theta}^{\varepsilon};\vec{v},\underline{\eta})+\varepsilon A_{\rm m}^N(\vec{u}^{\,\varepsilon},\underline{\theta}^{\varepsilon};\vec{v},\underline{\eta})\\ &\qquad\qquad=\varepsilon^{\rho}\int_{\omega} l\,\vec{G}_0\cdot\vec{v}\,dS,\qquad\forall(\vec{v},\underline{\eta})\in\mathcal{V}^N.\end{aligned}} \tag{5.209}$$

Note that the surface load of this s-m-b problem is set as the integral over the thickness of the first term in the Taylor expansion of the body forces.

More specifically, when the thickness parameter ε tends to zero, the solution of the basic shell model converges to the same limit solutions – for the same scalings of the loading applied – as the solution of the s-m-b problem (5.209), and with the same subspace of pure bending displacements that determines the type of asymptotic behavior. Namely, when pure bending is not inhibited, the solution converges to the solution of the pure bending limit

problem as defined in (5.156). By contrast, when pure bending is inhibited, the solution converges to the solution of the membrane problem (5.184), provided that the loading satisfies the condition (5.185).

Finally summarizing these conclusions and the discussion on the asymptotic equivalence of the s-m-b and m-b models, we can say that the three shell models that we discussed – namely the basic shell model, the s-m-b model and the m-b model – are all "asymptotically equivalent" and also – recalling Remark 5.1.10 – that these models are all "asymptotically equivalent" to the 3D elastic model.

5.4.2 Asymptotic analysis of the 3D-shell model

We now study the asymptotic behavior of the 3D-shell model, namely, of the solution of Problem (4.161). The primary objective here is to compare the 3D-shell model with classical shell models and with the basic shell model by means of the asymptotic behavior. We may refer to (Chapelle et al., 2004a) for a similar earlier analysis.

We introduce the space of pure bending displacements, defined in this case by

$$\mathcal{V}_0^{3Ds} = \{(\vec{v},\vec{\eta},\vec{\varsigma}) \in \mathcal{V}^{3Ds}, \text{ such that } \gamma_{\alpha\beta}(\vec{v}) = 0,\ \zeta_\alpha(\vec{v},\vec{\eta}) = 0,\ \delta(\vec{\eta}) = 0,\ \forall \alpha,\beta = 1,2\}. \tag{5.210}$$

Comparing with classical shell models and with the basic shell model, $\mathcal{V}_0^{3Ds}$ contains displacements for which pinching strains vanish, in addition to membrane and shear strains. Note that vanishing pinching strains simply means that the transverse component of $\vec{\eta}$ is identically zero.

Depending on the geometry and boundary conditions, the shell may or may not have non-zero pure-bending displacements. We then distinguish between the two situations; that is, when

$$\mathcal{V}_0^{3Ds} \cap \{(\vec{v},\vec{\eta},\vec{0}) \in \mathcal{V}^{3Ds}\} = \{(\vec{0},\vec{0},\vec{0})\},$$

pure bending is inhibited, and when

$$\mathcal{V}_0^{3Ds} \cap \{(\vec{v},\vec{\eta},\vec{0}) \in \mathcal{V}^{3Ds}\} \neq \{(\vec{0},\vec{0},\vec{0})\},$$

pure bending is non-inhibited.

As for the basic shell model, we seek a scaling of the loading in the form

$$\vec{F} = \varepsilon^{\rho-1}\vec{G}, \tag{5.211}$$

In this case, we will assume in our analysis that we take $\vec{G}$ in the form

$$\vec{G}(\xi^1,\xi^2,\xi^3) = \vec{G}_0(\xi^1,\xi^2) + \xi^3\vec{B}(\xi^1,\xi^2,\xi^3), \tag{5.212}$$

where $\vec{G}_0$ is in $L^2(\mathcal{S})$ and $\vec{B}$ is a bounded function over $\mathcal{B}$ (uniformly in t). This assumption is weaker than (5.152) considered for the basic shell model. We make this weaker assumption because we will in any case not be able to obtain the strong convergence results (that we obtained for the other shell models). We will only be able to give results for weak convergence, and hence may as well relax the regularity assumption used in (5.212).

Let us introduce some specific bilinear and linear forms that will be needed in the forthcoming discussion. We define

$$\begin{aligned} A_{\rm m}^{3Ds}(\vec{u},\vec{\theta};\vec{v},\vec{\eta}) \\ = \int_\omega l\Big[{}^0H^{\alpha\beta\lambda\mu}\gamma_{\alpha\beta}(\vec{u})\gamma_{\lambda\mu}(\vec{v}) + {}^0H^{\alpha\beta33}\big(\gamma_{\alpha\beta}(\vec{u})\delta(\vec{\eta}) + \gamma_{\alpha\beta}(\vec{v})\delta(\vec{\theta})\big) \\ +4{}^0H^{\alpha3\beta3}\zeta_\alpha(\vec{u},\vec{\theta})\zeta_\beta(\vec{v},\vec{\eta}) + {}^0H^{3333}\delta(\vec{\theta})\delta(\vec{\eta})\Big]\,dS, \end{aligned} \tag{5.213}$$

$$\begin{aligned} A_{\rm b}^{3Ds}(\vec{u},\vec{\theta},\vec{\varrho};\vec{v},\vec{\eta},\vec{\varsigma}) = \int_\omega \frac{l^3}{12}\Big[{}^0H^{\alpha\beta\lambda\mu}\hat{\chi}_{\alpha\beta}(\vec{u},\vec{\theta})\hat{\chi}_{\lambda\mu}(\vec{v},\vec{\eta}) \\ +{}^0H^{\alpha\beta33}\big(\hat{\chi}_{\alpha\beta}(\vec{u},\vec{\theta})p(\vec{\varsigma}) + \hat{\chi}_{\alpha\beta}(\vec{v},\vec{\eta})p(\vec{\varrho})\big) \\ +4{}^0H^{\alpha3\beta3}m_\alpha(\vec{\theta},\vec{\varrho})m_\beta(\vec{\eta},\vec{\varsigma}) + {}^0H^{3333}p(\vec{\varrho})p(\vec{\varsigma})\Big]\,dS, \end{aligned} \tag{5.214}$$

where the tensor ${}^0H$ is defined by

$${}^0H^{ijkl} = H^{ijkl}|_{\xi^3=0}, \tag{5.215}$$

and we also define

$$G^{3Ds}(\vec{v}) = \int_\omega l\vec{G}_0\cdot\vec{v}\,dS. \tag{5.216}$$

We henceforth denote – in the framework of this asymptotic analysis – the solution of Problem (4.161) for a given thickness parameter ε by $(\vec{u}^\varepsilon,\vec{\theta}^\varepsilon,\vec{\varrho}^\varepsilon)$ and we now discuss the cases of non-inhibited versus inhibited pure bending separately.

The case of non-inhibited pure bending. Assuming that $\mathcal{V}_0^{3Ds}$ contains some non-zero elements, we have a model that can be directly compared to the basic shell model with non-inhibited pure bending. Namely, the terms of order zero in ξ^3 in the strain expressions (4.74) tend to vanish (via a penalization mechanism) and the appropriate scaling factor is then $\rho = 3$.

We define the norm

$$\|\vec{v},\vec{\eta},\vec{\varsigma}\|_{\rm b}=\Big(\|\vec{v}\|_1^2+\|\underline{\eta}\|_1^2+\|\eta_3\|_0^2+\|\varsigma_3\|_0^2+\|\underline{\varsigma}+\frac{1}{2}\underline{\nabla}\eta_3\|_0^2\Big)^{\frac{1}{2}},\qquad(5.217)$$

for which we expect the convergence to occur. This norm is not equivalent to the original norm of the displacement space (namely, the H^1-norm, recall Proposition 4.3.8), since we – in essence – lose in the energy all the strain terms of degree higher than 1 in the ξ^3-expansions (4.74) when ε goes to zero. This norm is, indeed, weaker than the H^1 norm, hence $\mathcal{V}^{3Ds}$ is not complete with respect to $\|\cdot\|_{\rm b}$. We define $\mathcal{V}_{\rm b}^{3Ds}$ as the completion of $\mathcal{V}^{3Ds}$ for this new norm. We will also use the space $\mathcal{V}_{0\rm b}^{3Ds}$, defined as the completion of $\mathcal{V}_0^{3Ds}$ for $\|\cdot\|_{\rm b}$, which is identified as

$$\mathcal{V}_{0\rm b}^{3Ds}=\{(\vec{v},\vec{\eta},\vec{\varsigma})\in\mathcal{V}_{\rm b}^{3Ds}\text{ such that }\gamma_{\alpha\beta}(\vec{v})=0,$$
$$\zeta_\alpha(\vec{v},\vec{\eta})=0,\delta(\vec{\eta})=0,\forall\alpha,\beta=1,2\}.\qquad(5.218)$$

Using the proposed scaling $\rho=3$ the tentative limit problem reads: *Find* $(\vec{u}^0,\vec{\theta}^0,\vec{\varrho}^0)\in\mathcal{V}_{0\rm b}^{3Ds}$ *such that*

$$\boxed{A_{\rm b}^{3Ds}(\vec{u}^0,\vec{\theta}^0,\vec{\varrho}^0;\vec{v},\vec{\eta},\vec{\varsigma})=G^{3Ds}(\vec{v}),\qquad\forall(\vec{v},\vec{\eta},\vec{\varsigma})\in\mathcal{V}_{0\rm b}^{3Ds}.}\qquad(5.219)$$

We point out that we use a similar notation for the tentative limit solution here as for the basic shell model for the sake of simplicity, but this does not mean that we are presuming any connection between the two limit solutions at this stage. Note that the right-hand side of this variational formulation defines a linear form in $\mathcal{V}_{0\rm b}^{3Ds}$ (although this completed space may contain elements that do not belong to $\mathcal{V}^{3Ds}$) since

$$\begin{aligned}\Big|\int_\omega l\vec{G}_0\cdot\vec{v}\,dS\Big| &\le C\|\vec{G}_0\|_0\|\vec{v}\|_0\\ &\le C\|\vec{G}_0\|_0\|\vec{v},\vec{\eta},\vec{\varsigma}\|_{\rm b},\ \forall(\vec{v},\vec{\eta},\vec{\varsigma})\in\mathcal{V}_{\rm b}^{3Ds}.\end{aligned}\qquad(5.220)$$

We will then establish the following convergence.

Proposition 5.4.3 *The solution* $(\vec{u}^\varepsilon,\vec{\theta}^\varepsilon,\vec{\varrho}^\varepsilon)$ *of Problem (4.161) converges weakly in* $\mathcal{V}_{\rm b}^{3Ds}$*, as* ε *goes to* 0*, to* $(\vec{u}^0,\vec{\theta}^0,\vec{\varrho}^0)$ *solution of (5.219).*

In order to prove this result we will need the following lemma, in which we will use the same compact notation for the strains as in the proof of Proposition 4.3.8, and the semi-norm defined by

$$\|\vec{v},\vec{\eta}\,\|_{\rm m}=A_{\rm m}^{3Ds}(\vec{v},\vec{\eta};\vec{v},\vec{\eta})^{\frac{1}{2}}.$$

Lemma 5.4.1. *We have the following equivalence relations of norms and semi-norms:*

1. *Whether these expressions define norms (when pure bending is inhibited) or semi-norms (otherwise), $\|\vec{v},\vec{\eta}\|_{\rm m}$ is equivalent to $\Big(\|\underline{\underline{\gamma}}\|_0^2+\|\underline{\zeta}\|_0^2+\|\delta\|_0^2\Big)^{1/2}$.*
2. *The norms $\|\vec{v},\vec{\eta},\vec{\varsigma}\|_{\rm b}$, $\Big(\|\underline{\underline{\gamma}}\|_0^2+\|\underline{\zeta}\|_0^2+\|\delta\|_0^2+\|\underline{\underline{\hat{\chi}}}\|_0^2+\|\underline{m}\|_0^2+\|p\|_0^2\Big)^{1/2}$, and $\big(A_{\rm m}^{3Ds}(\vec{v},\vec{\eta};\vec{v},\vec{\eta})+A_{\rm b}^{3Ds}(\vec{v},\vec{\eta},\vec{\varsigma};\vec{v},\vec{\eta},\vec{\varsigma})\big)^{1/2}$, are all equivalent.*
3. *The norms $\|\vec{v},\vec{\eta},\vec{\varsigma}\|_1$ and $\Big(\|\underline{\underline{\gamma}}\|_0^2+\|\underline{\zeta}\|_0^2+\|\delta\|_0+\|\underline{\underline{\hat{\chi}}}\|_0^2+\|\underline{m}\|_0^2+\|p\|_0^2+\|\underline{\underline{k}}\|_0^2+\|\underline{n}\|_0^2\Big)^{1/2}$ are equivalent.*

Proof of Lemma 5.4.1. We split the proof according to the items in the statement of the lemma.
i) From the definition of $\|\cdot\|_{\rm m}$ we have

$$\begin{aligned}\|\vec{v},\vec{\eta}\|_{\rm m}^2 &= \int_\omega l\Big[{}^0H^{\alpha\beta\lambda\mu}\gamma_{\alpha\beta}\gamma_{\lambda\mu}+{}^0H^{3333}(\delta)^2\\ &\qquad +2{}^0H^{\alpha\beta33}\gamma_{\alpha\beta}\delta+4{}^0H^{\alpha3\beta3}\zeta_\alpha\zeta_\beta\Big]\,dS\\ &\geq L\int_\omega\Big[{}^0H^{\alpha\beta\lambda\mu}\gamma_{\alpha\beta}\gamma_{\lambda\mu}+{}^0H^{3333}(\delta)^2\\ &\qquad +2{}^0H^{\alpha\beta33}\gamma_{\alpha\beta}\delta+4{}^0H^{\alpha3\beta3}\zeta_\alpha\zeta_\beta\Big]\,dS. \qquad (5.221)\end{aligned}$$

Then

$$\begin{aligned}\int_\omega {}^0H^{\alpha\beta\lambda\mu}\gamma_{\alpha\beta}\gamma_{\lambda\mu}\,dS &= \frac{E\nu}{(1+\nu)(1-2\nu)}\int_\omega a^{\alpha\beta}a^{\lambda\mu}\gamma_{\alpha\beta}\gamma_{\lambda\mu}\,dS+\\ &\quad+\frac{E}{2(1+\nu)}\int_\omega(a^{\alpha\lambda}a^{\beta\mu}+a^{\alpha\mu}a^{\beta\lambda})\gamma_{\alpha\beta}\gamma_{\lambda\mu}\,dS\\ &= \frac{E\nu}{(1+\nu)(1-2\nu)}\|{\rm tr}\underline{\underline{\gamma}}\|_0^2+\frac{E}{1+\nu}\|\underline{\underline{\gamma}}\|_0^2. \qquad (5.222)\end{aligned}$$

Likewise,

$$\int_\omega {}^0H^{\alpha3\beta3}\zeta_\alpha\zeta_\beta\,dS=\frac{E}{2(1+\nu)}\|\underline{\zeta}\|_0^2, \qquad (5.223)$$

$$\int_\omega {}^0H^{3333}(\delta)^2\,dS = \frac{E(1-\nu)}{(1+\nu)(1-2\nu)}\|\delta\|_0^2, \tag{5.224}$$

$$\int_\omega {}^0H^{\alpha\beta 33}\gamma_{\alpha\beta}\delta\,dS = \frac{E\nu}{(1+\nu)(1-2\nu)}\langle \mathrm{tr}\underline{\underline{\gamma}}, \delta\rangle_{L^2(\mathcal{S})}. \tag{5.225}$$

Hence,

$$\|\vec{v},\vec{\eta}\,\|_{\mathrm{m}}^2 \geq \frac{LE\nu}{(1+\nu)(1-2\nu)}\|\mathrm{tr}\underline{\underline{\gamma}} + \delta\|_0^2 + \frac{LE}{1+\nu}\|\underline{\underline{\gamma}}\|_0^2 + \frac{2LE}{(1+\nu)}\|\underline{\zeta}\|_0^2 + \frac{LE}{1+\nu}\|\delta\|_0^2. \tag{5.226}$$

which implies

$$\|\vec{v},\vec{\eta}\,\|_{\mathrm{m}}^2 \geq \gamma\Big[\|\underline{\underline{\gamma}}\|_0^2 + \|\underline{\zeta}\|_0^2 + \|\delta\|_0^2\Big]. \tag{5.227}$$

Furthermore, since $\|\mathrm{tr}\underline{\underline{\gamma}}\|_0 \leq C\|\underline{\underline{\gamma}}\|_0$ and

$$l \leq l_{\max} = \sup_{(\xi^1,\xi^2)\in\omega} l(\xi^1,\xi^2),$$

a similar argument would lead to

$$\|\vec{v},\vec{\eta}\,\|_{\mathrm{m}}^2 \leq C\Big[\|\underline{\underline{\gamma}}\|_0^2 + \|\underline{\zeta}\|_0^2 + \|\delta\|_0^2\Big], \tag{5.228}$$

hence, the equivalence holds.

ii) We have

$$\begin{aligned}\|\vec{v},\vec{\eta},\vec{\varsigma}\,\|_{\mathrm{b}}^2 &= \|\vec{v}\|_1^2 + \|\underline{\eta}\|_1^2 + \|\eta_3\|_0^2 + \|\varsigma_3\|_0^2 + \|\underline{\varsigma} + \frac{1}{2}\underline{\nabla}\eta_3\|_0^2 \\ &= \|\vec{v}\|_1^2 + \|\underline{\eta}\|_1^2 + \|\underline{m}\|_0^2 + \|\delta\|_0^2 + \frac{1}{4}\|p\|_0^2.\end{aligned} \tag{5.229}$$

Using the H^1-coercivity of the bilinear form of the s-m-b model, we have

$$\gamma(\|\vec{v}\|_1^2 + \|\underline{\eta}\|_1^2) \leq \|\underline{\underline{\gamma}}\|_0^2 + \|\underline{\zeta}\|_0^2 + \|\underline{\underline{\hat{\chi}}}(\vec{v},\underline{\eta},0)\|_0^2, \tag{5.230}$$

and

$$\begin{aligned}\|\underline{\underline{\hat{\chi}}}(\vec{v},\underline{\eta},0)\|_0 &= \|\underline{\underline{\hat{\chi}}} - \underline{\underline{b}}\eta_3\|_0 \\ &\leq \|\underline{\underline{\hat{\chi}}}\|_0 + \|\underline{\underline{b}}\eta_3\|_0 \\ &\leq C(\|\underline{\underline{\hat{\chi}}}\|_0 + \|\delta\|_0).\end{aligned} \tag{5.231}$$

From (5.229), (5.230) and (5.231), we obtain

$$\|\vec{v},\vec{\eta},\vec{\varsigma}\|_{\mathrm{b}}^2 \leq C\big(\|\underline{\underline{\gamma}}\|_0^2 + \|\underline{\varsigma}\|_0^2 + \|\underline{\underline{\hat{\chi}}}\|_0^2 + \|\underline{m}\|_0^2 + \|\delta\|_0^2 + \|p\|_0^2\big). \tag{5.232}$$

Furthermore, from the definition of the norm $\|\cdot\|_{\mathrm{b}}$ we obtain by straightforward bounds

$$\|\underline{\underline{\gamma}}\|_0^2 + \|\underline{\varsigma}\|_0^2 + \|\underline{\underline{\hat{\chi}}}\|_0^2 + \|\underline{m}\|_0^2 + \|\delta\|_0^2 + \|p\|_0^2 \leq C\|\vec{v},\vec{\eta},\vec{\varsigma}\|_{\mathrm{b}}^2, \tag{5.233}$$

hence the equivalence of $\|\cdot\|_{\mathrm{b}}$ and $\Big(\|\underline{\underline{\gamma}}\|_0^2+\|\underline{\varsigma}\|_0^2+\|\delta\|_0^2+\|\underline{\underline{\hat{\chi}}}\|_0^2+\|\underline{m}\|_0^2+\|p\|_0^2\Big)^{1/2}$ is proven. To prove the equivalence of $\|\cdot\|_{\mathrm{b}}$ and $\big(A_{\mathrm{m}}^{3Ds}(\cdot,\cdot)+A_{\mathrm{b}}^{3Ds}(\cdot,\cdot)\big)^{1/2}$, we recall that $\|\underline{\underline{\gamma}}\|_0^2 + \|\underline{\varsigma}\|_0^2 + \|\delta\|_0^2$ is equivalent to $A_{\mathrm{m}}^{3Ds}(\cdot,\cdot)$. Hence to complete the proof it suffices to show that

$$\gamma(\|\underline{\underline{\hat{\chi}}}\|_0^2 + \|\underline{m}\|_0^2 + \|p\|_0^2) \leq A_{\mathrm{b}}^{3Ds}(\vec{v},\vec{\eta},\vec{\varsigma};\vec{v},\vec{\eta},\vec{\varsigma}) \leq C(\|\underline{\underline{\hat{\chi}}}\|_0^2 + \|\underline{m}\|_0^2 + \|p\|_0^2),$$

which is achieved exactly like in Step i) above.

iii) The equivalence of $\|\cdot\|_1$ and $\Big(\|\underline{\underline{\gamma}}\|_0^2+\|\underline{\varsigma}\|_0^2+\|\delta\|_0+\|\underline{\underline{\hat{\chi}}}\|_0^2+\|\underline{m}\|_0^2+\|p\|_0^2+\|\underline{\underline{k}}\|_0^2 + \|\underline{n}\|_0^2\Big)^{1/2}$ directly follows from the proof of Proposition 4.3.8. ∎

Remark 5.4.1. Using Eqs. (4.23), (4.24), (4.74), and the change of variables $\xi^3 = \varepsilon\xi$, the bilinear form A^{3Ds} can be expressed as

$$A^{3Ds}(\vec{u},\vec{\theta},\vec{\varrho};\vec{v},\vec{\eta},\vec{\varsigma}) = I_1 + I_2 + I_3 + I_4 + I_5, \tag{5.234}$$

with

$$\begin{aligned} I_1 = \varepsilon\int_\omega\int_{-l/2}^{l/2} H^{\alpha\beta\lambda\mu}\big[&\gamma_{\alpha\beta}(\vec{u}) + \varepsilon\xi\hat{\chi}_{\alpha\beta}(\vec{u},\vec{\theta}) + \varepsilon^2(\xi)^2 k_{\alpha\beta}(\vec{\theta},\vec{\varrho}) \\ &+\varepsilon^3(\xi)^3 l_{\alpha\beta}(\vec{\varrho})\big] \times \big[\gamma_{\lambda\mu}(\vec{v}) + \varepsilon\xi\hat{\chi}_{\lambda\mu}(\vec{v},\vec{\eta}) + \varepsilon^2(\xi)^2 k_{\lambda\mu}(\vec{\eta},\vec{\varsigma}) \\ &+\varepsilon^3(\xi)^3 l_{\lambda\mu}(\vec{\varsigma})\big]\sqrt{g}\,d\xi d\xi^1 d\xi^2, \end{aligned} \tag{5.235}$$

$$\begin{aligned} I_2 = \varepsilon\int_\omega\int_{-l/2}^{l/2} 4H^{\alpha 3\beta 3}\big[&\zeta_\alpha(\vec{u},\vec{\theta}) + \varepsilon\xi m_\alpha(\vec{\theta},\vec{\varrho}) + \varepsilon^2(\xi)^2 n_\alpha(\vec{\varrho})\big] \\ &\times\big[\zeta_\beta(\vec{v},\vec{\eta}) + \varepsilon\xi m_\beta(\vec{\eta},\vec{\varsigma}) + \varepsilon^2(\xi)^2 n_\beta(\vec{\varsigma})\big]\sqrt{g}\,d\xi d\xi^1 d\xi^2, \end{aligned} \tag{5.236}$$

$$I_3 = \varepsilon \int_\omega \int_{-l/2}^{l/2} H^{3333}\big[\delta(\vec{\theta}) + \varepsilon\xi p(\vec{\varrho})\big] \times \big[\delta(\vec{\eta}) + \varepsilon\xi p(\vec{\varsigma})\big]\sqrt{g}\, d\xi d\xi^1 d\xi^2, \tag{5.237}$$

$$I_4 = \varepsilon \int_\omega \int_{-l/2}^{l/2} H^{\alpha\beta 33}\big[\gamma_{\alpha\beta}(\vec{u}) + \varepsilon\xi\hat{\chi}_{\alpha\beta}(\vec{u},\vec{\theta}) + \varepsilon^2(\xi)^2 k_{\alpha\beta}(\vec{\theta},\vec{\varrho}) + \varepsilon^3(\xi)^3 l_{\alpha\beta}(\vec{\varrho})\big] \times \big[\delta(\vec{\eta}) + \varepsilon\xi p(\vec{\varsigma})\big]\sqrt{g}\, d\xi d\xi^1 d\xi^2, \tag{5.238}$$

$$I_5 = \varepsilon \int_\omega \int_{-l/2}^{l/2} H^{\alpha\beta 33}\big[\gamma_{\alpha\beta}(\vec{v}) + \varepsilon\xi\hat{\chi}_{\alpha\beta}(\vec{v},\vec{\eta}) + \varepsilon^2(\xi)^2 k_{\alpha\beta}(\vec{\eta},\vec{\varsigma}) + \varepsilon^3(\xi)^3 l_{\alpha\beta}(\vec{\varsigma})\big] \times \big[\delta(\vec{\theta}) + \varepsilon\xi p(\vec{\varrho})\big]\sqrt{g}\, d\xi d\xi^1 d\xi^2. \tag{5.239}$$

Similarly, the linear form F^{3Ds} becomes

$$F^{3Ds}(\vec{v},\vec{\eta},\vec{\varsigma}) = \varepsilon \int_\omega \int_{-l/2}^{l/2} \vec{F}\cdot\big[\vec{v} + \varepsilon\xi\vec{\eta} + \varepsilon^2(\xi)^2\vec{\varsigma}\big]\sqrt{g}\, d\xi d\xi^1 d\xi^2. \tag{5.240}$$

■

Proof of Proposition 5.4.3. We follow the same approach as for the basic shell model. We divide the proof into 3 steps.

i) *Uniform bound on the solution.* We start by noting that, in the coercivity proof of Proposition 4.3.8, from (4.165) and (4.166)–(4.168), the inequality (4.169) can be restated as

$$A^{3Ds}(\vec{v},\vec{\eta},\vec{\varsigma};\vec{v},\vec{\eta},\vec{\varsigma}) \geq \gamma \int_\omega t\Big\{a^{\alpha\lambda}a^{\beta\mu}[\gamma_{\alpha\beta}\gamma_{\lambda\mu} + t^2\hat{\chi}_{\alpha\beta}\hat{\chi}_{\lambda\mu} + t^4 k_{\alpha\beta}k_{\lambda\mu} + t^6 l_{\alpha\beta}l_{\lambda\mu}] + a^{\alpha\beta}[\zeta_\alpha\zeta_\beta + t^2 m_\alpha m_\beta + t^4 n_\alpha n_\beta] + [\delta^2 + t^2 p^2]\Big\}\, dS, \tag{5.241}$$

with γ independent of ε. Hence,

$$A^{3Ds}(\vec{v},\vec{\eta},\vec{\varsigma};\vec{v},\vec{\eta},\vec{\varsigma}) \geq \gamma\varepsilon \int_\omega L\Big\{a^{\alpha\lambda}a^{\beta\mu}[\gamma_{\alpha\beta}\gamma_{\lambda\mu} + \varepsilon^2L^2\hat{\chi}_{\alpha\beta}\hat{\chi}_{\lambda\mu} + \varepsilon^4L^4 k_{\alpha\beta}k_{\lambda\mu} + \varepsilon^6L^6 l_{\alpha\beta}l_{\lambda\mu}] + a^{\alpha\beta}[\zeta_\alpha\zeta_\beta + \varepsilon^2L^2 m_\alpha m_\beta + \varepsilon^4L^4 n_\alpha n_\beta] + [\delta^2 + \varepsilon^2L^2p^2]\Big\}\, dS, \tag{5.242}$$

which implies

$$\begin{aligned} A^{3Ds}(\vec{v},\vec{\eta},\vec{\varsigma};\vec{v},\vec{\eta},\vec{\varsigma}) &\geq \gamma\varepsilon^3\Big[\frac{1}{\varepsilon^2}(\|\underline{\underline{\gamma}}\|_0^2+\|\underline{\zeta}\|_0^2+\|\delta\|_0^2) \\ &\quad +\|\underline{\underline{\hat{\chi}}}\|_0^2+\|\underline{m}\|_0^2+\|p\|_0^2+\varepsilon^2\big(\|\underline{\underline{k}}\|_0^2+\|\underline{n}\|_0^2\big)\Big] \\ &\geq \gamma\Big[\varepsilon^3\big(\|\underline{\underline{\gamma}}\|_0^2+\|\underline{\zeta}\|_0^2+\|\delta\|_0^2+\|\underline{\underline{\hat{\chi}}}\|_0^2+\|\underline{m}\|_0^2+\|p\|_0^2\big) \\ &\quad +\varepsilon^5\big(\|\underline{\underline{k}}\|_0^2+\|\underline{n}\|_0^2\big)\Big], \end{aligned}$$

provided that $\varepsilon \leq 1$. Then, using the equivalences given in Lemma 5.4.1 we infer

$$A^{3Ds}(\vec{v},\vec{\eta},\vec{\varsigma};\vec{v},\vec{\eta},\vec{\varsigma}) \geq \gamma\Big[\varepsilon^3\|\vec{v},\vec{\eta},\vec{\varsigma}\|_{\mathrm{b}}^2+\varepsilon^5\|\vec{v},\vec{\eta},\vec{\varsigma}\|_1^2\Big]. \tag{5.243}$$

In addition, recalling $\vec{F}=\varepsilon^2\vec{G}$, using (2.155), (5.212), (5.240) and integrating through the thickness, we obtain

$$\begin{aligned} &\int_\Omega \vec{F}\cdot(\vec{v}+\xi^3\vec{\eta}+(\xi^3)^2\vec{\varsigma})\,dV \\ &\quad = \varepsilon^3\int_\omega\int_{-l/2}^{l/2}(\vec{G}_0+\varepsilon\xi\vec{B})(\vec{v}+\varepsilon\xi\vec{\eta}+\varepsilon^2(\xi)^2\vec{\varsigma})\sqrt{g}\,d\xi d\xi^1 d\xi^2 \\ &\quad = \varepsilon^3\int_\omega L\vec{G}_0\cdot\vec{v}\sqrt{a}\,d\xi^1 d\xi^2+R, \end{aligned} \tag{5.244}$$

where the remainder R is bounded as

$$|R| \leq C\varepsilon^4\|\vec{v},\vec{\eta},\vec{\varsigma}\|_0. \tag{5.245}$$

Recalling (5.220), this gives

$$\int_\Omega \vec{F}\cdot(\vec{v}+\xi^3\vec{\eta}+(\xi^3)^2\vec{\varsigma})\,dV \leq C\varepsilon^3\|\vec{v},\vec{\eta},\vec{\varsigma}\|_{\mathrm{b}}+C\varepsilon^4\|\vec{v},\vec{\eta},\vec{\varsigma}\|_0. \tag{5.246}$$

Using then $(\vec{v},\vec{\eta},\vec{\varsigma})=(\vec{u}^\varepsilon,\vec{\theta}^\varepsilon,\vec{\varrho}^\varepsilon)$ in the variational formulation, with (5.243) and (5.246) we infer

$$\|\vec{u}^\varepsilon,\vec{\theta}^\varepsilon,\vec{\varrho}^\varepsilon\|_{\mathrm{b}}+\varepsilon\|\vec{u}^\varepsilon,\vec{\theta}^\varepsilon,\vec{\varrho}^\varepsilon\|_1 \leq C. \tag{5.247}$$

ii) *Weak convergence in* $\mathcal{V}_{0\mathrm{b}}^{3Ds}$. Since $(\vec{u}^\varepsilon,\vec{\theta}^\varepsilon,\vec{\varrho}^\varepsilon)$ is uniformly bounded in the norm $\|\cdot\|_{\mathrm{b}}$, we can extract a subsequence (for which we will use the same

notation) converging weakly in $\mathcal{V}_{\mathrm{b}}^{3Ds}$ to a limit $(\vec{u}^{\,w}, \vec{\theta}^{\,w}, \vec{\varrho}^{\,w})$. Of course, $\varepsilon\|\cdot\|_1$ remains bounded for this subsequence also, due to (5.247). Since the geometry is smooth, we can expand the constitutive tensor as

$$H^{ijkl}(\xi^1,\xi^2,\xi^3) = {}^0H^{ijkl}(\xi^1,\xi^2) + \xi^3 \bar{H}^{ijkl}(\xi^1,\xi^2,\xi^3), \tag{5.248}$$

where $\bar{H}^{ijkl}(\xi^1,\xi^2,\xi^3)$ is bounded over $\mathcal{B}$. Using the change of variable $\xi^3 = \varepsilon\xi$, for any $(\vec{v},\vec{\eta},\vec{\varsigma}) \in \mathcal{V}^{3Ds} \subset \mathcal{V}_{\mathrm{b}}^{3Ds}$,

$$A^{3Ds}(\vec{u}^{\,\varepsilon}, \vec{\theta}^{\,\varepsilon}, \vec{\varrho}^{\,\varepsilon}; \vec{v},\vec{\eta},\vec{\varsigma}) = I_1 + I_2 + I_3 + I_4 + I_5, \tag{5.249}$$

where I_1, I_2, I_3, I_4, I_5 are defined by Eqs. (5.235)–(5.239). Since $(\vec{u}^{\,\varepsilon}, \vec{\theta}^{\,\varepsilon}, \vec{\varrho}^{\,\varepsilon})$ is weakly converging in $\mathcal{V}_{\mathrm{b}}^{3Ds}$, we have weak convergence in $L^2(\mathcal{S})$ of

$$\Big(\underline{\underline{\gamma}}(\vec{u}^{\,\varepsilon}), \underline{\zeta}(\vec{u}^{\,\varepsilon}, \vec{\theta}^{\,\varepsilon}), \delta(\vec{\theta}^{\,\varepsilon}), \underline{\underline{\hat{\chi}}}(\vec{u}^{\,\varepsilon}, \vec{\theta}^{\,\varepsilon}), \underline{m}(\vec{\theta}^{\,\varepsilon}, \vec{\varrho}^{\,\varepsilon}), p(\vec{\varrho}^{\,\varepsilon})\Big)$$

to

$$\Big(\underline{\underline{\gamma}}(\vec{u}^{\,w}), \underline{\zeta}(\vec{u}^{\,w}, \vec{\theta}^{\,w}), \delta(\vec{\theta}^{\,w}), \underline{\underline{\hat{\chi}}}(\vec{u}^{\,w}, \vec{\theta}^{\,w}), \underline{m}(\vec{\theta}^{\,w}, \vec{\varrho}^{\,w}), p(\vec{\varrho}^{\,w})\Big).$$

Therefore, using the uniform boundedness of $\varepsilon\|\vec{u}^{\,\varepsilon}, \vec{\theta}^{\,\varepsilon}, \vec{\varrho}^{\,\varepsilon}\|_1$, we obtain

$$\lim_{\varepsilon\to 0} \frac{1}{\varepsilon} I_1 = \int_\omega l\, {}^0H^{\alpha\beta\lambda\mu} \gamma_{\alpha\beta}(\vec{u}^{\,w}) \gamma_{\lambda\mu}(\vec{v}) \sqrt{a}\, d\xi^1 d\xi^2, \tag{5.250}$$

$$\lim_{\varepsilon\to 0} \frac{1}{\varepsilon} I_2 = \int_\omega l\, {}^0H^{\alpha 3\beta 3} \zeta_\alpha(\vec{u}^{\,w}, \vec{\theta}^{\,w}) \zeta_\beta(\vec{v},\vec{\eta}) \sqrt{a}\, d\xi^1 d\xi^2, \tag{5.251}$$

$$\lim_{\varepsilon\to 0} \frac{1}{\varepsilon} I_3 = \int_\omega l\, {}^0H^{3333} \delta(\vec{\theta}^{\,w}) \delta(\vec{\eta}) \sqrt{a}\, d\xi^1 d\xi^2, \tag{5.252}$$

$$\lim_{\varepsilon\to 0} \frac{1}{\varepsilon} I_4 = \int_\omega l\, {}^0H^{\alpha\beta 33} \gamma_{\alpha\beta}(\vec{u}^{\,w}) \delta(\vec{\eta}) \sqrt{a}\, d\xi^1 d\xi^2, \tag{5.253}$$

$$\lim_{\varepsilon\to 0} \frac{1}{\varepsilon} I_5 = \int_\omega l\, {}^0H^{\alpha\beta 33} \gamma_{\alpha\beta}(\vec{v}) \delta(\vec{\theta}^{\,w}) \sqrt{a}\, d\xi^1 d\xi^2, \tag{5.254}$$

hence,

$$\lim_{\varepsilon\to 0} \frac{1}{\varepsilon} A^{3Ds}(\vec{u}^{\,\varepsilon}, \vec{\theta}^{\,\varepsilon}, \vec{\varrho}^{\,\varepsilon}; \vec{v},\vec{\eta},\vec{\varsigma}) = A_{\mathrm{m}}^{3Ds}(\vec{u}^{\,w}, \vec{\theta}^{\,w}; \vec{v},\vec{\eta}). \tag{5.255}$$

On the other hand, recalling (5.246) we have

$$\begin{aligned}\left|\frac{1}{\varepsilon}A^{3Ds}(\vec{u}^{\,\varepsilon},\vec{\theta}^{\,\varepsilon},\vec{\varrho}^{\,\varepsilon};\vec{v},\vec{\eta},\vec{\varsigma})\right| &= \left|\frac{1}{\varepsilon}\int_{\Omega}\vec{F}\cdot(\vec{v}+\xi^3\vec{\eta}+(\xi^3)^2\vec{\varsigma})\,dV\right| \\ &\leq C\varepsilon^2\|\vec{v},\vec{\eta},\vec{\varsigma}\|_{\rm b}+C\varepsilon^3\|\vec{v},\vec{\eta},\vec{\varsigma}\|_0, \quad (5.256)\end{aligned}$$

and, since $(\vec{v},\vec{\eta},\vec{\varsigma})$ is fixed in $\mathcal{V}^{3Ds}$, the left-hand side of this inequality tends to zero with ε. Therefore,

$$A^{3Ds}_{\rm m}(\vec{u}^{\,w},\vec{\theta}^{\,w};\vec{v},\vec{\eta})=0, \quad \forall(\vec{v},\vec{\eta},\vec{\varsigma})\in\mathcal{V}^{3Ds}, \tag{5.257}$$

and by density this also holds for any $(\vec{v},\vec{\eta},\vec{\varsigma})\in\mathcal{V}^{3Ds}_{\rm b}$, hence in particular for $(\vec{u}^{\,w},\vec{\theta}^{\,w},\vec{\varrho}^{\,w})$. From Lemma 5.4.1 (first equivalence statement) we then infer that $(\vec{u}^{\,w},\vec{\theta}^{\,w},\vec{\varrho}^{\,w})\in\mathcal{V}^{3Ds}_{\rm 0b}$.

iii) *Characterization of* $(\vec{u}^{\,w},\vec{\theta}^{\,w},\vec{\varrho}^{\,w})$. Let us now choose $(\vec{v},\vec{\eta},\vec{\varsigma})\in\mathcal{V}^{3Ds}_0$, namely,

$$\gamma_{\alpha\beta}(\vec{v})=0,\ \zeta_\alpha(\vec{v},\vec{\eta})=0,\ \delta(\vec{\eta})=0. \tag{5.258}$$

Since

$$\frac{1}{\varepsilon^3}A^{3Ds}(\vec{u}^{\,\varepsilon},\vec{\theta}^{\,\varepsilon},\vec{\varrho}^{\,\varepsilon};\vec{v},\vec{\eta},\vec{\varsigma})=\frac{1}{\varepsilon^3}I_1+\frac{1}{\varepsilon^3}I_2+\frac{1}{\varepsilon^3}I_3+\frac{1}{\varepsilon^3}I_4+\frac{1}{\varepsilon^3}I_5, \tag{5.259}$$

we analyse separately each term in the right-hand side. Using (5.258), we have

$$\begin{aligned}\frac{1}{\varepsilon^3}I_1=\frac{1}{\varepsilon^2}\int_\omega\int_{-l/2}^{l/2}H^{\alpha\beta\lambda\mu}\big[&\gamma_{\alpha\beta}(\vec{u}^{\,\varepsilon})+\varepsilon\xi\hat{\chi}_{\alpha\beta}(\vec{u}^{\,\varepsilon},\vec{\theta}^{\,\varepsilon})+\varepsilon^2(\xi)^2k_{\alpha\beta}(\vec{\theta}^{\,\varepsilon},\vec{\varrho}^{\,\varepsilon}) \\ &+\varepsilon^3(\xi)^3l_{\alpha\beta}(\vec{\varrho}^{\,\varepsilon})\big]\times\big[\varepsilon\xi\hat{\chi}_{\lambda\mu}(\vec{v},\vec{\eta})+\varepsilon^2(\xi)^2k_{\lambda\mu}(\vec{\eta},\vec{\varsigma}) \\ &+\varepsilon^3(\xi)^3l_{\lambda\mu}(\vec{\varsigma})\big]\sqrt{g}\,d\xi d\xi^1d\xi^2. \quad (5.260)\end{aligned}$$

Developing in powers of ε by using (2.155) and (5.248), we obtain that the only term in $\frac{1}{\varepsilon}$ is

$$\frac{1}{\varepsilon^2}\int_\omega\int_{-l/2}^{l/2}\varepsilon\xi\,{}^0H^{\alpha\beta\lambda\mu}\gamma_{\alpha\beta}(\vec{u}^{\,\varepsilon})\hat{\chi}_{\lambda\mu}(\vec{v},\vec{\eta})\sqrt{a}\,d\xi d\xi^1d\xi^2, \tag{5.261}$$

which vanishes because of the integration on ξ. The other terms in the expansion of $\dfrac{1}{\varepsilon^3}I_1$ converge to zero, except for

$$\int_\omega\frac{l^3}{12}\,{}^0H^{\alpha\beta\lambda\mu}\hat{\chi}_{\alpha\beta}(\vec{u}^{\,w},\vec{\theta}^{\,w})\hat{\chi}_{\lambda\mu}(\vec{v},\vec{\eta})\sqrt{a}\,d\xi^1d\xi^2. \tag{5.262}$$

To prove this claim, we use the weak convergence of $(\vec{u}^{\varepsilon}, \vec{\theta}^{\varepsilon}, \vec{\varrho}^{\varepsilon})$, the uniform bound on $\varepsilon\|\vec{u}^{\varepsilon}, \vec{\theta}^{\varepsilon}, \vec{\varrho}^{\varepsilon}\|_1$ and the fact that $(\vec{u}^{w}, \vec{\theta}^{w}, \vec{\varrho}^{w}) \in \mathcal{V}_{0\mathrm{b}}^{3Ds}$. For example,

$$\lim_{\varepsilon\to 0}\frac{1}{\varepsilon^2}\int_{\omega}\int_{-l/2}^{l/2}\varepsilon^2\,{}^0H^{\alpha\beta\lambda\mu}\gamma_{\alpha\beta}(\vec{u}^{\varepsilon})((\xi)^2 k_{\lambda\mu}(\vec{\eta},\vec{\varsigma}))\sqrt{a}\,d\xi d\xi^1 d\xi^2$$

$$= \int_{\omega}\frac{l^3}{12}\,{}^0H^{\alpha\beta\lambda\mu}\gamma_{\alpha\beta}(\vec{u}^{w})k_{\lambda\mu}(\vec{\eta},\vec{\varsigma})\sqrt{a}\,d\xi^1 d\xi^2 = 0, \tag{5.263}$$

because $\gamma_{\alpha\beta}(\vec{u}^{w}) = 0$. Note also that for the same reason, and using the boundedness of $\bar{H}^{\alpha\beta\lambda\mu}$, we have

$$\lim_{\varepsilon\to 0}\frac{1}{\varepsilon^2}\int_{\omega}\int_{-l/2}^{l/2}\varepsilon\xi\bar{H}^{\alpha\beta\lambda\mu}\gamma_{\alpha\beta}(\vec{u}^{\varepsilon})\varepsilon\xi\hat{\chi}_{\lambda\mu}(\vec{v},\vec{\eta})\sqrt{a}\,d\xi d\xi^1 d\xi^2$$

$$= \lim_{\varepsilon\to 0}\int_{\omega}\int_{-l/2}^{l/2}(\xi)^2\bar{H}^{\alpha\beta\lambda\mu}\gamma_{\alpha\beta}(\vec{u}^{\varepsilon})\hat{\chi}_{\lambda\mu}(\vec{v},\vec{\eta})\sqrt{a}\,d\xi d\xi^1 d\xi^2 = 0. \tag{5.264}$$

By similar arguments, we obtain

$$\lim_{\varepsilon\to 0}\frac{1}{\varepsilon^3}I_2 = \int_{\omega}\frac{l^3}{3}\,{}^0H^{\alpha 3\beta 3}m_{\alpha}(\vec{\theta}^{w},\vec{\varrho}^{w})m_{\beta}(\vec{\eta},\vec{\varsigma})\sqrt{a}\,d\xi^1 d\xi^2, \tag{5.265}$$

$$\lim_{\varepsilon\to 0}\frac{1}{\varepsilon^3}I_3 = \int_{\omega}\frac{l^3}{12}\,{}^0H^{3333}p(\vec{\varrho}^{w})p(\vec{\varsigma})\sqrt{a}\,d\xi^1 d\xi^2, \tag{5.266}$$

$$\lim_{\varepsilon\to 0}\frac{1}{\varepsilon^3}(I_4+I_5) = \int_{\omega}\frac{l^3}{12}\,{}^0H^{\alpha\beta 33}\Big(\hat{\chi}_{\alpha\beta}(\vec{u}^{w},\vec{\theta}^{w})p(\vec{\varsigma})$$

$$+\hat{\chi}_{\alpha\beta}(\vec{v},\vec{\eta})p(\vec{\varrho}^{w})\Big)\sqrt{a}\,d\xi^1 d\xi^2. \tag{5.267}$$

Therefore,

$$\lim_{\varepsilon\to 0}\frac{1}{\varepsilon^3}A^{3Ds}(\vec{u}^{\varepsilon},\vec{\theta}^{\varepsilon},\vec{\varrho}^{\varepsilon};\vec{v},\vec{\eta},\vec{\varsigma}) = A_{\mathrm{b}}^{3Ds}(\vec{u}^{w},\vec{\theta}^{w},\vec{\varrho}^{w};\vec{v},\vec{\eta},\vec{\varsigma}). \tag{5.268}$$

Furthermore, recalling (5.244) and (5.245) we have

$$\frac{1}{\varepsilon^3}\int_{\Omega}\vec{F}\cdot(\vec{v}+\xi^3\vec{\eta}+(\xi^3)^2\vec{\varsigma})dV = \int_{\omega}l\vec{G}_0\cdot\vec{v}\sqrt{a}\,d\xi^1 d\xi^2 + \frac{R}{\varepsilon^3},$$

with

$$\Big|\frac{R}{\varepsilon^3}\Big| \le C\varepsilon\|\vec{v},\vec{\eta},\vec{\varsigma}\|_0.$$

We infer

$$\lim_{\varepsilon\to 0}\frac{1}{\varepsilon^3}\int_\Omega \vec{F}\cdot(\vec{v}+\xi^3\vec{\eta}+(\xi^3)^2\vec{\varsigma})dV = G^{3Ds}(\vec{v}),$$

hence,

$$A_{\rm b}^{3Ds}(\vec{u}^{\,w},\vec{\theta}^{\,w},\vec{\varrho}^{\,w};\vec{v},\vec{\eta},\vec{\varsigma}) = G^{3Ds}(\vec{v}),\ \forall(\vec{v},\vec{\eta},\vec{\varsigma})\in\mathcal{V}_0^{3Ds}. \tag{5.269}$$

By density, this equation also holds for any $(\vec{v},\vec{\eta},\vec{\varsigma})\in\mathcal{V}_{0\rm b}^{3Ds}$ and therefore coincides with Equation (5.219). From the uniqueness of the solution, it follows that $(\vec{u}^{\,w},\vec{\theta}^{\,w},\vec{\varrho}^{\,w}) = (\vec{u}^{\,0},\vec{\theta}^{\,0},\vec{\varrho}^{\,0})$. As this holds for any weakly-converging subsequence $(\vec{u}^{\,\varepsilon},\vec{\theta}^{\,\varepsilon},\vec{\varrho}^{\,\varepsilon})$, we conclude that the whole sequence converges weakly to $(\vec{u}^{\,0},\vec{\theta}^{\,0},\vec{\varrho}^{\,0})$. ∎

Remark 5.4.2. Unlike for classical shell models or for the basic shell model, in the present case we also have a singular perturbation problem arising from the higher order terms in the bilinear form A^{3Ds}, in addition to the penalization mechanism. Strong convergence cannot be established under these circumstances, because the terms corresponding to penalization and singular perturbation are coupled in the expression of the total strain energy, see Eqs. (5.234)-(5.239). We also refer to (Lions, 1973, Th. 10.3) for a similar problem. ∎

Remark 5.4.3. Even though we have a very weak control on $\underline{\varrho}^{\varepsilon}$ in $\|\cdot\|_{\rm b}$ (since we only prove a convergence result for the quantity $(\underline{\varrho}^{\varepsilon}+\frac{1}{2}\underline{\nabla}\theta_3^{\varepsilon})$ in the L^2-norm), the scaled vector $\varepsilon^2\vec{\varrho}^{\,\varepsilon}$ – arising in the expression of the 3D displacements – converges to zero in the norm $\|\cdot\|_1$ when ε tends to zero, see (5.247). ∎

The case of inhibited pure bending. We define

$$\mathcal{V}^{\natural} = \{(\vec{v},\vec{\eta}) \text{ such that } (\vec{v},\vec{\eta},\vec{0})\in\mathcal{V}^{3Ds}\}. \tag{5.270}$$

Since pure bending is inhibited $\|\cdot\|_{\rm m}$ provides a norm in $\mathcal{V}^{\natural}$, and according to Lemma 5.4.1 this norm is equivalent to

$$\|\underline{\underline{\gamma}}(\vec{v})\|_0 + \|\underline{\varsigma}(\vec{v},\vec{\eta})\|_0 + \|\delta(\vec{\eta})\|_0. \tag{5.271}$$

Comparing with the similar norms used for classical shell models and for the basic shell model, we note that in this case the norm $\|\cdot\|_{\rm m}$ additionally contains the pinching strain terms.

Proceeding like for the basic shell model, we introduce $\mathcal{V}_{\rm m}^{3Ds}$ as the completion of $\mathcal{V}^{\natural}$ with respect to the norm $\|\cdot\|_{\rm m}$. The convergence of the asymptotic behavior is then obtained in this space for the scaling $\rho = 1$, and the limit problem reads:
Find $(\vec{u}^{\,\rm m}, \vec{\theta}^{\,\rm m}) \in \mathcal{V}_{\rm m}^{3Ds}$ *such that*

$$\boxed{A_{\rm m}^{3Ds}(\vec{u}^{\,\rm m}, \vec{\theta}^{\,\rm m}; \vec{v}, \vec{\eta}) = G^{3Ds}(\vec{v}), \quad \forall (\vec{v}, \vec{\eta}) \in \mathcal{V}_{\rm m}^{3Ds},} \tag{5.272}$$

with again a similar notation for the tentative limit solution as for the basic shell model. We point out that, in order to obtain a well-posed limit problem we need to enforce that $G^{3Ds} \in (\mathcal{V}_{\rm m}^{3Ds})'$, namely that

$$|\int_\omega l\vec{G}_0 \cdot \vec{v}\, dS| \leq C\|\vec{v}, \vec{\eta}\,\|_{\rm m}, \quad \forall (\vec{v}, \vec{\eta}) \in \mathcal{V}_{\rm m}^{3Ds}, \tag{5.273}$$

which is the same condition as with the basic shell model. We can then prove the following convergence result.

Proposition 5.4.4 *Assuming that* $G^{3Ds} \in (\mathcal{V}_{\rm m}^{3Ds})'$, *we have that* $\big(\vec{u}^{\,\varepsilon} + \frac{t^2}{12}\vec{\varrho}^{\,\varepsilon}, \vec{\theta}^{\,\varepsilon}\big)$ *converges weakly in* $\mathcal{V}_{\rm m}^{3Ds}$, *as* ε *goes to* 0, *to* $(\vec{u}^{\,\rm m}, \vec{\theta}^{\,\rm m})$ *solution of (5.272).*

Proof. We divide the proof into two steps.
i) *Uniform bound on the solution.* We start like in the proof of Proposition 5.4.3, using Eq.(5.242) and Lemma 5.4.1 to obtain

$$\begin{aligned} &A^{3Ds}(\vec{v}, \vec{\eta}, \vec{\varsigma}; \vec{v}, \vec{\eta}, \vec{\varsigma}) \\ &\qquad \geq \quad \gamma\Big(\varepsilon\|\vec{v}, \vec{\eta}\,\|_{\rm m}^2 + \varepsilon^3\|\vec{v}, \vec{\eta}, \vec{\varsigma}\|_{\rm b}^2 + \varepsilon^5\|\vec{v}, \vec{\eta}, \vec{\varsigma}\|_1^2\Big). \end{aligned} \tag{5.274}$$

Recalling that $\vec{F} = \vec{G}_0 + \varepsilon\xi\vec{B}$ and integrating through the thickness we have

$$\int_\Omega \vec{F} \cdot (\vec{v} + \xi^3\vec{\eta} + (\xi^3)^2\vec{\varsigma})\, dV = \varepsilon \int_\omega l\vec{G}_0 \cdot \vec{v}\, dS + R, \tag{5.275}$$

where the remainder R is bounded as

$$\begin{aligned} |R| \quad &\leq \quad C\big(\varepsilon^2\|\vec{v}, \vec{\eta}\|_0 + \varepsilon^3\|\vec{\varsigma}\|_0\big) \\ &\leq \quad C\big(\varepsilon^2\|\vec{v}, \vec{\eta}, \vec{\varsigma}\|_{\rm b} + \varepsilon^3\|\vec{v}, \vec{\eta}, \vec{\varsigma}\|_1\big). \end{aligned} \tag{5.276}$$

Since $\vec{G}_0 \in (\mathcal{V}_{\rm m}^{3Ds})'$, from (5.275) we have

$$\int_\Omega \vec{F}\cdot(\vec{v}+\xi^3\vec{\eta}+(\xi^3)^2\vec{\varsigma})\,dV$$
$$\leq C\varepsilon(\|\vec{v},\vec{\eta}\,\|_{\rm m}+\varepsilon\|\vec{v},\vec{\eta},\vec{\varsigma}\|_{\rm b}+\varepsilon^2\|\vec{v},\vec{\eta},\vec{\varsigma}\|_1). \tag{5.277}$$

Considering $(\vec{v},\vec{\eta},\vec{\varsigma})=(\vec{u}^\varepsilon,\vec{\theta}^\varepsilon,\vec{\varrho}^\varepsilon)$ in the variational formulation and using (5.274) and (5.277), we infer

$$\|\vec{u}^\varepsilon,\vec{\theta}^\varepsilon\|_{\rm m}+\varepsilon\|\vec{u}^\varepsilon,\vec{\theta}^\varepsilon,\vec{\varrho}^\varepsilon\|_{\rm b}+\varepsilon^2\|\vec{u}^\varepsilon,\vec{\theta}^\varepsilon,\vec{\varrho}^\varepsilon\|_1\leq C. \tag{5.278}$$

ii) *Weak convergence.* Since $(\vec{u}^\varepsilon,\vec{\theta}^\varepsilon)$ is uniformly bounded in $\mathcal{V}_{\rm m}^{3Ds}$ and $\varepsilon^2(\vec{u}^\varepsilon,\vec{\theta}^\varepsilon,\vec{\varrho}^\varepsilon)$ is uniformly bounded in $H^1(\mathcal{S})$, we infer that the sequence $\big(\vec{u}^\varepsilon+\frac{t^2}{12}\vec{\varrho}^\varepsilon,\vec{\theta}^\varepsilon\big)$ is also uniformly bounded in $\mathcal{V}_{\rm m}^{3Ds}$. Therefore, we can extract a subsequence (of the latter) converging weakly to a limit $(\vec{u}^w,\vec{\theta}^w)$ in $\mathcal{V}_{\rm m}^{3Ds}$. Of course, for this subsequence $\varepsilon\|\vec{u}^\varepsilon,\vec{\theta}^\varepsilon,\vec{\varrho}^\varepsilon\|_{\rm b}$ and $\varepsilon^2\|\vec{u}^\varepsilon,\vec{\theta}^\varepsilon,\vec{\varrho}^\varepsilon\|_1$ are also bounded. We again use the expansion (5.248) in the decomposition (5.249) for an arbitrary $(\vec{v},\vec{\eta},\vec{\varsigma})\in\mathcal{V}^{3Ds}\subset\mathcal{V}_{\rm m}^{3Ds}$, noting that we now have, due to the weak convergence in $\mathcal{V}_{\rm m}^{3Ds}$,

$$\Big(\underline{\underline{\gamma}}\big(\vec{u}^\varepsilon+\frac{t^2}{12}\vec{\varrho}^\varepsilon\big),\underline{\zeta}\big(\vec{u}^\varepsilon+\frac{t^2}{12}\vec{\varrho}^\varepsilon,\vec{\theta}^\varepsilon\big),\delta(\vec{\theta}^\varepsilon)\Big)\overset{\varepsilon\to0}{\longrightarrow}\Big(\underline{\underline{\gamma}}(\vec{u}^w),\underline{\zeta}(\vec{u}^w,\vec{\theta}^w),\delta(\vec{\theta}^w)\Big),$$

weakly in $L^2(\mathcal{S})$. Taking into account the uniform boundedness of $\varepsilon\|\vec{u}^\varepsilon,\vec{\theta}^\varepsilon,\vec{\varrho}^\varepsilon\|_{\rm b}$ and $\varepsilon^2\|\vec{u}^\varepsilon,\vec{\theta}^\varepsilon,\vec{\varrho}^\varepsilon\|_1$, we obtain

$$\lim_{\varepsilon\to0}\frac{1}{\varepsilon}I_1=\int_\omega l\,{}^0H^{\alpha\beta\lambda\mu}\gamma_{\alpha\beta}(\vec{u}^w)\gamma_{\lambda\mu}(\vec{v})\sqrt{a}\,d\xi^1d\xi^2,$$

$$\lim_{\varepsilon\to0}\frac{1}{\varepsilon}I_2=\int_\omega 4l\,{}^0H^{\alpha3\beta3}\zeta_\alpha(\vec{u}^w,\vec{\theta}^w)\zeta_\beta(\vec{v},\vec{\eta})\sqrt{a}\,d\xi^1d\xi^2,$$

$$\lim_{\varepsilon\to0}\frac{1}{\varepsilon}I_3=\int_\omega l\,{}^0H^{3333}\delta(\vec{\theta}^w)\delta(\vec{\eta})\sqrt{a}\,d\xi^1d\xi^2,$$

$$\lim_{\varepsilon\to0}\frac{1}{\varepsilon}I_4=\int_\omega l\,{}^0H^{\alpha\beta33}\gamma_{\alpha\beta}(\vec{u}^w)\delta(\vec{\eta})\sqrt{a}\,d\xi^1d\xi^2,$$

$$\lim_{\varepsilon\to0}\frac{1}{\varepsilon}I_5=\int_\omega l\,{}^0H^{\alpha\beta33}\gamma_{\alpha\beta}(\vec{v})\delta(\vec{\theta}^w)\sqrt{a}\,d\xi^1d\xi^2.$$

Hence, for any $(\vec{v},\vec{\eta},\vec{\varsigma})$ fixed in $\mathcal{V}^{3Ds}$, we infer

$$\lim_{\varepsilon\to0}\frac{1}{\varepsilon}A^{3Ds}(\vec{u}^\varepsilon,\vec{\theta}^\varepsilon,\vec{\varrho}^\varepsilon;\vec{v},\vec{\eta},\vec{\varsigma})=A_{\rm m}^{3Ds}(\vec{u}^w,\vec{\theta}^w;\vec{v},\vec{\eta}). \tag{5.279}$$

On the other hand, recalling (5.275) we have

$$\begin{aligned}\frac{1}{\varepsilon}A^{3Ds}(\vec{u}^{\,\varepsilon},\vec{\theta}^{\,\varepsilon},\vec{\varrho}^{\,\varepsilon};\vec{v},\vec{\eta},\vec{\varsigma}) &= \frac{1}{\varepsilon}\int_{\Omega}\vec{F}\cdot(\vec{v}+\xi^3\vec{\eta}+(\xi^3)^2\vec{\varsigma})\,dV \\ &= G^{3Ds}(\vec{v})+\frac{R}{\varepsilon}, \end{aligned} \tag{5.280}$$

where R satisfies (5.276), hence R/ε converges to zero as $\varepsilon \to 0$ since $(\vec{v},\vec{\eta},\vec{\varsigma})$ is fixed. We then infer

$$A^{3Ds}_{\rm m}(\vec{u}^{\,w},\vec{\theta}^{\,w};\vec{v},\vec{\eta}) = G^{3Ds}(\vec{v}), \quad \forall\,(\vec{v},\vec{\eta})\in\mathcal{V}^{3Ds}. \tag{5.281}$$

By density, this holds for any $(\vec{v},\vec{\eta})\in\mathcal{V}^{3Ds}_{\rm m}$. Since (5.272) has a unique solution, we have that $(\vec{u}^{\,w},\vec{\theta}^{\,w}) = (\vec{u}^{\,\rm m},\vec{\theta}^{\,\rm m})$. Finally, as this identity holds for any weakly-converging subsequence we conclude that the whole sequence $\big(\vec{u}^{\,\varepsilon}+\frac{t^2}{12}\vec{\varrho}^{\,\varepsilon},\vec{\theta}^{\,\varepsilon}\big)$ converges weakly to $(\vec{u}^{\,\rm m},\vec{\theta}^{\,\rm m})$ in $\mathcal{V}^{3Ds}_{\rm m}$. ∎

Remark 5.4.4. The term $\vec{u}^{\,\varepsilon}+\frac{t^2}{12}\vec{\varrho}^{\,\varepsilon}$ is the mean value of the displacement vector across the thickness, hence this convergence result is consistent with the asymptotic analysis performed on the 3D problem in (Ciarlet, 2000). In fact, we cannot prove the convergence of $\vec{u}^{\,\varepsilon}$ by itself, since we only show that $\varepsilon^2\vec{\varrho}^{\,\varepsilon}$ is bounded in the H^1-norm and that $\|\varepsilon^2\varrho_3^\varepsilon\|_0$ vanishes when ε tends to zero, see (5.278). ∎

Conclusions on the asymptotic analysis of the 3D-shell model. We can further analyze the variational formulations of the limit problems for both asymptotic behaviors.

When pure bending is not inhibited, using in Problem (5.219) a test function with $\vec{v}=\vec{0},\vec{\eta}=\vec{0},\underline{\varsigma}=\underline{0}$ and ς_3 arbitrary, we have

$${}^0H^{\alpha\beta33}\hat{\chi}_{\alpha\beta}(\vec{u}^{\,0},\vec{\theta}^{\,0}) + {}^0H^{3333}p(\vec{\varrho}^{\,0}) = 0, \tag{5.282}$$

and this can be used to eliminate $p(\vec{\varrho}^{\,0}) = 2\varrho_3^0$ in the variational formulation. Similarly, taking $\vec{\varsigma}$ such that $\varsigma_3=0$ with $\vec{v}=\vec{\eta}=\vec{0}$ we obtain

$$m_\alpha(\vec{\theta}^{\,0},\vec{\varrho}^{\,0}) = 0, \qquad \alpha=1,2. \tag{5.283}$$

Furthermore, the transverse component of $\vec{\eta}$ for $(\vec{v},\vec{\eta},\vec{\varsigma})\in\mathcal{V}^{3Ds}_{\rm 0b}$ is zero by definition of $\mathcal{V}^{3Ds}_{\rm 0b}$. Finally, the variational formulation (5.219) is equivalent to

$$\int_\omega \frac{l^3}{12} {}^0C^{\alpha\beta\lambda\mu}\chi_{\alpha\beta}(\vec{u}^0,\underline{\theta}^0)\chi_{\lambda\mu}(\vec{v},\underline{\eta})\,dS = G^{3Ds}(\vec{v}), \qquad \forall(\vec{v},\underline{\eta}) \in \mathcal{V}_{0\mathrm{b}}^{3Ds}, \tag{5.284}$$

which is the same limit problem as for classical shell models and for the basic shell model when pure bending is not inhibited.

Remark 5.4.5. This argument shows why the quadratic kinematical assumption provides a consistent asymptotic behavior with non-inhibited pure bending, whereas a linear assumption does not. In fact, with a linear kinematical assumption we do not have (5.282), hence the asymptotic behavior (without plane stress assumption) directly yields (5.284) with

$${}^0H^{\alpha\beta\lambda\mu} = \frac{E\nu}{(1+\nu)(1-2\nu)}a^{\alpha\beta}a^{\lambda\mu} + \frac{E}{2(1+\nu)}(a^{\alpha\lambda}a^{\beta\mu} + a^{\alpha\mu}a^{\beta\lambda})$$

substituted for ${}^0C^{\alpha\beta\lambda\mu}$, which – of course – gives a different limit solution. Note that, in particular, the behavior of these coefficients in the incompressible limit $\nu \to 0.5$ is dramatically different. ■

Similarly, when pure bending is inhibited, choosing test functions such that $\vec{v} = \vec{0}$, $\underline{\eta} = \underline{0}$ with η_3 arbitrary in the limit problem (5.272), we obtain

$${}^0H^{\alpha\beta 33}\gamma_{\alpha\beta}(\vec{u}^{\mathrm{m}}) + {}^0H^{3333}\delta(\vec{\theta}^{\mathrm{m}}) = 0. \tag{5.285}$$

Using this equation to substitute $\delta(\vec{\theta}^{\mathrm{m}}) = \theta_3^m$ in (5.272), we have

$$\int_\omega l\Big[{}^0C^{\alpha\beta\lambda\mu}\gamma_{\alpha\beta}(\vec{u}^{\mathrm{m}})\gamma_{\lambda\mu}(\vec{v}) + {}^0D^{\alpha\beta}\zeta_\alpha(\vec{u}^{\mathrm{m}},\vec{\theta}^{\mathrm{m}})\zeta_\beta(\vec{v},\vec{\eta})\Big]\,dS = G^{3Ds}(\vec{v}),$$

for all $(\vec{v},\vec{\eta}) \in \mathcal{V}_{\mathrm{m}}^{3Ds}$. Therefore, in this case also, we note that the limit problem corresponds to the limit problem obtained with classical shell models and with the basic shell model.

Finally, for both asymptotic categories of shell problems, the mathematical shell model corresponding to 3D-shell elements is *asymptotically consistent* with classical shell models, i.e. the solutions converge – when ε tends to zero and with proper load scaling factors – to the solutions of the same limit problems. Hence, by analogy to the asymptotic behavior of classical shell models, me may say that the shell structure described by the 3D-shell model analyzed here is *bending-dominated* when pure bending is non-inhibited, and that it is *membrane-dominated* when pure bending is inhibited and provided that (5.273) holds.

In addition, the above analysis shows how the elimination of the transverse components of the first and second order terms in the quadratic kinematical assumption leads to transformations of the elasticity tensor identical to those induced by the plane stress assumption in classical shell models, see

e.g. (Pitkäranta et al., 1995; Delfour, 1999; Bischoff & Ramm, 2000) for other discussions on this issue. Hence, this asymptotic analysis is valuable both as a theoretical substantiation of the model introduced in this paper, and to provide insight into the plane stress assumption used in other models.

5.5 Asymptotic Considerations in Dynamic Analysis

As can be expected, the previously-discussed asymptotic considerations – although based on the analysis of static formulations – have strong consequences in dynamic analysis also. This can be analyzed in particular by investigating the properties of the related spectral – i.e. eigenvalue – problem. Some detailed analyses are available in the classical mechanics literature, see in particular (Leissa, 1973; Soedel, 2004) and references therein, but here we also aim at providing some mathematical insight.

Let us introduce the corresponding inertia bilinear form

$$\varepsilon I_d + \varepsilon^3 I_r,$$

where I_d represents the translational inertia while I_r denotes the – sometimes neglected – rotational inertia. For Reissner-Mindlin type models, the classical expressions of these inertia bilinear forms are

$$I_d(\vec{u},\vec{v}) = \int_\omega l\,\mu\,\vec{u}\cdot\vec{v}\,dS, \quad I_r(\underline{\theta},\underline{\eta}) = \int_\omega \frac{l^3}{12}\mu\,\underline{\theta}\cdot\underline{\eta}\,dS, \tag{5.286}$$

where μ denotes the material density, namely, mass per unit volume.

Hence, we are concerned with the behavior of the eigenpairs $(\Phi^\varepsilon,\lambda^\varepsilon)$ which satisfy

$$A_{\rm m}(\Phi^\varepsilon,V)+\varepsilon^2 A_{\rm b}(\Phi^\varepsilon,V) = \lambda^\varepsilon\big(I_d(\Phi^\varepsilon,V)+\varepsilon^2 I_r(\Phi^\varepsilon,V)\big), \quad \forall V\in\mathcal{V}. \tag{5.287}$$

In our discussion of the shell spectral problem, we will again distinguish the cases of inhibited and non-inhibited pure bending.

5.5.1 Non-inhibited pure bending

When considering non-inhibited pure bending problems, it can be shown that the spectral problem behaves exactly as we can expect. Namely, we define the following candidate limit spectral problem in the pure bending subspace: *Find* $(\Phi,\lambda)\in\mathcal{V}_0\times\mathbb{R}^+$ *such that*

$$A_{\rm b}(\Phi,V) = \lambda\, I_d(\Phi,V), \quad \forall V\in\mathcal{V}_0. \tag{5.288}$$

It is then proven in (Sanchez-Palencia, 1992) that the appropriately rescaled eigenvalues of Problem (5.287) – namely, $\lambda^\varepsilon/\varepsilon^2$ – converge to the eigenvalues of (5.288). In other words, the eigenvalues of the bending-dominated shell "behave like ε^2" – as is natural. In addition, the corresponding eigenspaces also converge in the sense of distances between subspaces, which addresses the case of eigenvalues of arbitrary multiplicity. Namely, considering an eigenvalue of multiplicity m in the limit problem – where m can be one – there are exactly m eigenvalues (counting each of them with its corresponding multiplicity) of the problem (5.287) that converge to this eigenvalue; and the subspace S_m^ε spanned by associated eigenvectors converges to the eigenspace S_m corresponding to the limit multiple eigenvalue with

$$\sup_{V\in S_m^\varepsilon}\inf_{W\in S_m}\frac{\|V-W\|_{\mathcal{V}}}{\|V\|_{\mathcal{V}}}=\sup_{V\in S_m}\inf_{W\in S_m^\varepsilon}\frac{\|V-W\|_{\mathcal{V}}}{\|V\|_{\mathcal{V}}}\quad\stackrel{\varepsilon\to 0}{\longrightarrow}0.$$

For a general discussion on multiple eigenvalues in frequency analysis, see also (Bathe, 1996).

5.5.2 Inhibited pure bending

For inhibited pure bending problems, the asymptotic behavior of the shell spectral problem is much more complex, although the dominant parts of the elastic energy and inertia bilinear forms – namely, $\varepsilon A_{\rm m}$ and εI_d, respectively – have the same scaling in ε. This is due to the fact that the tentative limit problem

$$A_{\rm m}(\Phi,V)=\lambda\, I_d(\Phi,V),\quad\forall V\in\mathcal{V},$$

is not well-posed. Note in particular that we cannot – in general – formulate this problem in the completed space $\mathcal{V}_{\rm m}$ since the inertia bilinear form I_d typically requires L^2-regularity for the fields considered. Hence, this is clearly related to the asymptotic behaviors of membrane-dominated shell problems when non-admissible loadings are considered, see Section 5.3.2. The resulting behavior is then strongly dependent on the geometry of the shell midsurface and on the specific boundary conditions.

The diversity of the resulting asymptotic behaviors has been exemplified in (Artioli et al., 2008) for clamped axisymmetric shells of various geometries. Considering the fundamental eigenpair $(\Phi_1^\varepsilon,\lambda_1^\varepsilon)$, and the corresponding bending energy ratio R_{b1}^ε, namely,

$$R_{b1}^\varepsilon=\frac{\varepsilon^3 A_{\rm b}(\Phi_1^\varepsilon,\Phi_1^\varepsilon)}{\varepsilon A_{\rm m}(\Phi_1^\varepsilon,\Phi_1^\varepsilon)+\varepsilon^3 A_{\rm b}(\Phi_1^\varepsilon,\Phi_1^\varepsilon)}$$

the main results of (Artioli et al., 2008) can be summarized as follows, depending on the geometric type of the midsurface

- Elliptic midsurface: $\lambda_1^\varepsilon \sim \varepsilon^0$, $\lim_{\varepsilon\to 0} R_{b1}^\varepsilon = 0$.
- Parabolic midsurface: $\lambda_1^\varepsilon \sim \varepsilon$, $\lim_{\varepsilon\to 0} R_{b1}^\varepsilon = \frac{1}{2}$.
- Hyperbolic midsurface: $\lambda_1^\varepsilon \sim \varepsilon^{\frac{2}{3}}$, $\lim_{\varepsilon\to 0} R_{b1}^\varepsilon = \frac{1}{3}$.

Note that we write here $\lambda_1^\varepsilon \sim \varepsilon^\rho$ to more precisely express that

$$\forall \eta > 0, \quad \lim_{\varepsilon\to 0} \frac{\lambda_1^\varepsilon}{\varepsilon^{\rho-\eta}} = 0, \quad \lim_{\varepsilon\to 0} \frac{\lambda_1^\varepsilon}{\varepsilon^{\rho+\eta}} = +\infty,$$

hence, for instance in the elliptic case $\lambda_1^\varepsilon \sim \varepsilon^0$ does not mean that λ_1^ε converges to a finite limit. The above results show that although the problem is pure-bending inhibited – and only membrane stresses would resist the loading if that loading can be carried only by membrane stresses (see Fig. 5.1) – due to the nature of the inertia forces significant bending can be present. We also refer to (Beirão da Veiga et al., 2008) for a more detailed mathematical analysis of the fundamental eigenpair for a clamped cylindrical shell.

These mathematical results are limited to the asymptotic behavior of the smallest eigenvalue, but we will give a more detailed illustration of an overall spectral behavior in the following section.

5.5.3 Detailed numerical illustration for a clamped cylinder

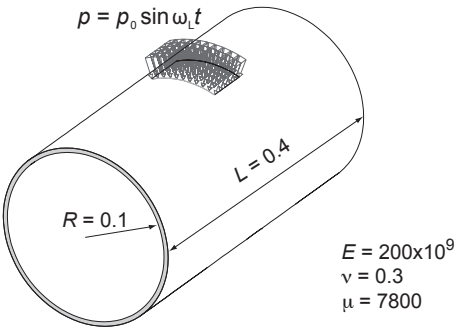

Fig. 5.18. Cylindrical shell model; both ends are clamped

We now present some more detailed illustrations of the spectral asymptotic behavior for the case of a clamped circular cylinder. Figure 5.18 shows the shell structure considered. We solve for the lowest 20 frequencies and mode shapes for different shell thicknesses, using a fine mesh of 240×120 – along the circumferential and longitudinal directions, respectively – MITC4 elements (see Chapter 8), and consider $t = 0.01$, 0.001, 0.0001, and 0.00001. Table 5.2 lists the frequencies and the number of longitudinal "half" waves (N) and number of circumferential full waves (M) in each mode. The name

Fig. 5.19. Shapes of fundamental modes for $t = 0.01$ (left) and $t = 0.00001$ (right)

$t = 0.01$				$t = 0.001$				$t = 0.0001$				$t = 0.00001$			
	Freq. (Hz)	M	N		Freq. (Hz)	M	N		Freq. (Hz)	M	N		Freq. (Hz)	M	N
1	1701	2	1	1	676.3	4	1	1	227.3	8	1	1	74.78	14	1
2	1701	2	1	2	676.3	4	1	2	227.3	8	1	2	74.78	14	1
3	2184	3	1	3	708.7	5	1	3	237.8	9	1	3	74.79	15	1
4	2184	3	1	4	708.7	5	1	4	237.8	9	1	4	74.79	15	1
5	2625	1	1	5	894.7	3	1	5	243.4	7	1	5	77.36	16	1
6	2625	1	1	6	894.7	3	1	6	243.4	7	1	6	77.36	16	1
7	3174	3	2	7	906.5	6	1	7	267.3	10	1	7	77.83	13	1
8	3174	3	2	8	906.5	6	1	8	267.3	10	1	8	77.83	13	1
9	3306	2	2	9	1148	5	2	9	294.4	6	1	9	82.00	17	1
10	3306	2	2	10	1148	5	2	10	294.4	6	1	10	82.00	17	1
11	3676	4	1	11	1155	6	2	11	309.9	11	1	11	84.49	12	1
12	3676	4	1	12	1155	6	2	12	309.9	11	1	12	84.49	12	1
13	3926	Torsion		13	1199	7	1	13	361.9	12	1	13	88.30	18	1
14	4316	4	2	14	1199	7	1	14	361.9	12	1	14	88.30	18	1
15	4316	4	2	15	1346	7	2	15	381.7	10	2	15	95.42	11	1
16	4566	3	3	16	1346	7	2	16	381.7	10	2	16	95.42	11	1
17	4566	3	3	17	1388	4	2	17	386.7	11	2	17	95.96	19	1
18	4936	1	2	18	1388	4	2	18	386.7	11	2	18	95.96	19	1
19	4936	1	2	19	1452	2	1	19	392.1	5	1	19	104.8	20	1
20	5014	2	3	20	1452	2	1	20	392.1	5	1	20	104.8	20	1

M = number of circumferential waves
N = number of longitudinal "half" waves

Table 5.2. Frequencies of the cylindrical shell as t decreases

"half" wave is used to describe the shape, although the slope is zero at the ends. We can make the following interesting and sometimes surprising observations.

- The number of circumferential full waves is almost always larger than the number of longitudinal half waves. Only when $t = 0.01$ (the moderately thick shell case) do we have that for some mode shapes $N = M$, and only for the 18th and 19th frequencies, do we have that the number of full longitudinal and circumferential waves is the same.
- As the thickness decreases, the number of longitudinal half waves remains at 1 ($N = 1$) for an increasing number of frequencies, and the number of circumferential waves increases. For the very thin shell ($t = 0.00001$), the lowest frequency corresponds to one longitudinal half wave and 14 circumferential full waves. For the moderately thick shell, the lowest frequency corresponds to $N = 1$ and $M = 2$ only, see Figure 5.19. This is consistent with the asymptotic property $M \sim \varepsilon^{-\frac{1}{4}}$ established in (Beirão da Veiga et al., 2008).
- For the moderately thick shell, we have one torsional mode, which does not exist among the lowest 20 modes of the thinner shells.
- Of course, because of symmetry we have almost all frequencies appearing in pairs. However, these pairs of frequencies also become closer in spacing as t decreases. For example, whereas for $t = 0.01$ we have f1 = 1701 and f3 = 2184, we have for $t = 0.00001$ the values f1 = 74.78, f3 = 74.79. Figure 5.19 shows the mode shapes corresponding to f1 = 1701 and f1 = 74.78.

These changes in spectral behavior with a change in shell thickness can be related to our above fundamental discussion. In particular, we can see that the computed fundamental eigenvalues[3] – namely, $\lambda_1^\varepsilon = 1.142\,10^8$, $1.806\,10^7$, $2.040\,10^6$, and $2.208\,10^5$ s^{-2} for $\varepsilon = t/R = 0.1$, 0.01, 0.001, and 0.0001, respectively – tend to scale like ε as predicted. In addition, the fact that membrane and bending energies are asymptotically equally balanced in the fundamental modes – whereas the bending energy scales cubically with ε while the membrane and shear energies scale linearly with ε – is reflected in the increasing number of circumferential waves which clearly induce more bending than membrane and shear action.

Of course, these changes in physical behavior require in finite element analysis that the mesh used for the solution of a dynamic response must depend significantly on the thickness of the shell. For example, whereas for the moderately thick shell ($\varepsilon = 0.1$) the number of elements used circumferentially could be only twice the number used for the longitudinal direction, this ratio should be much larger for the very thin shell (or many elements could be used in both directions, which would be computationally more expensive). These numerical considerations will now be illustrated by some further simulation examples.

[3] Eigenvalues λ and eigenfrequencies f are related by the formula $\lambda = (2\pi\,\mathrm{f})^2$.

A region of the shell is subjected to a uniform time-varying pressure load, see Figure 5.18. Three values of thickness are considered ($t = 0.01$, 0.001, 0.0001) to cover typical shell thicknesses. An implicit transient dynamic analysis shall be performed. Hence the first objective is to find an appropriate mesh for the analyses. Three different mesh densities that might typically be used in engineering practice are investigated, all using the MITC4 shell element. The number of elements along the circumferential and longitudinal directions are 40×20 for the coarse mesh, 80×40 for the intermediate mesh and 240×120 for the fine mesh.

The appropriate mesh for a dynamic analysis should be able to accurately capture the static response of the model, and the highest natural frequency content of the dynamic excitation (Bathe, 1996). A mesh that is suitable for a static analysis may therefore not be suitable for dynamics. Also, a mesh suitable for a certain shell thickness may not be suitable for a thinner shell of otherwise identical geometry. Both concepts will be demonstrated in this example[4].

	$t = 0.01$	$t = 0.001$	$t = 0.0001$
Coarse mesh	2.57	2.51	23.5
Intermediate mesh	0.800	0.785	7.10
Fine mesh	0.0370	0.0719	0.0864

Table 5.3. Errors in maximum displacements in static analysis (in percentage)

The errors for the maximum displacements in the static analyses are shown in Table 5.3. All reference solutions for the errors have been obtained by solving the problems with a very fine mesh of 480×240 elements. By setting an upper error limit of 5%, it is clear that the coarse mesh gives acceptable accuracy for $t = 0.01$ and $t = 0.001$, and the fine mesh is required for $t = 0.0001$.

	$t = 0.01$	$t = 0.001$	$t = 0.0001$
Coarse mesh	1.49	8.73	31.5
Intermediate mesh	1.11	0.353	10.1
Fine mesh	0.170	1.01	3.01

Table 5.4. Errors in maximum displacements in dynamic analysis (in percentage)

[4] These results have been obtained using the MITC4 shell element with displacement incompatible modes to improve the plane stress behavior, that is, only the membrane behavior is affected (Bathe, 1996).

Dynamic analyses using implicit direct time integration are then performed with an excitation frequency $\omega_L = 2\omega_{\min}$, where $\omega_{\min}$ is the lowest natural frequency (different for each shell thickness), and 2% Rayleigh damping around ω_L. In each solution, a very small time step is used for the time integration. The errors in the maximum displacements (now also over time) are shown in Table 5.4. The errors, in most cases, have increased compared to the errors in the static analysis. The coarse mesh is still acceptable for $t = 0.01$. The intermediate mesh is acceptable for $t = 0.001$, while for $t = 0.0001$ the fine mesh is needed to satisfy the displacement error.

In the above, we throughout considered linear analysis conditions. In nonlinear analysis, the same observations hold but additional effects can enter. In particular, in large deformation analysis, membrane stresses (in tension or compression) are usually present in the current configuration and can highly affect the dynamic behavior. We will now demonstrate the effect of initial tensile hoop and longitudinal stresses on these frequencies and mode shapes. The shell geometry, boundary conditions, and material properties are all as before. Using Pa as the implicit stress unit, an initial hoop stress of $20.\,10^6$ and an initial longitudinal stress of $10.\,10^6$ are applied to all four cylindrical shells with different thicknesses. These initial stresses closely resemble the stress state in a pressure vessel with an internal applied pressure of $p = 20.\,10^6 \times t/R$.

Fig. 5.20. Fundamental mode in pre-stressed state for $t = 0.00001$

Table 5.5 lists the first 20 frequencies and number of longitudinal half waves (N) and number of circumferential full waves (M) for each pre-stressed cylindrical shell, to be compared with the corresponding results for the unstressed shell in Table 5.2. The mode shape corresponding to the lowest frequency for $t = 0.00001$ with initial stresses is shown in Figure 5.20, to be compared with Figure 5.19 (right) without initial stresses. The results warrant some interesting observations:

$t = 0.01$				$t = 0.001$				$t = 0.0001$				$t = 0.00001$			
	Freq. (Hz)	M	N		Freq. (Hz)	M	N		Freq. (Hz)	M	N		Freq. (Hz)	M	N
1	1705	2	1	1	738.6	4	1	1	547.7	5	1	1	544.2	5	1
2	1705	2	1	2	738.6	4	1	2	547.7	5	1	2	544.2	5	1
3	2194	3	1	3	805.3	5	1	3	551.7	6	1	3	544.8	6	1
4	2194	3	1	4	805.3	5	1	4	551.7	6	1	4	544.8	6	1
5	2626	1	1	5	918.8	3	1	5	601.4	7	1	5	589.7	7	1
6	2626	1	1	6	918.8	3	1	6	601.4	7	1	6	589.7	7	1
7	3182	3	2	7	1019	6	1	7	636.3	4	1	7	634.7	4	1
8	3182	3	2	8	1019	6	1	8	636.3	4	1	8	634.7	4	1
9	3309	2	2	9	1212	5	2	9	672.3	8	1	9	654.3	8	1
10	3309	2	2	10	1212	5	2	10	672.3	8	1	10	654.3	8	1
11	3688	4	1	11	1248	6	2	11	753.7	9	1	11	727.8	9	1
12	3688	4	1	12	1248	6	2	12	753.7	9	1	12	727.8	9	1
13	3927	Torsion		13	1319	7	1	13	787.0	8	2	13	770.4	8	2
14	4327	4	2	14	1319	7	1	14	787.0	8	2	14	770.4	8	2
15	4327	4	2	15	1422	4	2	15	788.7	7	2	15	778.6	7	2
16	4572	3	3	16	1422	4	2	16	788.7	7	2	16	778.6	7	2
17	4572	3	3	17	1456	7	2	17	825.6	9	2	17	800.5	9	2
18	4936	1	2	18	1456	7	2	18	825.6	9	2	18	800.5	9	2
19	4936	1	2	19	1457	2	1	19	841.2	10	1	19	805.4	10	1
20	5017	2	3	20	1457	2	1	20	841.2	10	1	20	805.4	10	1

M = number of circumferential waves
N = number of longitudinal "half" waves

Table 5.5. Frequencies of the pre-stressed cylindrical shell as t decreases

- For $t = 0.01$ there is a small increase in the frequencies but no change in the mode shapes (N and M are unchanged).
- For $t = 0.001$ there is a larger increase in the frequencies and a minor change in the mode shapes (the 15th and 16th frequencies now correspond to $M = 4$, $N = 2$ instead of the 17th and 18th frequencies in the unstressed shell).
- For $t = 0.0001$ there is a significant increase in all reported frequencies and also a significant change in the mode shapes. The lowest four frequencies correspond to fewer circumferential waves when compared to the results from the unstressed shell.
- For $t = 0.00001$ the results are very similar to the results for $t = 0.0001$, in terms of frequency values and mode shapes. The shell is significantly stiffer than the unstressed shell of the same thickness.
- The asymptotic behavior of the shell (as its thickness is reduced) is different for the unstressed and pre-stressed shells. For the unstressed shell, the lowest frequency scales approximately as $\sqrt{t}$, while the initially stressed shell results converge to a thickness invariant lowest frequency, that is, the frequency stabilizes at a value above 500 Hz.

This last observation can be easily explained by noting that the behavior of pre-stressed structures is described with an additional term εA_{ps} in the stiffness bilinear form. A typical expression for this additional term would be

$$A_{ps}(\vec{u},\vec{v}) = \int_\omega m_{ps}^{\alpha\beta}\, \vec{u}_{,\alpha} \cdot \vec{v}_{,\beta}\, dS,$$

where $\underline{\underline{m}}_{ps}$ denotes the membrane stress tensor corresponding to the pre-stressed state. Formally, the tentative limit spectral problem is now

$$A_{\rm m}(\Phi, V) + A_{ps}(\Phi, V) = \lambda\, I_d(\Phi, V), \quad \forall V \in \mathcal{V}.$$

Hence, when the membrane initial stress tensor $\underline{\underline{m}}_{ps}$ is positive definite – namely, when it corresponds to tensile stresses in all principal directions – the bilinear form A_{ps} brings coercivity that makes this spectral problem well-posed, which corresponds to the limit behavior seen in the numerical computations.

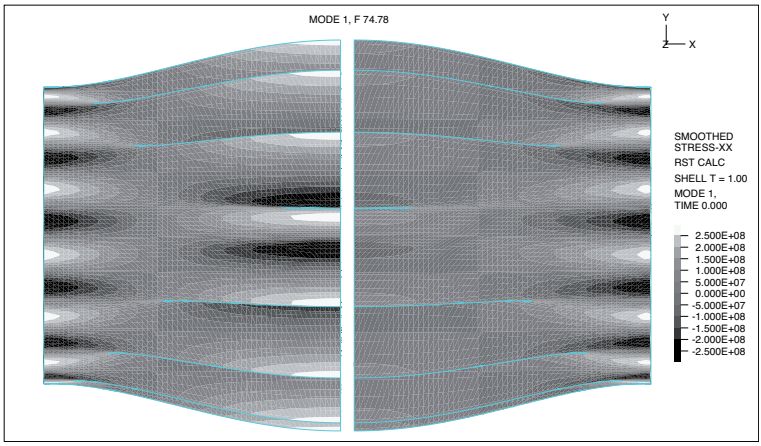

Fig. 5.21. Axial modal stresses for lowest frequency for cylinder with $t = 0.00001$: unstressed case

Further physical insight is obtained by considering the axial modal stresses for the same two cases as shown in the Figures 5.21 and 5.22. The left half in each Figure shows the stress on the cylinder's outer surface and the right half shows the stress on the inner surface (shown side by side in the figure for ease of comparison). For the pre-stressed cylinder there is little difference between the two sides indicating a predominantly membrane deformation mode. For the unstressed case, close to the center of the cylinder there are both bending and membrane deformations, as evident by the difference in

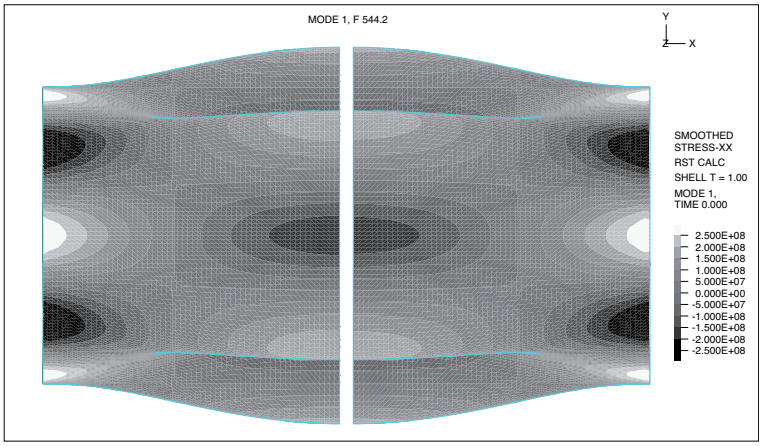

Fig. 5.22. Axial modal stresses for lowest frequency for cylinder with $t = 0.00001$: pre-stressed case

the axial modal stress. Near the fixed ends, however, there is little difference between the stresses at the top and bottom surfaces indicating mostly membrane deformations in those regions.

6. Displacement-Based Shell Finite Elements

In this chapter, we describe and analyze the main strategies that have been proposed and used to formulate *displacement-based* finite element procedures for shells. By displacement-based we mean that the finite element solution is obtained by directly applying the variational principle in the finite element space which discretizes the space of admissible displacements for the structure. In particular, this implies that no "numerical trick" – such as reduced integration – is used in the formulation.

We start by considering the straightforward approach that consists in directly discretizing the shell mathematical models introduced in Chapter 4. We then turn to the analysis of seemingly very different finite element strategies based on engineering considerations, namely the *facet-shell element* approach and the *general shell element* approach.

We recall that the symbol C is used to denote generic positive constants, while γ denotes generic strictly positive constants. Of course, when a finite element problem is concerned all constants are assumed to be independent of the mesh considered, hence independent of the mesh parameter h.

6.1 Discretizations of Shell Mathematical Models

In this approach, a specific shell mathematical model is considered and the components of the model unknowns in the coordinate system used are approximated with finite element functions. It is then the 2D reference domain ω which is meshed, and we thus obtain a classical finite element problem posed in this reference domain. Using the Céa Lemma (Proposition 3.2.2), we then have for the shell models considered in Chapter 4

$$\boxed{\|\vec{u} - \vec{u}_h\|_{\mathcal{V}^K} \leq C \inf_{\vec{v} \in \mathcal{V}_h^K} \|\vec{u} - \vec{v}\|_{\mathcal{V}^K}} \tag{6.1}$$

for the m-b model, while we obtain for the s-m-b model

$$\boxed{\|\vec{u} - \vec{u}_h, \underline{\theta} - \underline{\theta}_h\|_{\mathcal{V}^N} \leq C \inf_{(\vec{v}, \underline{\eta}) \in \mathcal{V}_h^N} \|\vec{u} - \vec{v}, \underline{\theta} - \underline{\eta}\|_{\mathcal{V}^N},} \tag{6.2}$$

D. Chapelle, K.-J. Bathe, *The Finite Element Analysis of Shells – Fundamentals*,
Computational Fluid and Solid Mechanics, 2nd ed., DOI 10.1007/978-3-642-16408-8_6,

and a similar estimate for the basic shell model. In order to carry the analysis further, we can see that we need to address the technical difficulty that surface Sobolev norms are used in the above relations. For such norms, however, we cannot apply any existing interpolation estimates. However, we can prove that the surface norms are equivalent to classical Sobolev norms defined in the reference domain.

Proposition 6.1.1 *The norms* $\|\cdot\|_{\mathcal{V}^N}$ *and* $\|\cdot\|_{\mathcal{V}^K}$ *are equivalent to the norms* $\|\cdot\|_{\tilde{\mathcal{V}}^N}$ *and* $\|\cdot\|_{\tilde{\mathcal{V}}^K}$*, respectively, with*

$$\|\vec{v},\underline{\eta}\|^2_{\tilde{\mathcal{V}}^N} = \sum_{i=1}^{3} \|v_i\|^2_{H^1(\omega)} + \sum_{\alpha=1}^{2} \|\eta_\alpha\|^2_{H^1(\omega)}, \tag{6.3}$$

$$\|\vec{v}\|^2_{\tilde{\mathcal{V}}^K} = \sum_{\alpha=1}^{2} \|v_\alpha\|^2_{H^1(\omega)} + \|v_3\|^2_{H^2(\omega)}. \tag{6.4}$$

Proof. From the definitions of surface Sobolev norms and the fact that covariant derivatives involve classical derivatives up to an order no greater than their own order, and using the boundedness of all geometric coefficients, we clearly have that

$$\|\vec{v},\underline{\eta}\|_{\mathcal{V}^N} \leq C\|\vec{v},\underline{\eta}\|_{\tilde{\mathcal{V}}^N} \tag{6.5}$$

for any $(\vec{v},\underline{\eta})$ such that $\|\vec{v},\underline{\eta}\|_{\tilde{\mathcal{V}}^N}$ is well-defined. Similarly,

$$\|\vec{v}\|_{\mathcal{V}^K} \leq C\|\vec{v}\|_{\tilde{\mathcal{V}}^K} \tag{6.6}$$

for any $\vec{v}$ such that $\|\vec{v}\|_{\tilde{\mathcal{V}}^K}$ is well-defined. To prove the reversed inequalities, we start by considering a scalar function ϕ in $L^2(\mathcal{S})$. We have

$$\|\phi\|^2_{L^2(\mathcal{S})} = \int_\omega \phi^2 \sqrt{a}\, d\xi^1 d\xi^2. \tag{6.7}$$

We recall that $\sqrt{a} = \|\vec{a}^1 \wedge \vec{a}^2\|$ and that the vectors $(\vec{a}^1,\vec{a}^2)$ are assumed to be linearly independent all over $\bar{\omega}$, hence $\sqrt{a}$ admits a strictly positive lower bound γ. Therefore, ϕ is in $L^2(\omega)$ and

$$\|\phi\|_{L^2(\omega)} \leq \frac{1}{\sqrt{\gamma}}\|\phi\|_{L^2(\mathcal{S})}. \tag{6.8}$$

Consider now a first-order tensor $\underline{\eta}$ in $L^2(\mathcal{S})$. By definition

$$\|\underline{\eta}\|^2_{L^2(\mathcal{S})} = \int_\omega a^{\alpha\beta}\eta_\alpha\eta_\beta\sqrt{a}\, d\xi^1 d\xi^2. \tag{6.9}$$

Using an argument similar to that in the proof of Lemma 4.3.4, we have for any $(\xi^1, \xi^2) \in \omega$

$$c\big((X_1)^2 + (X_2)^2\big) \leq a^{\alpha\beta}(\xi^1, \xi^2) X_\alpha X_\beta \leq C\big((X_1)^2 + (X_2)^2\big), \quad \forall (X_1, X_2) \in I\!R^2, \tag{6.10}$$

where c and C are two strictly positive constants. Combining the left inequality with the lower bound on $\sqrt{a}$, we infer that (η_1, η_2) is in $L^2(\omega)$, with

$$\|\eta_1, \eta_2\|_{L^2(\omega)} \leq \frac{1}{\sqrt{c\gamma}} \|\underline{\eta}\|_{L^2(\mathcal{S})}. \tag{6.11}$$

Next, considering ϕ in $H^1(\mathcal{S})$ with

$$\|\phi\|^2_{H^1(\mathcal{S})} = \|\phi\|^2_{L^2(\mathcal{S})} + \int_\omega a^{\alpha\beta} \phi_{,\alpha} \phi_{,\beta} \sqrt{a}\, d\xi^1 d\xi^2, \tag{6.12}$$

using the previous results we have that ϕ is in $L^2(\omega)$ with the bound (6.8), and that $(\phi_{,1}, \phi_{,2})$ is in $L^2(\omega)$ with

$$\|\phi_{,1}, \phi_{,2}\|_{L^2(\omega)} \leq C \|\underline{\nabla} \phi\|_{L^2(\mathcal{S})} \tag{6.13}$$

(applying (6.11) with $\underline{\eta} = \underline{\nabla}\phi$). Therefore ϕ is in $H^1(\omega)$ and

$$\|\phi\|_{H^1(\omega)} \leq C \|\phi\|_{H^1(\mathcal{S})}. \tag{6.14}$$

For a first-order tensor $\underline{\eta}$ in $H^1(\mathcal{S})$, we have by definition

$$\|\underline{\eta}\|^2_{H^1(\mathcal{S})} = \|\underline{\eta}\|^2_{L^2(\mathcal{S})} + \int_\omega a^{\alpha\lambda} a^{\beta\mu} \eta_{\alpha|\beta} \eta_{\lambda|\mu} \sqrt{a}\, d\xi^1 d\xi^2. \tag{6.15}$$

We already know that (η_1, η_2) is in $L^2(\omega)$ with

$$\|\eta_1, \eta_2\|_{L^2(\omega)} \leq C \|\underline{\eta}\|_{L^2(\mathcal{S})}. \tag{6.16}$$

By arguments of the type used to obtain the inequalities of Lemmas 4.3.4 and 4.3.5, we have that for any $(\xi^1, \xi^2) \in \omega$

$$\begin{aligned} c\big((Y_{11})^2 + (Y_{12})^2 + (Y_{21})^2 + (Y_{22})^2\big) \\ \leq a^{\alpha\lambda}(\xi^1, \xi^2) a^{\beta\mu}(\xi^1, \xi^2) Y_{\alpha\beta} Y_{\lambda\mu} \\ \leq C\big((Y_{11})^2 + (Y_{12})^2 + (Y_{21})^2 + (Y_{22})^2\big), \\ \forall (Y_{11}, Y_{12}, Y_{21}, Y_{22}) \in I\!R^4, \end{aligned} \tag{6.17}$$

where c and C are strictly positive constants. Hence, using the left inequality and the lower bound on $\sqrt{a}$ we have

$$\int_\omega \left((\eta_{1|1})^2 + (\eta_{1|2})^2 + (\eta_{2|1})^2 + (\eta_{2|2})^2\right) d\xi^1 d\xi^2 \leq C \int_\omega a^{\alpha\lambda} a^{\beta\mu} \eta_{\alpha|\beta} \eta_{\lambda|\mu} \sqrt{a}\, d\xi^1 d\xi^2. \tag{6.18}$$

Therefore $(\eta_{1|1}, \eta_{1|2}, \eta_{2|1}, \eta_{2|2})$ is in $L^2(\omega)$, which implies that the vector of standard derivatives $(\eta_{1,1}, \eta_{1,2}, \eta_{2,1}, \eta_{2,2})$ is also in $L^2(\omega)$, since we recall

$$\eta_{\alpha,\beta} = \eta_{\alpha|\beta} + \Gamma^\lambda_{\alpha\beta} \eta_\lambda, \tag{6.19}$$

(η_1, η_2) is in $L^2(\omega)$, and the Christoffel symbols are bounded. Moreover,

$$\|\eta_{1,1}, \eta_{1,2}, \eta_{2,1}, \eta_{2,2}\|_{L^2(\omega)} \leq C \|\underline{\eta}\|_{H^1(\mathcal{S})}. \tag{6.20}$$

As a consequence, (η_1, η_2) is seen to be in $H^1(\omega)$, and a combination of (6.16) and (6.20) gives

$$\|\eta_1, \eta_2\|_{H^1(\omega)} \leq C \|\underline{\eta}\|_{H^1(\mathcal{S})}. \tag{6.21}$$

The last preliminary step in this proof pertains to zero-th order tensors in $H^2(\mathcal{S})$. Consider then ϕ in $H^2(\mathcal{S})$. We have

$$\|\phi\|^2_{H^2(\mathcal{S})} = \|\phi\|^2_{H^1(\mathcal{S})} + \|\underline{\nabla}\phi\|^2_{H^1(\mathcal{S})}. \tag{6.22}$$

Setting $\underline{\eta} = \underline{\nabla}\phi$ in the previous argument, we directly obtain that ϕ is in $H^2(\omega)$ with

$$\|\phi\|_{H^2(\omega)} \leq C \|\phi\|_{H^2(\mathcal{S})}. \tag{6.23}$$

Finally, the desired reversed inequalities

$$\|\vec{v}, \underline{\eta}\|_{\tilde{\mathcal{V}}^N} \leq C \|\vec{v}, \underline{\eta}\|_{\mathcal{V}^N} \qquad \forall (\vec{v}, \underline{\eta}) \in \mathcal{V}^N \tag{6.24}$$

$$\|\vec{v}\|_{\tilde{\mathcal{V}}^K} \leq C \|\vec{v}\|_{\mathcal{V}^K} \qquad \forall \vec{v} \in \mathcal{V}^K \tag{6.25}$$

are direct consequences of these preliminary results. ∎

Remark 6.1.1. The norms $\|\cdot\|_{\tilde{\mathcal{V}}^N}$ and $\|\cdot\|_{\tilde{\mathcal{V}}^K}$ are clearly dependent on the curvilinear coordinate system, i.e. on the chart that is used. They are considered here for the purpose of mathematical analysis only, in the absence

of interpolation results for surface Sobolev spaces. This indicates that these coordinate-dependent norms should not be used to obtain sharp estimates of invariant quantities. In particular, errors made by approximating the exact solution by a finite element solution are most likely to be more meaningful when computed using the original norms $\|\cdot\|_{\mathcal{V}^N}$ and $\|\cdot\|_{\mathcal{V}^K}$, e.g. with a view to mesh adaptation. ■

As a consequence, error estimates for *direct discretizations* of shell mathematical models can be derived within the classical theory of finite elements, see e.g. (Ciarlet, 1978). For the s-m-b model, since the functional space in consideration is H^1 for all components of the unknowns, using a Lagrange-type discretization of the p-th degree (namely P_p for triangles and Q_p for quadrilaterals) we thus obtain

$$\boxed{\|\vec{u} - \vec{u}_h, \underline{\theta} - \underline{\theta}_h\|_{\mathcal{V}^N} \leq Ch^p,} \tag{6.26}$$

where h denotes the largest diameter of all elements in the mesh. We refer to Chapter 3 for a discussion on the conditions to be satisfied by the mesh and the numerical integration rules in order to obtain such estimates. We again emphasize that this estimate can only hold if the exact solution is sufficiently regular, namely is in H^{p+1}. If this regularity condition is not satisfied, adequate mesh refinement (in the vicinity of singularities of the exact solution) must be used to recover this optimal estimate (Verfürth, 1996; Frey & George, 2000). Note that – in principle – the basic shell model and the 3D-shell model can also be directly discretized in a similar manner, see (Lee & Bathe, 2005), but as discussed below some much more effective finite element formulations are available in association with these models, namely, general shell elements and 3D-shell elements, respectively.

For the m-b model the situation is more complicated due to the fact that the transverse displacement is in H^2. This implies that C^1 finite elements must be used to obtain a conforming discretization of the model, at least for the transverse component of the displacement. We do not dwell upon such procedures, since our emphasis in this book is – to a large extent – on shell models based on the Reissner-Mindlin kinematical assumption, and in particular on the basic shell model, which are much more widely used in engineering practice. In fact, a major reason for this preference can be seen by considering an example of a C^1-conforming finite element known as the Argyris triangle, see e.g. (Ciarlet, 1978). This element features, as degrees of freedom, the values of the discretized function and of all its derivatives up to order 2 at the vertices and the normal derivatives at the middle of each edge, namely in total 21 degrees of freedom for one single component of the unknown. This discretization is, however, very accurate since the local approximation space is then P_5. Note indeed that a Hermite-type element with

only first-order derivatives given at the vertices would not be C^1-conforming, as the gradients would not be continuous along the edges in general. Some further developments have been performed to obtain "lighter" C^1-conforming elements (Bernadou, 1996). In addition, special non-conforming elements can also be used for these models, e.g. the DKT elements, see (Batoz et al., 1980; Bernadou et al., 1994b; Carrive et al., 1995) and the references therein. Nevertheless, finite element procedures for Kirchhoff-Love type models all have non-Lagrange degrees of freedom, which makes them much less attractive to use than isoparametric elements.

Remark 6.1.2. It should be noted that what would seem the most natural discretization of mathematical shell models, namely, using standard finite element shape functions to discretize the components of the displacement and rotation fields in the *local basis* (in covariant components, typically) leads to discrete fields that cannot – in general – represent rigid body modes with exactly zero strains. This is unacceptable because, in practice, we should be able to achieve the accurate representation of rigid body translations and rotations using very coarse meshes. This accurate representation can be achieved by instead interpolating the *Cartesian components* of the displacement and rotation vectors, see also (Lee & Bathe, 2005). ■

6.2 Facet-Shell Elements

Facet-shell elements have been introduced with the earliest finite element procedures to analyze shell structures, and they are still used in engineering practice. The facet-shell element approach consists in approximating the shell structure by an assemblage of planar triangular or quadrilateral (frequently composed of triangles) elements. These finite elements are formulated to superimpose plate bending stiffness (in the transverse direction) with membrane stiffness (in the tangential directions), see e.g. (Zienkiewicz & Taylor, 1989/1991; Bathe, 1996), and also (Chapelle, 1997) for a similar approach applied to curved rods. Clearly, a specific technical difficulty arises as to how to enforce compatibility conditions for the rotations of different facets – with different normal vectors – at common vertices of the mesh.

Considering this approach, an important issue is the physical relevance in conjunction with the mathematical convergence. In particular, when decreasing the sizes of the facets – namely, when refining the mesh – we would like the finite element solutions to converge to the exact solution of a well-defined mathematical model, the mechanical validity of which could be assessed by various means (including by performing physical experiments). In fact, this convergence issue has been mathematically analyzed in (Bernadou & Trouvé, 1989), see also (Bernadou & Trouvé, 1990a,b), and serious doubt is cast in

these references as to the ability of facet-shell elements to satisfy the required mathematical properties of convergence and consistency.

This question can be further investigated by conducting some numerical experiments. We thus consider the case of a hyperbolic paraboloid for which the midsurface is given by

$$\vec{\phi}(\xi^1, \xi^2) = \begin{pmatrix} \xi^1 \\ \xi^2 \\ (\xi^1)^2 - (\xi^2)^2 \end{pmatrix}, \qquad \omega = \left]-\frac{1}{2}, \frac{1}{2}\right[^2. \tag{6.27}$$

We computed the solutions obtained when a uniform vertical distributed force is applied (Poisson's ratio $\nu = 0.3$), with the edge corresponding to $\xi^1 = -1/2$ clamped, and for various values of the thickness. For visualization purposes, Figure 6.1 shows the original and deformed (normalized) shape obtained for $t = 0.001$ with a regular mesh of 64×64 MITC4 elements (note the almost rigid region originating from the clamped boundary, see Section 5.2.2 for an interpretation of this phenomenon). We also obtained further results using

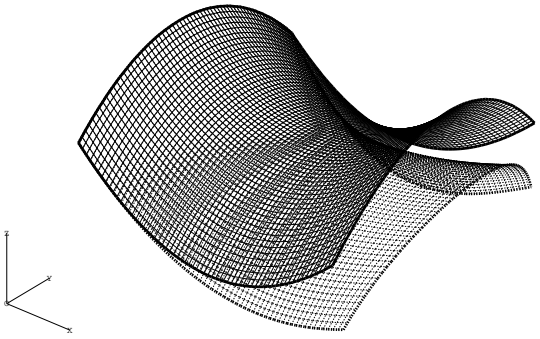

Fig. 6.1. Original and deformed hyperbolic paraboloid

a finer mesh of 144×144 MITC4 elements and these results are used as a reference in the computations performed with facet-shell elements.

The facet-shell element that we used in our computations is the 3-node triangular DKT plate bending element, see (Batoz et al., 1980), superimposed with the constant strain membrane element, with a mesh pattern as shown in Figure 6.2. We display in Figure 6.3 the displacement obtained at the middle of the free boundary $\xi^1 = 1/2$ (namely, opposite the clamped boundary), for various meshes of increasing refinement (note the log scale for the mesh parameter h). This displacement is scaled by the corresponding value for the reference solution and each curve corresponds to a given value

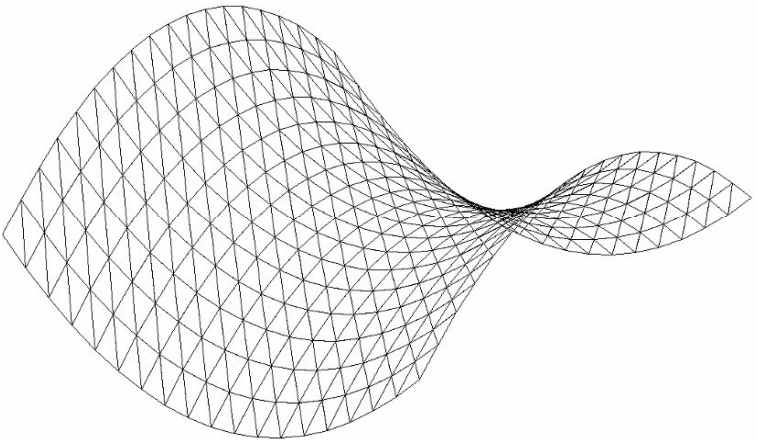

Fig. 6.2. Mesh pattern used for facet-shell elements

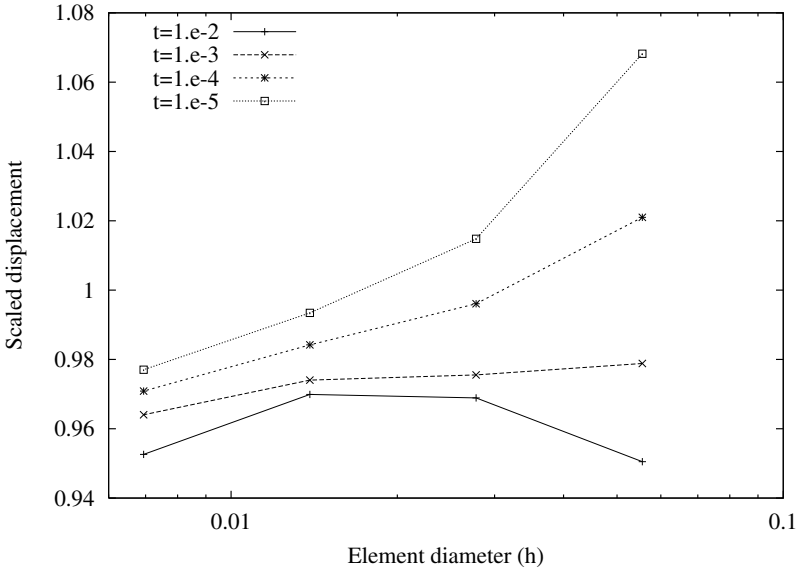

Fig. 6.3. Scaled displacement (middle of edge $\xi^1 = 1/2$)

of the thickness. We can see that the facet-element solutions do not appear to converge to the reference values when the mesh is refined, although all results shown lie within a few percent of the reference. Moreover, these curves do not exhibit a converging behavior (to any value that may be other than the reference used), since their slopes do not significantly decrease as the mesh is refined. A very similar behavior is observed with the computed strain energies (also scaled using the reference solutions) that we represent in Figure 6.4.

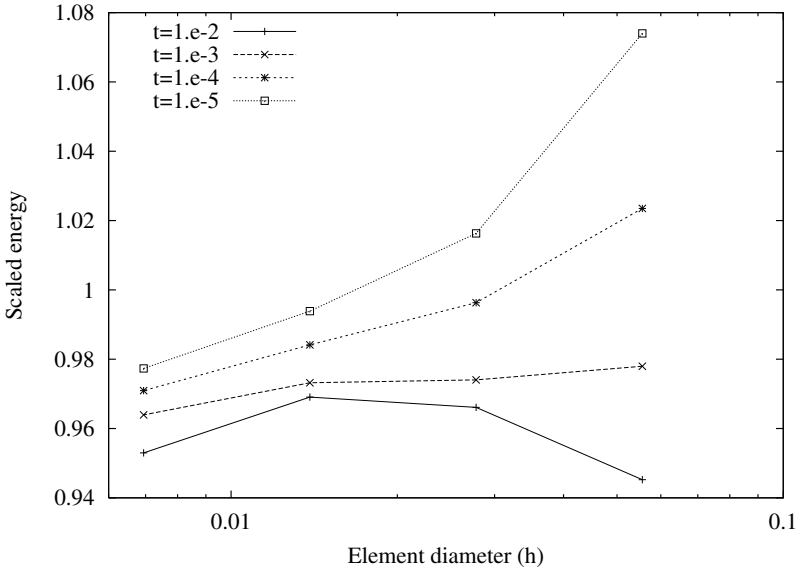

Fig. 6.4. Scaled deformation energy

Therefore, although facet-shell elements can produce reasonably accurate solutions (e.g. in the above hyperbolic paraboloid test problem, which is a difficult problem to solve, see Chapters 7 and 8), there is evidence that they fail to satisfy the basic convergence properties that should be expected from sound finite element procedures in general. In fact, although not focused on the solutions given above, despite their flat geometry these elements have also been proven to suffer from deficiencies related to membrane locking, a numerical phenomenon we discuss in Chapter 7, see (Akian & Sanchez-Palencia, 1992). Finally, while some time ago the solution accuracy obtained with these elements was judged to be adequate, at present much more effective shell finite elements are available, as will be seen in the forthcoming discussions. Hence we cannot recommend the use of facet-shell elements for general shell analyses, and can also not recommend that new shell elements be formulated by superimposing plate bending and membrane elements. Instead, general

shell elements are best formulated using a general shell theory or, even better, based on a general 3D continuum mechanics approach incorporating shell theory assumptions (see Section 6.3 and Chapters 7 to 9).

6.3 General Shell Elements

Most shell finite element procedures now used in engineering practice fall into this category. Unlike the previously discussed procedures, general shell elements are not derived from a shell (or plate-bending) model, but instead from a 3D variational formulation. More specifically, a basic general shell element procedure is constructed as follows (Bathe, 1996).

1. Consider a general 3D variational formulation posed on the 3D geometrical domain $\mathcal{B}$ and infer a modified variational problem from the *stress assumption*

$$\boxed{\sigma^{33} \equiv 0.} \tag{6.28}$$

We symbolically denote this modified problem by

$$A^{3D}(\vec{U}, \vec{V}) = F^{3D}(\vec{V}), \quad \forall \vec{V} \in \mathcal{V}^{3D}, \tag{6.29}$$

where A^{3D} and F^{3D} respectively represent the external and internal virtual works, and $\mathcal{V}^{3D}$ denotes the appropriate functional space taking into account the essential boundary conditions. Note that we performed such a modification of the 3D variational formulation (specifically with Hooke's law) when constructing our basic shell model, see Section 4.2.1.

2. Consider a special mesh of $\mathcal{B}$ defined by nodes located on the midsurface of the shell body and the following relation between local coordinates $(r, s, z) \in [-1, 1]^3$ and the position vector $\vec{x}$ inside an element

$$\boxed{\vec{x} = \sum_{i=1}^{k} \lambda_i(r, s)\big(\vec{x}^{(i)} + z\frac{t^{(i)}}{2}\vec{a}_3^{(i)}\big),} \tag{6.30}$$

where the functions λ_i are 2D Lagrange shape functions associated with the k nodes of the element considered, and the quantities $\vec{x}^{(i)}$, $t^{(i)}$ and $\vec{a}_3^{(i)}$ denote the position, thickness and unit normal vector at the nodes, respectively. Of course, the 2D shape functions λ_i depend on the polynomial order chosen and on the geometric type of the element (namely whether quadrilateral or triangular elements are used). Hence, with this

strategy we obtain a 3D mesh for $\mathcal{B}$ with a single layer of elements through the thickness of the shell, using shape functions based on 2D shape functions, and in which all the edges across the thickness are normal to the midsurface, see Figure 6.5. We also note that, setting $z = 0$ in (6.30) and varying (r, s) in $[-1, 1]^2$ we obtain an approximation of the midsurface[1] lying inside the element.

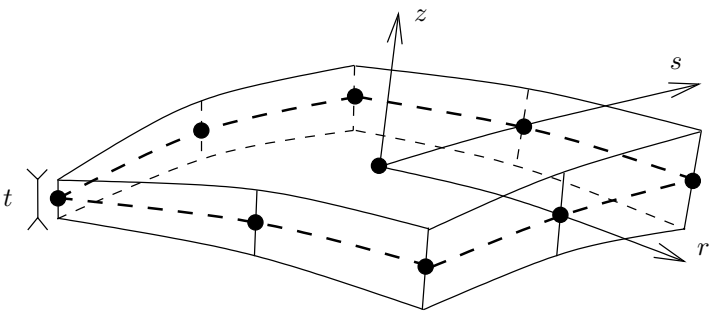

Fig. 6.5. 9-node general shell element with local coordinate system

3. Following now a standard isoparametric approach, we allow for displacements that are obtained by varying the nodal quantities pertaining to position, namely the nodal position vectors $\vec{x}^{(i)}$ and the nodal unit normal vectors $\vec{a}_3^{(i)}$. We thus obtain displacements given by

$$\boxed{\vec{V} = \sum_{i=1}^{k} \lambda_i(r,s)\big(\vec{v}^{(i)} + z\frac{t^{(i)}}{2}\vec{\eta}^{(i)}\big),} \tag{6.31}$$

where, since $\vec{\eta}^{(i)}$ corresponds to the variation of the unit vector $\vec{a}_3^{(i)}$,

$$\boxed{\vec{\eta}^{(i)} \cdot \vec{a}_3^{(i)} = 0.} \tag{6.32}$$

We denote this finite element displacement space by $\mathcal{V}_h^{3D}$. Note that (6.31) implies that the finite element displacement function satisfies *Reissner-Mindlin kinematics* at all nodes of the mesh, i.e. along the fibers normal to the midsurface at the nodes.

[1] We henceforth reserve the terminology "the midsurface" to refer to the *exact midsurface* of the shell, and we specify "approximate midsurface" or "finite element interpolated midsurface" when appropriate.

4. Finally, the general shell element procedure consists in solving for $\vec{U}_h$ in $\mathcal{V}_h^{3D}$, i.e. given inside each element by

$$\vec{U}_h = \sum_{i=1}^{k} \lambda_i(r,s)\big(\vec{u}_h^{(i)} + z\frac{t^{(i)}}{2}\vec{\theta}_h^{(i)}\big), \tag{6.33}$$

that satisfies

$$\boxed{A_h^{3D}(\vec{U}_h, \vec{V}) = F_h^{3D}(\vec{V}), \quad \forall \vec{V} \in \mathcal{V}_h^{3D},} \tag{6.34}$$

where the subscript h in A_h^{3D} and F_h^{3D} signifies that we are using the approximated geometry defined by (6.30) to compute the external and internal virtual works, as usual in isoparametric finite element procedures.

As can be seen from this description, general shell elements are based on the idea of "degenerating" a 3D solid finite element into a shell element by using special shape functions that are related to the Reissner-Mindlin kinematical assumption and by also using a stress assumption. This is indeed why these elements are sometimes also called "degenerated solid shell elements", see in particular the seminal work (Ahmad et al., 1970). Clearly, a major advantage of this approach is that, since the only model used is the 3D model in consideration, *general 3D constitutive laws can be employed*. In addition, the practical methodology corresponds to an isoparametric finite element procedure, hence the implementation is straightforward. In particular it does not require the datum of a chart describing the midsurface, but only the nodal positions and normal vectors. This is effective in practice as most shell structures analyzed are defined using computer-aided design systems that do not provide charts.

Note that the degrees of freedom utilized in a general shell element procedure – namely the displacement of the midsurface and the rotation of the normal fibers at the nodes – are exactly the same as those of a direct discretization of a shell model based on the Reissner-Mindlin kinematical assumption. However, since general shell elements are not based on an explicit shell model, their mathematical analysis is not as straightforward. This analysis is the objective of the following discussion.

In order to perform the numerical analysis of general shell elements, we first need to identify a candidate mathematical model, the solution of which would be the limit of the finite element solution as the mesh is refined. Based on the above description of the general shell element procedure, a natural candidate for the corresponding mathematical model is obtained by using the 3D variational formulation (6.29) inferred from the plane stress assumption (6.28), and displacement functions that satisfy the Reissner-Mindlin kinematical assumption everywhere. Namely, the variational formulation considered

is

$$\boxed{A^{3D}(\vec{U},\vec{V}) = F^{3D}(\vec{V}),} \tag{6.35}$$

where $\vec{U}$ is the unknown that satisfies the Reissner-Mindlin kinematical assumption and boundary conditions, and $\vec{V}$ denotes any corresponding test function. Therefore we can write like in Chapter 4

$$\vec{U}(\xi^1,\xi^2,\xi^3) = \vec{u}(\xi^1,\xi^2) + \xi^3\theta_\lambda(\xi^1,\xi^2)\vec{a}^\lambda(\xi^1,\xi^2), \tag{6.36}$$

$$\vec{V}(\xi^1,\xi^2,\xi^3) = \vec{v}(\xi^1,\xi^2) + \xi^3\eta_\lambda(\xi^1,\xi^2)\vec{a}^\lambda(\xi^1,\xi^2), \tag{6.37}$$

and we can define $\mathcal{V}^G$ as the space spanned by $(\vec{v},\underline{\eta})$ when $\vec{V}$ takes all possible values of admissible test functions that give a bounded internal energy. We recall that if the 3D formulation corresponds to an isotropic material we thus obtain the *basic shell model* introduced and analyzed in Chapter 4. In this case, of course, $\mathcal{V}^G$ is the same as $\mathcal{V}^B$.

Then, in order to analyze the convergence of the finite element procedure, we need to consider *sequences of finite element solutions* obtained by refining the mesh. We assume that these sets of meshes are such that all nodes are exactly located on the given midsurface (even though it may not be known in practice) to which the nodal normal vectors are also exactly orthogonal. We can then recast the methodology described above into a framework more adapted to numerical analysis. First of all, to compare the finite element solution to the exact solution of the candidate limit problem, we need to *relate the finite element solution to a displacement field and a rotation field given on the whole midsurface*, i.e. in the variables (ξ^1,ξ^2). To that purpose, we set the following one-to-one relation between (ξ^1,ξ^2) and the local coordinates (r,s) inside each element:

$$\boxed{\begin{pmatrix} \xi^1 \\ \xi^2 \end{pmatrix} = \sum_{i=1}^{k} \lambda_i(r,s) \begin{pmatrix} \xi^1_{(i)} \\ \xi^2_{(i)} \end{pmatrix},} \tag{6.38}$$

where $(\xi^1_{(i)},\xi^2_{(i)})$ denote the nodal coordinates in ω. For any quantity defined in the local coordinates (r,s), i.e. implicitly given on the approximate midsurface, we can then use the above relation to *transport* this quantity onto the exact midsurface parametrized in the (ξ^1,ξ^2)-variables. In particular, from a finite element displacement function that satisfies (6.31) we can infer two transported vector fields given in the (ξ^1,ξ^2) variables, namely

$$\left\{\begin{array}{l} T_1(\vec{V})(\xi^1,\xi^2) = \displaystyle\sum_{i=1}^{k} \lambda_i(r,s)\vec{v}^{(i)} \\ T_2(\vec{V})(\xi^1,\xi^2) = \displaystyle\sum_{i=1}^{k} \lambda_i(r,s)\vec{\eta}^{(i)} \end{array}\right. \tag{6.39}$$

inside each element. These two vector fields correspond to the interpolation of nodal displacements and rotations via the transport operation. The field $T_1(\vec{V})$ can be identified as a displacement of the midsurface. The second field $T_2(\vec{V})$, however, does not directly provide a rotation field since we do not have – in general – the orthogonality property "$T_2(\vec{V}) \cdot \vec{a}_3 = 0$" exactly satisfied, except at the nodes, see Eq.(6.32). Indeed, *the interpolation of a tangential vector is not a tangential vector*, except in very specific situations (e.g. for a plate). In order to recover this tangential character everywhere, we will use the projection onto the tangential plane, i.e. the operator π defined by

$$\boxed{\pi(\vec{w}) = \vec{w} - (\vec{w} \cdot \vec{a}_3)\vec{a}_3,} \tag{6.40}$$

for any vector field $\vec{w}$ defined on the midsurface. We can then define

$$\boxed{\mathcal{V}_h^G = \Big\{ \big(T_1(\vec{V}), \pi\big(T_2(\vec{V})\big)\big) \mid \vec{V} \in \mathcal{V}_h^{3D} \Big\}.} \tag{6.41}$$

Note that $\mathcal{V}_h^G$ is a (finite-dimensional) *subspace* of $\mathcal{V}^G$, since we can now identify the second 3D vector field of any element of $\mathcal{V}_h^G$ as a rotation surface tensor. We show the transport of interpolated displacement and rotation vectors in Figure 6.6.

The issue that we want to address is therefore the approximation of $(\vec{u}, \underline{\theta})$ (corresponding to the solution of (6.35)) by $(\vec{u}_h, \vec{\theta}_h)$ defined inside each element by

$$\left\{\begin{array}{l} \vec{u}_h(\xi^1,\xi^2) = T_1(\vec{U}_h) \\ \vec{\theta}_h(\xi^1,\xi^2) = \pi\big(T_2(\vec{U}_h)\big) \end{array}\right. \tag{6.42}$$

We then introduce the interpolation operator $\mathcal{I}$ associated with the finite element shape functions, namely defined inside each element by

$$\boxed{\mathcal{I}(\phi)(\xi^1,\xi^2) = \sum_{i=1}^{k} \lambda_i(r,s)\phi(\xi^1_{(i)}, \xi^2_{(i)}),} \tag{6.43}$$

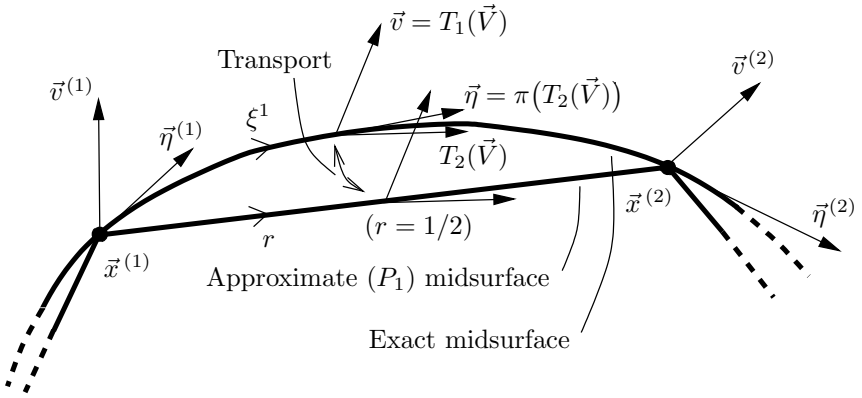

Fig. 6.6. Transport of interpolated displacement and rotation vectors

for any continuous scalar or vector function ϕ. Note that, for any $(\vec{v}, \vec{\eta}) \in \mathcal{V}_h^G$, we have

$$\begin{cases} \vec{v}(\xi^1, \xi^2) = \displaystyle\sum_{i=1}^{k} \lambda_i(r,s)\vec{v}^{(i)} = \mathcal{I}(\vec{v}) \\ \vec{\eta}(\xi^1, \xi^2) = \pi\Big(\displaystyle\sum_{i=1}^{k} \lambda_i(r,s)\vec{\eta}^{(i)}\Big) = \pi\big(\mathcal{I}(\vec{\eta})\big) \end{cases} \tag{6.44}$$

Therefore, for any $\vec{V}$ in $\mathcal{V}_h^{3D}$ with $(\vec{v}, \vec{\eta}) = \big(T_1(\vec{V}), \pi\big(T_2(\vec{V})\big)\big)$, we have

$$\begin{aligned} \vec{V} &= \sum_{i=1}^{k} \lambda_i(r,s)\big(\vec{v}^{(i)} + z\frac{t^{(i)}}{2}\vec{\eta}^{(i)}\big), \\ &= \mathcal{I}(\vec{v}) + \frac{z}{2}\mathcal{I}(t\vec{\eta}), \\ &= \vec{v} + \xi^3\frac{\mathcal{I}(t\vec{\eta})}{t}, \end{aligned} \tag{6.45}$$

setting the following one-to-one correspondence

$$\boxed{\xi^3 = z\frac{t}{2}.} \tag{6.46}$$

Using similar relations for $\vec{U}_h$, we can now reformulate – for the purpose of mathematical analysis – the finite element problem (6.34) as
Find $(\vec{u}_h, \vec{\theta}_h) \in \mathcal{V}_h^G$ *such that*

$$A_h^{3D}\Big(\vec{u}_h + \xi^3\frac{\mathcal{I}(t\vec{\theta}_h)}{t}, \vec{v} + \xi^3\frac{\mathcal{I}(t\vec{\eta})}{t}\Big) = F_h^{3D}\Big(\vec{v} + \xi^3\frac{\mathcal{I}(t\vec{\eta})}{t}\Big), \quad \forall (\vec{v},\vec{\eta}) \in \mathcal{V}_h^G. \tag{6.47}$$

Note that, in fact, the combination of (6.38) and (6.46) provides a complete one-to-one correspondence between the local coordinates (r, s, z) and the global (3D) curvilinear coordinates (ξ^1, ξ^2, ξ^3), hence also a means to transport quantities from the 3D approximate geometry to the exact 3D shell body $\mathcal{B}$. Indeed, the mapping between (ξ^1, ξ^2, ξ^3) and the approximate 3D geometry is given by

$$\vec{x} = \mathcal{I}(\vec{\phi}) + \xi^3\frac{\mathcal{I}(t\vec{a}_3)}{t}, \tag{6.48}$$

directly inferred from (6.30). This equation gives a characterization – in the variables (ξ^1, ξ^2, ξ^3) – of the geometric approximation involved in A_h^{3D} and F_h^{3D}. We can see that this approximation consists in using the approximate chart

$$\vec{\Phi}_h(\xi^1, \xi^2, \xi^3) = \mathcal{I}(\vec{\phi})(\xi^1, \xi^2) + \xi^3\frac{\mathcal{I}(t\vec{a}_3)(\xi^1, \xi^2)}{t}, \tag{6.49}$$

instead of the exact chart $\vec{\Phi}$ to derive all geometric quantities. We summarize the relations between the coordinate systems and the geometries in the diagram given in Figure 6.7, where the transport operation is represented by a dashed arrow because it is *implicitly* defined by the other relations featured in the diagram.

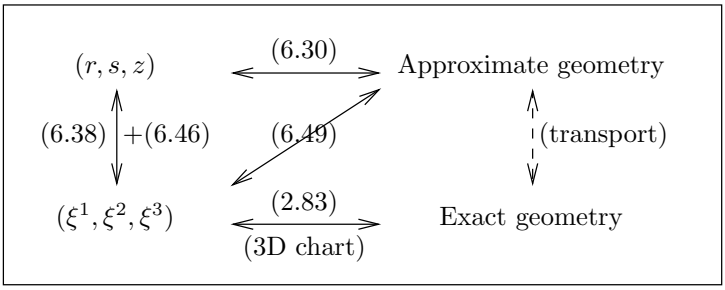

Fig. 6.7. Relations between coordinate systems and geometries

We can also reformulate the mathematical model as
Find $(\vec{u}, \vec{\theta}) \in \mathcal{V}^G$ *such that*

$$A^{3D}(\vec{u}+\xi^3\vec{\theta},\vec{v}+\xi^3\vec{\eta}) = F(\vec{v}+\xi^3\vec{\eta}), \qquad \forall(\vec{v},\vec{\eta}) \in \mathcal{V}^G. \tag{6.50}$$

Comparing the finite element problem (6.47) with this mathematical model, we can see that we have consistency errors coming from two sources:

1. The approximation of the geometry corresponding to (6.49);
2. The presence of the interpolation operator $\mathcal{I}$ in (6.47), with the projection used in (6.44).

Remark 6.3.1. For the purpose of mathematical analysis we needed to recast the finite element problem in a form using the surface unknowns $(\vec{u}_h, \vec{\theta}_h)$, in order to directly compare the finite element solution with the solution of the continuous problem (6.50). Note that $(\vec{u}_h, \vec{\theta}_h)$ relate to the discrete 3D displacements by the equations (6.42), and to the actual finite element nodal degrees of freedom by (6.44). ■

Remark 6.3.2. In the early work of Ciarlet (1976), consistency errors arising from the approximation of the geometry by interpolation of nodal positions were already analyzed, albeit in the context of the discretization of an explicit shell model, namely the m-b model. For this same model, Destuynder & Salaün (1998) later proposed a low-order approximation of the geometry (linear for the positions and the normal vectors) combined with a mixed formulation using the shear stresses as auxiliary unknowns (see also Destuynder & Salaün, 1995a,b, 1996). Here, our approach is different due to the three-dimensional character of the variational formulation, and the consistency errors that arise are indeed more complex. ■

In order to fully analyze the finite element approximation errors, and in particular the above consistency errors, we need to consider specific 3D formulations. Let us focus on the case of an isotropic elastic material. Then, of course, the mathematical model given by (6.50) is the *basic shell model* analyzed in Chapter 4. Also, we can use this specific case as an example to further point out how the plane stress assumption may be implemented in practice, recalling that the exact normal vector is not known except at the nodes. We consider two possible strategies:

S-1. The internal virtual work is directly obtained by using the left-hand side of Equation (4.30) and by substituting the approximate chart for the exact one to derive all the geometric coefficients. Namely, we use

$$A_h^{3D}(\vec{V},\vec{W}) = \int_\Omega \big[\bar{C}^{\alpha\beta\lambda\mu}\bar{e}_{\alpha\beta}(\vec{V})\bar{e}_{\lambda\mu}(\vec{W}) + \bar{D}^{\alpha\lambda}\bar{e}_{\alpha 3}(\vec{V})\bar{e}_{\lambda 3}(\vec{W})\big]\sqrt{\bar{g}}\,d\xi^1 d\xi^2 d\xi^3, \tag{6.51}$$

in which we write with a bar-symbol the quantities that are affected by the geometric approximation. The components of the constitutive tensors $\bar{C}^{\alpha\beta\lambda\mu}$ and $\bar{D}^{\alpha\lambda}$ depend on the approximate geometry through the use of the approximate metric tensor of components $\bar{g}^{\alpha\beta}$, instead of $g^{\alpha\beta}$. The effect on the strains is characterized in the expression

$$\bar{e}_{ij}(\vec{V}) = \frac{1}{2}\Big(\frac{\partial\vec{V}}{\partial\xi^i}\cdot\vec{\bar{g}}_j + \frac{\partial\vec{V}}{\partial\xi^j}\cdot\vec{\bar{g}}_i\Big), \tag{6.52}$$

with

$$\vec{\bar{g}}_i = \frac{\partial\vec{\Phi}_h}{\partial\xi^i}. \tag{6.53}$$

Note that, in practice, this strategy is implemented by equivalently using the local coordinate system (r,s,z) within each element. Indeed, since the mappings from (r,s) to (ξ^1,ξ^2) on the one hand and from z to ξ^3 on the other hand are defined independently, we can use the local (r,s,z) coordinate system instead of (ξ^1,ξ^2,ξ^3) in the integral of (6.51) and the same expression holds due to tensorial invariance.

S-2. The internal virtual work is computed by taking the interpolated normal direction (corresponding to the z local coordinate) as the direction for which stresses vanish due to the plane stress assumption, using a transformed $(\bar{r},\bar{s},z)$ coordinate system for which the z-direction is orthogonal to the $(\bar{r},\bar{s})$-plane (Bathe, 1996). The value of the internal energy in the (r,s,z) coordinate system is then inferred from that in the other coordinate system by using change of frames formulas. Note that, compared to the former strategy *S-1*, this strategy gives a (slightly) different result because the plane-stress constitutive law is now used in a frame for which the third direction is *exactly orthogonal* to the other directions, as it is indeed in the mathematical model.

In the forthcoming analysis, we start by considering the first strategy, and then address the alternative one (in Prop. 6.3.3).

Proposition 6.3.1 *Using Equation* (6.51) *(namely the strategy* S-1*), Problem* (6.47) *has a unique solution. Furthermore, assuming that the solution of the basic shell model is smooth we have the following error estimate*

$$\|\vec{u}-\vec{u}_h,\vec{\theta}-\vec{\theta}_h\|_{\mathcal{V}^B} \le Ch^{\min\{p,2\}}. \tag{6.54}$$

In order to prove this proposition, we first tackle the consistency errors. To that purpose, the following technical lemma is crucial.

Lemma 6.3.1. *Consider a continuous vector field $\vec{\psi}$ tangent to the midsurface at all points (i.e. $\vec{\psi} \cdot \vec{a}_3 \equiv 0$), and let $\vec{\psi}_{\rm int} = \mathcal{I}(\vec{\psi})$. Then*

$$\|\vec{\psi}_{\rm int} \cdot \vec{a}_3\|_{H^1(\omega)} \leq Ch \|\vec{\psi}_{\rm int}\|_{H^1(\omega)}, \tag{6.55}$$

$$\|\vec{\psi}_{\rm int} \cdot \vec{a}_3\|_{L^2(\omega)} \leq Ch^2 \|\vec{\psi}_{\rm int}\|_{H^1(\omega)}. \tag{6.56}$$

Proof. We denote by $\mathcal{M}$ the "piecewise-mean" operator. Namely, on each element K,

$$\mathcal{M}(\phi)|_K = \frac{1}{|K|} \int_K \phi \, dS, \tag{6.57}$$

for any scalar or vector function ϕ, where $|K|$ denotes the area of the surface comprised within K, viz.

$$|K| = \int_K dS. \tag{6.58}$$

Defining now

$$\vec{\psi}_{\rm m} = \pi\big(\mathcal{M}(\vec{\psi}_{\rm int})\big), \tag{6.59}$$

we have

$$\begin{aligned} \vec{\psi}_{\rm int} \cdot \vec{a}_3 &= (\vec{\psi}_{\rm int} - \vec{\psi}_{\rm m}) \cdot \vec{a}_3 \\ &= (\vec{\psi}_{\rm int} - \mathcal{I}(\vec{\psi}_{\rm m})) \cdot \vec{a}_3 + (\mathcal{I}(\vec{\psi}_{\rm m}) - \vec{\psi}_{\rm m}) \cdot \vec{a}_3. \end{aligned} \tag{6.60}$$

We start by bounding the second term of the right-hand side of Eq.(6.60). Standard interpolation estimates give

$$\|\mathcal{I}(\vec{\psi}_{\rm m}) - \vec{\psi}_{\rm m}\|_{H^l(K)} \leq C h_K^{p+1-l} |\vec{\psi}_{\rm m}|_{H^{p+1}(K)}, \qquad l = 0, 1, \tag{6.61}$$

where h_K is the diameter of element K and p is the order of approximation of the finite element shape functions. Furthermore, recalling that $\mathcal{M}(\vec{\psi}_{\rm int})$ is constant over K and that, for any vector field $\vec{v}$,

$$\pi(\vec{v}) = \vec{v} - (\vec{v} \cdot \vec{a}_3)\vec{a}_3, \tag{6.62}$$

we have, assuming that the chart is sufficiently regular,

$$|\vec{\psi}_{\rm m}|_{H^{p+1}(K)} \leq C\sqrt{|K|}\,\|\mathcal{M}(\vec{\psi}_{\rm int})\|. \tag{6.63}$$

By the Cauchy-Schwarz inequality, we have

$$\|\mathcal{M}(\vec{\psi}_{\rm int})\| = \frac{1}{|K|}\|\int_K \vec{\psi}_{\rm int}\,dS\| \leq \frac{1}{\sqrt{|K|}}\|\vec{\psi}_{\rm int}\|_{L^2(K)}. \tag{6.64}$$

Hence, combining (6.61)–(6.64), we obtain

$$\|(\mathcal{I}(\vec{\psi}_{\rm m}) - \vec{\psi}_{\rm m})\cdot\vec{a}_3\|_{H^l(K)} \leq Ch_K^{p+1-l}\|\vec{\psi}_{\rm int}\|_{L^2(K)}, \qquad l = 0, 1. \tag{6.65}$$

We then focus on the first term of the right-hand side of Eq.(6.60). We have on each element K

$$\begin{aligned}(\vec{\psi}_{\rm int} - \mathcal{I}(\vec{\psi}_{\rm m}))\cdot\vec{a}_3|_K &= \sum_i \lambda_i(\vec{\psi}^{(i)} - \vec{\psi}_{\rm m}^{(i)})\cdot\vec{a}_3 \\ &= \sum_i \lambda_i(\vec{\psi}^{(i)} - \vec{\psi}_{\rm m}^{(i)})\cdot(\vec{a}_3 - \vec{a}_3^{(i)}),\end{aligned} \tag{6.66}$$

since $\vec{\psi}^{(i)}\cdot\vec{a}_3^{(i)} = \vec{\psi}_{\rm m}^{(i)}\cdot\vec{a}_3^{(i)} = 0$. We tackle this expression by first bounding the Euclidean norm of $(\vec{\psi}^{(i)} - \vec{\psi}_{\rm m}^{(i)})$. We write

$$\|\vec{\psi}^{(i)} - \vec{\psi}_{\rm m}^{(i)}\| = \|\vec{\psi}_{\rm int}^{(i)} - \vec{\psi}_{\rm m}^{(i)}\| \leq \|\vec{\psi}_{\rm int}^{(i)} - \mathcal{M}(\vec{\psi}_{\rm int})\| + \|\mathcal{M}(\vec{\psi}_{\rm int}) - \vec{\psi}_{\rm m}^{(i)}\|. \tag{6.67}$$

Using standard scaling arguments, we get

$$\sup_i \|\vec{\psi}_{\rm int}^{(i)} - \mathcal{M}(\vec{\psi}_{\rm int})\| \leq C|\vec{\psi}_{\rm int}|_{H^1(K)}. \tag{6.68}$$

For the second term of Equation (6.67), we have

$$\begin{aligned}\|\mathcal{M}(\vec{\psi}_{\rm int}) - \vec{\psi}_{\rm m}^{(i)}\| &= |\mathcal{M}(\vec{\psi}_{\rm int})\cdot\vec{a}_3^{(i)}| = \frac{1}{|K|}\left|\int_K \vec{\psi}_{\rm int}\cdot\vec{a}_3^{(i)}\,dS\right| \\ &\leq \frac{1}{|K|}\left(\left|\int_K \vec{\psi}_{\rm int}\cdot\vec{a}_3\,dS\right| + \left|\int_K \vec{\psi}_{\rm int}\cdot(\vec{a}_3^{(i)} - \vec{a}_3)\,dS\right|\right) \\ &\leq \frac{C}{\sqrt{|K|}}\,(\|\vec{\psi}_{\rm int}\cdot\vec{a}_3\|_{L^2(K)} + h_K\|\vec{\psi}_{\rm int}\|_{L^2(K)}),\end{aligned} \tag{6.69}$$

since

$$\|\vec{a}_3^{(i)} - \vec{a}_3\|_{L^\infty(K)} \leq Ch_K. \tag{6.70}$$

Therefore, combining Equations (6.67)–(6.69), we get

$$\sup_i \|\vec{\psi}^{(i)} - \vec{\psi}_{\mathrm{m}}^{(i)}\| \leq C(h_K^{-1}\|\vec{\psi}_{\mathrm{int}} \cdot \vec{a}_3\|_{L^2(K)} + \|\vec{\psi}_{\mathrm{int}}\|_{H^1(K)}), \tag{6.71}$$

We will now use Equation (6.66) twice consecutively to obtain first (6.56), then (6.55). For (6.56), we directly bound the right-hand side of Equation (6.66) by using (6.70) and (6.71). We have

$$\begin{aligned}
&\|(\vec{\psi}_{\mathrm{int}} - \mathcal{I}(\vec{\psi}_{\mathrm{m}})) \cdot \vec{a}_3\|_{L^2(K)} \\
&\qquad \leq \quad C\sqrt{|K|}\sup_i \big\{ \|\lambda_i\|_{L^\infty(K)} \, \|\vec{\psi}^{(i)} - \vec{\psi}_{\mathrm{m}}^{(i)}\| \, \|\vec{a}_3^{(i)} - \vec{a}_3\|_{L^\infty(K)} \big\} \\
&\qquad \leq \quad C(h_K\|\vec{\psi}_{\mathrm{int}} \cdot \vec{a}_3\|_{L^2(K)} + h_K^2\|\vec{\psi}_{\mathrm{int}}\|_{H^1(K)}).
\end{aligned} \tag{6.72}$$

Combining this bound with Equations (6.60) and (6.65) for $l = 0$, we have for any $p \geq 1$

$$\|\vec{\psi}_{\mathrm{int}} \cdot \vec{a}_3\|_{L^2(K)} \leq C(h_K\|\vec{\psi}_{\mathrm{int}} \cdot \vec{a}_3\|_{L^2(K)} + h_K^2\|\vec{\psi}_{\mathrm{int}}\|_{H^1(K)}). \tag{6.73}$$

Hence, for h small enough,

$$\|\vec{\psi}_{\mathrm{int}} \cdot \vec{a}_3\|_{L^2(K)} \leq Ch_K^2\|\vec{\psi}_{\mathrm{int}}\|_{H^1(K)}, \tag{6.74}$$

and, squaring this inequality and summing over all elements, we obtain (6.56).

We then use (6.66) again to bound the H^1 semi-norm as follows.

$$\begin{aligned}
&|\vec{\psi}_{\mathrm{int}} - \mathcal{I}(\vec{\psi}_{\mathrm{m}})) \cdot \vec{a}_3|_{H^1(K)} \\
&\quad \leq \quad C\sqrt{|K|} \, \sup_i \big\{ \|\vec{\psi}^{(i)} - \vec{\psi}_{\mathrm{m}}^{(i)}\| \, (\|\lambda_i\|_{W^{1,\infty}(K)} \, \|\vec{a}_3^{(i)} - \vec{a}_3\|_{L^\infty(K)}, \\
&\qquad\qquad\qquad\qquad + \|\lambda_i\|_{L^\infty(K)} \, \|\vec{a}_3\|_{W^{1,\infty}(K)}) \big\}
\end{aligned}$$

Hence,

$$\begin{aligned}
&|\vec{\psi}_{\mathrm{int}} - \mathcal{I}(\vec{\psi}_{\mathrm{m}})) \cdot \vec{a}_3|_{H^1(K)} \\
&\quad \leq \quad Ch_K(h_K^{-1}\|\vec{\psi}_{\mathrm{int}} \cdot \vec{a}_3\|_{L^2(K)} + \|\vec{\psi}_{\mathrm{int}}\|_{H^1(K)})(h_K^{-1} \times h_K + 1 \times 1) \\
&\quad \leq \quad C(\|\vec{\psi}_{\mathrm{int}} \cdot \vec{a}_3\|_{L^2(K)} + h_K \, \|\vec{\psi}_{\mathrm{int}}\|_{H^1(K)}) \\
&\quad \leq \quad Ch_K\|\vec{\psi}_{\mathrm{int}}\|_{H^1(K)},
\end{aligned} \tag{6.75}$$

using Equation (6.74). Finally, combining (6.75) with (6.60) and (6.65) for $l = 1$ we obtain

$$|\vec{\psi}_{\mathrm{int}} \cdot \vec{a}_3|_{H^1(K)} \leq Ch_K\|\vec{\psi}_{\mathrm{int}}\|_{H^1(K)}, \tag{6.76}$$

and Equation (6.55) immediately follows. ∎

Remark 6.3.3. Equations (6.55) and (6.56) closely resemble interpolation estimates, since

$$\vec{\psi}_{\text{int}} \cdot \vec{a}_3 = \mathcal{I}(\vec{\psi}) \cdot \vec{a}_3 = \big(\mathcal{I}(\vec{\psi}) - \vec{\psi}\big) \cdot \vec{a}_3. \tag{6.77}$$

Note, however, that we would need one more degree of regularity in the right-hand side of (6.55) and (6.56), namely $\|\vec{\psi}\|_{H^2(\omega)}$, to obtain such orders of convergence directly from interpolation estimates. This "superconvergence" result only holds because $\vec{\psi}$ is a tangential vector field, of course. In addition, it can be shown by considering specific examples that these estimates are optimal. ∎

In the following lemma we examine the impact of a thickness parameter that varies (over the midsurface) on the consistency, through the interpolation operator as it appears in (6.47).

Lemma 6.3.2. *For any* $(\vec{v}, \vec{\eta})$ *in* $\mathcal{V}_h^B$,

$$\|t\mathcal{I}(\vec{\eta}) - \mathcal{I}(t\vec{\eta})\|_{L^2(\mathcal{S})} \leq C(h^2 \|\underline{\nabla} t\|_{L^\infty(\omega)} + h^{p+1}) \|\vec{\eta}\|_{H^1(\omega)}, \tag{6.78}$$

$$\|t\mathcal{I}(\vec{\eta}) - \mathcal{I}(t\vec{\eta})\|_{H^1(\mathcal{S})} \leq C(h \|\underline{\nabla} t\|_{L^\infty(\omega)} + h^{p}) \|\vec{\eta}\|_{H^1(\omega)}. \tag{6.79}$$

Proof. We only show (6.79), as (6.78) can be shown using similar (and simpler) arguments. We use the piecewise-mean operator $\mathcal{M}$ defined in the proof of Lemma 6.3.1 to construct

$$\vec{\eta}_{\text{m}} = \mathcal{M}(\vec{\eta}). \tag{6.80}$$

We then have, in each element K,

$$\begin{aligned} t\mathcal{I}(\vec{\eta}) - \mathcal{I}(t\vec{\eta}) &= t\mathcal{I}(\vec{\eta} - \vec{\eta}_{\text{m}}) - \mathcal{I}\big(t(\vec{\eta} - \vec{\eta}_{\text{m}})\big) + \big(t - \mathcal{I}(t)\big)\vec{\eta}_{\text{m}} \\ &= \sum_i \lambda_i (t - t^{(i)})(\vec{\eta}^{(i)} - \vec{\eta}_{\text{m}}) \; + \big(t - \mathcal{I}(t)\big)\vec{\eta}_{\text{m}}. \end{aligned} \tag{6.81}$$

Standard scaling arguments give

$$\sup_i \|\vec{\eta}^{(i)} - \vec{\eta}_{\text{m}}\| \leq C|\vec{\eta}|_{H^1(K)}, \tag{6.82}$$

and by the Cauchy-Schwarz inequality we have

$$\|\vec{\eta}_{\mathrm{m}}\| \leq \frac{1}{\sqrt{|K|}}\|\vec{\eta}\|_{L^2(K)}. \tag{6.83}$$

Therefore

$$\begin{aligned}
&\|t\mathcal{I}(\vec{\eta}) - \mathcal{I}(t\vec{\eta})\|_{H^1(K)} \\
&\quad\leq\quad C\sqrt{|K|}\,|\vec{\eta}|_{H^1(K)}\,\sup_i\big\{\|\lambda_i\|_{W^{1,\infty}(K)}\,\|t - t^{(i)}\|_{L^\infty(K)} \\
&\qquad\qquad\qquad\qquad +\|\lambda_i\|_{L^\infty(K)}\|\underline{\nabla} t\|_{L^\infty(K)}\big\} \\
&\qquad +C\|t - \mathcal{I}(t)\|_{W^{1,\infty}(K)}\|\vec{\eta}\|_{L^2(K)} \\
&\quad\leq\quad C\big(h_K\|\underline{\nabla} t\|_{L^\infty(K)}|\vec{\eta}|_{H^1(K)} + h_K^p\|\vec{\eta}\|_{L^2(K)}\big),
\end{aligned} \tag{6.84}$$

since $\|t - t^{(i)}\|_{L^\infty(K)} \leq h_K\|\underline{\nabla} t\|_{L^\infty(K)}$. To conclude the proof we square this inequality and sum over all elements. ∎

Remark 6.3.4. From the last step of the above proof, we can see that $h\|\underline{\nabla} t\|_{L^\infty(\omega)}$ can be substituted by $\sup_K h_K\|\underline{\nabla} t\|_{L^\infty(K)}$ in (6.79). Similarly, of course, $h^2\|\underline{\nabla} t\|_{L^\infty(\omega)}$ can be substituted by $\sup_K h_K^2\|\underline{\nabla} t\|_{L^\infty(K)}$ in (6.79). This shows that the consistency error due to the interpolation of the thickness can be controlled *a priori* by adapting the mesh so that these local indicators are appropriately bounded. ∎

The following lemma establishes the required interpolation estimates.

Lemma 6.3.3. *Assume that* $(\vec{u}, \vec{\theta})$ *is in* $\mathcal{V}^B \cap H^{p+1}(\omega)$*, then*

$$\|\vec{u} - \mathcal{I}(\vec{u}), \vec{\theta} - \pi\big(\mathcal{I}(\vec{\theta})\big)\|_{H^1(\mathcal{V}^B)} \leq Ch^p\|\vec{u}, \vec{\theta}\|_{H^{p+1}(\omega)}. \tag{6.85}$$

Proof. For $\vec{u}$, standard interpolation estimates directly give

$$\|\vec{u} - \mathcal{I}(\vec{u})\|_{H^1(\omega)} \leq Ch^p\|\vec{u}\|_{H^{p+1}(\omega)}. \tag{6.86}$$

For $\vec{\theta}$, we have

$$\begin{aligned}
\|\vec{\theta} - \pi\big(\mathcal{I}(\vec{\theta})\big)\|_{H^1(\omega)} &= \|\pi\big(\vec{\theta} - \mathcal{I}(\vec{\theta})\big)\|_{H^1(\omega)} \\
&\leq C\|\vec{\theta} - \mathcal{I}(\vec{\theta})\|_{H^1(\omega)} \\
&\leq Ch^p\|\vec{\theta}\|_{H^{p+1}(\omega)}.
\end{aligned} \tag{6.87}$$

∎

Remark 6.3.5. The key point in this result is that, when $(\vec{u}, \vec{\theta})$ is in $\mathcal{V}^B$, $\big(\mathcal{I}(\vec{u}), \pi\big(\mathcal{I}(\vec{\theta})\big)\big)$ is in $\mathcal{V}_h^B$. Hence this shows that there exists an element of $\mathcal{V}_h^B$ which approximates $(\vec{u}, \vec{\theta})$ with an optimal error bound with respect to the finite element shape functions considered. ∎

Defining the notation

$$C_h(\vec{v}, \vec{\eta}; \vec{w}, \vec{\tau}) = \\ A^{3D}(\vec{v} + \xi^3\vec{\eta}, \vec{w} + \xi^3\vec{\tau}) - A_h^{3D}\Big(\vec{v} + \xi^3\frac{\mathcal{I}(t\vec{\eta})}{t}, \vec{w} + \xi^3\frac{\mathcal{I}(t\vec{\tau})}{t}\Big), \tag{6.88}$$

for any $\big((\vec{v}, \vec{\eta}), (\vec{w}, \vec{\tau})\big)$ in $\mathcal{V}_h^B \times \mathcal{V}_h^B$, we can now derive the consistency errors.

Proposition 6.3.2 *For any smooth $(\vec{v}_s, \vec{\eta}_s)$ in $\mathcal{V}^B$, we have*

$$\inf_{(\vec{v},\vec{\eta})\in\mathcal{V}_h^B}\Big\{\|\vec{v}_s - \vec{v}, \vec{\eta}_s - \vec{\eta}\|_{\mathcal{V}^B} + \sup_{(\vec{w},\vec{\tau})\in\mathcal{V}_h^B}\frac{C_h(\vec{v}, \vec{\eta}; \vec{w}, \vec{\tau})}{\|\vec{w}, \vec{\tau}\|_{\mathcal{V}^B}}\Big\} \\ \leq Ch^{\min\{2,p\}}\|\vec{v}_s, \vec{\eta}_s\|_{H^{\min\{3,p+1\}}}. \tag{6.89}$$

In addition,

$$\sup_{(\vec{w},\vec{\tau})\in\mathcal{V}_h^B}\frac{\Big|F^{3D}(\vec{w} + \xi^3\vec{\tau}) - F_h^{3D}\big(\vec{w} + \xi^3\frac{\mathcal{I}(t\vec{\tau})}{t}\big)\Big|}{\|\vec{w}, \vec{\tau}\|_{\mathcal{V}^B}} \leq Ch^{\min\{2,p\}}. \tag{6.90}$$

Proof. Set $(\vec{v}, \vec{\eta}) = \big(\mathcal{I}(\vec{v}_s), \pi\big(\mathcal{I}(\vec{\eta}_s)\big)\big)$. We then have by Lemma 6.3.3

$$\|\vec{v}_s - \vec{v}, \vec{\eta}_s - \vec{\eta}\|_{\mathcal{V}^B} \leq Ch^p\|\vec{v}_s, \vec{\eta}_s\|_{H^{p+1}}, \tag{6.91}$$

and also, of course,

$$\|\vec{v}_s - \vec{v}, \vec{\eta}_s - \vec{\eta}\|_{\mathcal{V}^B} \leq Ch^2\|\vec{v}_s, \vec{\eta}_s\|_{H^3}, \tag{6.92}$$

when $p \geq 2$. We want to bound the consistency error $|C_h(\vec{v}, \vec{\eta}; \vec{w}, \vec{\tau})|$. We have

$$|C_h(\vec{v}, \vec{\eta}; \vec{w}, \vec{\tau})| \leq I + II, \tag{6.93}$$

with

$$I = \Big|A^{3D}(\vec{v} + \xi^3\vec{\eta}, \vec{w} + \xi^3\vec{\tau}) - A^{3D}\Big(\vec{v} + \xi^3\frac{\mathcal{I}(t\vec{\eta})}{t}, \vec{w} + \xi^3\frac{\mathcal{I}(t\vec{\tau})}{t}\Big)\Big|, \tag{6.94}$$

$$II = \Big| A^{3D}\Big(\vec{v} + \xi^3 \frac{\mathcal{I}(t\vec{\eta})}{t}, \vec{w} + \xi^3 \frac{\mathcal{I}(t\vec{\tau})}{t}\Big) - A_h^{3D}\Big(\vec{v} + \xi^3 \frac{\mathcal{I}(t\vec{\eta})}{t}, \vec{w} + \xi^3 \frac{\mathcal{I}(t\vec{\tau})}{t}\Big)\Big| \tag{6.95}$$

We proceed to bound these two terms separately. The term II represents the error due to the interpolation of the geometry, i.e. due to the use of the approximate chart defined by (6.49). Note that the integrals involved in A^{3D} and A_h^{3D} are taken over the same domains, so that the difference between the two expressions comes only from the use of approximate geometric coefficients. Recalling (6.51), and since clearly

$$\|\vec{\bar{g}}_i - \vec{g}_i\|_{L^\infty}(\omega) \leq Ch^p, \tag{6.96}$$

we infer

$$II \leq Ch^p \|\vec{v}, \frac{\mathcal{I}(t\vec{\eta})}{t}\|_{H^1(\omega)} \|\vec{w}, \frac{\mathcal{I}(t\vec{\tau})}{t}\|_{H^1(\omega)}. \tag{6.97}$$

Using the standard interpolation continuity inequality

$$\|\mathcal{I}(t\vec{\tau})\|_{H^1(\omega)} \leq C\|t\vec{\tau}\|_{H^1(\omega)}, \tag{6.98}$$

and the fact that t is smooth and bounded away from zero, we have

$$\|\frac{\mathcal{I}(t\vec{\tau})}{t}\|_{H^1(\omega)} \leq C\|\vec{\tau}\|_{H^1(\omega)}, \tag{6.99}$$

and similarly for $\vec{\eta}$. Therefore,

$$II \leq Ch^p \|\vec{v}, \vec{\eta}\|_{H^1(\omega)} \|\vec{w}, \vec{\tau}\|_{H^1(\omega)}. \tag{6.100}$$

For the term I, we have

$$I \leq III + IV, \tag{6.101}$$

with

$$III = \Big| A^{3D}\Big(\vec{v} + \xi^3\vec{\eta}, \xi^3(\vec{\tau} - \frac{\mathcal{I}(t\vec{\tau})}{t})\Big)\Big|, \tag{6.102}$$

$$IV = \Big| A^{3D}\Big(\xi^3(\vec{\eta} - \frac{\mathcal{I}(t\vec{\eta})}{t}), \vec{w} + \xi^3 \frac{\mathcal{I}(t\vec{\tau})}{t}\Big)\Big|, \tag{6.103}$$

and we again tackle these two terms separately. Due to the boundedness of A^{3D} we have

$$\begin{aligned} IV &\leq C\|\vec{\eta} - \frac{\mathcal{I}(t\vec{\eta})}{t}\|_{H^1(\omega)}\|\vec{w}, \frac{\mathcal{I}(t\vec{\tau})}{t}\|_{H^1(\omega)} \\ &\leq C\|\vec{\eta} - \frac{\mathcal{I}(t\vec{\eta})}{t}\|_{H^1(\omega)}\|\vec{w}, \vec{\tau}\|_{H^1(\omega)}. \end{aligned} \tag{6.104}$$

Recalling that $\vec{\eta} = \pi\big(\mathcal{I}(\vec{\eta}_s)\big)$ we have

$$\vec{\eta} - \frac{\mathcal{I}(t\vec{\eta})}{t} = \vec{\eta} - \vec{\eta}_s - \frac{\mathcal{I}(t\vec{\eta}_s) - t\vec{\eta}_s}{t}, \tag{6.105}$$

hence Lemma 6.3.3 and standard interpolation results give

$$IV \leq Ch^p\|\vec{\eta}_s\|_{H^{p+1}(\omega)}\|\vec{w}, \vec{\tau}\|_{H^1(\omega)}, \tag{6.106}$$

and also

$$IV \leq Ch^2\|\vec{\eta}_s\|_{H^3(\omega)}\|\vec{w}, \vec{\tau}\|_{H^1(\omega)} \tag{6.107}$$

when $p \geq 2$.

The treatment of the remaining term (III) is more complicated. In order to discard the derivatives in the tangential variables of $(\vec{\tau} - \mathcal{I}(t\vec{\tau})/t)$ that would only give an estimate in $O(h)$ if they were to be directly bounded according to (6.55) and (6.79), we use integrations by parts in these variables on each element. We thus obtain

$$III \leq C(V + VI), \tag{6.108}$$

with

$$V = \sum_K \|\vec{v}, \vec{\eta}\|_{H^2(K)}\|\vec{\tau} - \frac{\mathcal{I}(t\vec{\tau})}{t}\|_{L^2(K)}, \tag{6.109}$$

$$VI = \sum_E \|[\![\vec{v}_{,1}]\!], [\![\vec{v}_{,2}]\!], [\![\vec{\eta}_{,1}]\!], [\![\vec{\eta}_{,2}]\!]\|_{L^2(E)}\|\vec{\tau} - \frac{\mathcal{I}(t\vec{\tau})}{t}\|_{L^2(E)}, \tag{6.110}$$

and where the sum over K represents the summation over all elements of the mesh, the sum over E the summation over all the edges of the mesh, and the symbol $[\![\phi]\!]$ denotes the absolute value of the jump in the quantity ϕ between two adjacent elements. Note that $\vec{v}$ and $\vec{\eta}$ are continuous across element edges, but not their derivatives. For the term V, interpolation results give

$$\|\vec{v}, \vec{\eta}\|_{H^2(K)} \leq \|\vec{v}_s, \vec{\eta}_s\|_{H^2(K)} + \|\vec{v} - \vec{v}_s, \vec{\eta} - \vec{\eta}_s\|_{H^2(K)} \leq C\|\vec{v}_s, \vec{\eta}_s\|_{H^2(K)}, \tag{6.111}$$

hence, by the Cauchy-Schwarz inequality,

$$V \leq C\|\vec{v}_s, \vec{\eta}_s\|_{H^2(\omega)}\|\vec{\tau} - \frac{\mathcal{I}(t\vec{\tau})}{t}\|_{L^2(\omega)}. \tag{6.112}$$

Moreover,

$$\begin{aligned} \vec{\tau} - \frac{\mathcal{I}(t\vec{\tau})}{t} &= \vec{\tau} - \mathcal{I}(\vec{\tau}) + \frac{t\mathcal{I}(\vec{\tau}) - \mathcal{I}(t\vec{\tau})}{t} \\ &= -(\mathcal{I}(\vec{\tau}) \cdot \vec{a}_3)\vec{a}_3 + \frac{t\mathcal{I}(\vec{\tau}) - \mathcal{I}(t\vec{\tau})}{t}, \end{aligned} \tag{6.113}$$

recalling the following property of the rotation term in the finite element space

$$\vec{\tau} = \pi\big(\mathcal{I}(\vec{\tau})\big). \tag{6.114}$$

Therefore, using (6.56) and (6.78), we obtain

$$V \leq Ch^2\|\vec{v}_s, \vec{\eta}_s\|_{H^2(\omega)}\|\vec{\tau}\|_{H^1(\omega)}. \tag{6.115}$$

As for the term VI, we have by a Cauchy-Schwarz inequality

$$\begin{aligned} VI \leq \Big(\sum_E h_E\|[\![\vec{v}_{,1}]\!], [\![\vec{v}_{,2}]\!], [\![\vec{\eta}_{,1}]\!], [\![\vec{\eta}_{,2}]\!]\|^2_{L^2(E)}\Big)^{\frac{1}{2}} \\ \times \Big(\sum_E (h_E)^{-1}\|\vec{\tau} - \frac{\mathcal{I}(t\vec{\tau})}{t}\|^2_{L^2(E)}\Big)^{\frac{1}{2}}. \end{aligned} \tag{6.116}$$

Using again the decomposition (6.113) we have

$$\mathcal{I}(\vec{\tau}) \cdot \vec{a}_3 = \sum_i \lambda_i \vec{\tau}^{(i)} \cdot \vec{a}_3 = \sum_i \lambda_i \vec{\tau}^{(i)} \cdot (\vec{a}_3 - \vec{a}_3^{(i)}), \tag{6.117}$$

where the sum over i denotes the summation over all the nodes of the edge considered. Of course,

$$\|\vec{a}_3 - \vec{a}_3^{(i)}\| \leq Ch_E, \tag{6.118}$$

hence, scaling arguments give

$$\begin{aligned} (h_E)^{-1}\|(\mathcal{I}(\vec{\tau}) \cdot \vec{a}_3)\vec{a}_3\|^2_{L^2(E)} &\leq C(h_E)^{-1}\|\mathcal{I}(\vec{\tau}) \cdot \vec{a}_3\|^2_{L^2(E)} \\ &\leq C(h_E)^2\big(\max_E |\vec{\tau}^{(i)}|\big)^2, \end{aligned} \tag{6.119}$$

where the "max" term represents the largest of the nodal values of $\vec{\tau}$ on the edge E, in absolute value. Likewise, we have

$$t\mathcal{I}(\vec{\tau}) - \mathcal{I}(t\vec{\tau}) = \sum_i \lambda_i (t - t^{(i)}) \vec{\tau}^{(i)}, \tag{6.120}$$

and $|t - t^{(i)}| \leq C h_E$, hence

$$(h_E)^{-1} \|t\mathcal{I}(\vec{\tau}) - \mathcal{I}(t\vec{\tau})\|^2_{L^2(E)} \leq C (h_E)^2 \big(\max_E |\vec{\tau}^{(i)}|\big)^2. \tag{6.121}$$

Therefore, by other scaling arguments,

$$\begin{aligned}
\sum_E (h_E)^{-1} \|\vec{\tau} - \frac{\mathcal{I}(t\vec{\tau})}{t}\|^2_{L^2(E)} &\leq C \sum_E (h_E)^2 \big(\max_E |\vec{\tau}^{(i)}|\big)^2 \\
&\leq C \sum_K (h_K)^2 \big(\max_K |\vec{\tau}^{(i)}|\big)^2 \\
&\leq C \sum_K \|\vec{\tau}\|^2_{L^2(K)} \\
&\leq C \|\vec{\tau}\|^2_{L^2(\omega)}.
\end{aligned} \tag{6.122}$$

We now consider a jump term of the form

$$J_E = h_E \big(\|[\![\rho_{,1}]\!]\|^2_{L^2(E)} + \|[\![\rho_{,2}]\!]\|^2_{L^2(E)} \big), \tag{6.123}$$

where ρ is the interpolant of a smooth function ρ_s (representing a component of $\vec{v}_s$ or $\vec{\eta}_s$). We also have

$$J_E = h_E \big(\|[\![\rho_{,1} - \rho_{s,1}]\!]\|^2_{L^2(E)} + \|[\![\rho_{,2} - \rho_{s,2}]\!]\|^2_{L^2(E)} \big), \tag{6.124}$$

since the jumps of the derivatives of ρ_s vanish. Then,

$$\sum_E J_E \leq 2 \sum_K \sum_{E \in \partial K} h_E \big(\|\rho_{,1} - \rho_{s,1}\|^2_{L^2(E)} + \|\rho_{,2} - \rho_{s,2}\|^2_{L^2(E)} \big). \tag{6.125}$$

Denoting by $\hat{K}$ the reference element, by $\hat{E}$ the image of the edge E in this reference element, and by $\hat{\rho}$ and $\hat{\rho}_s$ the images of ρ and ρ_s we have, using scaling arguments and the fundamental trace inequality (3.58),

$$\begin{aligned}
&\sum_{E \in \partial K} h_E \big(\|\rho_{,1} - \rho_{s,1}\|^2_{L^2(E)} + \|\rho_{,2} - \rho_{s,2}\|^2_{L^2(E)} \big) \\
&\quad \leq C \sum_{\hat{E} \in \partial \hat{K}} \big(\|\hat{\rho}_{,1} - \hat{\rho}_{s,1}\|^2_{L^2(\hat{E})} + \|\hat{\rho}_{,2} - \hat{\rho}_{s,2}\|^2_{L^2(\hat{E})} \big) \\
&\quad \leq C \|\hat{\rho} - \hat{\rho}_s\|^2_{H^2(\hat{K})} \\
&\quad \leq C \big((h_K)^{-2} \|\rho - \rho_s\|^2_{L^2(K)} + \|\rho - \rho_s\|^2_{H^1(K)} + (h_K)^2 \|\rho - \rho_s\|^2_{H^2(K)} \big) \\
&\quad \leq C (h_K)^{2p} \|\rho_s\|^2_{H^{p+1}(K)}
\end{aligned} \tag{6.126}$$

the last bound being obtained by invoking standard interpolation estimates. Note that, even when ρ corresponds to a component of $\vec{\eta}$, which is obtained from $\vec{\eta}_s$ by

$$\vec{\eta} = \pi\big(\mathcal{I}(\vec{\eta}_s)\big), \tag{6.127}$$

the proof of Lemma 6.3.3 shows that standard interpolation bounds hold. Combining this bound with (6.116) and (6.122), we infer

$$VI \leq Ch^p \|\vec{v}_s, \vec{\eta}_s\|_{H^{p+1}(\omega)} \|\vec{\tau}\|_{L^2(\omega)}. \tag{6.128}$$

Note that we also have

$$VI \leq Ch^2 \|\vec{v}_s, \vec{\eta}_s\|_{H^3(\omega)} \|\vec{\tau}\|_{L^2(\omega)}, \tag{6.129}$$

when $p \geq 2$.

Finally, gathering the equations (6.93), (6.100), (6.101), (6.106)/(6.107), (6.108), (6.115) and (6.128)/(6.129), we obtain

$$\sup_{(\vec{w},\vec{\tau})\in\mathcal{V}_h^B} \frac{C_h(\vec{v},\vec{\eta};\vec{w},\vec{\tau})}{\|\vec{w},\vec{\tau}\|_{\mathcal{V}^B}} \leq Ch^{\min\{2,p\}} \|\vec{v}_s, \vec{\eta}_s\|_{H^{\min\{3,p+1\}}}, \tag{6.130}$$

which, together with (6.91)/(6.92), implies (6.89). The estimate (6.90) is obtained by similar (but simpler) arguments. ∎

Remark 6.3.6. We note that the consistency errors given in this proposition are optimal with respect to the approximation capabilities of the shape functions used when linear or quadratic shape functions are considered, but not for higher-order elements. Namely, the best error estimate it provides is in $O(h^2)$. From the above proof, we can see that the $O(h^2)$ error comes from two sources, namely the need to resort to estimates (6.56) and (6.78), because test functions are only in H^1. By contrast, the approximation of the geometry used in the expression of the constitutive tensors produces a consistency error which is of optimal order $O(h^p)$, like the interpolation estimate in Lemma 6.3.3. ∎

We are now in a position to prove Proposition 6.3.1.

Proof of Proposition 6.3.1. We use a standard stability/consistency argument. Since A^{3D} is coercive, the consistency bound (6.89) implies that A_h^{3D} provides a coercive bilinear form on $\mathcal{V}_h^B$, namely that

$$A_h^{3D}(\vec{v}+\xi^3\vec{\eta}, \vec{v}+\xi^3\vec{\eta}) \geq \gamma \|\vec{v},\vec{\eta}\|^2_{\mathcal{V}^B}, \qquad \forall (\vec{v},\vec{\eta}) \in \mathcal{V}_h^B, \tag{6.131}$$

at least for h sufficiently small. Therefore, Problem (6.47) has a unique solution (at least for h sufficiently small also).

Then, the proof follows that of the first Strang Lemma (see e.g. Ciarlet, 1978). Consider $(\vec{v},\vec{\eta})$ in $\mathcal{V}_h^B$. By (6.131) we have

$$\begin{aligned}
&\|\vec{u}_h-\vec{v},\vec{\theta}_h-\vec{\eta}\|^2_{\mathcal{V}^B}\\
&\quad\le\; C\,A_h^{3D}(\vec{u}_h-\vec{v}+\xi^3(\vec{\theta}_h-\vec{\eta}),\vec{u}_h-\vec{v}+\xi^3(\vec{\theta}_h-\vec{\eta}))\\
&\quad=\; C\Big[\,A^{3D}(\vec{u}-\vec{v}+\xi^3(\vec{\theta}-\vec{\eta}),\vec{u}_h-\vec{v}+\xi^3(\vec{\theta}_h-\vec{\eta}))\\
&\qquad +C_h(\vec{v},\vec{\eta};\vec{u}_h-\vec{v},\vec{\theta}_h-\vec{\eta})\\
&\qquad +F_h^{3D}\Big(\vec{u}_h-\vec{v}+\xi^3\frac{\mathcal{I}(t(\vec{\theta}_h-\vec{\eta}))}{t}\Big)-F^{3D}(\vec{u}_h-\vec{v}+\xi^3(\vec{\theta}_h-\vec{\eta}))\Big],
\end{aligned}$$

using Equations (6.47) and (6.50) with $(\vec{u}_h-\vec{v},\vec{\theta}_h-\vec{\eta})$ instead of $(\vec{v},\vec{\eta})$ as a test function. Note that $\mathcal{V}_h^B\subset\mathcal{V}^B$, so that a test function of $\mathcal{V}_h^B$ can indeed be used in (6.50). The boundedness of A^{3D} implies

$$\begin{aligned}
&A^{3D}(\vec{u}-\vec{v}+\xi^3(\vec{\theta}-\vec{\eta}),\vec{u}_h-\vec{v}+\xi^3(\vec{\theta}_h-\vec{\eta}))\\
&\qquad\qquad\le C\|\vec{u}-\vec{v},\vec{\theta}-\vec{\eta}\|_{\mathcal{V}^B}\|\vec{u}_h-\vec{v},\vec{\theta}_h-\vec{\eta}\|_{\mathcal{V}^B},
\end{aligned}\tag{6.132}$$

hence dividing the previous inequality by $\|\vec{u}_h-\vec{v},\vec{\theta}_h-\vec{\eta}\|_{\mathcal{V}^B}$ gives

$$\begin{aligned}
&\|\vec{u}_h-\vec{v},\vec{\theta}_h-\vec{\eta}\|_{\mathcal{V}^B}\\
&\qquad\le\; C\Big\{\|\vec{u}-\vec{v},\vec{\theta}-\vec{\eta}\|_{\mathcal{V}^B}+\sup_{(\vec{w},\vec{\tau})\in\mathcal{V}_h^B}\frac{C_h(\vec{v},\vec{\eta};\vec{w},\vec{\tau})}{\|\vec{w},\vec{\tau}\|_{\mathcal{V}^B}}\\
&\qquad\quad+\sup_{(\vec{w},\vec{\tau})\in\mathcal{V}_h^B}\frac{\Big|F^{3D}(\vec{w}+\xi^3\vec{\tau})-F_h^{3D}\big(\vec{w}+\xi^3\frac{\mathcal{I}(t\vec{\tau})}{t}\big)\Big|}{\|\vec{w},\vec{\tau}\|_{\mathcal{V}^B}}\Big\}.
\end{aligned}\tag{6.133}$$

Then we conclude the proof by applying Proposition 6.3.2 and a triangle inequality. ∎

We again emphasize that the above result indicates that the convergence obtained with general shell elements is no better than $O(h^2)$, due to the consistency errors. So far, however, one could argue that our estimates only give an *upper bound* of the error, hence that these suboptimal bounds (for finite elements of degree greater than 2) do not really imply that the actual errors will not be smaller. This could indeed happen due to limitations in the mathematical analysis, the complexity of which may be suspected to cloud

the understanding. In order to further investigate this matter, we introduce a model problem that contains the consistency error related to the interpolation of rotation vectors (namely that requiring the use of (6.56)), but does not contain undue technicalities. We consider the problem
Find $\vec{\theta}$ *in* $\mathcal{R}$ *such that*

$$a(\vec{\theta}, \vec{\eta}) = f(\vec{\eta}), \qquad \forall \vec{\eta} \in \mathcal{R}, \tag{6.134}$$

with

$$a(\vec{\theta}, \vec{\eta}) = \int_I \frac{d\vec{\theta}}{d\xi} \cdot \frac{d\vec{\eta}}{d\xi}\, d\xi, \tag{6.135}$$

$$f(\vec{\eta}) = \int_I \vec{p} \cdot \vec{\eta}\, d\xi, \qquad \vec{p} \in L^2(I)^3, \tag{6.136}$$

$$\mathcal{R} = \{\vec{\eta} \in H_0^1(I)^3 \mid \vec{\eta} \cdot \vec{a}_3 \equiv 0\}, \tag{6.137}$$

where I is an interval of $\mathbb{R}$, and $\vec{a}_3$ is a smooth vector field of unit length defined over I. Note that, for simplicity, we assume "clamped" boundary conditions. Then, like for the general shell element procedure, we define the discrete rotation space as the space of the projections (onto the plane perpendicular to $\vec{a}_3$) of continuous functions of $\mathcal{R}$, viz.

$$\mathcal{R}_h = \big\{\pi\big(\mathcal{I}(\vec{\eta})\big) \mid \vec{\eta} \in \mathcal{R} \cap \mathcal{C}^0(\omega)^3\big\}, \tag{6.138}$$

and the resulting finite element problem is
Find $\vec{\theta}_h$ *in* $\mathcal{R}_h$ *such that*

$$a\big(\mathcal{I}(\vec{\theta}_h), \mathcal{I}(\vec{\eta})\big) = f\big(\mathcal{I}(\vec{\eta})\big), \qquad \forall \vec{\eta} \in \mathcal{R}_h. \tag{6.139}$$

The error analysis of this finite element procedure can be carried out by the same arguments as for general shell elements, and we thus obtain an error estimate which is only quadratic for shape functions quadratic or of higher degree (assuming, as usual, sufficient regularity of the exact solution). In order to determine whether this estimate is optimal (namely, the best that can be obtained in general), we have performed some numerical experiments on a cubic finite element scheme. We considered for the geometry a quarter of the unit circle, and the loading was designed so that the exact solution is known and given by $\sin(4\xi)$ times the unit tangential vector, for $\xi \in \big[0, \frac{\pi}{2}\big]$. The convergence curve – shown in Figure 6.8 with the caption "original" – clearly displays an $O(h^2)$ asymptotic error, which confirms that the above error estimate is indeed optimal.

In order to circumvent this suboptimal consistency error and recover a nominal convergence behavior, we would like to use the projections of the

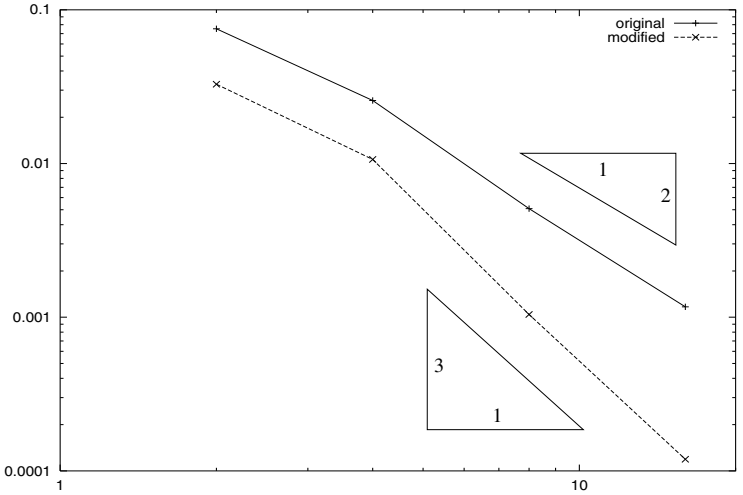

Fig. 6.8. Error in H^1-semi-norm vs. number of elements

interpolated rotation vectors in (6.139), namely $\vec{\theta}_h$ and $\vec{\eta}$ themselves. This is impossible because the geometry is not known – hence neither is the projection operator – except at the nodes. However, we can use the interpolated normal vector $\mathcal{I}(\vec{a}_3)$ to define an approximate projection operator π_h, which leads to considering

$$a\big(\pi_h\big(\mathcal{I}(\vec{\theta}_h)\big), \pi_h\big(\mathcal{I}(\vec{\eta})\big)\big) = f\big(\pi_h\big(\mathcal{I}(\vec{\eta})\big)\big), \qquad \forall \vec{\eta} \in \mathcal{R}_h, \tag{6.140}$$

instead of (6.139). It is then straightforward to establish an $O(h^p)$ consistency estimate for this modified formulation, and the corresponding curve in Figure 6.8 indeed shows that optimal convergence is achieved. Of course, this simple modification can be used with general shell elements too.

Remark 6.3.7. In the above model problem, we have focused on the consistency error arising from the interpolation of rotation vectors. As regards the other source of consistency error – namely the interpolation of the thickness performed together with the rotation – we could also consider a specific model problem. Furthermore, a similar treatment can be devised to recover nominal convergence, by employing a *separate* interpolation of the thickness. Finally, the combination of these modifications leads to considering finite element displacement functions of the form

$$\boxed{\vec{V} = \sum_{i=1}^{k} \lambda_i(r,s)\Big(\vec{v}^{(i)} + z\frac{\mathcal{I}(t)}{2}\pi_h(\vec{\eta}^{(i)})\Big),} \tag{6.141}$$

in each element, or equivalently

$$\vec{V} = \vec{v} + \xi^3\frac{\mathcal{I}(t)}{t}\pi_h\big(\mathcal{I}(\vec{\eta})\big). \tag{6.142}$$

■

We now examine the approximation procedure provided by the alternative strategy *S-2* (see p.236), for which we establish a similar error bound.

Proposition 6.3.3 *Denoting by* $(\vec{\hat{u}}_h, \vec{\hat{\theta}}_h)$ *the finite element solution obtained using the strategy* S-2 *and assuming that the exact solution is smooth, we have the following error estimate*

$$\boxed{\|\vec{u} - \vec{\hat{u}}_h, \vec{\theta} - \vec{\hat{\theta}}_h\|_{\mathcal{V}^B} \leq Ch^{\min\{p,2\}}.} \tag{6.143}$$

Proof. We consider the covariant base vectors $(\vec{\bar{g}}_1, \vec{\bar{g}}_2, \vec{\bar{g}}_3)$ corresponding to the approximate chart $\vec{\Phi}_h$ given by (6.49). We have

$$\begin{cases} \vec{\bar{g}}_\alpha = \dfrac{\partial\mathcal{I}(\vec{\phi})}{\partial\xi^\alpha} + \xi^3\dfrac{\partial}{\partial\xi^\alpha}\Big(\dfrac{\mathcal{I}(t\vec{a}_3)}{t}\Big), \qquad \alpha = 1,2 \\ \vec{\bar{g}}_3 = \dfrac{\mathcal{I}(t\vec{a}_3)}{t} \end{cases} \tag{6.144}$$

to be compared with (2.152)/(2.153) for the exact covariant base vectors. Here, we do not exactly have that $\vec{\bar{g}}_3$ is a unit vector orthogonal to $\vec{\bar{g}}_1$ and $\vec{\bar{g}}_2$. Nevertheless, standard interpolation estimates give

$$\begin{cases} \|\vec{\bar{g}}_3\|^2 = \bar{g}_{33} = 1 + O(h^{p+1}) \\ \vec{\bar{g}}_\alpha \cdot \vec{\bar{g}}_3 = \bar{g}_{\alpha 3} = O(h^p), \qquad \alpha = 1,2 \end{cases} \tag{6.145}$$

Following now the prescribed strategy, we locally define an alternative coordinate system for which $\vec{\bar{g}}_3$ is the third base vector and is orthogonal to the others. To that purpose, we choose

$$\begin{cases} \vec{\hat{g}}_\alpha = \vec{\bar{g}}_\alpha - \dfrac{\bar{g}_{\alpha 3}}{\bar{g}_{33}}\vec{\bar{g}}_3, \qquad \alpha = 1,2 \\ \vec{\hat{g}}_3 = \vec{\bar{g}}_3 \end{cases} \tag{6.146}$$

We note that the corresponding contravariant base vectors are

$$\vec{\bar{g}}^{\alpha} = \vec{\bar{g}}\,^{\alpha}, \qquad \alpha = 1, 2, \tag{6.147}$$

(check that $\vec{\bar{g}}^{\alpha} \cdot \vec{\hat{g}}_i = \delta_i^{\alpha}$) and also that

$$\vec{\hat{g}}\,^{3} = \frac{\vec{\bar{g}}_3}{\bar{g}_{33}}. \tag{6.148}$$

We use the expression of the internal virtual work density given by

$$\hat{C}^{\alpha\beta\lambda\mu}\hat{e}_{\alpha\beta}(\vec{U})\hat{e}_{\lambda\mu}(\vec{V}) + \hat{D}^{\alpha\lambda}\hat{e}_{\alpha 3}(\vec{U})\hat{e}_{\lambda 3}(\vec{V}), \tag{6.149}$$

where the hat symbol denotes tensorial components in the modified $(\vec{\hat{g}}_1, \vec{\hat{g}}_2, \vec{\hat{g}}_3)$ coordinate system. Of course, $\hat{C}^{\alpha\beta\lambda\mu}$ and $\hat{D}^{\alpha\lambda}$ are defined according to (4.28) and (4.29) using components in the modified coordinate system for all tensors. Hence, from (6.147) we infer

$$\begin{cases} \hat{C}^{\alpha\beta\lambda\mu} = \dfrac{E}{2(1+\nu)}(\bar{g}^{\alpha\lambda}\bar{g}^{\beta\mu} + \bar{g}^{\alpha\mu}\bar{g}^{\beta\lambda} + \dfrac{2\nu}{1-\nu}\bar{g}^{\alpha\beta}\bar{g}^{\lambda\mu}) = \bar{C}^{\alpha\beta\lambda\mu}, \\ \hat{D}^{\alpha\lambda} = \dfrac{2E}{1+\nu}\bar{g}^{\alpha\lambda} = \bar{D}^{\alpha\lambda} \end{cases} \tag{6.150}$$

i.e. the components of the constitutive tensors are the same as those used for strategy *S-1*. Next, in order to compare the components of the strain tensors we use change of bases formulas. Namely,

$$\hat{e}_{ij}\vec{\hat{g}}^{i} \otimes \vec{\hat{g}}^{j} = \bar{e}_{kl}\vec{\bar{g}}^{\,k} \otimes \vec{\bar{g}}^{\,l} \tag{6.151}$$

implies

$$\hat{e}_{ij} = (\vec{\hat{g}}_i \cdot \vec{\bar{g}}^{\,k})(\vec{\hat{g}}_j \cdot \vec{\bar{g}}^{\,l})\,\bar{e}_{kl}. \tag{6.152}$$

Hence, using (6.146) we obtain

$$\begin{cases} \hat{e}_{\alpha\beta} = \bar{e}_{\alpha\beta} - \dfrac{\bar{g}_{\alpha 3}}{\bar{g}_{33}}\bar{e}_{\beta 3} - \dfrac{\bar{g}_{\beta 3}}{\bar{g}_{33}}\bar{e}_{\alpha 3} + \dfrac{\bar{g}_{\alpha 3}\,\bar{g}_{\beta 3}}{(\bar{g}_{33})^2}\bar{e}_{33} \\ \hat{e}_{\alpha 3} = \bar{e}_{\alpha 3} - \dfrac{\bar{g}_{\alpha 3}}{\bar{g}_{33}}\bar{e}_{33} \end{cases} \tag{6.153}$$

We thus observe that the expression of the density of internal virtual work used with this strategy is very similar to that used with the first strategy, since the only difference lies in the presence of additional strain terms with coefficients of order at least $O(h^p)$ (recall (6.145)) in the above system. In addition, note that for displacements functions of the type

$$\vec{V} = \vec{v} + \xi^3 \vec{\eta}, \tag{6.154}$$

we have

$$\bar{e}_{33}(\vec{V}) = \frac{\partial \vec{V}}{\partial \xi^3} \cdot \vec{g}_3 = \vec{\eta} \cdot \vec{g}_3. \tag{6.155}$$

Hence,

$$\|\bar{e}_{33}(\vec{V})\|_{L^2} \leq C \|\vec{\eta}\|_{L^2}. \tag{6.156}$$

Finally, denoting by $\hat{A}_h^{3D}$ the bilinear form obtained by using the above density of virtual work, (6.153) directly leads to

$$\left| A_h^{3D}\Big(\vec{v} + \xi^3 \frac{\mathcal{I}(t\vec{\eta})}{t}, \vec{w} + \xi^3 \frac{\mathcal{I}(t\vec{\tau})}{t}\Big) - \hat{A}_h^{3D}\Big(\vec{v} + \xi^3 \frac{\mathcal{I}(t\vec{\eta})}{t}, \vec{w} + \xi^3 \frac{\mathcal{I}(t\vec{\tau})}{t}\Big) \right| \leq C h^p \|\vec{v}, \vec{\eta}\|_{\mathcal{V}^B} \|\vec{w}, \vec{\tau}\|_{\mathcal{V}^B}, \tag{6.157}$$

for all $(\vec{v}, \vec{\eta})$ and $(\vec{w}, \vec{\tau})$ in $\mathcal{V}_h^B$, which implies that a consistency estimate similar to (6.89) holds for $\hat{A}_h^{3D}$. The approximation error can then be derived by the exact same argument as in the proof of Proposition 6.3.1. ∎

Remark 6.3.8. Clearly, the same modification of the shape functions as for Strategy *S-1* can be used in order to recover error estimates of the same order as interpolation estimates, for finite elements of degree higher than two. Namely, we can use the approximate projection operator for the rotation term, and a separate interpolation of the thickness parameter, see Remark 6.3.7. ∎

6.4 3D-Shell Elements

General shell elements can be extended to higher-order kinematical assumptions concerning the displacements across the thickness, as we did for mathematical shell models. In particular, we will now introduce and analyze *3D-shell elements* designed to approximate the second-order 3D-shell model. In the following description we more particularly emphasize the differences with the above general shell elements.

1. We consider a general *full* 3D variational formulation – that is, a 3D formulation in stress and strain without any modification or assumption on the stress state – represented by

$$A^{3D\text{full}}(\vec{U}, \vec{V}) = F^{3D}(\vec{V}), \quad \forall \vec{V} \in \mathcal{V}^{3D}. \tag{6.158}$$

2. The mesh is defined exactly as for *general shell elements* in (6.30) by nodal positions, normal vectors and thicknesses, as summarized in

$$\vec{x} = \sum_{i=1}^{k} \lambda_i(r,s)\big(\vec{x}^{(i)} + z\frac{t^{(i)}}{2}\vec{a}_3^{(i)}\big), \quad (r,s,z) \in [-1,1]^3. \tag{6.159}$$

3. The kinematical assumption is quadratic with respect to the transverse coordinates at the nodes, namely, we consider finite element displacement shape functions of the type

$$\boxed{\vec{V} = \sum_{i=1}^{k} \lambda_i(r,s)\left(\vec{v}^{(i)} + z\frac{t^{(i)}}{2}\vec{\eta}^{(i)} + z^2\frac{(t^{(i)})^2}{4}\vec{\varsigma}^{(i)}\right),} \tag{6.160}$$

which characterizes the finite element displacement space denoted by $\mathcal{V}_h^{3D\text{quad}}$.

4. Finally the 3D-shell element procedure consists in solving for $\vec{U}_h$ in $\mathcal{V}_h^{3D\text{quad}}$, i.e. given inside each element by

$$\vec{U}_h = \sum_{i=1}^{k} \lambda_i(r,s)\left(\vec{u}_h^{(i)} + z\frac{t^{(i)}}{2}\vec{\theta}_h^{(i)} + z^2\frac{(t^{(i)})^2}{4}\vec{\varrho}_h^{(i)}\right), \tag{6.161}$$

that satisfies

$$\boxed{A_h^{3D\text{full}}(\vec{U}_h,\vec{V}) = F_h^{3D}(\vec{V}), \quad \forall \vec{V} \in \mathcal{V}_h^{3D\text{quad}},} \tag{6.162}$$

where the subscript h in $A_h^{3D\text{full}}$ and F_h^{3D} signifies that we are using the approximated geometry defined by (6.159) to compute the external and internal virtual works.

We may compare (6.160) with (6.31) and see that the quadratic term has been added. We also note that, as in Section 6.3, the finite element nodal variables – $(\vec{u}_h^{(i)}, \vec{\theta}_h^{(i)}, \vec{\varrho}_h^{(i)})$ and $(\vec{v}^{(i)}, \vec{\eta}^{(i)}, \vec{\varsigma}^{(i)})$ – are described by the notation used for the kinematic variables in the shell theory to which we connect the finite element formulation (the basic shell model in Section 6.3 and the 3D-shell theory now).

Remark 6.4.1. The 3D-shell element shape functions can equivalently be written as

$$\vec{V} = \sum_{i=1}^{k} \lambda_i(r,s)\Big(\frac{(z-1)z}{2}\vec{V}^{(i)}_{\text{lower}} + (1-z^2)\vec{V}^{(i)}_{\text{mid}} + \frac{(z+1)z}{2}\vec{V}^{(i)}_{\text{upper}}\Big), \tag{6.163}$$

with

$$\vec{v}^{\,(i)} = \vec{V}^{\,(i)}_{\text{mid}}, \tag{6.164}$$

$$\vec{\eta}^{\,(i)} = \frac{1}{t^{(i)}}\big(\vec{V}^{\,(i)}_{\text{upper}} - \vec{V}^{\,(i)}_{lower}\big), \tag{6.165}$$

$$\vec{\varsigma}^{(i)} = \frac{4}{(t^{(i)})^2}\Big[\frac{1}{2}\big(\vec{V}^{\,(i)}_{\text{upper}} + \vec{V}^{\,(i)}_{\text{lower}}\big) - \vec{V}^{\,(i)}_{\text{mid}}\Big], \tag{6.166}$$

where $\vec{V}^{\,(i)}_{\text{lower}}$, $\vec{V}^{\,(i)}_{\text{mid}}$ and $\vec{V}^{\,(i)}_{\text{upper}}$ denote the corresponding displacements at the points lying on the lower, middle and upper surfaces on the same transverse material fiber as node i. This is obviously equivalent to the expression

$$\vec{V} = \sum_{j=1}^{3k} \lambda_j^{3D}(r,s,z)\vec{V}^{(j)}, \tag{6.167}$$

in which the functions λ_j^{3D} are quadratic in z and represent the Lagrange shape functions associated with 3D nodes laid out on the two outer surfaces and on the midsurface. Therefore, the proposed shell elements can be formulated in the form of brick elements that have the same essential features as 3D elements, namely the same node layouts, shape functions and unknowns (nodal displacements). Note that – in particular – when the shape functions are also quadratic in the (r,s) variables they correspond to *standard* Q_2 3D shape functions, hence the practical implementation of these elements is straightforward. Moreover, using the 3D-shell elements in this form with top and bottom nodes can be very valuable in practice when the shell structure is coupled to another surrounding medium, such as in fluid-structure or soil-structure interaction, in contact problems, or in sandwich structures. However, when the shell considered is very thin this leads to degenerated 3D elements with nodal distances across the thickness much smaller than in-plane distances, which induces ill-conditioning in the stiffness matrix, see (Kim & Bathe, 2008). ■

Remark 6.4.2. In large deformation analyses using the Total and Updated Lagrangian formulations (Bathe, 1996), initially straight fibres described by (6.159) become in general curved fibres. The deformed shell geometry is obtained by adding the calculated displacements to the initial geometry (see e.g. (Kim & Bathe, 2008)), hence the interpolation in (6.159) is only valid for the initial geometry. The updated geometry and total and incremental displacements can be calculated using (6.159) and (6.161), in the same way as in the incremental solutions of 3D solids. ■

In order to perform the convergence analysis of 3D-shell elements we will use the same mapping from the global coordinates (ξ^1, ξ^2, ξ^3) to the local

coordinates (r, s, z) as for general shell elements, with in particular $\xi^3 = zt/2$. Hence, we can rewrite the shape functions (6.160) as

$$\vec{V} = \vec{v} + \xi^3 \vec{\eta} + (\xi^3)^2 \vec{\varsigma}, \tag{6.168}$$

with the usual interpolation rule for $\vec{v}$ inside each element

$$\vec{v} = \sum_{i=1}^{k} \lambda_i(r, s) \vec{v}^{(i)}, \tag{6.169}$$

but slightly modified expressions for $\vec{\eta}$ and $\vec{\varsigma}$, namely,

$$\vec{\eta} = \sum_{i=1}^{k} \lambda_i(r, s) \frac{t^{(i)}}{t} \vec{\eta}^{(i)}, \quad \vec{\varsigma} = \sum_{i=1}^{k} \lambda_i(r, s) \left(\frac{t^{(i)}}{t} \right)^2 \vec{\varsigma}^{(i)}. \tag{6.170}$$

Therefore, comparing (6.168) with (4.77) we can see that the finite element shape functions directly satisfy the 3D-shell model kinematical assumptions, provided we consider $\vec{\eta}$ and $\vec{\varsigma}$ in the polynomial (finite element) space *weighted* by the functions $1/t$ and $1/t^2$, respectively. Namely, we need to consider (slightly) non-standard approximation spaces in this case. This will have to be dealt with at the final approximation stage of the mathematical analysis, but the fact that the discrete functions are directly in the adequate variational space – which means that we have an *internal* Galerkin approximation in the numerical analysis terminology – will make the rest of the convergence analysis much simpler than for general shell elements.

Denoting this finite element space by $\mathcal{V}_h^{3Ds}$, we can now reformulate the finite element problem as
Find $(\vec{u}_h, \vec{\theta}_h, \vec{\varrho}_h) \in \mathcal{V}_h^{3Ds}$ *such that*

$$A_h^{3Ds}(\vec{u}_h, \vec{\theta}_h, \vec{\varrho}_h; \vec{v}, \vec{\eta}, \vec{\varsigma}) = F_h^{3Ds}(\vec{v}, \vec{\eta}, \vec{\varsigma}), \quad \forall (\vec{v}, \vec{\eta}, \vec{\varsigma}) \in \mathcal{V}_h^{3Ds}, \tag{6.171}$$

with the natural definitions

$$A_h^{3Ds}(\vec{u}_h, \vec{\theta}_h, \vec{\varrho}_h; \vec{v}, \vec{\eta}, \vec{\varsigma}) = A_h^{3D\text{full}}\big(\vec{u}_h + \xi^3 \vec{\theta}_h + (\xi^3)^2 \vec{\varrho}_h, \vec{v} + \xi^3 \vec{\eta} + (\xi^3)^2 \vec{\varsigma}\big),$$

$$F_h^{3Ds}(\vec{v}, \vec{\eta}, \vec{\varsigma}) = F_h^{3D}\big(\vec{v} + \xi^3 \vec{\eta} + (\xi^3)^2 \vec{\varsigma}\big),$$

which simply means that we are using the approximate geometry instead of the exact one in the variational expressions considered for the 3D-shell model in Chapter 4. We will then show the following existence and convergence result.

Proposition 6.4.1 *Problem* (6.171) *has a unique solution. Furthermore, assuming that the solution of the 3D-shell model is sufficiently smooth we have the following optimal error estimate*

$$\boxed{\|\vec{u}-\vec{u}_h,\vec{\theta}-\vec{\theta}_h,\vec{\varrho}-\vec{\varrho}_h\|_1 \le Ch^p.} \tag{6.172}$$

This result is very important, because it effectively establishes that the 3D-shell model is the mathematical model underlying 3D-shell elements, and we have shown in Sections 4.3.4 and 5.4.2 that the 3D-shell model features adequate mathematical properties, in particular from an asymptotic point of view. Note also that this estimate is now optimal, unlike (6.54) for general shell elements in which we did not have an internal Galerkin approximation. The proof of Proposition 6.4.1 will essentially rely on the following consistency lemma.

Lemma 6.4.1. *For any smooth* $(\vec{v}_s,\vec{\eta}_s,\vec{\varsigma}_s)$ *in* $\mathcal{V}^{3Ds}$*, we have*

$$\begin{aligned}\inf_{(\vec{v},\vec{\eta},\vec{\varsigma})\in\mathcal{V}_h^{3Ds}}\Big\{&\|\vec{v}_s-\vec{v},\vec{\eta}_s-\vec{\eta},\vec{\varsigma}_s-\vec{\varsigma}\|_1\\ &+\sup_{(\vec{w},\vec{\tau},\vec{\sigma})\in\mathcal{V}_h^{3Ds}}\frac{(A^{3Ds}-A_h^{3Ds})(\vec{v},\vec{\eta},\vec{\varsigma};\vec{w},\vec{\tau},\vec{\sigma})}{\|\vec{w},\vec{\tau},\vec{\sigma}\|_1}\Big\}\\ &\le Ch^p\|\vec{v}_s,\vec{\eta}_s,\vec{\varsigma}_s\|_{H^{p+1}}.\end{aligned} \tag{6.173}$$

In addition,

$$\sup_{(\vec{w},\vec{\tau},\vec{\sigma})\in\mathcal{V}_h^{3Ds}}\frac{\Big|(F^{3Ds}-F_h^{3Ds})(\vec{w},\vec{\tau},\vec{\sigma})\Big|}{\|\vec{w},\vec{\tau},\vec{\sigma}\,\|_1}\le Ch^p. \tag{6.174}$$

Proof. We handle the geometric approximation exactly like in the proof of Proposition 6.3.2 to obtain (6.174) and

$$\sup_{(\vec{w},\vec{\tau},\vec{\sigma})\in\mathcal{V}_h^{3Ds}}\frac{(A^{3Ds}-A_h^{3Ds})(\vec{v},\vec{\eta},\vec{\varsigma};\vec{w},\vec{\tau},\vec{\sigma})}{\|\vec{w},\vec{\tau},\vec{\sigma}\|_1}\le Ch^p\|\vec{v},\vec{\eta},\vec{\varsigma}\|_1. \tag{6.175}$$

Then, recalling (6.170) we can choose

$$(\vec{v},\vec{\eta},\vec{\varsigma})=\Big(\mathcal{I}(\vec{v}_s),\frac{\mathcal{I}(t\vec{\eta}_s)}{t},\frac{\mathcal{I}(t^2\vec{\varsigma}_s)}{t^2}\Big)\in\mathcal{V}_h^{3Ds}.$$

The resulting non-standard interpolation estimates are easy to handle since, for example for $\vec{\eta}$,

$$\begin{aligned}\|\vec{\eta}_s-\vec{\eta}\|_1 &= \|\big(t\vec{\eta}_s-\mathcal{I}(t\vec{\eta}_s)\big)/t\|_1\\ &\le C\|t\vec{\eta}_s-\mathcal{I}(t\vec{\eta}_s)\|_1\\ &\le Ch^p\|t\vec{\eta}_s\|_{H^{p+1}}\\ &\le Ch^p\|\vec{\eta}_s\|_{H^{p+1}},\end{aligned}$$

where we have repeatedly used the fact that t is smooth and bounded away from zero. The bound (6.173) directly follows. ■

Proof of Proposition 6.4.1. First, we use (6.175) to infer that the bilinear function A_h^{3Ds} is bounded and coercive. Similarly, F_h^{3Ds} is bounded due to (6.174). Therefore, (6.171) has a unique solution. Finally, we invoke a "first Strang Lemma" argument like in the proof of Proposition 6.3.1, and we use Lemma 6.4.1 to obtain the estimate (6.172). ■

7. Influence of the Thickness in the Finite Element Approximation

The influence of the thickness in the finite element analysis of thin structures is a crucial issue, as it is deeply interrelated with the motivation of modeling a 3D continuum as a shell in engineering. Why, indeed, should we use shell models and finite elements – instead of 3D models – to analyze a given structure? The answer to this question seems obvious: firstly, the use of a shell model is to reduce the analysis cost, and secondly, the use of the shell model is to reduce the complexity of the analysis including the interpretation of the results for engineering design. Clearly, the motivation to use shell models rests upon the fact that shell mathematical models and finite elements incorporate kinematical assumptions pertaining to the displacement distribution across the thickness of the structure, see previous chapters. Hence, we do not have to discretize the problem across the thickness, but only over the mid-surface (or equivalently in the 2D domain that corresponds to the in-plane coordinates). In other words, in shell analysis we "trade" the discretization in the transverse direction for a kinematical assumption in the same direction. Of course, by using a shell mathematical model instead of a 3D model we introduce a modeling error due to the difference between the exact solutions of the two mathematical models. The analysis of this modeling error goes beyond the scope of this book, but we recall that this error can be shown – under certain assumptions and using some specific convergence measures – to tend to zero when the thickness of the structure tends to zero, see Chapter 5 (and in particular Remark 5.1.10).

Therefore, an essential motivation for modeling a 3D continuum as a shell relies on the assumption that the accuracy of a corresponding finite element solution – compared to the exact solution of the *shell* model – only depends on criteria that prevail in 2D analysis, i.e. typically on the fineness of the surface mesh *regardless of the transverse direction*, i.e. *independently of the thickness* value. This means that we expect *uniform convergence* of the finite element solution with respect to the thickness parameter, i.e. relative error bounds of the type

$$\boxed{\frac{\|U^\varepsilon - U_h^\varepsilon\|_\star}{\|U^\varepsilon\|_\star} \leq Ch^p,} \tag{7.1}$$

D. Chapelle, K.-J. Bathe, *The Finite Element Analysis of Shells – Fundamentals*,
Computational Fluid and Solid Mechanics, 2nd ed., DOI 10.1007/978-3-642-16408-8_7,

where U_h^ε represents the finite element solution for a given thickness value ε (to be compared with the exact solution U^ε, see Chapter 5), and where the bounding constant C and the order of convergence p should not depend on ε. In the above equation we denote the norm with a "$\star$" symbol to indicate that the norm for which uniform convergence is expected remains to be specified, and the order p should then be the optimal order of convergence for this norm (namely the order of convergence of interpolation errors). Such a uniform estimate is very important to ensure the *reliability* of the finite element procedure considered.

However, it was soon recognized in the development of structural analysis procedures that standard finite element techniques – such as the displacement-based shell finite elements introduced in Chapter 6 – fail to display such uniformly converging behaviors in general, and that instead finite element approximations tend to dramatically deteriorate when the thickness of the structure decreases. This difficulty could then invoke the question as to whether the use of shell mathematical models in the finite element analysis of shells is actually effective from a computational point of view, when compared to a fully three-dimensional finite element analysis. It is the purpose of this chapter to analyze such difficulties and to examine some remedies to overcome these difficulties.

We emphasize that – throughout this chapter – the generic positive constants C and the generic strictly positive constants γ are all assumed to be independent of the thickness parameter ε (and also – of course – independent of the mesh parameter h).

7.1 Numerical Locking in Thin Structures

In order to illustrate the type of numerical difficulty that arises in the formulation of thin structures, we consider the example of a straight cantilever beam in plane strain conditions. The beam is of (constant) rectangular cross-section, clamped at $s = 0$ and loaded by a concentrated transverse force T at $s = L$, see Figure 7.1.

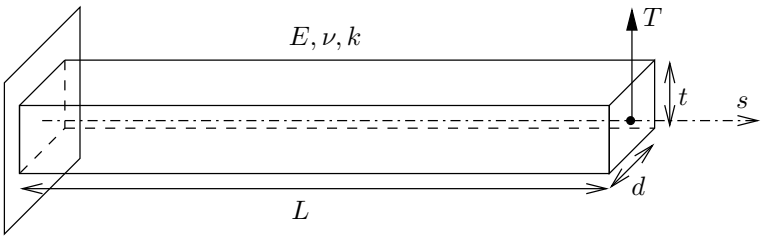

Fig. 7.1. Beam loaded by transverse tip load

The variational formulation for this problem can be derived from the Reissner-Mindlin plate model (4.67) by using the assumption that the displacement and rotation quantities do not change in the direction orthogonal to the plane of the beam, and that the rotation causing displacements in this orthogonal direction is zero. We thus obtain the problem
Find (u, θ) *in* $\mathcal{V}^T$ *such that*

$$\boxed{\begin{aligned}\frac{Et^3 d}{12(1-\nu^2)} \int_0^L \theta' \eta' \, ds + \frac{Etdk}{2(1+\nu)} \int_0^L (\theta + u')(\eta + v') \, ds \\ = Tv(L), \qquad \forall (v, \eta) \in \mathcal{V}^T,\end{aligned}} \tag{7.2}$$

with

$$\mathcal{V}^T = \big\{(v, \eta) \in \big(H^1(]0, L[)\big)^2 \mid v(0) = 0, \ \eta(0) = 0\big\}, \tag{7.3}$$

and where d denotes the depth of the beam in the out-of-plane direction. Here, u represents the transverse displacement and θ the rotation of a cross-section. Note that the mathematical model is – in fact – the plane strain Timoshenko beam model, see e.g. (Bathe, 1996).

Remark 7.1.1. We recall that H^1 functions are continuous *in 1D* hence their pointwise values used in the above boundary conditions and external virtual work are indeed meaningful. ■

Following the approach used in Chapter 5, we define

$$\varepsilon = \frac{t}{L} \tag{7.4}$$

and

$$\boxed{\mathcal{V}_0^T = \big\{(v, \eta) \in \mathcal{V}^T \mid \eta + v' = 0\big\}.} \tag{7.5}$$

Clearly, $\mathcal{V}_0^T$ is not limited to the zero function, hence we are always in a *bending-dominated situation*. Therefore, an appropriate sequence of problems parametrized by ε can be defined by scaling the loading as

$$T = \varepsilon^3 \tilde{T}, \tag{7.6}$$

with $\tilde{T}$ independent of ε. We then consider

Find $(u^\varepsilon, \theta^\varepsilon)$ *in* $\mathcal{V}^T$ *such that*

$$\frac{EL^3d}{12(1-\nu^2)}\int_0^L \theta^{\varepsilon\prime}\eta'\,ds + \varepsilon^{-2}\frac{ELdk}{2(1+\nu)}\int_0^L (\theta^\varepsilon + u^{\varepsilon\prime})(\eta + v')\,ds = \tilde{T}v(L), \qquad \forall (v,\eta) \in \mathcal{V}^T. \tag{7.7}$$

From Chapter 5 (see Proposition 5.1.2), we know that the sequence of solutions converges – for the norm of $\mathcal{V}^T$, namely the H^1-norm – to the solution of the limit problem
Find (u^0, θ^0) *in* $\mathcal{V}_0^T$ *such that*

$$\frac{EL^3d}{12(1-\nu^2)}\int_0^L \theta^{0\prime}\eta'\,ds = \tilde{T}v(L), \qquad \forall (v,\eta) \in \mathcal{V}_0^T, \tag{7.8}$$

which is, in fact, the formulation of a (plane strain) Bernoulli beam problem (Bathe, 1996).

We now consider the discretization of the above sequence of problems by P_1-Lagrange finite elements (i.e. with linear interpolation between nodes), namely
Find $(u_h^\varepsilon, \theta_h^\varepsilon)$ *in* $\mathcal{V}_h^T$ *such that*

$$\frac{EL^3d}{12(1-\nu^2)}\int_0^L \theta_h^{\varepsilon\prime}\eta'\,ds + \varepsilon^{-2}\frac{ELdk}{2(1+\nu)}\int_0^L (\theta_h^\varepsilon + u_h^{\varepsilon\prime})(\eta + v')\,ds = \tilde{T}v(L), \qquad \forall (v,\eta) \in \mathcal{V}_h^T, \tag{7.9}$$

where $\mathcal{V}_h^T$ denotes the corresponding finite element space. If we keep $\mathcal{V}_h^T$ fixed (namely the mesh is unchanged) and make ε go to zero, we can apply Proposition 5.1.2 with the finite-dimensional space $\mathcal{V}_h^T$ substituted for the general displacement space. We thus obtain that $(u_h^\varepsilon, \theta_h^\varepsilon)$ converges – for the H^1-norm – to the solution of the limit problem
Find (u_h^0, θ_h^0) *in* $\mathcal{V}_h^T \cap \mathcal{V}_0^T$ *that satisfies*

$$\frac{EL^3d}{12(1-\nu^2)}\int_0^L \theta_h^{0\prime}\eta'\,ds = \tilde{T}v(L), \qquad \forall (v,\eta) \in \mathcal{V}_h^T \cap \mathcal{V}_0^T. \tag{7.10}$$

However we can easily see that the contents of $\mathcal{V}_h^T \cap \mathcal{V}_0^T$ are reduced to the zero function in this case. Namely, considering (v,η) in $\mathcal{V}_h^T \cap \mathcal{V}_0^T$, it satisfies

$$\eta + v' = 0 \tag{7.11}$$

in the whole interval $[0, L]$. Therefore, since v is piecewise-linear we infer that η must be piecewise-constant, hence a fixed constant since it is a continuous function. Due to the clamped boundary condition this constant is zero, therefore (7.11) now tells us that v is piecewise-constant, hence zero by the same reasoning. As a consequence, the solution of (7.10) – the limit solution of (7.9) – is the trivial $(0, 0)$ function, whereas the limit solution of the continuous problem is clearly non-zero. Of course, in practice the thickness parameter is never exactly zero, but the argument shows that, for a set finite element subspace, the amplitude of the finite element solution will decrease and tend to zero as the thickness decreases, which does not correctly represent the behavior of the exact solution.

Table 7.1. Values of $u_h^\varepsilon(L)/u^\varepsilon(L)$

N	$\varepsilon = 1.$	$\varepsilon = 0.1$	$\varepsilon = 0.01$
1	0.7742	0.0331	0.0003
10	0.9971	0.7742	0.0331
100	1.0000	0.9971	0.7742

The numerical results presented in Table 7.1 provide some practical evidence of this phenomenon. They are obtained for the above example of the beam (with $\nu = 0.3$ and $k = 5/6$ here) discretized by N P_1-elements of equal lengths, and we give the value of the computed deflection at the tip of the beam scaled by the corresponding exact value for the same thickness (of course the closed-form exact solution can be obtained in this case). We recall that – in 1D – convergence in the H^1-norm entails convergence in pointwise values, hence the measure of convergence that we are using is adequate. The behavior predicted by theory is confirmed, namely the structure as seen through the finite element analysis appears increasingly stiffer as the thickness decreases, which can be observed by looking at any row of the table. For example, for a discretization of the beam into 10 elements, which we would expect to be a reasonable discretization, the deflection of the tip is underestimated by more than an order of magnitude for $\varepsilon = 0.01$. In Figure 7.2 we show the computed deflection of the beam along its length compared to the exact solution and the same behavior is observed at the global level. Due to the exceedingly stiff behavior exhibited in the numerical solution, this phenomenon is known as *numerical locking*. In this particular case, it is more specifically referred to as "shear locking" since it is induced by the constraint of vanishing shear strains.

We considered here the problem described in Fig. 7.1, but the same behavior is illustrated in (Bathe, 1996) considering the cantilever beam model

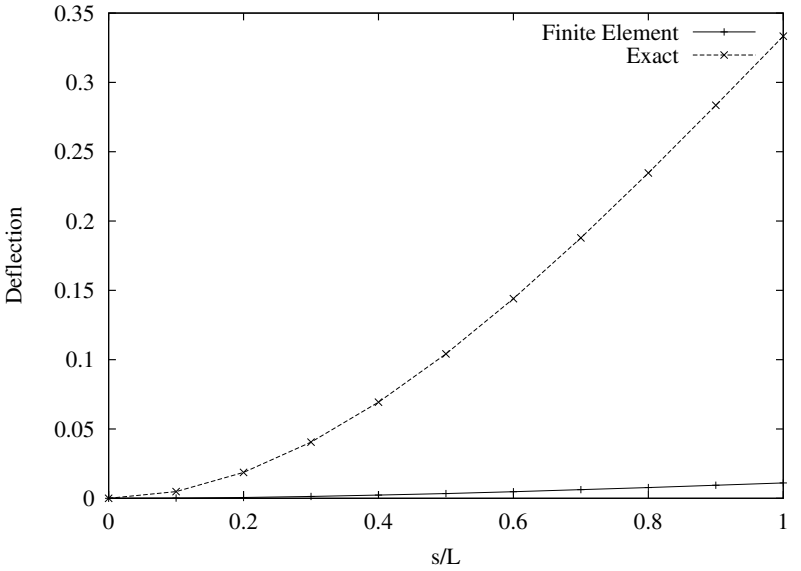

Fig. 7.2. Finite element vs. exact deflection for $\varepsilon = 0.01$

subjected to a tip moment. This underlines that – of course – the numerical locking occurs for any loading that activates the pure bending displacements (as expressed by the condition "$\exists V \in \mathcal{V}_0,\ G(V) \neq 0$" in the diagram given in Fig. 5.2).

A direct consequence of locking is that the objective of uniform convergence stated in the above introduction is – obviously – not achieved. For example, in the above numerical results we can see that, for a prescribed accuracy of 25% for the tip deflection, we must vary the element lengths as εL (see the diagonal of the table). Non-uniform convergence can also be visualized by comparing convergence behaviors for various values of the parameter ε. Such a comparison is displayed in Figure 7.3 and we clearly see that the convergence behavior dramatically deteriorates (namely the convergence curve is shifted upwards) when ε decreases (note that a log-log scale is used).

Remark 7.1.2. We should note that a fully 3D analysis does not circumvent the problem of locking in an effective way when pursuing a shell solution. Specifically, let us consider the 3D discretization that we may associate with a shell element discretization, namely using 3D elements with top and bottom nodes only and only one layer through the shell thickness. Then the finite element problem considered is similar to the finite element problem obtained using the s-m-b or basic shell mathematical models, as follows from the discussion given in Chapter 6. In order not to have locking in the 3D analysis of

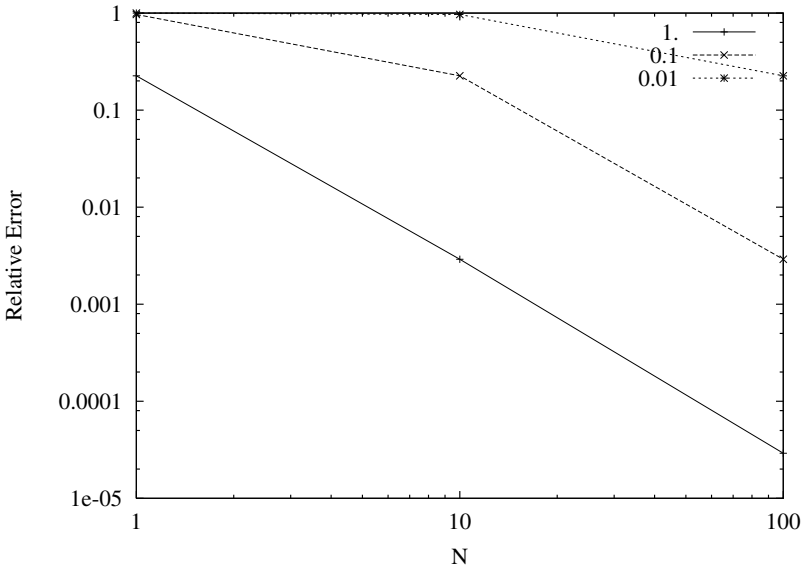

Fig. 7.3. Relative error in tip deflection for various values of ε

a shell, it is – indeed – necessary to resort to a discretization strategy in which the lengths of the element sides in the tangential and transverse directions are almost equal, see Figure 7.4. This observation is consistent with the results given in Table 7.1 (consider the diagonal entries). Such a discretization – while accurate – is increasingly expensive as the thickness decreases, which is not in accordance with the objective of a shell analysis. ■

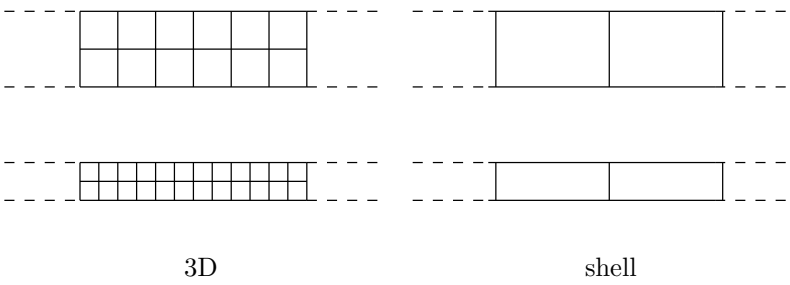

Fig. 7.4. Compared "natural" discretizations when t varies for 3D vs. shell solutions

Remark 7.1.3. We should further note that – while the stress and kinematic assumptions used to formulate the mathematical shell models are specifically

directed towards avoiding certain solution difficulties that arise in fully 3D finite element discretizations, see Section 4.1 – the numerical behavior of shear locking described here is present in the 3D solutions and – unfortunately – is not bypassed by using the Reissner-Mindlin kinematical assumptions. The problem of shear locking is bypasssed by using the m-b shell model (reducing here to the Bernoulli beam model) but then other finite element discretization difficulties arise, see Section 6.1 and (Bathe, 1996). Also, the problem of membrane locking is of course still present in curved structures discretized using the m-b shell model. ■

The numerical locking phenomenon was already discussed and illustrated on the example of the Timoshenko beam formulation in (Bathe, 1996), where also the remedies of using a mixed formulation are presented. However, we are here considering the formulation in the general mathematical context presented earlier, which leads to further insight into the formulation and how to circumvent the locking difficulties.

7.2 Treatments of Numerical Locking by Mixed Formulations

Numerical locking is a pathological phenomenon that has been long known and investigated, not only in the formulation of thin structures but also, in particular, in incompressible (or nearly incompressible) mechanics for fluids and solids. In incompressible problems, it is the incompressibility constraint – enforced exactly or approximately – which induces the difficulty. In this context some very effective treatments have been devised by using formulations in which the constraints are taken into account by means of Lagrange multipliers which need also be discretized in the resulting finite element formulation, see in particular the seminal works (Brezzi, 1974; Babuška, 1973), and also (Kardestuncer & Norrie, 1987) and the references therein. Such approches are known as *mixed formulations*, since the Lagrange multipliers represent additional unknowns – of a type different from displacement type unknowns – in these formulations. This strategy has proven to be very powerful, as the mixed finite element formulations that have been shown to be well-posed have provided some effective *locking-free* procedures – in particular for incompressible mechanics – which are now very widely used in engineering practice (Brezzi & Fortin, 1991; Bathe, 1996).

We now outline the basic principles of mixed finite element formulations, before examining how (and how far) they can be applied to the formulations of thin structures, and shells in particular.

7.2.1 Basic principles: the Timoshenko beam example

We introduce the basic approach of using a mixed formulation with the example of the "Timoshenko beam" formulation considered above, namely Equation (7.7). We define the additional unknown

$$\boxed{q^\varepsilon = \varepsilon^{-3}\frac{Etdk}{2(1+\nu)}(\theta^\varepsilon + u^{\varepsilon\prime}),} \tag{7.12}$$

which can be interpreted as the internal shear force scaled by the same factor (namely ε^{-3}) as the external transverse force in (7.6). Substituting into (7.7) we obtain

$$\frac{EL^3d}{12(1-\nu^2)}\int_0^L \theta^{\varepsilon\prime}\eta'\,ds + \int_0^L q^\varepsilon(\eta+v')\,ds = \tilde{T}v(L), \qquad \forall (v,\eta)\in\mathcal{V}^T. \tag{7.13}$$

Noting that $(u^\varepsilon,\theta^\varepsilon)$ being in $\mathcal{V}^T$ implies that q^ε is in L^2, we define

$$\mathcal{T}^T = L^2(]0,L[), \tag{7.14}$$

and we rewrite (7.12) in the equivalent variational form

$$\int_0^L q^\varepsilon r\,ds = \varepsilon^{-2}\frac{ELdk}{2(1+\nu)}\int_0^L(\theta^\varepsilon + u^{\varepsilon\prime})r\,ds, \qquad \forall r\in\mathcal{T}^T. \tag{7.15}$$

Gathering (7.13) and (7.15), we obtain a mixed variational formulation equivalent to the displacement-based formulation (7.7), viz.
Find $\big((u^\varepsilon,\theta^\varepsilon),q^\varepsilon\big)$ *in* $\mathcal{V}^T\times\mathcal{T}^T$ *such that*

$$\boxed{\begin{cases} \dfrac{EL^3d}{12(1-\nu^2)}\displaystyle\int_0^L \theta^{\varepsilon\prime}\eta'\,ds + \int_0^L(\eta+v')q^\varepsilon\,ds = \tilde{T}v(L), \\ \qquad\qquad\qquad\qquad\qquad\qquad \forall (v,\eta)\in\mathcal{V}^T, \\ \displaystyle\int_0^L(\theta^\varepsilon+u^{\varepsilon\prime})r\,ds - \varepsilon^2\frac{2(1+\nu)}{ELdk}\int_0^L q^\varepsilon r\,ds = 0, \quad \forall r\in\mathcal{T}^T. \end{cases}} \tag{7.16}$$

We note that the small parameter ε now appears with a positive exponent, and that we have indeed obtained a formulation of the type of (3.153). It is then natural to consider the following candidate limit problem

Find $\big((u^0,\theta^0),q^0\big)$ *in* $\mathcal{V}^T\times\mathcal{T}^T$ *such that*

$$\left\{\begin{array}{l} \dfrac{EL^3d}{12(1-\nu^2)}\displaystyle\int_0^L \theta^{0\prime}\eta'\,ds+\int_0^L(\eta+v')q^0\,ds=\tilde{T}v(L),\\ \qquad\qquad\qquad\qquad\qquad\qquad\qquad\qquad \forall(v,\eta)\in\mathcal{V}^T,\\ \displaystyle\int_0^L(\theta^0+u^{0\prime})r\,ds=0,\qquad \forall r\in\mathcal{T}^T. \end{array}\right. \tag{7.17}$$

This formulation is a mixed formulation of the type considered in (3.92). We also note that the subspace $\mathcal{V}_0^T$ defined in (7.5) corresponds to the subspace used in Proposition 3.2.3, namely that

$$\mathcal{V}_0^T=\big\{(v,\eta)\in\mathcal{V}^T\mid \int_0^L(\eta+v')r\,ds=0,\qquad \forall r\in\mathcal{T}^T\big\}. \tag{7.18}$$

We can then show the well-posedness of the mixed formulation (7.17) using Proposition 3.2.3.

Proposition 7.2.1 *The problem given by* (7.17) *has a unique solution and this solution* $\big((u^0,\theta^0),q^0\big)$ *satisfies*

$$\|u^0,\theta^0\|_{\mathcal{V}^T}+\|q^0\|_{\mathcal{T}^T}\le C\tilde{T}. \tag{7.19}$$

Proof. We will show that the two conditions of Prop. 3.2.3 are satisfied.

For the first condition, we need to show that

$$|\eta|_{H^1}\ge\gamma\|v,\eta\|_{\mathcal{V}^T},\qquad \forall(v,\eta)\in\mathcal{V}_0^T. \tag{7.20}$$

Consider any (v,η) in $\mathcal{V}_0^T$. Using the Poincaré inequality (3.61) we have that

$$|\eta|_{H^1}\ge\gamma\|\eta\|_{H^1}\ge\gamma\|\eta\|_{L^2}. \tag{7.21}$$

In addition, recalling the constraint enforced in $\mathcal{V}_0^T$ we have

$$|v|_{H^1}=\|\eta\|_{L^2}, \tag{7.22}$$

hence

$$|\eta|_{H^1}\ge\gamma|v|_{H^1}. \tag{7.23}$$

Using again the Poincaré inequality (with v) we obtain

$$|\eta|_{H^1} \geq \gamma \|v\|_{H^1}, \tag{7.24}$$

and (7.20) follows by combining this with the first inequality in (7.21).

For the continuous inf-sup condition, we need to show that there exists a constant $\delta > 0$ such that

$$\sup_{(v,\eta)\in\mathcal{V}^T,\,(v,\eta)\neq 0} \frac{\int_0^L (\eta + v')r\,ds}{\|v,\eta\|_{\mathcal{V}^T}} \geq \delta \|r\|_{\mathcal{T}^T}, \qquad \forall r \in \mathcal{T}^T. \tag{7.25}$$

Consider then any r in $\mathcal{T}^T$ and set

$$(v,\eta) = \Big(\int_0^s r\,ds\ ,\ 0 \Big), \tag{7.26}$$

(note that this is consistent with the boundary conditions) so that $v' = r$ and

$$\int_0^L (\eta + v')r\,ds = \|r\|^2_{\mathcal{T}^T}. \tag{7.27}$$

In addition, using again the Poincaré inequality we also have

$$\|v,\eta\|_{\mathcal{V}^T} = \|v\|_{H^1} \leq C|v|_{H^1} = C\|r\|_{\mathcal{T}^T}. \tag{7.28}$$

Therefore, with this choice of (v,η) we have

$$\frac{\int_0^L (\eta + v')r\,ds}{\|v,\eta\|_{\mathcal{V}^T}} \geq \delta \|r\|_{\mathcal{T}^T}, \tag{7.29}$$

for some strictly positive constant δ, hence (7.25) holds, and the proposition is proved. ∎

We can see that – for the case considered here – we have "$\mathcal{T}^+ = \mathcal{T}$" in the framework of Section 3.2, meaning that the continuous inf-sup condition holds in $\mathcal{T}^+$, namely, in L^2. This does not hold for plate and shell models, as we discuss later in this Chapter. Since for the Timoshenko beam model the assumptions of Proposition 3.2.10 hold (taking, for example, $\varepsilon_{\max} = 1$), we then have the following result.

Proposition 7.2.2 *The problem given by* (7.16) *has a unique solution and this solution* $\big((u^\varepsilon, \theta^\varepsilon), q^\varepsilon\big)$ *is such that*

$$\|u^0 - u^\varepsilon, \theta^0 - \theta^\varepsilon\|_{\mathcal{V}^T} + \|q^0 - q^\varepsilon\|_{\mathcal{T}^T} \xrightarrow{\varepsilon\to 0} 0. \tag{7.30}$$

Remark 7.2.1. Taking $(v,\eta) \in \mathcal{V}_0^T$ in the first equation of (7.17) we obtain (7.8) which we have already shown to be the limit problem of the displacement-based formulation. However, we have now shown that the scaled shear force also converges in the mixed formulation. The limit q^0 is – in fact – the Lagrange multiplier of the constraint that prevails in the displacement-based limit problem, namely the constraint of vanishing shear strains. ■

Remark 7.2.2. The mixed formulation (7.16) can also be derived by using the Hu-Washizu or Hellinger-Reissner variational principles, see (Bathe, 1996) and the references therein. ■

So far, we have introduced a mixed formulation which is exactly equivalent to the original displacement-based formulation (7.7). Since the mixed formulation involves one additional unknown field, the advantage is not obvious at this stage. However, the analysis of the discretized problem will show the effectiveness of the approach.

Consider then a finite-element discretization of the mixed problem (7.16) using P_p (continuous) shape functions for the deflection and the rotation, and $P_{(p-1)}$ *discontinuous* shape functions for the scaled shear force, for any $p \geq 1$. Denoting by $\mathcal{V}_h^T$ and $\mathcal{T}_h^T$ the corresponding finite element subspaces, we thus consider the sequence of problems
Find $\left((u_h^\varepsilon, \theta_h^\varepsilon), q_h^\varepsilon\right)$ *in* $\mathcal{V}_h^T \times \mathcal{T}_h^T$ *such that*

$$\left\{\begin{array}{l} \dfrac{EL^3 d}{12(1-\nu^2)} \displaystyle\int_0^L {\theta_h^\varepsilon}' \eta' \, ds + \int_0^L (\eta + v') q_h^\varepsilon \, ds = \tilde{T} v(L), \\ \qquad\qquad\qquad\qquad\qquad\qquad\qquad\qquad \forall (v,\eta) \in \mathcal{V}_h^T, \\ \displaystyle\int_0^L (\theta_h^\varepsilon + {u_h^\varepsilon}') r \, ds - \varepsilon^2 \frac{2(1+\nu)}{ELdk} \int_0^L q_h^\varepsilon r \, ds = 0, \quad \forall r \in \mathcal{T}_h^T. \end{array}\right. \tag{7.31}$$

We now show that this finite element procedure "works" for the limit problem (7.17), namely that the assumptions of Proposition 3.2.4 are satisfied for the finite element problem
Find $\left((u_h^0, \theta_h^0), q_h^0\right)$ *in* $\mathcal{V}_h^T \times \mathcal{T}_h^T$ *such that*

$$\left\{\begin{array}{l} \dfrac{EL^3 d}{12(1-\nu^2)} \displaystyle\int_0^L {\theta_h^0}' \eta' \, ds + \int_0^L (\eta + v') q_h^0 \, ds = \tilde{T} v(L), \\ \qquad\qquad\qquad\qquad\qquad\qquad\qquad\qquad \forall (v,\eta) \in \mathcal{V}_h^T, \\ \displaystyle\int_0^L (\theta_h^0 + {u_h^0}') r \, ds = 0, \quad \forall r \in \mathcal{T}_h^T. \end{array}\right. \tag{7.32}$$

Recalling that the analysis of this limit finite element problem involves the subspace

$$\mathcal{V}_{h0}^T = \Big\{(v,\eta) \in \mathcal{V}_h^T \mid \int_0^L (\eta + v')r\, ds = 0, \quad \forall r \in \mathcal{T}_h^T\Big\}, \tag{7.33}$$

we note that the constraint prevailing in this subspace can also be written as

$$\Pi_h(\eta) + v' = 0, \tag{7.34}$$

where Π_h denotes the L^2-projection onto the subspace $\mathcal{T}_h^T$, namely onto the subspace of discontinuous piecewise $P_{(p-1)}$ polynomials. We point out that this projection operator does not need to be applied on v' which is already in this subspace.

We can now state and prove the convergence result.

Proposition 7.2.3 *The problem given by* (7.32) *has a unique solution and this solution* $\big((u_h^0, \theta_h^0), q_h^0\big)$ *satisfies*

$$\begin{aligned} &\|u^0 - u_h^0, \theta^0 - \theta_h^0\|_{\mathcal{V}^T} + \|q^0 - q_h^0\|_{\mathcal{T}^T} \\ &\qquad \le C \inf_{(v,\eta)\in\mathcal{V}_h^T, r\in\mathcal{T}_h^T} \big\{\|u^0 - v, \theta^0 - \eta\|_{\mathcal{V}^T} + \|q^0 - r\|_{\mathcal{T}^T}\big\}. \end{aligned} \tag{7.35}$$

Proof. We will show that the conditions of Proposition 3.2.4 are satisfied, with arguments very similar to those used in the proof of Proposition 7.2.1.

For the first condition, we need to show that

$$|\eta|_{H^1} \ge \gamma \|v, \eta\|_{\mathcal{V}^T}, \quad \forall (v,\eta) \in \mathcal{V}_{h0}^T. \tag{7.36}$$

Consider any (v,η) in $\mathcal{V}_{h0}^T$. Using the Poincaré inequality (3.61) we have that

$$|\eta|_{H^1} \ge \gamma \|\eta\|_{H^1} \ge \gamma \|\eta\|_{L^2}. \tag{7.37}$$

In addition, recalling the constraint enforced in $\mathcal{V}_{h0}^T$ we have

$$|v|_{H^1} = \|\Pi_h(\eta)\|_{L^2}, \tag{7.38}$$

and, by the fundamental properties of the projection,

$$\|\Pi_h(\eta)\|_{L^2} \le \|\eta\|_{L^2}. \tag{7.39}$$

Therefore,

$$|\eta|_{H^1} \geq \gamma |v|_{H^1}. \tag{7.40}$$

We now apply the Poincaré inequality on v and (7.36) follows.

For the discrete inf-sup condition, we need to show that there exists a constant $\delta > 0$ such that

$$\sup_{(v,\eta)\in\mathcal{V}_h^T,\,(v,\eta)\neq 0} \frac{\int_0^L (\eta + v')r\,ds}{\|v,\eta\|_{\mathcal{V}^T}} \geq \delta \|r\|_{\mathcal{T}^T}, \qquad \forall r \in \mathcal{T}_h^T. \tag{7.41}$$

Consider then any r in $\mathcal{T}_h^T$ and set

$$(v,\eta) = \Big(\int_0^s r\,ds\ ,\ 0 \Big). \tag{7.42}$$

Again, this is consistent with the boundary conditions *and* we have that (v,η) is in $\mathcal{V}_h^T$. We conclude like in the proof of Prop. 7.2.1. ∎

By Proposition 3.2.11, it directly follows that a similar result holds for the mixed formulation with finite ε, namely (7.31).

Proposition 7.2.4 *The problem given by* (7.31) *has a unique solution and this solution* $\big((u_h^\varepsilon, \theta_h^\varepsilon), q_h^\varepsilon\big)$ *satisfies*

$$\begin{aligned} &\|u^\varepsilon - u_h^\varepsilon, \theta^\varepsilon - \theta_h^\varepsilon\|_{\mathcal{V}^T} + \|q^\varepsilon - q_h^\varepsilon\|_{\mathcal{T}^T} \\ &\qquad \leq C \inf_{(v,\eta)\in\mathcal{V}_h^T, r\in\mathcal{T}_h^T} \big\{ \|u^\varepsilon - v, \theta^\varepsilon - \eta\|_{\mathcal{V}^T} + \|q^\varepsilon - r\|_{\mathcal{T}^T} \big\}, \end{aligned} \tag{7.43}$$

with a constant C independent of ε.

We also point out that the second equation of the system (7.31) can be rewritten as

$$q_h^\varepsilon = \varepsilon^{-2} \frac{ELdk}{2(1+\nu)} \Pi_h(\theta_h^\varepsilon + u_h^{\varepsilon\prime}). \tag{7.44}$$

Substituting into the first equation, we can see that $(u_h^\varepsilon, \theta_h^\varepsilon)$ is the solution of the problem
Find $(u_h^\varepsilon, \theta_h^\varepsilon)$ *in* $\mathcal{V}_h^T$ *such that*

$$\begin{aligned} \frac{EL^3 d}{12(1-\nu^2)} \int_0^L \theta_h^{\varepsilon\prime} \eta'\,ds + \varepsilon^{-2} \frac{ELdk}{2(1+\nu)} \int_0^L \Pi_h\big(\theta_h^\varepsilon + u_h^{\varepsilon\prime}\big)(\eta + v')\,ds \\ = \tilde{T} v(L), \qquad \forall (v,\eta) \in \mathcal{V}_h^T. \end{aligned} \tag{7.45}$$

Note that this elimination of the shear force unknown is a specific case of the general procedure presented in Section 3.2.1 to derive a purely displacement-based formulation from a mixed formulation, and indeed Eqs. (7.44)-(7.45) correspond to (3.185)-(3.184), respectively. We can check that the second integral in (7.45) – corresponding to A_0^h in Section 3.2.1 – gives a *symmetric* bilinear form (hence provides a symmetric finite element matrix), by using the definition of the projection Π_h, namely

$$\int_0^L \Pi_h(\phi) r \, ds = \int_0^L \phi r \, ds, \qquad \forall r \in \mathcal{T}^T, \tag{7.46}$$

and taking $r = \Pi_h(\theta_h^\varepsilon + u_h^{\varepsilon\prime})$ and $\phi = \eta + v'$ we obtain

$$\int_0^L \Pi_h\big(\theta_h^\varepsilon + u_h^{\varepsilon\prime}\big)(\eta + v') \, ds = \int_0^L \Pi_h\big(\theta_h^\varepsilon + u_h^{\varepsilon\prime}\big)\Pi_h\big(\eta + v'\big) \, ds. \tag{7.47}$$

Remark 7.2.3. This displacement-based form of the mixed formulation suggests a natural interpretation of how locking is overcome. Namely, the effect of the projection operator Π_h is to relax the constraint that the discrete solution tends to satisfy when ε is small. Indeed, in the asymptotic limit we only enforce (7.34) instead of

$$\eta + v' = 0,$$

which would induce numerical locking. However, we emphasize that this projection operation must be chosen very carefully in order for convergence to be ensured. Namely, constraint relaxation should not be performed using a generic procedure – such as reduced numerical integration – without any deep mathematical insight into how this relaxation can affect the global convergence behavior. In fact, it is generally only by satisfying the inf-sup and ellipticity conditions that we can prove that the projection is tailored to the specific constraint and finite element spaces considered. ■

In addition, due to the discontinuous character of the shape functions in $\mathcal{T}_h^T$, the effect of the projection can be calculated at the element level, namely by using functions r that vanish outside a given element in the definition (7.46). Therefore, the mixed finite element procedure – which we have shown to be free of locking – can be implemented as easily and efficiently as the original displacement-based finite element procedure. In fact we can show that, in order to compute the second integral in (7.45), it suffices to use the Gauss numerical integration scheme with p points per element on the quantity $(\theta_h^\varepsilon + u_h^{\varepsilon\prime})(\eta + v')$, as was already demonstrated in (Bathe, 1996). This is – indeed – a direct consequence of the following result.

Proposition 7.2.5 *For any continuous piecewise-P_p function η, inside each element $\Pi_h(\eta)$ is the (unique) $P_{(p-1)}$ polynomial that takes the same values as η at the p points of the Gauss numerical integration scheme.*

Proof. Consider any continuous piecewise-P_p function η. The function $\Pi_h(\eta)$ is defined by $\Pi_h(\eta) \in \mathcal{T}_h^T$ and

$$\int_0^L \Pi_h(\eta) r \, ds = \int_0^L \eta r \, ds, \qquad \forall r \in \mathcal{T}_h^T. \tag{7.48}$$

On the other hand, considering the Gauss integration rule with p points (valid for polynomials of order up to $2p-1$) and denoting by $\tilde{\eta}$ the unique $P_{(p-1)}$ piecewise-polynomial that takes the same values as η at the Gauss points we have that

$$\int_0^L \tilde{\eta} r \, ds = \int_0^L \eta r \, ds, \qquad \forall r \in \mathcal{T}_h^T, \tag{7.49}$$

because both integrals can be exactly evaluated by using the Gauss integration rule, namely using the values of the functions at the Gauss points only. Therefore $\tilde{\eta}$ satisfies the same equation as $\Pi_h(\eta)$ and $\tilde{\eta} \in \mathcal{T}_h^T$, hence the uniqueness of the projection implies

$$\Pi_h(\eta) = \tilde{\eta}. \tag{7.50}$$

■

In order to illustrate our discussion and to demonstrate the efficiency of finite element procedures obtained via mixed formulations, we compute finite element solutions with the scheme corresponding to P_1 displacements and rotations, and P_0 shear forces, to be compared with the displacement-based P_1 procedure used in Section 7.1 (with the same values of all parameters). We obtain the results shown in Table 7.2 and in Figure 7.5. Although we observe a slight sensitivity of the errors with respect to the thickness parameter in these numerical results, this sensitivity is clearly very limited as – for example – the convergence curves corresponding to $\varepsilon = 0.1$ and $\varepsilon = 0.01$ can hardly be distinguished in Figure 7.5. This is obviously very different from locking, for which the deterioration of convergence is unlimited when the thickness parameter tends to zero (compare with Figure 7.3). Therefore, the theoretical error analysis performed above is well confirmed by numerical results, in that the mixed formulation has indeed provided a very efficient (and easily implemented) treatment to locking in this case.

Remark 7.2.4. A direct consequence of the uniform convergence featured by the above mixed finite element method is that we have the convergence

Table 7.2. Values of $u_h^\varepsilon(L)/u^\varepsilon(L)$

N	$\varepsilon = 1.$	$\varepsilon = 0.1$	$\varepsilon = 0.01$
1	0.8654	0.7521	0.7500
10	0.9986	0.9975	0.9975
100	1.0000	1.0000	1.0000

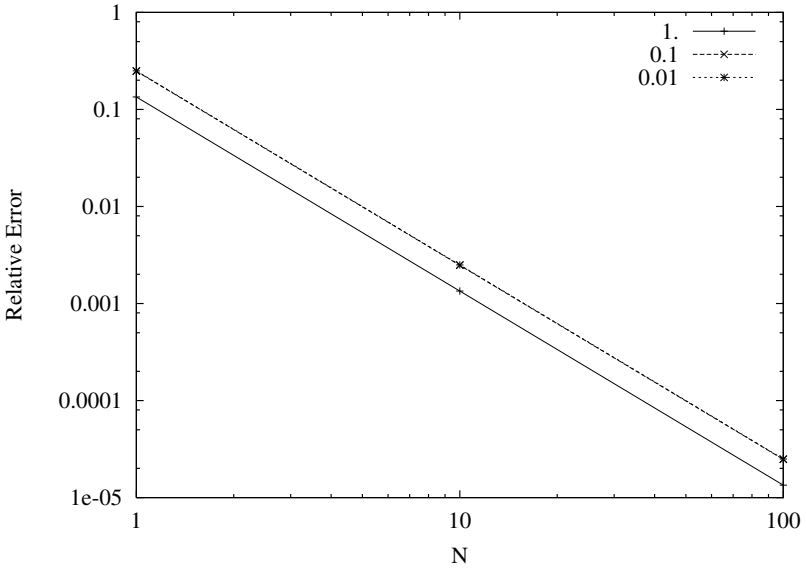

Fig. 7.5. Relative error in tip deflection for various values of ε

diagram given in Figure 7.6. This is called a commuting diagram, as the term in the bottom-right position can be reached from the upper-left term by two ways (namely, by making h and ε tend to zero in the two alternate orders). This is in contrast with the displacement-based formulation, for which we

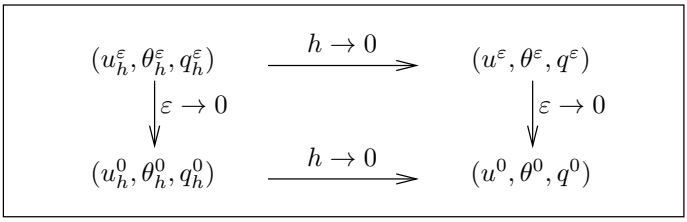

Fig. 7.6. Convergence diagram for mixed method

have the incomplete diagram given in Figure 7.7. ■

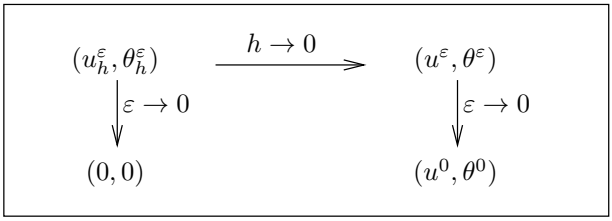

Fig. 7.7. Convergence diagram for displacement-based method

Remark 7.2.5. A very natural and important question to raise is whether the above-discussed difficulties related to small thickness parameters – i.e. numerical locking – and the corresponding remedies – namely, carefully designed mixed formulations satisfying the ellipticity and inf-sup conditions – are also applicable in dynamic analysis. Physically, we would expect this to be the case. This issue was addressed in detail in (Boffi et al., 1997) based on a spectral analysis of mixed formulations. The conclusion is that, considering the limit problem (i.e. vanishing thickness in the structural models considered here), the same ellipticity and inf-sup conditions governing static analysis are also *sufficient conditions* to ensure the convergence of the eigenvalues and eigenspaces of the mixed formulation. Note that the analysis of (Boffi et al., 1997) only covers the limit mixed formulation. Indeed, we conjecture that when considering the sequence of parameter-dependent mixed problems sufficient conditions for ensuring *uniform convergence* of eigenvalues and eigenspaces are instead given by the inf-sup condition and the specific coercivity condition (3.188). ■

7.2.2 Applications to the Reissner-Mindlin plate model

The purpose of this section is to demonstrate how mixed formulations can be used to "unlock" finite element approximations of the Reissner-Mindlin plate model. This can be seen as a preliminary step to the analysis of shell formulations since – compared to the Timoshenko beam model considered above – the plate model features the same two-dimensional character as the s-m-b shell model from which it can be derived (see Section 4.2.4).

We recall that the Reissner-Mindlin plate model can be expressed as
Find $(u, \underline{\theta})$ *in* $\mathcal{V}^{RM}$ *such that*

$$\int_\omega \frac{t^3}{12} {}^0C^{\alpha\beta\lambda\mu}\chi_{\alpha\beta}(\underline{\theta})\chi_{\lambda\mu}(\underline{\eta})\, dS + \int_\omega t\, {}^0D^{\alpha\lambda}\zeta_\alpha(u,\underline{\theta})\zeta_\lambda(v,\underline{\eta})\, dS = \int_\omega tFv\, dS, \quad \forall (v,\underline{\eta}) \in \mathcal{V}^{RM}. \tag{7.51}$$

Note that we have dropped the "3" subscript denoting the transverse components of the displacements and forces, since we are not concerned with the tangential components in this model. Setting

$$\boxed{\mathcal{V}^{RM} = \big\{(v,\underline{\eta}) \in H^1(\mathcal{S}) \times H^1(\mathcal{S})\big\} \cap \mathcal{BC},} \tag{7.52}$$

with the essential boundary conditions chosen in compatibility with H^1 and so that no global rigid body motion is possible, the mathematical analysis of the s-m-b shell model performed in Section 4.3.1 applies in this special case and shows that the Reissner-Mindlin plate model is well-posed (with, e.g., $F \in L^2$). Without loss of generality we will choose an orthonormal coordinate system with a fixed basis to describe the geometry, in which case we recall the simplified expression of the strain tensors

$$\begin{cases} \chi_{\alpha\beta}(\underline{\eta}) = \frac{1}{2}(\eta_{\alpha,\beta} + \eta_{\beta,\alpha}) \\ \zeta_\alpha(v,\underline{\eta}) = \frac{1}{2}(\eta_\alpha + v_{,\alpha}) \end{cases} \tag{7.53}$$

Following now the approach of Chapter 5 we define

$$\varepsilon = \frac{t}{L}, \tag{7.54}$$

where we assume – for simplicity – that t is constant. We also define

$$\boxed{\mathcal{V}_0^{RM} = \big\{(v,\underline{\eta}) \in \mathcal{V}^{RM} \mid \underline{\zeta}(v,\underline{\eta}) = \underline{0}\big\}.} \tag{7.55}$$

Here again, the pure bending displacement subspace $\mathcal{V}_0^{RM}$ is never restricted to the zero element, hence we are in a *bending-dominated situation*. As a consequence, we can scale the loading as

$$F = \varepsilon^3 G, \tag{7.56}$$

and we consider the sequence of problems
Find $(u^\varepsilon, \underline{\theta}^\varepsilon)$ *in* $\mathcal{V}^{RM}$ *such that*

$$\frac{L^3}{12}\int_\omega {}^0C^{\alpha\beta\lambda\mu}\chi_{\alpha\beta}(\underline{\theta}^\varepsilon)\chi_{\lambda\mu}(\underline{\eta})\,dS + \varepsilon^{-2}L\int_\omega {}^0D^{\alpha\lambda}\zeta_\alpha(u^\varepsilon,\underline{\theta}^\varepsilon)\zeta_\lambda(v,\underline{\eta})\,dS = L\int_\omega Gv\,dS, \quad \forall (v,\underline{\eta})\in \mathcal{V}^{RM}. \tag{7.57}$$

Clearly, we also have shear locking in this case when using displacement-based finite element procedures. In order to address this difficulty we define the auxiliary unknown $\underline{q}^\varepsilon$ such that

$$q_\alpha^\varepsilon\,(=q^{\varepsilon\alpha}) = \frac{\varepsilon^{-2}L}{2}{}^0D^{\alpha\lambda}\zeta_\alpha(u^\varepsilon,\underline{\theta}^\varepsilon), \tag{7.58}$$

namely,

$$\underline{q}^\varepsilon = \varepsilon^{-3}\frac{Et}{2(1+\nu)}(\underline{\theta}^\varepsilon + \underline{\nabla}u^\varepsilon), \tag{7.59}$$

which can be interpreted as a scaled shear force distribution, similarly to the Timoshenko beam model (compare with (7.12)). The quantity $\underline{q}^\varepsilon$ is in $L^2(\mathcal{S})$, and we have the equivalent mixed formulation
Find $\big((u^\varepsilon,\underline{\theta}^\varepsilon),\underline{q}^\varepsilon\big)$ *in* $\mathcal{V}^{RM}\times L^2(\mathcal{S})$ *such that*

$$\begin{cases} \dfrac{L^3}{12}\displaystyle\int_\omega {}^0C^{\alpha\beta\lambda\mu}\chi_{\alpha\beta}(\underline{\theta}^\varepsilon)\chi_{\lambda\mu}(\underline{\eta})\,dS + \int_\omega (\underline{\eta}+\underline{\nabla}v)\cdot\underline{q}^\varepsilon\,dS \\ \qquad\qquad = L\displaystyle\int_\omega Gv\,dS, \quad \forall (v,\underline{\eta})\in\mathcal{V}^{RM}, \\ \displaystyle\int_\omega (\underline{\theta}^\varepsilon+\underline{\nabla}u^\varepsilon)\cdot\underline{r}\,dS - \varepsilon^2\frac{2(1+\nu)}{EL}\int_\omega \underline{q}^\varepsilon\cdot\underline{r}\,dS = 0, \\ \qquad\qquad \forall \underline{r}\in L^2(\mathcal{S}). \end{cases} \tag{7.60}$$

We now have a mixed formulation of the type given in (3.153) and can denote

$$A_{\rm b}^{RM}(\underline{\theta},\underline{\eta}) = \frac{L^3}{12}\int_\omega {}^0C^{\alpha\beta\lambda\mu}\chi_{\alpha\beta}(\underline{\theta})\chi_{\lambda\mu}(\underline{\eta})\,dS, \tag{7.61}$$

$$B^{RM}(v,\underline{\eta};\underline{r}) = \int_\omega (\underline{\eta} + \underline{\nabla} v)\cdot \underline{r}\, dS, \tag{7.62}$$

$$D^{RM}(\underline{q},\underline{r}) = \frac{2(1+\nu)}{EL}\int_\omega \underline{q}^\varepsilon \cdot \underline{r}\, dS. \tag{7.63}$$

Compared to the strategy followed for the Timoshenko beam problem, however, we are now facing two difficulties:

- We *do not* have the continuous inf-sup condition

$$\inf_{\underline{r}\in\mathcal{T}^{RM},\underline{r}\neq\underline{0}}\ \sup_{(v,\underline{\eta})\in\mathcal{V}^{RM},(v,\underline{\eta})\neq(0,\underline{0})} \frac{B^{RM}(v,\underline{\eta};\underline{r})}{\|v,\underline{\eta}\|_{\mathcal{V}^{RM}}\|\underline{r}\|_{\mathcal{T}^{RM}}} \geq \delta > 0 \tag{7.64}$$

  for $\mathcal{T}^{RM} = L^2(\mathcal{S})$, see Example 7.2.1 below;
- We *do not* have the coercivity of the bilinear form $A_{\rm b}^{RM}$ over the *whole space* $\mathcal{V}^{RM}$, since this bilinear form does not contain the transverse displacement. Of course, it is coercive over $\mathcal{V}_0^{RM}$ since the coercivity of the s-m-b shell model for any finite value of the thickness implies in this case, for $\varepsilon = 1$,

$$A_{\rm b}^{RM}(\underline{\eta},\underline{\eta}) + L\int_\omega {}^0D^{\alpha\lambda}\zeta_\alpha(v,\underline{\eta})\zeta_\lambda(v,\underline{\eta})\, dS \geq \gamma\|v,\underline{\eta}\|_{\mathcal{V}^{RM}}, \forall (v,\underline{\eta})\in\mathcal{V}^{RM}, \tag{7.65}$$

  which – in turn – immediately implies

$$A_{\rm b}^{RM}(\underline{\eta},\underline{\eta}) \geq \gamma\|v,\underline{\eta}\|_{\mathcal{V}^{RM}}, \qquad \forall (v,\underline{\eta})\in\mathcal{V}_0^{RM}. \tag{7.66}$$

  So, even if we find a space $\mathcal{T}^{RM}$ (different from $L^2(\mathcal{S})$) in which the inf-sup condition holds, this partial coercivity will not allow us to apply Propositions 3.2.5 and 3.2.6. In addition, even when only considering the limit mixed problem of the type (3.92) and its finite element approximations, we will then have to enforce the corresponding discrete partial coercivity condition, namely

$$A_{\rm b}^{RM}(\underline{\eta},\underline{\eta}) \geq \gamma\|v,\underline{\eta}\|_{\mathcal{V}^{RM}}, \qquad \forall (v,\underline{\eta})\in\mathcal{V}_{h0}^{RM}, \tag{7.67}$$

  which together with the discrete inf-sup condition is difficult to achieve in practice.

The purpose of the discussion below will be to see how we can circumvent these two difficulties.

Example 7.2.1

Consider for instance the case of a fully clamped plate, namely $\mathcal{V}^{RM} =$

$H_0^1(\mathcal{S}) \times H_0^1(\mathcal{S})$. We want to show that the continuous inf-sup condition (7.64) does not hold with $\mathcal{T}^{RM} = L^2(\mathcal{S})$.

Let us assume that it holds. We then have, for any $\underline{r} \in \mathcal{T}^{RM}$,

$$\gamma \|\underline{r}\|_{L^2} \leq \sup_{(v,\underline{\eta}) \in \mathcal{V}^{RM}, (v,\underline{\eta}) \neq (0,\underline{0})} \frac{B^{RM}(v, \underline{\eta}; \underline{r})}{\|v, \underline{\eta}\|_{\mathcal{V}^{RM}}} \leq C \|\underline{r}\|_{L^2}, \tag{7.68}$$

where the lower bound is directly inferred from the inf-sup condition and the upper bound is obtained by simply applying the Cauchy-Schwarz inequality. This shows that the "sup" expression gives a norm equivalent to the L^2 norm. Consider now specific choices of $\underline{r}$ as

$$\underline{r} = \underline{\nabla}^{\perp} \phi, \tag{7.69}$$

for any ϕ in $H^1(\mathcal{S})$, viz.

$$r_1 = \phi_{,2}, \qquad r_2 = -\phi_{,1}. \tag{7.70}$$

Defining

$$\tilde{\phi} = \phi - \frac{\int_\omega \phi \, dS}{\int_\omega dS}, \tag{7.71}$$

we have, by construction,

$$\underline{\nabla}^{\perp} \phi = \underline{\nabla}^{\perp} \tilde{\phi}, \qquad \int_\omega \tilde{\phi} \, dS = 0. \tag{7.72}$$

Then, from (7.68),

$$\gamma |\tilde{\phi}|_{H^1} \leq \sup_{(v,\underline{\eta}) \in \mathcal{V}^{RM}, (v,\underline{\eta}) \neq (0,\underline{0})} \frac{B^{RM}(v, \underline{\eta}; \underline{\nabla}^{\perp} \phi)}{\|v, \underline{\eta}\|_{\mathcal{V}^{RM}}} \leq C |\tilde{\phi}|_{H^1}, \tag{7.73}$$

and this implies, by a standard "Poincaré type" inequality,

$$\gamma \|\tilde{\phi}\|_{H^1} \leq \sup_{(v,\underline{\eta}) \in \mathcal{V}^{RM}, (v,\underline{\eta}) \neq (0,\underline{0})} \frac{B^{RM}(v, \underline{\eta}; \underline{\nabla}^{\perp} \phi)}{\|v, \underline{\eta}\|_{\mathcal{V}^{RM}}} \leq C \|\tilde{\phi}\|_{H^1}. \tag{7.74}$$

On the other hand, it is straightforward to see that

$$\int_\omega \underline{\nabla} v \cdot \underline{\nabla}^{\perp} \phi \, dS = 0, \tag{7.75}$$

hence

$$\sup_{(v,\underline{\eta})\in\mathcal{V}^{RM},(v,\underline{\eta})\neq(0,\underline{0})} \frac{B^{RM}(v,\underline{\eta};\underline{\nabla}^{\perp}\phi)}{\|v,\underline{\eta}\|_{\mathcal{V}^{RM}}}$$

$$= \sup_{\underline{\eta}\in H_0^1(\mathcal{S}),\underline{\eta}\neq\underline{0}} \frac{\int_\omega \underline{\eta}\cdot\underline{\nabla}^{\perp}\phi\, dS}{\|\underline{\eta}\|_{H^1}}$$

$$= \sup_{\underline{\eta}\in H_0^1(\mathcal{S}),\underline{\eta}\neq\underline{0}} \frac{\int_\omega (\mathrm{rot}\,\underline{\eta})\,\phi\, dS}{\|\underline{\eta}\|_{H^1}}, \tag{7.76}$$

after integrating by part (with $\mathrm{rot}\,\underline{\eta} = \eta_{2,1} - \eta_{1,2}$). It is a classical result (see in particular (Ladyzhenskaya, 1969; Temam, 1977) where the equivalent form with the divergence operator was established and used for the analysis of the Stokes problem) that

$$\sup_{\underline{\eta}\in H_0^1(\mathcal{S}),\underline{\eta}\neq\underline{0}} \frac{\int_\omega (\mathrm{rot}\,\underline{\eta})\,\phi\, dS}{\|\underline{\eta}\|_{H^1}} \geq \gamma\|\tilde{\phi}\|_{L^2}, \tag{7.77}$$

and, of course, a Cauchy-Schwarz inequality provides the upper bound in

$$\gamma\|\tilde{\phi}\|_{L^2} \leq \sup_{(v,\underline{\eta})\in\mathcal{V}^{RM},(v,\underline{\eta})\neq(0,\underline{0})} \frac{B^{RM}(v,\underline{\eta};\underline{\nabla}^{\perp}\phi)}{\|v,\underline{\eta}\|_{\mathcal{V}^{RM}}} \leq C\|\tilde{\phi}\|_{L^2}. \tag{7.78}$$

Comparing (7.74) and (7.78) this implies that the H^1 and L^2 norms would be equivalent over the space of functions with zero mean value, which is – of course – wrong. Therefore, the continuous inf-sup condition cannot hold for $\mathcal{T}^{RM} = L^2(\mathcal{S})$. ∎

In the framework of the Reissner-Mindlin plate model, it is possible to identify the "natural norm" in the shear force space such that the continuous inf-sup condition holds, and a complete analysis of the corresponding functional space can be achieved. In particular, when the plate is totally clamped we have (Bathe & Brezzi, 1985; Brezzi & Fortin, 1991; Brezzi et al., 1991; Chapelle, 1993; Iosilevich et al., 1997).

$$\mathcal{T}^{RM} = H^{-1}(\mathrm{div};\mathcal{S}) = \left\{\underline{r}\in H^{-1}(\mathcal{S}) \mid \mathrm{div}\underline{r}\in H^{-1}(\mathcal{S})\right\}, \tag{7.79}$$

and also

$$\mathcal{T}^{RM} = \left(H_0(\mathrm{rot};\mathcal{S})\right)', \tag{7.80}$$

where

$$H_0(\mathrm{rot};\mathcal{S}) = \left\{\underline{\beta}\in L^2(\mathcal{S}) \mid \mathrm{rot}\underline{\beta}\in L^2(\mathcal{S}),\ \underline{\beta}\cdot\underline{t} = 0 \text{ on } \partial\mathcal{S}\right\}, \tag{7.81}$$

in which $\underline{t}$ denotes the unit tangent vector to the boundary $\partial\mathcal{S}$.

However, for shell mathematical models such an analysis does not appear to be at hand due to various complications. This difficulty can be circumvented by using the abstract norm introduced in Remark 3.2.8, namely,

$$\boxed{\|\underline{r}\|_{IS} = \sup_{(v,\underline{\eta})\in\mathcal{V}^{RM},(v,\underline{\eta})\neq(0,\underline{0})} \frac{B^{RM}(v,\underline{\eta};\underline{r})}{\|v,\underline{\eta}\|_{\mathcal{V}^{RM}}}.} \tag{7.82}$$

Note that this is – indeed – a norm in $L^2(\mathcal{S})$ since $\|\underline{r}\|_{IS} = 0$ gives

$$\int_\omega (\underline{\eta} + \underline{\nabla} v)\cdot \underline{r}\; dS = 0, \tag{7.83}$$

for any $(v,\underline{\eta}) \in \mathcal{V}^{RM}$, which implies that $\underline{r} = 0$. Of course, we have

$$\inf_{\underline{r}\in L^2(\mathcal{S}),\underline{r}\neq\underline{0}} \sup_{(v,\underline{\eta})\in\mathcal{V}^{RM},(v,\underline{\eta})\neq(0,\underline{0})} \frac{B^{RM}(v,\underline{\eta};\underline{r})}{\|v,\underline{\eta}\|_{\mathcal{V}^{RM}}\|\underline{r}\|_{IS}} = 1, \tag{7.84}$$

hence the continuous inf-sup condition is trivially satisfied for this norm, by construction. Therefore, we can invoke the coercivity of the Reissner-Mindlin bilinear form – which holds in particular for $\varepsilon = 1$ – to directly apply Proposition 3.2.7, which provides a uniform bound on the sequence of solutions as given in the following proposition.

Proposition 7.2.6 *The sequence of solutions* $\big((u^\varepsilon,\underline{\theta}^\varepsilon),\underline{q}^\varepsilon\big) \in \mathcal{V}^{RM}\times L^2(\mathcal{S})$ *satisfies the uniform bound*

$$\boxed{\|u^\varepsilon,\underline{\theta}^\varepsilon\|_{\mathcal{V}^{RM}} + \|\underline{q}^\varepsilon\|_{IS} + \varepsilon\|\underline{q}^\varepsilon\|_{L^2} \le C\|G\|_{L^2}.} \tag{7.85}$$

Remark 7.2.6. The uniform bound (7.85) is consistent with our above discussion on the fact that the L^2 norm is not appropriate for the shear space. Here we can see that – although $\underline{q}^\varepsilon$ is in L^2 for all finite values of ε – the L^2 estimate "blows up" when ε tends to zero, whereas the estimate on $\|\underline{q}^\varepsilon\|_{IS}$ is uniform in ε. Nevertheless, we have

$$\|\underline{r}\|_{IS} = \sup_{(v,\underline{\eta})\in\mathcal{V}^{RM},(v,\underline{\eta})\neq(0,\underline{0})} \frac{B^{RM}(v,\underline{\eta};\underline{r})}{\|v,\underline{\eta}\|_{\mathcal{V}^{RM}}} \ge \sup_{\underline{\eta}\neq\underline{0}} \frac{\int_\omega \underline{\eta}\cdot\underline{r}\; dS}{\|\underline{\eta}\|_{H^1}},$$

where $\underline{\eta}$ can be any admissible rotation vector satisfying the boundary conditions. Assuming for simplicity that the plate is completely clamped, we have

$$\sup_{\underline{\eta}\in H_0^1,\, \underline{\eta}\neq\underline{0}} \frac{\int_\omega \underline{\eta}\cdot\underline{r}\, dS}{\|\underline{\eta}\|_{H^1}} = \|\underline{r}\|_{H^{-1}}.$$

Hence

$$\|\underline{r}\|_{H^{-1}} \leq \|\underline{r}\|_{IS},$$

which shows that we can measure the solution $\underline{q}^\varepsilon$ in the H^{-1}-norm. This norm cannot be computed explicitly, but we can approximate its value based on the fact that

$$\|\underline{r}\|_{H^{-1}} = \|\underline{\theta}(\underline{r})\|_{H^1},$$

where $\underline{\theta}(\underline{r})$ is the vector of H_0^1 which satisfies the variational problem

$$\langle\, \underline{\theta}(\underline{r}), \underline{\eta}\,\rangle_{H^1} = \langle\, \underline{r}, \underline{\eta}\,\rangle_{H^{-1}\times H^1}, \quad \forall \underline{\eta}\in H_0^1.$$

An approximation of $\|\underline{r}\|_{H^{-1}}$ is then obtained by solving a finite element approximation of this variational problem using the same finite element space as for the plate problem. ■

We then consider the corresponding discrete inf-sup condition

$$\inf_{\underline{r}\in\mathcal{T}_h^{RM},\underline{r}\neq\underline{0}} \sup_{(v,\underline{\eta})\in\mathcal{V}_h^{RM},(v,\underline{\eta})\neq(0,\underline{0})} \frac{B^{RM}(v,\underline{\eta};\underline{r})}{\|v,\underline{\eta}\|_{\mathcal{V}^{RM}}\|\underline{r}\|_{IS}} \geq \gamma > 0, \tag{7.86}$$

to be satisfied for a given choice of discretization spaces $(\mathcal{V}_h^{RM}, \mathcal{T}_h^{RM})$. This condition looks difficult to work with due to the abstract character of the shear space norm. However, we can write the inf-sup condition in the equivalent – simpler – form

$$\begin{aligned} &\sup_{(v,\underline{\eta})\in\mathcal{V}_h^{RM},(v,\underline{\eta})\neq(0,\underline{0})} \frac{B^{RM}(v,\underline{\eta};\underline{r})}{\|v,\underline{\eta}\|_{\mathcal{V}^{RM}}} \\ &\qquad \geq \gamma \sup_{(v,\underline{\eta})\in\mathcal{V}^{RM},(v,\underline{\eta})\neq(0,\underline{0})} \frac{B^{RM}(v,\underline{\eta};\underline{r})}{\|v,\underline{\eta}\|_{\mathcal{V}^{RM}}}, \quad \forall \underline{r}\in\mathcal{T}_h^{RM}. \end{aligned} \tag{7.87}$$

The following result (sometimes referred to as "Fortin's trick" in the numerical analysis literature) then gives a convenient sufficient condition for this condition to hold.

Proposition 7.2.7 *Suppose that there exists a family of uniformly continuous linear operators Λ_h from $\mathcal{V}^{RM}$ to $\mathcal{V}_h^{RM}$, namely,*

$$\|\Lambda_h(v,\underline{\eta})\|_{\mathcal{V}^{RM}} \leq C\|v,\underline{\eta}\|_{\mathcal{V}^{RM}}, \tag{7.88}$$

and such that, for any $(v,\underline{\eta}) \in \mathcal{V}^{RM}$,

$$B^{RM}(v,\underline{\eta};\underline{r}) = B^{RM}(\Lambda_h(v,\underline{\eta});\underline{r}), \qquad \forall \underline{r} \in \mathcal{T}_h^{RM}. \tag{7.89}$$

Then (7.87) *holds.*

Proof. Consider an arbitrary $\underline{r} \in \mathcal{T}_h^{RM}$. Then, for any $(w,\underline{\tau}) \neq (0,\underline{0})$ in $\mathcal{V}^{RM}$, successively using (7.89) and (7.88) we have

$$\frac{B^{RM}(w,\underline{\tau};\underline{r})}{\|w,\underline{\tau}\|_{\mathcal{V}^{RM}}} = \frac{B^{RM}(\Lambda_h(w,\underline{\tau});\underline{r})}{\|w,\underline{\tau}\|_{\mathcal{V}^{RM}}} \leq C\frac{B^{RM}(\Lambda_h(w,\underline{\tau});\underline{r})}{\|\Lambda_h(w,\underline{\tau})\|_{\mathcal{V}^{RM}}}, \tag{7.90}$$

provided that $\Lambda_h(w,\underline{\tau}) \neq (0,\underline{0})$. Then, under this same condition we have

$$\frac{B^{RM}(w,\underline{\tau};\underline{r})}{\|w,\underline{\tau}\|_{\mathcal{V}^{RM}}} \leq C \sup_{(v,\underline{\eta})\in\mathcal{V}_h^{RM},(v,\underline{\eta})\neq(0,\underline{0})} \frac{B^{RM}(v,\underline{\eta};\underline{r})}{\|v,\underline{\eta}\|_{\mathcal{V}^{RM}}}. \tag{7.91}$$

Note furthermore that this bound still holds when $(w,\underline{\tau})$ is such that $\Lambda_h(w,\underline{\tau}) = (0,\underline{0})$ because (7.89) then implies

$$B^{RM}(w,\underline{\tau};\underline{r}) = 0. \tag{7.92}$$

Therefore, since the bound holds for any non-zero $(w,\underline{\tau})$ it also holds for the sup, i.e.

$$\sup_{(v,\underline{\eta})\in\mathcal{V}^{RM},(v,\underline{\eta})\neq(0,\underline{0})} \frac{B^{RM}(v,\underline{\eta};\underline{r})}{\|v,\underline{\eta}\|_{\mathcal{V}^{RM}}} \leq C \sup_{(v,\underline{\eta})\in\mathcal{V}_h^{RM},(v,\underline{\eta})\neq(0,\underline{0})} \frac{B^{RM}(v,\underline{\eta};\underline{r})}{\|v,\underline{\eta}\|_{\mathcal{V}^{RM}}}, \tag{7.93}$$

which directly implies (7.87). ∎

Remark 7.2.7. In fact, it can be shown that the existence of the operator defined in Proposition 7.2.7 is also a necessary condition for (7.87), see in particular (Brezzi & Fortin, 1991), hence we have a complete equivalence. ∎

As emphasized above, we are also concerned with the partial coercivity of A_{b}^{RM}. Recalling the proofs of the general convergence results given in

Propositions 3.2.6 and 3.2.11 we can see that the difficulty will be to establish the stability of the bilinear form

$$\boxed{\begin{aligned} &M_\varepsilon^{RM}\big((u,\underline{\theta}),\underline{q};(v,\underline{\eta}),\underline{r}\big) = \\ &\quad A_{\mathrm{b}}^{RM}(\underline{\theta},\underline{\eta}) + B^{RM}(v,\underline{\eta};\underline{q}) + B^{RM}(u,\underline{\theta};\underline{r}) - \varepsilon^2 D^{RM}(\underline{q},\underline{r}) \end{aligned}} \tag{7.94}$$

in the finite element displacement subspace $\mathcal{V}_h^{RM}$. Although this has been achieved for specific discretizations, it is very difficult to achieve when looking for practical and effective finite element discretizations, especially since it must be obtained *in conjunction* with the inf-sup condition (7.87). As discussed in Section 3.2.1, it is possible, however, to circumvent this difficulty by considering the modified bilinear form

$$\boxed{\begin{aligned} &\tilde{M}_\varepsilon^{RM}\big((u,\underline{\theta}),\underline{q};(v,\underline{\eta}),\underline{r}\big) = M_\varepsilon^{RM}\big((u,\underline{\theta}),\underline{q};(v,\underline{\eta}),\underline{r}\big) \\ &+ \frac{2\alpha EL}{1+\nu}\int_\omega \Big(\underline{\zeta}(u,\underline{\theta}) - \varepsilon^2\frac{1+\nu}{EL}\underline{q}\Big)\cdot\Big(\underline{\zeta}(v,\underline{\eta}) - \varepsilon^2\frac{1+\nu}{EL}\underline{r}\Big)\,dS, \end{aligned}} \tag{7.95}$$

where α is a strictly positive parameter to be specified. As noted in Section 3.2.1, the perturbation added to the original bilinear form is *consistent*, namely, we have for the exact solution $\big((u^\varepsilon,\underline{\theta}^\varepsilon),\underline{q}^\varepsilon\big)$

$$\tilde{M}_\varepsilon^{RM}\big((u^\varepsilon,\underline{\theta}^\varepsilon),\underline{q}^\varepsilon;(v,\underline{\eta}),\underline{r}\big) = M_\varepsilon^{RM}\big((u^\varepsilon,\underline{\theta}^\varepsilon),\underline{q}^\varepsilon;(v,\underline{\eta}),\underline{r}\big), \tag{7.96}$$

for any $\big((v,\underline{\eta}),\underline{r}\big) \in \mathcal{V}^{RM}\times L^2(\mathcal{S})$, since

$$\underline{\zeta}(u^\varepsilon,\underline{\theta}^\varepsilon) = \varepsilon^2\frac{1+\nu}{EL}\underline{q}^\varepsilon. \tag{7.97}$$

Therefore, we have that $\big((u^\varepsilon,\underline{\theta}^\varepsilon),\underline{q}^\varepsilon\big)$ satisfies the variational problem

$$\begin{aligned} \tilde{M}_\varepsilon^{RM}\big(((u^\varepsilon,\underline{\theta}^\varepsilon),\underline{q}^\varepsilon;(v,\underline{\eta}),\underline{r}\big) &= L\int_\omega Gv\,dS, \\ &\forall\big((v,\underline{\eta}),\underline{r}\big)\in\mathcal{V}^{RM}\times L^2(\mathcal{S}). \end{aligned} \tag{7.98}$$

and we can take this formulation (rather than the original formulation (7.60)) as the basis for a finite element discretization which thus writes
Find $\big((u_h^\varepsilon,\underline{\theta}_h^\varepsilon),\underline{q}_h^\varepsilon\big)$ *in* $\mathcal{V}_h^{RM}\times\mathcal{T}_h^{RM}$ *such that*

$$\tilde{M}_\varepsilon^{RM}\big((u_h^\varepsilon,\underline{\theta}_h^\varepsilon),\underline{q}_h^\varepsilon;(v,\underline{\eta}),\underline{r}\big)=L\int_\omega Gv\,dS,\qquad \forall\big((v,\underline{\eta}),\underline{r}\big)\in\mathcal{V}_h^{RM}\times\mathcal{T}_h^{RM}. \tag{7.99}$$

With this discrete problem we have the following convergence result, directly implied by Proposition 3.2.8.

Proposition 7.2.8 *Assume that* (7.87) *holds and that* $0<\alpha<1$. *Then, for any* $\varepsilon\le 1$ *the discrete problem* (7.99) *has a unique solution and this solution satisfies*

$$\begin{aligned}\|u^\varepsilon-u_h^\varepsilon,\underline{\theta}^\varepsilon-\underline{\theta}_h^\varepsilon\|_{\mathcal{V}^{RM}}+\|\underline{q}^\varepsilon-\underline{q}_h^\varepsilon\|_{IS}+\varepsilon\|\underline{q}^\varepsilon-\underline{q}_h^\varepsilon\|_{L^2}\\ \le C\inf_{\big((v,\underline{\eta}),\underline{r}\big)\in\mathcal{V}_h^{RM}\times\mathcal{T}_h^{RM}}\Big\{\|u^\varepsilon-v,\underline{\theta}^\varepsilon-\underline{\eta}\|_{\mathcal{V}^{RM}}\\ +\|\underline{q}^\varepsilon-\underline{r}\|_{IS}+\varepsilon\|\underline{q}^\varepsilon-\underline{r}\|_{L^2}\Big\}.\end{aligned} \tag{7.100}$$

Remark 7.2.8. In numerical practice, it is usually better to avoid – whenever possible – adding stabilization terms to a formulation in mechanics, in particular when these terms depend on parameters for which the numerical analysis gives no (or very little) information as to how they should be chosen. However, for the stabilization term considered here the bounds within which this parameter may vary are clearly identified (namely, the interval $]0,1[$) and do not depend on the particular problem analyzed (only L, the overall characteristic dimension is problem-dependent, but this is a physical quantity). In addition, numerical experiments show that the performance is not very sensitive to the choice of α (Chapelle & Stenberg, 1998a), so we can choose, for example, $\alpha=1/2$. ■

For practical implementation purposes, we can perform an elimination of the shear force unknown in the discrete problem, as in the case of the Timoshenko beam mixed formulation. Varying only $\underline{r}$ in (7.99) we obtain

$$2(1-\alpha\varepsilon^2)\Big(\Pi_h\big(\underline{\zeta}(u^\varepsilon,\underline{\theta}^\varepsilon)\big)-\varepsilon^2\frac{1+\nu}{EL}\underline{q}_h^\varepsilon\Big)=\underline{0}, \tag{7.101}$$

hence, with $0<\alpha<1$ and $\varepsilon\le 1$,

$$\underline{q}_h^\varepsilon=\varepsilon^{-2}\frac{EL}{1+\nu}\Pi_h\big(\underline{\zeta}(u^\varepsilon,\underline{\theta}^\varepsilon)\big), \tag{7.102}$$

where Π_h denotes – as before – the L^2-projection onto the space $\mathcal{T}_h^{RM}$. Here also, this projection can be calculated element-wise when the discrete space $\mathcal{T}_h^{RM}$ consists of functions which can be chosen independently in each element (namely, discontinuously). Substituting then $\underline{q}_h^\varepsilon$ in (7.99) and varying only $(v, \underline{\eta})$ we have

$$\begin{aligned} &A_{\mathrm{b}}^{RM}(\underline{\theta}_h^\varepsilon, \underline{\eta}) \\ &+ (\varepsilon^{-2} - \alpha)\frac{2EL}{1+\nu}\int_\omega \Pi_h\big(\underline{\zeta}(u_h^\varepsilon, \underline{\theta}_h^\varepsilon)\big)\cdot \Pi_h\big(\underline{\zeta}(v, \underline{\eta})\big)\, dS \\ &+ \alpha\frac{2EL}{1+\nu}\int_\omega \underline{\zeta}(u_h^\varepsilon, \underline{\theta}_h^\varepsilon)\cdot \underline{\zeta}(v, \underline{\eta})\, dS = L\int_\omega Gv\, dS, \end{aligned} \tag{7.103}$$

for all $(v, \underline{\eta})$ in $\mathcal{V}_h^{RM}$. This shows that the mixed formulation is easy to implement (provided that the shear is discretized discontinuously), and that it does not induce much additional computational cost since the above discrete problem is purely displacement-based.

Remark 7.2.9. Setting $\alpha = 0$ in (7.103), we would obtain a discrete problem similar to that deduced from the Timoshenko beam mixed formulation, see Eq. (7.45). However, with the projection operator acting on the shear strains this formulation would not be stable in general. From this equation, we see that the effect of the additional term in the mixed formulation is to retain a fraction of the original – unprojected – shear deformation energy to preserve the coercivity, which is how the stabilization works. This stabilization strategy has been proposed in several references, see e.g. (Pitkäranta, 1992; Chapelle, 1993; Arnold & Brezzi, 1993; Bathe, 1996). ■

Remark 7.2.10. The full equivalence between the mixed formulation and "reduced integration" mentioned already above only holds for very specific formulations, and also depends on the geometry of the elements and material properties used. The value of the equivalence lies in that in these specific cases the equivalence can be used to evaluate in an efficient manner the element matrices of the mixed formulation, for an example see Section 7.2.1. Since this full equivalence is rather rare, some other analysis of a reduced integration scheme, even of an approximate nature, to identify whether a stable and convergent method is obtained needs to be pursued before the reduced integration scheme can be employed with confidence. For examples

of what can go wrong in the use of reduced integration, see (Bathe, 1996, pp. 472–478). ■

We now consider an example to show how we can construct finite element spaces $\mathcal{V}_h^{RM}$ and T_h^{RM} such that the crucial inf-sup condition (7.87) holds. Say that we want to use triangular elements and piecewise-constant shear forces, namely

$$\boxed{T_h^{RM} = \big\{\underline{r} \in L^2(\mathcal{S}) \mid \ \underline{r}|_K \in P_0 \ \forall K\big\},} \tag{7.104}$$

where "$\forall K$" means "in each element K in the mesh". This is the "simplest choice" for the discrete shear space. We then need to find a space $\mathcal{V}_h^{RM}$ and an operator Λ_h such that (7.88) and (7.89) hold. Let us look for an operator that acts independently on v and $\underline{\eta}$, so that we write (by a slight abuse of notation)

$$\Lambda_h(v, \underline{\eta}) = \big(\Lambda_h(v), \Lambda_h(\underline{\eta})\big). \tag{7.105}$$

Then (7.89) reduces to imposing for all $(v, \underline{\eta})$ in $\mathcal{V}^{RM}$

$$\int_K \Lambda_h(\underline{\eta})\, dS = \int_K \underline{\eta}\, dS, \qquad \forall K, \tag{7.106}$$

and

$$\begin{aligned} &\int_K \underline{\nabla} \Lambda_h(v)\, dS = \int_K \underline{\nabla} v\, dS, \qquad \forall K, \\ \iff \quad &\int_{\partial K} \Lambda_h(v)\, \underline{n}\, ds = \int_{\partial K} v\, \underline{n}\, ds, \qquad \forall K, \end{aligned} \tag{7.107}$$

where ds here denotes the integration along the boundary parametrized by arc-length, and $\underline{n}$ the outward unit normal vector to the boundary (note that (7.107) was obtained by an integration by parts). In order to enforce (7.106) it is then natural to use internal degrees of freedom for the rotation, whereas we will use edge degrees of freedom for the displacement in order to obtain (7.107). We thus use the following displacement space

$$\boxed{\mathcal{V}_h^{RM} = \{(v, \underline{\eta}) \in \mathcal{V}^{RM} \mid \ v|_K \in P_2,\ \underline{\eta}|_K \in P_1 \oplus B_3,\ \forall K\},} \tag{7.108}$$

where B_3 denotes the cubic bubble inside each element. Figure 7.8 summarizes the finite element spaces considered. This finite element method was originally proposed and analyzed in (Arnold & Brezzi, 1993; Chapelle, 1993). We now show that it satisfies the inf-sup condition.

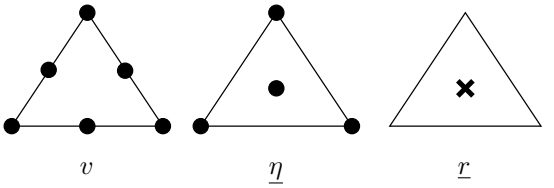

Fig. 7.8. Finite element spaces used

Proposition 7.2.9 *With the choices given in* (7.104) *and* (7.108)*, the inf-sup condition* (7.87) *is satisfied.*

Proof. We will construct an operator Λ_h acting indepently on the displacement and rotation and satisfying (7.88), (7.106) and (7.107) (hence also (7.89)).

i) *Construction of* $\Lambda_h(\underline{\eta})$. We start by defining Λ_1 as the classical Clément interpolation operator[1] into the space of continuous piecewise-P_1 functions. On each triangle K in the mesh, this operator satisfies (Clément, 1975)

$$\|\underline{\eta}-\Lambda_1(\underline{\eta})\|_{L^2(K)}+h_K|\underline{\eta}-\Lambda_1(\underline{\eta})|_{H^1(K)} \leq C \sum_{\partial K'\cap\partial K\neq\emptyset} h_{K'}|\underline{\eta}|_{H^1(K')}, \quad (7.109)$$

where the summation sign applies on every element K' adjacent to K and on K itself. We then construct Λ_2 as the operator from $H^1(\mathcal{S})$ into the space of piecewise-polynomials whose restriction to each element is a cubic bubble, by imposing that

$$\int_K \big(\underline{\eta} - \Lambda_2(\underline{\eta})\big)\, dS = 0, \qquad \forall K. \quad (7.110)$$

A standard scaling argument then gives

$$\|\underline{\eta} - \Lambda_2(\underline{\eta})\|_{H^1(K)} \leq C\big(h_K^{-1}\|\underline{\eta}\|_{L^2(K)} + |\underline{\eta}|_{H^1(K)}\big). \quad (7.111)$$

Setting next

$$\Lambda_h(\underline{\eta}) = \Lambda_1(\underline{\eta}) + \Lambda_2\big(\underline{\eta} - \Lambda_1(\underline{\eta})\big), \quad (7.112)$$

we have $\Lambda_h(\underline{\eta}) \in \mathcal{V}_h^{RM}$ when $\underline{\eta} \in \mathcal{V}^{RM}$, and combining (7.109) and (7.111) we get

[1] The Clément interpolation operator is most valuable when considering functions that cannot be interpolated in the usual sense, such as for H^1 functions which are not continuous, in general. Instead of using pointwise values which are not available in such cases, it is defined by considering (integrated) mean values of the function over neighboring elements.

$$\|\Lambda_h(\underline{\eta})\|_{H^1} \leq C\|\underline{\eta}\|_{H^1}. \tag{7.113}$$

In addition, (7.110) implies that (7.106) is satisfied.

ii) *Construction of* $\Lambda_h(v)$ *and conclusion.* We again use the Clément operator to define Λ_3 satisfying

$$\|v-\Lambda_3(v)\|_{L^2(K)}+h_K|v-\Lambda_3(v)|_{H^1(K)} \leq C \sum_{\partial K'\cap\partial K\neq\emptyset} h_{K'}|v|_{H^1(K')}. \tag{7.114}$$

Then we construct Λ_4 from $H^1(\mathcal{S})$ into the space of continuous piecewise-P_2 functions (corresponding to the discrete transverse displacement space) by setting the degrees of freedom at all vertices to zero and the mid-edge degrees of freedom so that

$$\int_E \big(v - \Lambda_4(v)\big)\, ds = 0, \tag{7.115}$$

on any internal edge E in the mesh. A scaling argument provides a bound similar to (7.111), namely

$$\|v - \Lambda_4(v)\|_{H^1(K)} \leq C\big(h_K^{-1}\|v\|_{L^2(K)} + |v|_{H^1(K)}\big). \tag{7.116}$$

Taking

$$\Lambda_h(v) = \Lambda_3(v) + \Lambda_4\big(v - \Lambda_3(v)\big), \tag{7.117}$$

$\Lambda_h(v)$ is in $\mathcal{V}_h^{RM}$, and we have by combining (7.114) and (7.116)

$$\|\Lambda_h(v)\|_{H^1} \leq C\|v\|_{H^1}. \tag{7.118}$$

Finally, (7.115) implies that Λ_h satisfies (7.107). ∎

We have thus obtained a locking-free finite element procedure for Reissner-Mindlin plates, as implied by the uniform error estimate (7.100). Numerical experiments also demonstrate that this finite element procedure performs well (Chinosi & Lovadina, 1995; Chapelle & Stenberg, 1998a). However, an important shortcoming of this scheme is that the approximation spaces are unbalanced, so that the error estimate provided by (7.100) will be limited by the space of lowest approximation capability, namely the error will be $O(h)$ here due to the approximation of the rotation and of the shear stress whereas the transverse displacement is approximated by quadratic functions. Although this finite element procedure can be improved (Chapelle & Stenberg, 1998a), it is nevertheless unpractical to work with an element which does not have all its degrees of freedom (at least for the transverse displacement and the rotation) at the same nodes.

7.2.3 Basic principles of *stabilized* mixed formulations

The approach that we have demonstrated using the example of the Reissner-Mindlin plate problem is very general and can be also applied – in principle – to shell models. In particular, the results given in Propositions 7.2.6 to 7.2.8 only make use of the general expression of the variational problem in the form of (5.38). But, of course, in shell models the expression of A_{m} is different because

- it contains the membrane energy in addition to the shear energy present in plates;
- the strain terms – including the shear strains – contain some geometric coefficients that account for the fact that the shell is not planar (e.g. the curvature terms).

Therefore – of course – the analysis performed on the finite element procedure considered in Proposition 7.2.9 does not hold for shells.

In fact, due to the above two complications present in shells, the crucial inf-sup condition (7.87) has so far resisted all attempts of proofs for general shell geometries (even by using the convenient methodology provided by Fortin's trick, namely Prop. 7.2.7). This is why it may be valuable to design finite element procedures that do not require an inf-sup condition to hold, which is a major motivation of *stabilized mixed formulations*. We now give a simplified analysis of an example of mixed stabilized formulation, using again the Reissner-Mindlin plate model to demonstrate the basic principles. We refer to (Lyly & Stenberg, 1999) for a comprehensive analysis of such formulations for plates and for a detailed bibliography regarding stabilized mixed formulations in general, see also (Hughes & Franca, 1988). In addition, we refer to (Chapelle & Stenberg, 1998b) where such schemes are proposed and analyzed for the s-m-b shell model.

First, let us denote by $\underline{\mathcal{L}}$ the second-order differential operator such that

$$\frac{L^3}{12}\int_\omega {}^0C^{\alpha\beta\lambda\mu}\chi_{\alpha\beta}(\underline{\theta})\chi_{\lambda\mu}(\underline{\eta})\,dS = -\int_\omega \underline{\mathcal{L}}(\underline{\theta})\cdot\underline{\eta}\,dS, \tag{7.119}$$

for any smooth functions $\underline{\theta}$ and $\underline{\eta}$ with zero boundary conditions all around the domain. Note that $\underline{\mathcal{L}}$ is obtained by an integration by parts, and that the same manipulation performed in the first equation of (7.60) gives the equilibrium equation

$$-\underline{\mathcal{L}}(\underline{\theta}^\varepsilon) + \underline{q}^\varepsilon = \underline{0}, \tag{7.120}$$

corresponding to the test function $\underline{\eta}$. We also point out that $\underline{\mathcal{L}}(\underline{\theta})$ contains derivatives of $\underline{\theta}$ of order two only. Introducing the notation

$$d_K = \frac{h_K}{L}, \tag{7.121}$$

we define the new bilinear form

$$\begin{aligned}\tilde{M}^{RM}_{\varepsilon,h}\big((u,\underline{\theta}),\underline{q};(v,\underline{\eta}),\underline{r}\big) &= M^{RM}_{\varepsilon}\big((u,\underline{\theta}),\underline{q};(v,\underline{\eta}),\underline{r}\big)\\ &+\alpha\sum_K(\varepsilon^2+d_K^2)^{-1}\frac{2EL}{1+\nu}\int_K\Big(\underline{\zeta}(u,\underline{\theta})-\varepsilon^2\frac{1+\nu}{EL}\underline{q}\Big)\\ &\qquad\cdot\Big(\underline{\zeta}(v,\underline{\eta})-\varepsilon^2\frac{1+\nu}{EL}\underline{r}\Big)\,dS\\ &-\beta\sum_K\frac{d_K^2}{EL}\int_K\big(\underline{q}-\underline{\mathcal{L}}(\underline{\theta})\big)\cdot\big(\underline{r}-\underline{\mathcal{L}}(\underline{\eta})\big)\,dS,\end{aligned}\tag{7.122}$$

Note that we have retained the same kind of stabilization parameter as in (7.95), but we have "substituted" $\alpha(\varepsilon^2+d_K^2)^{-1}$ for α as a weight for this term, i.e. we have increased the weight of this stabilization term since ε and d_K are intended to be small. In addition, we have introduced a new term using the equilibrium equation (7.120), with a coefficient β to be specified also. We point out that – like for $\tilde{M}^{RM}_{\varepsilon}$ in (7.95) – the modifications introduced here are consistent, i.e. they vanish for the exact solution. Then we consider the new finite element problem
Find $\big((u_h^\varepsilon,\underline{\theta}_h^\varepsilon),\underline{q}_h^\varepsilon\big)$ *in* $\mathcal{V}_h^{RM}\times\mathcal{T}_h^{RM}$ *such that*

$$\begin{aligned}\tilde{M}^{RM}_{\varepsilon,h}\big((u_h^\varepsilon,\underline{\theta}_h^\varepsilon),\underline{q}_h^\varepsilon;(v,\underline{\eta}),\underline{r}\big) &= L\int_\omega Gv\,dS,\\ &\qquad\forall\big((v,\underline{\eta}),\underline{r}\big)\in\mathcal{V}_h^{RM}\times\mathcal{T}_h^{RM}.\end{aligned}\tag{7.123}$$

In this formulation we denote the (tentative) solution by $\big((u_h^\varepsilon,\underline{\theta}_h^\varepsilon),\underline{q}_h^\varepsilon\big)$ like in (7.99) for simplicity of notation, but of course the two formulations are different and will lead to different solutions in general. We show below that the new bilinear form $\tilde{M}^{RM}_{\varepsilon,h}$ is bounded and stable for a specific norm, given by

$$\begin{aligned}\|(v,\underline{\eta}),\underline{r}\|_{\varepsilon,h} &=\\ &\Big(\|v,\underline{\eta}\|^2_{RM}+\sum_K(\varepsilon^2+d_K^2)^{-1}\|\underline{\zeta}(v,\underline{\eta})\|^2_{L^2(K)}\\ &\qquad+\varepsilon^2\|\underline{r}\|^2_{L^2}+\sum_K d_K^2\|\underline{r}\|^2_{L^2(K)}\Big)^{\frac12},\end{aligned}\tag{7.124}$$

which can be used to obtain a uniform error estimate.

Remark 7.2.11. Although the coefficient $(\varepsilon^2 + d_K^2)^{-1}$ featured in the above norm is large, the corresponding part of the norm is not expected to dominate the whole expression *for the displacements and rotations of interest* since for the exact solution, in particular, $\varepsilon^{-2}\|\underline{\zeta}(u^\varepsilon, \underline{\theta}^\varepsilon)\|_{L^2}$ tends to zero with ε (recall Chapter 5). In fact, denoting by

$$\underline{r}^{DB}(v, \underline{\eta}) = \varepsilon^{-2} \frac{EL}{1+\nu} \underline{\zeta}(v, \underline{\eta}) \tag{7.125}$$

the shear force directly computed from the displacements and rotations, the specific part considered in the above norm is equivalent to

$$\sum_K \frac{\varepsilon^4}{\varepsilon^2 + d_K^2} \|\underline{r}^{DB}(v, \underline{\eta})\|^2_{L^2(K)} \tag{7.126}$$

and (using $\varepsilon^2 + d_K^2 > \varepsilon^2$) this expression is bounded by $\varepsilon^2 \|\underline{r}^{DB}(v, \underline{\eta})\|^2_{L^2}$, to be compared with the term $\varepsilon^2 \|\underline{r}\|^2_{L^2}$ used in the norm. ■

The stability argument given below will require the inequality

$$\frac{d_K^2}{EL} \|\underline{\mathcal{L}}(\underline{\eta})\|^2_{L^2(K)} \leq C_I \frac{L^3}{12} \int_K {}^0C^{\alpha\beta\lambda\mu} \chi_{\alpha\beta}(\underline{\eta}) \chi_{\lambda\mu}(\underline{\eta})\, dS, \qquad \forall K, \tag{7.127}$$

for any $\underline{\eta}$ in the *finite element space*. This is called an *inverse inequality* and it can be established by scaling arguments (see e.g. (Ciarlet, 1978)). We then have the following result.

Proposition 7.2.10 *Assume that* $0 < \alpha < 1$ *and that* $0 < \beta < C_I^{-1}$. *Then the bilinear form* $\tilde{M}^{RM}_{\varepsilon,h}$ *is bounded and stable for the norm* $\|\cdot\|_{\varepsilon,h}$.

Proof. We only sketch this proof, and refer to (Lyly & Stenberg, 1999) for more details. The boundedness is straightforward and we focus on the stability. For any $\big((v, \underline{\eta}), \underline{r}\big) \in \mathcal{V}_h^{RM} \times \mathcal{T}_h^{RM}$, take $(w, \underline{\tau}) = (v, \underline{\eta})$ and $\underline{s} = -\underline{r}$. We then have

$$\|(w, \underline{\tau}), \underline{s}\|_{\varepsilon,h} = \|(v, \underline{\eta}), \underline{r}\|_{\varepsilon,h}, \tag{7.128}$$

and

$$
\begin{aligned}
&\tilde{M}^{RM}_{\varepsilon,h}\big((v,\underline{\eta}),\underline{r};(w,\underline{\tau}),\underline{s}\big)\\
&\quad= A^{RM}_{\mathrm{b}}(\underline{\eta},\underline{\eta})+\alpha\frac{2EL}{1+\nu}\sum_K(\varepsilon^2+d_K^2)^{-1}\|\underline{\zeta}(v,\underline{\eta})\|^2_{L^2(K)}\\
&\qquad+\frac{1}{EL}\sum_K\Big(2(1+\nu)\varepsilon^2\big(1-\alpha\frac{\varepsilon^2}{\varepsilon^2+d_K^2}\big)+\beta d_K^2\Big)\|\underline{r}\|^2_{L^2(K)}\\
&\qquad-\beta\sum_K\frac{d_K^2}{EL}\|\underline{\mathcal{L}}(\underline{\eta})\|^2_{L^2(K)}\\
&\quad\geq\ \gamma\|(v,\underline{\eta}),\underline{r}\|^2_{\varepsilon,h},
\end{aligned}
\tag{7.129}
$$

using the inverse inequality (7.127), $\beta C_I<1$, and

$$
1-\alpha\frac{\varepsilon^2}{\varepsilon^2+d_K^2}>1-\alpha>0. \tag{7.130}
$$

■

We emphasize that Proposition 7.2.10 is valid *without any particular assumption* on the finite element spaces $\mathcal{V}_h^{RM}$ and $\mathcal{T}_h^{RM}$. Therefore we have indeed succeeded in circumventing *both* the coercivity condition in the displacement space *and* the inf-sup condition (7.87), with the use of the above two stabilization terms. This is precisely the objective of stabilized mixed formulations. On the other hand, while the same comments as in Remark 7.2.8 hold for the choice of the α parameter, the choice of β is more difficult because it depends on the inverse inequality constant C_I, which itself depends on the finite element spaces (and on the meshes) used.

Remark 7.2.12. In each element K, the best constant (namely, the smallest) that satisfies (7.127) is the solution of a local eigenvalue problem. Therefore, in practice β could be chosen by computing – during the assembling process – this smallest eigenvalue $C_{I,K}$ and by taking in each element, e.g., $(C_{I,K}^{-1})/2$ as a local value for β. It can then be checked that the stability proof still holds. Of course, this methodology induces some significant additional cost.

■

Remark 7.2.13. If we choose a discontinuous finite element space for the shear, the corresponding degrees of freedom can still be eliminated at the element level, thereby providing an equivalent problem with displacement degrees of freedom only. Compared to (7.103), however, the second part of

the modified bilinear form is much more complicated and – in particular – also contains terms in $\underline{\mathcal{L}}(\underline{\theta})$ (and not only shear strain terms). ■

Remark 7.2.14. With the mixed stabilized formulation considered here, there is a difficulty which does not appear in the above stability argument. This difficulty indeed arises when seeking an interpolation estimate in the norm defined in (7.124). This can be seen by considering the limit case "$\varepsilon = 0$". Then, focusing on the displacement and rotation, an interpolation estimate is given by the quantity

$$\Big(\|u^0 - v, \underline{\theta}^0 - \underline{\eta}\|_{RM}^2 + \sum_K d_K^{-2} \|\underline{\zeta}(u^0 - v, \underline{\theta}^0 - \underline{\eta})\|_{L^2(K)}^2\Big)^{\frac{1}{2}}, \tag{7.131}$$

for the limit solution $(u^0, \underline{\theta}^0)$ and a well-chosen finite element displacement/rotation couple. Recalling the expression of the shear strain, we infer that – in essence – the interpolation estimate is governed by

$$h^{-1}\|u^0 - v\|_{H^1} + \|\underline{\theta}^0 - \underline{\eta}\|_{H^1}. \tag{7.132}$$

This leads to using higher-order discretizations for the displacement than for the rotation (note that, in particular, piecewise-linear displacements cannot be used), which is not convenient in practice. However, this limitation can be circumvented by considering more complex stabilized formulations, see (Lyly & Stenberg, 1999). ■

7.2.4 MITC plate elements

The family of plate elements named MITC plate elements (MITC standing for "Mixed Interpolation of Tensorial Components") is based on ideas that were inspired from the formulation of similar shell elements (Dvorkin & Bathe, 1984; Bathe & Dvorkin, 1986), see also (Bathe & Dvorkin, 1985; Bathe, 1996). Compared with the formulation (7.103), we now consider the problem
Find $(u_h^\varepsilon, \underline{\theta}_h^\varepsilon)$ *in* $\mathcal{V}_h^{RM}$ *such that*

$$\begin{aligned} A_{\mathrm{b}}^{RM}(\underline{\theta}_h^\varepsilon, \underline{\eta}) + \varepsilon^{-2}\frac{2EL}{1+\nu}\int_\omega R_h\big(\underline{\zeta}(u_h^\varepsilon, \underline{\theta}_h^\varepsilon)\big) \cdot R_h\big(\underline{\zeta}(v, \underline{\eta})\big)\, dS \\ = L\int_\omega Gv\, dS, \qquad \forall (v, \underline{\eta}) \in \mathcal{V}_h^{RM}. \end{aligned} \tag{7.133}$$

In this new formulation, R_h denotes what we call a *reduction operator* that is intended to allow for relaxing the constraint of vanishing shear strain in the

discrete displacements. The operator R_h has values in a discrete space $\mathcal{T}_h^{RM}$ but – unlike with Π_h in (7.103) – R_h is not defined as the L^2-projection onto $\mathcal{T}_h^{RM}$. However, R_h is chosen so that it reduces to the identity when applied in $\mathcal{T}_h^{RM}$, like a projection operator. Another important difference with (7.103) is that stabilization terms are not used in MITC formulations.

In order to specify how to build the finite element spaces and the reduction operator for MITC plate elements, we need to distinguish between the transverse displacement and the rotation, for which we respectively define the finite element subspaces $\mathcal{V}_{dh}^{RM}$ and $\mathcal{V}_{rh}^{RM}$, so that

$$\mathcal{V}_h^{RM} = \mathcal{V}_{dh}^{RM} \times \mathcal{V}_{rh}^{RM}. \tag{7.134}$$

The design of the MITC plate elements is based on an analogy between the constraints of vanishing shear strains in plate bending problems and the possible incompressibility in elasticity problems (Bathe & Brezzi, 1985, 1987). Accordingly, we need an auxiliary discrete space (which is not used in the actual finite element computations) denoted by $\mathcal{Q}_h$ and consisting of scalar fields in L^2. Defining P_h as the L^2-projection onto $\mathcal{Q}_h$, the conditions that need be satisfied in order to construct a suitable MITC plate element are the following (Brezzi et al., 1989; Bathe et al., 1990)

P1. $\underline{\nabla}\mathcal{V}_{dh}^{RM} \subset \mathcal{T}_h^{RM}$;

P2. $\operatorname{rot} \mathcal{T}_h^{RM} \subset \mathcal{Q}_h$;

P3. $\forall \underline{\eta} \in \left[H^1(\mathcal{S})\right]^2$, $\operatorname{rot}\big(R_h\underline{\eta}\big) = P_h\big(\operatorname{rot}\underline{\eta}\big)$;

P4. If $\underline{r} \in \mathcal{T}_h^{RM}$ satisfies $\operatorname{rot}\underline{r} = 0$, then there exists $v \in \mathcal{V}_{dh}^{RM}$ s.t. $\underline{r} = \underline{\nabla} v$;

P5. The pair of discrete spaces $\big(\mathcal{V}_{rh}^{RM}, \mathcal{Q}_h\big)$ satisfies the inf-sup condition

$$\sup_{\underline{\eta}\in\mathcal{V}_{rh}^{RM}\setminus\{\underline{0}\},\, \underline{\eta}|_{\partial\omega}=\underline{0}} \frac{\int_\omega s \operatorname{rot}\underline{\eta}\, dS}{\|\underline{\eta}\|_1} \geq \gamma \|s\|_{L_0^2}, \qquad \forall s \in \mathcal{Q}_h. \tag{7.135}$$

Note that the norm $\|\cdot\|_{L_0^2}$ appearing in (7.135) denotes the L^2-norm of a function with the mean value subtracted.

Remark 7.2.15. Property P3 can be summarized by the commuting diagram given in Figure 7.9. ■

Remark 7.2.16. Due to the similarity of the "div" and "rot" operators, the inf-sup condition (7.135) is *equivalent* to that arising in the Stokes (or incompressible elasticity) problem (Brezzi & Fortin, 1991; Bathe, 1996). Hence from a pair of spaces (displacement and pressure) that is suitable for 2D in-

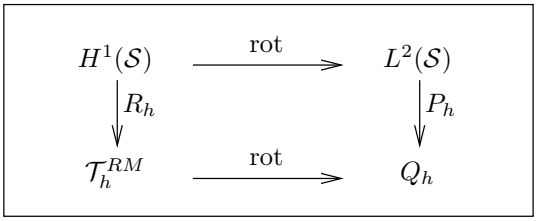

Fig. 7.9. Property P3 represented as a commuting diagram

compressible problems we can directly infer spaces that satisfy the condition P5 above. ■

Before giving examples of actual finite element formulations that satisfy the above five conditions, we comment upon the essential significance of these conditions. First, the condition P1 ensures that the finite element formulation is stable, namely that the bilinear form appearing in the left-hand side of (7.133) is coercive. Due to P1 we have, for all $(v, \underline{\eta}) \in \mathcal{V}_h^{RM}$,

$$R_h\big(\underline{\zeta}(v, \underline{\eta})\big) = \underline{\nabla} v + R_h(\underline{\eta}), \tag{7.136}$$

and this clearly implies coercivity, provided that R_h is continuous in H^1 which is a natural (and easily satisfied) property for a reduction operator. Note that this coercivity property is equivalent to the coercivity of the bilinear form A_{b}^{RM} in the subspace

$$\tilde{V}_{h0}^{RM} = \{(v, \underline{\eta}) \in \mathcal{V}_h^{RM} \mid R_h\big(\underline{\zeta}(v, \underline{\eta})\big) = \underline{0}\}, \tag{7.137}$$

which is similar to (3.108), namely the first crucial condition that arises in general mixed formulations.

Then, in order to provide insight into the other four conditions we consider an arbitrary smooth element $(v, \underline{\eta}) \in \mathcal{V}^{RM}$ that satisfies the vanishing shear strain constraint, i.e. $(v, \underline{\eta}) \in \mathcal{V}_0^{RM}$, viz.

$$\underline{\nabla} v + \underline{\eta} = \underline{0}, \tag{7.138}$$

and we argue that – for locking to be avoided – we need to be able to find an optimal approximation of $(v, \underline{\eta})$ in the finite element subspace $\tilde{V}_{h0}^{RM}$, namely with the relaxed constraint imposed. We thus seek $(v_h, \underline{\eta}_h) \in \mathcal{V}_h^{RM}$ as an approximation of $(v, \underline{\eta})$ that satisfies

$$R_h\big(\underline{\zeta}(v_h, \underline{\eta}_h)\big) = \underline{\nabla} v_h + R_h(\underline{\eta}_h) = \underline{0}. \tag{7.139}$$

By P2, we can consider the "rot" of $R_h\big(\underline{\zeta}(v_h, \underline{\eta}_h)\big)$, hence we obtain

$$\operatorname{rot} R_h(\underline{\eta}_h) = 0, \tag{7.140}$$

since the term $\underline{\nabla} v_h$ gives zero. We then apply P3 and infer

$$P_h\big(\operatorname{rot} \underline{\eta}_h\big) = 0. \tag{7.141}$$

Noting that $(v, \eta) \in \mathcal{V}_0^{RM}$ implies, also by an application of the "rot" operator,

$$\operatorname{rot} \underline{\eta} = 0, \tag{7.142}$$

we directly have from P5 that there exists an optimal approximation of $\underline{\eta}$ that satisfies the relaxed constraint (7.141). With $\underline{\eta}_h$ being thus chosen, (7.140) and P4 imply that there exists v_h in $\mathcal{V}_{dh}^{RM}$ such that

$$\underline{\nabla} v_h = -R_h(\underline{\eta}_h). \tag{7.143}$$

Comparing this with (7.138) we obtain, using a Poincaré inequality,

$$\begin{aligned} \|v - v_h\|_1 &\leq C\|\underline{\eta} - R_h(\underline{\eta}_h)\|_0 \\ &\leq C\big(\|\underline{\eta} - R_h(\underline{\eta})\|_0 + \|\underline{\eta} - \underline{\eta}_h\|_0\big), \end{aligned} \tag{7.144}$$

using also the continuity of R_h in L^2 which provides

$$\|R_h(\underline{\eta}) - R_h(\underline{\eta}_h)\|_0 \leq C\|\underline{\eta} - \underline{\eta}_h\|_0. \tag{7.145}$$

Therefore, whether or not v_h is an optimal approximation of v depends on the consistency of the reduction operator R_h through the error term $\|\underline{\eta} - R_h(\underline{\eta})\|_0$. This is not a consequence of the assumed conditions P1–P5, but will follow from specific choices of R_h as interpolation operators (see examples below).

Numerical experiments illustrating the performance of MITC plate elements have been published in (Bathe et al., 1990, 1989). A complete error analysis of the MITC plate elements is available in (Brezzi et al., 1991), see also (Brezzi et al., 1989; Peisker & Braess, 1992). The error analysis crucially relies on the application of the Helmholtz decomposition principle on the shear force. This decomposition leads to considering a sequence of problems, one of which being defined by a mixed formulation similar to those arising in incompressible problems. In fact, P5 is the inf-sup condition corresponding to this particular mixed formulation. This approach based on the Helmholtz decomposition takes advantage of the specific nature of the shear force space in plate problems hence it is not applicable to shell problems, which is why we do not provide the detailed analysis here.

Remark 7.2.17. We can also consider the mixed formulation equivalent to (7.133) obtained by introducing the discrete shear force

$$\underline{q}_h^\varepsilon = \varepsilon^{-3}\frac{Et}{2(1+\nu)}R_h(\underline{\theta}_h^\varepsilon + \underline{\nabla} u_h^\varepsilon), \tag{7.146}$$

as an auxiliary unknown. This formulation reads

$$\begin{aligned} M_{\varepsilon,h}^{RM}\big((u_h^\varepsilon, \underline{\theta}_h^\varepsilon), \underline{q}_h^\varepsilon; (v, \underline{\eta}), \underline{r}\big) &= L\int_\omega Gv\, dS, \\ &\forall\big((v, \underline{\eta}), \underline{r}\big) \in \mathcal{V}_h^{RM} \times \mathcal{T}_h^{RM}, \end{aligned} \tag{7.147}$$

with

$$\begin{aligned} &M_{\varepsilon,h}^{RM}\big((u, \underline{\theta}), \underline{q}; (v, \underline{\eta}), \underline{r}\big) = \\ &\quad A_{\mathrm{b}}^{RM}(\underline{\theta}, \underline{\eta}) + B_h^{RM}(v, \underline{\eta}; \underline{q}) + B_h^{RM}(u, \underline{\theta}; \underline{r}) - \varepsilon^2 D^{RM}(\underline{q}, \underline{r}), \end{aligned} \tag{7.148}$$

in which

$$B_h^{RM}(v, \underline{\eta}; \underline{r}) = \int_\omega R_h(\underline{\eta} + \underline{\nabla} v) \cdot \underline{r}\, dS. \tag{7.149}$$

Comparing with the mixed bilinear form in (7.94) we can see that we have introduced a consistency error source due to the presence of the reduction operator in B_h^{RM}. As discussed above, the consistency errors caused by R_h are "small" in practice. As regards the stability of the mixed bilinear form $M_{\varepsilon,h}^{RM}$, the general theory shows that it relies on the coercivity condition and on the inf-sup condition. As already pointed out, the coercivity condition is automatically satisfied due to P1. The inf-sup condition for $M_{\varepsilon,h}^{RM}$ reads

$$\sup_{(v,\underline{\eta})\in\mathcal{V}_h^{RM},(v,\underline{\eta})\neq(0,\underline{0})} \frac{B_h^{RM}(v, \underline{\eta}; \underline{r})}{\|v, \underline{\eta}\|_{\mathcal{V}^{RM}}} \geq \gamma\|\underline{r}\|_{IS}. \tag{7.150}$$

However, the above-mentioned complete error analysis of MITC plate elements uses the decomposition principle rather than a direct analysis of (7.133) or (7.147) and – in fact – a mathematical proof that the MITC elements satisfy the inf-sup condition (7.150) is still missing, see (Brezzi et al., 1991; Brezzi & Fortin, 1991). ■

We proceed to present the formulation of the main elements in the MITC plate elements family. In order to define the corresponding reduction operators we use *tying points*, namely specific points in which some well-chosen components of the reduced shear strain are taken equal to the same components of the shear strain directly calculated from the displacements. For the quadrilateral elements, these components are covariant components in the local (r, s) coordinate system – whence the name MITC – which is expected

to make these elements more robust with respect to distortions. These covariant components are denoted by ζ_r and ζ_s. We also use the following compact notation for the reduced shear strains

$$\underline{\zeta}^R = R_h(\underline{\zeta}). \tag{7.151}$$

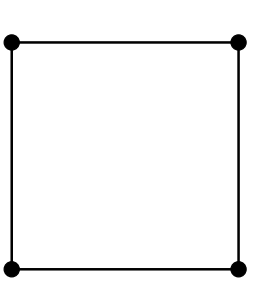

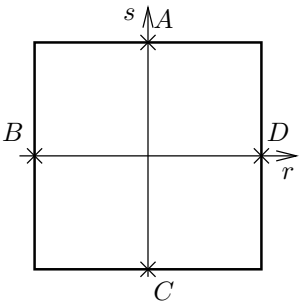

● $\underline{\theta}$ and u interpolation

$\zeta_r^R = a_1 + b_1 s$; tying at points A and C
$\zeta_s^R = a_2 + b_2 r$; tying at points B and D

Fig. 7.10. MITC4 plate element

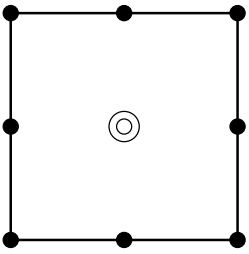

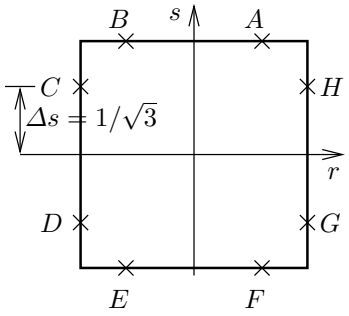

● $\underline{\theta}$ and u interpolation
◎ $\underline{\theta}$ interpolation

$\zeta_r^R = a_1 + b_1 r + c_1 s + d_1 rs + e_1 s^2$;
tying at points A, B, E, F

$\zeta_s^R = a_2 + b_2 r + c_2 s + d_2 rs + e_2 r^2$;
tying at points C, D, G, H

plus integral tying $\int_K (\underline{\zeta} - \underline{\zeta}^R) dS = \underline{0}$

Fig. 7.11. MITC9 plate element

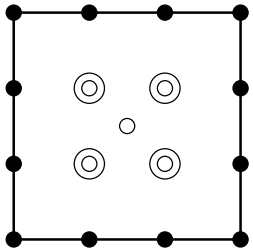

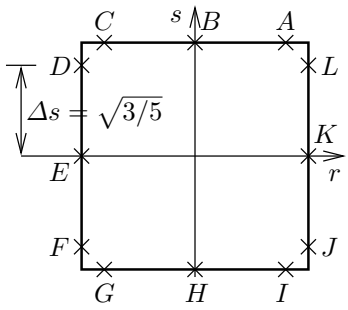

● $\underline{\theta}$ and u interpolation
◎ $\underline{\theta}$ interpolation
○ u interpolation

$$\zeta_r^R = a_1 + b_1 r + c_1 s + d_1 r^2 + e_1 rs + f_1 s^2 + g_1 r^2 s + h_1 rs^2 + i_1 s^3$$
tying at points A, B, C, G, H, I

$$\zeta_s^R = a_2 + b_2 r + c_2 s + d_2 r^2 + e_2 rs + f_2 s^2 + g_2 r^2 s + h_2 rs^2 + i_2 r^3$$
tying at points D, E, F, J, K, L

plus integral tying $\int_K (\underline{\zeta} - \underline{\zeta}^R) dS = \int_K (\underline{\zeta} - \underline{\zeta}^R) x \, dS = \int_K (\underline{\zeta} - \underline{\zeta}^R) y \, dS = \underline{0}$

Fig. 7.12. MITC16 plate element

The quadrilateral MITC4, MITC9 and MITC16 plate elements are described in Figures 7.10, 7.11, and 7.12, respectively. In these figures, the local coordinates r and s are assumed to range in $[-1, +1]$. In addition, in Figure 7.12 x and y denote an arbitrary cartesian coordinate system given in the plane of the structure. It can be shown that the MITC9 and MITC16 plate elements satisfy Conditions P1 to P5 when rectangular elements are considered (Brezzi et al., 1989). The underlying discrete spaces suitable for incompressible problems correspond to the Q_2/P_1 and Q_3/P_2 elements, respectively. In addition, optimal consistency is obtained with the reduction operators of the MITC9 and MITC16 plate elements, hence optimal *thickness-independent* error estimates can be derived both for the displacements/rotations and for the shear forces. The MITC4 plate element – on the other hand – does not satisfy Condition P5, since the corresponding incompressible element would be Q_1/P_0 that does not satisfy the inf-sup condition for incompressible analysis in general, see (Brezzi & Fortin, 1991; Bathe, 1996) and references therein. However, by a specific analysis it can be shown that an optimal error estimate holds for the displacements and rotations, again for rectangular elements (Bathe & Brezzi, 1985).

The triangular MITC7 and MITC12 elements are described in Figures 7.13 and 7.14. In these figures (x, y) denotes an arbitrary cartesian coordinate system and $\underline{\tau}$ the unit vector tangent to the element boundary. It can be shown that these elements satisfy the five conditions P1 to P5, and

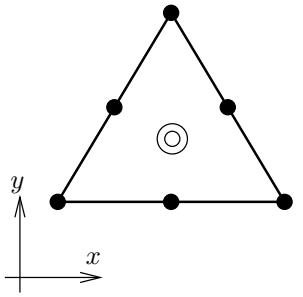

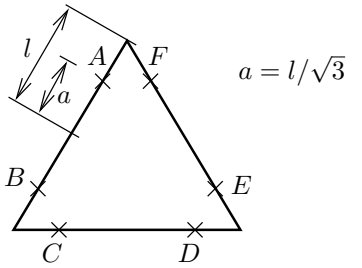

● $\underline{\theta}$ and u interpolation
◎ $\underline{\theta}$ interpolation

$\zeta_x^R = a_1 + b_1 x + c_1 y + y(dx + ey)$;
$\zeta_y^R = a_2 + b_2 x + c_2 y - x(dx + ey)$;
tying of $\underline{\zeta} \cdot \underline{\tau}$ at points A, B, C, D, E, F
plus integral tying $\int_K (\underline{\zeta} - \underline{\zeta}^R) dS = \underline{0}$

Fig. 7.13. MITC7 plate element

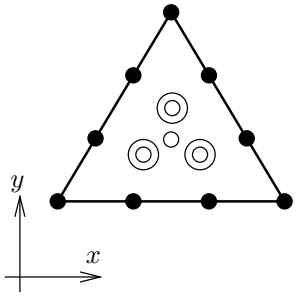

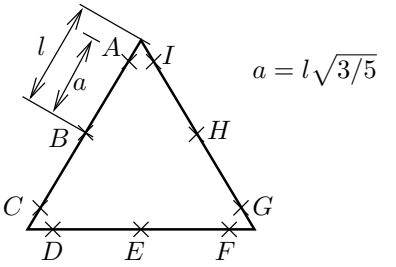

● $\underline{\theta}$ and u interpolation
◎ $\underline{\theta}$ interpolation
○ u interpolation

$\zeta_x^R = a_1 + b_1 x + c_1 y + d_1 x^2 + e_1 xy$
$\quad + f_1 y^2 + y(gx^2 + hxy + iy^2)$;
$\zeta_y^R = a_2 + b_2 x + c_2 y + d_2 x^2 + e_2 xy$;
$\quad + f_2 y^2 - x(gx^2 + hxy + iy^2)$;
tying of $\underline{\zeta} \cdot \underline{\tau}$ at all points A to I
plus integral tying $\int_K (\underline{\zeta} - \underline{\zeta}^R) dS$
$= \int_K (\underline{\zeta} - \underline{\zeta}^R) x \, dS = \int_K (\underline{\zeta} - \underline{\zeta}^R) y \, dS = \underline{0}$

Fig. 7.14. MITC12 plate element

that optimal consistency also holds, hence optimal error estimates for the displacements/rotations and for the shear forces are obtained (Brezzi et al., 1989, 1991).

Remark 7.2.18. We observe that – for all the MITC plate elements presented here – the tangential component of $\underline{\zeta}^R$ is continuous across interele-

ment boundaries. This is indeed required in order to have $\mathrm{rot}\mathcal{T}_h^{RM} \subset L^2$, which is implied by Condition P2. ■

For illustration and validation purposes, we now present some assessment results – taken from (Lee & Bathe, 2010) – obtained with the quadratic MITC plate elements, for a test problem consisting of a clamped square plate subjected to uniform pressure. Soft clamping was used – namely, the rotations along the boundaries were left free – and due to symmetry the computational domain was restricted to one fourth of the plate. The quadrilateral element meshes correspond to a regular $N \times N$ subdivision of the computational domain, and the triangular element meshes are obtained by splitting the quadrilateral elements along a fixed diagonal.

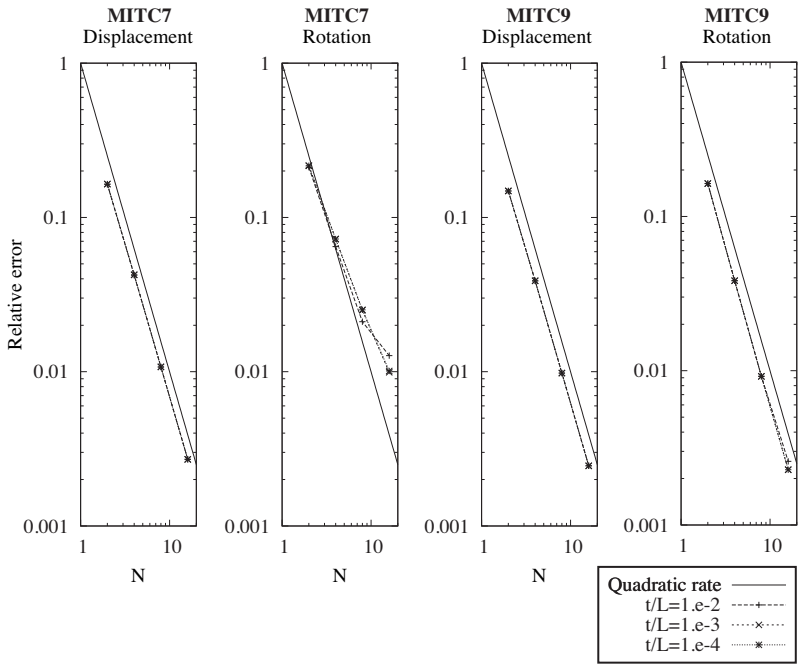

Fig. 7.15. Clamped square plate under uniform pressure ($\nu = 0.3$): displacement error in H^1-semi-norm and rotation error in H^1-norm

Figure 7.15 shows the computed relative errors for sequences of increasingly refined meshes (obtained by increasing the subdivision parameter N), and for several values of the thickness ratio t/L, L being here the half-length of the square. Two error indicators are considered separately, namely, the H^1-semi-norm for the transverse displacement and the H^1-norm for the rotations, and the reference solution used in the errors was computed with a fine mesh of 96×96 MITC9 elements. As we can see in the figure, except for

the MITC7 rotations, the convergence rates are optimal and no dependence on the thickness is observed. As regards the MIT7 rotation errors, the slightly suboptimal convergence is likely due to a soft boundary layer associated with the clamping, see Section 8.1.

7.3 Specific Difficulties Arising in the Analysis of Shells

We recall that our objective is to obtain shell finite element procedures that behave uniformly well with respect to the thickness parameter, i.e. for which the finite element solution U_h^ε satisfies an estimate of the type

$$\boxed{\frac{\|U^\varepsilon - U_h^\varepsilon\|_\star}{\|U^\varepsilon\|_\star} \leq Ch^p,} \tag{7.152}$$

where the norm used remains to be specified. In the light of the discussion of Chapter 5 regarding the asymptotic behaviors of shell models, it is natural to require that a uniform convergence estimate hold in the norm for which the solution remains uniformly bounded (and may also converge to a limit solution) when the thickness parameter tends to zero. Namely, we are led to require that

1. In a bending-dominated case such a uniform estimate hold in the norm of the displacement space $\mathcal{V}$;
2. In a membrane-dominated case such a uniform estimate hold in the membrane energy norm.

Let us start by considering a standard displacement-based finite element procedure obtained by discretizing the variational formulation (5.4), namely the problem
Find $U_h^\varepsilon \in \mathcal{V}_h$ *such that*

$$\boxed{\varepsilon^3 A_{\rm b}(U_h^\varepsilon, V) + \varepsilon A_{\rm m}(U^\varepsilon, V) = F^\varepsilon(V), \qquad \forall V \in \mathcal{V}_h,} \tag{7.153}$$

where $\mathcal{V}_h$ denotes the finite element displacement space used. For a *membrane-dominated* problem, as shown in Chapter 5 we – in fact – need to consider the scaled problem

$$\boxed{A_{\rm m}(U_h^\varepsilon, V) + \varepsilon^2 A_{\rm b}(U_h^\varepsilon, V) = G(V), \qquad \forall V \in \mathcal{V}_h.} \tag{7.154}$$

Note that we are now writing $A_{\rm m}$ first in the left-hand side of this equation because it corresponds to the major part of the energy in the membrane-dominated asymptotic behavior. Assuming that G is an admissible loading in the membrane energy space – namely that $G \in \mathcal{V}'_{\rm m}$ – so that the asymptotic convergence result of Proposition 5.1.3 holds, we can then show that we have a uniform convergence property for the above finite element solution.

Proposition 7.3.1 *Assume that there exist two interpolation operators $\mathcal{I}$ and $\mathcal{J}$, defined respectively in $\mathcal{V}_{\rm m}$ and $\mathcal{V}$ and both with values in $\mathcal{V}_h$, such that*

$$\left\{\begin{array}{ll} \|\mathcal{I}(V)\|_{\rm m} \leq C\|V\|_{\rm m}, & \forall V \in \mathcal{V}_{\rm m} \\ \|\mathcal{I}(V)\|_{\mathcal{V}} \leq C\|V\|_{\mathcal{V}}, & \forall V \in \mathcal{V} \\ \lim\limits_{h\to 0} \|V - \mathcal{I}(V)\|_{\rm m} = 0, & \forall V \in \mathcal{V}_{\rm m} \end{array}\right. \tag{7.155}$$

$$\left\{\begin{array}{ll} \|\mathcal{J}(V)\|_{\mathcal{V}} \leq C\|V\|_{\mathcal{V}}, & \forall V \in \mathcal{V} \\ \lim\limits_{h\to 0} \|V - \mathcal{J}(V)\|_{\mathcal{V}} = 0, & \forall V \in \mathcal{V} \end{array}\right. \tag{7.156}$$

Then for any fixed $\varepsilon_{max} > 0$ we have

$$\boxed{\lim_{h\to 0} \sup_{\varepsilon\in]0,\varepsilon_{max}]} \left\{\|U^\varepsilon - U_h^\varepsilon\|_{\rm m} + \varepsilon\|U^\varepsilon - U_h^\varepsilon\|_{\mathcal{V}}\right\} = 0.} \tag{7.157}$$

Proof. In this proof, we will need to handle the actual values of some bounding constants (and not only to invoke the existence of such constants), so we will denote these specific quantities with indices. In particular we will use, from (7.155),

$$\|\mathcal{I}(V)\|_{\mathcal{V}} \leq C_1\|V\|_{\mathcal{V}}, \quad \forall V \in \mathcal{V}. \tag{7.158}$$

We now choose $\varepsilon_{\max} > 0$. Recalling that the bilinear form "$A_{\rm m} + \varepsilon^2 A_{\rm b}$" gives a $\mathcal{V}$-coercive bilinear form for any $\varepsilon > 0$ (see Chapter 5), we have in particular,

$$\gamma\|V\|^2_{\mathcal{V}} \leq A_{\rm m}(V,V) + \varepsilon^2_{\max} A_{\rm b}(V,V) \leq C\|V\|^2_{\mathcal{V}}, \quad \forall V \in \mathcal{V}. \tag{7.159}$$

Hence, using

$$A_{\rm m}(V,V) = \|V\|^2_{\rm m}, \tag{7.160}$$

we infer that, for any $\varepsilon \in [0, \varepsilon_{\max}]$ and for any $V \in \mathcal{V}$,

$$\gamma\big\{\|V\|_{\rm m}+\varepsilon\|V\|_{\mathcal V}\big\}^2 \leq A_{\rm m}(V,V)+\varepsilon^2 A_{\rm b}(V,V)\leq C\big\{\|V\|_{\rm m}+\varepsilon\|V\|_{\mathcal V}\big\}^2. \tag{7.161}$$

Therefore, standard properties of Galerkin approximations give

$$\|U^\varepsilon-U_h^\varepsilon\|_{\rm m}+\varepsilon\|U^\varepsilon-U_h^\varepsilon\|_{\mathcal V} \leq C_2\inf_{V\in\mathcal V_h}\big\{\|U^\varepsilon-V\|_{\rm m}+\varepsilon\|U^\varepsilon-V\|_{\mathcal V}\big\}. \tag{7.162}$$

Furthermore, we also obtain from (7.159) that

$$\varepsilon^2\|V\|_{\mathcal V}^2\leq C\,\varepsilon^2\big[A_{\rm m}(V,V)+A_{\rm b}(V,V)\big],\qquad \forall V\in\mathcal V, \tag{7.163}$$

so that, using the property (5.63) and the fact (inferred from Prop. 5.1.3) that $A_{\rm m}(U^\varepsilon,U^\varepsilon)$ is uniformly bounded, we have

$$\lim_{\varepsilon\to 0}\varepsilon\|U^\varepsilon\|_{\mathcal V}=0. \tag{7.164}$$

Consider now an arbitrary real number $\eta>0$. In order to prove (7.157) we need to show that there exists $h_\eta>0$ such that, for any $h<h_\eta$,

$$\sup_{\varepsilon\in]0,\varepsilon_{\max}]}\big\{\|U^\varepsilon-U_h^\varepsilon\|_{\rm m}+\varepsilon\|U^\varepsilon-U_h^\varepsilon\|_{\mathcal V}\big\}\leq\eta. \tag{7.165}$$

It follows from (7.164) that there exists $\varepsilon_\eta>0$ such that, for all $\varepsilon\in]0,\varepsilon_\eta]$,

$$C_2(1+C_1)\,\varepsilon\|U^\varepsilon\|_{\mathcal V}\leq\frac{\eta}{2}, \tag{7.166}$$

which, combined with (7.162) and (7.158), gives

$$\begin{aligned}\sup_{\varepsilon\in]0,\varepsilon_\eta]}&\big\{\|U^\varepsilon-U_h^\varepsilon\|_{\rm m}+\varepsilon\|U^\varepsilon-U_h^\varepsilon\|_{\mathcal V}\big\}\\ &\leq \sup_{\varepsilon\in]0,\varepsilon_\eta]}C_2\big\{\|U^\varepsilon-\mathcal I(U^\varepsilon)\|_{\rm m}+\varepsilon\|U^\varepsilon-\mathcal I(U^\varepsilon)\|_{\mathcal V}\big\}\\ &\leq \sup_{\varepsilon\in]0,\varepsilon_\eta]}C_2\big\{\|U^\varepsilon-\mathcal I(U^\varepsilon)\|_{\rm m}+(1+C_1)\,\varepsilon\|U^\varepsilon\|_{\mathcal V}\big\}\\ &\leq C_2\sup_{\varepsilon\in]0,\varepsilon_\eta]}\|U^\varepsilon-\mathcal I(U^\varepsilon)\|_{\rm m}\ +\frac{\eta}{2}.\end{aligned} \tag{7.167}$$

The mapping $\varepsilon\mapsto U^\varepsilon$ is clearly continuous from $]0,\varepsilon_{\max}]$ into $\mathcal V$, hence into $\mathcal V_{\rm m}$, and Proposition 5.1.3 shows that this extends to continuity from $[0,\varepsilon_{\max}]$ into $\mathcal V_{\rm m}$ provided that we let

$$U^{\varepsilon}(\varepsilon = 0) = U^{\mathrm{m}}. \tag{7.168}$$

Therefore, Equation (7.155-a) implies that the family of functions

$$\big(\varepsilon \mapsto \|U^{\varepsilon} - \mathcal{I}(U^{\varepsilon})\|_{\mathrm{m}}\big)_h$$

is equicontinuous from $[0, \varepsilon_{\max}]$ into $\mathbb{R}$ since, by using (3.8),

$$\begin{aligned} \big|\|U^{\varepsilon_1} - \mathcal{I}(U^{\varepsilon_1})\|_{\mathrm{m}} - \|U^{\varepsilon_2} - \mathcal{I}(U^{\varepsilon_2})\|_{\mathrm{m}}\big| &\leq \|U^{\varepsilon_1} - U^{\varepsilon_2} - \mathcal{I}(U^{\varepsilon_1} - U^{\varepsilon_2})\|_{\mathrm{m}} \\ &\leq C\|U^{\varepsilon_1} - U^{\varepsilon_2}\|_{\mathrm{m}}, \end{aligned} \tag{7.169}$$

where the final right-hand side does not depend on h. Further, for any $\varepsilon \geq 0$ we have, by (7.155-c),

$$\lim_{h \to 0} \|U^{\varepsilon} - \mathcal{I}(U^{\varepsilon})\|_{\mathrm{m}} = 0, \tag{7.170}$$

so that the Ascoli theorem (see e.g. Rudin, 1991; Yosida, 1980) implies that we have uniform convergence when h tends to zero, namely,

$$\lim_{h \to 0} \sup_{\varepsilon \in [0, \varepsilon_\eta]} \|U^{\varepsilon} - \mathcal{I}(U^{\varepsilon})\|_{\mathrm{m}} = 0. \tag{7.171}$$

It follows that there exists $h_\eta^{(1)} > 0$ such that, for all $h < h_\eta^{(1)}$,

$$C_2 \sup_{\varepsilon \in [0, \varepsilon_\eta]} \|U^{\varepsilon} - \mathcal{I}(U^{\varepsilon})\|_{\mathrm{m}} \leq \frac{\eta}{2}. \tag{7.172}$$

Hence, from (7.167), for all $h < h_\eta^{(1)}$,

$$\sup_{\varepsilon \in]0, \varepsilon_\eta]} \big\{\|U^{\varepsilon} - U_h^{\varepsilon}\|_{\mathrm{m}} + \varepsilon\|U^{\varepsilon} - U_h^{\varepsilon}\|_{\mathcal{V}}\big\} \leq \eta. \tag{7.173}$$

It remains to obtain a similar bound for $\varepsilon \in [\varepsilon_\eta, \varepsilon_{\max}]$. Using again (7.162) we obtain

$$\begin{aligned} &\sup_{\varepsilon \in [\varepsilon_\eta, \varepsilon_{\max}]} \big\{\|U^{\varepsilon} - U_h^{\varepsilon}\|_{\mathrm{m}} + \varepsilon\|U^{\varepsilon} - U_h^{\varepsilon}\|_{\mathcal{V}}\big\} \\ &\qquad \leq \sup_{\varepsilon \in [\varepsilon_\eta, \varepsilon_{\max}]} C_2\big\{\|U^{\varepsilon} - \mathcal{J}(U^{\varepsilon})\|_{\mathrm{m}} + \varepsilon\|U^{\varepsilon} - \mathcal{J}(U^{\varepsilon})\|_{\mathcal{V}}\big\} \\ &\qquad \leq C_3 \sup_{\varepsilon \in [\varepsilon_\eta, \varepsilon_{\max}]} \|U^{\varepsilon} - \mathcal{J}(U^{\varepsilon})\|_{\mathcal{V}}. \end{aligned} \tag{7.174}$$

From (7.156-a) we have that the family of functions

$$\big(\varepsilon \mapsto \|U^\varepsilon - \mathcal{J}(U^\varepsilon)\|_{\mathrm{m}}\big)_h$$

is equicontinuous from $[\varepsilon_\eta, \varepsilon_{\max}]$ into $\mathbb{R}$, hence (7.156-b) and the Ascoli theorem imply

$$\lim_{h\to 0} \sup_{\varepsilon\in[\varepsilon_\eta,\varepsilon_{\max}]} \|U^\varepsilon - \mathcal{J}(U^\varepsilon)\|_{\mathcal{V}} = 0. \tag{7.175}$$

As a consequence, there exists $h_\eta^{(2)} > 0$ such that, for all $h < h_\eta^{(1)}$,

$$C_3 \sup_{\varepsilon\in[\varepsilon_\eta,\varepsilon_{\max}]} \|U^\varepsilon - \mathcal{J}(U^\varepsilon)\|_{\mathcal{V}} \le \eta, \tag{7.176}$$

hence,

$$\sup_{\varepsilon\in[\varepsilon_\eta,\varepsilon_{\max}]} \big\{\|U^\varepsilon - U_h^\varepsilon\|_{\mathrm{m}} + \varepsilon\|U^\varepsilon - U_h^\varepsilon\|_{\mathcal{V}}\big\} \le \eta. \tag{7.177}$$

Now, letting

$$h_\eta = \min\big(h_\eta^{(1)}, h_\eta^{(2)}\big), \tag{7.178}$$

we have (7.165). ∎

Remark 7.3.1. We point out that (7.155) and (7.156) represent rather unrestrictive interpolation assumptions. For instance, in the case of a uniformly elliptic shell based on the m-b shell model and clamped along the whole boundary, we have $\mathcal{V} = H_0^1(\mathcal{S})^2 \times H_0^2(\mathcal{S})$ and $\mathcal{V}_{\mathrm{m}} = H_0^1(\mathcal{S})^2 \times L^2(\mathcal{S})$ (see Section 5.2.1), and we can choose for both $\mathcal{I}$ and $\mathcal{J}$ the interpolation operator given in (Clément, 1975). This interpolator provides the required interpolation properties in H^1 and L^2, whereas standard interpolation cannot be used (since these spaces contain non-continuous functions, see Section 3.1.2). ∎

Remark 7.3.2. The uniform convergence result (7.157) – although weaker than an estimate as sought in (7.152) – is clearly the "best" result that can be obtained without using additional specific regularity properties on the solutions U^ε. In the present case, we would then require *uniform* regularity bounds since we are seeking uniform error estimates for the sequences of exact and corresponding finite element solutions. Such uniform regularity bounds would typically provide

$$\inf_{V\in\mathcal{V}_h} \big\{\|U^\varepsilon - V\|_{\mathrm{m}} + \varepsilon\|U^\varepsilon - V\|_{\mathcal{V}}\big\} \le Ch^p, \tag{7.179}$$

with C (and p) independent of ε, so that a uniform error estimate would then directly follow from (7.162). However, regularity results for shell solutions

are very scarce, and it is clear that uniform regularity cannot hold in general situations due to the presence of strong boundary layers that depend on the thickness value (see in particular (Pitkäranta et al., 2001; Dauge & Yosibash, 2000) and the references therein), hence it is necessary to resort to appropriate mesh refinement to obtain optimal errors. ■

We conclude from Proposition 7.3.1 and the interpretations given in the above remarks that displacement-based elements provide – for well-posed *membrane-dominated* shell problems – uniform convergence results that are similar to classical results for the finite element approximations of elliptic boundary value problems.

We now turn to the analysis of *bending-dominated* shell problems discretized using displacement-based finite elements. The finite element problem to be considered is then

$$\boxed{A_{\rm b}(U_h^\varepsilon, V) + \frac{1}{\varepsilon^2} A_{\rm m}(U_h^\varepsilon, V) = G(V), \qquad \forall V \in \mathcal{V}_h.} \tag{7.180}$$

As discussed in the previous sections of this chapter, the major difficulty with this type of finite element formulation is the *numerical locking* phenomenon. As exemplified in the approximation of the Timoshenko beam problem by piecewise-linear displacement-base finite elements, locking is – in particuliar – critical when

$$\mathcal{V}_h \cap \mathcal{V}_0 = \{0\}. \tag{7.181}$$

The specific difficulty with shells is that – unlike with beams and plates – the situation characterized by (7.181) prevails in general. This is illustrated in the following result.

Proposition 7.3.2 *Consider a shell with a regular hyperbolic midsurface and fixed on some part of its boundary. Assume that the problem is discretized – in the framework of* (7.180) *– with a finite element procedure by which the components of the midsurface displacements are approximated using continuous piecewise-polynomial functions. Assume further that no element edge in the mesh is part of an asymptotic line of the midsurface. Then* (7.181) *holds.*

Proof. We will show that, for any inextensional midsurface displacement $\vec{v}$, if $\vec{v}$ is zero on some edge of any element of the mesh, then $\vec{v}$ is identically zero over the whole element. This being granted, the result is immediately obtained by "propagating" the zero displacements from the boundary conditions to the whole domain.

Consider an arbitrary element of the mesh, with $\vec{v}$ set to zero on any of its edges, then we have two possibilities:

1. Either the lattice of asymptotic lines originating from this edge covers the element completely (like in Figure 7.16-a) and the conclusion directly follows from Proposition 5.2.1.
2. Or the element is only partially covered as in Figure 7.16-b (note that a degenerate case is impossible due to the assumption made on the element edges), but in this case we still have $\vec{v} = 0$ on a part of non-zero area of the element. Recalling that the displacement components are given by polynomial functions, this implies that they are zero over the whole element.

■

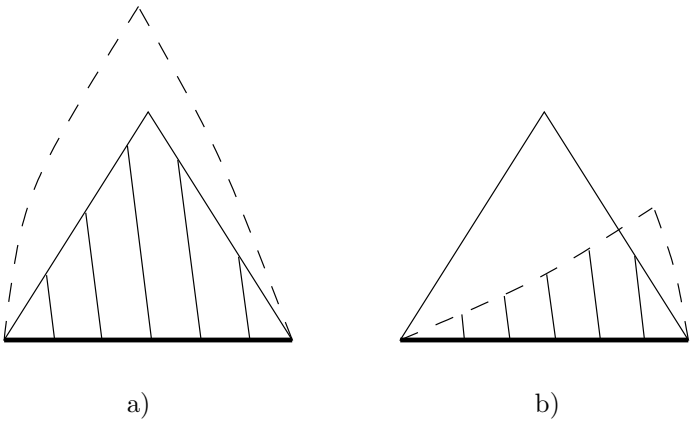

a) b)

Fig. 7.16. Asymptotic lines and inhibited region for an element

In order to make the statement of this property simpler, we assumed that no single element edge lies along an asymptotic curve. It is obvious, however, that this result carries over to any case in which the same propagation technique can be applied, which is much more general. A practical consequence of this discussion is that, when using benchmark problems to numerically detect locking phenomena in shells, we should not align the mesh with the asymptotic lines of the midsurface when such lines exist, in order to avoid inhibiting the locking mechanism identified in the above proof. This holds in particular for *cylindrical test problems* for which the (very strong) temptation to align the mesh along the axis should also be resisted when seeking conclusions of general significance (note that, in industrial computations, aligning meshes along lines of specific geometric properties is impossible in general).

We further emphasize that Proposition 7.3.2 reveals a significant difference between finite element methods for shells and for other structures. For beams and plates, it is indeed always possible to avoid (7.181) by raising the polynomial degrees of the discretization spaces, see in particular (Arnold,

1981; Paumier, 1992). Here our argument is independent of the polynomial degree, hence *locking always occurs using displacement-based finite element formulations*, in particular due to the constraint that membrane strains vanish – which induces the specific type of locking called *membrane locking*. But of course, for a given thickness the errors in the solution may be acceptably small if the order of the polynomials is sufficiently high and the mesh is sufficiently fine.

Remark 7.3.3. Locking in shell finite elements has been proven to arise in various conditions other than those considered in Prop. 7.3.2, see in particular (Choï et al., 1998; Sanchez-Hubert & Sanchez-Palencia, 1997). ■

When trying to circumvent locking in shell finite element approximations, it is natural to resort to *mixed formulations*, as already discussed for beams and plates. We then introduce the membrane stresses (and the shear stresses for models based on the Reissner-Mindlin kinematical assumption) as auxiliary unknowns. As an example the membrane stress tensor in classical shell models (e.g., in the m-b and s-m-b models) is given by

$$\underline{\underline{m}} = t\,{}^{0}_{4}\mathbb{C} : \underline{\underline{\gamma}}(\vec{u}). \tag{7.182}$$

We thus obtain a mixed formulation of the form

$$\boxed{\begin{cases} A_{\rm b}(U^\varepsilon, V) + B(V, \Sigma^\varepsilon) = G(V), & \forall V \in \mathcal{V} \\ B(U^\varepsilon, \Xi) - \varepsilon^2 D(\Sigma^\varepsilon, \Xi) = 0, & \forall \Xi \in \mathcal{T}^+ \end{cases}} \tag{7.183}$$

in which the second equation expresses the stress-strain relationship for the additional unknowns, and $\mathcal{T}^+$ corresponds to L^2 for all components of the stress unknowns. Then, both fields (displacements and stresses) are discretized in the finite element procedure (in general, discontinuous shape functions are used for the stresses in order to allow the elimination of the stress degrees of freedom at the element level). After performing an elimination of the stress unknowns, the finite element formulation can be written as

$$\boxed{A_{\rm b}(U_h^\varepsilon, V) + \frac{1}{\varepsilon^2} A_{\rm m}^h(U_h^\varepsilon, V) = G(V), \quad \forall V \in \mathcal{V}_h,} \tag{7.184}$$

in which $A_{\rm m}^h$ is a "perturbed" form of $A_{\rm m}$ (see (7.45) in the example of the beam).

Remark 7.3.4. We can now see why mixed methods may "work" in the solution of bending-dominated shell problems. We have shown with Proposition

7.3.2 that any order of displacement interpolation using (7.180) yields (7.181), that is, imposed zero displacements on the boundary propagate along the asymptotic lines and constrain the shell elements to not deform in bending, even when they should, like in the region outside the area ABC of Fig. 5.3. On the other hand, with a mixed method we use A_m^h instead of A_m to represent the membrane energy (and the shear energy in the s-m-b model). The mixed method must be designed so that the membrane strains (and if applicable, the shear strains) can be zero while the bending strains are accurately represented when the physical situation so demands (like in the region outside the area ABC in Fig. 5.3). As in Remark 7.2.3, we again emphasize that the discrete spaces in the mixed formulation must be chosen very carefully and that – ideally – the inf-sup condition should be proven to ensure convergence. ■

In order to obtain an error estimate (uniform in ε) for the finite element approximation of the mixed shell problem (7.183), we need to establish the crucial corresponding inf-sup condition that we can rewrite, similarly to (7.87),

$$\sup_{V\in\mathcal{V}_h, V\neq 0} \frac{B(V;\Xi)}{\|V\|_{\mathcal{V}}} \geq \gamma \sup_{V\in\mathcal{V}, V\neq 0} \frac{B(V;\Xi)}{\|V\|_{\mathcal{V}}}, \qquad \forall \Xi \in \mathcal{T}_h. \tag{7.185}$$

Note that we have chosen to write the inf-sup condition in the form that does not use the norm of $\mathcal{T}$ explicitly. In fact, the problem of characterizing the space $\mathcal{T}$ and the associated norm for *general* geometries and boundary conditions is still open. A considerable difficulty in this direction arises from the presence of geometric coefficients (in particular coefficients related to the curvatures) in the bilinear form B, and more specifically in the part of B that corresponds to the membrane energy. Furthermore, although the characterization of $\mathcal{T}$ is bypassed in (7.185), the problem of finding pairs of finite element spaces $\mathcal{V}_h$ and $\mathcal{T}_h$ that satisfy (7.185) (for instance by tentatively using Prop. 7.2.7 like in Section 7.2.2) – again, for general geometries and boundary conditions – still remains to be solved, see in particular (Arnold & Brezzi, 1997a) in which an inf-sup condition is obtained albeit under some restrictive assumptions on the geometry. In this respect, the influence of the geometry in the membrane part of B is a major obstacle.

Remark 7.3.5. Given the considerable difficulty to prove an inf-sup condition for shell finite elements, Bramble & Sun (1998) have proposed and analyzed an interesting idea, which consists in relaxing the inf-sup condition while tolerating some degree of non-uniformity in the convergence of the approximate solutions. Namely a mixed method is used for which a stability condition weaker than the inf-sup condition (7.185) is shown to hold, and a

uniform error estimate is then obtained *under the condition*

$$h \leq C\sqrt{\varepsilon}. \tag{7.186}$$

This means that locking should not appear unless a very small thickness (or a coarse mesh) is used. However, a thorough numerical assessment of this finite element procedure is lacking, as regards locking as well as other difficulties featured by mixed finite elements for shells (see below). ■

Finally, as regards the mathematical analysis of the locking of shell problems, the only shell finite element method for which an analysis *valid for general geometries* has provided a uniform error estimate for *bending-dominated* problems is the method given in (Chapelle & Stenberg, 1998a). This method corresponds to a *mixed-stabilized* formulation in which additional stabilizing terms are added to the mixed formulation in order to by-pass the inf-sup condition.

In the framework of shell models, mixed formulations feature another – still more critical – difficulty, which is that they are clearly tailored to the approximation of a problem in which a constraint is enforced by penalization. But for shell problems to fall into that category, according to our above discussion the asymptotic behavior must be of the bending-dominated type. On the other hand, if the problem solved using a mixed method happens to be of the membrane-dominated type, instead of (7.184) we – in fact – need to consider

$$\boxed{A_{\mathrm{m}}^h(U_h^\varepsilon, V) + \varepsilon^2 A_{\mathrm{b}}(U_h^\varepsilon, V) = G(V), \qquad \forall V \in \mathcal{V}_h,} \tag{7.187}$$

Hence, compared to Equation (7.154) satisfied by the exact solution, the mixed formulation leads to a perturbation of the *leading term* of the formulation. Therefore, convergence (and in particular uniform convergence) cannot be expected in this case unless the *consistency* of A_{m}^h with respect to A_{m} is strictly controlled. This condition is very difficult to enforce, in particular because mixed methods are not designed to that purpose. As a matter of fact, for the above-mentioned mixed-stabilized scheme that works well in bending-dominated cases, uniform convergence is not obtained in membrane-dominated situations, hence the element cannot be used for general shell analysis. There is also some numerical evidence that the same difficulty holds for the lowest-order finite element procedure proposed in (Arnold & Brezzi, 1997a), see (Bucalem & Shimura da Nóbrega, 2000).

Therefore, it appears that we are facing a dilemma caused by the dramatic discrepancy between the two major asymptotic states of shell problems. Indeed, in the above discussion, we have shown that there are elements (the classical displacement-based elements) that work well in the membrane-dominated case but fail in the bending-dominated case. Also, we have shown

that there are elements (the mixed elements referred to above) that work well in the bending-dominated case but fail in the membrane-dominated case. The real challenge lies in designing elements that perform well in both cases and are practical and effective, and therefore can be used for general shell analysis.

8. Towards the Formulation of Effective General Shell Elements

In Chapter 7 we discussed the difficulties encountered in the formulation of reliable and effective shell elements. These difficulties are summarized in the synopsis of Figure 8.1 in correspondence with the various types of shell asymptotic behaviors that can be encountered, as addressed in Chapter 5. The objective of the present chapter is to propose some strategies to evaluate shell finite element discretizations in the search for improved schemes. With general analytical proofs not available for the convergence behavior, the numerical assessment is a key ingredient in these strategies. As an example we present the formulation of the MITC shell elements and demonstrate how the numerical assessment of these elements can be performed.

8.1 Guidelines for Assessing and Improving the Reliability of Shell Finite Elements

Whereas the complete mathematical analysis required to design and justify a general uniformly and optimally converging[1] finite element procedure for shell problems still seems out of reach, we believe that it is crucial – in the search for improved shell elements – to combine the physical and mathematical insight provided by the analysis of mathematical shell models and, as far as possible, of their discretizations on the one hand, with extensive numerical testing on the other hand. In this interaction, *test problems* (also often called "benchmarks") are both an essential interface and an invaluable means of assessing the performance and the reliability of shell finite element methods, hence also of improving these methods.

8.1.1 Considerations on proper selection and use of test problems

Of course, in order to provide a rigorous and meaningful assessment tool, test problems must be very carefully chosen, and properly used. It is clear from the conclusions of Chapter 7 that the design of a general finite element

[1] Recall that by "uniformly and optimally converging" we mean that the convergence behavior satisfies an estimate of the type (7.1) (with p being the optimal rate of convergence and C a constant independent of ε).

D. Chapelle, K.-J. Bathe, *The Finite Element Analysis of Shells – Fundamentals*,
Computational Fluid and Solid Mechanics, 2nd ed., DOI 10.1007/978-3-642-16408-8_8,

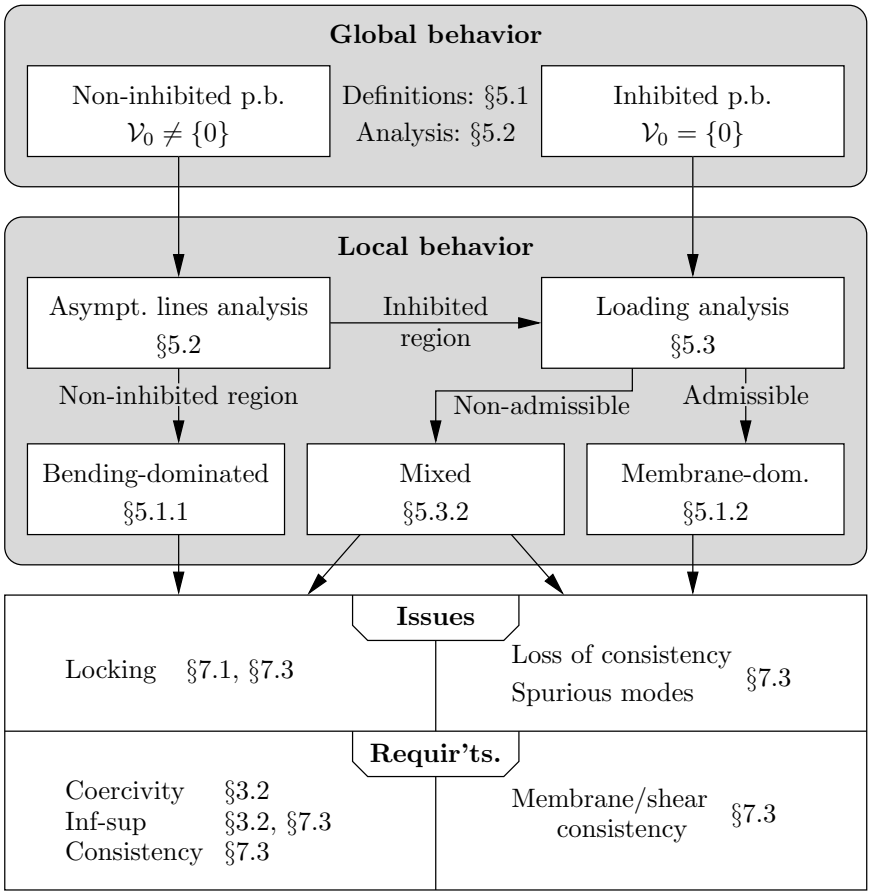

Fig. 8.1. Issues and requirements for finite elements to represent shell behaviors (note: "p.b." stands for pure bending)

procedure for shell analysis must aim at overcoming two major difficulties: locking must not occur in bending-dominated cases, and consistency must not be lost, in particular in the membrane and shear terms when attempting to remedy locking.

As discussed in (Chapelle & Bathe, 1998), a suitable selection of test problems should therefore fulfill the following essential requirements:

- A basic set of test problems must contain instances of the two fundamental asymptotic behaviors of shell structures;
- Several types of geometries (namely, at least one instance for each of the elliptic, parabolic and hyperbolic types) must be considered, since the asymptotic behavior is highly sensitive to the geometry of the midsurface (for example a set of test problems only based on cylinders is not satisfactory);

- Numerical computations must be performed and reported upon for several values of h (since we are concerned with the whole convergence behavior and not only with the accuracy in one specific instance) and for several values of ε (in order to assess the robustness of the convergence with respect to this parameter).
- Test cases corresponding to well-posed variational problems with well-posed limit problems should be preferably employed, as only such problems allow a straightforward interpretation of any numerical difficulties.

We also emphasize that a deep insight into the behavior of the exact solutions is an essential prerequisite in the assessment procedure, i.e. in the proper use of test problems. A particularly important feature of these solutions is the development of boundary layers which vary in amplitude and width when the thickness of the shell varies. If these boundary layers are not properly taken into account in the choice of the discretization scheme (in particular by refining the mesh when and where appropriate), they can strongly affect the convergence behavior and may lead to wrong conclusions in the reliability assessment. This insight, available for plates (see e.g. (Häggblad & Bathe, 1990; Arnold & Falk, 1996; Dauge & Yosibash, 2000)), has more recently been developed for shells also, see in particular (Karamian et al., 2000; Pitkäranta et al., 2001).

Once a good set of test problems has been selected, it is crucial to evaluate the error made in the numerical computations using proper *error measures*. We now review and evaluate some possible choices, including the currently most widely used measures (see also Chapelle, 2001). We point out that we always consider *relative errors*, namely errors normalized by an absolute value corresponding to the reference solution, as in the left-hand side of (7.1) when the error measure is given by a norm.

Pointwise displacements. This error measure is most extensively used, especially in the engineering literature. It is, however, likely to be misleading, since the pointwise convergence of finite element methods is not guaranteed in general (namely, when the energy norm is not compatible with pointwise displacements, see in particular Remark 4.3.5). For example, when analyzing the Scordelis-Lo roof (see Section 5.3.2), it is common practice to only measure the displacement in the middle of the free edge (and only for one given thickness value). This is valuable but clearly not sufficient to fully measure the error in the solution and thus evaluate a finite element discretization scheme.

Energy norm. This norm corresponds to $[\varepsilon^2 A_{\mathrm{b}}(V,V) + A_{\mathrm{m}}(V,V)]^{\frac{1}{2}}$ (in the framework of Chapter 7). Note that we can scale the energy by any given power of ε (and indeed any other coefficient) since we are only concerned with relative errors. Clearly, if a displacement-based element were assessed with this norm, in membrane-dominated problems the norm would be an appropriate measure of the solution quality. Consider next that we use this

norm for a bending-dominated problem. Then the error measured for the displacement based element discretization would depend on the shell thickness and the convergence curves would considerably shift as the shell thickness decreases, see for example Figure 8.46 below. Assume further that we actually have a "perfect locking-free element". Then the convergence curves must be expected to look worse because the error for the displacement-based element is smallest in this norm, hence the optimal character of the numerical procedure would not be reflected.

Modified energy norm. This norm incorporates the modification introduced by the mixed formulation, namely we would now use $[\varepsilon^2 A_{\rm b}(V,V) + A_{\rm m}^h(V,V)]^{\frac{1}{2}}$ in the notation of Chapter 7. This choice is advocated in (Malinen & Pitkäranta, 2000), in particular. With this norm, the error measure is dependent on the specific finite element procedure used. This means that the quality of an element is evaluated by using its own formulation. Hence two different elements would be evaluated using two different criteria. However our objective is to use, instead, an absolute – that is element formulation independent – error assessment. Moreover, we point out that this norm can conceal spurious zero membrane energy modes – namely, discrete displacement fields $V \in \mathcal{V}_h$ such that $A_{\rm m}^h(V,V) = 0$ whereas $A_{\rm m}(V,V)$ is "finite" – hence this norm may be unreliable in measuring the quality of an element, in particular in membrane-dominated cases.

Energy variation. This measure corresponds to using

$$\frac{\mathcal{W} - \mathcal{W}_h}{\mathcal{W}}, \tag{8.1}$$

where $\mathcal{W}$ is the energy that corresponds to the exact (or reference) solution, namely

$$\mathcal{W} = \varepsilon^2 A_{\rm b}(U^\varepsilon, U^\varepsilon) + A_{\rm m}(U^\varepsilon, U^\varepsilon), \tag{8.2}$$

and $\mathcal{W}_h$ the energy of the finite element solution, namely

$$\mathcal{W}_h = \varepsilon^2 A_{\rm b}(U_h^\varepsilon, U_h^\varepsilon) + A_{\rm m}(U_h^\varepsilon, U_h^\varepsilon), \tag{8.3}$$

for displacement-based methods and

$$\mathcal{W}_h = \varepsilon^2 A_{\rm b}(U_h^\varepsilon, U_h^\varepsilon) + A_{\rm m}^h(U_h^\varepsilon, U_h^\varepsilon), \tag{8.4}$$

for mixed methods. For displacement-based methods, it can be shown that this measure equals the square of the error in the energy norm, see e.g. (Bathe, 1996). However, this property does not hold for mixed methods, which makes the interpretation of this indicator more difficult. In fact, in actual solutions using mixed formulations we may well see positive and negative values of the

error measure (which is not a norm). For this reason, an absolute value was used in (Bathe et al., 2000a). Therefore it may well happen that a "nearly zero" value is obtained although the complete solution field is not yet accurate. A further mesh refinement would very likely show this fact. Hence, while this error measure has clearly some value to identify the behavior of approximate solutions, the measure is not an ideal one to use. In particular, this error measure not being a norm cannot be employed in an error analysis within the framework of Eq. (7.1), see also (Malinen & Pitkäranta, 2000).

Asymptotic convergence norms. We consider here the norms in which exact solutions are proven to converge to limit solutions, i.e. the norm of the displacement space for bending-dominated problems and the membrane energy norm for membrane-dominated problems. Since our objective is to assess whether the convergence behavior (when refining the mesh) is uniform as the thickness decreases, this particular choice of norms is very natural (see also Section 7.3), and indeed we cannot expect uniform convergence in stronger norms.

The "s-norm". We call "s-norm" (denoted by the symbol $\|\cdot\|_s$) the error measure obtained by comparing the approximate and reference strains by means of the governing energy, see (Bathe et al., 2002; Hiller & Bathe, 2003). Clearly, if the finite element procedure is purely displacement-based and when no approximation of the geometry is involved (as, e.g., in discretizations of the m-b and s-m-b models), this corresponds to the energy norm discussed above. When a mixed finite element procedure is used, however, we have a different error measure. For example, in the case of the MITC elements for the Reissner-Mindlin plate model – recall Eq. (7.133) – the s-norm would be defined as

$$\begin{aligned}&\|u^\varepsilon - u_h^\varepsilon, \underline{\theta}^\varepsilon - \underline{\theta}_h^\varepsilon\|_s^2 = \\ &\quad A_{\mathrm{b}}^{RM}(\underline{\theta}^\varepsilon - \underline{\theta}_h^\varepsilon, \underline{\theta}^\varepsilon - \underline{\theta}_h^\varepsilon) + \varepsilon^{-2}\frac{2EL}{1+\nu}\|\underline{\zeta}(u^\varepsilon, \underline{\theta}^\varepsilon) - R_h\big(\underline{\zeta}(u_h^\varepsilon, \underline{\theta}_h^\varepsilon)\big)\|_0^2.\end{aligned} \tag{8.5}$$

We note that – although this error measure uses the mixed strains like the modified energy norm above – the s-norm considered here has an absolute character since we compare the approximate finite element strains with the *exact reference strains*. We also emphasize that this error measure is of particular value for application purposes since it assesses the accuracy of the strains – hence also of the *stresses* – as provided by the finite element procedure employed. For a general shell element procedure (such as for MITC shell elements, see Section 8.2), recalling Eq. (4.30) in the case of an isotropic material we can define

$$\begin{aligned}\|\vec{U}^\varepsilon - \vec{U}_h^\varepsilon\|_s^2 = \int_\Omega \Big[&C^{\alpha\beta\lambda\mu}\big(e_{\alpha\beta}(\vec{U}^\varepsilon) - \tilde{e}_{\alpha\beta}(\vec{U}_h^\varepsilon)\big)\big(e_{\lambda\mu}(\vec{U}^\varepsilon) - \tilde{e}_{\lambda\mu}(\vec{U}_h^\varepsilon)\big) \\ &+ D^{\alpha\lambda}\big(e_{\alpha 3}(\vec{U}^\varepsilon) - \tilde{e}_{\alpha 3}(\vec{U}_h^\varepsilon)\big)\big(e_{\lambda 3}(\vec{U}^\varepsilon) - \tilde{e}_{\lambda 3}(\vec{U}_h^\varepsilon)\big)\Big]\, dV,\end{aligned} \tag{8.6}$$

where the "˜" notation refers to the use of the approximate geometry (see Sections 6.3 and 8.2) and also – when applicable – of the reduction operator corresponding to the mixed formulation considered.

As a conclusion to this discussion on error measures, our recommendation for the assessment of shell finite element procedures is to use primarily the *asymptotic convergence norms* and the *s-norm*.

When evaluating finite element schemes, particular attention needs to be given to boundary layers in the test problems; namely, we should ascertain that these boundary layers (i.e. the "non-smooth part" of the exact solutions) are properly resolved in the numerical solutions. To discuss the need for proper meshing of the boundary layers, consider that we use the asymptotic convergence norms. Then, for well-posed membrane-dominated problems approximated using displacement-based finite elements, the proof of Prop. 7.3.1 also shows that, recalling Eq. (7.162),

$$\begin{aligned} &\|U^\varepsilon - U_h^\varepsilon\|_{\mathrm{m}} + \varepsilon \|U^\varepsilon - U_h^\varepsilon\|_{\mathcal{V}} \\ &\qquad \leq C \inf_{V \in \mathcal{V}_h} \big\{ \|U^\varepsilon - V\|_{\mathrm{m}} + \varepsilon \|U^\varepsilon - V\|_{\mathcal{V}} \big\}, \end{aligned} \tag{8.7}$$

which means that a displacement-based finite element procedure is *uniformly optimal* with respect to ε for the norm $\|\cdot\|_{\mathrm{m}} + \varepsilon\|\cdot\|_{\mathcal{V}}$. Therefore, if the mesh is refined so that the boundary layers of a given test problem are properly resolved for this norm, uniform optimal convergence is obtained. This is illustrated in Figures 8.2 to 8.4, where the case of a clamped circular cylinder is considered (as described in details in Fig. 8.5). The s-m-b model is used, and Q2 (that is, 9-node) displacement-based elements are employed to discretize the problem. Figure 8.2 shows the convergence curves obtained for the membrane norm (i.e. $\|\cdot\|_{\mathrm{m}}$) and for decreasing values of ε (here, we take $L = 2R$, hence $\varepsilon = t/2R$) when as many layers of elements are used within the layer of width $\sqrt{\varepsilon}L$ along the boundaries (i.e. the boundary layers) as in the rest of the domain. We can see that the convergence rate is optimal for all values of the thickness, and that there is very little sensitivity of the convergence behavior on the value of ε. By contrast, if no particular treatment of the boundary layers is applied, we obtain the convergence curves displayed in Figure 8.3 where some significant sensitivity with respect to ε is observed. Also, if the original norm of $\mathcal{V}$ is used instead of the membrane norm (see Figure 8.4) we again detect some marked sensitivity. All these numerical results are in complete agreement with Equation (8.7).

Likewise, for bending-dominated problems classical results for mixed formulations show that, when the inf-sup condition is satisfied, we have the following optimal error bound, see Section 3.2:

$$\|U^\varepsilon - U_h^\varepsilon\|_{\mathcal{V}} + \|\Sigma^\varepsilon - \Sigma_h^\varepsilon\|_{\mathcal{T}} \leq C \inf_{\substack{V \in \mathcal{V}_h \\ \Xi \in \mathcal{T}_h}} \{\|U^\varepsilon - V\|_{\mathcal{V}} + \|\Sigma^\varepsilon - \Xi\|_{\mathcal{T}}\}. \tag{8.8}$$

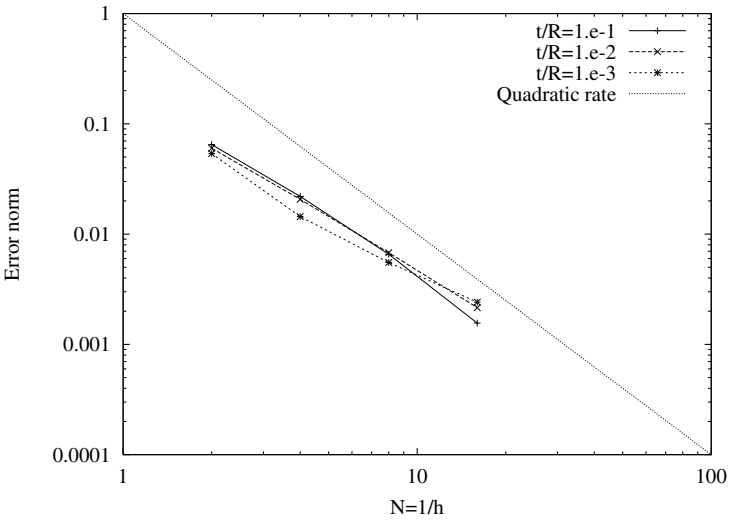

Fig. 8.2. Clamped cylinder: adapted mesh, membrane norm

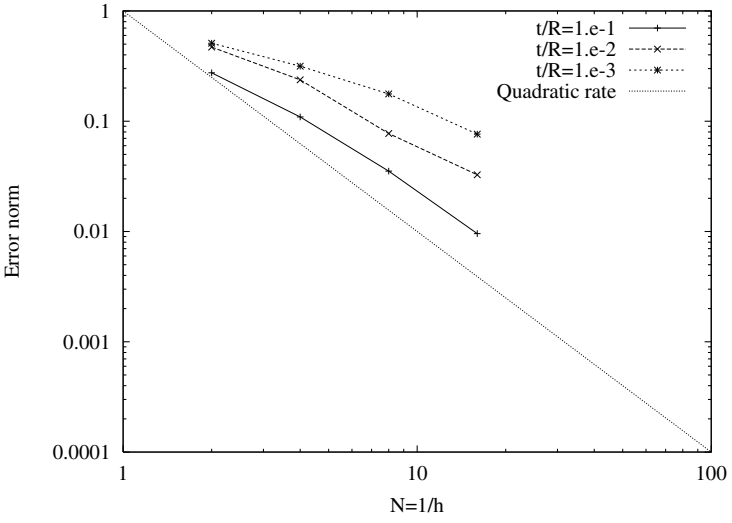

Fig. 8.3. Clamped cylinder: non-adapted mesh, membrane norm

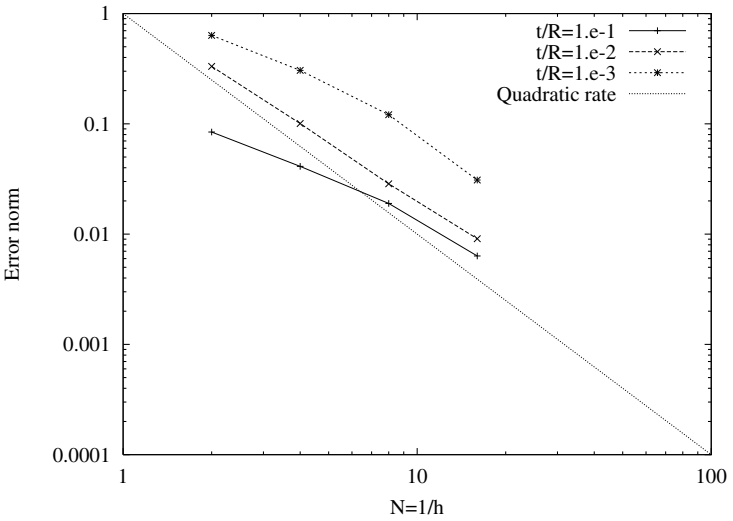

Fig. 8.4. Clamped cylinder: adapted mesh, H^1 norm

As previously mentioned we do not know of any mixed finite element procedure for shells that is mathematically proven to satisfy the inf-sup condition. Nevertheless, this estimate is very useful to determine how the meshes should be refined. Namely, we want to have an optimal uniform (with respect to ε) value in the right-hand side of Eq. (8.8), which is governed by the regularity of the exact displacements and stresses. This ensures that – if the inf-sup condition were to be satisfied – the finite element error corresponding to the left-hand side of Eq. (8.8) would also be uniformly optimal. Note that the norm $\|\cdot\|_{\mathcal{T}}$ is difficult to evaluate in practice, and that we may use instead the stronger L^2-norm (see e.g. Chapelle & Stenberg, 1998b; Bathe et al., 2000b) to ascertain the optimality in the right-hand side of Eq. (8.8).

Remark 8.1.1. In the above discussion regarding the asymptotic convergence norms used for numerical evaluation purposes, we do not mention the error made in the stress variables measured in the norm $\|\cdot\|_{\mathcal{T}}$, as appearing in (8.8). This is because the evaluation of this norm is out of reach in practice, in general. We could – of course – assess this error using instead the L^2 norm, but since the stresses do not in general converge in the L^2 norm the assessment results may then be misleading. ■

While therefore the importance of satisfying the inf-sup condition is apparent, mathematically proving this condition for arbitrary geometries and boundary conditions is a great challenge, and as mentioned above has not been accomplished for generally applicable finite element discretizations. Hence a numerical procedure to assess whether the inf-sup condition is satis-

fied is of primary interest. Such a numerical scheme was proposed and demonstrated in (Bathe et al., 2000b) and, in fact, numerical inf-sup tests are of general value to assess mixed formulations (Chapelle & Bathe, 1993; Bathe, 2001b).

8.1.2 Proposed set of test problems

Based on the above discussion, we now propose a set of suitable test problems designed to assess the effectiveness of shell finite elements and their robustness with respect to thickness variations. We divide these test problems according to their asymptotic behaviors.

As *bending-dominated test problems* we propose the following test cases:

Cylinder with free ends. The cylinder described in Figure 8.5 is loaded by a periodic pressure as shown in the figure (where ξ^2 denotes the circumferential arc-length as in Fig. 5.4). No boundary conditions are prescribed, and rigid body modes are discarded by enforcing appropriate symmetry conditions in the computational domain (namely, one sixteenth of the whole structure). Recalling Section 5.2.3, pure bending is clearly non-inhibited. This example was already proposed by (Pitkäranta et al., 1995) who also presented a procedure to obtain numerical solutions of arbitrary precision for shell models like the s-m-b model, see also (Brias-soulis, 2002b).

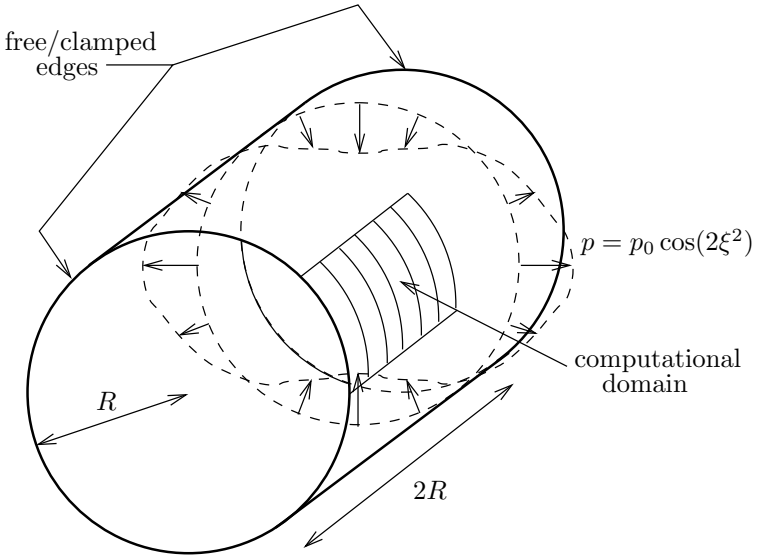

Fig. 8.5. Cylinder loaded by periodic pressure

Axisymmetric hyperboloid with free ends. This type of structure, shown in Figure 8.6, is used in actual shell designs, and in particular in the design of cooling towers for power plants. The specific geometry that we consider is defined by the equation

$$x^2 + y^2 = R^2 + z^2, \qquad z \in [-R, R], \tag{8.9}$$

(Oz) being the axis of symmetry. This is a hyperbolic surface and – when leaving the ends free – we obtain a structure with non-inhibited pure-bending (recall Section 5.2.2). We can, e.g., load this structure by a periodic pressure as for the above cylinder and then discard the rigid body modes using symmetry conditions. This is a more difficult test problem – especially as regards locking – than the free cylinder problem because the present surface features two non-zero principal curvatures (of opposite sign, due to the hyperbolic geometry).

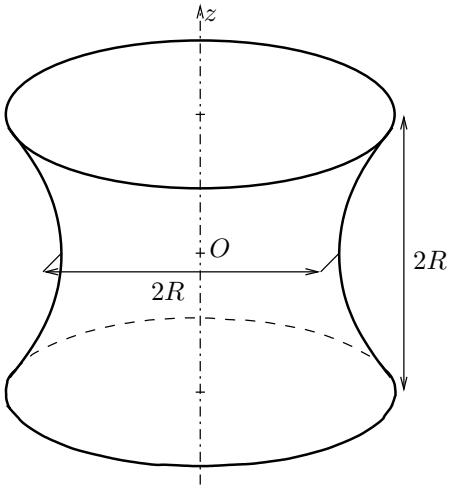

Fig. 8.6. Axisymmetric hyperboloid

Open hemisphere with free ends. We consider the open hemisphere shown in Figure 8.7, where the cutout is designed to avoid meshing difficulties with the top of the structure. When leaving the two boundaries free we have a bending-dominated structure, see Section 5.2.1. We can choose to apply, e.g., a periodic pressure loading such as for the above cylindrical structure.

As *membrane-dominated test problems* we propose the following test cases:

Cylinder with clamped ends. The geometric definition of this problem and the loading are the same as for the first proposed test above, see

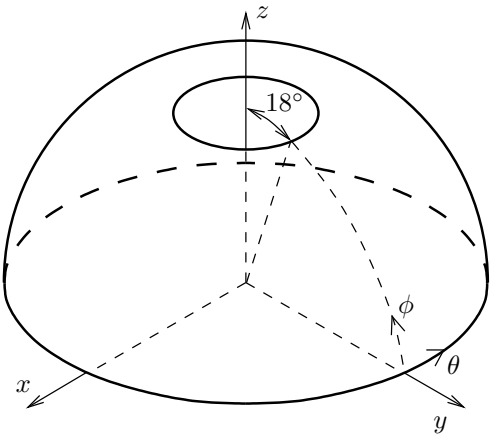

Fig. 8.7. Hemispherical shell under axisymmetric loading

Fig. 8.5, but we now consider fully-clamped ends. This problem for which pure bending is inhibited (see Section 5.2.3) is also analyzed in (Pitkäranta et al., 1995), where it is shown that the membrane limit problem is well-posed and how numerical solutions of arbitrary precision can be computed.

Axisymmetric hyperboloid with clamped ends. By considering the above-presented axisymmetric hyperboboid under periodic pressure and now imposing clamped boundary conditions, we obtain a well-posed membrane-dominated test problem (since the space of finite membrane energy $\mathcal{V}_{\mathrm{m}}$ is a Sobolev space and the loading is indefinitely smooth in this case, see Remark 5.2.1), see (Bathe et al., 2002; Hiller & Bathe, 2003) for further numerical evidence of this well-posedness.

Open hemisphere with clamped ends. For this structure with clamped top and bottom edges (like for a clamped full hemisphere) we recall from Section 5.2.1 that the space $\mathcal{V}_{\mathrm{m}}$ in which the membrane limit problem is posed is rather regular so that any "reasonable" loading (in L^2, say) will provide a well-posed limit problem (unlike for a similar structure with only one of the boundaries clamped, recall Section 5.3.2). If we choose an axisymmetric loading, we can also compare the numerical results of the shell analysis procedure with the results of some reliable axisymmetric analysis scheme.

We emphasize that for all the above-proposed test problems well-defined asymptotic limits exist, and more specifically for a given problem the asymptotic behavior is either membrane-dominated or bending-dominated. As previously discussed, other types of asymptotic behaviors (as defined in Chapter 5) do exist, and in particular in cases when pure bending is inhibited and "$G \notin \mathcal{V}'_{\mathrm{m}}$", see in particular Section 5.3.2 for examples. As also seen

in this section, a major difficulty in such cases is that – since we do not know of a norm for which an asymptotic limit exists – we cannot define a proper error measure for assessing the finite element approximation. This is why the use of such problems cannot be primarily recommended to assess the reliability of finite element procedures. However, as discussed in Section 5.3.2 these cases feature mixed characteristics of both bending-dominated and membrane-dominated behaviors, hence we may expect that a given finite element procedure that would perform well (namely, converge uniformly and optimally) for these two fundamental categories of asymptotic behaviors would also perform well in "more complex" cases.

In the evaluation of finite element procedures using the above test problems, reference solutions need be employed. Clearly, it is crucial to use reference solutions that actually correspond to the mathematical model underlying the finite element scheme employed. Different mathematical models will in general result into different exact solutions, and this should be reflected in the reference solutions. However, as emphasized in Chapter 5 any valid shell mathematical model should be asymptotically consistent with 3D continuum mechanics and therefore as the shell thickness decreases all exact solutions should converge to the same limit solutions. Of course, analytical solutions of shell mathematical models are frequently out of reach, and even when available only correspond to a mathematical model that may not be applicable to the finite element scheme used. Hence we need to resort to numerical reference solutions. These solutions are usually provided by finite element solutions obtained with very fine meshes.

8.2 Formulation of MITC Shell Elements

MITC[2] shell elements are general shell elements, namely, they are obtained using a 3D variational formulation, hence they differ significantly from the MITC plate elements presented in Section 7.2.4, although they are based on similar ideas. We introduce these elements here with the objective to demonstrate how mixed general shell elements can be constructed, how these elements relate to the theory discussed in this book, and to give some assessment results using the guidelines presented in the above section. Our purpose is not to give a complete assessment of these elements but only to show how the above-presented methodology would be applied using one membrane-dominated problem and one bending-dominated problem.

8.2.1 Formulation of quadrilateral MITC elements

Considering the (covariant) components of the strain tensor in the *local coordinate system* (r, s, z), the MITC shell elements are formulated by using – instead of the strain components directly computed from the displacements

[2] Recall that "MITC" stands for "Mixed Interpolation of Tensorial Components"

– an interpolation of these strain components within each element with a specific interpolation strategy for each component, see (Dvorkin & Bathe, 1984; Bathe & Dvorkin, 1986; Bucalem & Bathe, 1993; Bathe et al., 2003b) and see also (Bathe, 1996) with the references therein. The corresponding interpolation points where the tying of the interpolated strain components to the displacement-based strain components is performed – called the tying points – are shown in Figures 8.8, 8.9 and 8.10 for the MITC4, MITC9 and MITC16 shell elements, respectively[3]. Note that, in the MITC4 shell element – like in the MITC4 plate element – only the transverse shear strains are subjected to the interpolation procedure.

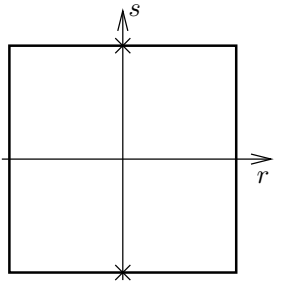

Component e_{rz}

Fig. 8.8. MITC4 shell element

8.2.2 Formulation of triangular MITC elements

In practice, triangular shell elements are also of utmost interest, in particular when complex geometries requiring unstructured automatic mesh generation are to be considered. In order to formulate triangular MITC elements using tied strain components, it is important that strain interpolations and a tying procedure be used that render the element 'isotropic', i.e. the element behavior shall be independent of the specific local coordinate system chosen (implicitly) within each element, hence independent of the order in which the nodes are listed in the element data. We refer to (Lee & Bathe, 2004; Lee et al., 2007) for more detailed discussions and related assessments regarding the isotropy of shell elements. Of course, these discussions apply to any other triangular shell element formulation as well.

In order to enforce the isotropy requirement, we recall that the tying procedure is applied to the covariant components of the strains in the basis $(\vec{g}_r, \vec{g}_s, \vec{g}_z)$. In this basis, the first two vectors $(\vec{g}_r, \vec{g}_s)$ are the images through the finite element geometric chart of the vectors $(\underline{\imath}_r, \underline{\imath}_s)$ connecting the element

[3] Of course, the components e_{sz} and e_{ss} are processed using symmetric rules

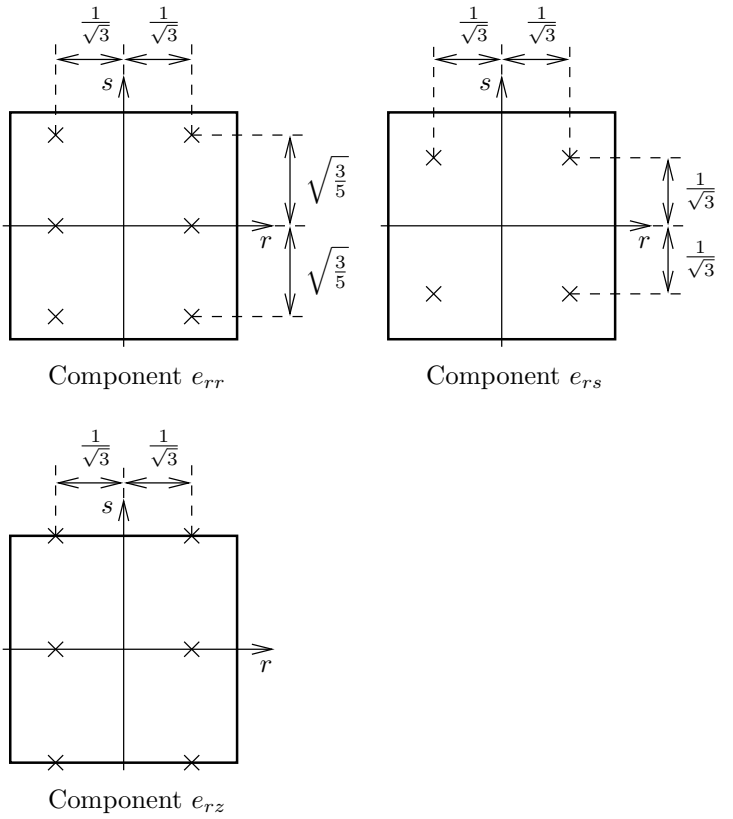

Fig. 8.9. MITC9 shell element

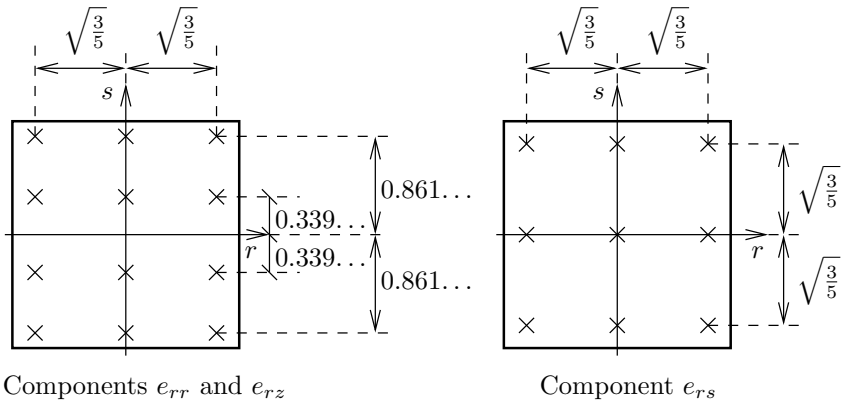

Fig. 8.10. MITC16 shell element

nodes in the (r, s) plane as shown in Figure 8.11. Clearly, we will impose the isotropy by requiring that – in the tying procedure – the third direction given by $\underline{\imath}_q = \underline{\imath}_s - \underline{\imath}_r$ – or equivalently $\vec{\bar{g}}_q = \vec{\bar{g}}_s - \vec{\bar{g}}_r$ in the physical space – is treated in exactly the same manner as the first two.

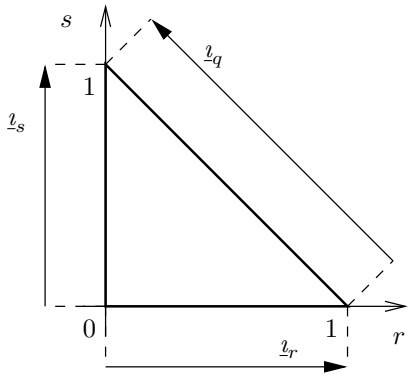

Fig. 8.11. Three director vectors in (r, s) coordinate system

Regarding the mixed interpolation of transverse shear strains, we note that the component of the shear strain tensor in the q-direction is given by, according to tensorial changes,

$$e_{qz} = e_{sz} - e_{rz}. \tag{8.10}$$

Therefore, isotropy is ensured by using tying points for e_{qz} in a symmetric manner with the tying points chosen for e_{rz} and e_{sz}, and by imposing that the corresponding interpolation spaces are also taken symmetrically, see examples below.

As concerns in-plane strains, we have the identity

$$e_{qq} = e_{ss} + e_{rr} - 2e_{rs}. \tag{8.11}$$

Hence, in this case isotropy is enforced by considering symmetric tying points and interpolation spaces for e_{rr}, e_{ss} and e_{qq}. Note that we then do not need to specifically prescribe an interpolation procedure for e_{rs} which is instead solved for in (8.11).

Remark 8.2.1. Note that the third coordinate could be alternatively defined by applying a rotation transformation on the (r, s) coordinate system, which would introduce different factors in Eqs. (8.10) and (8.11) as in (Lee & Bathe, 2004). ■

MITC3 element. We now present the formulation of an effective 3-node general shell element – referred to as the MITC3 shell element (Lee & Bathe, 2004) – satisfying the above-discussed isotropy requirements. We use mid-edge tying points as shown in Figure 8.12 for e_{rz}, e_{sz} and e_{qz}, and the corresponding mixed-interpolated strains $\tilde{e}_{rz}$, $\tilde{e}_{sz}$ and $\tilde{e}_{qz}$ are taken linear in (r, s) with each of them constant along the edge of their associated tying point. This means that for

$$\tilde{e}_{rz} = a_1 + b_1 r + c_1 s, \quad \tilde{e}_{sz} = a_2 + b_2 r + c_2 s,$$

we have six (independent) linear relations prescribed on the six coefficients, including the two constraints applied on

$$\tilde{e}_{qz} = \tilde{e}_{sz} - \tilde{e}_{rz}.$$

Namely, the linear relations yield

$$a_1 = e_{rz}^{(1)}, \quad b_1 = 0, \quad c_1 = e_{sz}^{(2)} - e_{rz}^{(1)} - e_{qz}^{(3)},$$

$$a_2 = e_{sz}^{(2)}, \quad b_2 = -c_1, \quad c_2 = 0.$$

Furthermore, for this 3-node shell element we leave the in-plane strains unmodified. This means that we implicitly rely on the effect of geometry approximation in the membrane strains – see Section 8.2.3 below – to alleviate membrane locking.

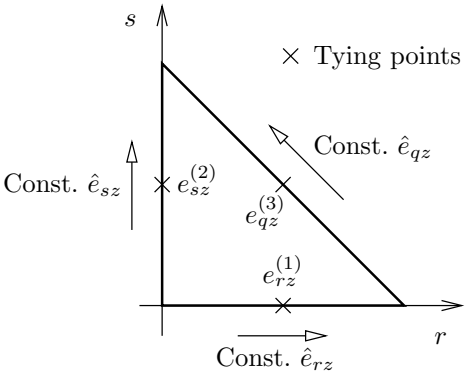

Fig. 8.12. MITC3 tying points and strain interpolations

MITC6 element. The formulation of the 6-node MITC6 shell element is more complex. One noteworthy difference is that the strain components that we interpolate are not the components of the strain tensor in the $(\vec{g}_r, \vec{g}_s, \vec{g}_z)$ basis which varies within each element, but instead the components in the fixed basis associated with the barycenter

$$(\vec{g}_r^{(b)}, \vec{g}_s^{(b)}, \vec{g}_z^{(b)}) = (\vec{g}_r, \vec{g}_s, \vec{g}_z)\big|_{r=1/3, s=1/3, z}.$$

Denoting these strain components by $\hat{e}_{ij}$ – with (i, j) standing for (r, s, z) in this case – the standard change of coordinates formulae give

$$\hat{e}_{ij} = \tilde{e}_{kl}\,(\vec{g}_i^{(b)} \cdot \vec{g}^k)\,(\vec{g}_j^{(b)} \cdot \vec{g}^l), \tag{8.12}$$

and of course we can also define

$$\vec{g}_q^{(b)} = \vec{g}_s^{(b)} - \vec{g}_r^{(b)},$$

leading to

$$\hat{e}_{qz} = \hat{e}_{sz} - \hat{e}_{rz}, \quad \hat{e}_{qq} = \hat{e}_{ss} + \hat{e}_{rr} - 2\hat{e}_{rs},$$

in order to enforce the isotropy of the interpolation procedures. We then summarize the MITC6 interpolation procedure in Figure 8.13. The shear strains $(\hat{e}_{rz}, \hat{e}_{sz}, \hat{e}_{qz})$ are taken quadratic, with linear variations along the edges corresponding to the associated tying points located according to the 2-point Gauss rule. With the barycenter used as a tying point for each component, this gives 4 linear relations for each, hence 12 relations for 12 coefficients in total. Regarding the in-plane strain components $(\hat{e}_{rr}, \hat{e}_{ss}, \hat{e}_{qq})$, they are taken linear with three tying points for each.

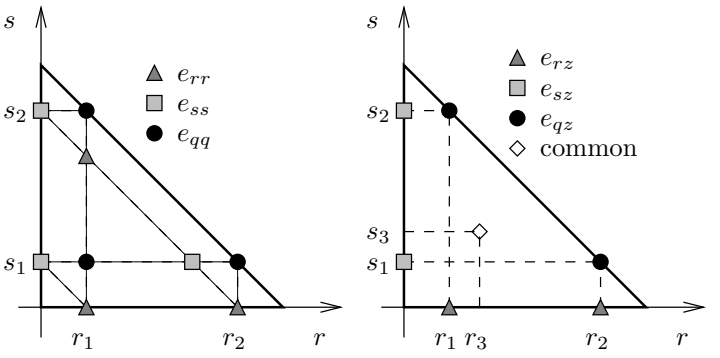

Fig. 8.13. MITC6 tying points

Remark 8.2.2. In the original MITC6 element proposed in (Lee & Bathe, 2004), the above-described interpolation procedures were directly applied with the components associated with the varying basis $(\vec{g}_r, \vec{g}_s, \vec{g}_z)$. However, this element – named MITC6a in (Lee & Bathe, 2004) – was later found to display spurious membrane modes in some specific membrane-dominated configurations, see (Chapelle & Paris Suarez, 2008; Beirão da Veiga et al., 2007). Thereafter the modification associated with the fixed basis $(\vec{g}_r^{(b)}, \vec{g}_s^{(b)}, \vec{g}_z^{(b)})$ was proposed and shown to be effective in (Kim & Bathe, 2009). ■

8.2.3 Insight into MITC shell formulations

The above-described tying point procedures clearly correspond to a reduction operator acting on the strains, similarly to the reduction operators introduced in Section 7.2.4 for MITC plate elements. However, the reduction operators for MITC shell elements act on *3D strains* instead of shell strains since – of course – general shell elements are based on 3D variational formulations, recall Section 6.3. This amounts to modifying the bilinear form A_h^{3D} in (6.47). This procedure can be related to a mixed formulation, although one that differs from the mixed formulations introduced and analyzed in Chapter 7, since by modifying the 3D tangential strains we – in essence – modify both the membrane, shear, *and bending* strains in the shell formulation, recall Eq. (4.9).

Remark 8.2.3. MITC procedures can also be related to mixed formulations by means of the Hellinger-Reissner principle, see (Dvorkin & Bathe, 1984; Bathe, 1996; Bathe et al., 2000a). ■

In order to get more insight into the connections of MITC formulations to the general framework of mixed formulations discussed in Chapter 7, we may observe – from the direct correspondence between the basic shell model summarized in (6.35) and the discrete formulation (6.47) on which general shell elements are based – that an asymptotic analysis similar to that performed for the basic shell model can also be performed for the discrete problem characterizing MITC solutions – at least formally. Considering sequences of problems obtained when decreasing the thickness parameter while keeping the nodal data (hence the approximate midsurface) unchanged, we obtain two different limit problems depending on the contents of the subspace

$$\mathcal{V}_{0h} = \{V \in \mathcal{V}_h \mid A_{\mathrm{m}}^h(V, V) = 0\}, \tag{8.13}$$

where A_{m}^h denotes an approximation of the A_{m} bilinear form arising in the general shell element formulation (see below discussion). We can say that $\mathcal{V}_{0h}$ is a subspace of finite element displacements that satisfy the inextensional

constraints approximately. The two limit problems are then similar to the continuous case, namely,

1. When $\mathcal{V}_{0h} = \{0\}$, we need to consider
   Find $U_h^{\mathrm{m}} \in \mathcal{V}_h$ *such that*

$$A_{\mathrm{m}}^h(U_h^{\mathrm{m}}, V) = G^h(V), \qquad \forall V \in \mathcal{V}_h, \tag{8.14}$$

   where G_h denotes the general shell element approximation of G.
2. When $\mathcal{V}_{0h} \neq \{0\}$, the limit problem is
   Find $U_h^0 \in \mathcal{V}_{0h}$ *such that*

$$A_{\mathrm{b}}^h(U_h^0, V) = G^h(V), \qquad \forall V \in \mathcal{V}_h, \tag{8.15}$$

   where A_{b}^h is an approximation of the A_{b} bilinear form.

Remark 8.2.4. In general we do not have $\mathcal{V}_{0h}$ equal to $\mathcal{V}_h \cap \mathcal{V}_0$ since A_{m}^h differs from A_{m}. As already mentioned, the primary objective of mixed procedures is to relax the constraints prevailing in $\mathcal{V}_0$ at the finite element level, so we typically expect $\mathcal{V}_{0h}$ to be "larger than" $\mathcal{V}_h \cap \mathcal{V}_0$ in bending-dominated situations. ■

Summarizing the above asymptotic considerations, we can see that the finite element formulation considered is asymptotically equivalent to the following unique problem
Find $\tilde{U}_h^\varepsilon \in \mathcal{V}_h$ *such that*

$$\boxed{\varepsilon^3 A_{\mathrm{b}}^h(\tilde{U}_h^\varepsilon, V) + \varepsilon A_{\mathrm{m}}^h(\tilde{U}_h^\varepsilon, V) = F_h^\varepsilon(V), \qquad \forall V \in \mathcal{V}_h.} \tag{8.16}$$

In this equation F_h^ε carries ε as a superscript to recall that a scaling is required, and h as a subscript because the specific expression used is based on geometric approximations (when compared with the exact form F^ε).

In order to illustrate this discussion, we now show how the expressions of A_{b}^h and A_{m}^h can be derived for the example of a shell of constant thickness and when using Strategy *S-1* to implement the plane stress assumption (recall Section 6.3). Then the governing bilinear form is given by (6.51). With a view to discussing the MITC procedure, we use the local (r, s, z) coordinate system instead of (ξ^1, ξ^2, ξ^3) in this expression. Due to tensorial invariance, this simply gives

$$\begin{aligned} A_h^{3D}(\vec{V}, \vec{W}) = \sum_K \int_{K,z} \big[& \bar{C}^{\alpha\beta\lambda\mu} \bar{e}_{\alpha\beta}(\vec{V}) \bar{e}_{\lambda\mu}(\vec{W}) \\ & + \frac{4}{t^2} \bar{D}^{\alpha\lambda} \bar{e}_{\alpha z}(\vec{V}) \bar{e}_{\lambda z}(\vec{W}) \big] \sqrt{\bar{g}}\, dr ds dz, \end{aligned} \tag{8.17}$$

where the Greek dummy indices are now associated with (r, s) and $\sqrt{\bar{g}}$ denotes the Jacobian corresponding to (r, s, z). The factor $4/t^2$ comes from the change of variables from ξ^3 to z. Recalling (6.49) we have

$$\vec{\bar{g}}_\alpha = \left(\vec{\Phi}_h\right)_{,\alpha} = \vec{\bar{a}}_\alpha + z\frac{t}{2}\vec{\bar{a}}_{3,\alpha}, \tag{8.18}$$

$$\vec{\bar{g}}_z = \frac{t}{2}\vec{\bar{a}}_3, \tag{8.19}$$

defining

$$\vec{\bar{a}}_\alpha = \left[\mathcal{I}(\vec{\phi})\right]_{,\alpha}, \qquad \vec{\bar{a}}_3 = \mathcal{I}(\vec{a}_3). \tag{8.20}$$

Therefore

$$\begin{aligned} \bar{e}_{\alpha\beta}(\vec{V}) &= \frac{1}{2}(\vec{V}_{,\alpha}\cdot\vec{\bar{g}}_\beta + \vec{V}_{,\beta}\cdot\vec{\bar{g}}_\alpha) \\ &= \gamma^h_{\alpha\beta}(\vec{v}) + z\frac{t}{2}\chi^h_{\alpha\beta}(\vec{v},\vec{\eta}) + z^2\frac{t^2}{8}(\vec{\eta}_{,\alpha}\cdot\vec{\bar{a}}_{3,\beta} + \vec{\eta}_{,\beta}\cdot\vec{\bar{a}}_{3,\alpha}), \end{aligned} \tag{8.21}$$

for

$$\vec{V} = \vec{v} + \frac{zt}{2}\vec{\eta}, \tag{8.22}$$

and with

$$\gamma^h_{\alpha\beta}(\vec{v}) = \frac{1}{2}(\vec{v}_{,\alpha}\cdot\vec{\bar{a}}_\beta + \vec{v}_{,\beta}\cdot\vec{\bar{a}}_\alpha), \tag{8.23}$$

$$\chi^h_{\alpha\beta}(\vec{v},\vec{\eta}) = \frac{1}{2}(\vec{\eta}_{,\alpha}\cdot\vec{\bar{a}}_\beta + \vec{\eta}_{,\beta}\cdot\vec{\bar{a}}_\alpha + \vec{v}_{,\alpha}\cdot\vec{\bar{a}}_{3,\beta} + \vec{v}_{,\beta}\cdot\vec{\bar{a}}_{3,\alpha}). \tag{8.24}$$

These expressions can be compared with those of the membrane and bending strain components in (4.10), of which they are approximate forms owing to the approximation of the geometry characterized in (8.20) and to the fact that we do not have exact orthogonality between $\vec{\bar{a}}_3$ and $\vec{\eta}$. Likewise, we have

$$\bar{e}_{\alpha z}(\vec{V}) = \frac{t}{2}\left[\zeta^h_\alpha(\vec{v},\vec{\eta}) + z\frac{t}{2}o^h_\alpha(\vec{\eta})\right] \tag{8.25}$$

with the approximate shear strain

$$\zeta^h_\alpha(\vec{v},\vec{\eta}) = \frac{1}{2}(\vec{v}_{,\alpha}\cdot\vec{\bar{a}}_3 + \vec{\eta}\cdot\vec{\bar{a}}_\alpha) \tag{8.26}$$

which can be compared to the exact expression in (4.10). In (8.25) we also have the additional term

$$o_\alpha^h(\vec{\eta}) = \frac{1}{2}(\vec{\eta}\cdot\vec{a}_3)_{,\alpha}, \tag{8.27}$$

which has no direct counterpart in the exact expressions (4.9) since at the continuous level we have $\vec{\eta}\cdot\vec{a}_3 = 0$. However this term has a limited impact since we have, by Lemma 6.3.1,

$$\|\vec{\eta}\cdot\vec{a}_3\|_{H^1(\omega)} \le \|\vec{\eta}\cdot\vec{a}_3\|_{H^1(\omega)} + \|\vec{\eta}\cdot(\vec{a}_3-\vec{a}_3)\|_{H^1(\omega)} \le Ch\|\vec{\eta}\,\|_{H^1(\omega)}. \tag{8.28}$$

We can now infer the expressions of $A_{\rm m}^h$ and $A_{\rm b}^h$:

$$\begin{aligned} A_{\rm m}^h(\vec{v},\vec{\eta};\vec{w},\vec{\tau}) = \sum_K L\int_K \big[&{}^0\bar{C}^{\alpha\beta\lambda\mu}\tilde{\gamma}_{\alpha\beta}^h(\vec{v})\tilde{\gamma}_{\lambda\mu}^h(\vec{w}) \\ &+ {}^0\bar{D}^{\alpha\lambda}\tilde{\zeta}_\alpha^h(\vec{v},\vec{\eta})\tilde{\zeta}_\lambda^h(\vec{w},\vec{\tau})\big]\sqrt{\bar{a}}\,drds, \end{aligned} \tag{8.29}$$

$$\begin{aligned} A_{\rm b}^h(\vec{v},\vec{\eta};\vec{w},\vec{\tau}) = \sum_K \frac{L^3}{12}\int_K \big[&{}^0\bar{C}^{\alpha\beta\lambda\mu}\tilde{\chi}_{\alpha\beta}^h(\vec{v},\vec{\eta})\tilde{\chi}_{\lambda\mu}^h(\vec{w},\vec{\tau}) \\ &+ \frac{{}^0\bar{D}^{\alpha\lambda}}{4}\tilde{o}_\alpha^h(\vec{\eta})\tilde{o}_\lambda^h(\vec{\tau})\big]\sqrt{\bar{a}}\,drds, \end{aligned} \tag{8.30}$$

where the "0" left superscript is used to denote the value of the quantity on the (approximate) midsurface, and the "˜" notation means that we are using the MITC rules of strain interpolation described above. These expressions can be compared with the corresponding exact expressions in the s-m-b model, recall (5.6) and (5.7).

Remark 8.2.5. Note that the above expressions of $A_{\rm m}^h$ and $A_{\rm b}^h$ can be used directly in the variational formulation (8.16) as a shell finite element procedure, and a closely-related approach is followed in (Chapelle et al., 2003b). This is – however – mostly valuable for the purpose of mathematical analysis, since in practice we lose the advantage of the flexibility of general shell elements by – in essence – integrating the constitutive law across the thickness *a priori*. ■

We are now in a position to better understand the connections of MITC shell formulations with the mixed formulations presented in the previous chapters, as well as the difficulties involved in the mathematical analysis of these finite element procedures. Comparing the asymptotically equivalent "conceptual" formulation (8.16) with the generic mixed formulation discussed in Chapter 7 and written in the alternate scaled forms (7.184) and (7.187), the main difference lies in the substitution of $A_{\rm b}^h$ for $A_{\rm b}$. This substitution itself is – however – not likely to lead to serious difficulties. Indeed, the consistency error introduced can be decomposed into two sources, namely, the geometric approximations which we showed to be well-controlled in Chapter

6 and the MITC interpolation procedure of the strains. Although the impact of this interpolation procedure is difficult to analyze mathematically in itself (see below), it can be quite easily assessed numerically by using for comparison purposes special MITC elements in which only the first term in the z-expansion of each strain component (see (8.21) and (8.25)) is interpolated at the tying points according to the MITC procedure, which takes care of the terms that induce locking without affecting the approximate bending strains.

Furthermore, the above expressions (8.29)-(8.30) and the related discussion provide an illustration of the difficulties hindering a mathematical analysis of shell mixed formulations, beyond that concerning a formal proof of the inf-sup condition which has not been achieved for any general shell finite element procedure so far. As highlighted in Chapter 7, it is important to assess the consistency of A_{m}^h with respect to A_{m} in membrane-dominated situations. This consistency should then hold in the norm that prevails in the asymptotic limit – namely, the membrane energy norm – which means that we are seeking an estimate of the kind needed in the first Strang Lemma, see e.g. (Ciarlet, 1978), viz.

$$|A_{\mathrm{m}}(V,W) - A_{\mathrm{m}}^h(V,W)| \leq Ch^p A_{\mathrm{m}}(V,V)^{\frac{1}{2}} A_{\mathrm{m}}(W,W)^{\frac{1}{2}}, \tag{8.31}$$

for all (V,W) in $(\mathcal{V}_h)^2$. This type of consistency estimate is particularly difficult to establish for two reasons:

1. With the strategy used in Chapter 6 to analyze the consistency errors of general shell elements we can also bound here the consistency errors arising from all sources of geometric approximations, including from the differences between exact and approximate membrane and shear strains. However these consistency errors are then naturally bounded in the H^1-norm, not in the required membrane norm.
2. Concerning the consistency error arising from the MITC tying point procedure, the analysis in Sobolev norms (let alone in the membrane norm) is still an open issue.

Therefore, although the difficulties to be confronted with in the mathematical analysis of MITC shell elements are identified in the above discussion, these difficulties appear to be quite considerable and a complete analysis is not yet at hand, although some preliminary results are available, see in particular (Malinen, 2001; Havu & Pitkäranta, 2002; Niemi, 2009). Nevertheless, the fundamental principles stated above for the numerical testing of shell finite elements are – of course – applicable to MITC elements in order to perform a reliable and thorough assessment of these elements.

8.2.4 Considerations regarding 3D-shell elements

Regarding the 3D-shell elements introduced in Section 6.4, we have seen by analyzing the asymptotic behavior of the 3D-shell model – namely, the

mathematical model underlying 3D-shell elements – in Section 5.4.2 that in bending-dominated structures the same constraints – namely of vanishing membrane and shear strains – are also present in the variational formulation of the proposed shell element, recall (5.210). Hence, it is straightforward to use the same treatments – namely, the MITC approach – to address the induced locking phenomena. In addition, we can see in (5.210) that a new constraint applies, which is that a displacement field expressed in the form

$$\vec{V}(\xi^1,\xi^2,\xi^3) = \vec{v}(\xi^1,\xi^2) + \xi^3\vec{\eta}(\xi^1,\xi^2) + (\xi^3)^2\vec{\varsigma}(\xi^1,\xi^2),$$

should also satisfy

$$\vec{\eta}\cdot\vec{a}_3 \equiv 0, \tag{8.32}$$

in the asymptotic pure-bending limit. Hence, this constraint creates an additional source of locking that we call *pinching locking*, due to the nature of the quantity that tends to vanish, namely, the pinching strain.

In order to circumvent the pinching locking phenomenon, a natural idea inspired from the MITC approach is to use tying points for the corresponding e_{zz} tensorial component. In particular, when using the nodes themselves as tying points (as proposed e.g. in (Betsch & Stein, 1995; Bischoff & Ramm, 1997)) we can see that the relaxed constraint imposed is that

$$\vec{\eta}\cdot\vec{a}_3 = 0 \tag{8.33}$$

at the nodes only, which is easily satisfied by the discrete displacements. In fact, it can be mathematically proven that this strategy effectively remedies the pinching locking phenomenon, see (Chapelle et al., 2003a).

Another specific concern with 3D-shell elements arises when analyzing structures made of nearly-incompressible materials. Indeed, when using classical shell models and associated adequate finite element procedures, the plane stress assumption – in essence – cancels the incompressible singularity (the "$1-2\nu$" term does not appear in the denominator of the constitutive law), and these models and their numerical discretizations are compatible with the incompressible limit, as fully mathematically substantiated in (Chapelle et al., 2004b). In 3D-shell models and finite elements, however, the plane stress assumption is not used, hence the incompressible singularity is still present, and it is shown in (Chapelle et al., 2004b) that a specific treatment is *required* in order to recover proper consistency with the incompressible limit. This treatment consists in projecting the trace of the strain tensor – namely, the volumetric strain – onto the space of functions linear across the thickness, which can be very effectively performed in 3D-shell elements by using a 2-point integration rule in the thickness direction. When this treatment is not applied, the incompressible solution is wrong for the *continuous* 3D-shell model itself, hence even increased mesh refinement cannot

compensate for the error in this case. Some preliminary numerical illustrations of this strategy are given in (Chapelle et al., 2004b), and some more detailed validations using a pressure interpolation allowing any integration order – as, for example, needed for general nonlinear analysis – are presented in (Kim & Bathe, 2008).

8.3 Assessment Results

In this section we present some assessment results of the above-described MITC shell elements with test problems based on two types of geometries:

- Planar structures, primarily with the motivation of comparing MITC shell and plate elements with each other;
- The axisymmetric hyperboloid, a doubly-curved surface which allows to obtain both membrane-dominated and bending-dominated behaviors, depending on the boundary conditions considered.

8.3.1 Shell elements used in plate bending

The MITC plate elements, discussed in Section 7.2.4 and constructed in principle like the shell elements, have a strong mathematical basis for linear plate analyses and show optimal convergence behavior, independent of the plate thickness, in mathematical analyses and numerical tests. The disadvantage of these elements is that they have internal nodes that only carry rotational degrees of freedom. As the shell elements are used in practice for both plates and shells, a natural question to ask is therefore "How much more powerful are the MITC plate bending elements when compared to the MITC shell elements in the linear analysis of plates?". This question was analyzed in detail in (Lee & Bathe, 2010) from which the numerical results given below are taken.

In Figures 8.14 to 8.16 we compare the errors obtained with the quadratic MITC plate and shell elements, for the softly clamped square plate test problem already considered in Section 7.2.4, recall Fig. 7.15. In addition to the H^1-semi-norm for the displacement errors and to the H^1-norm for the rotation errors, we also plot the s-norm relative errors. For all the error indicators considered the MITC9 plate and shell elements behave almost identically, namely, they achieve an optimal rate of convergence without any sensitivity with respect to the thickness parameter. As regards the triangular elements, we observe that the MITC6 shell element convergence is more significantly suboptimal than for the MITC7 plate element, with a slight sensitivity on the thickness parameter which may indicate some attenuated locking. When looking at the displacement and rotation errors separately we can see that MITC6 deficiencies are mainly due to rotation convergence. Nevertheless, the MITC6 convergence behavior is reasonable on the whole.

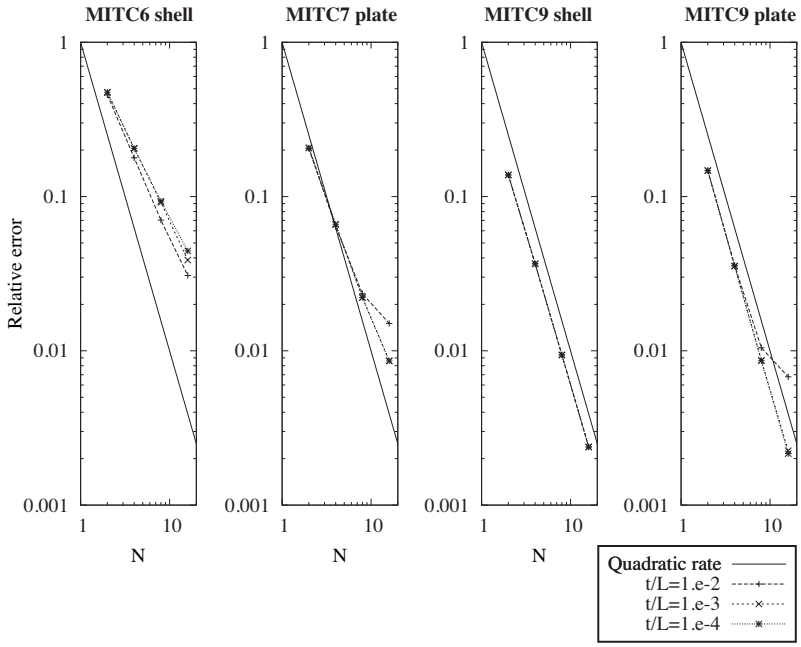

Fig. 8.14. Square plate: s-norm

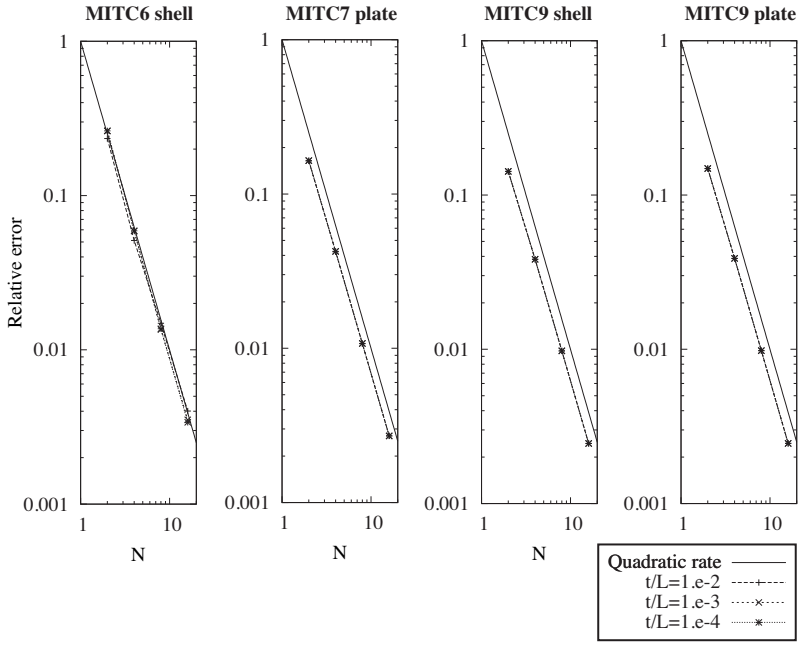

Fig. 8.15. Square plate: displacement H^1-semi-norm

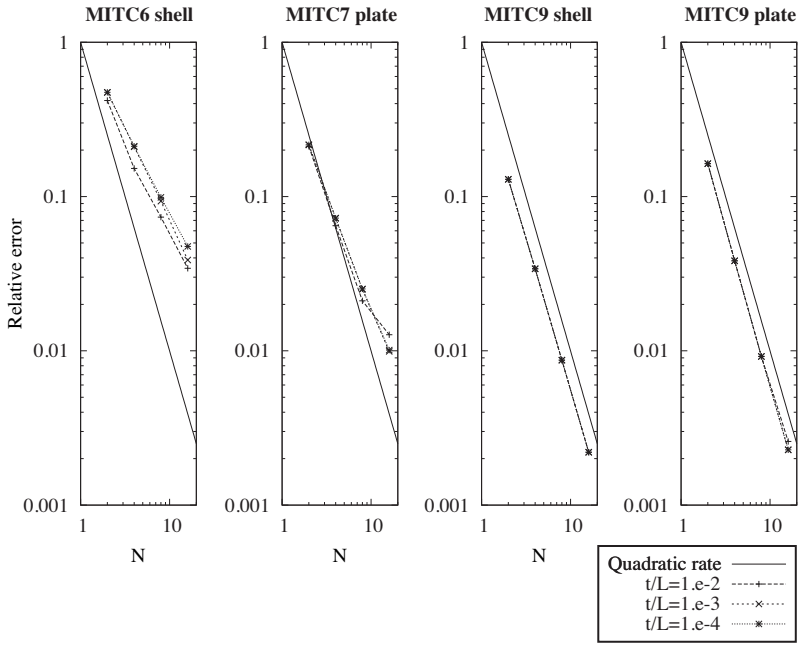

Fig. 8.16. Square plate: rotations H^1-norm

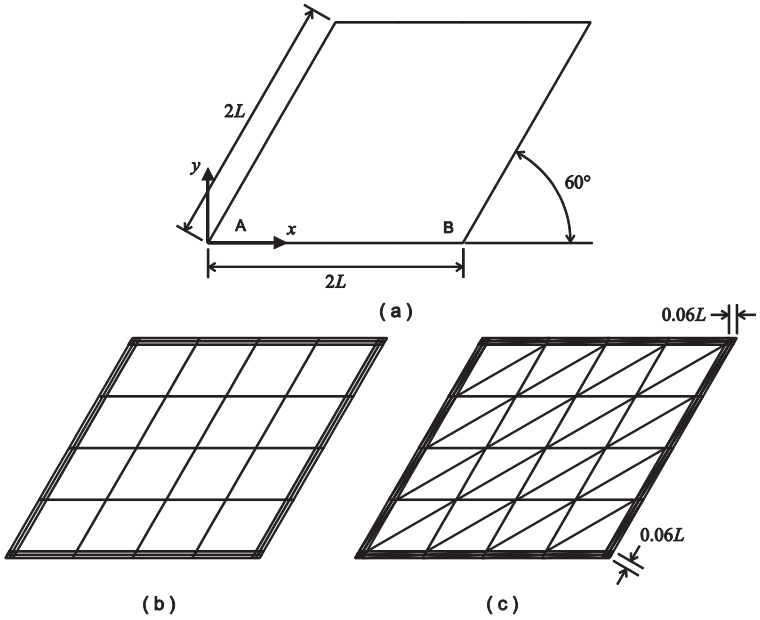

Fig. 8.17. Skewed plate: (a) geometry, (b) quadrilateral and (c) triangular mesh

We now consider a more difficult test problem consisting of the skewed simply-supported plate shown in Figure 8.17, again with $\nu = 0.3$. In such a case, strong boundary layers are present and a stress singularity arises at the obtuse corner B. In order to approximately capture the boundary layers, the graded mesh pattern shown in Fig. 8.17 was used, with the same boundary layer meshing for all thickness values considered.

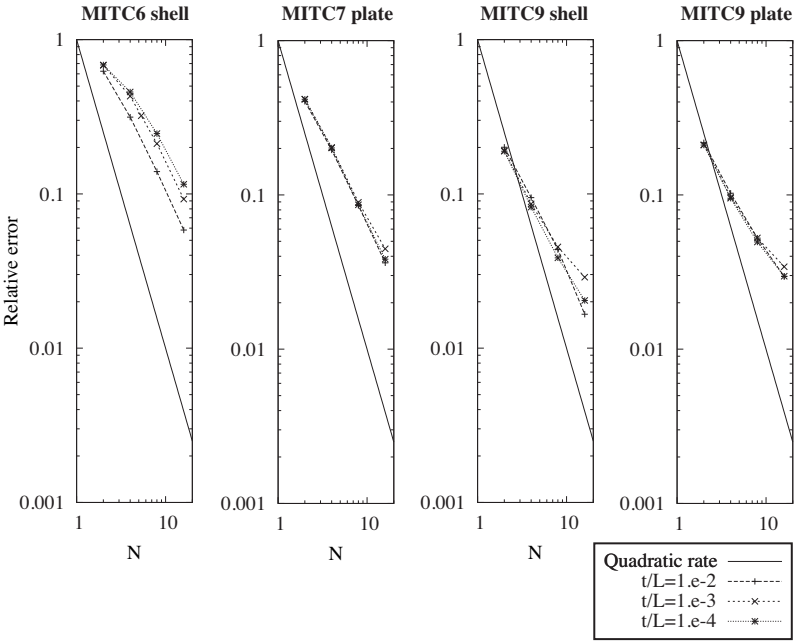

Fig. 8.18. Skewed plate: s-norm

The relative errors are shown in Figures 8.18 to 8.20, for a reference solution computed with a fine mesh ($N = 128$) of MITC9 shell elements. Optimal convergence is not obtained in this case, except for the displacement convergence of the MITC7 and MITC9 (plate and shell) elements. This suboptimal convergence is probably due to the stress singularity and the approximate boundary layer resolution. In this case too, the convergence behaviors of the MITC9 plate and shell elements are very similar, but the shell element performs even better. And as before the MITC6 shell element does not perform as well as the MITC7 element, albeit still reasonably well.

Finally, we show the transverse shear computed along the edge AB depicted in Figure 8.17. The shear yz-component (i.e. orthogonal to the edge) is plotted in Figure 8.21 for the thickness ratio $t/L = 1/100$. Note that the numerical values are normalized using the yy-component of the bending stress at the center of the plate. This figure clearly reveals the stress singularity at

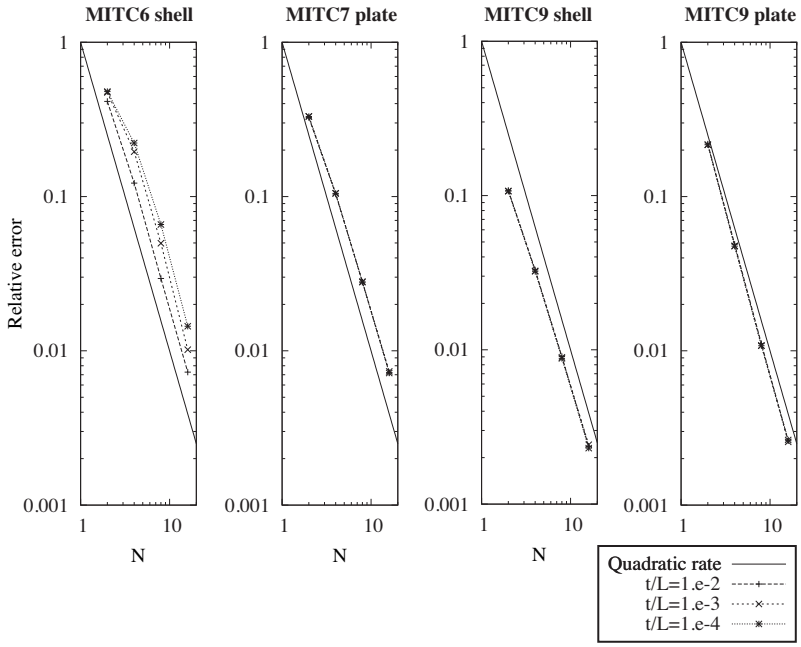

Fig. 8.19. Skewed plate: displacement H^1-semi-norm

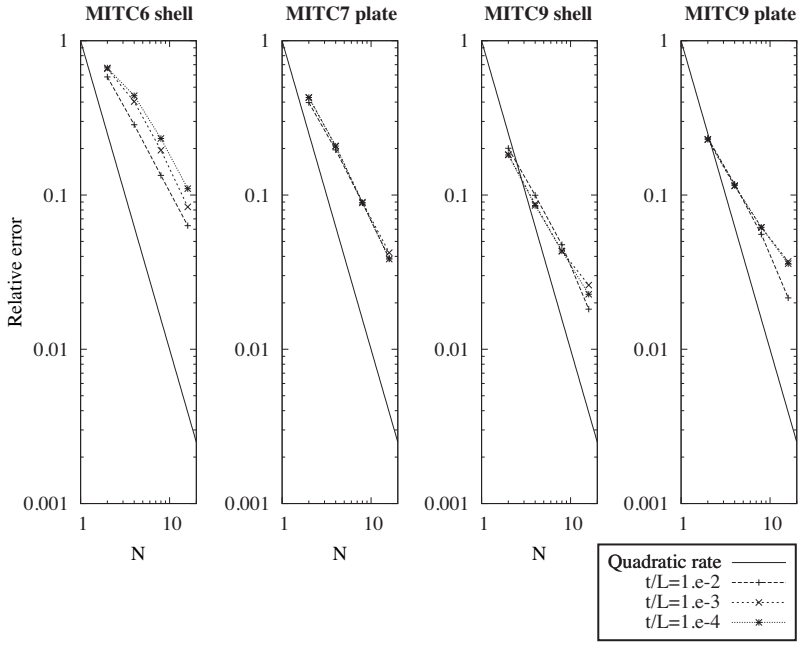

Fig. 8.20. Skewed plate: rotations H^1-norm

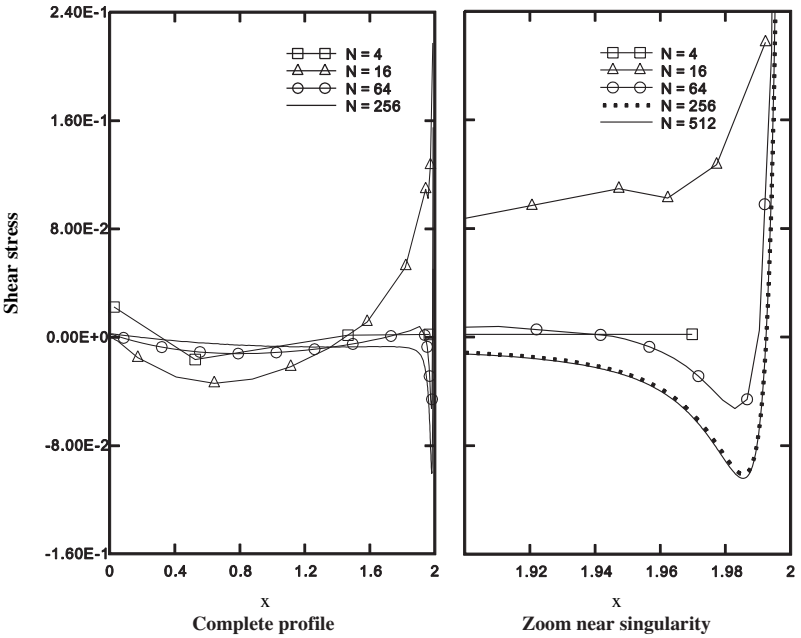

Fig. 8.21. Skewed plate: convergence of the normalized transverse yz-shear stress (left: complete profile; right: zoom near B) for the MITC9 shell element solutions. The stress is sampled at the mid-points of the element edges.

the corner B, and the great difficulty to accurately capture the shear stresses in this case, since only with a very fine mesh corresponding to $N = 256$ do we reach shear stress results that do not change significantly with further mesh refinement.

As conclusions to these numerical assessments of the quadratic shell elements in plate bending, we can summarize:

- the MITC7 plate element performs better than the MITC6 shell element, which is to be expected since the MITC7 element carries additional degrees of freedom; however the MITC6 shell element performs reasonably well on the whole;
- the MITC9 plate and shell elements both provided excellent results, with optimal rates of convergence in the square plate test problem, and virtually no dependence on the thickness in all convergence results; in fact, the MITC9 shell element performed even slightly better than the MITC9 plate element in the skewed plate test problem.

8.3.2 Axisymmetric hyperboloid

In this section, we consider one bending-dominated problem and one membrane-dominated problem based on the same geometry, namely the axisymmetric hyperboloid defined above. We select this specific geometry because

- by merely changing the boundary conditions the two fundamental asymptotic behaviors (with well-posed limit problems) are reached;
- two non-zero principal curvatures of opposite signs are present, hence it is a complex geometry, leading necessarily to the use of distorted elements;
- there are no corner singularities[4], which means that no special grading is necessary (other than that used for capturing the boundary layers).

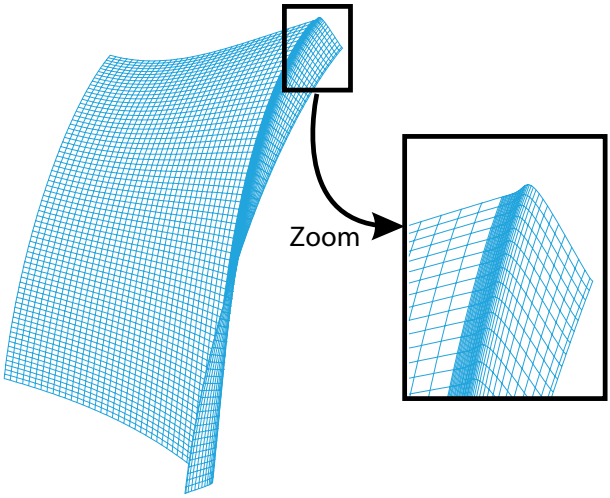

Fig. 8.22. Boundary layer in the clamped hyperboloid

In both cases, boundary layers are present along the edges of the structure and it can be shown that their width is of order $L\sqrt{\varepsilon}$ (Karamian et al., 2000; Pitkäranta et al., 2001). These boundary layers need to be meshed appropriately as was already discussed in Section 8.1.1. Hence the above theoretical result regarding the width of boundary layers is useful but – of course – involves an unknown constant, and numerical experiments can be performed to determine the actual width. As an example we show in Figure 8.22 the boundary layer obtained under clamped conditions (Hiller & Bathe, 2003).

[4] This is – in fact – the reason why we prefer to use this test problem rather than the hyperbolic paraboloid shell problem previously advocated in (Chapelle & Bathe, 1998).

The numerical results given below – most of which being taken from (Bathe & Lee, 201x), see also (Bathe et al., 2002; Hiller & Bathe, 2003) for the quadrilateral elements, and (Lee & Bathe, 2004; Lee et al., 2007; Kim & Bathe, 2009) for the triangular elements – were obtained using sequences of meshes with increased degrees of fineness. The symmetries featured in the geometry were taken advantage of by restricting the computational domain to one eighth of the whole structure, namely, one half along the axis, and one fourth in the circumferential direction.

Earlier evaluation results of the MITC elements were given in (Bathe et al., 2000a), using the energy variation error measure discussed in Section 8.1.1 and following the guidelines presented in (Chapelle & Bathe, 1998). The results that we present below follow a stronger approach of assessment in that actual error norms are used.

Structure with clamped ends. Following our above discussion (see Section 8.1.1) the convergence behavior of the MITC shell elements is assessed using two different error measures, namely the membrane energy norm and the s-norm. In order to compute the membrane energy norm (recall that we are dealing with general shell elements, hence the bilinear form A_{m} is not explicitly defined) a one point integration of the energy through the thickness was used in the displacement-based formulation corresponding to each element in consideration. The boundary layer was numerically identified to be of width $6\sqrt{\varepsilon}R$, approximately, and the sequence of meshes was constructed accordingly.

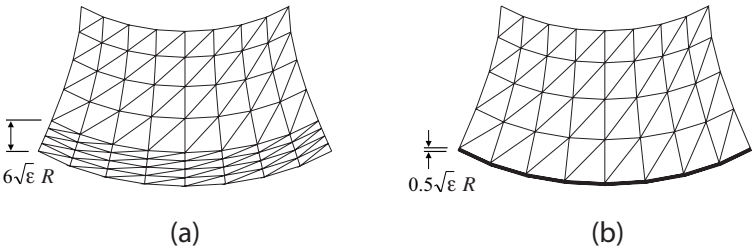

Fig. 8.23. Typical meshes for axisymmetric hyperboloid (1/8th of structure, $N = 4$) with clamped (a) and free (b) boundary layers

For the quadrilateral elements (MITC4, MITC9 and MITC16), the computational domain corresponding to one eighth of the whole structure was discretized into N (axial direction) by $2N$ (circumferential direction) elements for the area *outside of the boundary layer* – N being an integer that is increased to observe the convergence behavior – and into N (axial) by $2N$ (circumferential) elements in the boundary layer area. As regards triangular meshes, they were obtained by subdividing the quadrilateral elements into triangles along a consistent diagonal direction. Note that this discretization

yields elements of well-balanced (isotropic) dimensions outside of the boundary layer, see Figure 8.23. For the numerical results given below, the reference solutions used in error computations are obtained with a fine mesh (namely, $N = 48$) of MITC9 elements, unless otherwise specified.

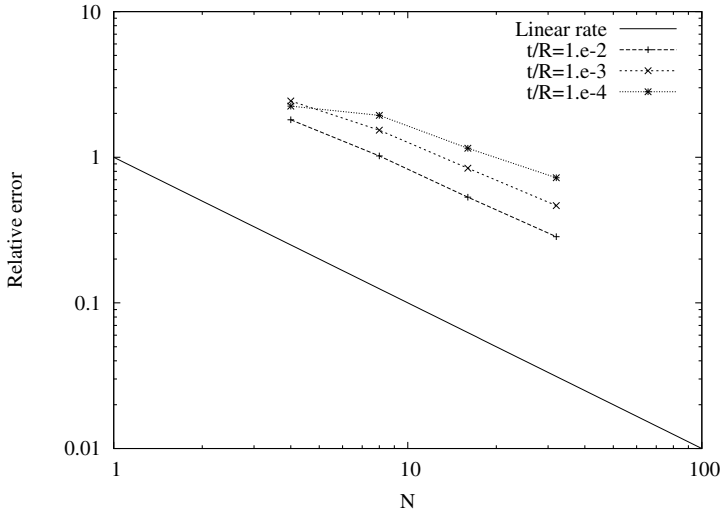

Fig. 8.24. Clamped ends, MITC4 element: membrane energy norm

We display in Figure 8.24 the convergence curves obtained for the MITC4 element with the membrane energy norm. We can see that the errors in this norm are quite large, and that they grow when the thickness decreases, although the convergence curves approximately follow the linear rate. In order to track the origin of these large errors more precisely, we plot in Figure 8.25 similar curves when the shear terms are discarded from the energy. We observe that the errors obtained are much smaller and with little sensitivity when decreasing the thickness parameter. Hence, the large errors obtained in the membrane energy norm come from the shear energy, namely from the approximation of the rotation fields. On the other hand the displacement *per se* is well predicted (as seen through the membrane energy norm).

We also show in Figure 8.26 the results obtained with the s-norm. These results are very similar to those obtained with the membrane norm without shear. Hence, the strains and stresses are well predicted by the MITC4 element.

We observe a similar behavior for the MITC9 solutions, for which the convergence curves are shown in Figures 8.27, 8.28 and 8.29, also for the membrane energy norm, the membrane energy norm without shear, and the s-norm, respectively. Namely, errors are large in the membrane energy norm

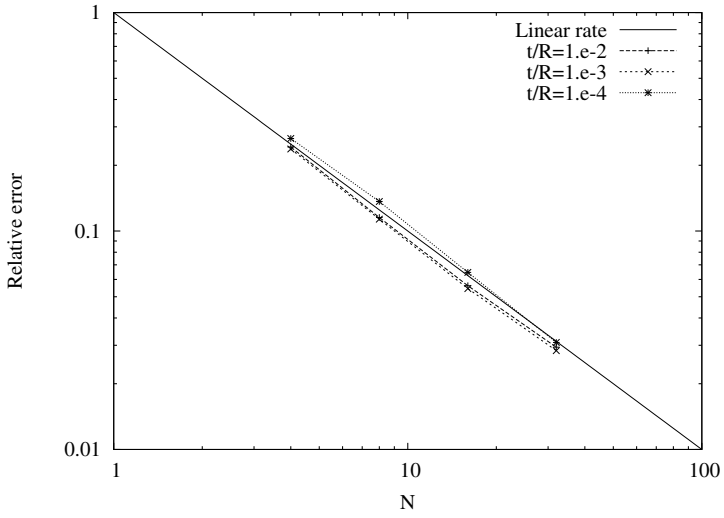

Fig. 8.25. Clamped ends, MITC4 element: membrane norm without shear

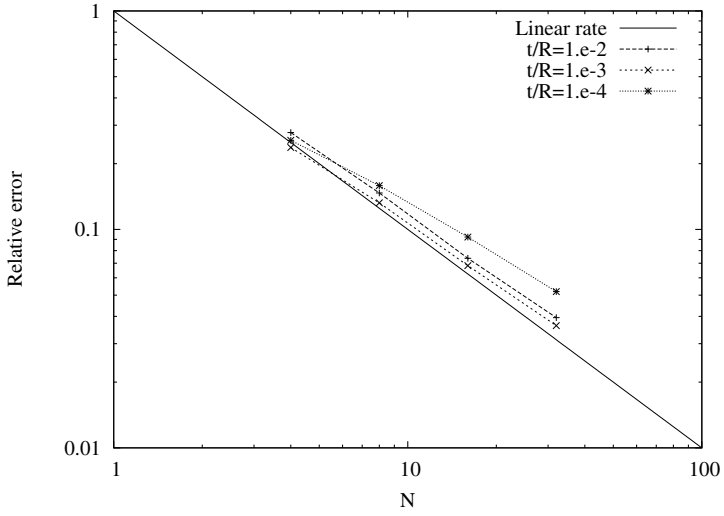

Fig. 8.26. Clamped ends, MITC4 element: s-norm

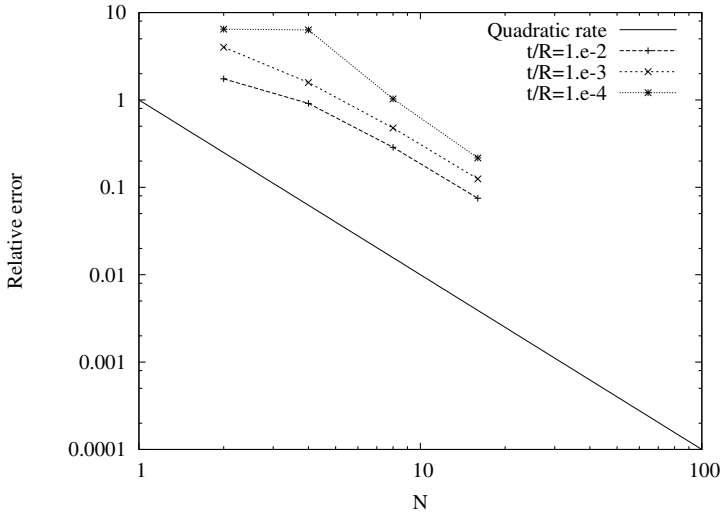

Fig. 8.27. Clamped ends, MITC9 element: membrane energy norm

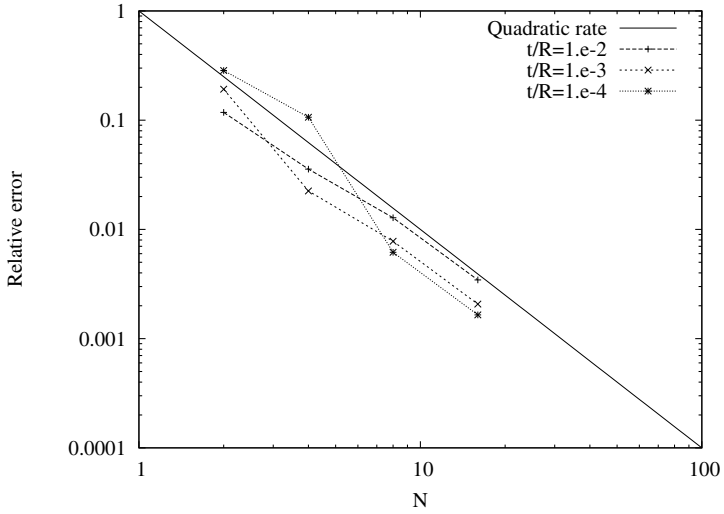

Fig. 8.28. Clamped ends, MITC9 element: membrane norm without shear

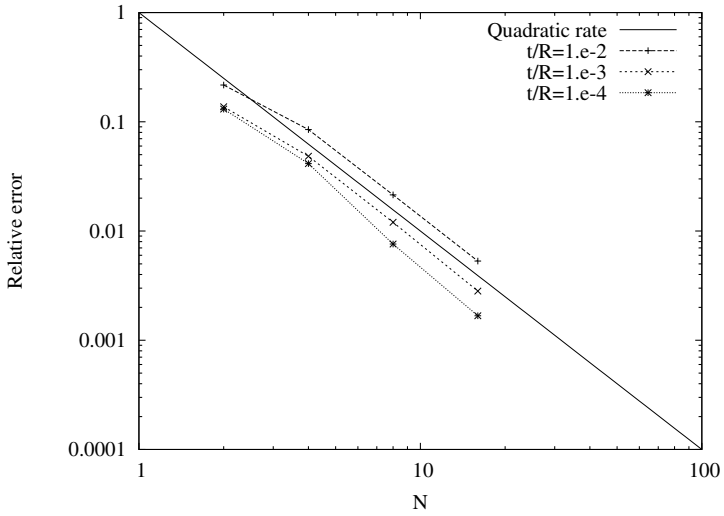

Fig. 8.29. Clamped ends, MITC9 element: s-norm

and grow when the thickness decreases, but when discarding the shear terms or when considering the s-norm the errors obtained are much smaller and – in fact – even decrease with the thickness. In addition all convergence curves display a clear quadratic rate of convergence.

Very similar observations also hold for the MITC16 element, see Figures 8.30 and 8.31, but virtually a cubic convergence rate with relatively small shifting upwards is measured.

We now turn our attention to the triangular elements, namely, the MITC3 and MITC6 shell elements.

The errors for the MITC3 element are shown in Figures 8.32 to 8.34. Like for the quadrilateral MITC shell elements, the errors are quite large in the membrane energy norm, and much smaller when discarding the shear energy or in the s-norm. In Figures 8.33 and 8.34 some sensitivity with respect to the thickness parameter is observed, albeit to a reasonable extent, indeed.

Similar observations hold for the MITC6 element, for which errors are displayed in Figures 8.35 to 8.37. In this case too, the convergence behavior is much improved – although still sub-optimal – when considering the errors in the membrane norm without shear or in the s-norm. Nevertheless, these errors should be compared to the reference results obtained with displacement-based P2 elements, see Figs. 8.38–8.40. Note that some significant thickness sensitivity is also present in the membrane norm results for the P2 element, which confirms that further mesh grading in the boundary layer is required in order to obtain optimal errors due to the shear energy, as discussed in (Chapelle & Paris Suarez, 2008) and further in (Bathe & Lee, 201x).

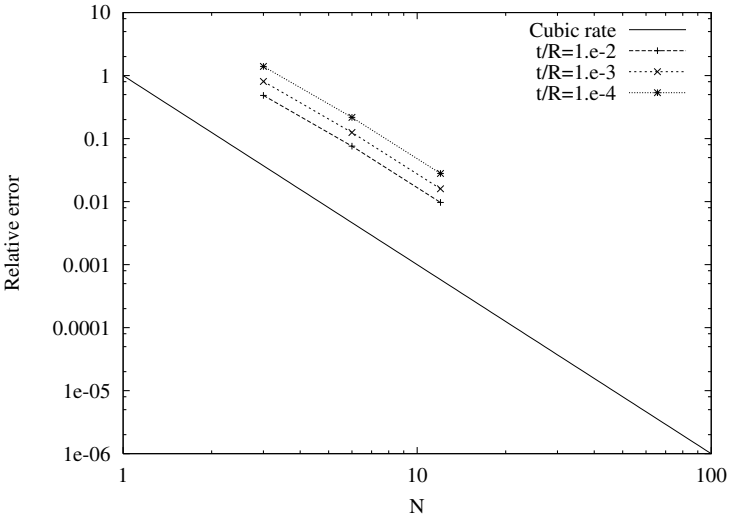

Fig. 8.30. Clamped ends, MITC16 element: membrane energy norm

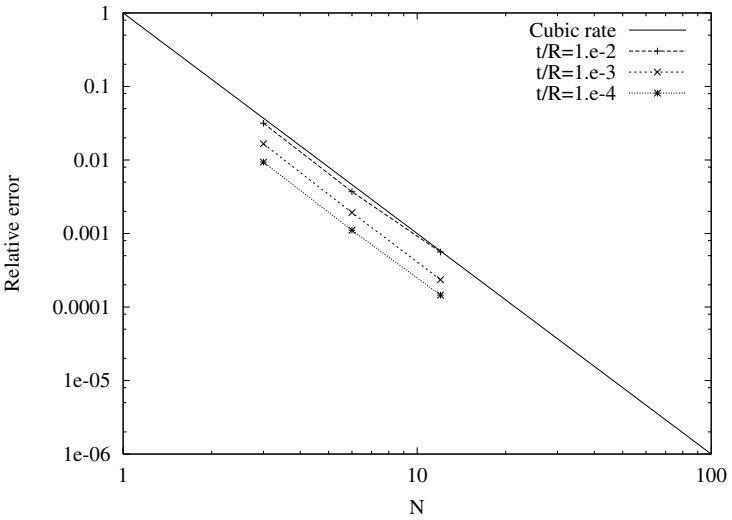

Fig. 8.31. Clamped ends, MITC16 element: s-norm

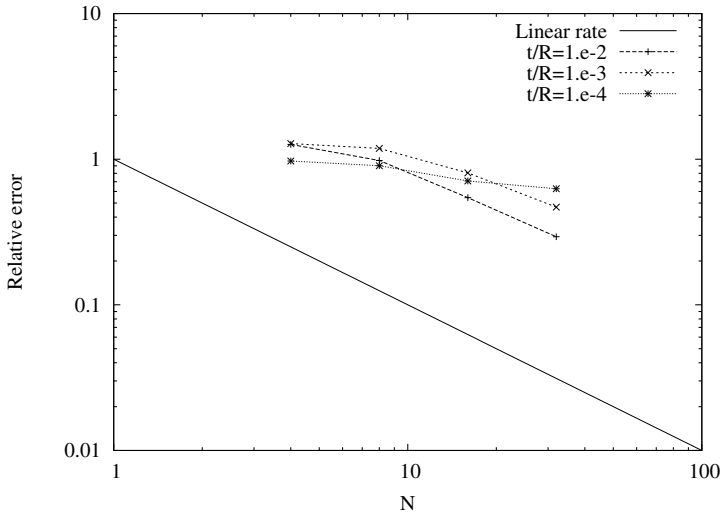

Fig. 8.32. Clamped ends, MITC3 element: membrane energy norm

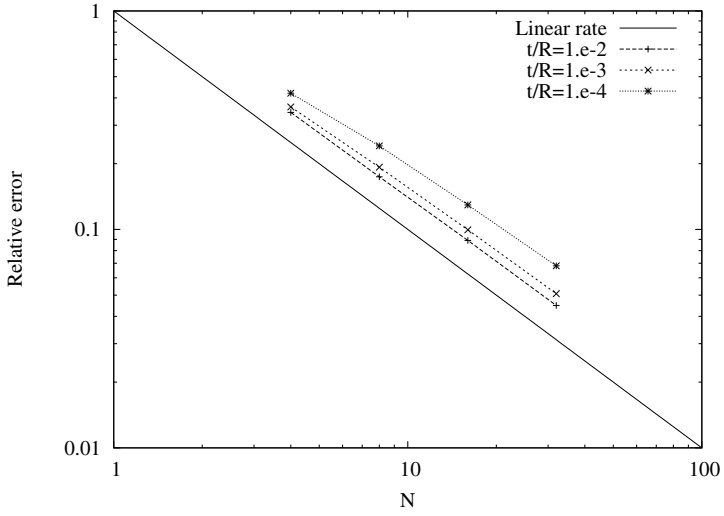

Fig. 8.33. Clamped ends, MITC3 element: membrane norm without shear

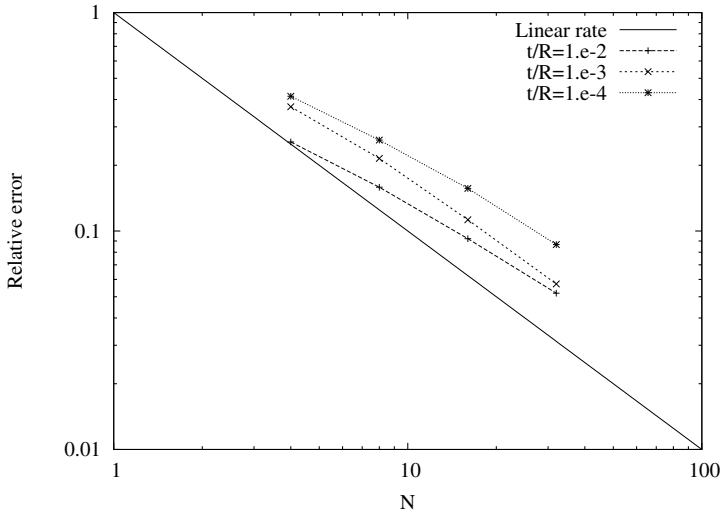

Fig. 8.34. Clamped ends, MITC3 element: s-norm

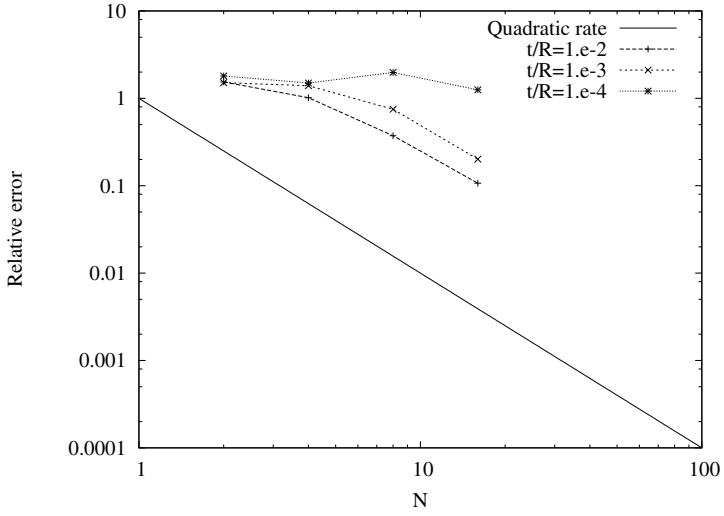

Fig. 8.35. Clamped ends, MITC6 element: membrane energy norm

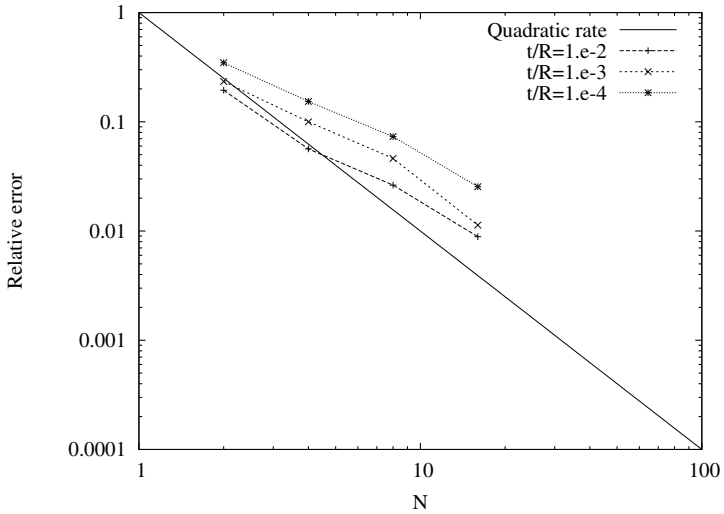

Fig. 8.36. Clamped ends, MITC6 element: membrane norm without shear

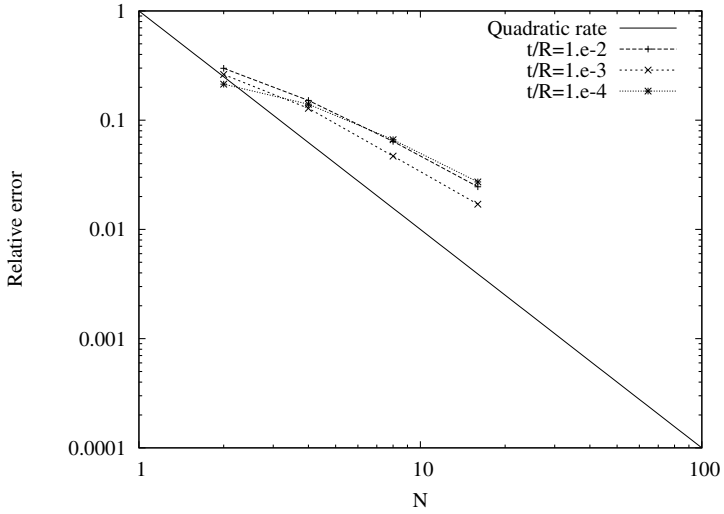

Fig. 8.37. Clamped ends, MITC6 element: s-norm

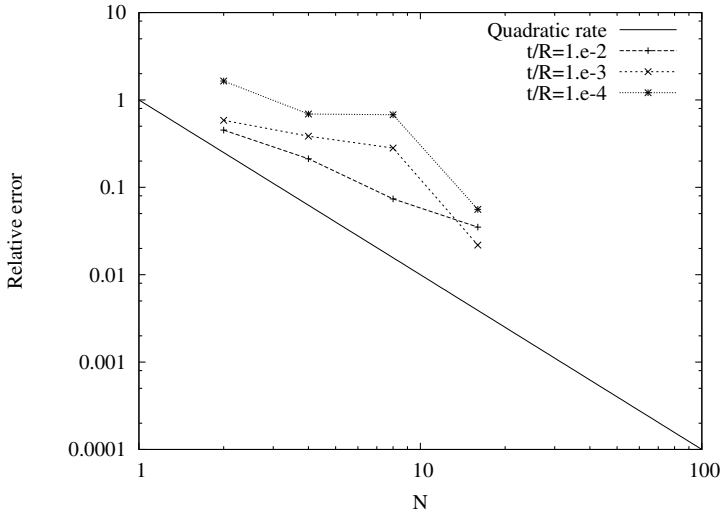

Fig. 8.38. Clamped ends, P2 element: membrane energy norm

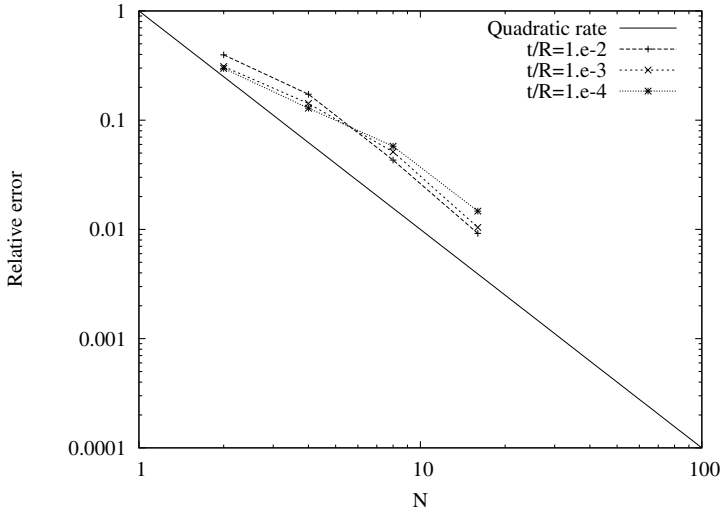

Fig. 8.39. Clamped ends, P2 element: membrane norm without shear

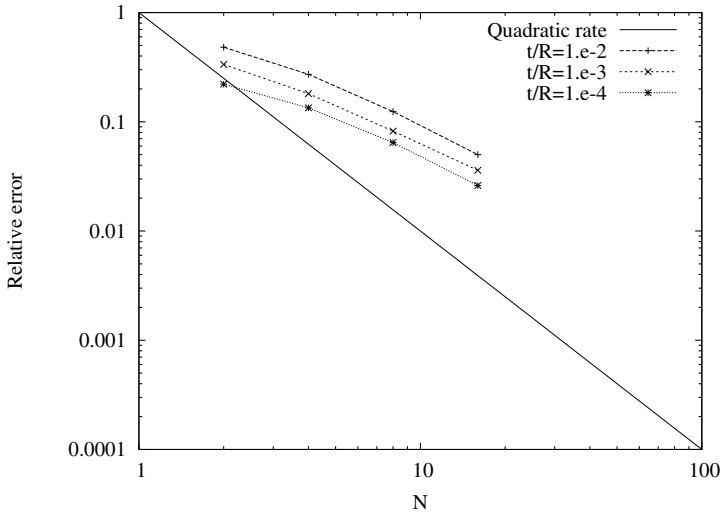

Fig. 8.40. Clamped ends, P2 element: s-norm

The above results indicate that the MITC shell elements perform rather well in membrane-dominated cases, except when the full membrane energy norm is considered. More precisely, with the exception of the rotations all mechanical quantities – namely, the displacements per se, the strains and the stresses – display convergence behaviors that are in good agreement with a uniform optimal convergence estimate of the kind (7.1) for the norms considered.

Structure with free ends. In this case we consider as discussed above the two error measures corresponding to the s-norm and the norm of the displacement space. For the basic shell model, we know that the norm of the displacement space is equivalent to the H^1 Sobolev norm applied on the displacements and rotations (see Chapter 5), but we want to use an equivalent norm that would be more practical for numerical computations and more closely related to the shell mechanics formulations. For the s-m-b model we could use instead the norm given by the bilinear form $A_{\rm m} + A_{\rm b}$, see Chapter 5, hence for general shell elements we use the bilinear form given by the displacement-based mechanical formulation for $\varepsilon = 1$ (or with a smaller finite value if $\varepsilon = 1$ does not allow condition (2.161) to be fulfilled). We subsequently refer to this norm as the "$A_{\rm m} + A_{\rm b}$" norm.

Similar mesh sequences and reference solutions as for the clamped structure were considered for the quadrilateral and triangular MITC elements, except that the boundary layer – much weaker in amplitude than in the clamped case – was estimated to be of width $0.5\sqrt{\varepsilon}R$, see Figure 8.23.

We show the results obtained with the MITC4 element in Figure 8.41 and 8.42. For both norms all convergence curves follow the optimal linear rate and

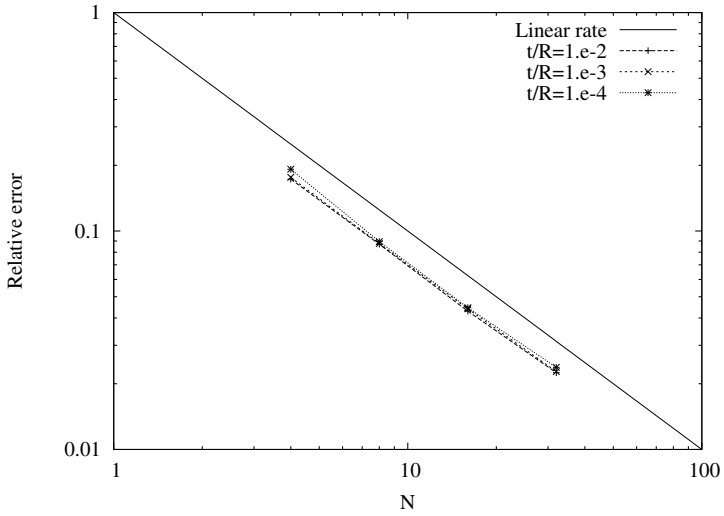

Fig. 8.41. Free ends, MITC4 element: "$A_{\mathrm{b}} + A_{\mathrm{m}}$" norm

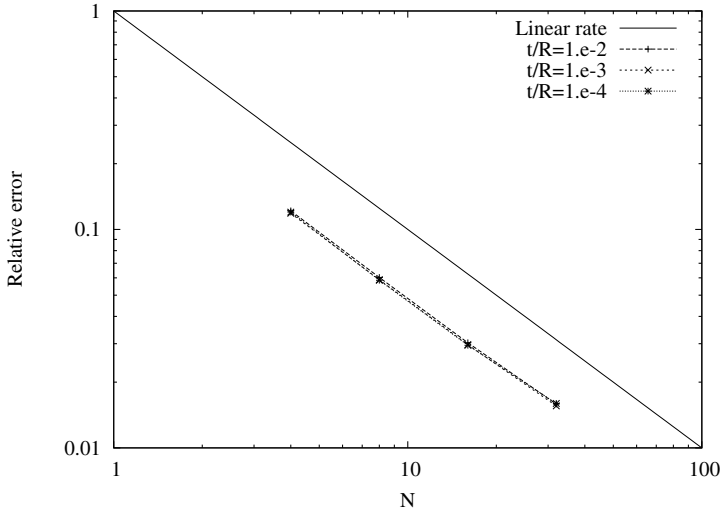

Fig. 8.42. Free ends, MITC4 element: s-norm

hardly vary when the thickness is decreased, hence the MITC4 element does not appear to suffer from locking in this case.

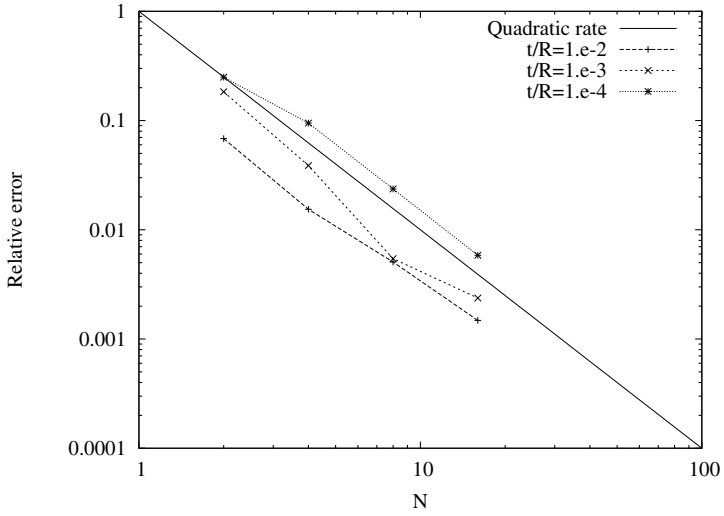

Fig. 8.43. Free ends, MITC9 element: "$A_{\mathrm{b}} + A_{\mathrm{m}}$" norm

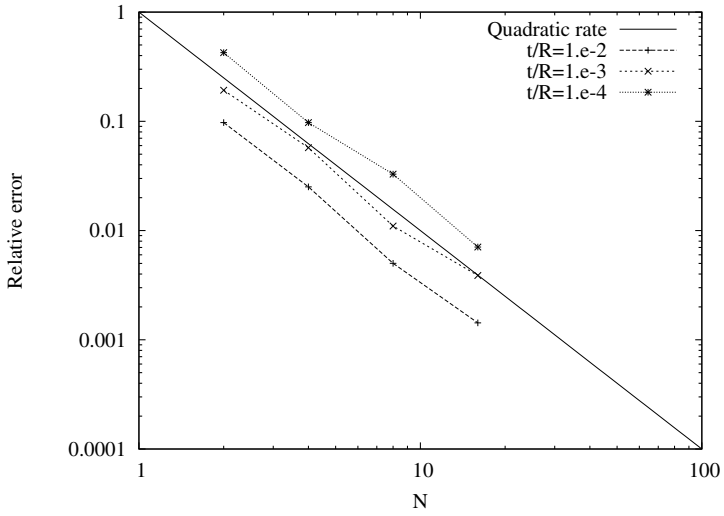

Fig. 8.44. Free ends, MITC9 element: s-norm

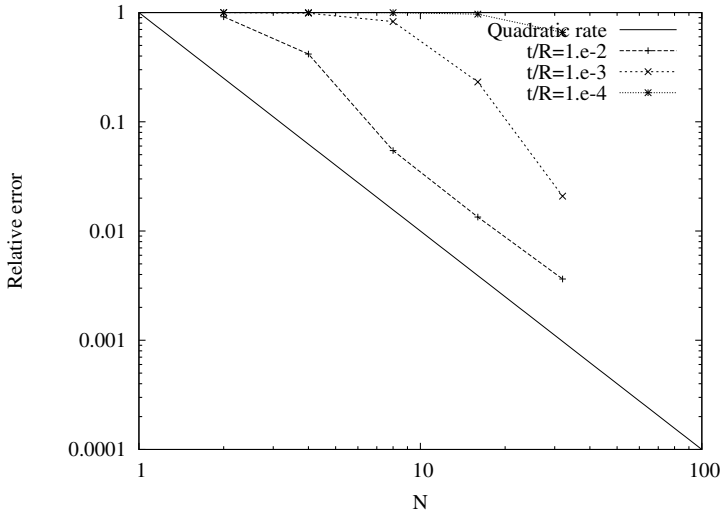

Fig. 8.45. Free ends, Q2 element: "$A_{\mathrm{b}} + A_{\mathrm{m}}$" norm

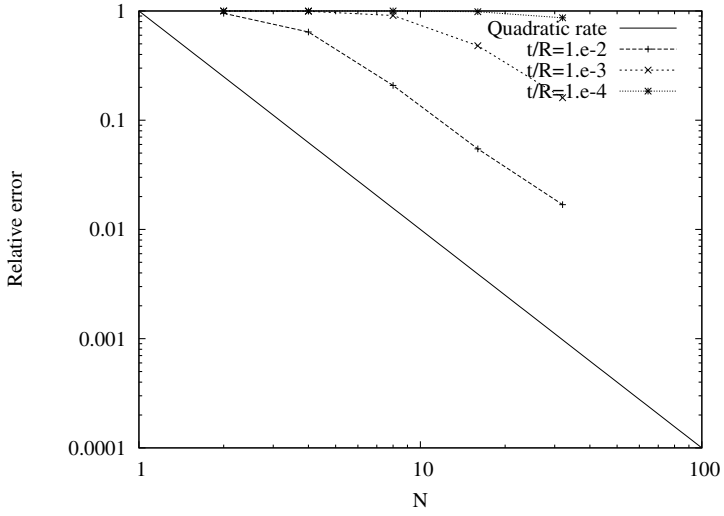

Fig. 8.46. Free ends, Q2 element: s-norm

The convergence behavior of the MITC9 element is displayed in Figures 8.43 and 8.44. Unlike for the MITC4, we note here in both norms a deterioration of convergence when the thickness decreases, which means that some locking occurs. However, for comparison purposes we also show in Figures 8.45 and 8.46 the corresponding convergence curves for the Q2 displacement-based elements (note that the s-norm is equivalent to the energy norm in this case, of course) and we can see that locking is very limited in the MITC9 element compared to its displacement-based counterpart. Furthermore, it should be stressed that the behavior of the MITC9 element in this bending-dominated test problem has been much improved compared to the previous version of this element, see (Bucalem & Bathe, 1993). This improvement – proposed in (Bathe et al., 2003b) – has been spurred by the thorough numerical assessments based on physical and mathematical insight that we are advocating here.

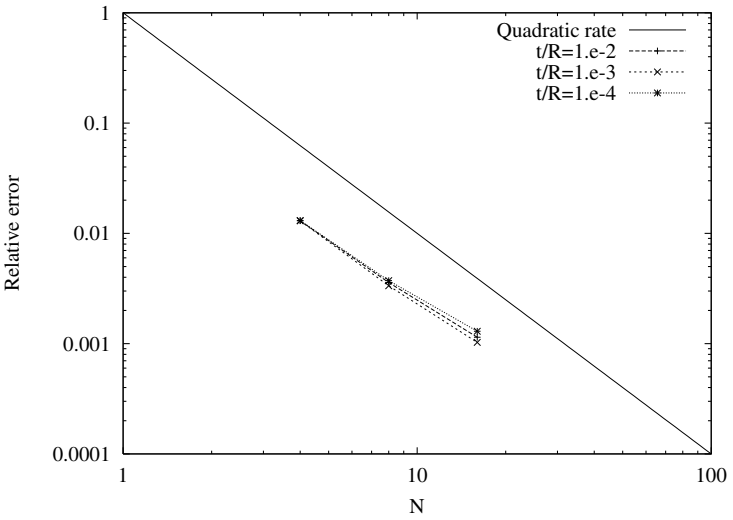

Fig. 8.47. Free cylinder, MITC9 element: "$A_\mathrm{b} + A_\mathrm{m}$" norm

Remark 8.3.1. These numerical results obtained with the MITC9 element in a bending-dominated situation underline the importance of selecting test problems of sufficiently complex geometry in order to assess the efficiency and reliability of shell procedures. In fact, when considering the above-described cylindrical test problem with free ends we obtain the convergence curves of Figure 8.47 which hardly show any sign of locking. ■

The results obtained for the MITC16 element are shown in Figures 8.48 and 8.49 (reference solution with $N = 36$, MITC16). The convergence curves

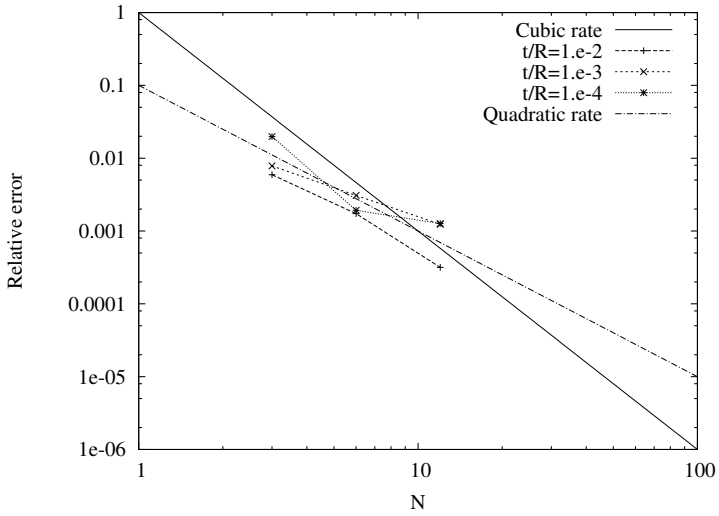

Fig. 8.48. Free ends, MITC16 element: "$A_{\mathrm{b}} + A_{\mathrm{m}}$" norm

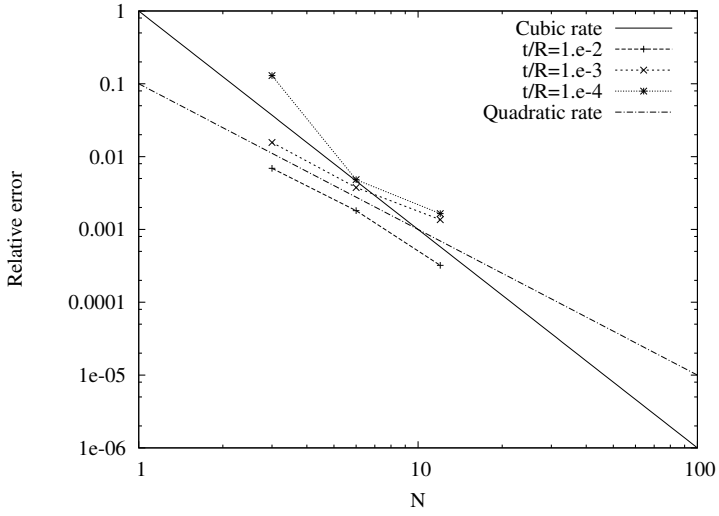

Fig. 8.49. Free ends, MITC16 element: s-norm

display an overall satisfactory behavior for both norms considered, although some sensitivity of the errors on the thickness parameter is observed. In addition, the convergence rates appear to match the quadratic curve better than the cubic reference, as could be expected from the discussion of Section 6.3. Note, indeed, that the interpolation of the rotations enters the shell bending energy exactly like in the model problem considered in Figure 6.8.

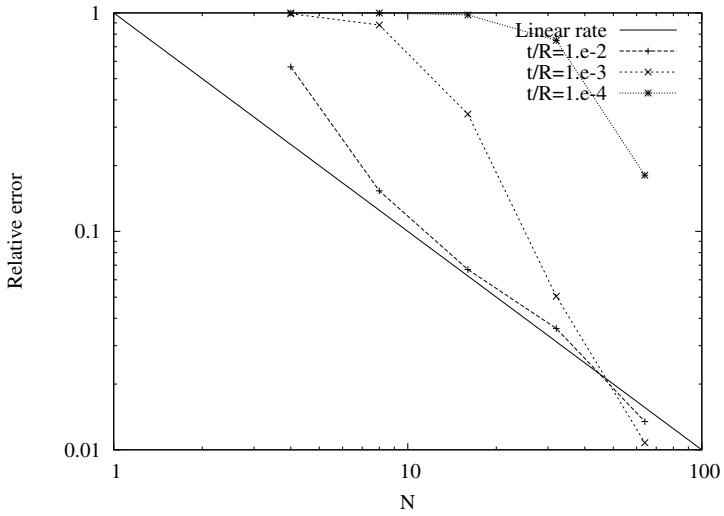

Fig. 8.50. Free ends, MITC3 element: "$A_{\mathrm{b}} + A_{\mathrm{m}}$" norm

Regarding the triangular MITC3 shell element, the error results are shown in Figures 8.50 and 8.51. As can be expected from such a low-order element – with a low-order approximation of the geometry – locking occurs quite severely in the convergence curves.

In the case of the triangular MITC6 element, some locking is also clearly present, in particular for the smallest thickness values, see Figures 8.52 and 8.53.

Concluding remarks on the assessment results. Of course we can only draw partial conclusions from these assessment results since other problem solutions – with different geometries, in particular – need be considered for comprehensiveness.

From these numerical results the quadrilateral MITC elements appear to perform well both in membrane-dominated and bending-dominated situations. In particular, a very good locking-free behavior of the MITC4 element in the bending-dominated case has been observed. On the other hand, the MITC6 element showed some locking (in the bending dominated case) which indicates that improvements in this element are still desirable. Regarding the

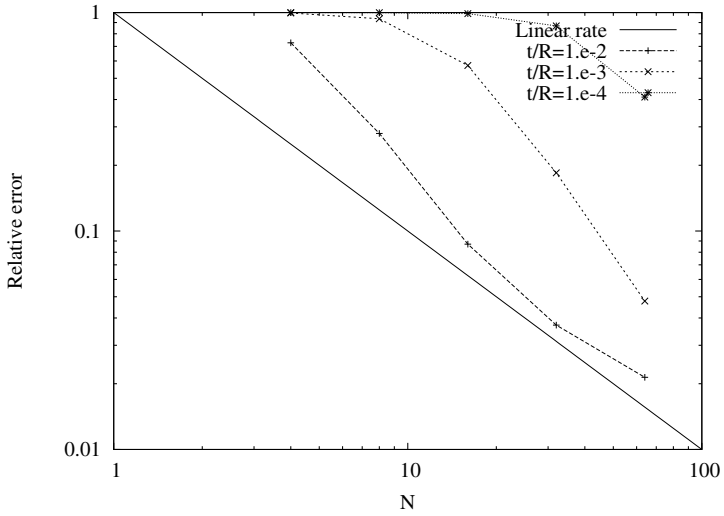

Fig. 8.51. Free ends, MITC3 element: s-norm

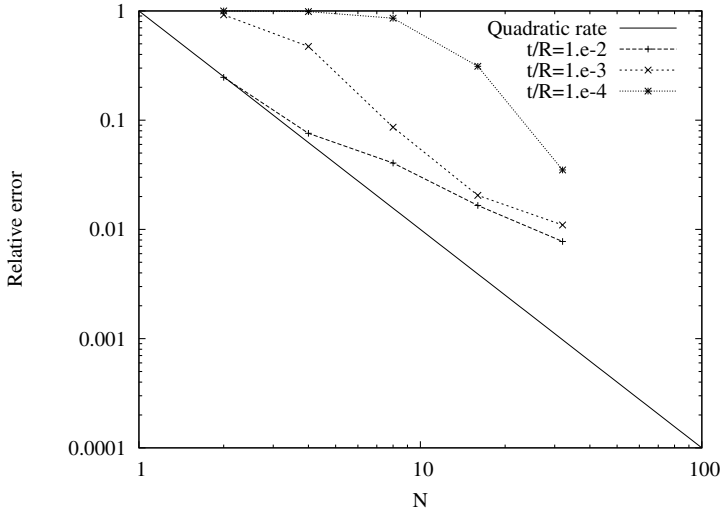

Fig. 8.52. Free ends, MITC6 element: "$A_{\mathrm{b}} + A_{\mathrm{m}}$" norm

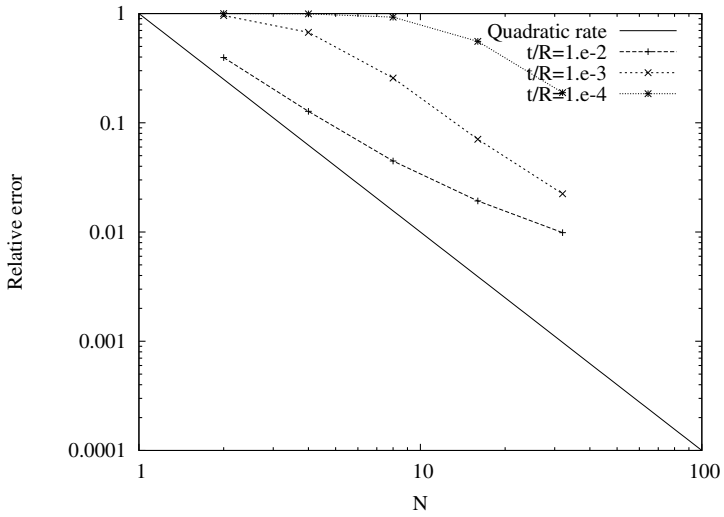

Fig. 8.53. Free ends, MITC6 element: s-norm

MITC3 element, the assessment results show quite undesirable locking in the bending-dominated case, but for a linear element it is rather unlikely that significant improvements can be achieved in this respect.

From the results obtained in the membrane-dominated case with the full membrane energy norm – compared with those without the shear energy – it appears that the approximation of the rotation is not uniformly optimal through the error measure corresponding to the transverse shear energy. However, the shear strains – hence also the shear stresses – are well predicted as shown by the good behavior observed for the s-norm.

As regards the s-norm in general, we conclude that it is a valuable error measure. Its capability as regards locking detection is demonstrated in the case of the MITC6 element – and to some extent also for the MITC9 element – for which the locking behavior is revealed as clearly as with the "$A_{\mathrm{m}} + A_{\mathrm{b}}$" norm. Most importantly this error measure assesses the quality of strains and stresses, which is very valuable from a physical standpoint.

9. On the Nonlinear Analysis of Shells

The nonlinear analysis of shells is today clearly a very large field, in which much research and development has taken place, so that at present many nonlinear analyses can be performed with confidence in engineering practice, see for example (Bathe, 1999, 2001a; Ibrahimbegović & Krätzig, 2002).

Our objective in this chapter is to merely outline the process of nonlinear shell analysis, and to thus indicate that all the theory regarding the fundamentals of shell analysis presented in the previous chapters is directly applicable to the nonlinear analysis of shells as well.

9.1 The Incremental Analysis to Obtain Nonlinear Response Solutions

So far we assumed in the book that the displacements of the shell structure are infinitesimally small and that the constitutive tensor relating the stresses to the strains is constant. This means that the structural response is assumed to be "linear", in the sense that linear equations in the unknown displacements govern the response[1].

If the displacements are large or the constitutive relation is not constant, then a nonlinear analysis is needed in order to solve for the response of the shell. A nonlinear analysis is also required if the displacement boundary conditions on the shell structure change during the response, such as encountered in contact analysis. In all these cases an incremental solution is performed in order to solve for the response of the shell structure.

As described in detail in (Bathe, 1996), it is then effective to use the time variable "t" to measure the response. The loads are applied as a function of time and, correspondingly, the response of the shell is measured as a function of time. In a static analysis when the loads are applied very slowly and inertia forces are neglected (and when the constitutive relation is not time-dependent), the time variable is simply a dummy variable used to describe

[1] Indeed, we also assumed that the material considered is isotropic (governed by a single Young's modulus and a single Poisson's ratio only), although this assumption could be easily removed.

D. Chapelle, K.-J. Bathe, *The Finite Element Analysis of Shells – Fundamentals*,
Computational Fluid and Solid Mechanics, 2nd ed., DOI 10.1007/978-3-642-16408-8_9,

the incremental load application and corresponding response solution, but otherwise t is of course an actual physical variable[2].

Consider a general shell structure undergoing large displacements and possibly a nonlinear constitutive response. We assume that the incremental response for times $0, \Delta t, \ldots, t$, where Δt is the time step increment, has been solved for, and that next the response for time $t + \Delta t$ shall be calculated. The governing continuum mechanics equations for the shell viewed as a 3D continuum at time $t + \Delta t$ can be written as
Find ${}^{t+\Delta t}\vec{U} \in \mathcal{V}^{3D}$ *such that*

$$\boxed{{}^{t+\Delta t}A^{3D}({}^{t+\Delta t}\vec{U}, \vec{V}) = {}^{t+\Delta t}F(\vec{V}), \qquad \forall \vec{V} \in \mathcal{V}^{3D}.} \tag{9.1}$$

Of course the operator ${}^{t+\Delta t}A^{3D}$ can be highly nonlinear due to nonlinear material behavior and large deformations. In (9.1) we consider the loading to be independent of the deformations, but this restriction can of course be easily removed (see Bathe, 1996).

For the solution of (9.1), we incrementally decompose the displacements into the just calculated values ${}^{t}\vec{U}$ and the unknown increments

$${}^{t+\Delta t}\vec{U} = {}^{t}\vec{U} + \vec{U}. \tag{9.2}$$

A linearization to calculate the incremental displacements is performed, such that

$${}^{t+\Delta t}\vec{U} \approx {}^{t}\vec{U} + \Delta\vec{U}. \tag{9.3}$$

Hence, with the solution at time t being known, the governing incremental variational form is

$$\Delta^{t}A^{3D}({}^{t}\vec{U}, \Delta\vec{U}, \vec{V}) = {}^{t+\Delta t}F(\vec{V}) - {}^{t}A^{3D}({}^{t}\vec{U}, \vec{V}), \tag{9.4}$$

where $\Delta^{t}A^{3D}$ is established from the linearization of the nonlinear operator ${}^{t+\Delta t}A^{3D}$ about the configuration at time t. We note that $\Delta^{t}A^{3D}$ is a *bilinear form* just as encountered in linear analysis but of course the individual terms are now different due to the geometric and material nonlinearities. For example, the current stresses at time t may result into stress-stiffening or stress-softening effects, and the constitutive relations in general depend on the stress state.

This incremental decomposition corresponds in fact to the first iteration of a full Newton-Raphson iteration, which we can write as

[2] Of course, we use the variable t also to denote the thickness of the shell; however, no confusion is possible since we use the *time variable* t quite distinctly as a left superscript to denote the time-dependence of a variable.

$$\Delta^{t+\Delta t}A^{3D(i-1)}({}^{t+\Delta t}\vec{U}^{(i-1)}, \Delta\vec{U}^{(i)}, \vec{V}) = {}^{t+\Delta t}F(\vec{V}) - {}^{t+\Delta t}A^{3D(i-1)}({}^{t+\Delta t}\vec{U}^{(i-1)}, \vec{V}), \tag{9.5}$$

$${}^{t+\Delta t}\vec{U}^{(i)} = {}^{t+\Delta t}\vec{U}^{(i-1)} + \Delta\vec{U}^{(i)}, \quad i = 1, 2, \ldots \tag{9.6}$$

with the iteration continuing until the right-hand side is small (in an appropriate norm). Then (9.1) is satisfied to sufficient accuracy. The important point to note is that (9.5) is for each iteration simply a *linear problem* of the kind we have considered in the previous chapters but naturally with some differences in the bilinear forms encountered. We elaborate on this fact by giving in the following some details of the finite element discretization. Of particular interest is, of course, in how far the differences in the bilinear forms (encountered in linear analysis and incremental nonlinear analysis) can affect the discussions and conclusions given in the previous chapters.

9.2 The Finite Element Discretization of a Shell for General Nonlinear Analysis

The above abstract variational formulation is quite general and indeed holds for any solid continuum. When applied to shell analysis, the formulation must clearly contain the specific assumptions pertaining to the shell model used. In the previous chapters we have used for linear analysis the Reissner-Mindlin kinematic assumption and the assumption of zero stress through the shell thickness (see Sections 4.1 and 4.2.1) to develop a general finite element solution procedure. We also identified that there is a "basic shell model" underlying this solution approach. This basic shell model can be used to derive the s-m-b model and the m-b model. We studied these models regarding well-posedness, asymptotic behaviors and so on. In addition we established a 3D-shell model and also studied this model. But in current practice, by far mostly finite element discretizations of the basic shell model – or variants thereof – are used, although finite element methods based on the 3D-shell model can be effective for analyses involving very large deformations, see (Bathe et al., 201x) and Sections 9.4.3 and 9.4.5.

For the nonlinear analysis, we could in principle use the same assumptions and develop the basic shell model equations to include the nonlinear large displacement, large strain and nonlinear material effects. We would then discretize the governing variational equation using finite element procedures. This would also enable us to study the related s-m-b and m-b models for large deformation analysis.

However, a more direct way to proceed is to incorporate the Reissner-Mindlin kinematic assumption and the through-the-thickness zero stress assumption directly into the continuum description through the finite element discretization. This is achieved in the same way as in linear analysis but now allowing for large deformations and nonlinear material response.

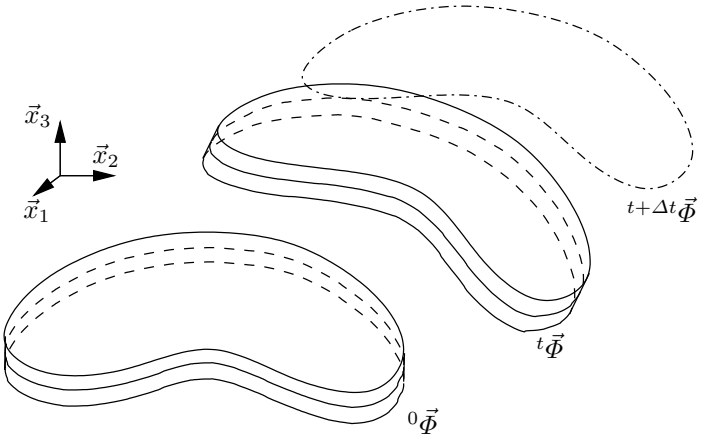

Fig. 9.1. Shell structure undergoing large displacements

Consider the generic shell displayed in Figure 9.1 (in the $t + \Delta t$ configuration we only show the midsurface). We assume that at any time t, the 3D medium of the shell is given by the equivalent of (2.83) but allowing for large deformations,

$$\boxed{{}^{t}\vec{\Phi}(\xi^1, \xi^2, \xi^3) = {}^{t}\vec{\phi}(\xi^1, \xi^2) + \xi^3 \, {}^{t}\vec{a}_3(\xi^1, \xi^2).} \tag{9.7}$$

We note that in this relation all variables are a function of time t (that is, a function of the shell deformations). The director vector ${}^{t}\vec{a}_3$ changes direction but, by definition, is of unit length as in Chapter 2. The change in thickness of the shell, due to large deformations, means that ξ^3 varies over a changing length with time, see (2.84).

Since the displacements of the material particles are given by the change in geometric locations between the current and original configurations of the shell, we have from (9.7) that

$${}^{t}\vec{U} = {}^{t}\vec{\Phi} - {}^{0}\vec{\Phi}. \tag{9.8}$$

Furthermore, the incremental displacements for the material particles from time t to time $t+\Delta t$ are obtained by considering the change in the respective configurations, that is,

$$\vec{U} = {}^{t+\Delta t}\vec{\Phi} - {}^{t}\vec{\Phi}. \tag{9.9}$$

The objective of the analysis is to calculate a sufficiently close approximation to ${}^{t+\Delta t}\vec{\Phi}$ with the shell deformation assumptions mentioned above.

To perform the analysis, it is effective to establish the operator in (9.1) with the shell assumptions, incorporate the finite element interpolations and then linearize the governing equations about the last calculated configuration by direct differentiation. This process yields (9.4) and (9.5) in discretized form with the shell assumptions and thus the incremental displacements in terms of the chosen solution variables (Bathe, 1996).

An effective way to proceed is to interpolate in (9.1) the geometry and displacements using the usual isoparametric interpolation functions, and to interpolate the strains using the MITC shell element formulation approach. The tying of the strain interpolations is performed as described in Chapter 8.

Assume that (9.1) has been discretized by these interpolations in the same manner as in linear analysis. We already mentioned that the incremental finite element equations are then obtained efficiently by *differentiation of the nodal variables with respect to the incremental solution variables*. The nodal variables are the nodal mid-surface displacements (from which the updated nodal positions can be calculated) and nodal director vectors, and the *incremental* solution variables are the incremental nodal displacements and the incremental / instantaneous rotations about the instantaneous director vectors. Note that the nodal rotations are only used *instantaneously* in the linearization to compute the new directions of the nodal director vectors, and solely the nodal mid-surface displacements with the nodal director vectors describe the large deformation response of the shell.

In this solution approach, the effects of large displacements/ large strains and large rotations are directly included, but clearly subject to the Reissner-Mindlin kinematic assumption and the assumption of zero stress through the shell thickness. Of course, for large displacement and / or large strain analysis an appropriate strain measure and corresponding energy-conjugate stress measure need be used (and to model general very large strain conditions a formulation based on the 3D-shell model is more appropriate, see Bathe & Lee, 201x).

In this formulation either the total Lagrangian or the updated Lagrangian formulation can be employed, and the given material stress-strain description will largely decide as to which formulation is more effective, see (Bathe, 1996).

Whatever the nonlinear effects that are incorporated in the solution, the resulting finite element equations obtained from (9.5) then have the form, for a single element or an assemblage of elements,

$$^{t+\Delta t}\mathbf{K}^{(i-1)}\Delta\mathbf{U}^{(i)} = {}^{t+\Delta t}\mathbf{R} - {}^{t+\Delta t}\mathbf{F}^{(i-1)}, \tag{9.10}$$

where, referring to (9.5),

- $^{t+\Delta t}\mathbf{K}^{(i-1)}$ is the tangent stiffness matrix evaluated from the expression $\Delta^{t+\Delta t}A^{3D(i-1)}({}^{t+\Delta t}\vec{U}^{(i-1)}, \Delta\vec{U}^{(i)}, \vec{V})$;
- $\Delta\mathbf{U}^{(i)}$ is the vector of nodal incremental solution variables;

- ${}^{t+\Delta t}\mathbf{R}$ is the vector of applied nodal forces and moments evaluated from ${}^{t+\Delta t}F(\vec{V})$;
- ${}^{t+\Delta t}\mathbf{F}^{(i-1)}$ is the nodal force vector corresponding to the element stresses evaluated from ${}^{t+\Delta t}A^{3D(i-1)}({}^{t+\Delta t}\vec{U}^{(i-1)}, \vec{V})$.

The updated nodal solution variables are then calculated as

$$ {}^{t+\Delta t}\mathbf{U}^{(i)} = {}^{t+\Delta t}\mathbf{U}^{(i-1)} + \Delta\mathbf{U}^{(i)}, \tag{9.11} $$

where, in this equation, there is some abuse of notation because, as mentioned above, instantaneous rotations at the nodes are actually used to update the directions of the nodal director vectors, for details see (Bathe, 1996).

While in this Newton-Raphson iterative solution, a linear solution is performed in each iteration, the actual response of the shell might be highly nonlinear (for some example solutions, see Section 9.4). In some nonlinear analyses, unique solutions exist as implied in the mapping of (9.7). However, even when the uniqueness of the mapping is violated and multiple solutions exist, the basic Newton-Raphson iteration scheme is still used in practice with enhancements to trace out possible solution paths.

The nonlinear phenomena might lead to buckling or collapse, snap-through response, and so on. These phenomena are a result of the nonlinear material behavior and / or the large deformations that take place. The Newton-Raphson iteration in (9.11) might then have difficulties to converge or not converge at all, but the enhancements using additional solution strategies, such as load-displacement constraint methods, automatic time / load stepping techniques and line searching, make it possible to still obtain physically valid solutions. The discussion of these phenomena and their analyses is beyond the scope of this book and we refer to (Bathe, 1996).

9.3 The Fundamental Considerations of Linear Analysis Used in Nonlinear Analysis

The objective of this book is to present fundamentals regarding the analysis of shells. These were presented in linear analysis and we might ask in how far these are applicable in nonlinear analysis. In fact, all the considerations given are completely applicable in nonlinear analysis as well.

Specifically, we identified different physical behaviors of shells depending on the shell geometry, boundary conditions and loading applied (see Fig. 5.2). Membrane-dominated, bending-dominated, mixed and ill-posed problems were identified and discussed. These types of problems are clearly also encountered in nonlinear analysis. However, we may note that, when including large deformation effects, the pure-bending state is rather seldom encountered in practice since membrane stresses are almost always generated.

In addition we need to realize that the character of a shell problem might change during the response solution.

Firstly, this change in physical behavior may come about because merely the spatial variation of the loading over the mid-surface of the shell changes incrementally with time. Consider for example the Scordelis-Lo roof shell structure, see Section 5.3.2 and Fig. 5.5. As we discussed, when the roof is subjected to its dead weight the problem is a mixed problem with $\rho = 1.75$. However, if the structure is subjected to a smooth loading with zero value at the free edge, it is a membrane-dominated problem with $\rho = 1$, see (Lee & Bathe, 2002).

Secondly, the character of a shell problem might change due to changes in the displacement boundary conditions, that may be due to contact being established with some other structure. For example, this situation is encountered if the Scordelis-Lo shell roof, subjected to a smooth loading, comes into contact, see Section 9.4.4.

And thirdly, the character of a shell problem can change in large deformations due to changes in the curvatures of the shell. For example, the pure-bending situation may not be possible at large displacements because in large displacement conditions, the structure will carry its loads in membrane and bending actions. Consider the rather simple case of the analysis of a clamped plate subjected to transverse loading in large displacements. In linear analysis, this is a bending-dominated problem and $\rho = 3$. Correspondingly, the loads are carried exclusively through bending stresses when the plate displacements are small. But as the plate is subjected to large displacements and their effects are included in the analysis, the structure (which now acts like a shell) carries the loads by membrane and bending stresses, see Section 9.4.2.

It is clear then that for the nonlinear analysis of shell structures, finite element schemes are needed that are effective for the various types of problems discussed in Chapter 5. Also, to be generally applicable, the finite element analysis scheme should not be based on a specific shell theory that would only be applicable for specific geometries and deformations. Of course, the finite element procedure should be reliable and, ideally, would be optimal in all the possible physical problems that can be encountered.

The fact that no specific shell theory is used – but only the basic Reissner-Mindlin shell kinematic assumption and the through-the-thickness zero stress assumption, or even not these assumptions as in the 3D-shell model – makes it possible to analyze very general shell structures in complex nonlinear response. The reliability of the shell discretization is clearly necessary in order to be able to interpret confidently the solution results. Hence, a shell finite element scheme must fulfill the ellipticity condition for any possible analysis to be encountered (and mesh to be used) for which the physical conditions require that the ellipticity condition hold. This means, for example, that as long as no buckling or collapse of the shell are encountered, the ellipticity

condition should be satisfied in the solution process. Furthermore, this condition should be satisfied without the use of artificial factors applied to certain stiffness values.

As we stated already in discussing linear shell analysis, no shell finite element scheme has so far been *analytically* proven to be optimal for all possible shell problems. Of course the same holds for nonlinear analysis since, as mentioned already, all considerations discussed for linear analysis are applicable in nonlinear analysis as well. In particular, in order to identify an effective shell discretization scheme for nonlinear analysis, it is very appropriate to evaluate the procedure in linear analysis, as discussed in the previous chapters. Then, provided the nonlinear deformation and material conditions are properly incorporated, consistently linearized and efficiently solved for, the shell discretization scheme will be effective for nonlinear analysis as well.

9.4 Demonstrative Solutions

We present the following example solutions to illustrate the observations given in the previous sections regarding nonlinear shell analyses.

9.4.1 The "Myth of No-Locking" in nonlinear analysis of shells

While the problem of locking is well accepted in the linear analysis of shells, there seems to be the myth – or misunderstanding – that this problem does not exist in the nonlinear analysis of shell structures. There is no basis for that misunderstanding: of course, an element which locks in linear analysis will also lock in nonlinear analysis and the consequences are just as severe. We demonstrate this fact in the solutions of two problems below.

In the first problem, we consider the nonlinear large-displacement analysis of a curved beam structure. The arch is modeled using 2-node Timoshenko beam elements. The pure displacement-based elements lock while the mixed elements do not lock, see Chapter 8 and (Bathe, 1996) where mathematical analyses and numerical results are presented. However, numerical results on locking are usually given for linear analysis, and perhaps this is the reason for the misunderstanding.

Figure 9.2 shows schematically the problem solved, and the deformed geometry for a non-locking solution. Figure 9.3 gives the relative error in the energy norm obtained for different beam thicknesses. Four meshes were used to obtain these results, with 4, 8, 16 and 32 Timoshenko theory based beam elements. It is clearly seen that, as expected, the displacement-based elements lock also in the nonlinear analysis. For example, for the case t/L = 0.01 , even with 32 2-node elements, the energy and tip displacement are only 28% of the accurate non-locking values.

In the second problem, we model the cantilever plate loaded by a moment shown in Fig. 9.4 using two meshes A and B of triangular elements, and two

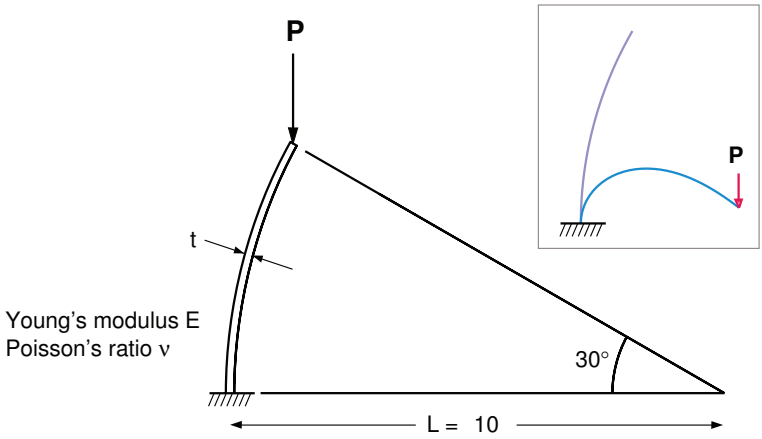

Fig. 9.2. Curved beam structure analyzed

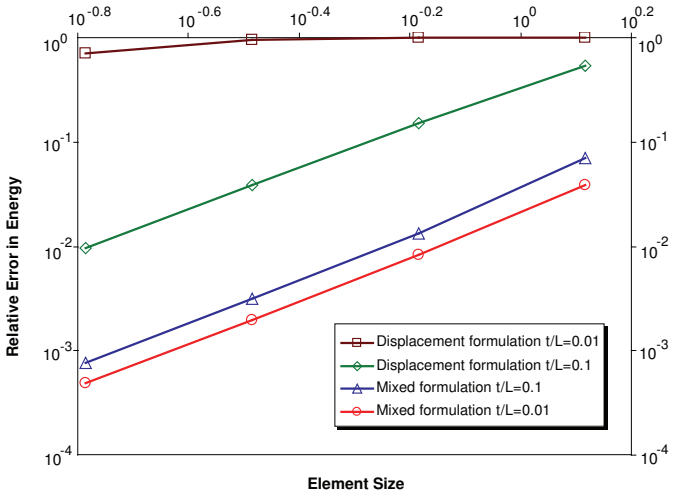

Fig. 9.3. Error in energy norm

meshes C and D of quadrilateral elements. Two types of elements are used: the MITC6 triangular shell element for meshes A and B, and the 9-node displacement-based shell element for meshes C and D. This displacement-based element is not recommended for general use, but we employ it here for illustrative purposes.

Figure 9.5 gives the results obtained for the various meshes and element types. Good solutions are obtained with the MITC6 element, and even when

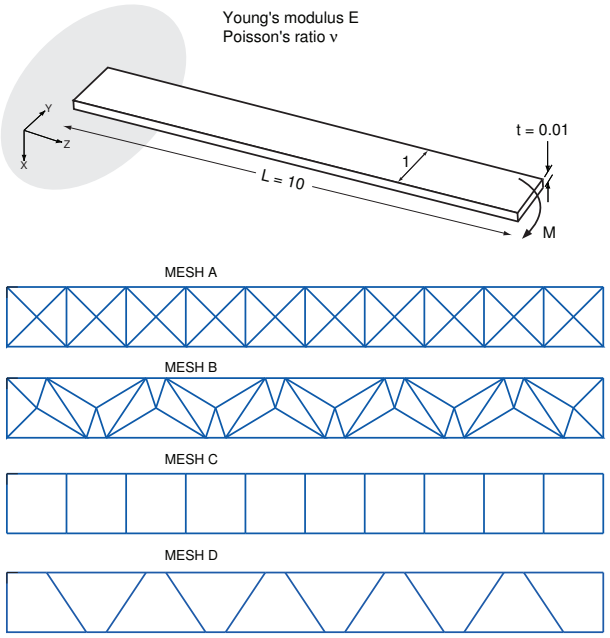

Fig. 9.4. Schematic of cantilever plate problem solved and meshes used

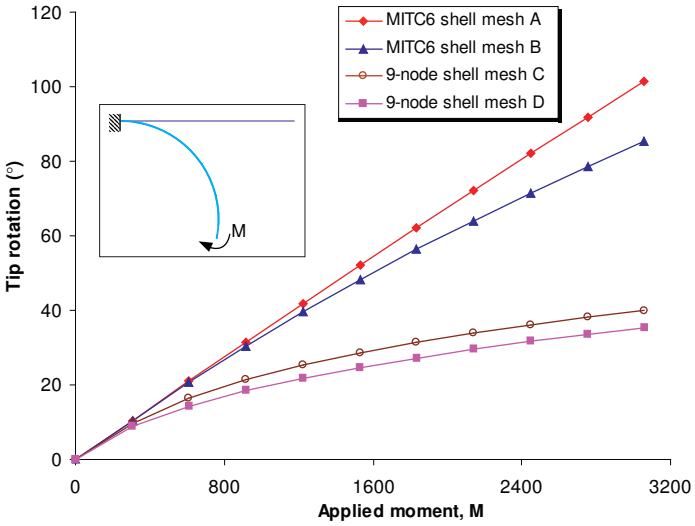

Fig. 9.5. Computed results using the 9-node displacement-based shell element and the MITC6 shell element in analysis of cantilever plate problem

the mesh is quite distorted as shown, the results are still reasonable. The solutions obtained using the displacement-based shell element are good for the first step (almost linear analysis results are obtained). However, they are very inaccurate due to locking when the load increases, even when using rectangular elements (mesh C). It is interesting to note that while locking occurs the mesh curves as it should, but the moment required for that curvature is much too high.

This example shows that while an element may seem to work quite well in linear analysis, in nonlinear analysis it may lock severely! In fact, a closer look would show that the 9-node displacement-based element also locks in linear analysis, by the definition of locking. Therefore, in this case locking is more apparent and – indeed – even more severe in nonlinear analysis.

The above solutions are given to help dispel the misconception that locking of elements and meshes does not exist in nonlinear analysis of shell structures. While the mathematical analyses pertain to linear solutions, the problem is of course at least just as severe in nonlinear analysis. Hence, it is important to always use general, reliable, and effective shell elements.

9.4.2 Large deformation analysis of a simply-supported plate

A square (1m×1m) simply-supported plate structure of (original) thickness 1mm is submitted to increasing uniform pressure. The material properties used, the center displacement and thickness of the plate are given in Fig. 9.6. In addition, Fig. 9.7 shows the effective stress at the top surface and at the midsurface for increasing values of the pressure, in the deformed configurations. Note that the plate initially, of course, acts in pure bending and then as the deformations increase, the structure, now acting like a shell, carries the pressure loading increasingly in membrane action. Hence, here the fundamental character of the shell problem changes from a bending-dominated to a membrane-dominated problem.

Since the elasto-plastic deformations are large, the structure gets thinner which cannot be neglected in the analysis, see Fig. 9.6. The response solution is obtained using the MITC4 shell element to solve the basic shell model equations, extended to include nonlinear large displacement and strain conditions. The updated Lagrangian Hencky elasto-plastic formulation assuming isotropic hardening is used, see (Bathe, 1996; Montans & Bathe, 2005; Kojic & Bathe, 2005), with the shell kinematic assumptions discussed in Sections 4.1 and 6.3. Hence, at each shell node the usual five degrees of freedom are employed. The thickness change is simply evaluated at the end of each incremental step from the current stress state using the condition that the normal stress through the thickness is to vanish. This procedure can be used for relatively simple large strain problems.

However, for difficult large strain problems, in which the elements may undergo large motions and distortions, a 3D-shell element formulation need be used (see Section 9.4.3). The results obtained with the MITC4 3D-shell

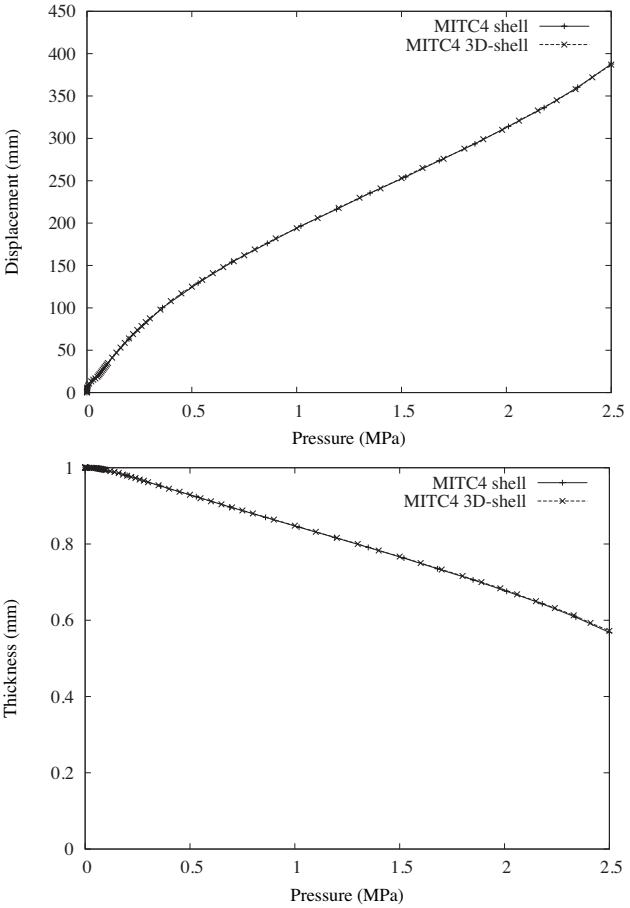

Fig. 9.6. Nonlinear response of plate structure: transverse displacement (top) and thickness (bottom) at center ($E = 2.e5$ MPa, $E_T = E/100$, $\sigma_Y = E/1000$, $\nu = 0.3$)

element (Bathe et al., 201x) are also shown in Fig. 9.6 and for this case almost coincide with those calculated using the MITC4 shell element.

9.4.3 Nonlinear analysis of thick cantilever beam

We give this example solution as an illustration of a case where a 3D-shell element must clearly be used to calculate the large deformation response. The thick cantilever beam considered is in plane strain conditions and the mesh of ten MITC4 3D-shell elements (Bathe et al., 201x) used is shown in Fig. 9.8. At its tip, the rotation is prescribed to incrementally reach 360 degrees. An incompressible Mooney-Rivlin material law is considered (actu-

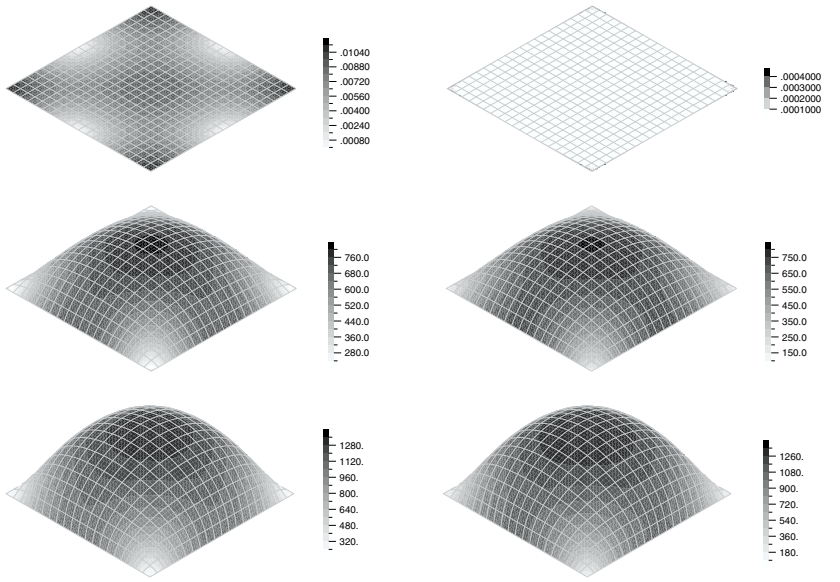

Fig. 9.7. Effective stress at top (left) and middle (right) surfaces for increasing pressure

ally, the Neo-Hookean assumption), hence a u/p formulation is used with 2 pressure variables through the thickness, see Section 8.2.4.

Figure 9.9 shows the response calculated and a comparison with a solution given by Rivlin (1949). The final deformation state is also shown in Fig. 9.8 where we see that the nodes originally located on the mid-surface of the beam have moved considerably due to the tension and compression states in the beam.

9.4.4 Contact analysis of Scordelis-Lo roof

The roof structure already considered in Section 5.3.2 is now analyzed when a smooth pressure loading is applied (making the problem a membrane-dominated problem in linear analysis, see (Lee & Bathe, 2002)) and contact is established with increasing load magnitude, see Fig. 9.10. The energy distributions when contact has not yet been established are shown in Fig. 9.11(a-b), which shows that the loading is almost exclusively carried by membrane stresses. However, once the roof is in contact with the longitudinal restraints, see Fig. 9.11(c-d), the shell contains significant bending stresses. Hence, in this case the fundamental character of the shell problem has changed from a purely membrane-dominated problem to a problem with significant bending actions.

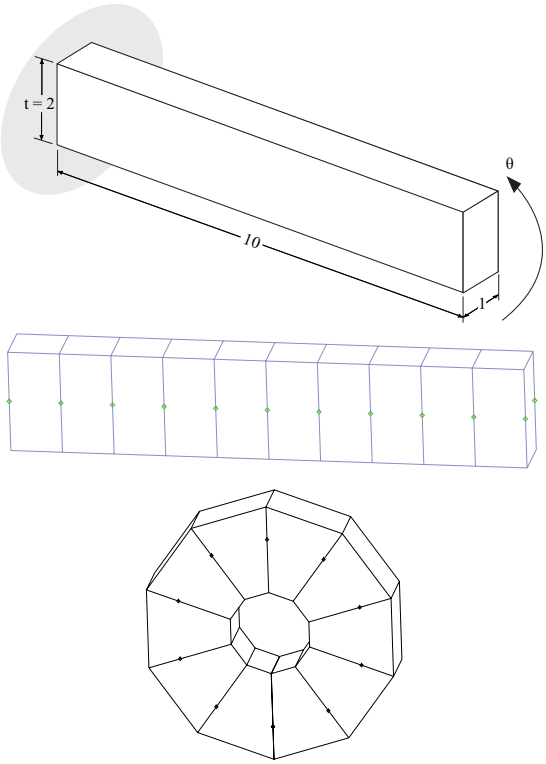

Fig. 9.8. Schematic of thick cantilever beam problem (top), with mesh in original (middle) and deformed (bottom) configurations (Neo-Hookean constant 1 MPa, lengths in cm)

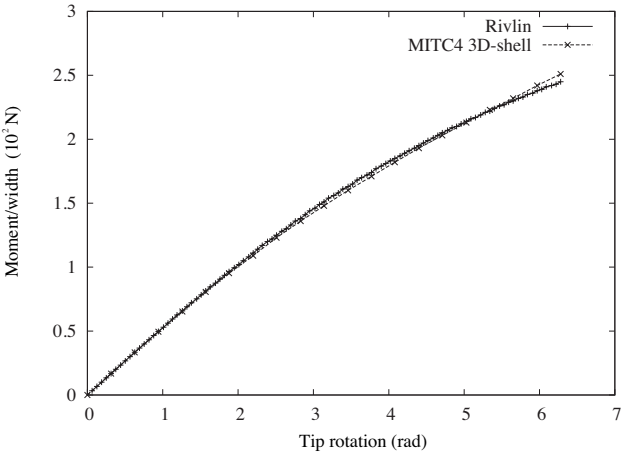

Fig. 9.9. Thick cantilever response: comparison of Rivlin and MITC4 3D-shell solutions

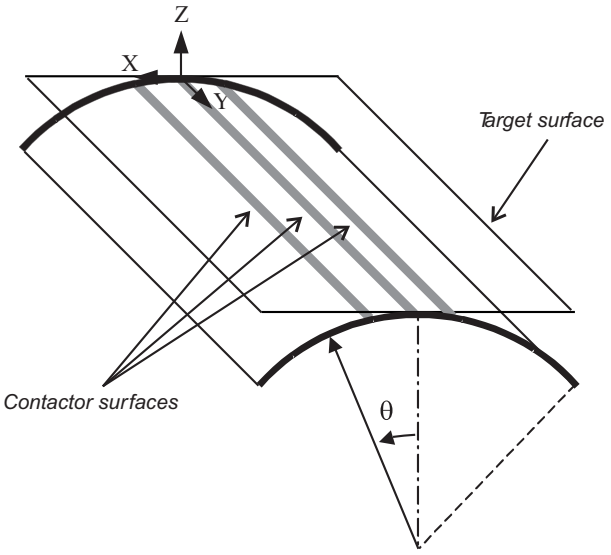

Fig. 9.10. Roof structure: problem definition

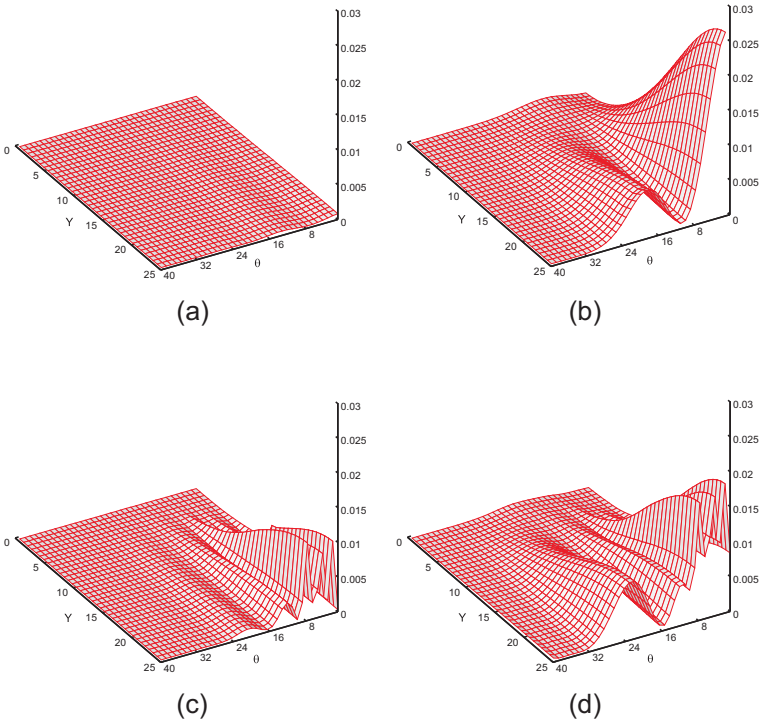

Fig. 9.11. Energy distributions in quarter of roof structure. Before contact: (a) bending energy, (b) total energy. With contact: (c) bending energy, (d) total energy

9.4.5 Crash analysis of a tube

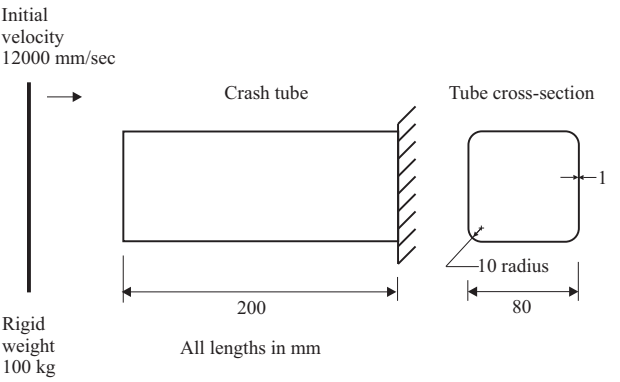

Material properties, plastic-cyclic material model:
E=207000 MPa
ν=0.3
ρ=7850 kg/m^3
σ_y=225 MPa
Nonlinear kinematic hardening:
h=280000 MPa
ζ=1300

Fig. 9.12. Crashed tube: problem definition

The steel tube shown in Figure 9.12 is crashed by a rigid weight given an initial velocity of 12 m.s^{-1} (Bathe et al., 201x). The steel material of the tube is modeled as elasto-plastic with kinematic hardening.

While the tube is quite thin, we model it using the MITC4 3D-shell element in order to capture the large strain behavior and the self-contact conditions which develop automatically during the response. This is of course a dynamic problem, and we use the implicit time integration scheme presented in Bathe (2007) with 1400 steps.

Figure 9.13 shows the contact force between the rigid plate and the tube as a function of the tube tip (contact) displacement during the tube crashing. The initial, an intermediate deformed and the final deformed meshes are shown in Fig. 9.14 As a check on the analysis results, the integrated energy under the force-deflection curve is virtually equal to the initial kinetic energy of the rigid plate.

For the solution of this problem, the 3D-shell element is effective because large strain conditions during the folding process need be simulated (see Fig. 9.14 for typical accumulated effective plastic strain values) and the self-contact can be modeled directly. Note that the ratio of thickness to radius of curvature changes drastically during the large deformation response of the shell.

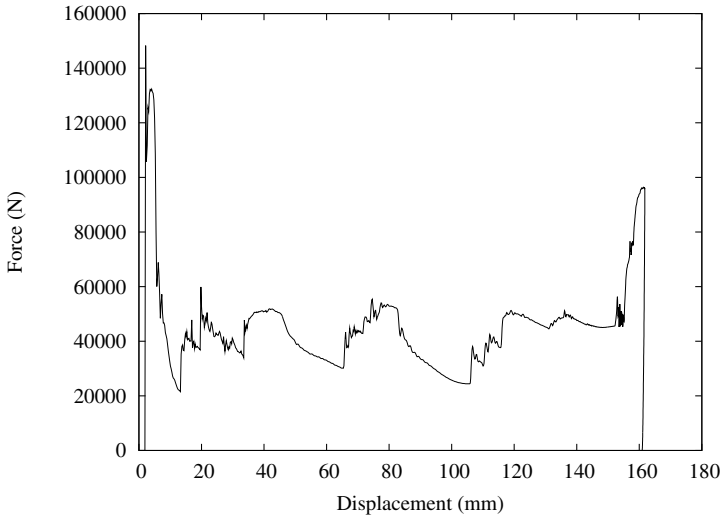

Fig. 9.13. Crashed tube: contact force as function of displacement

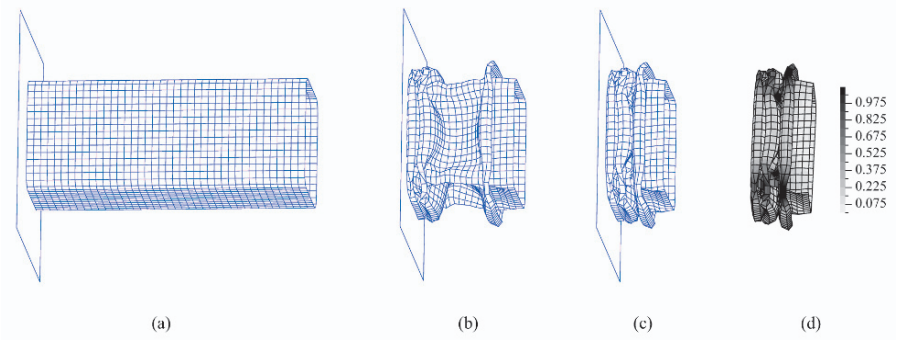

Fig. 9.14. Crashed tube: undeformed configuration (a), intermediate (b) and final (c) solutions, with accumulated effective plastic strains (d)

A. Tables of symbols

In this appendix, we recall the meaning of the main symbols used in this book, with the number of the page where their definition is introduced (when relevant). We recall that Latin dummy indices implicitly vary between 1 and 3, whereas Greek dummy indices implicitly vary between 1 and 2.

We point out that the same notation may be used to refer to different quantities provided that there is no possible confusion in a given context.

A.1 Latin Symbols

	Symbol, meaning and page number	
A^{3Ds}	bilinear form in the 3D-shell model	130
A_h^{3Ds}	id. with approximate geometry	256
A^B	bilinear form in the basic model	125
A^K	bilinear form in the m-b model	123
A^N	bilinear form in the s-m-b model	114
$A_{\rm b}$	scaled bending virtual work	137
$A_{\rm b}^{3Ds}$	id. in 3D-shell model	193
$A_{\rm m}$	scaled membrane (and shear if any) virtual work	137
$A_{\rm m}^{3Ds}$	id. in 3D-shell model	193
A^{3D}	3D plane-stress internal virtual work	228
A_h^{3D}	id. with approximate geometry	230
a	determinant of matrix $(a_{\alpha\beta})$	27
$\underline{\underline{a}}$	first fundamental form	26
$\vec{a}_1, \vec{a}_2$	2D covariant basis	25

continued on next page

D. Chapelle, K.-J. Bathe, *The Finite Element Analysis of Shells – Fundamentals*, Computational Fluid and Solid Mechanics, 2nd ed., DOI 10.1007/978-3-642-16408-8,

continued from previous page

Symbol, meaning and page number		
$\vec{a}^1, \vec{a}^2$	2D contravariant basis	25
$\vec{a}_3$	unit normal vector	24
$\underline{\underline{b}}$	second fundamental form	27
$\underline{\underline{c}}$	third fundamental form	30
C, c	generic positive constants	
$C^{\alpha\beta\lambda\mu}$	plane-stress in-plane constitutive coef.	101
${}^0_4C$	shell in-plane constitutive tensor	103
d	depth of beam structure	261
$D^{\alpha\lambda}$	plane-stress transverse constitutive coef.	101
${}^0\underline{\underline{D}}$	shell transverse constitutive tensor	103
dS	surface infinitesimal	27
dV	volume infinitesimal	19
E	Young's modulus	
$\vec{\vec{e}}$	3D linearized strain tensor	96
F^{3Ds}	linear form in the 3D-shell model	130
F_h^{3Ds}	id. with approximate geometry	256
F^B	linear form in the basic model	125
F^K	linear form in the m-b model	123
F^N	linear form in the s-m-b model	114
F^ε	generic external virtual work	137
F^{3D}	3D external virtual work	228
F_h^{3D}	id. with approximate geometry	230
G	scaled external virtual work	138
$\vec{\vec{g}}$	3D metric tensor	13
g	determinant of matrix (g_{mn})	19
$\vec{g}_1, \vec{g}_2, \vec{g}_3$	3D covariant basis	17
$\vec{g}^1, \vec{g}^2, \vec{g}^3$	3D contravariant basis	19

continued on next page

continued from previous page

Symbol, meaning and page number		
H	mean curvature	29
H^p	Sobolev space of order p	50
${}^{(4)}H$	Hooke's law tensor	100
h	mesh parameter	60
K	Gaussian curvature	29
k	shear correction factor	104
L	overall characteristic dimension	136
L^2	fundamental Sobolev space	48
L_1, L_2	Lamé constants	100
l	thickness profile	136
p	approximation order of the FE shape functions	223
q^ε	scaled shear force in Timoshenko beam	267
$\underline{q}^\varepsilon$	scaled shear force in RM plate	278
R_h	reduction operator	295
(r, s)	tangential local coordinates	228
$\vec{x}_1, \vec{x}_2, \vec{x}_3$	reference orthonormal basis	25
t	thickness of the shell	24
$t_{\min}$	minimum thickness	121
U^ε	generic shell solution for given ε	137
U^0	generic limit bending solution	142
U^{m}	generic limit membrane solution	147
$\vec{U}$	3D displacement solution	95
$\vec{U}_h$	3D displacement FE-solution	230
$\vec{u}$	midsurface displacement solution	95
$\vec{u}_h$	midsurface displacement FE-solution	230
V	generic shell displacement test function	137
$\vec{V}$	3D displacement test function	102

continued on next page

continued from previous page

Symbol, meaning and page number		
$\vec{v}$	midsurface displacement test function	95
$T, \tilde{T}$	original/scaled tip load in Timoshenko beam	261
z	transverse local coordinate	228

A.2 Greek Symbols

Symbol, meaning and page number		
δ^n_m	Kronecker symbol	
$\underline{\underline{\epsilon}}$	symmetrized gradient tensor	117
ε	non-dimensional thickness parameter	136
$\underline{\eta}, \vec{\eta}$	rotation test function	102
$\vec{\Phi}$	3D chart	17
$\vec{\phi}$	surface chart	24
$\bar{\Gamma}^k_{nm}$	3D Christoffel symbols	21
$\Gamma^\lambda_{\beta\alpha}$	surface Christoffel symbols	31
γ	generic *strictly positive* constant	
$\underline{\underline{\gamma}}$	membrane strain tensor	97
$\lambda_i(r,s)$	2D finite element shape function	228
ν	Poisson's ratio	
Ω	3D reference domain	17
ω	surface reference domain	24
π	projection operator onto tangential plane	232
$\underline{\underline{\bar{\rho}}}$	linearized change of curvature tensor	106
ρ	scaling exponent for loading	138
$\vec{\vec{\sigma}}$	3D stress tensor	
$\underline{\theta}, \vec{\theta}$	rotation solution	95

continued on next page

continued from previous page

Symbol, meaning and page number		
$\vec{\theta}_h$	rotation FE-solution	230
ξ^1, ξ^2, ξ^3	curvilinear coordinates	17
$\underline{\underline{\chi}}$	bending strain tensor	97
$\underline{\zeta}$	shear strain tensor	97

A.3 Special Symbols

Symbol, meaning and page number		
$\mathcal{B}$	3D shell body	24
$\mathcal{BC}$	boundary conditions	
$\mathcal{E}$	Euclidean (physical) space	9
$\mathcal{I}$	FE-interpolation operator	232
$\mathbb{R}$	set of real numbers	
$\mathcal{S}$	shell midsurface	24
$\mathcal{T}$	generic stress space in mixed formulations	62
$\mathcal{T}^+$	generic L^2-type stress space	74
$\mathcal{T}^{RM}$	shear space in RM-plate model	279
$\mathcal{T}_h^{RM}$	FE shear space in RM-plate model	283
$\mathcal{T}^T$	shear space in Timoshenko model	267
$\mathcal{T}_h^T$	FE shear space in Timoshenko model	270
$\mathcal{V}$	generic shell displacement space	137
$\mathcal{V}^{3D}$	3D displ. space (shell domain)	228
$\mathcal{V}_h^{3D}$	3D FE displ. space	229
$\mathcal{V}^{3Ds}$	displ. space in the 3D-shell model	130
$\mathcal{V}^B$	displ. space in the basic model	125
$\mathcal{V}^G$	displ. space for general Reissner-Mindlin kinematics	231

continued on next page

continued from previous page

Symbol, meaning and page number		
$\mathcal{V}_h^G$	general shell element displ. space	232
$\mathcal{V}^K$	displ. space in the m-b model	123
$\mathcal{V}^N$	displ. space in the s-m-b model	114
$\mathcal{V}^{RM}$	displ. space in Reissner-Mindlin plate model	277
$\mathcal{V}^T$	displ. space in Timoshenko model	261
$\mathcal{V}_h^T$	FE displ. space in Timoshenko model	262
$\mathcal{V}_0$	generic subspace of pure bending displ.	141
$\mathcal{V}^{3Ds}$	pure bending subspace in 3D-shell model	192
$\mathcal{V}_0^K$	pure bending subspace in m-b model	152
$\mathcal{V}_0^N$	pure bending subspace in s-m-b model	152
$\mathcal{V}_0^T$	pure bending subspace in Timoshenko model	261

B. Some Useful Mathematical Formulas

We first recall an elementary bound.

Proposition B.1 *For any two real numbers a and b, we have*

$$|ab| \leq \frac{1}{2}\left(\eta\, a^2 + \frac{1}{\eta}\, b^2\right), \qquad \forall \eta > 0. \tag{B.1}$$

Proof. This inequality directly follows from the positiveness of the expressions $\left(\sqrt{\eta}\, a + b/\sqrt{\eta}\right)^2$ and $\left(\sqrt{\eta}\, a - b/\sqrt{\eta}\right)^2$. ∎

The following result is very useful when manipulating norms in product spaces.

Proposition B.2 *For any set of n real numbers $(a_i)_{1\leq i\leq n}$, we have*

$$\frac{1}{\sqrt{n}} \sum_{i=1}^{n} |a_i| \leq \left(\sum_{i=1}^{n} (a_i)^2\right)^{\frac{1}{2}} \leq \sum_{i=1}^{n} |a_i|. \tag{B.2}$$

Proof. Noting that (B.2) expresses the equivalence of two norms in $\mathbb{R}^n$, the equivalence itself directly follows because all norms are equivalent in finite-dimensional vector spaces, hence

$$\gamma \sum_{i=1}^{n} |a_i| \leq \left(\sum_{i=1}^{n} (a_i)^2\right)^{\frac{1}{2}} \leq C \sum_{i=1}^{n} |a_i|, \tag{B.3}$$

for *some constants* γ and C. In order to obtain actual values for these constants, we develop

$$\begin{aligned}\left(\sum_{i=1}^{n}|a_i|\right)^2 &= \sum_{i=1}^{n}(a_i)^2 + 2\sum_{1\le i<j\le n}|a_i a_j| \\ &\le \sum_{i=1}^{n}(a_i)^2 + \sum_{1\le i<j\le n}(|a_i|^2+|a_j|^2) \\ &\le n\sum_{i=1}^{n}(a_i)^2, \end{aligned} \tag{B.4}$$

where we have used (B.1) with $a = a_i$, $b = a_j$ and $\eta = 1$, and the fact that each given index appears exactly $(n-1)$ times in a summation over $1 \le i < j \le n$. The other inequality directly follows from the first line of (B.4). We can see that these bounding constants are sharp by choosing all numbers equal for C, and all numbers but one equal to zero for γ. We also see how the equivalence "degenerates" (with the growth of $\sqrt{n}$) when the dimension of the vector space increases. ■

C. Distributions: Basic Definitions and Properties

This appendix aims at recalling the fundamental concepts and results of the theory of distributions that are strictly necessary for the understanding of our discussions in this book. For more details, we refer to (Schwartz, 1966; Dautray & Lions, 1988–1993).

Considering an open set $\mathcal{O}$ in $\mathbb{R}^n$, we denote by $C_0^\infty(\mathcal{O})$ the space of indefinitely differentiable functions with compact support in $\mathcal{O}$ (namely, each function vanishes outside of a compact subset of $\mathcal{O}$). In addition, for any compact subset Q we denote by C_Q^∞ the space of functions of $C_0^\infty(\mathcal{O})$ that vanish outside of Q.

Given a linear real-valued operator ϕ defined on $C_0^\infty(\mathcal{O})$, we say that ϕ is a *distribution* in $\mathcal{O}$ if, for any compact subset Q of $\mathcal{O}$, there exist an integer p and a constant C such that

$$\boxed{\forall u \in C_Q^\infty, \qquad |\phi(u)| \leq C \sup_{\xi \in Q,\, |\mathbf{m}| \leq p} |\partial_{\mathbf{m}} u(\xi)|.} \tag{C.1}$$

Note that the integer p reflects the regularity of the distribution, namely, with a lower p the distribution is more regular. The space of all distributions in $\mathcal{O}$ is a vector space that we denote by $\mathcal{D}'(\mathcal{O})$. In the sequel, we denote the action of distributions on functions of $C_0^\infty(\mathcal{O})$ by

$$\langle\, \phi, u \,\rangle_{\mathcal{D}'(\mathcal{O}) \times C_0^\infty(\mathcal{O})} = \phi(u). \tag{C.2}$$

We point out that the notation $\mathcal{D}(\mathcal{O})$ is also often found instead of $C_0^\infty(\mathcal{O})$ in the literature.

We now give some basic examples of distributions.

Example C.1
Consider a continuous function f defined in $\mathcal{O}$, and any function $u \in C_Q^\infty$ for Q arbitrary. We have

$$\left| \int_{\mathcal{O}} f u \, d\mathcal{O} \right| \leq \left(\int_{\mathcal{O}} |f| \, d\mathcal{O} \right) \sup_{\xi \in Q} |u(\xi)|, \tag{C.3}$$

hence f defines a distribution through

$$\langle f, u \rangle_{\mathcal{D}'(\mathcal{O}) \times C_0^\infty(\mathcal{O})} = \int_{\mathcal{O}} f u \, d\mathcal{O}. \tag{C.4}$$

In fact, the use of integration such as in this equation is the basic means of constructing distributions based on regular functions. ■

The following example shows that distributions can be built using less regular functions.

Example C.2
Consider $\phi \in L^2(\mathcal{O})$ and take, for any compact subset Q of $\mathcal{O}$, a function $u \in C_Q^\infty$. Clearly $u \in L^2(\mathcal{O})$, and by the Cauchy-Schwarz inequality we have

$$\left| \int_{\mathcal{O}} \phi u \, d\mathcal{O} \right| \leq \|\phi\|_{L^2(\mathcal{O})} \left(\int_{\mathcal{O}} u^2 \, d\mathcal{O} \right)^{\frac{1}{2}} \leq \|\phi\|_{L^2(\mathcal{O})} \sqrt{|Q|} \sup_{\xi \in Q} |u(\xi)|. \tag{C.5}$$

Hence, ϕ defines a distribution by

$$\langle \phi, u \rangle_{\mathcal{D}'(\mathcal{O}) \times C_0^\infty(\mathcal{O})} = \int_{\mathcal{O}} \phi u \, d\mathcal{O} \tag{C.6}$$

and therefore we can write

$$L^2(\mathcal{O}) \subset \mathcal{D}'(\mathcal{O}). \tag{C.7}$$

Of course, this inclusion also holds for higher-order Sobolev spaces, recall (3.52). ■

We can also define distributions without resorting to actual functions, as can be seen in the next example.

Example C.3
Consider the Dirac delta "function". Assuming that $\mathcal{O}$ contains 0, by definition for any function u in C_Q^∞ we have $\delta(u) = u(0)$. Therefore

$$|\delta(u)| \leq \sup_{\xi \in Q} |u(\xi)|, \tag{C.8}$$

and the delta "function" thus defines a distribution. Clearly, this distribution is not a function (since it cannot be defined by its point values), which is why we used quotes above. It is – indeed – one of the primary objectives of distributions to extend the classical functional framework. ■

We now come to the definition of differentiation for distributions. Considering a C^1 function f, the classical derivatives of f are distributions, see Example C.1, and we have for any u in $C_0^\infty(\mathcal{O})$

$$\begin{aligned}\langle \frac{\partial f}{\partial \xi^i}, u \rangle_{\mathcal{D}'(\mathcal{O})\times C_0^\infty(\mathcal{O})} &= \int_{\mathcal{O}} \frac{\partial f}{\partial \xi^i} u \, d\mathcal{O} \\ &= -\int_{\mathcal{O}} f \frac{\partial u}{\partial \xi^i} \, d\mathcal{O} \\ &= -\langle f, \frac{\partial u}{\partial \xi^i} \rangle_{\mathcal{D}'(\mathcal{O})\times C_0^\infty(\mathcal{O})}, \end{aligned} \tag{C.9}$$

where we have used Green's formula. Note that the last expression in (C.9) can be written because $\frac{\partial u}{\partial \xi^i}$ is also in $C_0^\infty(\mathcal{O})$. The general definition of the derivatives of a distribution is a direct extension of this identity. Namely, for any distribution ϕ in $\mathcal{D}'(\mathcal{O})$ we define $\frac{\partial \phi}{\partial \xi^i}$ as the distribution given by, for any $u \in C_0^\infty(\mathcal{O})$,

$$\boxed{\langle \frac{\partial \phi}{\partial \xi^i}, u \rangle_{\mathcal{D}'(\mathcal{O})\times C_0^\infty(\mathcal{O})} = -\langle \phi, \frac{\partial u}{\partial \xi^i} \rangle_{\mathcal{D}'(\mathcal{O})\times C_0^\infty(\mathcal{O})},} \tag{C.10}$$

and it is – indeed – easily seen that $\frac{\partial \phi}{\partial \xi^i}$ thus-defined fulfills the above definition property of distributions.

We demonstrate the power and the flexibility of this extended differentiation concept in the following example.

Example C.4
Assume that $\mathcal{O}$ is bounded and consider the variational problem
Find u in $H_0^1(\mathcal{O})$ such that

$$\int_{\mathcal{O}} \vec{\nabla} u \cdot \vec{\nabla} v \, d\mathcal{O} = \int_{\mathcal{O}} f v \, d\mathcal{O}, \qquad \forall v \in H_0^1(\mathcal{O}), \tag{C.11}$$

where $f \in L^2(\mathcal{O})$. We know from Chapter 3 that this problem has a unique solution. Of course $C_0^\infty(\mathcal{O}) \subset H_0^1(\mathcal{O})$, and considering an arbitrary test function $v \in C_0^\infty(\mathcal{O})$ we obtain

$$\begin{aligned}\int_{\mathcal{O}} \vec{\nabla} u \cdot \vec{\nabla} v \, d\mathcal{O} &= \sum_{i=1}^{n} \langle \frac{\partial u}{\partial \xi^i}, \frac{\partial v}{\partial \xi^i} \rangle_{\mathcal{D}'(\mathcal{O})\times C_0^\infty(\mathcal{O})} \\ &= -\langle \Delta u, v \rangle_{\mathcal{D}'(\mathcal{O})\times C_0^\infty(\mathcal{O})}, \end{aligned} \tag{C.12}$$

using the above rule of differentiation of distributions. Also

$$\int_{\mathcal{O}} f v \, d\mathcal{O} = \langle f, v \rangle_{\mathcal{D}'(\mathcal{O})\times C_0^\infty(\mathcal{O})}. \tag{C.13}$$

We infer that

$$-\Delta u = f, \tag{C.14}$$

where the equality holds in the distribution sense (note that Δu is not *a priori* in L^2, since u is only in H^1). Conversely, if we seek u in $H_0^1(\mathcal{O})$ that satisfies (C.14) we – of course – obtain by the same chain of equalities that

$$\int_{\mathcal{O}} \vec{\nabla} u \cdot \vec{\nabla} v \, d\mathcal{O} = \int_{\mathcal{O}} f v \, d\mathcal{O}, \tag{C.15}$$

for any $v \in C_0^\infty(\mathcal{O})$. Therefore, since $C_0^\infty(\mathcal{O})$ is dense in $H_0^1(\mathcal{O})$ (Adams, 1975), we infer that (C.11) holds. Finally, we found that the two equations (C.11) and (C.14) are equivalent (when seeking a solution in $H_0^1(\mathcal{O})$). For comments regarding the physical meaning of the equivalence, we refer to (Bathe, 1996). ■

Bibliography

Adams, R.A. (1975). *Sobolev Spaces*. New York: Academic Press.

Ahmad, S., Irons, B.M., & Zienkiewicz, O.C. (1970). Analysis of thick and thin shell structures by curved finite elements. *Internat. J. Numer. Methods Engrg.*, *2*, 419–451.

Ainsworth, M., & Oden, J.T. (2000). *A Posteriori Error Estimation in Finite Element Analysis*. New York: John Wiley & Sons.

Akian, J.L., & Sanchez-Palencia, E. (1992). Approximation de coques élastiques minces par facettes planes. Phénomènes de blocage membranaire. *C. R. Acad. Sci. Paris*, *t.315*, 363–369. Série I.

Alessandrini, S.M., Arnold, D.N., Falk, R.S., & Madureira, A. L. (1999). Derivation and justification of plate models by variational methods. In *Plates and shells (Québec, QC, 1996)*, vol. 21 of *CRM Proc. Lecture Notes*, (pp. 1–20). Providence: Amer. Math. Soc.

Argyris, J.H. (1954). Energy theorems and structural analysis, part I. *Aircraft Engineering*, *26*.

Argyris, J.H., & Kelsey, S. (1955). Energy theorems and structural analysis, part II. *Aircraft Engineering*, *27*.

Arnold, D.N. (1981). Discretization by finite elements of a model parameter dependent problem. *Numer. Math.*, *37*, 405–421.

Arnold, D.N., & Brezzi, F. (1993). Some new elements for the Reissner-Mindlin plate model. In J. Lions, & C. Baiocchi (Eds.) *Boundary Value Problems for Partial Differential Equations and Applications*, (pp. 287–292). Paris: Masson.

Arnold, D.N., & Brezzi, F. (1997a). Locking-free finite element methods for shells. *Math. Comp.*, *66*(217), 1–14.

Arnold, D.N., & Brezzi, F. (1997b). The partial selective reduced integration method and applications to shell problems. *Comput. & Structures*, *64*(1-4), 879–880.

Arnold, D.N., & Falk, R.S. (1996). Asymptotic analysis of the boundary layer for the Reissner-Mindlin plate model. *SIAM J. Math. Anal.*, *27*(2), 486–514.

Artioli, E., Beirão da Veiga, L., Hakula, H., & Lovadina, C. (2008). Free vibrations for some Koiter shells of revolution. *Appl. Math. Lett.*, *21*, 1245—1248.

Babuška, I. (1973). The finite element method with Lagrangian multipliers. *Numer. Math.*, *20*, 179–192.

Babuška, I., & Strouboulis, T. (2001). *The Finite Element Method and its Reliability*. New York: The Clarendon Press, Oxford University Press.

Başar, Y., & Krätzig, W.B. (2000). Theory of shell structures. Research Report 258, Institut für Konstruktiven Ingenieurbau, Ruhr-Universität Bochum.

Baiocchi, C., & Lovadina, C. (2002). A shell classification by interpolation. *Math. Models Methods Appl. Sci.*, *12*(10), 1359–1380.

Banach, S. (1932). *Théorie des Opérations Linéaires*. Warszawa.

Bathe, K.J. (1996). *Finite Element Procedures*. Englewood Cliffs: Prentice Hall.

Bathe, K.J. (Ed.) (1999). *Nonlinear Finite Element Analysis and ADINA*, vol. 72 of *Computers & Structures*.

Bathe, K.J. (Ed.) (2001a). *Computational Fluid and Solid Mechanics, Proceedings of the First M.I.T. Conference on Computational Fluid and Solid Mechanics*. Elsevier.

Bathe, K.J. (2001b). The inf-sup condition and its evaluation for mixed finite element methods. *Comput. & Structures*, *79*, 243–252, 971.

Bathe, K.J. (2007). Conserving energy and momentum in nonlinear dynamics: A simple implicit time integration scheme. *Comput. & Structures*, *85*, 437–445.

Bathe, K.J. (2009). The finite element method. In B. Wah (Ed.) *Encyclopedia of Computer Science and Engineering*, (pp. 1253–1264). John Wiley & Sons.

Bathe, K.J., & Brezzi, F. (1985). On the convergence of a four-node plate bending element based on Mindlin-Reissner plate theory and a mixed interpolation. In J. Whiteman (Ed.) *The Mathematics of Finite Elements and Applications V*, (pp. 491–503). New York: Academic Press.

Bathe, K.J., & Brezzi, F. (1987). A simplified analysis of two plate bending elements—the MITC4 and MITC9 elements. In *Proceedings, Numerical Methods in Engineering: Theory and Applications*.

Bathe, K.J., Brezzi, F., & Cho, S.W. (1989). The MITC7 and MITC9 plate bending elements. *Comput. & Structures*, *32*(3/4), 797–814.

Bathe, K.J., Bucalem, M.L., & Brezzi, F. (1990). Displacement and stress convergence of our MITC plate bending elements. *Eng. Comput.*, *7*, 291–302.

Bathe, K.J., Chapelle, D., & Lee, P.S. (2003a). A shell problem 'highly sensitive' to thickness changes. *Internat. J. Numer. Methods Engrg.*, *57*, 1039–1052.

Bathe, K.J., & Dvorkin, E.N. (1985). A four-node plate bending element based on Mindlin/Reissner plate theory and a mixed interpolation. *Internat. J. Numer. Methods Engrg.*, *21*, 367–383.

Bathe, K.J., & Dvorkin, E.N. (1986). A formulation of general shell elements—the use of mixed interpolation of tensorial components. *Internat. J. Numer. Methods Engrg.*, *22*, 697–722.

Bathe, K.J., Hiller, J.F., & Zhang, H. (2002). On the finite element analysis of shells and their full interaction with Navier-Stokes fluid flows. In B. Topping, & Z. Bittnar (Eds.) *Computational Structures Technology*. Edinburgh: Civil-Comp Press.

Bathe, K.J., Iosilevich, A., & Chapelle, D. (2000a). An evaluation of the MITC shell elements. *Comput. & Structures*, *75*(1), 1–30.

Bathe, K.J., Iosilevich, A., & Chapelle, D. (2000b). An inf-sup test for shell finite elements. *Comput. & Structures*, *75*(5), 439–456.

Bathe, K.J., & Lee, P.S. (201x). Measuring the convergence behavior of shell analysis schemes. In preparation.

Bathe, K.J., Lee, P.S., & Hiller, J.F. (2003b). Towards improving the MITC9 shell element. *Comput. & Structures*, *81*(8–11), 477–489.

Bathe, K.J., Sussman, T., & Walczak, J. (201x). Crash and crush shell analyses with implicit integration. In preparation.

Bathe, K.J., & Wilson, E.L. (1974). Thick shells. In W. Pilkey, K. Saczalski, & H. Schaeffer (Eds.) *Structural Mechanics Computer Programs*.

Batoz, J.L., Bathe, K.J., & Ho, L.W. (1980). A study of three-node triangular plate bending elements. *Internat. J. Numer. Methods Engrg.*, *15*(2), 1771–1812.

Beirão da Veiga, L., Chapelle, D., & Paris Suarez, I. (2007). Towards improving the MITC6 triangular shell element. *Comput. & Structures*, *85*, 1589–1610.

Beirão da Veiga, L., Hakula, H., & Pitkäranta, J. (2008). Asymptotic and numerical analysis of the eigenvalue problem for a clamped cylindrical shell. *Math. Models Methods Appl. Sci.*, *18*(11), 1983–2002.

Bernadou, M. (1996). *Finite Element Methods for Thin Shell Problems*. New York: John Wiley & Sons.

Bernadou, M., & Ciarlet, P.G. (1975). Sur l'ellipticité du modèle linéaire de coques de W.T. Koiter. In R. Glowinski, & J. Lions (Eds.) *Computing Methods in Applied Sciences and Engineering*. Heidelberg: Springer-Verlag.

Bernadou, M., Ciarlet, P.G., & Miara, B. (1994a). Existence theorems for two-dimensional linear shell theories. *J. Elasticity*, *34*(2), 111–138.

Bernadou, M., Mato Eiroa, P., & Trouvé, P. (1994b). On the convergence of a discrete Kirchhoff triangle method valid for shells of arbitrary shape. *Comput. Methods Appl. Mech. Engrg.*, *118*, 373–391.

Bernadou, M., & Trouvé, P. (1989). Approximation of general shell problems by flat plate elements. Part 1. *Comput. Mech.*, *5*, 175–208.

Bernadou, M., & Trouvé, P. (1990a). Approximation of general shell problems by flat plate elements. Part 2: Addition of a drilling degree of freedom. *Comput. Mech.*, *6*, 359–378.

Bernadou, M., & Trouvé, P. (1990b). Approximation of general shell problems by flat plate elements. Part 3: Extension to triangular facet elements. *Comput. Mech.*, *7*, 1–11.

Betsch, P., & Stein, E. (1995). An assumed strain approach avoiding artificial thickness straining for a non-linear 4-node shell element. *Commun. Numer. Meth. Engng.*, *11*, 899–909.

Bischoff, M., & Ramm, E. (1997). Shear deformable shell elements for large strains and rotations. *Internat. J. Numer. Methods Engrg.*, *40*, 4427–4449.

Bischoff, M., & Ramm, E. (2000). On the physical significance of higher order kinematic and static variables in a three-dimensional shell formulation. *Internat. J. Solids Structures*, *37*, 6933–6960.

Blouza, A., Brezzi, F., & Lovadina, C. (1999). Sur la classification des coques linéairement élastiques. *C. R. Acad. Sci. Paris, Série I*, *328*, 831–836.

Blouza, A., & Le Dret, H. (1999). Existence and uniqueness for the linear Koiter model for shells with little regularity. *Quart. Appl. Math.*, *57*, 317–337.

Boffi, D., Brezzi, F., & Gastaldi, L. (1997). On the convergence of eigenvalues for mixed formulations. *Annali Sc. Norm. Sup. Pisa Cl. Sci.*, *25*, 131–154.

Bramble, J.H., & Sun, T. (1998). A locking-free finite element method for Naghdi shells. *J. Comput. Appl. Math.*, *89*, 119–133.

Brenner, S.C., & Scott, L.R. (1994). *The Mathematical Theory of Finite Element Methods*. New York: Springer-Verlag.

Brezzi, F. (1974). On the existence, uniqueness and approximation of saddle-point problems arising from Lagrangian multipliers. *R.A.I.R.O., Anal. Numér.*, *8*, 129–151.

Brezzi, F., & Bathe, K.J. (1990). A discourse on the stability conditions for mixed finite element formulations. *Comput. Methods Appl. Mech. Engrg.*, *82*, 27–57.

Brezzi, F., Bathe, K.J., & Fortin, M. (1989). Mixed-interpolated elements for Reissner-Mindlin plates. *Internat. J. Numer. Methods Engrg.*, *28*, 1787–1801.

Brezzi, F., & Fortin, M. (1991). *Mixed and Hybrid Finite Element Methods*. New York: Springer-Verlag.

Brezzi, F., Fortin, M., & Stenberg, R. (1991). Error analysis of mixed-interpolated elements for Reissner-Mindlin plates. *Math. Models Methods Appl. Sci.*, *1*(2), 125–151.

Briassoulis, D. (2002a). Testing the asymptotic behaviour of shell elements - Part I: the classical benchmark tests. *Internat. J. Numer. Methods Engrg.*, *54*(3), 421–452.

Briassoulis, D. (2002b). Testing the asymptotic behaviour of shell elements - Part II: analytical solutions and the RFNS element case. *Internat. J. Numer. Methods Engrg.*, *54*(5), 631–670.

Bucalem, M.L., & Bathe, K.J. (1993). Higher-order MITC general shell elements. *Internat. J. Numer. Methods Engrg.*, *36*, 3729–3754.

Bucalem, M., & Bathe, K.J. (201x). *The Mechanics of Solids and Structures — Hierarchical Modeling and the Finite Element Solution*. Springer.

Bucalem, M.L., & Shimura da Nóbrega, S.H. (2000). A mixed formulation for general triangular isoparametric shell elements based on the degenerated solid approach. *Comput. & Structures*, *78*(1), 35–44.

Calladine, C.R. (1983). *Theory of Shell Structures*. Cambridge: Cambridge University Press.

Carrive, M., Le Tallec, P., & Mouro, J. (1995). Approximation par éléments finis d'un modèle de coques géométriquement exact. *Revue Européenne des Eléments Finis*, *4*(5–6), 633–662.

Céa, J. (1964). Approximation variationnelle des problèmes aux limites. *Annales de l'Institut Fourier*, *14*, 345–444.

Chapelle, D. (1993). Une formulation mixte de plaques où l'effort tranchant est approché dans son espace naturel. Research Report 2248, INRIA.

Chapelle, D. (1997). A locking-free approximation of curved rods by straight beam elements. *Numer. Math.*, *77*, 299–322.

Chapelle, D. (2001). Some new results and current challenges in the finite element analysis of shells. In *Acta Numerica*, (pp. 215–250). Cambridge: Cambridge University Press.

Chapelle, D., & Bathe, K.J. (1993). The inf-sup test. *Comput. & Structures*, *47*(4/5), 537–545.

Chapelle, D., & Bathe, K.J. (1998). Fundamental considerations for the finite element analysis of shell structures. *Comput. & Structures*, *66*, 19–36, 711–712.

Chapelle, D., & Bathe, K.J. (2000). The mathematical shell model underlying general shell elements. *Internat. J. Numer. Methods Engrg.*, *48*(2), 289–313.

Chapelle, D., & Bathe, K.J. (2010). On the ellipticity condition for model-parameter dependent mixed formulations. *Comput. & Structures*, *88*, 581–587. Doi:10.1016/j.compstruc.2010.01.009.

Chapelle, D., & Ferent, A. (2003). Modeling of the inclusion of a reinforcing sheet within a 3D medium. *Math. Models Methods Appl. Sci.*, *13*, 573–595.

Chapelle, D., Ferent, A., & Bathe, K.J. (2004a). 3D-shell finite elements and their underlying model. *Math. Models Methods Appl. Sci.*, *14*(1), 105–142.

Chapelle, D., Ferent, A., & Le Tallec, P. (2003a). The treatment of "pinching locking" in 3D-shell elements. *M2AN Math. Model. Numer. Anal.*, *37*, 143–158.

Chapelle, D., Mardare, C., & Münch, A. (2004b). Asymptotic considerations shedding light on incompressible shell models. *Journal of Elasticity*, *76*, 199–246.

Chapelle, D., Oliveira, D.L., & Bucalem, M.L. (2003b). MITC elements for a classical shell model. *Comput. & Structures*, *81*, 523–533.

Chapelle, D., & Paris Suarez, I. (2008). Detailed reliability assessment of triangular MITC elements for thin shells. *Comput. & Structures*, *86*, 2192–2202. Doi:10.1016/j.compstruc.2008.06.001.

Chapelle, D., & Stenberg, R (1998a). An optimal low-order locking-free finite element method for Reissner-Mindlin plates. *Math. Models Methods Appl. Sci.*, *8*(3), 407–430.

Chapelle, D., & Stenberg, R. (1998b). Stabilized finite element formulations for shells in a bending dominated state. *SIAM J. Numer. Anal.*, *36*(1), 32–73.

Chenais, D., & Paumier, J.-C. (1994). On the locking phenomenon for a class of elliptic problems. *Numer. Math.*, *67*, 427–440.

Chinosi, C., & Lovadina, C. (1995). Numerical analysis of some mixed finite element methods for Reissner-Mindlin plates. *Comput. Mech.*, *16*, 36–44.

Choï, D., Palma, F.J., Sanchez-Palencia, E., & Vilariño, M.A. (1998). Membrane locking in the finite element computation of very thin elastic shells. *M2AN Math. Model. Numer. Anal.*, *32*(2), 131–152.

Ciarlet, P.G. (1976). Conforming finite element methods for the shell problem. In J. Whiteman (Ed.) *Mathematics of Finite Elements and Applications II*, (pp. 105–123). London: Academic Press.

Ciarlet, P.G. (1978). *The Finite Element Method for Elliptic Problems*. Amsterdam: North-Holland.

Ciarlet, P.G. (1988). *Mathematical Elasticity - Volume I: Three-Dimensional Elasticity*. Amsterdam: North-Holland.

Ciarlet, P.G. (1998). *Introduction to Linear Shell Theory*. Series in Applied Mathematics. Gauthier-Villars & North-Holland.

Ciarlet, P.G. (2000). *Mathematical Elasticity - Volume III: Theory of Shells*. Amsterdam: North-Holland.

Ciarlet, P.G., & Raviart, P.A. (1972). The combined effect of curved boundaries and numerical integration in isoparametric finite element methods. In A. Aziz (Ed.) *The Mathematical Foundations of the Finite Element Method with Applications to Partial Differential Equations*, (pp. 409–474). New York: Academic Press.

Clément, P. (1975). Approximation by finite element functions using local regularization. *R.A.I.R.O., Anal. Numér.*, *8*, 77–84.

Coutris, N. (1978). Théorème d'existence et d'unicité pour un problème de coque élastique dans le cas d'un modèle linéaire de P.M. Naghdi. *R.A.I.R.O. Anal. Numér.*, *12*, 51–57.

Dauge, M., & Yosibash, Z. (2000). Boundary layer realization in thin elastic 3D domains and 2D hierarchic plate models. *Internat. J. Solids Structures*, *37*, 2443–2471.

Dautray, R., & Lions, J.L. (1988–1993). *Mathematical Analysis and Numerical Methods for Science and Technology*, vol. 1–6. Berlin: Springer-Verlag.

Delfour, M.C. (1999). Intrinsic $P(2,1)$ thin shell model and Naghdi's models without a priori assumption on the stress tensor. In K. Hoffmann,

G. Leugering, & F. Tröltzsch (Eds.) *Optimal Control of Partial Differential Equations*, (pp. 99–113). Basel: Birkhäuser.

Delfour, M.C. (2000). Tangential differential calculus and functional analysis on a $C^{1,1}$ submanifold. In R. Gulliver, W. Littman, & R. Triggiani (Eds.) *Differential-Geometric Methods in the Control of Partial Differential Equations*, (pp. 83–115). Providence: AMS.

Destuynder, P., & Salaün, M. (1995a). A mixed finite element for shell model with free edge boundary conditions. Part 1. The mixed variational formulation. *Comput. Methods Appl. Mech. Engrg.*, *120*, 195–217.

Destuynder, P., & Salaün, M. (1995b). A mixed finite element for shell model with free edge boundary conditions. Part 2. The numerical scheme. *Comput. Methods Appl. Mech. Engrg.*, *120*, 219–242.

Destuynder, P., & Salaün, M. (1996). A mixed finite element for shell model with free edge boundary conditions. Part 3. Numerical aspects. *Comput. Methods Appl. Mech. Engrg.*, *136*, 273–292.

Destuynder, P., & Salaün, M. (1998). Approximation of shell geometry for nonlinear analysis. *Comput. Methods Appl. Mech. Engrg.*, *156*, 111–148.

Dvorkin, E.N., & Bathe, K.J. (1984). A continuum mechanics based four-node shell element for general non-linear analysis. *Eng. Comput.*, *1*, 77–88.

Flügge, W. (1973). *Stresses in Shells*. New York, Heidelberg: Springer-Verlag, 2nd ed.

Frey, P.J., & George, P.L. (2000). *Mesh Generation*. Oxford: HERMES Science Publishing.

Glowinski, R., & Le Tallec, P. (1989). *Augmented Lagrangian and Operator-Splitting Methods in Nonlinear Mechanics*. SIAM Studies in Applied Mathematics. Philadelphia: SIAM.

Gol'denweizer, A.L. (1961). *Theory of Elastic Thin Shells*. Oxford: Pergamon Press.

Grätsch, T., & Bathe, K.J. (2005a). Influence functions and goal-oriented error estimation for finite element analysis of shell structures. *Internat. J. Numer. Methods Engrg.*, *63*, 709–736.

Grätsch, T., & Bathe, K.J. (2005b). A posteriori error estimation techniques in practical finite element analysis. *Comput. & Structures*, *83*, 235–265.

Green, A.E., & Zerna, W. (1968). *Theoretical Elasticity*. Oxford: Clarendon Press, 2nd ed.

Häggblad, B., & Bathe, K.J. (1990). Specifications of boundary conditions for Reissner/Mindlin plate bending finite elements. *Internat. J. Numer. Methods Engrg.*, *30*, 981–1011.

Havu, V., & Pitkäranta, J. (2002). Analysis of a bilinear finite element for shallow shells. I: Approximation of inextensional deformations. *Math. Comp.*, *71*, 923–943.

Hencky, H. (1947). Über die Berücksichtigung der Schubverzerrung in ebenen Platten. *Ingenieur Archiv*, *16*, 72–76.

Hiller, J.F., & Bathe, K.J. (2003). Measuring convergence of mixed finite element discretizations: an application to shell structures. *Comput. & Structures*, *81*(8–11), 639–654.

Hughes, T.J.R., & Franca, L.P. (1988). A mixed finite element formulation for Reissner-Mindlin plate theory: uniform convergence of all higher-order spaces. *Comput. Methods Appl. Mech. Engrg.*, *67*, 223–240.

Ibrahimbegović, A., & Krätzig, W.B. (Eds.) (2002). *Shells: Theoretical Formulation, Mathematical Analysis and Finite Element Implementation*, vol. 80(9–10) of *Computers & Structures*. Elsevier. Special issue.

Iosilevich, A., Bathe, K.J., & Brezzi, F. (1997). On evaluating the inf-sup condition for plate bending elements. *Internat. J. Numer. Methods Engrg.*, *40*, 3639–3663.

Karamian, P., Sanchez-Hubert, J., & Sanchez-Palencia, E. (2000). A model problem for boundary layers of thin elastic shells. *M2AN Math. Model. Numer. Anal.*, *34*(1), 1–30.

Kardestuncer, H., & Norrie, D.H. (Eds.) (1987). *Finite Element Handbook*. New York: McGraw-Hill.

Kikuchi, F. (1982). Accuracy of some finite element models for arch problems. *Comput. Methods Appl. Mech. Engrg.*, *35*, 315–345.

Kim, D.N., & Bathe, K.J. (2008). A 4-node 3D-shell element to model shell surface tractions and incompressible behavior. *Comput. & Structures*, *86*(21–22), 2027–2041.

Kim, D.N., & Bathe, K.J. (2009). A triangular six-node shell element. *Comput. & Structures*, *87*, 1451–1460.

Kirchhoff, G. (1876). *Vorlesungen über Mathematische Physik, Vol. 1, Mechanik*.

Kirmse, A. (1993). Bending-dominated deformation of thin spherical shells: analysis and finite element approximation. *SIAM J. Numer. Anal.*, *30*(4), 1015–1040.

Koiter, W.T. (1965). On the nonlinear theory of thin elastic shells. *Proc. Kon. Ned. Akad. Wetensch.*, *B69*, 1–54.

Kojic, M., & Bathe, K.J. (2005). *Inelastic Analysis of Solids and Structures*. Springer.

Ladyzhenskaya, O.A. (1969). *The Mathematical Theory of Viscous Incompressible Flow*. New York: Gordon and Breach.

Lax, P.D., & Milgram, A.N. (1954). Parabolic equations. In *Annals of Mathematics Studies*, 33, (pp. 167–190). Princeton: Princeton University Press.

Lee, N.S., & Bathe, K.J. (1993). Effects of element distortions on the performance of isoparametric elements. *Internat. J. Numer. Methods Engrg.*, *36*, 3553–3576.

Lee, P.S., & Bathe, K.J. (2002). On the asymptotic behavior of shell structures and the evaluation in finite element solutions. *Comput. & Structures*, *80*, 235–255.

Lee, P.S., & Bathe, K.J. (2004). Development of MITC isotropic triangular shell finite elements. *Comput. & Structures*, *82*, 945–962.

Lee, P.S., & Bathe, K.J. (2005). Insight into finite element shell discretizations by use of the "basic shell mathematical model". *Comput. & Structures*, *83*, 69–90.

Lee, P.S., & Bathe, K.J. (2010). The quadratic MITC plate and MITC shell elements in plate bending. *Advances in Engineering Software, in Press*.

Lee, P.S., Noh, H.C., & Bathe, K.J. (2007). Insight into 3-node triangular shell finite elements: the effect of element isotropy and mesh patterns. *Comput. & Structures*, *85*, 404–418.

Leissa, A.W. (1973). *Vibration of Shells*, vol. SP-288. NASA.

Lions, J.L. (1973). *Perturbations Singulières dans les Problèmes aux Limites et en Contrôle Optimal*. Berlin, New York: Springer-Verlag.

Lions, J.L., & Magenes, E. (1972). *Non-Homogeneous Boundary Value Problems and Applications*, vol. 1. Berlin: Springer-Verlag.

Lions, J.L., & Sanchez-Palencia, E. (1994). Problèmes aux limites sensitifs. *C. R. Acad. Sci. Paris, Série I*, *319*, 1021–1026.

Lions, J.L., & Sanchez-Palencia, E. (1996). Problèmes sensitifs et coques élastiques minces. In J. Céa, D. Chenais, G. Geymonat, & J. Lions (Eds.) *Partial Differential Equations and Functional Analysis - In Memory of Pierre Grisvard*, (pp. 207–220). Boston: Birkhäuser.

Lods, V., & Mardaré, C. (1998). The space of inextensional displacements for a partially clamped linear elastic shell with an elliptic middle surface. *J. Elasticity*, *51*, 127–144.

Love, A.E.H. (1927). *Mathematical Theory of Elasticity*. 4th ed.

Lyly, M., & Stenberg, R. (1999). Stabilized finite element methods for Reissner-Mindlin plates. Research Report 4-1999, Universität Innsbruck, Institut für Mathematik und Geometrie.

Malinen, M. (2001). On the classical shell model underlying bilinear degenerated shell finite elements. *Internat. J. Numer. Methods Engrg.*, *52*, 389–416.

Malinen, M., & Pitkäranta, J. (2000). A benchmark study of reduced-strain shell finite elements: quadratic schemes. *Internat. J. Numer. Methods Engrg.*, *48*, 1637–1671.

Mardaré, C. (1998). The generalized membrane problem for linearly elastic shells with hyperbolic or parabolic middle surface. *J. Elasticity*, *51*, 145–165.

Mindlin, R.D. (1951). Influence of rotary inertia and shear on flexural motion of isotropic elastic plates. *J. Appl. Mech.*, *18*, 31–38.

Montans, F.J., & Bathe, K.J. (2005). Computational issues in large strain elasto-plasticity: An algorithm for mixed hardening and plastic spin. *Internat. J. Numer. Methods Engrg.*, *63*, 159–196.

Naghdi, P.M. (1963). Foundations of elastic shell theory. In *Progress in Solid Mechanics*, vol. 4, (pp. 1–90). Amsterdam: North-Holland.

Niemi, A.H. (2009). A bilinear shell element based on a refined shallow shell model. *Internat. J. Numer. Methods Engrg.*, *81*(4), 485–512.

Novozhilov, V.V. (1970). *Thin Shell Theory*. Groningen: Wolters-Noordhoff Publishing, 2nd ed.

Paumier, J.C. (1992). On the locking phenomenon for a linearly elastic clamped plate. Research Report 76, L.M.C., Université Grenoble I.

Peisker, P., & Braess, D. (1992). Uniform convergence of mixed interpolated elements for Reissner-Mindlin plates. *M2AN Math. Model. Numer. Anal.*, *26*(5), 557–574.

Piila, J., & Pitkäranta, J. (1993a). Characterization of the membrane theory of a clamped shell. The parabolic case. *Math. Models Methods Appl. Sci.*, *3*(3), 417–442.

Piila, J., & Pitkäranta, J. (1993b). Energy estimates relating different linear elastic models of a thin cylindrical shell. I. The membrane-dominated case. *SIAM J. Math. Anal.*, *24*(1), 1–22.

Piila, J., & Pitkäranta, J. (1995). Energy estimates relating different linear elastic models of a thin cylindrical shell. II. The case of free boundary. *SIAM J. Math. Anal.*, *26*(4), 820–849.

Pitkäranta, J. (1992). The problem of membrane locking in finite element analysis of cylindrical shells. *Numer. Math.*, *61*, 523–542.

Pitkäranta, J., Leino, Y., Ovaskainen, O., & Piila, J. (1995). Shell deformation states and the finite element method: a benchmark study of cylindrical shells. *Comput. Methods Appl. Mech. Engrg.*, *128*, 81–121.

Pitkäranta, J., Matache, A.M., & Schwab, C. (2001). Fourier mode analysis of layers in shallow shell deformations. *Comput. Methods Appl. Mech. Engrg.*, *190*, 2943–2975.

Pitkäranta, J., & Sanchez-Palencia, E. (1997). On the asymptotic behaviour of sensitive shells with small thickness. *C. R. Acad. Sci. Paris, Série IIb*, *325*, 127–134.

Reissner, E. (1945). The effect of transverse shear deformation on the bending of elastic plates. *J. Appl. Mech.*, *67*, A69–A77.

Reissner, E. (1952). Stress strain relations in the theory of thin elastic shells. *J. Math. Phys.*, *31*, 109–119.

Rivlin, R.S. (1949). Large elastic deformations of isotropic materials VI. further results in the theory of torsion, shear and flexure. *Philosophical Transactions A*, *242*, 173–195.

Roberts, J.E., & Thomas, J.M. (1991). Mixed and hybrid methods. In P. Ciarlet, & J. Lions (Eds.) *Handbook of Numerical Analysis, Vol. II*. Amsterdam: North-Holland.

Rudin, W. (1991). *Functional Analysis*. New York: McGraw-Hill, 2nd ed.

Sanchez-Hubert, J., & Sanchez-Palencia, E. (1997). *Coques Elastiques Minces - Propriétés Asymptotiques*. Paris: Masson.

Sanchez-Hubert, J., & Sanchez-Palencia, E. (2001). Anisotropic finite element estimates and local locking for shells: parabolic case. *C. R. Acad. Sci. Paris, Série IIb*, *329*, 153–159.

Sanchez-Palencia, E. (1989a). Statique et dynamique des coques minces. I. Cas de flexion pure non inhibée. *C. R. Acad. Sci. Paris, Série I*, *309*, 411–417.

Sanchez-Palencia, E. (1989b). Statique et dynamique des coques minces. II. Cas de flexion pure inhibée - Approximation membranaire. *C. R. Acad. Sci. Paris, Série I*, *309*, 531–537.

Sanchez-Palencia, E. (1992). Asymptotic and spectral properties of a class of singular-stiff problems. *J. Math. Pures Appl.*, *71*, 379–406.

Sansour, C. (1995). A theory and finite element formulation of shells at finite deformations involving thickness change: circumventing the use of a rotation tensor. *Arch. Appl. Mech.*, *65*, 194–216.

Schwartz, L. (1966). *Théorie des Distributions*. Paris: Hermann.

Soedel, W. (2004). *Vibrations of Shells and Plates*. Marcel Dekker, 3rd ed.

Temam, R. (1977). *Navier-Stokes Equations*. Amsterdam: North-Holland.

Timoshenko, S., & Woinowsky-Krieger, S. (1959). *Theory of Plates and Shells*. New York: McGraw-Hill.

Turner, M.J., Clough, R.W., Martin, H.C., & Topp, L.J. (1956). Stiffness and deflection analysis of complex structures. *Journal of the Aeronautical Sciences*, *23*, 805–823.

Valid, R. (1995). *The Nonlinear Theory of Shells through Variational Principles*. Chichester: John Wiley & Sons.

Verfürth, R. (1996). *A Review of A Posteriori Error Estimation and Adaptive Mesh Refinement Techniques*. John Wiley & Sons and B.G. Teubner.

Wunderlich, W. (1980). On a consistent shell theory in mixed tensor formulation. In *Proc. 3rd IUTAM Symposium on Shell Theory: Theory of Shells*. Amsterdam: North Holland.

Yosida, K. (1980). *Functional Analysis*. Berlin, New York: Springer-Verlag, 6th ed.

Zienkiewicz, O.C., & Taylor, R.L. (1989/1991). *The Finite Element Method*, vol. 1&2. London: McGraw Hill, 4th ed.

Index